UNIVERSITY OF ILLINOIS AT URBANA-CHAMPAIGN

THE GRADUATE COLLEGE

AUGUST 1994

WE HEREBY RECOMMEND THAT THE THESIS BY

ROBERT MICHAEL McDAVID

ENTITLED FLUID FLOW AND HEAT TRANSFER BEHAVIOR OF TOP-SURFACE FLUX LAYERS IN STEEL CONTINUOUS CASTING

BE ACCEPTED IN PARTIAL FULFILLMENT OF THE REQUIREMENTS FOR THE DEGREE OF MASTER OF SCIENCE

Brian G. Thomas
Director of Thesis Research

R. L. Addy
Head of Department

Committee on Final Examination†

Chairperson

† Required for doctor's degree but not for master's.

O-517

FLUID FLOW AND HEAT TRANSFER BEHAVIOR OF TOP-SURFACE FLUX LAYERS IN STEEL CONTINUOUS CASTING

BY

ROBERT MICHAEL McDAVID

B.Sc., The University of the West Indies, 1990

THESIS

Submitted in partial fulfillment of the requirements
for the degree of Master of Science in Mechanical Engineering
in the Graduate College of the
University of Illinois at Urbana-Champaign, 1994

Urbana, Illinois

QUOTATION & DEDICATION

ABSTRACT

The surface quality of continuously cast steel slabs has been linked to the adequate supply of the liquid flux floating on the top surface. The flux performs several important functions including insulation, lubrication and facilitating uniform gap heat transfer, in addition to removal (i.e. fluxing) of inclusions. Despite its importance, the present work is one of the few studies on the behavior of the top surface flux layers.

The current work combines mathematical modeling and experiments to investigate the thermal distribution, flow pattern and thickness profile of the flux layers. Mathematical models include 1D steady state and transient and 2-D and 3-D steady state formulations. 1-D analytical and finite-element models were developed to study the heat transfer characteristics of the flux. The relationship between process parameters like casting speed, steel pour temperature, flux melting point, thermal conductivity and the steady-state depths of the solid and liquid flux layers was investigated. The results show that casting speed, enthalpy of fusion and melting point of the flux have the most significant effect on the thickness of the layers.

2-D and 3-D steady-state, coupled, finite-element models were created to investigate the effect of fluid flow and convection on the depths of the layers developed in different regions of the mold. The counter-current flow caused by the rapidly flowing steel beneath the flux, and the flux leaving the domain through the mold strand gap results in the formation of recirculation zones. These zones contribute to convective heat transport to the upper layers of the flux, making it thicker near the center of the mold and close to the SEN.

Flow separation in the flux layer results in a temperature distribution and flow pattern which leads to a depletion of liquid, centered at a location 150 mm from the narrowface of the mold. This depletion would result in the poor feeding of the mold-strand gap in general and in the off-corner wideface region in particular. The 3-D model also showed that a cold spot develops at the top suface of the flux, along the wideface wall, due to the flow separation. The resulting

variation in the vertical heat loss along the wideface will possibly result in a larger flux rim, which may lead to more severe quality problems.

The solidified flux rim on the narrowface wall forces colder, mobile flux (in the upper layers) to flow downwards towards the steel/flux interface, before it can enter the neighbouring mold-strand gap (see Figure 7.21). The result is a dip in the flux/melt interface, which corresponds to a decrease in liquid flux thickness at this point, the thinnest liquid layer occuring approximately 20 mm from the narrowface wall.

The flow in the liquid flux in the meniscus region is essentially one dimensional, normal to the heat flux direction. Thus convective heat transport is not significant in this region. As a further consequence, the predicted liquid depths in the meniscus region are very sensitive to the thermal material properties like thermal conductivity but not viscosity.

Enthalpy of fusion has a much less significant effect on layer depths over most of the mold than predicted by the 1-D model. Liquid thermal conductivity does have an effect on liquid layer depths, but the relationship is not proportional, due to the relatively more significant role of convective heat transport. Flux viscosity profiles and melting point have the largest effect. In general, increasing the flux viscosity, decreases the liquid depth due to reduction in liquid velocity and thus convective heat transport. The reduction in liquid layer depth is most significant at the characteristic location where the flow separates. Increasing the melting point decreases the liquid thickness approximately the same (proportionately) in all locations.

ACKNOWLEDGMENTS

First and foremost, I would like to thank Professor Brian G. Thomas for the opportunity to work with him on this complex but fundamentally important project. I am very grateful for his guidance and support over the past two years. Additionally, I would like to acknowledge the assistance of Professor Jonathan A. Dantzig. His insights were useful and greatly appreciated. I would also like to thank ARMCO Inc., Inland Steel, BHP, and LTV Steel for their financial support. Special thanks are extended to LTV Steel, Bill Emling and Lee Hendrix for providing their facilities and assistance with the plant measurements. Support for this project was also provided by the National Science Foundation and the National Center for Supercomputing Applications which allocated time on the CRAY 2 and CRAY Y-MP supercomputers.

I would like to acknowledge the assistance and support of present and recently past members of this research group namely Dr. Xiaoqing Huang, Dr. Avijit Moitra, Guowei Li. They were instrumental in getting me up to speed in the finer details of computational materials process modeling.

Of great importance to me was the truly exceptional friendships I have had the marvelous fortune to enjoy over the past three years. If it were not for the following, my experience to date would have been a shallow and mundane one, and for this I am indebted to them. To Kelly, Diana, Tom, Will, Wim, Laura, Nancy, Rich, Mark and Ed, I say a heartfelt thank you for your companionship, advice and, above all, willingness to party. I will remember each very fondly.

Whatever successes I have had in my life, I owe almost entirely to my immediate family. If it were not for the support, love and counsel of my parents, Richard and Juliet, and my siblings Anthony and Allyson and their indefatigable confidence in me, I would not be where I am today. I cannot begin to express my love and gratitude to them. Finally, and most importantly, I thank Almighty God for his unwavering assistance, guidance, companionship and inspiration throughout my life.

TABLE OF CONTENTS

LIST OF TABLES

LIST OF FIGURES

NOMENCLATURE

k	Thermal conductivity, $\frac{W}{mK}$
k_{eff}	Effective Thermal Conductivity, $\frac{W}{mK}$
k_s	Solid Flux Thermal Conductivity, $\frac{W}{mK}$
k_f, k_{liq}	Liquid Flux Thermal Conductivity, $\frac{W}{mK}$
k_p	Powder Flux Thermal Conductivity, $\frac{W}{mK}$
ΔH_L	Enthalpy of Fusion, $\frac{J}{kg}$
ρ	Density, $\frac{kg}{m^3}$
Π	Total Stress tensor
$\mathbf{V}$	Velocity
V	Volume
u_i	Velocity Component
$\mathbf{f}$	Unit Body Force, $\frac{m}{s^2}$
x_i	Cartesian Direction
δ	Kronecker Delta
Φ	Viscous Dissipation Rate, $\frac{W}{m^3}$
u	Internal Energy, \f(J/m^3)
τ	Shear Stress Tensor
two	Shear Stress at Wall, Pa
U+	Non-dimensionalized Velocity
y+	Non-dimensionalized Distance
K	Turbulent Kinetic Energy, J
C_μ, κ, E	Wall-Law Constants
H	Enthalpy, $\frac{J}{kg}$
c_p	Specific heat, $\frac{J}{kgK}$
T	Temperature, K
$\mathbf{T}$	Vector of Nodal Temperatures

q	Heat Flux, $\frac{W}{m^2}$
η, μ	Kinetic Viscosity, Pa.s
η_s	Kinetic Viscosity at shell surface temp, Pa.s
p	Pressure
$\mathbf{P}$	Vector of Nodal Pressures
Ni	Shape Functions
$\mathbf{N}$	Matrix of Shape Functions
$\{\mathbf{U}^e\}$	Matrix of Element Nodal Solutions
R^e	Element Residual
T_o	Boundary/Surface Temperature, °C
T_∞	Ambient Temperature, °C
T_{melt}	Melting Temperature, °C
T_{st}	Steel Temperature, °C
ΔT	Temperature Difference, K
h	Heat Transfer Coefficient, $\frac{W}{m^2K}$
h_{tot}	Total Heat Transfer Coefficient, $\frac{W}{m^2K}$
h_{rad}	Radiative Heat Transfer Coefficient, $\frac{W}{m^2K}$
ε	Emissivity
ε_{st}	Steel Emissivity
σ	Stefan-Boltzmann Constant, $\frac{W}{m^2K^4}$
β	Volumetric Expansion, $\frac{1}{K}$
φ	Velocity Interpolation Function
Ψ	Pressure Interpolation Function
ϑ	Temperature Interpolation Function
$\mathbf{K}$	Stiffness Matrix
$\mathbf{C}$	Capacitance Matrix
$\mathbf{M}$	Mass Matrix
t	Time
t_i	Surface Traction Component
E	Activation Energy, $\frac{J}{mol}$
Q_{tot}	Total Heat Transfer, W
Q_{cond}	Conductive Heat Transfer, W

Q_{rad}	Radiative Heat Transfer, W
Q_{fl}	Heat Transfer in Molten Flux, W
Q_p	Heat Transfer in Powder Flux, W
Λ	Phonon Mean Free Path, m
K_s	Melting Rate Constant
m_{sc}	Specific Flux Consumption, $\frac{kg}{m^2}$
$\dot{m}_c$	Flux Consumption Rate, $\frac{kg}{s}$
$\dot{M}_c$	Flux Consumption rate per meter of mold perimeter, $\frac{kg}{m.s}$
A	Area, m^2
V_c	Casting Speed, m/s

CHAPTER 1

INTRODUCTION

1.1 GENERAL

Continuously cast steel products currently account for approximately 65% of the total global steel production (Figure 1.1) [1]. In the U.S., roughly 70% of the 80 million metric tons of steel produced annually is manufactured using the continuous casting process. While most of the continuously cast products are in the form of rectangular slabs, blooms and billets, the trend domestically as well as internationally is towards increased use of the process, with future applications in the production of steel strip and other near net shape products. This trend is readily understandable given the beneficial attributes of the process which include high volume production rates, energy efficiency improvements over conventional ingot casting, the ability to vary product grade in-process and the reduction in the amount of post-production rolling required.

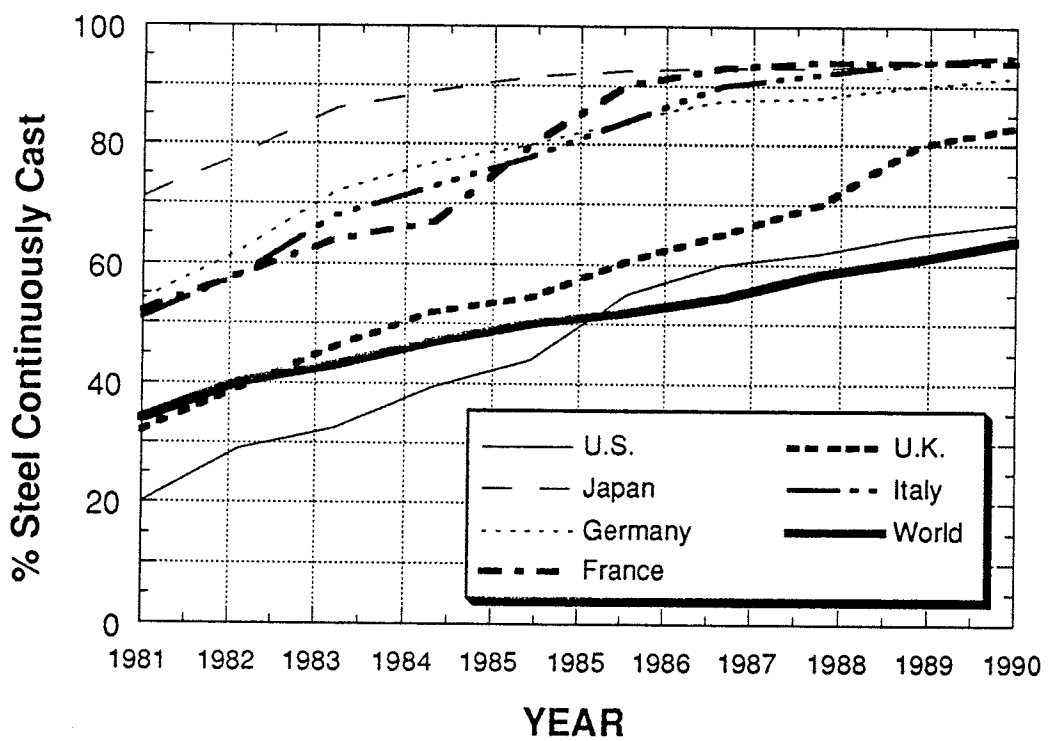

Figure 1.1 - Trend in Production of Continuously Cast Steel

Despite its many advantages over ingot casting, the continuous casting process has several shortcomings. Surface quality of the slab is highly dependent on casting practice and process parameters, as is the internal quality of the cast product. For example, slivers and cracks may form at the slab surface due to improper addition of the mold powder. Additionally, there are difficulties inherent in the process itself, typified by the need for lubrication between the steel shell and mold wall. These problems and associated defects frequently result in tons of scrapped or downgraded product annually, which is quite costly for the steel-producing companies, and ultimately the consumer. The consequences of undetected defects in the final product is potentially worse

Clearly, there is a need to more fully understand the specific process of continuous casting, due to its importance as a primary manufacturing process, which is based on its beneficial commercial features like high volume production rates, improved thermal efficiency and production flexibility. In addition, considerable improvement in product quality and productivity will be derived from a better understanding of the process. These reasons form the basic motivation for the considerable research being performed currently, both industrially and academically. Mathematical and physical models have been created to assess and quantify heat transfer, mass transfer, fluid flow, thermal stress and phase change phenomena which are all part of the continuous casting process. In this way insight into the most critical aspects of the process will be identified, with a view to achieving the productivity and quality goals mentioned above.

1.2 PROCESS OVERVIEW

Steel produced in the basic oxygen furnace is introduced into the refractory-lined ladle and tundish (Figure 1.2). In the continuous casting process, molten steel flows from the tundish under gravity, through the submerged entry nozzle (SEN) and into the casting mold. The steel freezes against the water-cooled copper mold forming a thin solidified shell. This shell acts as a container for the remaining liquid metal, and it grows in thickness as it travels down the mold. At the mold exit, the partially solidified strand is pulled along by giant rollers and, as such, is

continuously withdrawn from the mold. The slab enters the spray zone where it is further cooled by water jets. The completely solidified product is torch-cut into final slabs of varying lengths.

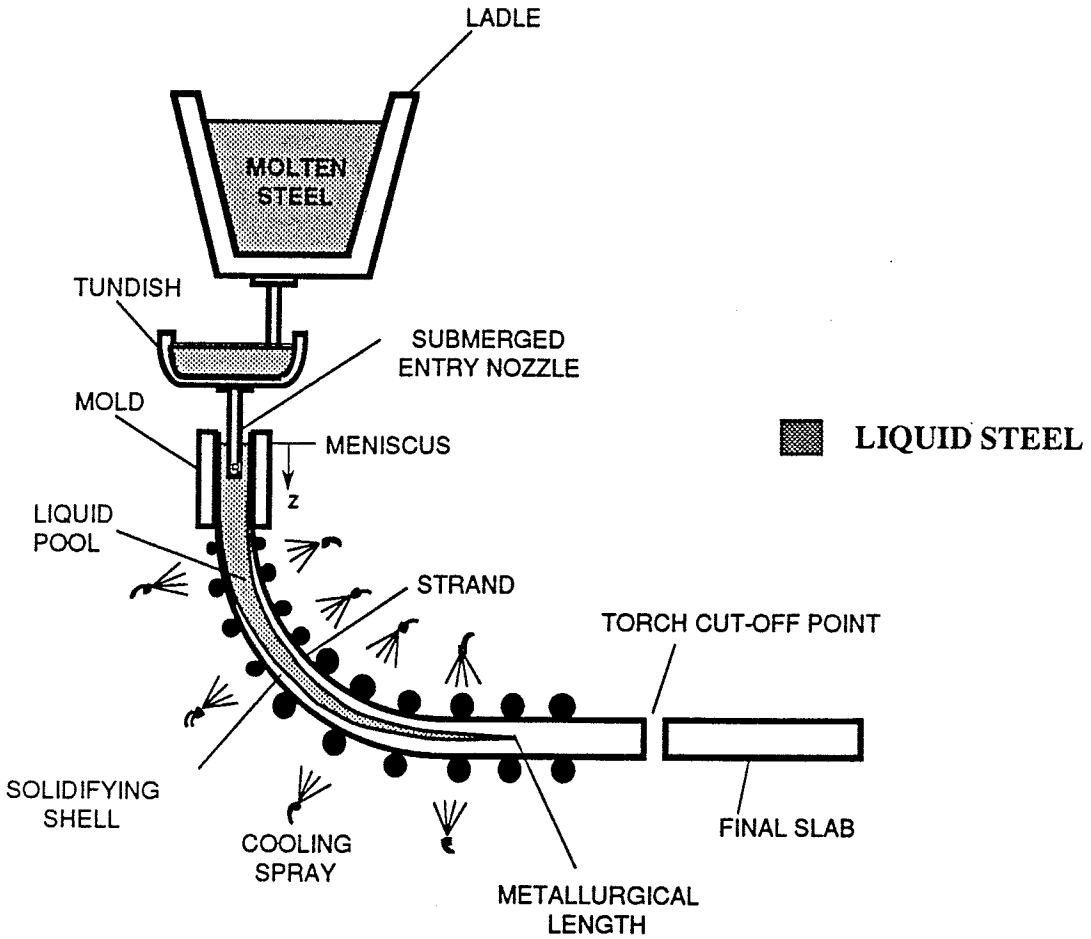

Figure 1.2 - Schematic Overview of the Continuous Casting Process

Perhaps the most critical aspects of the process are centered around the relatively short region of the actual mold. In the mold region, the steel flow is most turbulent, the peak heat flux is present and the thinnest, therefore weakest, shell occurs. In addition, the mold oscillates, producing significant dynamic effects of its own. Interaction between these phenomena results in a complex situation which is intrinsically worthy of study. It is therefore not surprising that most current research focuses on the mold region, as this also happens to be the area in which most casting defects originate.

Figure 1.3 is the typical representation of the situation inside the mold[2-4]. It shows the interaction of the liquid steel, solid steel, and lubricating flux with the mold wall.

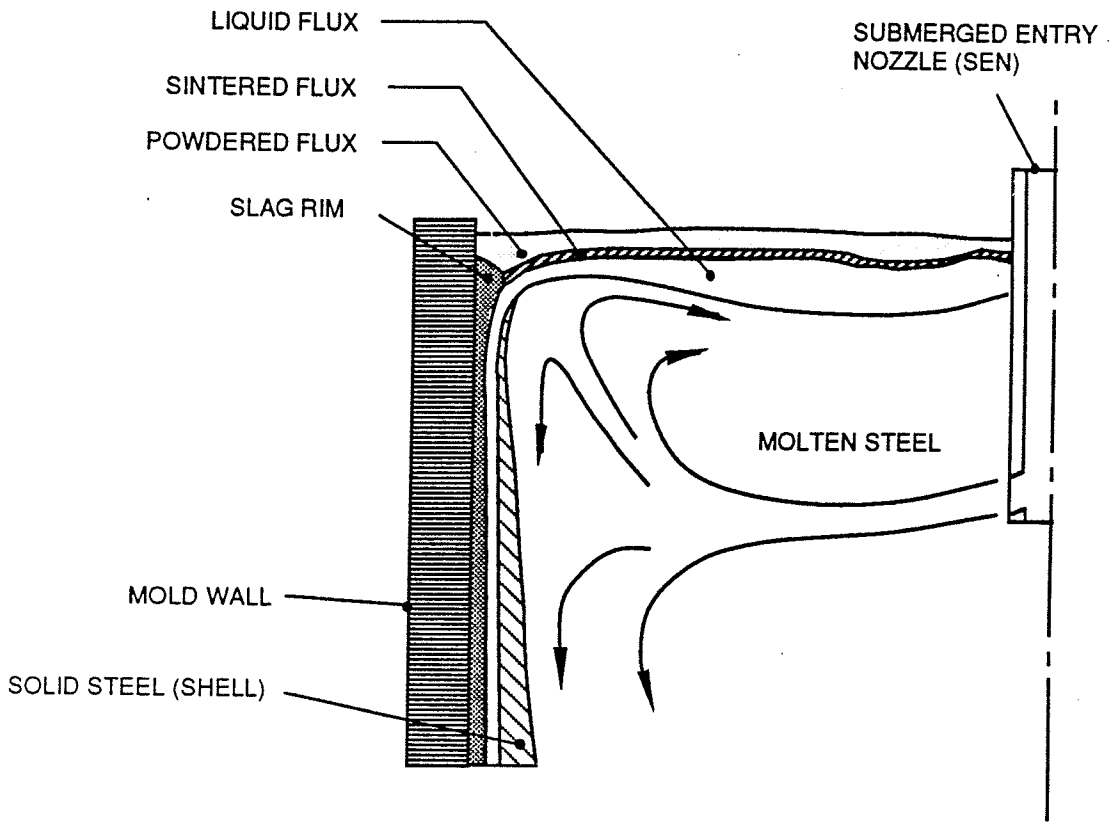

Figure 1.3 - Schematic of Mold-Flux-Steel Interaction

The physical relationship between the mold wall, steel shell and flux material is critical to the surface quality of the cast slab. Meniscus mark formation, heat transfer, lubrication and inclusion removal are some of the processes which occur in the mold region, based on the interaction of the materials present[4]. As the mold oscillates, liquid flux is pulled into the gap between the shell and mold, forming a thin lubricating film. This film prevents the shell from sticking to the mold wall, and thereby allows the slab to be withdrawn without tearing of the

shell. The depth of the oscillation marks is also dependent on the active phenomena in the mold region, forming yet another link to final surface quality. In the following paragraphs, a more detailed description of the mold region processes will be presented along with the motivation for this work.

1.3 MOTIVATION FOR STUDY

This study focuses on the lubricating flux material used in the continuous casting of steel. The flux is periodically introduced at the top of the mold as a powder. It covers the entire upper surface of the liquid steel which would have otherwise been exposed to the atmosphere. The flux material sinters and then melts due to the heat absorbed from the liquid steel pool below. During each oscillation cycle of the mold, the liquid flux infiltrates the gap between the mold and steel shell, the "consumption rate" of the flux being proportional to the "positive strip time" (i.e. portion of oscillation when the mold is moving in the casting direction) [5]. As the liquid flux travels down the mold, it solidifies as a function of the mold wall temperature. Thus, at any point below the meniscus, there exists re-solidified flux, which may be either glassy or crystalline[2, 6], and liquid flux. Depending on the amount of flux solidified and the amount of shrinkage of the steel shell that occurs, an air gap[6] may be present in the interface between the shell and mold wall.

Based on the preceding general description of the behavior of the flux material, several important functions can be identified. It is generally agreed[3, 7-11] that the flux is added to the mold to:

i) Provide lubrication between the mold and steel shell,

ii) Insulate the upper surface of the steel, preventing both solidification and oxidation,

iii) Promote uniform heat transfer between the shell and mold,

iv) Remove inclusions

The importance of each of these functions may be illustrated by the defects and problems caused in the absence of the flux. For example, improper lubrication may lead to a sticker type breakout where the shell adheres to the mold wall, tears as the strand is withdrawn, ultimately causing molten steel to flow out onto the casting machine. Secondly, if the upper surface of the steel were to solidify by being exposed to the atmosphere, at the very least, very deep meniscus marks will be formed[12]. Thirdly, if there is insufficient liquid flux in the gap between the mold and shell, an air gap will form as the shell shrinks away from the mold as it cools. This air gap will significantly reduce the heat extraction rate from the steel. Since heat is continuously being delivered to the shell from the superheated liquid, shell thinning will occur because heat is not being removed quickly enough on the mold side of the shell. Thinner shells may also lead to breakouts because the shell is insufficiently strong to contain the ferrostatic pressure. Finally, since many non-metallic particles that may be present in the liquid steel float to the surface, they can be conveniently removed by the liquid flux, and transported out of the mold.

It is clear therefore, that having a sufficiently deep and uniform liquid flux pool is critically important in avoiding casting problems like breakouts, and surface quality degradation problems like surface and sub-surface inclusions and deep meniscus marks[3, 13, 14]. In addition, having a deep liquid flux pool serves an additional function of decreasing the likelihood of powdered flux entrapment in the solidifying shell during metal level fluctuations which can result in severe sliver defects in the slab. It is significant to note that in practice, it has been observed that the liquid flux layer is quite thin close to the meniscus [10, 15], which is perhaps the most likely location for powder entrapment, and for fluid flow cut-off.

1.4 OBJECTIVES

Avoiding and minimizing casting problems and defects by maximizing the liquid flux thickness is generally agreed to be a feasible and desirable solution. It is the intent of this work to achieve the following:

(i) Development of a mathematical model that accurately calculates flow and temperature distribution in the top surface flux layer, as specified by comparison with experimental measurements,

(ii) Identification of the the physical phenomena which govern the behavior of the flux under actual casting conditions,

(iii) Identification of important thermal and flow features which develop in the flux,

(iv) Determination of the physical parameters which most significantly influence the thickness of the liquid pool,

(v) Specification of practice and material to achieve the maximum liquid depth in the top surface flux layers.

CHAPTER 2

LITERATURE SURVEY

2.1 MATERIAL CHARACTERIZATION

In general, the behavior of the flux material used in continuous casting of steel is governed by fluid flow and heat transfer phenomenon. The functions of hydrodynamic lubrication, thermal insulation, control of heat removal rate are determined by the thermal and flow properties of the material. It is therefore necessary to properly characterize the material as a precursor to a model of the flux's behavior. Immediately following is a summary of the available literature on the thermo-mechanical properties of the flux, including descriptions of flux compositions and classifications.

2.1.1 Flux Composition

Typically, continuous casting mold fluxes are silica-based (SiO_2) or Calcia-based (CaO) powders, to which other substances are added to vary the flux's melting and flow behavior. Typical flux composition ranges are given in the Table below[3, 12].

TABLE 2.1 - Composition Range of Typical Fluxes

CONSTITUENT	COMPOSITION RANGE (%)
SiO_2	20 - 50
CaO	25 - 45
Al_2O_3	0 - 10
Na_2O	1 - 20
C	1 - 25
MgO, MnO, BaO, B_2O_3	0 - 10
TiO_2, K_2O	0 - 5

While the combination of calcia and silica fundamentally determines the properties of the flux, the amounts used in a particular formulation will depend on the intended function. For

instance, by altering the ratio of CaO (wt. %) to SiO_2 (wt. %), the Basicity Index, a measure of the flux's ability to absorb alumina inclusions, can be varied [3].

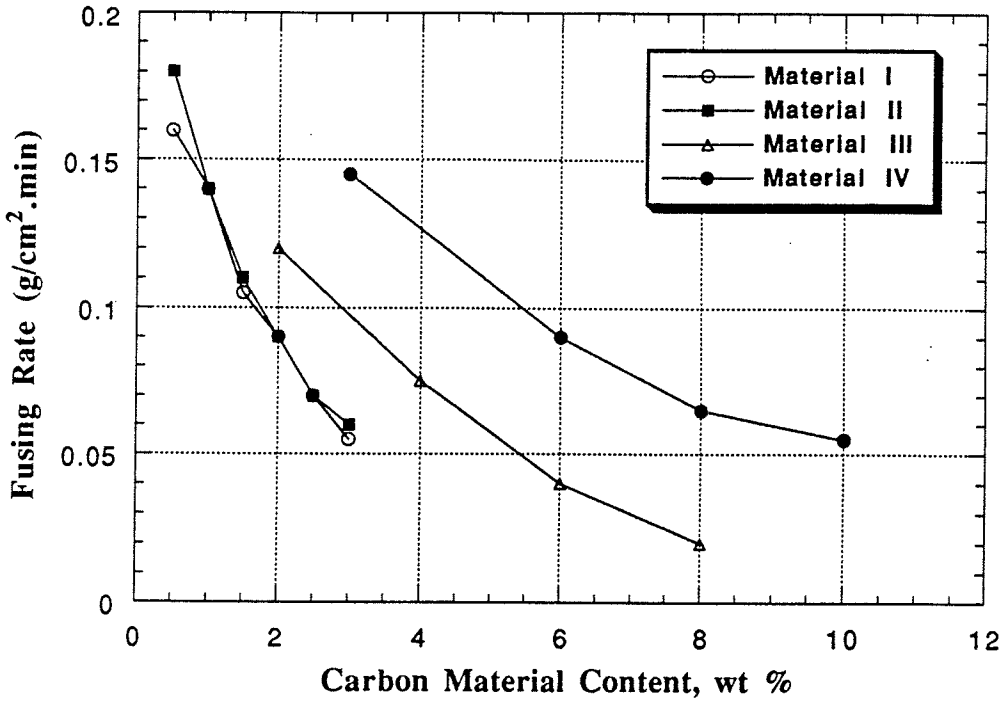

PROPERTY	C CONTENT, %	FIRING PT., °C
MATERIAL I	99.8	434
MATERIAL II	100	376
MATERIAL III	32.8	500
MATERIAL IV	76	500

Figure 2.1 - Effect of Carbon Content on Melting Rate of Flux[16]

Based on experimental results, the effect of each of the additives (i.e. apart from the major constituents of CaO and SiO_2) listed in Table 2.1 has been determined. It is generally agreed that fusion or melting rate can be adjusted by changing the amount and type of carbonaceous material added to the flux[3, 12, 16-19]. It has been suggested and verified by Xie *et. al.* [16] that the reason for the alteration of the fusion rate by carbon addition is due to the high interfacial surface tension between carbon and the base elements of Silica and Calcia. The

carbon materials therefore play a role in controlling the coalescence of partially fused flux droplets, thereby controlling the fusion into a homogeneous liquid pool. The so-called melting rate is probably a measure of the thermal diffusivity of the material (i.e. $k/(\rho c_p)$). Figure 2.1 illustrates the relationship between melting rate and the amount of carbon added to the flux. In experiments similar to those of Xie, Lee et. al. [18] measured the weight change of a specimen of flux which is maintained at 1200°C over a period of time. A schematic of the apparatus used may be found in the pertinent references for Xie and Lee. The melting rate is calculated as the ratio of weight change to the product of crucible cross-sectional area and time, and is characteristic for each sample of flux.

Most of the remaining oxide additives (Al_2O_3, MgO, MnO, BaO, B_2O_3, TiO_2, K_2O) are used to control the viscosity of the flux at elevated temperature. Work conducted by Turkdogan and Bills[20] has shown a direct correlation between the molar amount of alumina present and viscosity. In general, as the alumina content increases, the viscosity of the flux increases as well. However, all of the other oxide additives (MgO, MnO, BaO, B_2O_3, TiO_2, K_2O) decrease the flux viscosity as their content is increased[12]. Finally, according to the work performed by Moore *et. al.* [12] all the oxide additives except TiO_2 and Al_2O_3 decrease the melting point of the flux. Unlike the relationship between Basicity Index, Viscosity and the flux constituents like SiO_2, CaO and Al_2O_3, the quantitative relation between melting point, viscosity and the other oxide additives is unclear.

2.1.2 Flux Classification

In the virgin state, the solid flux may be classified into the following types according to Moore, *et. al.* [12]:

i) Fly Ash Powders
   - Mechanical blends incorporating fly ash

ii) Synthetic Powders
   - Mechanical blends of fine powdered raw materials (particle size - 200 mesh[3])

iii) Fritted Fluxes

- Sizable portion of flux is pre-melted and then sized

iv) Granular Fluxes

- Spherical or extruded granules (-35 mesh to +20 mesh[3])

Prior to melting, particle coalescence begins to occur. At this stage, the flux is referred to as sintered. The sintered state occurs when the softening temperature has been exceeded, and is not critically dependent on the time that the flux is held at the elevated temperature[21] .

Subsequent to melting, the liquid flux flows down the gap between the shell and mold. When the liquid flux contacts the mold, it re-solidifies. This re-solidified flux may be subdivided into two distinct layers:

i) The glassy slag layer

ii) The crystalline slag layer

The formation and growth of these layers depends on the cooling rate experienced by the liquid flux as it flow along the gap. As such, the existence of either layer is related to its location relative to the mold wall. Figure 2.2 schematically represents the division of the solid flux in the gap into crystalline and glassy layers.

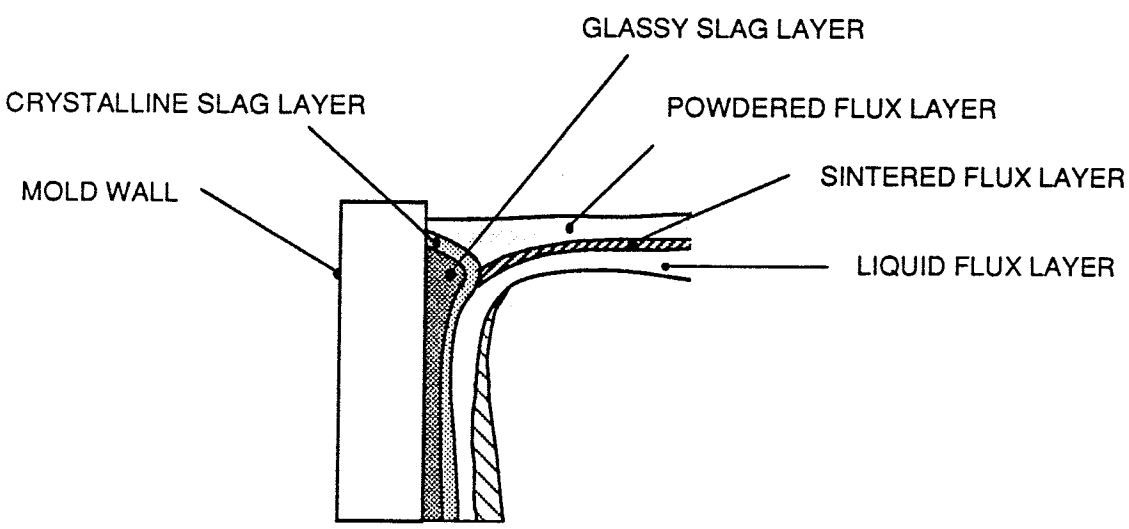

Figure 2.2 - Schematic Showing Various Forms of Mold Flux

Crystalline structure, as opposed to glassy structure, is characterized by a regularly repeating arrangement of atomic cells. There are several macroscopic differences in materials having these structures. For example, the glassy slag will not exhibit any clearly defined melting point as does crystalline slags. Furthermore, the melting point of the crystalline slag is independent of the cooling rate of the liquid flux, whereas the glass transition temperature for the glassy slag increases with increasing cooling rate. In the case of continuous casting, the preferential formation of glassy slag over crystalline slag is most likely a cooling rate effect. The glassy material is produced only when a crystalline structure is not developed when the melting point is attained during cooling. If no crystallization takes place, the liquid continues to cool with the same volumetric contraction as the liquid, forming what is known as a super cooled liquid. At some temperature, dependent on the cooling rate, there is a gradual reduction in the volumetric expansion coefficient. This marks the onset of glassy solid formation , at which time the liquid has a solid-like viscosity of approximately 10^{12} poise for silica-based slags[21].

2.1.3 Flux Properties

2.1.3.1 Viscosity

The viscosity of metallurgical fluxes is temperature dependent. The viscosity of the flux as a function of temperature as it solidifies from the melt has been show to be of the form of the Arrhenius-Andrade rate equation[3]. This equation takes the form :

$$\ln \eta = \ln A - \frac{E}{RT} \qquad (2.1)$$

where: η = Viscosity (Pa.s)

A = Frequency factor (constant) (Pa.s)

E = Activation energy for viscous flow (constant) $\frac{J}{mol}$

$$R \quad = \text{Gas Constant } \left(\frac{J}{mol.K}\right)$$

$$T \quad = \text{Absolute temperature (K)}$$

Therefore, a plot of ln η versus the reciprocal of absolute temperature should be a straight line with slope E/R and intercept of ln A. The experimental results of Branion and Bommaraju [3, 9, 22] show the Arrhenius relation to be approximately true until the flux solidification point. Close to the solidification point McCauley *et. al.* [23] and Turkdogan *et. al.* [20] observed deviations from linearity at high temperature. McCauley *et. al.* suggest that the empirical relation based on the Clausius-Clapeyron Equation more accurately describes the viscous behavior of the flux, as it accounts for the deviation from linearity[23]. The improved expression, called the Brostow Equation, takes the following form:

$$\ln \eta = a + \frac{b}{T} + c \ln T \tag{2.2}$$

where: a, b and c are constants to be determined experimentally.

The Clausius-Clapeyron Equation, upon which the Brostow Equation is based, relates pressure with temperature, enthalpy and volume. As a result the Brostow Equation itself is not totally empirical, but is based on thermodynamic theory as well.

A third expression relating viscosity to temperature has been used with some success by Saxton and Sherby [24] and Riboud *et. al.* [25]. The relation is similar to the Brostow Equation and is of the form:

$$\ln \eta = \ln A + \frac{b}{RT} + \ln T \tag{2.3}$$

Equation 2.2 therefore has one more adjustable coefficient, c, than does equation 2.3. Though equation 2.3 is considered to be more accurate that the Arrhenius-Andrade relation, it is less flexible than the Brostow Equation according to McCauley and Apelian [23].

Equations 2.1, 2.2 and 2.3 pertain to the flux in the liquid state. Below the solidification point, the viscosity increases sharply with decreasing temperature. The slope of the viscosity - temperature curve below the melting point is almost infinite. A simple power- law type equation has been suggested by Ho to model the viscosity of the flux both in the liquid and solid states [15]. This model, given below, accounts for the sharp changes in viscosity below the melting point.

$$\eta = \eta_s \left(\frac{T_s - T_{sol}}{T - T_{sol}} \right)^n \qquad (2.4)$$

where: η_s = Viscosity evaluated at $T = T_s$ (shell surface temperature)

T_{sol} = Solidification temperature of the liquid flux

n = Dimensionless empirical constant to fit measured data

All the models described above must be calibrated with actual experimental measurements.

2.1.3.2 Thermal Conductivity

Much of the most recent experimental work into the thermal properties of casting slags has focused on the determination of the thermal conductivity of the slag in the liquid state. When the slag is molten it is a semi-transparent medium across which heat energy may be transferred by radiation (thermal transport by photons) in addition to the usual phonon conduction [2, 26, 27]. Consequently, much work has been done to determine the absolute values of thermal conductivity of liquid slags minus the effect of heat transfer due to radiation.

The effect of radiation on the effective thermal conductivity or the significance of radiant heat transfer to the overall energy transport through a semi-transparent medium depends on whether the medium is optically thick[28]. If the mean photon penetration distance is small when compared to the characteristic dimension of the medium, the medium is considered to be optically thick. That is, radiant heat transfer is significant if the ratio of the characteristic length

of the medium to the photon extinction mean free path is greater than unity. If the pertinent ratio is denoted by R, then the following expression is used to determine optical thickness:

$$R = \frac{S}{l_m} \approx S \cdot \alpha_m \text{ [27]} \qquad (2.5)$$

where:

S	=	Characteristic length (m)
l_m	=	Photon Extinction Mean Free Path (m)
α_m	=	Mean absorption coefficient (m^{-1})

For the case of $40SiO_2$-$40CaO$-$20Al_2O_3$, a suggested value of α_m is 23 cm^{-1} [29].

If the medium is not optically thick, and only phonon conduction is considered relevant, the pure liquid thermal conductivity is required. However, heat transfer by radiation in the liquid flux used in steel continuous casting is significant, even over the very small thicknesses at the strand-mold gap[29].

The total heat transfer across the liquid layer, neglecting the effect of fluid motion is given by the following relation:

$$Q_{tot} = Q_{cond} + Q_{rad}$$

where:

Q_{tot}	=	Total radiant heat transfer (W)
Q_{cond}	=	Heat transfer due to phonon conduction (W)
Q_{rad}	=	Radiant Heat transfer due to photon conduction (W)

The lattice (phonon) or pure conduction is given by the following 1D heat conduction equation:

$$Q_{cond} = k_c \frac{\Delta T}{\Delta x} \qquad (2.6)$$

where:

k_c	=	Pure thermal conductivity $\left(\frac{W}{m.K}\right)$
ΔT	=	Temperature difference (K) = $T_{st} - T_{liq}$
T_{st}	=	Steel Surface Temperature (K)

T_{liq} = Flux Liquidus Temperature (K)
Δx = Liquid Layer Thickness (m)

The radiation portion of the transmitted energy may be estimated in several ways. The simplest method does not take into consideration specific medium properties such as its transmissivity. This first equation (equation 2.7) is generally used to calculate the radiant heat transfer between two surfaces. If the steel-flux interface and the liquid flux-solid flux interface are considered to be two surfaces between which the steel surface is emitting radiation, then equation 2.6 is applicable.

$$Q_{rad} = \left[\sigma \varepsilon_{st} n^2 (T_{st} + T_{liq})\left(T_{st}^2 + T_{liq}^2\right)\right] \Delta T \qquad (2.7)$$

where:
σ = Stefan-Boltzmann Constant
= $5.667 \times 10\text{-}8 \left(\frac{W}{m^2K^4}\right)$
ε_{st} = Emissivity of steel = 0.8
n = Refractive index of flux ≈ 1.5

Alternatively, the radiative portion of heat transfer may be calculated using the model of Czerny and Genzel[30], which treats radiant heat transfer as a three-dimensional phenomenon even though the net heat transfer is one-dimensional. The model is based on a consideration of the volume emissive power of the medium, i.e. the flux, and is given in equation 2.8 below.

$$Q_{rad} = \left[\frac{16}{3}\frac{n^2}{\gamma}\sigma Y (T_{st} + T_{liq})\left(T_{st}^2 + T_{liq}^2\right)\right]\frac{\Delta T}{\Delta x} \qquad (2.8)$$

where:
γ = Absorption coefficient of medium (m^{-1})
Y = Measure of the volume hemispherical emissivity of the medium

$$= \begin{cases} 1 & \delta \to 1 \\ \frac{3}{4}\frac{\varepsilon_{st}}{2-\varepsilon_{st}}\delta & \delta \to 0 \end{cases}$$

δ = Dimensionless thermal thickness $\left(= \frac{\Delta x}{\lambda}\right)$

λ = Wavelength of radiation corresponding to given γ

Finally, an expression similar to equation 2.8 was derived by Ohmiya *et. al.* [29] for the radiative heat flux through the glassy material. In this case, no interaction between radiation and conduction is assumed, so that for constant physical properties, the heat flux due to radiation may simply be added to that by conduction. Superposition of radiative and conductive heat fluxes has been demonstrated to underestimate the true heat flux, which is based on an interaction of the two modes of heat transfer. However, the discrepancy can be shown to be not significant [31]. This model incorporates the optical properties of the medium as well as those of the emitting and absorbing surfaces. Equation 2.9 below is a modification of the relation presented in the work of Ohmiya *et. al.* In equation 2.9, the surface emissivity of the solid flux replaces the emissivity of the mold surface. Thus, from the Ohmiya work, we have:

$$Q_{rad} = \left[\left(\frac{\sigma n^2}{0.75\gamma\Delta x + \varepsilon_{st}^{-1} + \varepsilon_{flux}^{-1} - 1}\right)(T_{st} + T_{liq})\left(T_{st}^2 + T_{liq}^2\right)\right]\Delta T \qquad (2.9)$$

where: ε_{flux} = Emissivity of solid flux surface

When the total heat flux is calculated by taking the sum of the radiation and conduction components, the effective or apparent thermal conductivity is found as follows:

$$Q_{tot} = Q_{cond} + Q_{rad} = k_{eff}\frac{\Delta T}{\Delta x}$$

$$\therefore \quad k_{eff} = \frac{Q_{cond} + Q_{rad}}{\Delta T}\Delta x \qquad (2.10)$$

This value of effective conductivity changes as the liquid layer thickness grows, both due to a decrease in the conductive portion of heat transfer as well as the change in the radiative heat transfer according to the models given above. The foregoing analysis, assumes that there is a

constant temperature gradient over the entire liquid thickness. However, it has been shown [32] that the temperature gradient is non-linear close to the boundaries of the medium. Additionally, there are a few variables in the relations above, which are not known with much reliability or accuracy. One such variable is the absorption coefficient, γ. Given these shortcomings in the models, it is difficult to apply them with any confidence. Ordinarily the alternative is to use experimental data. However, given the complex nature of the phenomenon of combined radiation and conduction, the value of thermal conductivity cannot be obtained without the use of one of the equations 2.7, 2.8 or 2.9. In other words, the effective thermal conductivity as determined from experiments is a value which is calculated to fit temperature and heat flux data to one of the models described above.

However, none of the models listed above can account for the trend in apparent thermal conductivity (k_{eff}) reported by several researchers [2, 26, 33] where the value of k_{eff} decreases with increasing temperature above the Debye temperature. This trend in the effective thermal conductivity is mirrored for the pure (i.e. phonon) thermal conductivity according to work by Kishimoto *et. al.*[26] and Taylor and Mills [2]. We may conclude, therefore, that the drop off in thermal conductivity is not due to the effect of radiation on thermal transport, as radiation is negligible in the method† used by Kishimoto and Taylor. Thus, the cause of the decline in pure thermal conductivity should be the same as that for the effective thermal conductivity. The mechanism of heat conduction for crystalline materials was explained by Debye in 1914 with an analogy to the kinetic theory of gases, whereby the thermal conductivity may be expressed as:

$$k = \frac{1}{3} C_p \rho v \Lambda \tag{2.11}$$

where:

C_p = Heat Capacity at constant pressure $\left(\frac{J}{kgK}\right)$

ρ = Density $\left(\frac{kg}{m^3}\right)$

v = Velocity of sound in solid $\left(\frac{m}{s}\right)$

Λ = Phonon mean free path (m)

In the molten state, it can be shown that the mean free path of phonons is inversely related to the temperature of flux [26]. The relation is of the form:

$$\frac{1}{\Lambda} = a + b\,T \tag{2.12}$$

where: a and b are constants

This trend in Λ would explain the decrease in the phonon thermal conductivity, k with increasing temperature when the temperature exceeds the Debye temperature.

The behavior of the flux in the solid state, when there is no radiation may also be explained in terms of the Debye model for thermal conductivity. Kittel [34] interpreted equation 2.11 for the behavior of glassy materials in terms of an approximately constant phonon mean free path in the solid state. Therefore, since Λ and v are constant, and according to equation 2.11, the increase in observed thermal conductivity in the solid state may be attributable to the increase in heat capacity, C_p, or density, ρ, with increasing temperature. This increase in C_p results in an approximately linear increase in the thermal conductivity according to Kishimoto *et. al.*[26]. Thus, an empirical model for thermal conductivity in the solid state, which seems to hold for many various slag compositions was determined, and is of the form:

$$k = C_1 + C_2\,T \tag{2.13}$$

where: C_1 and C_2 are experimentally determined constants

Typical values of C_1 and C_2 are given below:

$$0.7 < C_1 < 1.2 \quad \left(\frac{W}{mK}\right)$$
$$1\text{x}10^{-4} < C_2 < 3\text{x}10^{-4} \quad \left(\frac{W}{mK^2}\right)$$

Thus, according to Kishimoto *et. al.* [26], the thermal conductivity of the solid slag increases linearly with increasing temperature below the melting point. This is in sharp contrast

to other work by Nagata *et. al.* [33] in which thermal conductivity was shown to decrease with increasing temperature in a non-linear fashion for crystalline slags. However, that trend in thermal conductivity may have been particular to that composition of Na_2O-SiO_2 (50%-50% by mass). In fact, tests on other compositions of Na_2O and SiO_2 in the work by Nagata *et. al.* [33], resulted in the expected trend in thermal conductivity, in which thermal conductivity increases with increasing temperature in the solid state. In the solid and semi-solid states, radiation does not play a significant role in the transport of thermal energy when the medium is opaque. Thus the difference in the results presented by Kishimoto *et. al.* [26] and Nagata *et. al.* [33] for the flux thermal conductivity change with increasing temperature, below the melting point, is puzzling.

2.1.3.3 Specific Heat

The specific heat capacity of lubricating fluxes is usually measured as the specific heat at constant pressure, C_p. While the specific heat at constant volume, C_v, and the specific heat at constant pressure are approximately equal below the Debye temperature [21], there is a sharp deviation between the values at high temperature. The Debye temperature, Θ_D, is characteristic for each material and may be interpreted as the temperature at which atomic lattice vibrational frequency becomes a maximum. Above this temperature, the development of defects (Schottky and Frenkel type) in the crystalline lattice occur, leading to the rapid increase in C_p.

In general, the temperature dependence of specific heat, C_p, may be classified into three regions; the low temperature range or glassy state, the glass transition range or supercooled liquid state and the high temperature range or liquid state. These classifications are based on the changes in material structure with temperature which is illustrated in Figure 2.3. Alternatively if crystallization takes place upon cooling, there are only two regions, low temperature and high temperature. The transition from one structure to the other is sharp in this case, and occurs at the melting point.

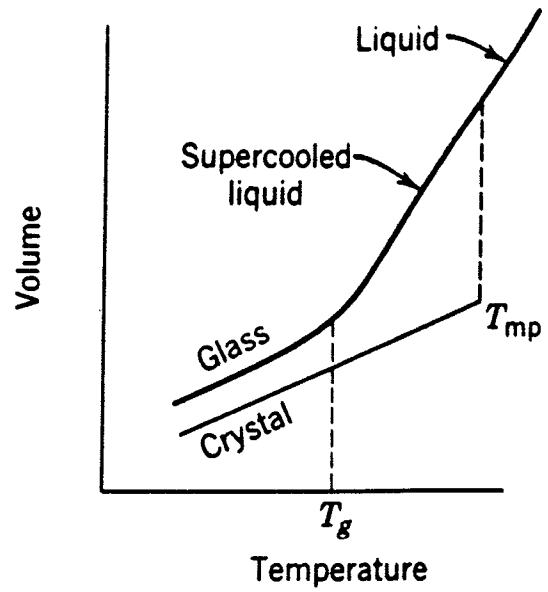

Figure 2.3: Flux Classification and Specific Volume as Functions of Temperature

In the low temperature range, below the Debye temperature, the specific heat is proportional to $(T/\Theta_D)^3$ where T is the absolute temperature [18].

In the glass transition region, there is rapid increase in heat capacity over a limited temperature range. This change corresponds to a transformation from an ordered to a disordered structure. The energy required to bring about this transformation is the latent heat of fusion ΔH_L. In the case of crystalline fluxes, this transformation occurs at the melting point. Typical values range from 250 J/g for glassy slags to 528 J/g for crystalline slags [33].

At elevated temperature, in the super-cooled liquid state, the heat capacity at constant pressure can be adequately represented as linearly increasing with increasing temperature [18]. This trend has been observed experimentally by Kishimoto *et. al.* [24] and has been attributed to an increase in atomic rotational kinetic energy as opposed to translational kinetic energy. Flux structure consists of long chains of molecules which are more likely to undergo vibration and rotation instead of translations.

2.2 MODELS OF FLUX BEHAVIOR

2.2.1 Heat Transfer Models

Most of the current mathematical modeling of the flux behavior has been done to analyze the heat transfer characteristics of the material. This stems primarily from a need to quantify the amount of heat removed from the steel by the mold across the mold-strand gap. By mathematically quantifying this gap heat flux, the heat removal rate can then be controlled to provide beneficial effects on the quality of the cast slab, based on a simulation using the mathematical model.

The majority of the heat transfer models developed by various researchers are based on the transient one-dimensional heat conduction equation:

$$\frac{1}{(k/\rho c_p)} \frac{\partial T}{\partial t} = \frac{\partial^2 T}{\partial x^2} \tag{2.14}$$

For example, by applying boundary and initial conditions to equation (2.14), expressed separately for the molten and solid flux, Nakato *et. al.* [35] have produced a mathematical model which, in effect, is a solution to equation (2.14). The solution is given below, where the only unknown variable is the rate constant of melting, K_s. Initial conditions follow.

$$\frac{k_p}{k_s}\sqrt{\frac{\alpha_s}{\alpha_p}}\left(\frac{T_o - T_{melt}}{T_{st} - T_{melt}}\right)\frac{e^{-\left(\alpha_s K_s^2/\alpha_p\right)}}{\mathrm{erf}\left(\sqrt{\alpha_s/\alpha_p}\,K_s\right)} + \frac{e^{-K_s^2}}{\mathrm{erf}\,(K_s)} - \frac{K_s \Delta H_L \sqrt{\pi}}{C_s\,(T_{st} - T_{melt})} = 0 \tag{2.15}$$

where: T_o = Initial temperature in domain (K)

T_{melt} = Flux melting point (K)

T_{st} = Steel surface temperature (K)

k_s and k_p are the thermal conductivities of solid and liquid flux respectively $\left(\frac{W}{m\,K}\right)$

α_s and α_p are the thermal diffusivities of solid and liquid flux respectively (where $\alpha = \frac{k}{\rho c_p}$)

Initial and Boundary Conditions:

$t = 0$ and $x > 0$ - $T_p = T_o$

$t > 0$ and $x = 0$ - $Ts = T_{st}$

$t > 0$ and $x = X_l(t)$: $T_s = T_p = T_{melt}$

$t > 0$ and $x = X_l(t)$: $k_s \frac{\partial T_s}{\partial x} - k_p \frac{\partial T_p}{\partial x} + \rho_s \frac{\partial X_l}{\partial t}$

The molten flux layer thickness, X_l, is then expressed as a function of the melting rate constant, when the consumption rate in the direction of the heat flux is nil. Whence:

$$X_l = 2K_s \sqrt{\alpha_s t} \qquad (2.16)$$

Thus, the liquid layer thickness can be determined at any point in time. In the Nagato work, this model was used to illustrate the effect of thermal conductivity, enthalpy of fusion, initial temperature and other parameters on the liquid layer thickness. Briefly, it was found that K_s increases with decreasing T_{melt}, k_p but increasing T_o and T_{st}.

Results for liquid layer thickness as a function of time, similar to those of Nakato [35] were obtained by Dehalle *et. al.* [10] whose model is also based on equation (2.14). Dehalle and co-workers [10] were also able to show that there is no significant change in the liquid layer thickness with powder additions when the surface temperature is kept relatively low (i.e. below 800 °C). Further, the liquid layer thickness appears to be insensitive to the frequency of the powder additions.

Nakano *et. al.* [36] took the one-dimensional heat conduction model further by discretizing the domain into a series of thin layers, the thickness of which depends on the accuracy desired. The heat conduction equation is then applied layer by layer, enabling the

temperature to be calculated at any location in the domain. Additionally, this model incorporates the heat transfer occurring at the surface of the flux, as well as variable flux properties. The variability in the flux properties is expressed as functions dependent on the sintering process occurring when the flux goes from a powdered form to the liquid. That is, thermal conductivity of the powder and the sintered layers are expressed as functions of the packing factor of the ith layer, f_i . For the powder we have

$$k_{p,i} = \frac{1}{\left[\frac{\left(1 - f_i^{1/3}\right)}{k_a} + \frac{f_i^{1/3}}{\left(1 - f_i^{2/3}\right) k_a + f_i^{2/3} k_s}\right]} \tag{2.17}$$

where: $k_{p,i}$ = Thermal conductivity of the ith powder layer $\left(\frac{W}{mK}\right)$

k_a = Thermal conductivity of air $\left(\frac{W}{mK}\right)$

k_s = Thermal conductivity of base material $\left(\frac{W}{mK}\right)$

f_i = Packing factor of the ith layer

$= 1 - \beta_i$

β_i = Void ratio of the ith layer

Similarly, for the sintered flux, we have:

$$k_{s,i} = \frac{1}{\left[\frac{\left(1 - \beta_i^{1/3}\right)}{k_s} + \frac{\beta_i^{1/3}}{\left(1 - \beta_i^{2/3}\right) k_s + \beta_i^{2/3} k_a}\right]} \tag{2.18}$$

The effective thermal conductivity of the liquid, $k_{l,i}$, in the Nakano model is expressed as a multiple of the base material thermal conductivity, k_s. The specific heat of the ith flux layer is also expressed in terms of the void ratio at that layer as:

$$C_i = C_{ps}\, x_i \left(1 - \beta_i\right) \rho_s + 28.8 C_{pa}\, x_i \left[\frac{\beta_i}{1.98(T_i + 273)}\right] \tag{2.19}$$

where: C_i = Heat Capacity of ith layer $\left(\frac{cal}{gK}\right)$

C_{ps} = Specific heat capacity of powder base material $\left(\frac{cal}{g\,K}\right)$

C_{pa} = Specific heat capacity of air $\left(\frac{cal}{gK}\right)$

x_i = Layer Thickness (m)

In this model, the values of C_{ps} and C_{pa} are expressed as functions of the absolute temperature. Critical to the model, however, is the need to mathematically express the sintering process. Nakano *et. al.* used the equation by Jander for the rate of the sintering reaction, and is given below as equation (2.20).

$$\left[1 - (1 - \zeta)^{1/3}\right]^2 = \kappa t \qquad (2.20)$$

where: ζ = Efficiency of the sintering reaction

κ = Rate quotient of the sintering reaction (s^{-1})

The efficiency of the sintering reaction is a measure of the consolidation that occurs in the powder as the temperature increases and is given by:

$$\zeta = 1 - \frac{\beta_i}{\beta_o} \qquad (2.21)$$

where: β_o = Initial void ratio of the powder

Introducing a new variable K, where $K = \sqrt{\kappa}$, the sintering reaction may be re-written as:

$$\beta = \beta_o \left(1 - K\sqrt{t}\right)^3 \qquad (2.22)$$

Finally, the rate constant K is a function of the flux composition, and can be expressed as follows:

$$K = A\,e^{-\left(\frac{E_s}{RT_k}\right)} \qquad (2.23)$$

where: A = constant

E_s = Activation Energy $\left(\frac{J}{mol}\right)$

T_k = Thermodynamic temperature (K)

$$R \quad = \text{Gas Constant} \left(\frac{J}{mol\,K}\right)$$

Using the preceding equations to account for property variability, Nakano *et. al.* [36] solved the one-dimensional conduction equation numerically. The model was verified under steady state conditions using experimental data. The temperature profile for zero net consumption (i.e consumption rate = melting rate = input rate) determined experimentally compared favorably with the model prediction, the only discrepancies occurring at the melt interface and at powder surface. However, the model predictions of liquid and solid layer thicknesses when consumption was imposed did not match the experimental results until the liquid conductivity in the model was increased. A value of six times the powder value was necessary to get agreement with the experimental data when consumption is incorporated. This increase was justified as being due to convection in the liquid, which requires that a larger heat transfer coefficient be used.

Further, using the same model, Nakano et. al. investigated the transient melting behavior of the flux. However, only the case where there is consumption was presented. For this case, the feed rate (i.e. the rate of addition of new powder) was made equal to the consumption rate. Their calculations show that it takes 20 minutes for the steady state value of liquid flux thickness to be achieved for a casting speed of 1.5 m/min and a flux consumption of 0.4 kg/ton of steel. Additionally, measurements of the liquid layer thickness as a function of time after addition of powder were made at an actual caster. These results showed, according to the authors, that the molten pool thickness remains practically constant, which is in contrast to their calculation, which shows the significant growth in liquid layer depth that occurs after new powder is added. Presumably the discrepancy occurs because the plant measurements were taken after the steady state had been achieved. That is, the time at which new powder is added, to initiate the measurements, is some time after the actual beginning of the cast.

2.2.2 Fluid Flow Models

It is generally understood that the thickness of liquid and solid flux layers developed in the continuous casting process is very strongly dependent on the heat transfer characteristics of the material. Heat transfer models such as those described in section 2.2.1 attempt to calculate the extent of the layers purely from a consideration of heat transfer phenomenon. Mass transport is included as a means of absorbing the latent heat of fusion. This imposed mass transfer of flux is calculated based on an overall consumption of mold flux, and does not consider how the flux is removed, nor variations in consumption rate at various locations around the mold. In short, no real consideration of the mechanism of infiltration into the mold-strand gap is given. Fluid flow models, such as those described below, attempt to complete the picture by predicting the flow of liquid into the gap based on casting conditions, which include the position of the solidifying shell. However, none of these models consider flow occurring in the top-surface flux layers, which presumably will affect how fluid enters the mold-strand gap. Following, therefore are flow models of previous work, which focus on the mold-strand gap only.

In recent work by Bommaraju *et. al.* [9], flux flow in the mold-strand gap is approximated by Couette flow between the stationary copper mold and the steel shell moving at the casting speed. In the work by Bommaraju, the Couette flow solution is used to determine the shear stress in the flux, and hence the normal stress produced in the steel shell. Additionally, the fluid flow model was coupled with a heat transfer model which was used to obtain the solidification shrinkage of the shell thus enabling calculation of the mold-strand gap size. Several conclusions were made about the effect of the powder viscosity on the stresses developed in the shell.

Despite the utility of the Bommaraju model of fluid flow, its physical significance may be limited because it differs significantly from the real situation, as the governing equation for Couette flow does not include any pressure terms. That is, the flow pattern is determined solely by a balance of viscous and inertia forces. The effect of fluid pressure on the flow pattern is ignored. However, work by Anzai *et. al.* [37] considers the general hydrodynamic lubrication by

the mold flux, in which the Navier-Stokes equation is solved. Additionally, the Anzai work assumes that the flow takes place between two rigid non-parallel plates, and the effect of the oscillation of one of the plates is incorporated. Consequently, the variation in pressure and flow rate for the flux in the mold strand gap is calculated. The results show that the trend in pressure and flow rate follow the same temporal pattern as the oscillation speed (not displacement) of the mold. Also, lower viscosities result in lower pressures but higher flow rate.

The Anzai work goes on to consider another more realistic case where the steel shell is not rigid. In this case, the Reynolds equation for lubrication and the two-dimensional plain strain elasticity equation for the steel shell are solved simultaneously using the finite element method. The results of this model show a similar trend in flow rate as developed when the steel shell is rigid. However, the flow rate profile is flatter than that given by the previous model.

2.3 DISCUSSION

Based on the review of current literature, there still remain several important shortcomings in the available models, and questions concerning the flow and thermal behavior of the lubricating flux. All of the heat transfer models reviewed are conduction models. Several authors [29, 31, 36] have confirmed the importance of radiation through the liquid flux, as well as the significance of convection in the liquid flux pool to heat transfer. Yet neither of these phenomena are incorporated into any of the models surveyed.

With the fluid flow models discussed, the effect of steel motion on the flux motion is not considered, nor has the flow pattern developed in the liquid flux pool above the steel been considered. Additionally, fluid flow and heat transfer in the flux material were never considered simultaneously. Thus, the significant effect that fluid flow has on heat transfer, as evidenced by the need to use an enhanced thermal conductivity in the presence of convection[36], and vice versa has not been evaluated either. It is therefore quite probable that none of the aforementioned models are capable of giving an accurate quantitative representation of the actual physical process of powder melting and liquid flux flow in an operating continuous casting mold.

CHAPTER 3

ONE-DIMENSIONAL MODEL

As an initial step in the process of developing a finite element model of the behavior of the lubricating flux, a simplified one dimensional heat transfer analysis was performed on the melting process. From this, a relationship between the molten flux layer thickness and the powdered flux layer thickness, under steady state conditions, was determined. This result will be used to verify the initial finite element model which consists of a steady state one-dimensional approximation of the actual physical situation. Once the initial finite element model is verified or determined to be self-consistent, it will be successively modified to eventually represent the actual physical state.

3.1 STEADY STATE MODEL

3.1.1 Analytical Derivation

Figure 3.1 below is a simplified schematic representation of the melting process for the lubricating flux. Introduced as a powder at some mass rate (= $\dot{m}_p$), the flux melts and flows into the mold-strand gaps at an equal, lesser or faster rate ($\dot{m}_c = \dot{m}_1 + \dot{m}_2$). The schematic shown in The two-dimensional mass flow is also simplified into one-dimensional mass inflow and outflow.

The following analysis is performed on a ***unit time basis*** . Considering one-dimensional heat conduction, and referring to Figure 3.1, we may write the following expressions for the flux layers:

For molten flux: $$Q_{fl} = \frac{k_f A(T_{st} - T_{melt})}{w_f} \quad (3.1)$$

For powder: $$Q_p = \frac{k_p A(T_{melt} - T_o)}{w_p} \quad (3.2)$$

$Q_{melt} = dm_p \Delta H_L$ (dm_p (kg) is the total mass of powder introduced in unit time) (3.3)

$Q_{conv} = h_{tot} A (T_o - T_\infty)$ (3.4)

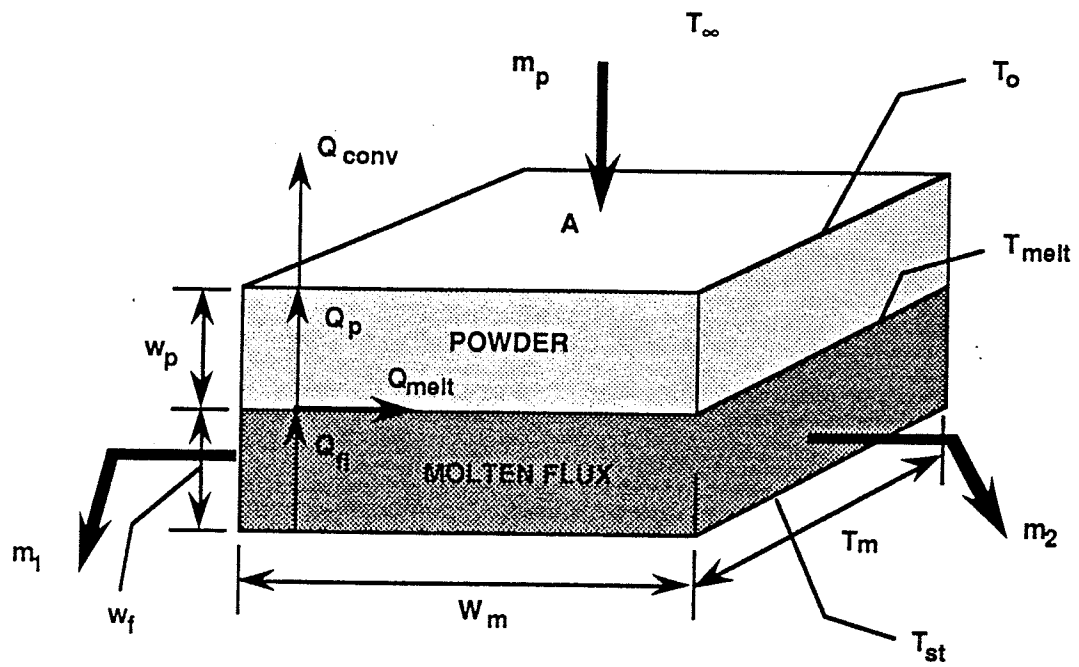

Figure 3.1 Schematic for Melting of Flux

NOMENCLATURE FOR ANALYTICAL MODEL

A	Cross-sectional Area of Mold, m^2
W_m	Width of mold, m
Tm	Thickness of Mold, m
w_p	Average Powder Thickness, m
w_f	Average Molten Flux Thickness, m
T_∞	Ambient Temperature, K
T_o	Temperature of top surface of Powder, K
T_{melt}	Melting Point of Powder, K
T_{st}	Steel Liquidus Temperature, C
ΔH_L	Latent Heat of Fusion of Flux, Jkg^{-1}
h_{tot}	Top Surface Heat Transfer Coefficient, $Wm^{-2}K^{-1}$
k_f	Thermal Conductivity of molten flux, $Wm^{-1}K^{-1}$
k_p	Thermal Conductivity of solid powder, $Wm^{-1}K^{-1}$

Q_{fl}	Heat Flux through molten flux, W
Q_p	Heat Flux through Powder, W
Q_{melt}	Heat absorbed in melting (i.e. Latent Heat), W
$m_1 + m_2$	Mass of molten flux leaving domain, kg

Expressing the heat balance across the flux layers, we may write

$$Q_p = Q_{conv} \tag{3.5}$$

$$Q_{fl} = Q_p + Q_{melt} \tag{3.6}$$

Similarly, the mass flow must be balanced in the domain such that the mass inflow, dm_p, equals the mass out, dm_c, plus the accumulation, dm_f. That is:

$$dm_p = dm_f + dm_c \tag{3.7}$$

where: dm_f (kg) is the change of mass of the flux &

dm_c (kg) is the mass leaving the domain = mass consumed

Combining equations 3.1 through 3.7, we get:

$$\frac{k_p(T_{melt} - T_o)}{w_p} = h_{tot}(T_o - T_\infty) \tag{3.8}$$

$$\frac{k_f A(T_{st} - T_{melt})}{w_f} = \frac{k_p A(T_{melt} - T_o)}{w_p} + dm_p \Delta H_L \tag{3.9}$$

and $$dm_p = dm_f + dm_c \tag{3.10}$$

We may eliminate T_o from equations 3.8 and 3.9, which would leave the variable h_{tot}. However, h_{tot} like T_o will be a function of w_p and w_f, but h_{tot} is more difficult to determine experimentally. Thus, we will leave T_o in the equations, but for future reference, T_o will be given by equation 1 as:

$$T_o = \frac{k_p T_{melt} + h_{tot}\, w_p T_\infty}{h_{tot} w_p + k_p} \tag{3.11}$$

From 3.9, $$\frac{k_f A(T_{st} - T_{melt})}{w_f} = \frac{k_p A(T_{melt} - T_o)}{w_p} + dm_f \Delta H_L + dm_c \Delta H_L$$

but $dm_f = \rho_f A dw_f$

Re-writing, we have

$$C_3\frac{dw_f}{dt} - \frac{C_1}{w_f} + \frac{C_2(T_{melt} - T_o)}{w_p} + \frac{dm_c}{dt}\Delta H_L = 0 \qquad (3.12)$$

where: $C_1 = k_f A(T_{st} - T_{melt})$

$C_2 = k_p A$

$C_3 = \rho_f A \Delta H_L$

Under steady-state conditions in which there is no variation of thicknesses with time, $\frac{dw_f}{dt} = 0$. To achieve this condition, the melting rate must equal the rate of powder consumption.

Re-writing equation 3.12 with $\frac{dw_f}{dt} = 0$, we get:

$$-\frac{C_1}{w_f} + \frac{C_2(T_{melt} - T_o)}{w_p} + \frac{dm_c}{dt}\Delta H_L = 0 \qquad (3.13)$$

$$\frac{C_1}{w_f} = \frac{\left[C_2(T_{melt} - T_o) + w_p\left(\frac{dm_c}{dt}\Delta H_L\right)\right]}{w_p} \qquad (3.14)$$

$$w_f = \frac{C_1 w_p}{\left[C_2(T_{melt} - T_o) + w_p\left(\frac{dm_c}{dt}\Delta H_L\right)\right]} \qquad (3.15)$$

Letting $\dot{m}_c$ denote the mass consumption rate $\frac{dm_c}{dt}$, and expressing C_1 and C_2 in terms of the physical constants, we get:

$$w_f = \frac{k_f A(T_{st} - T_{melt})w_p}{\left[k_p A(T_{melt} - T_o) + w_p \dot{m}_c L_{fusion}\right]} \qquad (3.16)$$

We therefore have the liquid flux thickness, w_f as a function of the powder thickness, w_p

Previously, an expression for T_o was obtained, in which T_o depended on h_{tot}, the heat transfer coefficient for the upper powder surface. h_{tot} has two components, one convective and one radiative. Thus, we may write:

$$h_{tot} = h_{conv} + h_{rad} \tag{3.17}$$

$$h_{rad} = \sigma\varepsilon(T_o + T_\infty)(T_o^2 + T_\infty^2)$$

The local convective heat transfer coefficient is given by equation (3.18)[38]:

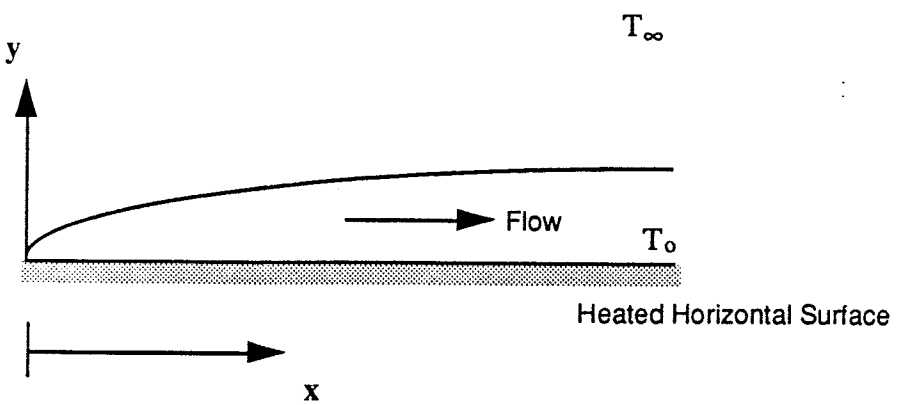

Figure 3.2 - Coordinate System for Natural-Convection Boundary Layer Flow over a Semi-infinite Plate [38]

$$Nu_x = \frac{h_x x}{k_{air}} = 0.5013\, Gr_x^{1/3}\, Pr^{1/4} \tag{3.18}$$

where:

Nu_x = Local Nusselt Number (convection vs. conduction)

h_x = Local convective heat transfer coefficient, W m^{-2} K^{-1}

k_{air} = Thermal conductivity of air, W m^{-1} K^{-1}

Gr_x = Local Grashof Number (buoyancy vs. viscosity)
$= \left(\frac{g\beta\Delta T x^3}{\nu^2}\right)$

Pr = Prandtl Number (momentum vs. thermal diffusion),
$= \frac{c_p\mu}{k_{air}}$

Expressing h_x as a function of x, we get:

$$h_x = \frac{0.5013\, k_{air}\, (Gr_x^{1/5}\, Pr^{1/4})}{x} \tag{3.19}$$

Expanding:

$$h_x = \left[\frac{0.5013\, k_{air} \left(\frac{g\beta\Delta T}{\nu^2}\right)^{1/5} x^{3/5} \left(\frac{c_p\mu}{k_{air}}\right)^{1/4}}{x} \right]$$

$$\Rightarrow \quad h_x = C_4\, x^{-2/5} \tag{3.20}$$

where: $$C_4 = 0.5013 k_{air}^{3/4} (c_p\mu)^{1/4} \left(\frac{g\beta\Delta T}{\nu^2}\right)^{1/5}$$

To determine the mean convective heat transfer coefficient h_m, equation 3.20 is integrated with respect to x over the entire width of the mold, W_m. That is:

$$h_m = \frac{C_4}{W_m} \int_0^{W_m} x^{-2/5}\, dx$$

$$\Rightarrow \quad h_m = \frac{5}{3} \frac{C_4}{W_m} W_m^{3/5}$$

$$\Rightarrow \quad h_m = \frac{5}{3} \frac{C_4}{W_m^{2/5}}$$

Substituting for C_4, we get:

$$h_m = \frac{5}{3} \left[\frac{0.5013 k_{air}^{3/4} (c_p\mu)^{1/4} (g\beta\Delta T)^{1/5}}{\nu^{2/5}\, W_m^{2/5}} \right] \tag{3.21}$$

where:

	c_p	= Specific heat capacity of air, J kg^{-1} K^{-1}
	μ	= Dynamic Viscosity, Pa•s
	g	= acceleration due to gravity, ms^{-2}
	β	= Coefficient of thermal expansion of air, K^{-1}
	ΔT	= Temperature difference (T_o - T_∞), K
	ν	= Kinematic viscosity, m^2s^{-1}
Note:	$\nu\rho$	$= \mu$

where ρ = density of air, kgm^{-3}

ν = Temperature dependent

μ = Temperature dependent [39]

c_p (air) = Temperature dependent

$\beta = \frac{1}{T_o}\ K^{-1}$

We may now express the total heat transfer coefficient at the surface of the powder, h_{tot} as $h_{tot} = h_{rad} + h_{conv}$, where h_{conv} is the mean heat transfer coefficient h_m given in 3.21

$$\Rightarrow \quad h_{tot} = \left[\sigma\varepsilon(T_o + T_\infty)(T_o^2 + T_\infty^2)\right] + \frac{5}{3}\left\{\frac{0.5013 k_{air}^{3/4}(c_p\mu)^{1/4}\left[g\beta(T_o - T_\infty)\right]^{1/5}}{\nu^{2/5}\, D^{2/5}}\right\} \tag{3.22}$$

Substituting for h_{tot} from equation 3.22 into equation 3.11, we get:

$$T_o = \frac{k_p T_{melt} + \left\{\left[\sigma\varepsilon(T_o + T_\infty)(T_o^2 + T_\infty^2)\right] + \frac{5}{3}\left\{\frac{0.5013(c_p\mu)^{1/4} k_{air}^{3/4}\left[g\beta(T_o - T_\infty)\right]^{1/5}}{\nu^{2/5}\, D^{2/5}}\right\}\right\} w_p T_\infty}{\left\{\left[\sigma\varepsilon(T_o + T_\infty)(T_o^2 + T_\infty^2)\right] + \frac{5}{3}\left\{\frac{0.5013(c_p\mu)^{1/4} k_{air}^{3/4}\left[g\beta(T_o - T_\infty)\right]^{1/5}}{\nu^{2/5}\, D^{2/5}}\right\}\right\} w_p + k_p} \tag{3.23}$$

TABLE 3.1 - Standard Simulation Conditions for 1-D Model

PROPERTY	VALUE	PROPERTY	VALUE
Solid Conductivity, $\mathbf{k_p}\left[\frac{W}{m.K}\right]$	0.9	Flux Consumption, $\left[\frac{kg}{m^2}\right]$	0.6
Flux Melting Point, $\mathbf{T_{melt}}$, [K]	1273	Slab Thickness, $\mathbf{T_m}$ [m]	0.2286
Stefan-Boltzman Cnst., $\sigma\left[\frac{W}{m^2.K^4}\right]$	5.67E-8	Casting Speed, $\mathbf{V_c}$ [m/min]	1.0
Flux Emissivity, ε	0.8	Consumption Rate, $\dot{\mathbf{m}}_\mathbf{c}\left[\frac{kg}{s}\right]^\dagger$	0.0326
Ambient Temperature, $\mathbf{T_\infty}$ [K]	300	Steel Temperature, $\mathbf{T_{st}}$ [K]	1823
Acceleration due to Gravity, $\mathbf{g}\left[\frac{m}{s^2}\right]$	9.81	Enthalpy of Fusion, $\Delta\mathbf{H_L}\left[\frac{J}{g}\right]$	350
Slab Width, $\mathbf{W_m}$ [m]	1.4	Liquid Flux Cond., $\mathbf{k_f}\left[\frac{W}{m.K}\right]$	1.5

† **Calculated Value**

3.1.2 Typical Results

Standard conditions for the simulation using this analytical model are given in Table 3.1. Figure 3.3 is a plot of W_p vs. T_o obtained using average values for the temperature range 200°C - 800°C [2]. To find a relation between the powder thickness, w_p and the molten flux thickness w_f, one unknown has to be eliminated from equation 3.9, i.e. T_o. However, according to equation 3.23, T_o cannot be explicitly expressed as a function of w_p. It is therefore impossible to obtain an analytical relationship for w_f solely as a function of w_p. However, the relationship may be illustrated through numerical means using a spreadsheet Figures 3.4 and 3.5 illustrate the relationship between w_p and w_f.

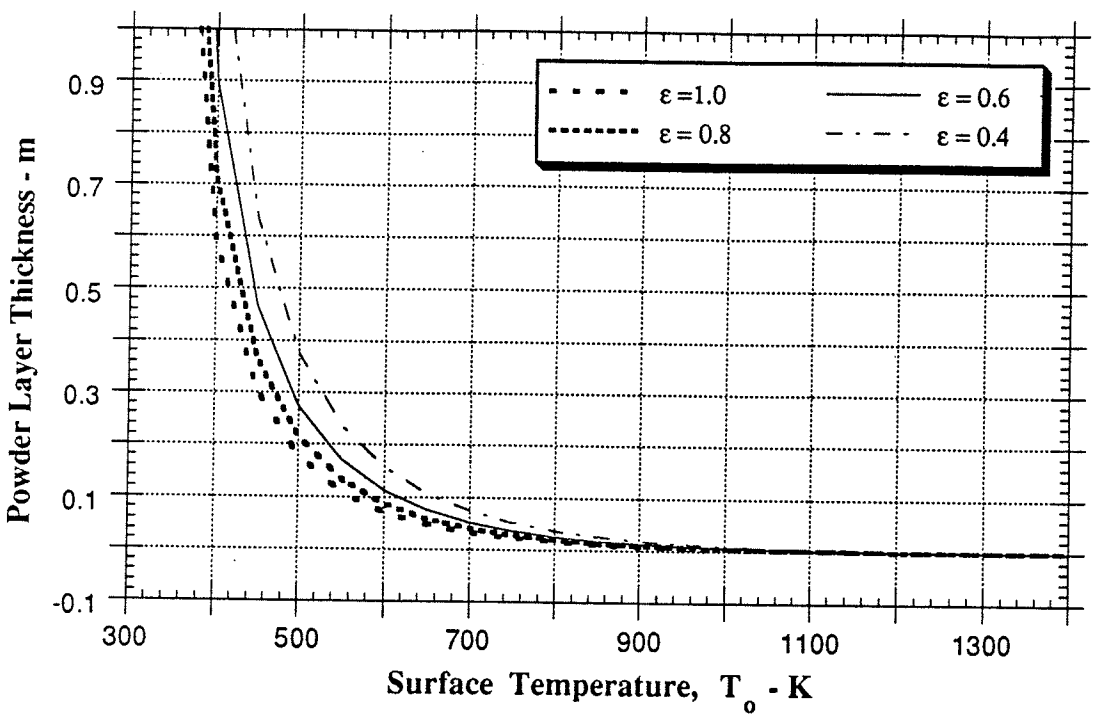

Figure 3.3 - Powder Thickness as a Function of Surface Temperature

3.1.3 Parametric Study

The preliminary results indicate that beyond a certain thickness of powder, the liquid pool no longer significantly increases in thickness with increasing powder thickness, which agrees with the findings of Dehalle and co-workers [10]. It can be seen from the equations, and from the spread sheet calculations that the term in the denominator of equation 3.16 containing the

melting rate (= consumption rate under steady state conditions) and the latent heat of fusion, dominates the relation. That is, the liquid flux thickness is relatively insensitive to changes in parameters other than the melting rate and/or the latent heat of fusion.

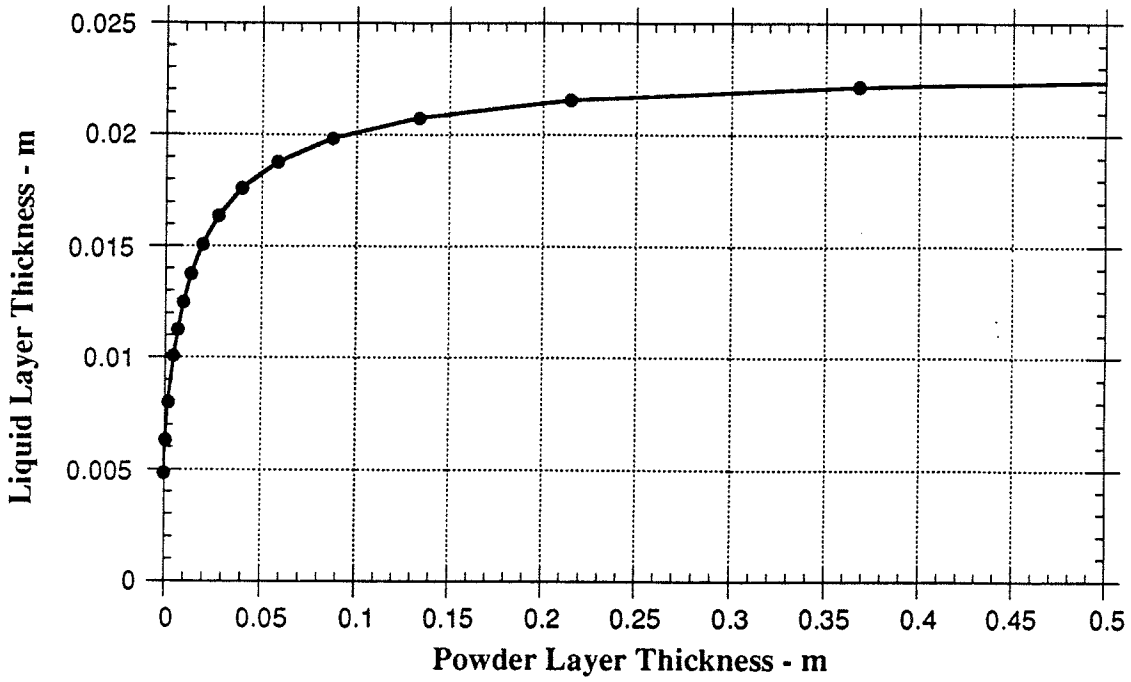

Figure 3.4 - Liquid Layer Thickness as a function of Powder Layer Thickness

Following is a study of the effect that changes in material properties have on the relationship between powder and liquid layer thicknesses. The material properties are chosen for a flux of the approximate composition given in Table 3.2 below. Figure 3.5 illustrates the effect of casting speed, V_c, and thus flux consumption rate $(\dot{m}_c)$ on the relationship between w_p and w_f, assuming constant specific consumption, m_{sc} of 0.6 kg/m^2.

TABLE 3.2 Standard Flux Composition for 1-D Model

Constituent	% by wt.	Constituent	% by wt.
SiO_2	35	Na_2O	5
CaO	35	F	6
Al_2O_3	6	C	4
MgO	1		

Figure 3.6 illustrates the effect of varying the flux powder emissivity on the relationship between the powder and liquid layer thicknesses. Based on Figure 3.6, the value of emissivity chosen does not appear to be critical in this analysis. Compare the effect of a change of 150% (0.4 -> 1.0) in emissivity from Figure 3.6, to a change of 150% (0.6 -> 1.5 kg/s) in consumption rate in Figure 3.5.

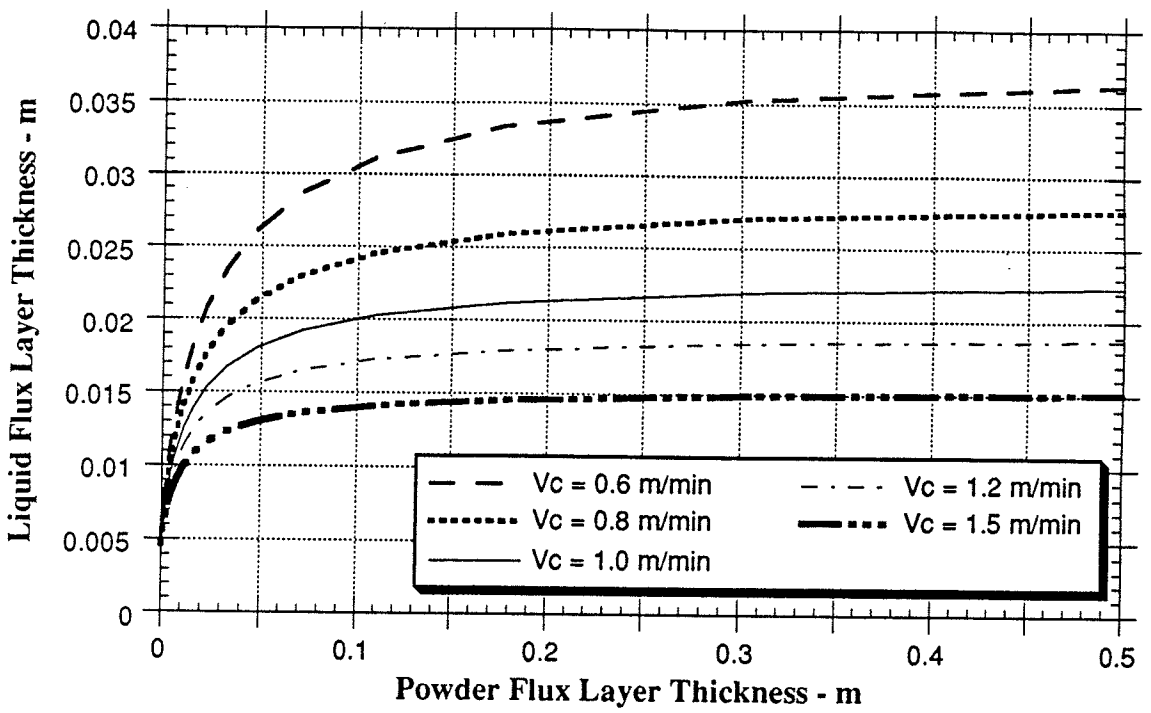

Figure 3.5 - Liquid Flux Layer Thickness as a Function of Powder Layer Thickness and Casting Speed, V_c.

In a similar way, the sensitivity of the wp-wf relation to changes in Latent heat of Fusion can also be investigated. The effect of such changes is illustrated in Figure 3.7 below. It is clear that the shift in the w_p - w_f relation for changes in ΔH_L is more significant than that for changes in emissivity. The values of ΔH_L used covers the range obtained for initially powdered or sintered material.

The effect of variation in the melting temperature of the flux is examined and is illustrated in Figure 3.8 below. Relatively small changes in flux composition can result in large variations in melting point, and thus in liquid layer thicknesses as well.

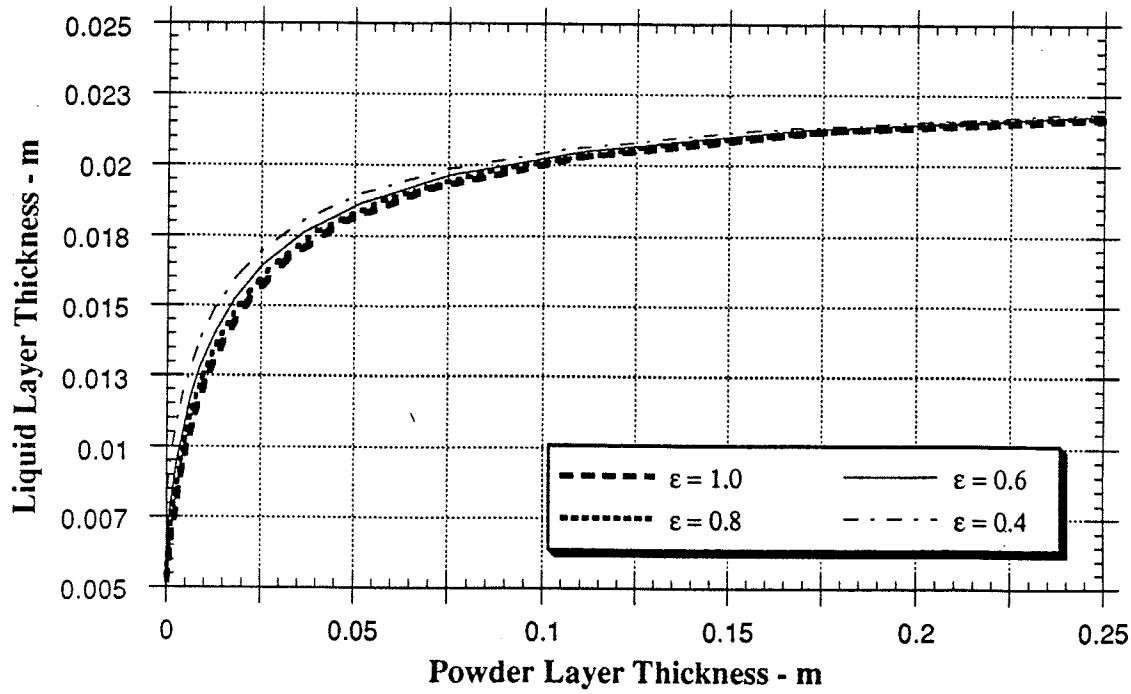

Figure 3.6 - Liquid Layer Thickness as a Function of Powder Layer Thickness and Powder Emissivity, ε

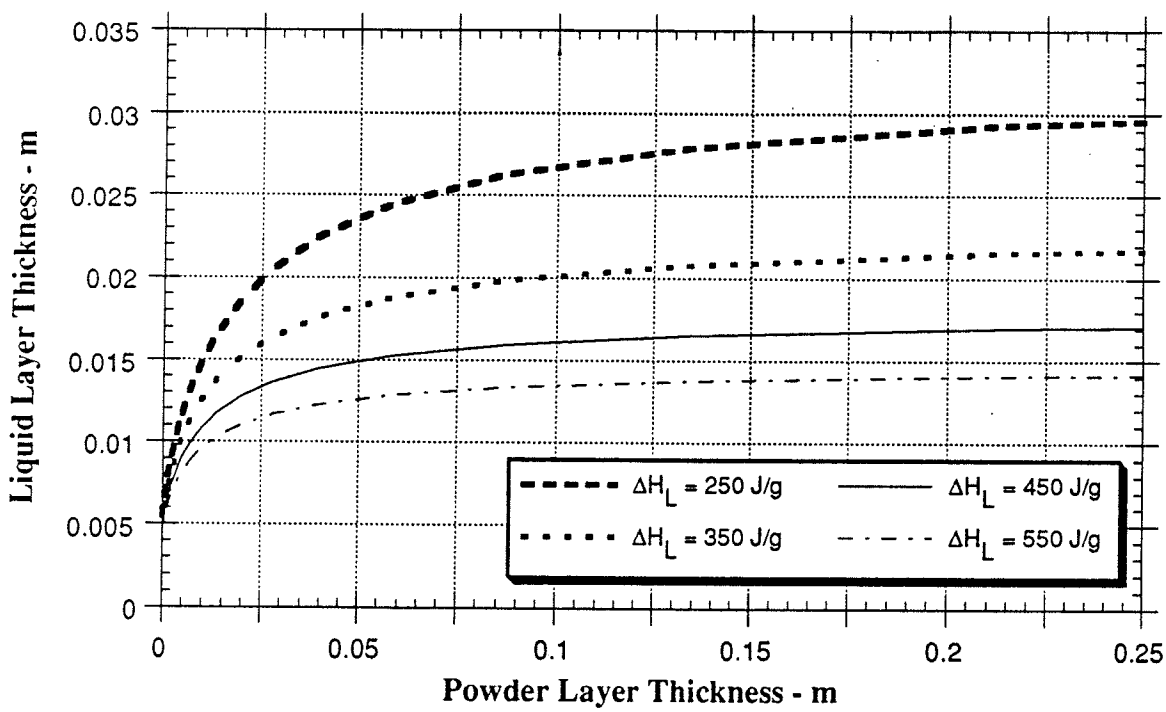

Figure 3.7 - Liquid Layer Thickness as a Function of Powder Layer Thickness and Enthalpy of Fusion, ΔH_L

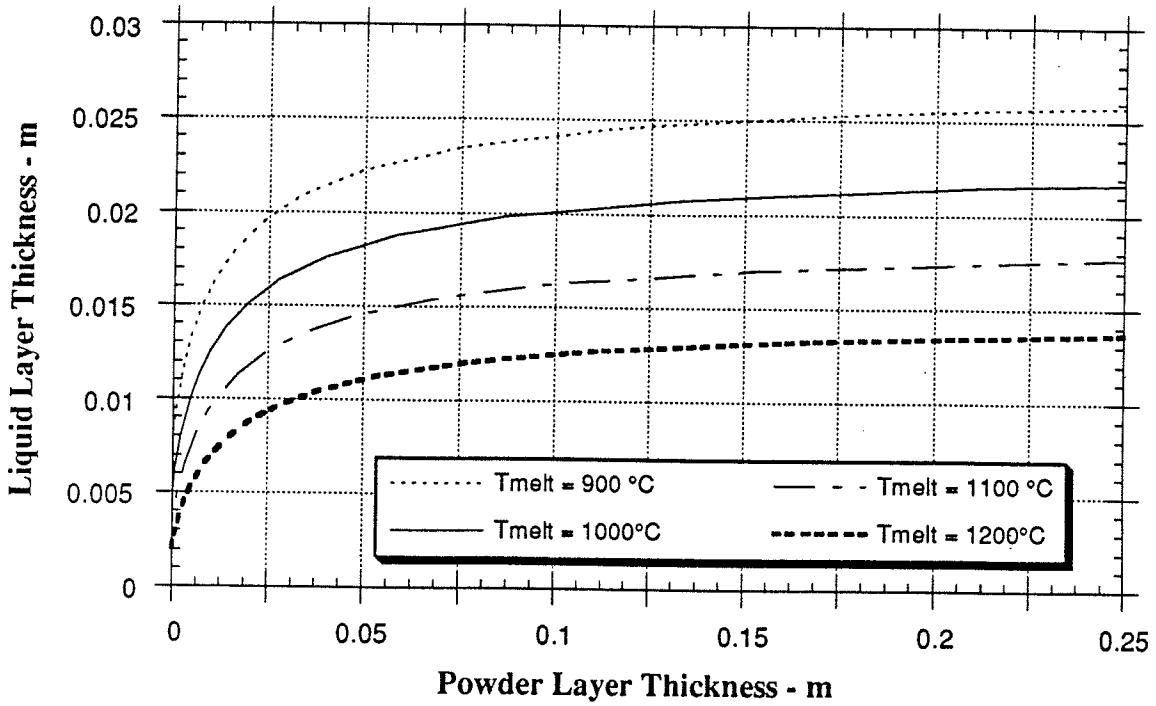

Figure 3.8 - Liquid Layer Thickness as a Function of Powder Layer Thickness and Flux Melting Point, T_{melt}

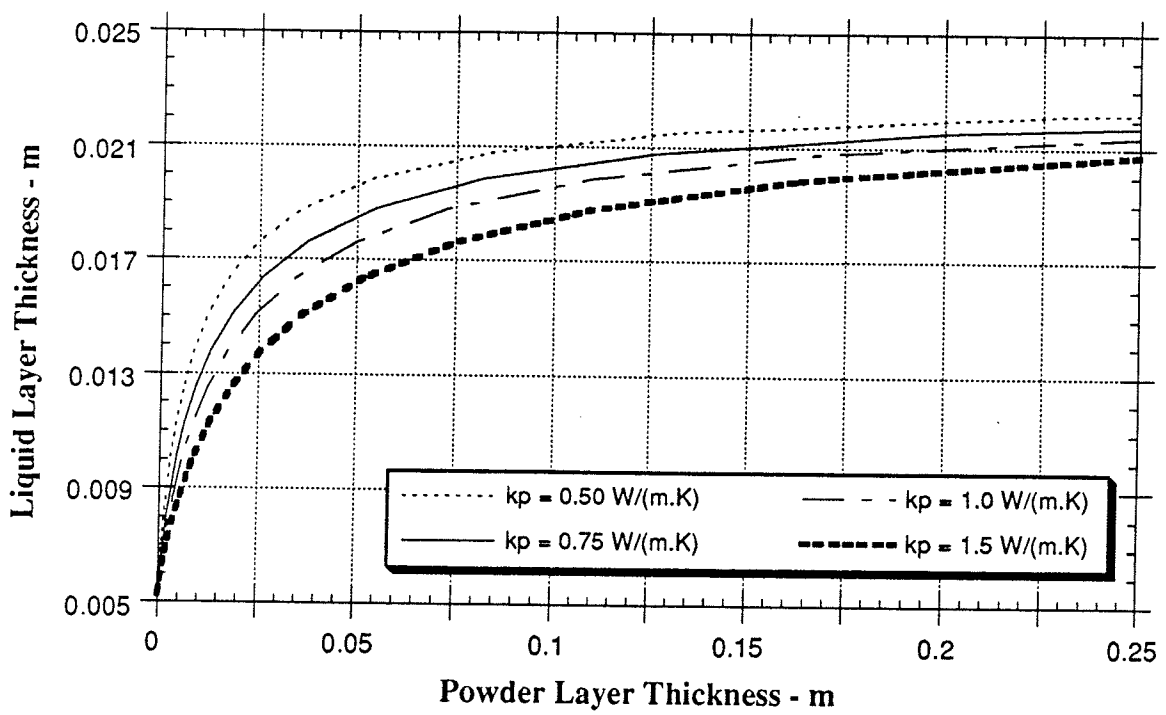

Figure 3.9 - Liquid Flux Layer Thickness as a function of Powder Layer Thickness and Average Powder Thermal Conductivity, k_p

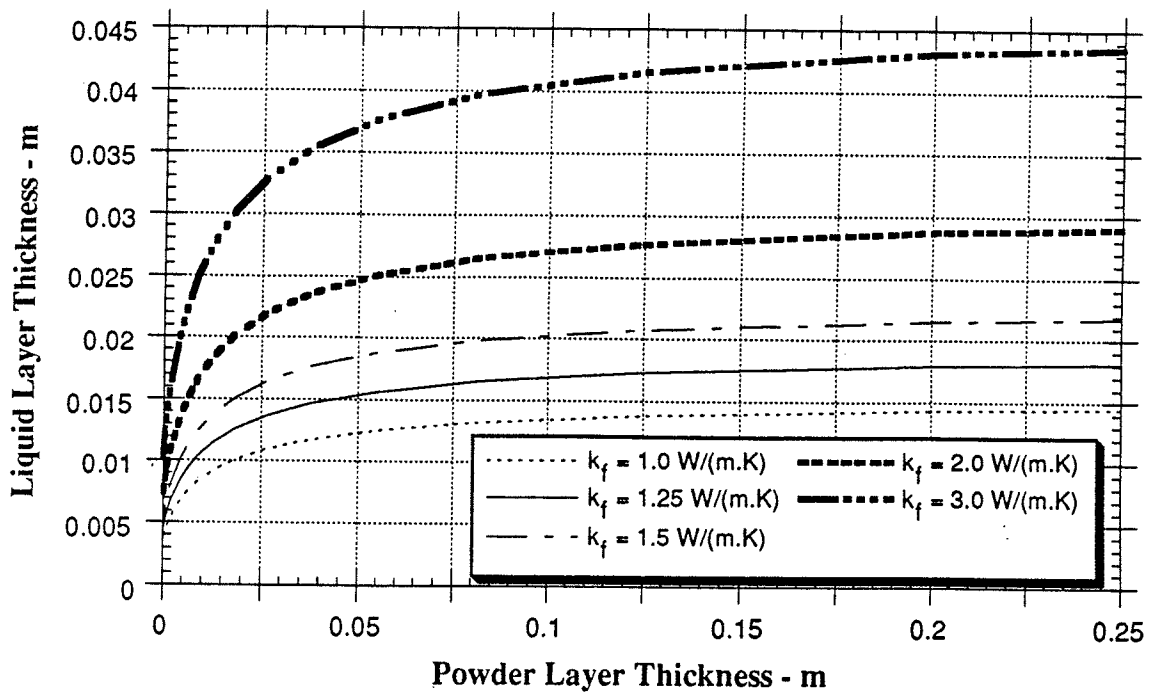

Figure 3.10 -Liquid Flux Layer Thickness as a Function of Powder Layer Thickness and Average Liquid Thermal Conductivity, k_f

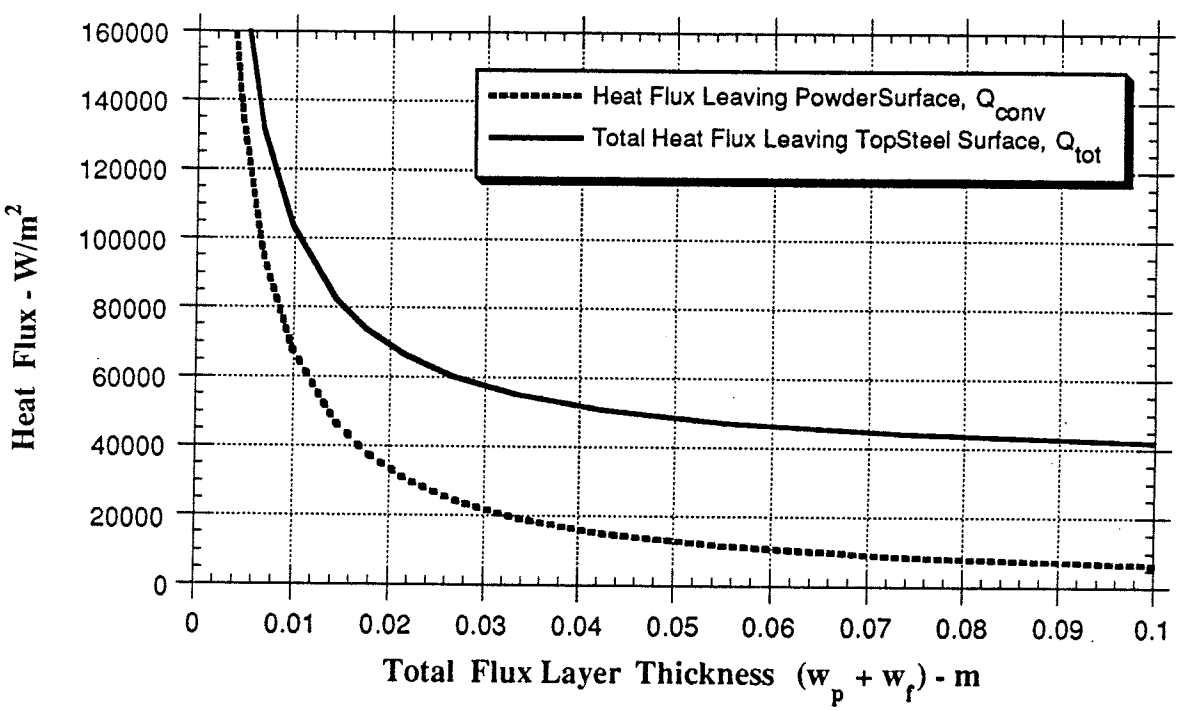

Figure 3.11 -Heat Flux Variation as a Function of Total Flux Layer Thickness for Standard Conditions

The result of changes in the thermal conductivites of the powdered (k_p) and molten fluxes (k_f) is illustrated in Figures 3.9 and 3.10. The conductivities are assumed to be constant over the entire thickness of powder or liquid, even though the temperatures vary. The effect of variation in liquid conductivity is more pronounced than that for powder conductivity.

Finally, in Figure 3.11 above, the variation in heat flux, both total and net, with respect to the molten flux layer shows that heat loss is greatly increased when flux thickness drops below 30 mm.

In summary, the three relations used to determine a relation between the molten flux and powdered flux thicknesses are:

$$T_o = \frac{k_p T_{melt} + h_{tot}\, w_p T_\infty}{h_{tot} w_p + k_p}$$

$$w_f = \frac{k_f A (T_{st} - T_{melt}) w_p}{\left[k_p A (T_{melt} - T_o) + w_p \dot{m}_c L_{fusion}\right]}$$

$$h_{tot} = \left[\sigma\varepsilon(T_o + T_\infty)(T_o^2 + T_\infty^2)\right] + \frac{5}{3}\left\{\frac{0.5013 k_{air}^{3/4} (c_p \mu)^{1/4} \left[g\beta(T_o - T_\infty)\right]^{1/5}}{\nu^{2/5} D^{2/5}}\right\}$$

Furthermore relations between any two of the four unknowns (T_o, h_{tot}, w_f and w_p) can be determined using these relations, but in the absence of a fourth independent equation, these unknowns cannot be solved for absolutely.

3.1.4 Comparison of Analytical Model with Finite Element Model

A finite element model in one dimension was constructed using the commercial code FIDAP™ (see Appendix B for input file). The results obtained using the finite element model were used in comparison with those obtained using the steady state analytical model described above. The purpose of this comparison is to simultaneously verify the analytical models, and to check the consistency of formulation of the finite element model.

3.1.4.1 Finite Element Model Description

The model domain with the boundary conditions is given in the Figure 3.12 below. The 1-D condition is simulated by using a single strip of 4 node quad elements. Refer to input files for material model definitions.

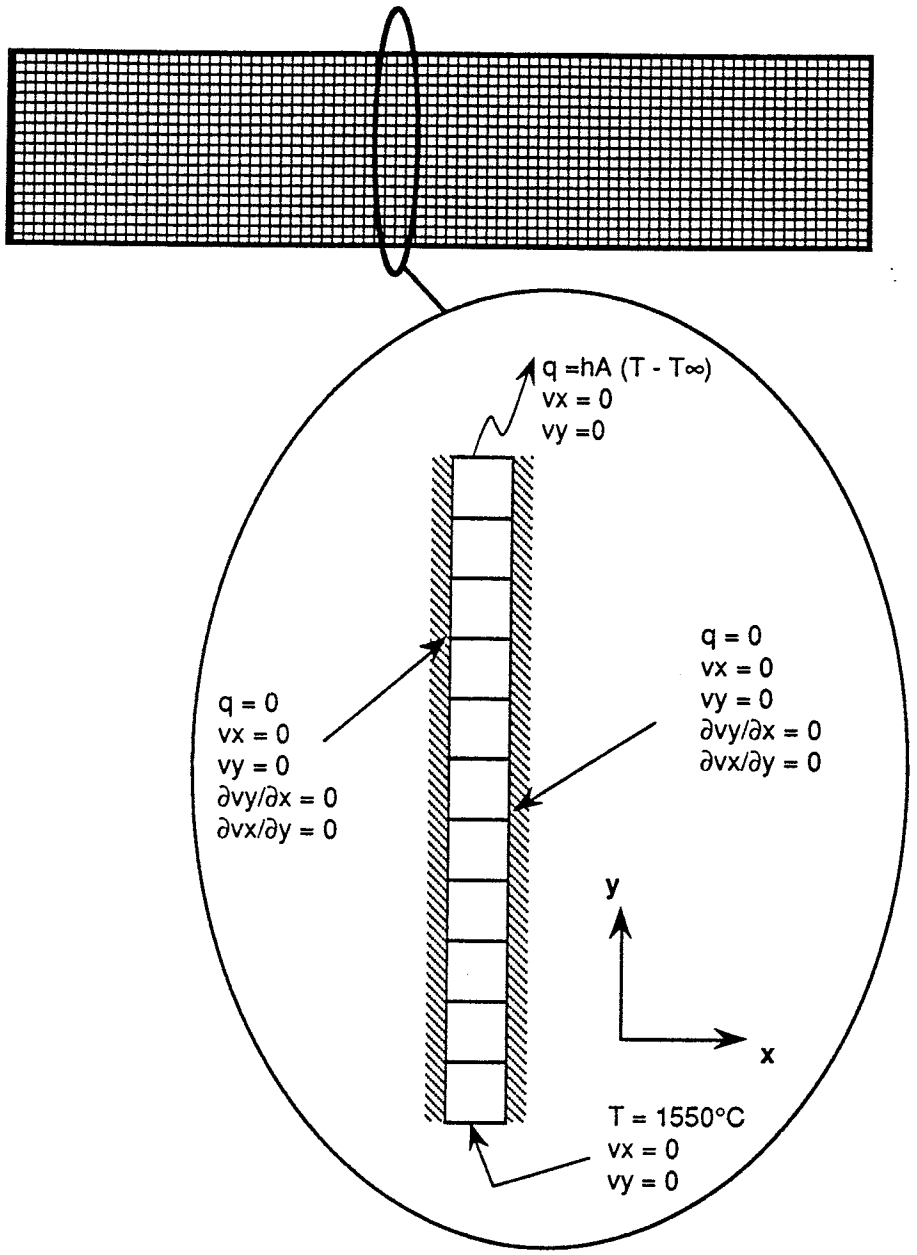

Figure 3.12 - Schematic of 1-D Finite Element Model Domain and Boundary Conditions

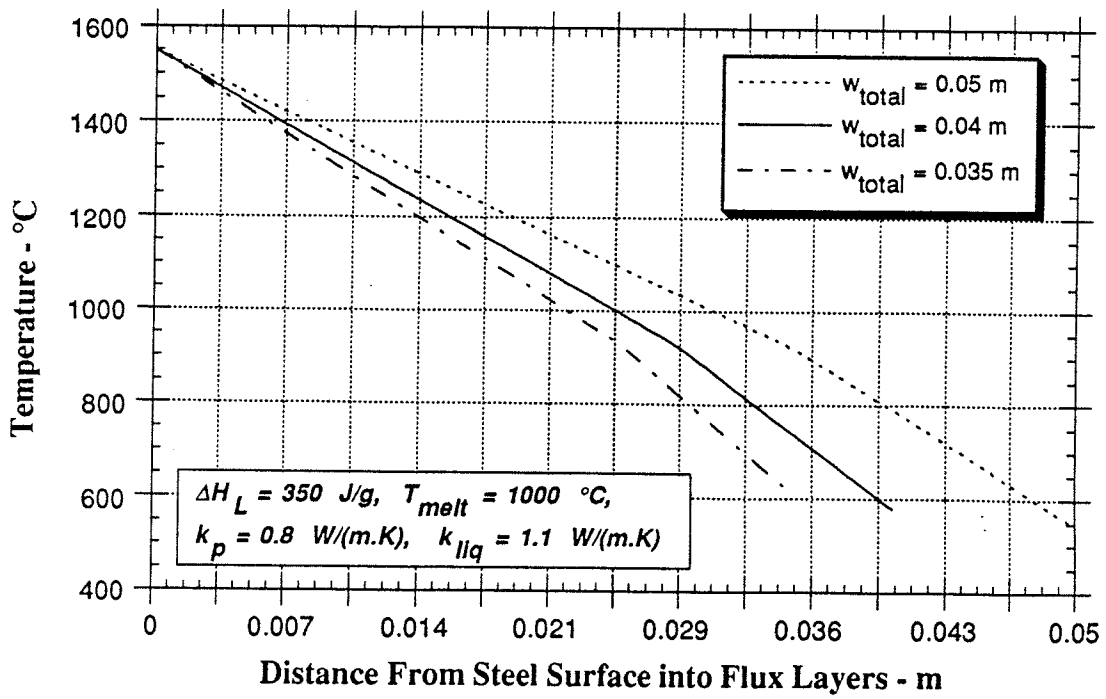

Figure 3.13 - Temperature Profile in Flux Layer as a Function of Total Flux Layer Thickness, w_{total}, as given by FIDAP for Zero Consumption

3.1.4.2 Results

The first finite element model simulates the steady state behavior of the flux as a function of overall flux layer thickness. The temperature profile through the flux thickness (i.e. in the y-direction) is given in Figure 3.13. The Figure also shows the effect of changing the overall layer thickness. This simulation was performed for the case where there is no consumption of flux, thus it essentially predicts the final location of the melt interface in a homogeneous material which is heated. The surface temperatures and liquid layer thicknesses obtained from several 'runs' of this model were compared to those obtained using the 1D analytical steady state model. These results are reproduced below in Figures 3.14 and 3.15. Note that this simulation is for the case of no consumption of flux ($dm_c/dt = 0$). The analytical values were obtained using the steady state spreadsheet model mentioned previously, and the input variables were adjusted to be more consistent with the flux for which material model data was available for use in FIDAP.

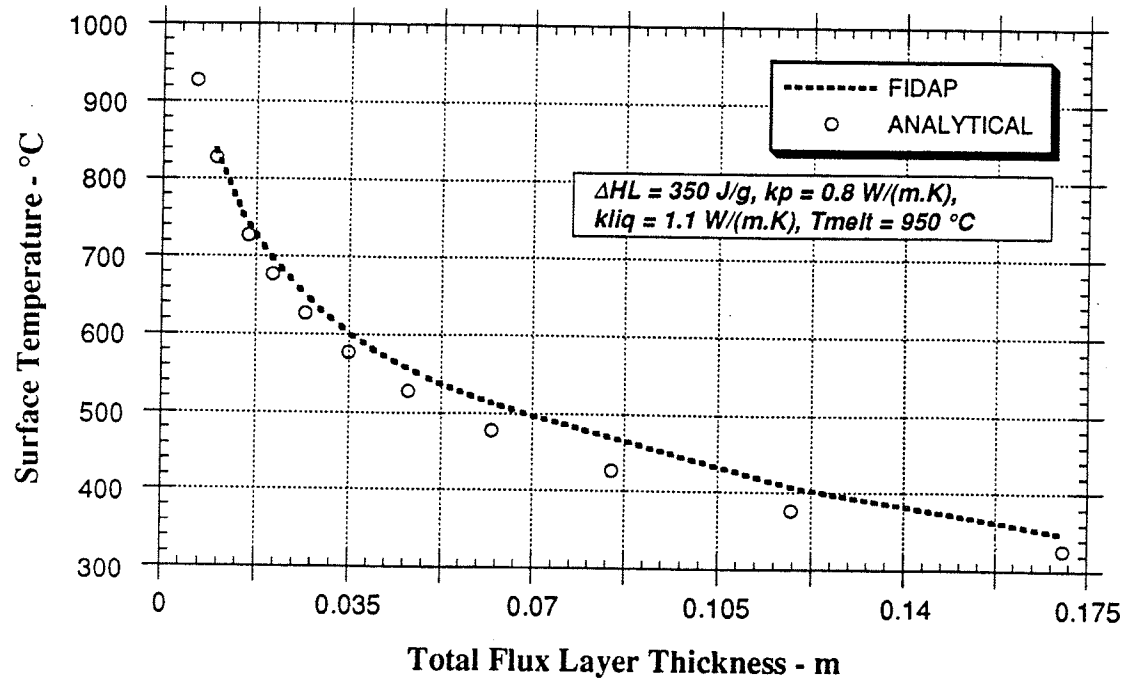

Figure 3.14 -Comparison of Surface Temperatures as a Function of Total Flux Thickness Between FIDAP and 1-D Analytical Model with Zero Consumption

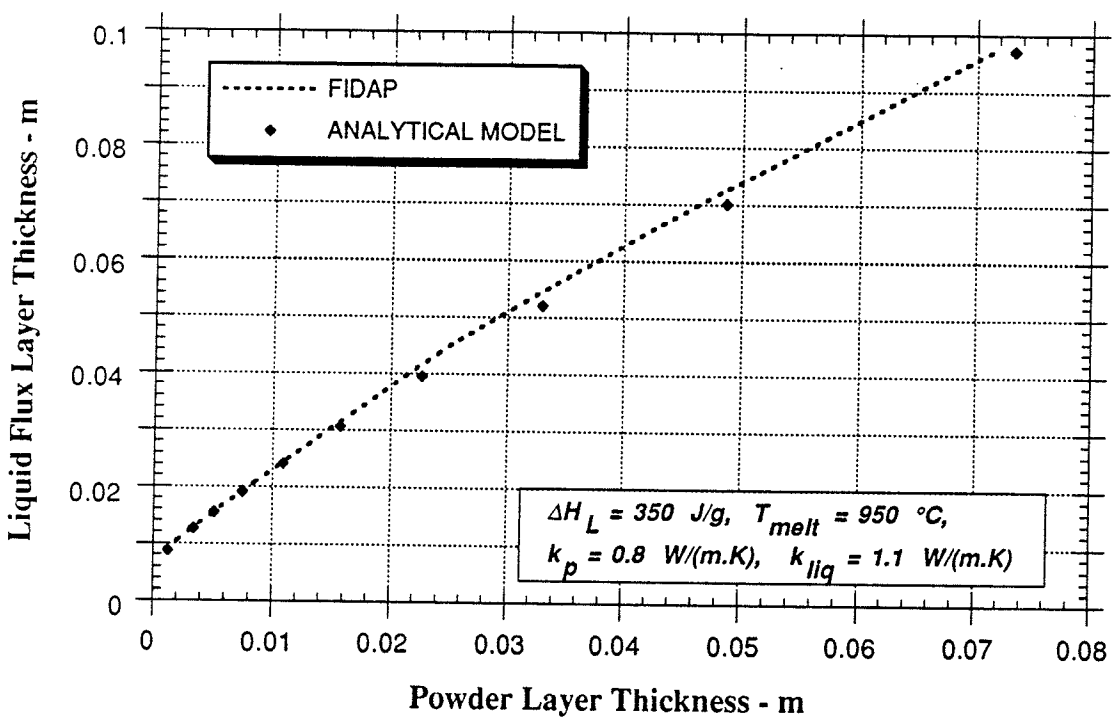

Figure 3.15 - Comparison of Liquid Layer Thickness as a Function of Powder Layer Thickness between FIDAP and 1-D Analytical Model.

Due to the good agreement shown in Figures 3.14 and 3.15, reasonable confidence in the formulation of the 1-D models is gained . This confidence may be extended to the results of the parametric study using the analytical model given in the previous sections. Additionally, because the finite element model appears to be correctly formulated it can be modified to perform a transient analysis

3.2 TRANSIENT 1-D FINITE ELEMENT MODEL

3.2.1 Model Development & Typical Results

The domain used for the transient one-dimensional finite element model is exactly the same as that used for the steady state analysis (see Figure 3.12). An implicit trapezoidal time integration scheme is used for the transient analysis. The reader is directed to Appendix A and to the FIDAP Theoretical Manual (pg. 7 -18) for full details of the scheme, and to Appendix C for the FIDAP input file.

Using similar material properties as in the analytical model as input to the transient finite element model, the time history of the liquid layer thickness was obtained (see Figure 3.16).

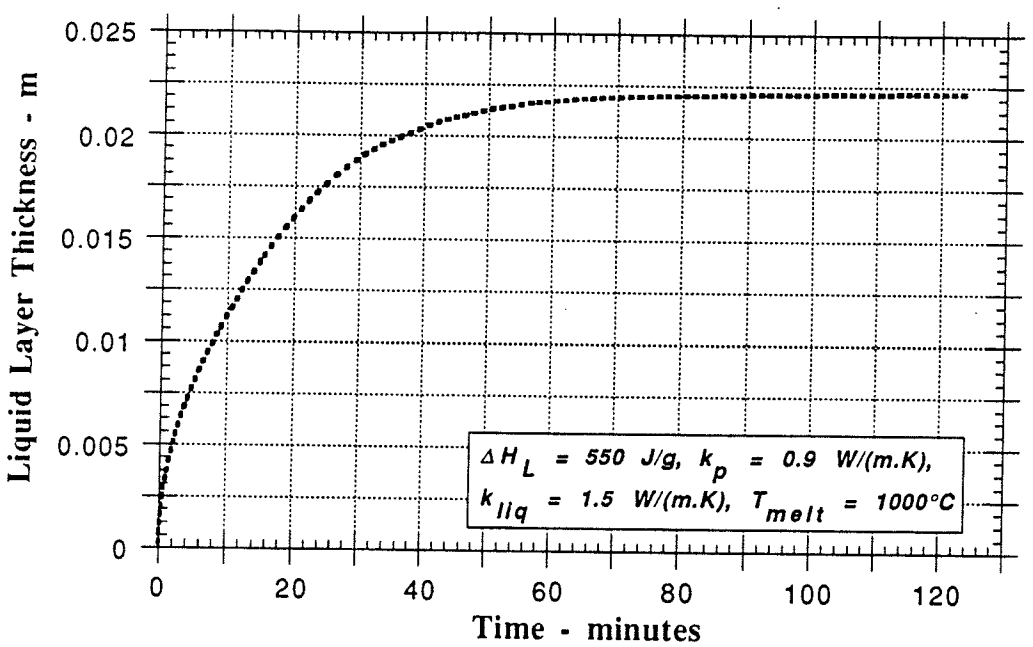

Figure 3.16 - Liquid Layer Thickness as a Function of Time

Unlike the steady state conduction problem, the governing equation for the transient conduction problem contains terms on the left hand side (i.e. LHS = 0 for steady state, but LHS = $\rho c_p \frac{\partial T}{\partial t}$ for transient). Thus, for the latter case, specific heat, or a specific heat model is required. The specific heat model is the same as is used in the 2-D and 3-D models, and is given in Figure 4.17. See chapter 4, section 4.2.3 for a complete explanation including references.

As can be seen from Figure 3.16, it takes about 2 hours for the melt interface to reach equilibrium position. This simulation was performed for zero consumption of flux. The rate of melting, calculated as the secant modulus of Figure 3.16, of 0.5 mm/minute is in very good agreement with the experimental value (after Xie *et. al.* [16]), calculated with reference to Figure 2.1, of 0.4 mm/minute. However, the total time to reach steady state of 120 minutes is in apparent contrast to the 20 - 25 minutes predicted by Nakano *et. al.*[36]. This difference is attributable to the difference in consumption rates used. In the Nakano paper, a flux consumption rate corresponding to casting speed of 1.5 m/min and a specific consumption of 0.4 kg/(tonne of steel) was used, while in the analysis presented here, the consumption rate is zero. The zero consumption state, however, more closely approximates the conditions under which the experimental Xie [16] data was taken, and hence the good agreement between that data and the present analysis.

If, however, consumption is included in the transient 1-D model, the effect on the time to reach steady state is clear. Figure 3.17 compares the transient response for the two cases of consumption and no consumption. A consumption rate equal to the one given in the Nakano paper was used. The consumption was incorporated as an imposed y-velocity. This velocity was calculated as follows:

$$\text{Specific consumption} = 0.4 \text{ kg/(tonne of steel)}$$

$$= 0.0004 \text{ kg/(kg of steel)} = \frac{\rho_{flux} \times V_{flux}}{\rho_{steel} \times V_{steel}}$$

$$\Rightarrow \quad V_{flux} = \frac{0.0004 \times \rho_{steel} \times V_{steel}}{\rho_{flux}} \tag{3.24}$$

where: V_{flux} = flux consumption velocity (m/min)

V_{steel} = V_c = casting speed = 1.5 m/min

ρ_{steel} = Steel Density = 7800 kg/m^3

ρ_{flux} = Flux Density = 2500 kg/m^3

Substituting these values into equation 3.24 -

$$V_{flux} = 0.001872 \text{ m/min}$$
$$= 0.0000312 \text{ m/s}$$

Note that for the Nakano paper, a casting speed of 1.5 m/min was used. Figure 3.17 illustrates the effect of imposing this consumption rate.

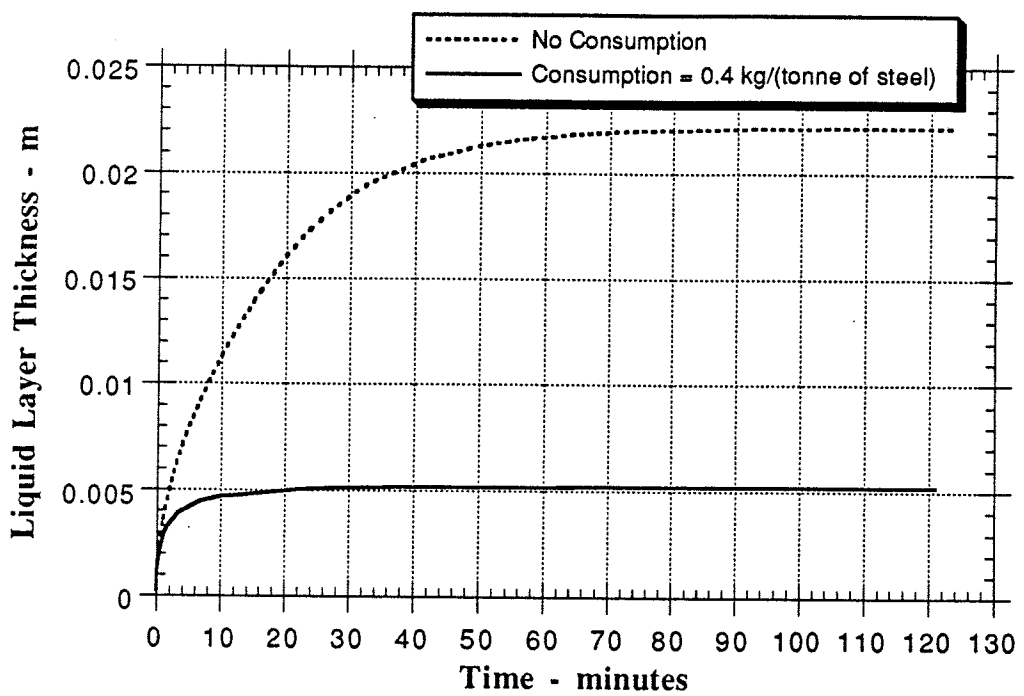

Figure 3.17 - Effect of Consumption on Time taken to Attain to Achieve Steady State

It can be seen that by incorporating the appropriate consumption, the time taken to achieve steady state is close to that predicted by Nakano of approximately 25 minutes. It should be noted however that there are differences between the material properties used in the model presented here and those of the Nakano model. The Nakano model utilizes the sintering model

to define material properties as discussed in section 2.2.1, while the model presented here uses constant values in the liquid and solid regions for thermal conductivity, and density.

Given the times calculated above, it seems reasonable that steady state can be achieved in practice. Nakano and co-workers validated this idea by taking measurements of liquid layer depth at an acutal caster. Their results show that the pool thickness exhibits a nearly constant value, which is determined by the casting parameters. However, the question arises as to what effect does the intermittent addition of powder have on the steady state achieved. Under some conditions, as predicted by Dehalle et. al. [10], intermittent addition of powder will have no effect on the liquid layer thickness, once the steady state is achieved. However, conditions can be envisaged where there may be small variations in the liquid layer thickness, even though, on average, the thickness is constant. Such a case is schematically represented in Figure 3.18.

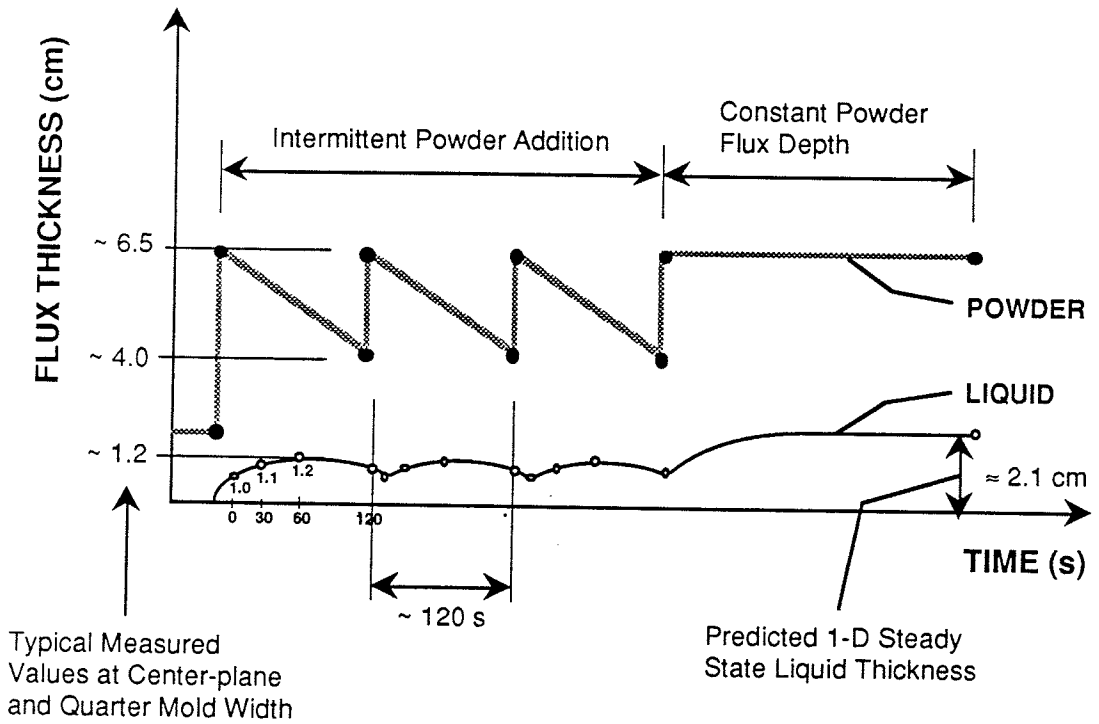

Figure 3.18 Schematic Showing Possible Effect of Intermittent Powder Additons on Liquid Layer thickness

In Figure 3.18, the flux thickness data points are typical values measured at LTV steel for a casting speed of 1.07 m/min, (refer to Figure 5.7, pg 100). The predicted 1-D

steady state liquid flux thickness (= 2.1 cm) was estimated from Figure 3.8, based on properties and casting parameters approximately the same as those for which the measured values were obtained. The schematic shows that under some conditions of intermittent powder addition, the liquid flux thickness can vary about some mean value, which is different from the steady state value predicted under conditions of constant powder level (or constant total flux thickness).

This mean value, for intermittent powder addition, is necessarily less than that for constant powder level, because of the time necessary for steady state to be achieved under the latter conditions. That is, if the powder level is assumed constant, the time taken to reach steady constant flux layer thickness is approximately 25 minutes as mentioned previously. However, in common practice, the time between powder additions is on the order of 3 minutes as shown in the figure. Therefore, there is not enough time for the full steady state liquid thickness (say for 5.0 cm of powder) of 2.1 cm to be developed. However, the time is sufficiently short so that the fluctuation in liquid depth is not significant.

Thus, even under these conditions of intermittent powder addition, a steady state assumption is still valid. Care must be taken in interpreting the results of model, however, in light of the fact that, under some conditions, the measured liquid layer thickness can be expected to be generically smaller than those predicted by the model.

CHAPTER 4

TWO-DIMENSIONAL MODEL

Two dimensional, steady state, coupled heat transfer and fluid flow models for the lubricating flux were constructed using the commercial finite element coded FIDAP™. While the physical problem is three dimensional in reality, several simplifying assumptions were used which attempt to make the two dimensional models physically reasonable. This chapter describes the development of these models in detail in addition to presenting some typical results obtained using the models.

4.1 MODEL DEVELOPMENT

Only symmetric halves of the mold were modeled to reduce the computing requirement. Figure 4.1 shows the planes A and B which contain the two-dimensional domains. The wide face model considers the two-dimensional fluid flow and heat transfer in the flux parallel to the mold wide face. Similarly, the narrow face model domain is contained in plane B. It is believed that the significant aspects of fluid flow and heat transfer in the lubricating flux may be revealed in these planes. The accuracy of the models, however, may depend on how out-of-plane phenomena are incorporated into each model, and on their relative importance. Refer to Appendix B for assumptions of the model and relevant background calculations.

4.1.1 Physical Description

To specify the overall geometry of the domain, a verification problem, for which measured data is available, is considered. The location of the steel surface and flux layer thickness data was taken from the thesis by Ho [15] which is based on measurements taken at LTV Steel Company. A schematic of the model domain for the wide face model is given in Figure 4.2

The model domain in Figure 4.2 shows one half of the sectional view contained in plane A in Figure 4.1. The shape of the flux-steel interface is assumed to be determined solely by the

flow pattern developed in the steel pool. Thus this boundary may be defined based on physical measurements for the particular conditions of casting, and not on any consideration of the flux. Similarly the boundaries with the mold wall and submerged entry nozzle may be geometrically defined independently of the flux.

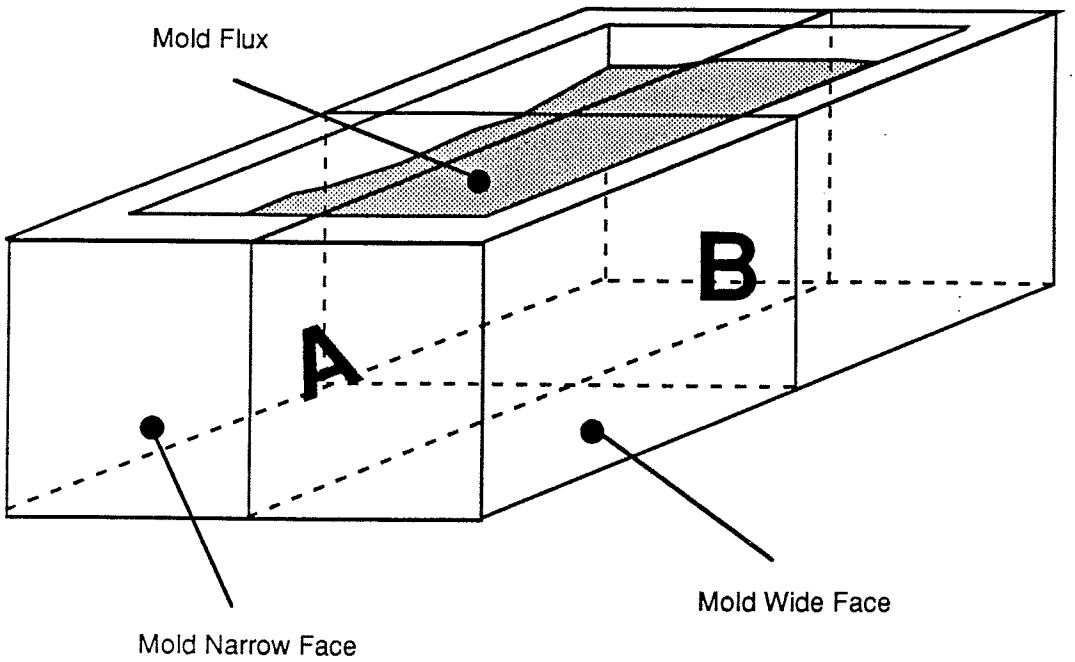

Figure 4.1 - Schematic Illustrating Modeling Domain Identification

The upper surface of the domain is the free surface of the flux, and thus cannot be defined independently of the flux behavior. Nevertheless, this surface is the only one which is unknown, which considerably simplifies the problem. Velocities and temperatures at the boundaries are dependent on the conditions in the steel and the mold. These boundary conditions will be discussed later. Refer to Appendix B for the consistent unit set used.

4.1.2 Geometry Definition

The dimensions of the model are based on measurements taken in the continuous casting mold at the steel plant. Specifically, overall width of the domain is approximately equal to half of the mold width, while the position and shape of the flux-steel interface are determined using a

"nail-board" test described in chapter 6. Figure 4.3 gives the dimensions of the standard wide face model.

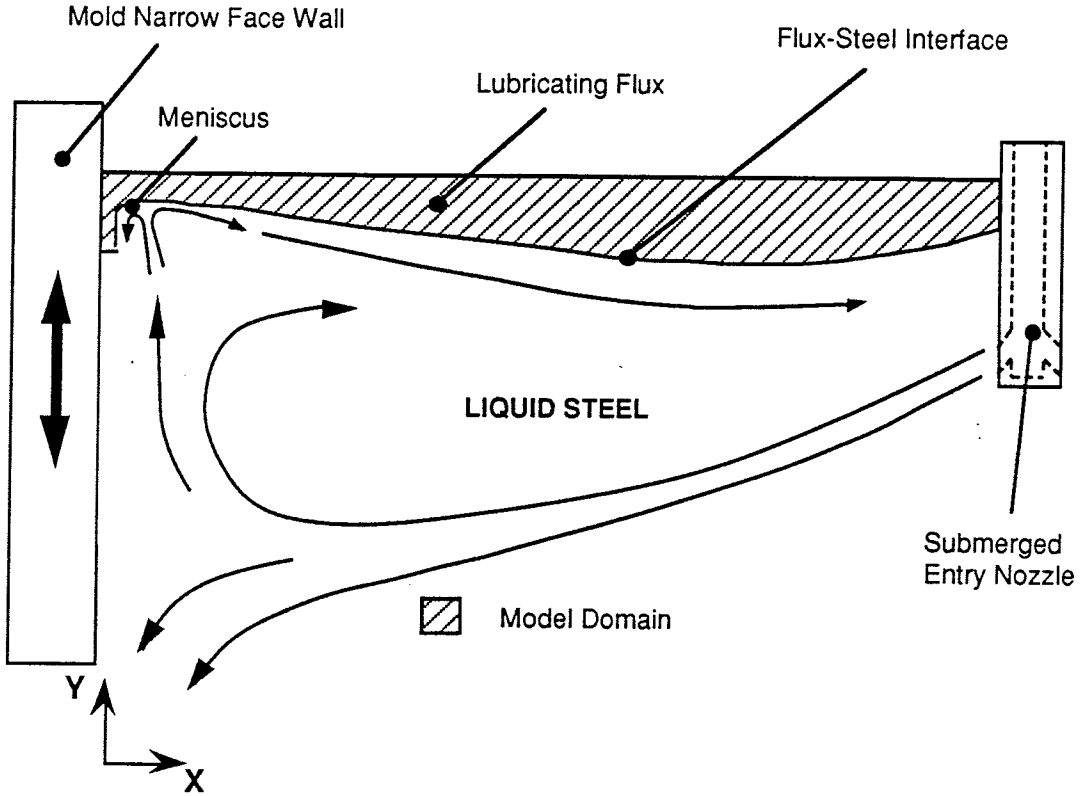

Figure 4.2 - Model Domain in Wide Face Direction

The domain does not extend to the full mold length (the left of Figure 4.3) because the behavior of the flux in the lower portion of the mold-strand gap is complicated and is not the focus of this study. Furthermore, it is an easier task to solve for the behavior of the flux in the gap and above the steel independently, coupling the regions only through the velocity and temperature outputs of each model. The cut-off point of the model is arbitrarily chosen to be 1 centimeter below the meniscus. The mold-strand gap width is chosen based on typical results of a two dimensional, step-wise, coupled elasto-viscoplastic thermo-mechanical model of the strand and mold [40], in addition to information gathered from available literature [9, 35, 41].

The shape of the meniscus is determined from an analytical solution of a modified version of the Young-Laplace Equation [7, 42] and is given below (equation 4.1).

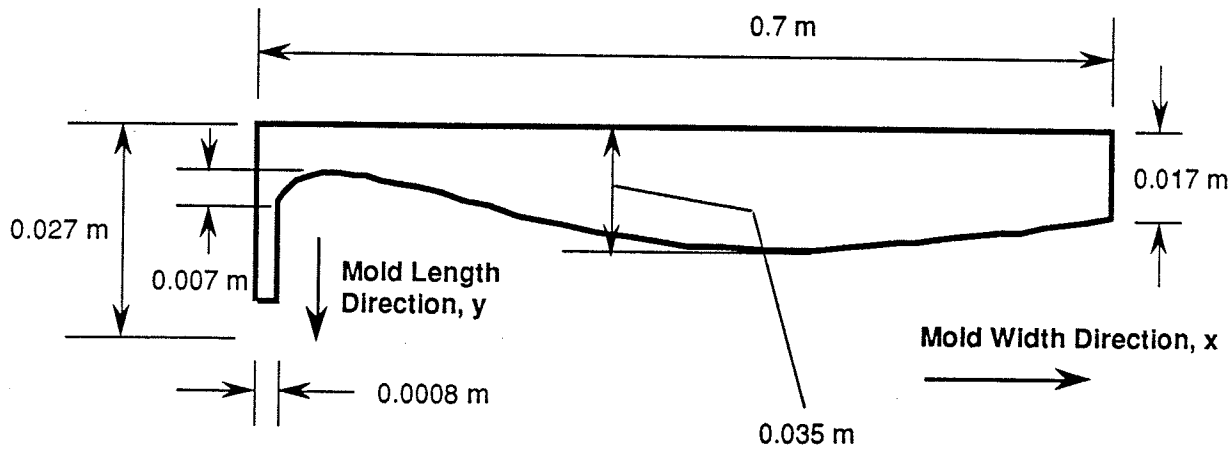

Figure 4.3 - Wide Face Model Dimensions

$$x = \frac{a}{\sqrt{2}} \ln \left[\frac{(-y)}{\sqrt{2}a - \sqrt{2a^2 - y^2}} \right] - \sqrt{2a^2 - y^2} + a \left[1 + \frac{\ln(\sqrt{2} - 1)}{\sqrt{2}} \right] \tag{4.1}$$

where:

a	= capillarity constant = $\sqrt{\frac{2\gamma}{\rho g}}$ m	
γ	= Surface tension ≈ 1.6 N/m for steel	
g	= Acceleration due to gravity = 9.8 m/s^2	
ρ	= Density of Steel = 2500 kg/m^3	

The variables x and y are illustrated in Figure 4.4.

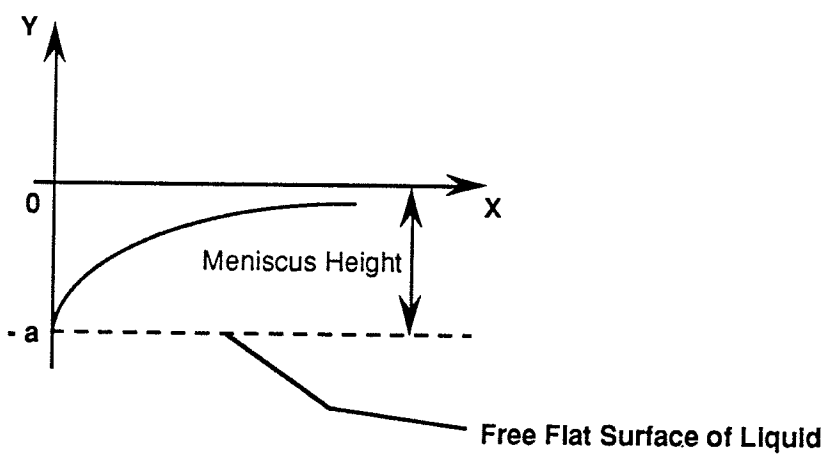

Figure 4.4 - Meniscus Shape Schematic

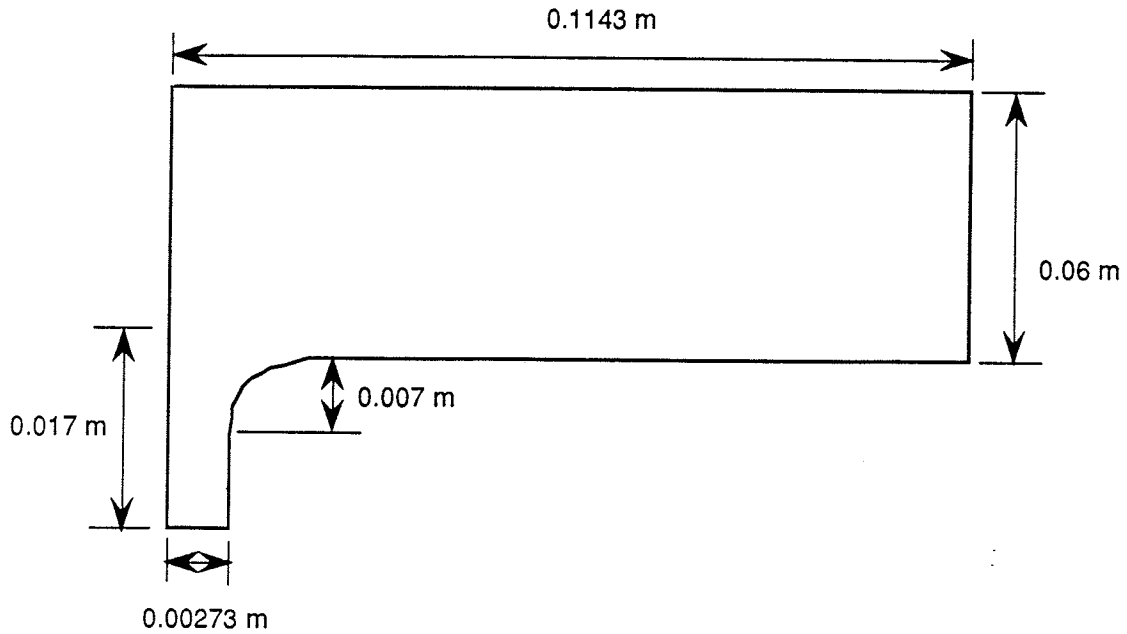

Figure 4.5 - Narrow Face Model Dimensions

4.1.3 Boundary Conditions

4.1.3.1 Mold Wall

4.1.3.1.1 Velocity and Stress Boundary Conditions

The boundary AF (refer to Figure 4.6) is formed with the mold wall. Because the flow of the flux is laminar, the necessary boundary condition at a solid interface is zero for both x and y velocities as given in Figure 4.6.

4.1.3.1.2 Temperature and Heat Flux Boundary Conditions

The temperatures down the mold wall calculated by a one-dimensional step-wise transient heat transfer model of the mold-gap-strand region [15], are imposed on boundary AF (see Figure 4.7).

4.1.3.2 Axis of Symmetry

4.1.3.2.1 Velocity and Stress Boundary Conditions

Velocity boundary conditions for axes of symmetry are zero normal velocity ($u_x = 0$) and zero tangential stress (σ_t). The normal stress and tangential velocity (u_y) is to be calculated by the program.

4.1.3.1.2 Temperature and Heat Flux Boundary Conditions

Zero heat flux is specified for axes of symmetry.

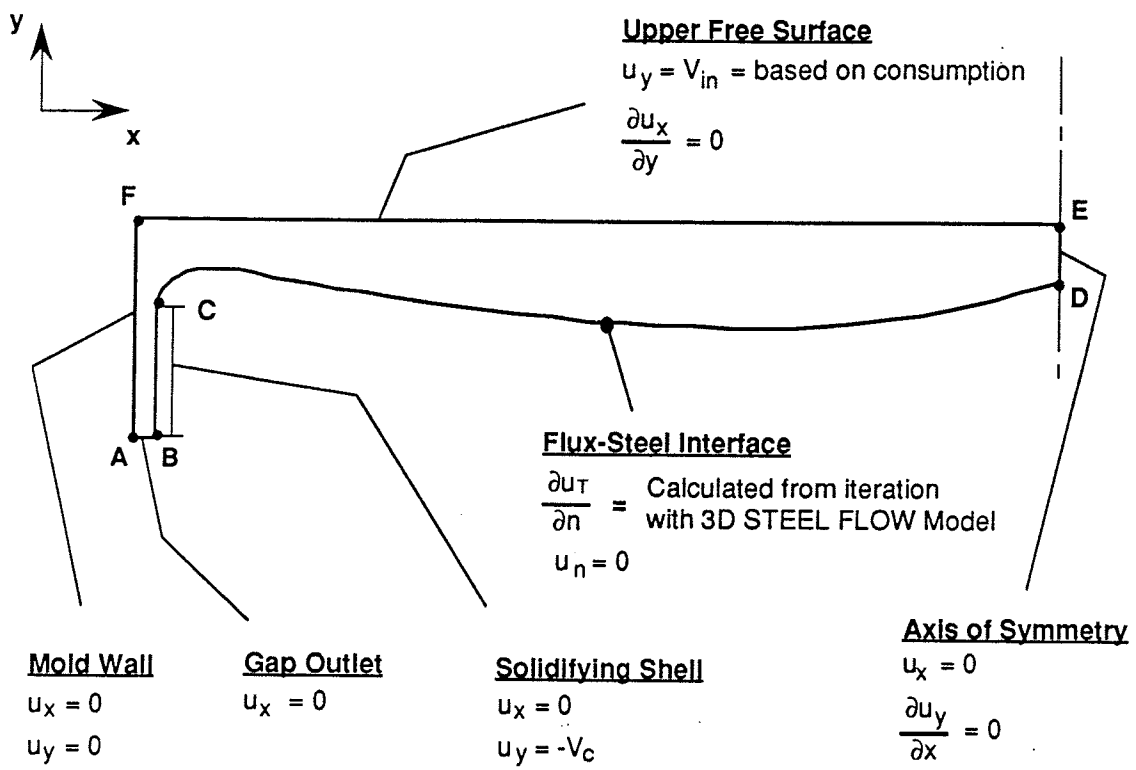

Figure 4.6 - Velocity and Velocity Gradient Boundary Conditions

4.1.3.3 Solidifying Steel Shell

4.1.3.3.1 Velocity and Stress Boundary Conditions

Along boundary BC the flux is in contact with the solidifying steel shell as shown in Figure 4.8. Even in the event that there is some degree of retardation in the flux speed just

adjacent to the shell, the casting speed is still a good approximation for the boundary BC because the finite element package is capable of calculating this flow retardation due to viscous forces.

4.1.3.3.2 Temperature and Heat Flux Boundary Conditions

The average steel temperature of 1550°C is used. Superheated temperatures may be imposed instead, but these values would differ by only a few degrees from the base used, and they would have a negligible effect on the results of this model.

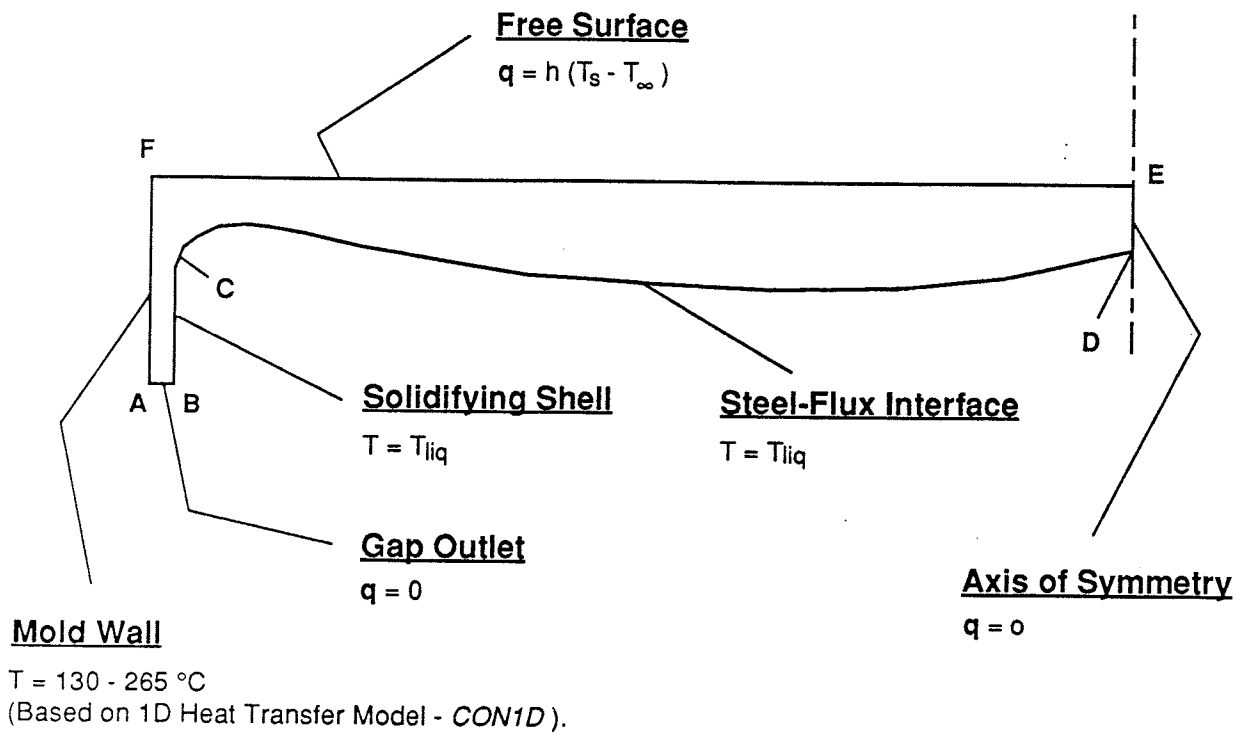

Figure 4.7 - Temperature Boundary Conditions

4.1.3.4 Mold-Strand Gap Outlet

4.1.3.4.1 Velocity and Stress Boundary Conditions

The flow of the flux must be in the y-direction at the outlet, so the x-component of velocity is specified to be zero. The normal stress is also specified to be zero. The model domain is truncated at the outlet location, thereby excluding the majority of the mold-strand gap. Thus just above and just below the boundary A-B the vertical velocity must be the same, just as if the rest of the mold-strand gap was present. Hence the zero stress boundary condition at A-B.

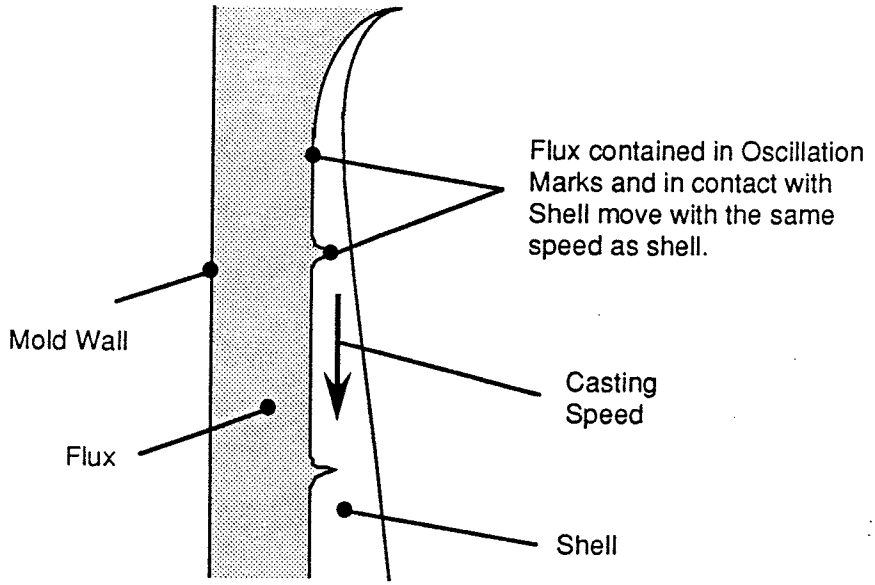

Figure 4.8 - Schematic Showing Velocity Boundary Condition at Shell

4.1.3.4.2 Temperature and Heat Flux Boundary Conditions

The gap continues for some distance down the mold below the cut-off point chosen for this domain. Hence, the temperature on either side of this boundary must be the same (similar to an axis of symmetry). Thus, zero heat flux boundary condition is specified.

4.1.3.5 Upper Free Surface

4.1.3.5.1 Velocity and Stress Boundary Conditions

The upper free surface velocity boundary condition is calculated to simulate an overall steady-state process, in which flux is consumed into the mold-strand gap at the same rate at which it is added, in powdered form, at the top surface. That is, while boundary FE is the mass inlet, boundary AB is the outlet. Implicit in this formulation is the assumption that all the flux added at the top surface is consumed through the *narrowface* gap. While this arrangement is necessary for the 2-D simulation, it is not physically accurate. In actuality, the majority of the flux is consumed through the wideface gap.

This inlet velocity is calculated as follows (refer to Figure 4.9)

Measured specific consumption at LTV Steel for casting speed (V_c) of 1m/min

$$= m_{sc} \left[\frac{kg}{m^2}\right]$$

Total consumption for mold shown in Figure 4.7, $\dot{m}_c$ $= m_{sc} \times 2(t_m + w_m) \times V_c \left[\frac{kg}{s}\right]$

(4.2)

But consumption per meter of Mold Perimeter, $\dot{M}_c$ $= \frac{\dot{m}_c}{2(t_m + w_m)} \left[\frac{kg}{m.s}\right]$

$\therefore$ Consumption to 1 Wide Face $= \dot{M}_c \times w_m$

$$= m_{sc} V_c w_m \left[\frac{kg}{s}\right] \quad (4.3)$$

and Consumption to 1 Narrow Face $= \dot{M}_c \times t_m$

$$= m_{sc} V_c w_m \left[\frac{kg}{s}\right] \quad (4.4)$$

With $V_c = 1.0 \frac{m}{min}$, $m_{sc} = 0.6 \frac{kg}{m^2}$ and using $w_m = 1.4$ m and $t_m = 0.2286$ m

Wide Face consumption $= 0.014$ kg/s

and Narrow Face consumption $= 0.002286$ kg/s

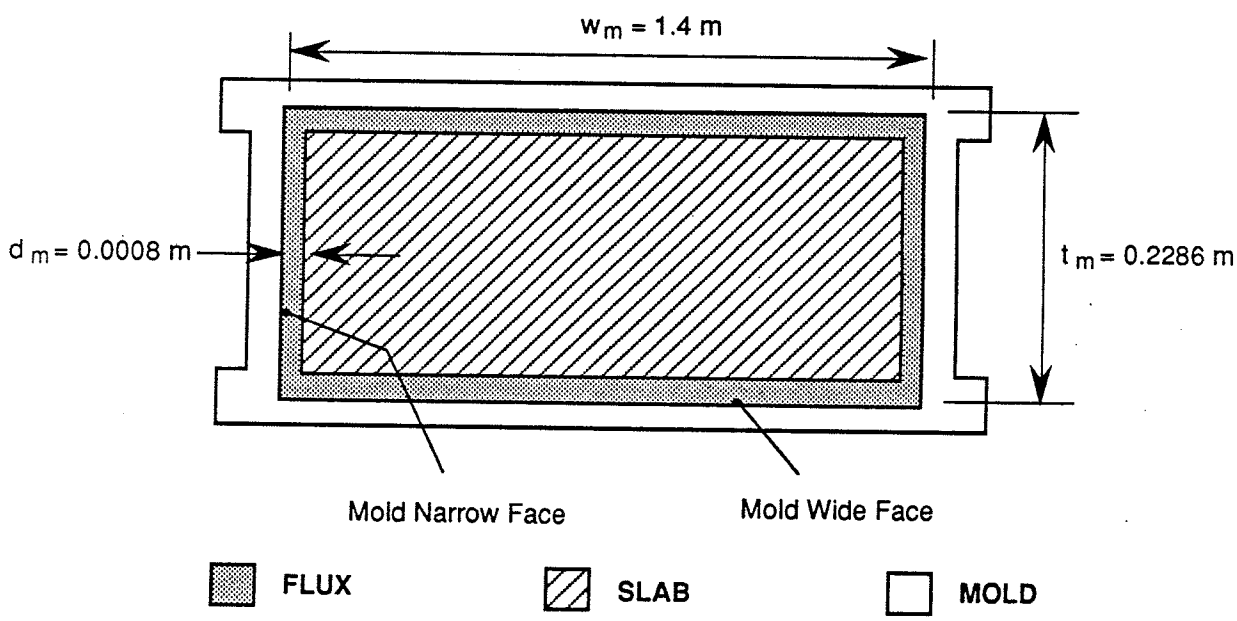

Figure 4.9 - Dimensions Used for Inlet Velocity Calculation (Top View)

Thus, the total mass flow in = (2x0.002286) + (2x0.014) = 0.0326 kg/s

Assuming constant density of 2500 kg/m^3, Volume flow in $= \frac{0.0326}{2500}$

$= 1.30288 \times 10^{-5}$ m^3/s

Ave. vertical velocity in at top surface therefore $= \frac{1.30288 \times 10^{-5}}{1.4 \times 0.2286}$

$= 4.070991 \times 10^{-5}$ m/s

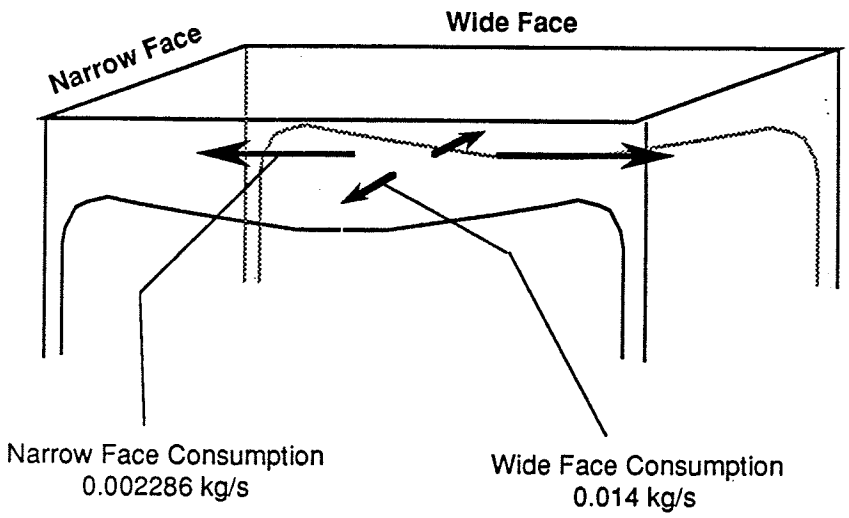

Figure 4.10 - Schematic Showing Distribution of Mass To Wide & Narrow Faces

This velocity, V_{in}, is applied uniformly along the top surface of the model in the y-direction (vertical) as given in Figure 4.6. The horizontal velocity component on the free surface is not specified. The free surface assumption of zero shear stress is imposed.

4.1.3.5.2 Temperature & Heat Flux Boundary Conditions

Along the free surface boundary EF, a heat transfer boundary condition is imposed by specifying a temperature-dependent heat transfer coefficient and an ambient temperature. The heat transfer coefficient is calculated as the sum of the radiative and convective components as shown below.

Average convective heat transfer coefficient based on an integration of the Local Nusselt number over the domain considered is given by [38]:

$$h_{conv} = \frac{5}{3}\left[\frac{0.5013k_{air}^{3/4}(c_p\mu)^{1/4}(g\beta\Delta T)^{1/5}}{\nu^{2/5}D^{2/5}}\right] \tag{4.5}$$

where:

c_p = Specific heat capacity of air, J kg^{-1} K^{-1}
μ = Dynamic Viscosity of air, Pa•s
g = acceleration due to gravity, ms^{-2}
β = Coefficient of thermal expansion of air, K^{-1}
ΔT = Temperature difference (T_o - T_∞), K
ν = Kinematic viscosity of air, m^2s^{-1}
D = Length of convecting surface, m

The radiative heat transfer coefficient is given as [39]:

$$h_{tot} = \left[\sigma\varepsilon(T_o + T_\infty)(T_o^2 + T_\infty^2)\right] \tag{4.6}$$

We may now express the total heat transfer coefficient at the surface of the powder, h_{tot} as follows:

$$h_{tot} = h_{rad} + h_{conv}$$

$$\Rightarrow \quad h_{tot} = \left[\sigma\varepsilon(T_o + T_\infty)(T_o^2 + T_\infty^2)\right] + \frac{5}{3}\left\{\frac{0.5013k_{air}^{3/4}(c_p\mu)^{1/4}\left[g\beta(T_o - T_\infty)\right]^{1/5}}{\nu^{2/5}D^{2/5}}\right\} \tag{4.7}$$

T_o is the surface temperature, which is unknown at any point in time. Therefore, to implement this coefficient in the model, a curve relating the value, h_{tot}, to temperature is given as an input to the finite element code. Linear interpolation between two points given in the transfer coefficient curve for any calculated temperature is used by the code. The ambient temperature is set at 30K.

4.1.3.6 Flux-Steel Interface Boundary Condition

4.1.3.6.1 Velocity and Stress Boundary Conditions

Particularly careful consideration must be given to the boundary condition applied to the flux-steel interface. For the wide face model being considered here, there is significant high

speed and turbulent motion in the steel at the interface for the plane shown. Results of a three-dimensional coupled heat transfer and fluid flow model of the steel slab are available [43] and may be used to determine the correct boundary condition for the flux.

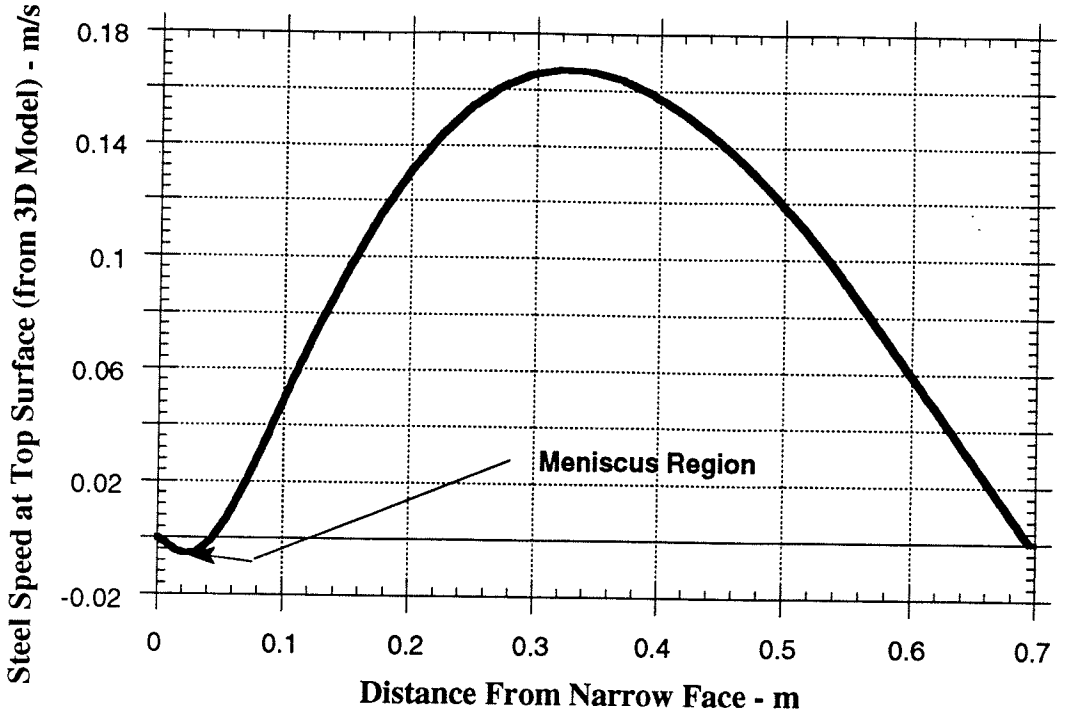

Figure 4.11 - Velocity Profile at Top Surface of Steel from 3D Slab Model[43]

There are basically three options for treatment of boundary conditions at the flux-steel interface. These are:

Option I: Ignore steel flow

Option II: Assume that the flux and steel act independently

Option III: Couple steel flow and flux flow

While Option I is approximately correct for the flux-steel interface parallel to the narrow face, it is inappropriate for the wide face model. Option II is the simplest choice for the

boundary condition to be applied at the flux-steel interface for the flux model, in which is the velocity calculated for the top surface of the steel by the three-dimensional slab model (see Figure 4.11) is imposed directly to the flux model. That is, the values of velocity obtained by the slab model at the interface, using the free surface assumption, may be applied directly to the flux model. However mold flux has a viscosity which is, at minimum, 10 times that of steel at 1550 °C, which leads to a completely different situation from that when steel is exposed to air. Referring to Figure 4.12, it can be shown that when the steel is in contact with air, the velocity gradient in the steel just below the interface is much less than that on the air side of the interface.

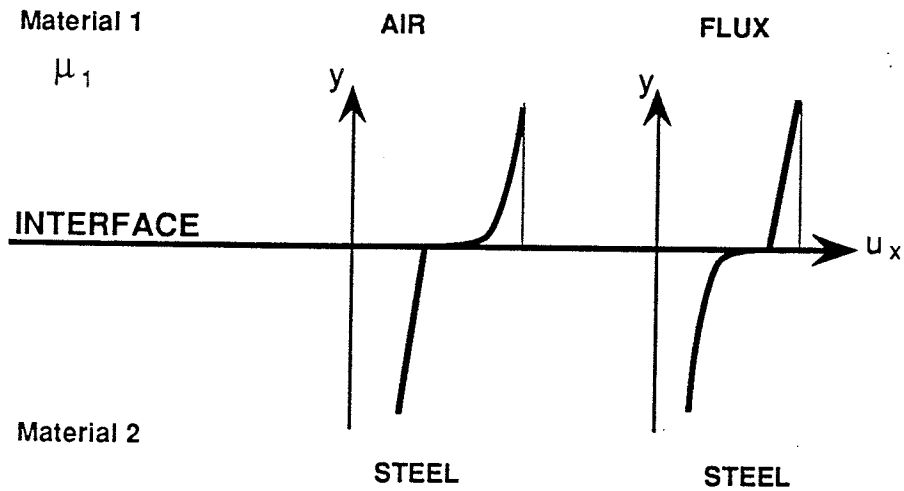

Figure 4.12 - Schematic Showing Variation of x-component Velocity across the Steel Interface

In general at an interface, the following must be satisfied:

$u_{x1} = u_{x2}$ and $\tau_1 = \tau_2$ (refer to Figure 4.11) which is first order continuity

$$\tau_1 = \tau_2 \quad \Rightarrow \quad \mu_1 \left(\frac{\partial u_x}{\partial y}\right)_1 = \mu_2 \left(\frac{\partial u_x}{\partial y}\right)_2$$

$$\Rightarrow \quad \frac{\left(\frac{\partial u_x}{\partial y}\right)_1}{\left(\frac{\partial u_x}{\partial y}\right)_2} = \frac{\mu_2}{\mu_1} \quad >> 1 \text{ for steel-air interaction}$$

=> Velocity gradient in steel (2) << Velocity gradient in air (1)

For example, at the meniscus region where the slab model calculates relatively low velocities in the negative x-direction (see Figure 4.11), the flux model gives large values of velocity at the interface at the same region. This occurs because the velocity of the fluid flowing in the layer between the interface and the boundary where the slab-model velocities are applied is calculated to balance the significant amount of mass flowing in the positive x-direction. Thus, the interfacial values calculated were not related to the imposed velocity at the edge of the shear layer as they should be. Additionally, a significant question arose as to the appropriate thickness of the shear layer. Clearly the value of the interfacial velocity is directly related to this thickness. However, there appeared to be no clear-cut method for determining the dimension of the steel layer. Finally, the flow of the steel is turbulent while the flux flow is laminar, posing numerical modeling difficulties. This method to determine the interfacial velocity was abandoned.

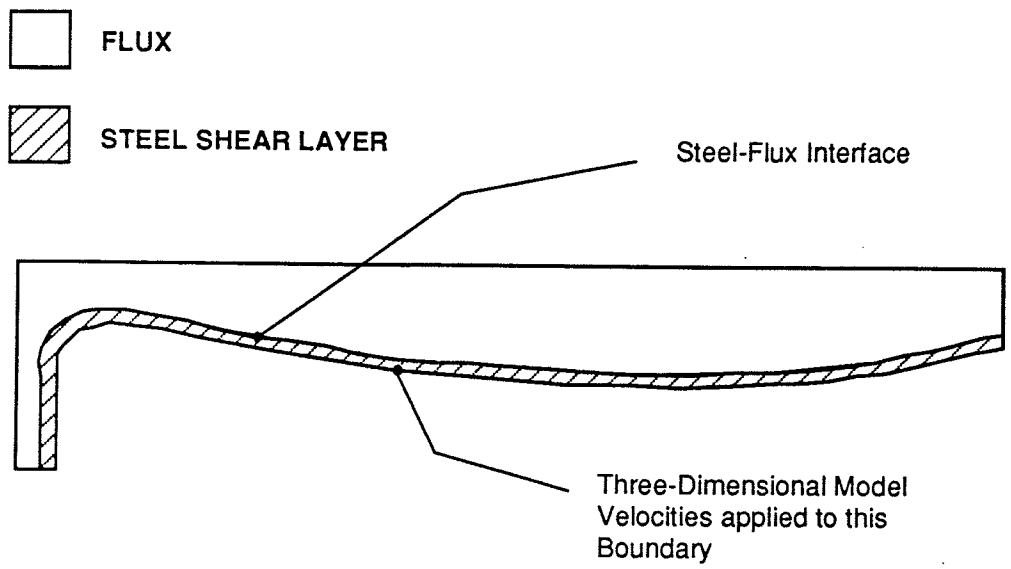

Figure 4.13 - Illustration of Steel Shear Layer Addition

Method 2:

At the interface, there is no slip between the liquids. Additionally, shear stress must be continuous across the interface. These conditions may be considered analogous to the temperature and heat flux boundary conditions at the junction between two solids of different thermal conductivities. With this in mind, an alternative approach to determine the correct

boundary condition at the interface was attempted. In this method an iterative procedure was utilized and it may be described as follows:

In principle we have the following at the interface between liquid steel (subscript, s) and the liquid flux (subscript, f):

$$u_s = u_f$$
$$\tau_s = \tau_f$$

As initial solution for the 3-D steel flow model,

$$u_s = u_s^1$$
$$\text{and} \quad \tau_s = 0$$

But for the flux, we have

$$u_f = u_f^1 = u_s^1 \text{ (imposed)}$$
$$\text{but} \quad \tau_f \neq 0$$

It is clear that these initial conditions do not satisfy the requirements at the interface, where the fluid flow equations must be satisfied simultaneously for the flux and the steel.

To converge on the correct solution therefore, the following strategy was used:

1. Impose $u_f^i = u_s^i$ in the isothermal flux model
2. Calculate τ_f^i from the isothermal flux model
3. Impose $\tau_f^i = \tau_s^{i+1}$ as a boundary condition in steel model
4. Recalculate $u_s = u_s^{i+1}$
4. Compare u_s^i and u_s^{i+1}
6. If $\dfrac{u_s^i - u_s^{i+1}}{u_s^i} > \text{Tol}$, repeat from step 1 with $u_f^{i+1} = u_s^{i+1}$
7. If $\dfrac{u_s^i - u_s^{i+1}}{u_s^i} < \text{Tol}$, convergence achieved, and $u_s \approx u_f$ = correct interface velocity.

While this methodology looked promising, there were several shortcomings and problems with its implementation. While it was possible to impose the shear stress as calculated by the flux model as a boundary condition in the steel flow (3D) model, the interfacial velocity then calculated by the steel model was based on a linear assumption relating the velocity at the node just below the interface and that at the interface. Ordinarily such an assumption is plausible, if the two liquids are similar. But because the flux viscosity is so high, modifications at the top surface of the steel model to account for this had to be made. This adjustment is also necessary because the flow in the steel is turbulent while the flux flow is laminar. This implies that in the region close to the interface in the steel, a transition occurs, and this must be taken into account.

Method 3:

To account for this retardation in the steel flow close to the interface, a Near-Wall Turbulence Model was examined. While the near-wall model assumes that the velocity at the interface (i.e. the wall) is zero, a frame-of-reference transformation will allow a movable boundary thereby allowing the interfacial velocity to be calculated with the model. The significant output of the model is the shear stress at the wall, and this can be utilized directly as a boundary condition in the flux model. A brief description of the Near-Wall Turbulence Model is given below [44-46].

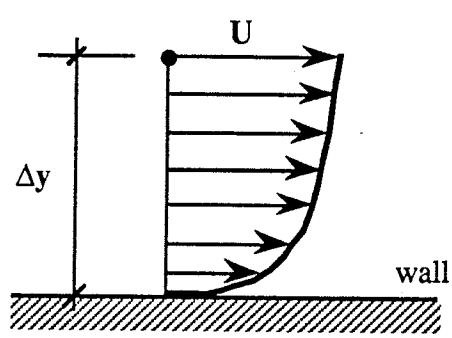

Figure 4.14 - Near-Wall Turbulent Velocity Profile

$$\tau_{wo} = \mu_o \left(\frac{\partial \bar{u}}{\partial y}\right)_w$$

$$= \mu_o \left(\frac{U}{\Delta y}\right)\left(\frac{y^+}{U^+}\right) \tag{4.8}$$

assuming that flow near to the wall approximates Couette flow

$$U^+ = \frac{1}{\kappa} \ln\left(Ey^+\right) \tag{4.9}$$

$$y^+ = (C_\mu)^{1/4} \left(\frac{\rho\, \Delta y}{\mu_o}\right) K^{1/2} \tag{4.10}$$

$$\tau_{wo} = \rho \left(\frac{U}{U^+}\right)^2 \tag{4.11}$$

where:

	τ_{wo}	= Shear Stress at Wall
	U^+	= Non-dimensionalized velocity
	y^+	= Non-dimensionalized distance
	K	= Turbulent kinetic energy
	C_μ, κ, E	= Wall-law constants

Using equations 4.8 - 4.11, the shear stress at the wall, or in this case, at the liquid-liquid interface is calculated using the three-dimensional slab model. With the resulting values of shear stress imposed as the boundary condition at the flux/steel interface in the flux model, instead of velocities, an iterative procedure similar to Method 2 was implemented. The converged solution of shear stress so obtained for the isothermal flux model will be used as the boundary condition for the coupled heat transfer model. It is assumed that the values obtained in the isothermal flux model, in which the constant viscosity of 0.05 Pa/s was used, is suitable for use in the coupled models. This may be assumed because the actual flux viscosity at the interface is the value at a temperature close to 1550°C (the steel liquidus temperature), which is approximately 0.035 Pa/s for the flux being studied.

The velocity normal to the flux-steel interface is set to zero to prevent penetration of liquid flux into the steel domain.

4.1.3.6.2 Temperature and Heat Flux Boundary Conditions

The temperature at the flux-steel interface is set constant at 1550 °C.

4.1.3.3 Mass Conservation

The appropriate mass flux for the problem is imposed by the inlet velocity boundary condition along line EF in Figure 4.6, and was discussed previously. The mass outlet is through the mold-strand gap. The finite element package calculates the velocity profile at outlet to balance the flow of mass out of the domain, with that flowing into the domain. This is a critical part of the analysis, because mass balance problems are frequently the cause of convergence difficulty.

4.1.3.6 Sources

There are no heat or mass sources used in this model

All the boundary conditions described are exactly the same for the narrowface model, except that the shear stress boundary condition for the steel-flux interface in this case is zero.

4.2 STANDARD INPUT MATERIAL PROPERTIES

4.2.1 Viscosity

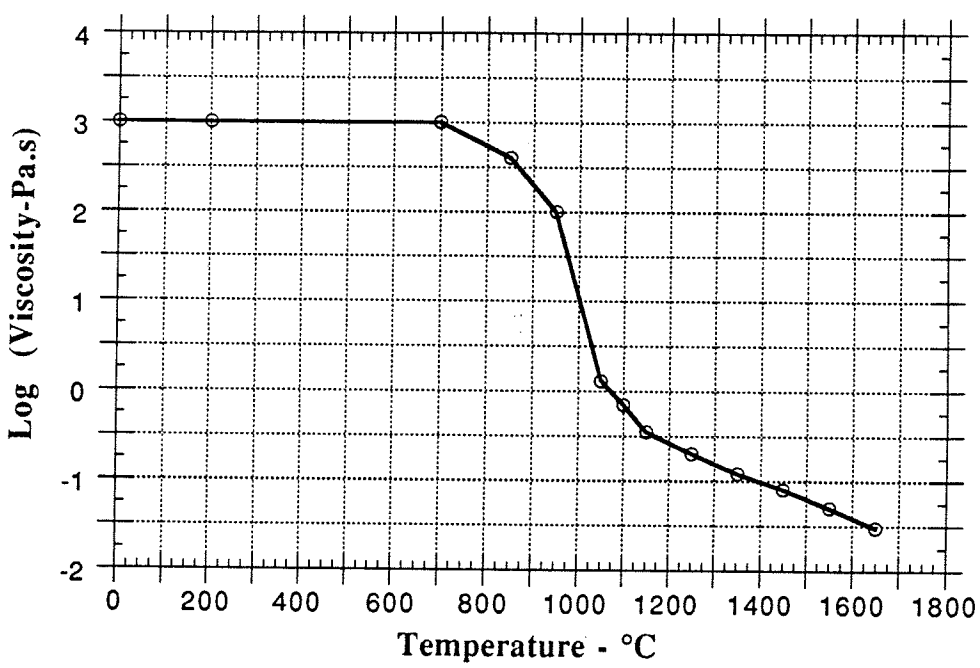

Figure 4.15 - Standard Viscosity - Temperature Input Curve

The viscosity below 900°C is held constant to assist the finite element code in converging on the correct solution. In actuality, the viscosity continues to increase below 900°C as the liquid flux solidifies. However, if that true curve is used, it introduces a large degree of numerical instability, because of the steep gradient in viscosity. The effect of this simplification is expected to be small because the truncation viscosity is large enough to simulate solid material, being 1000 times the value of the average liquid viscosity. The melting point of this flux is approximately 1000°C, while softening begins at about 950°C. Thus solidification is modeled in part by the sudden increase in viscosity around the melting point, and a large, constant value below the melting point.

4.2.2 Thermal Conductivity

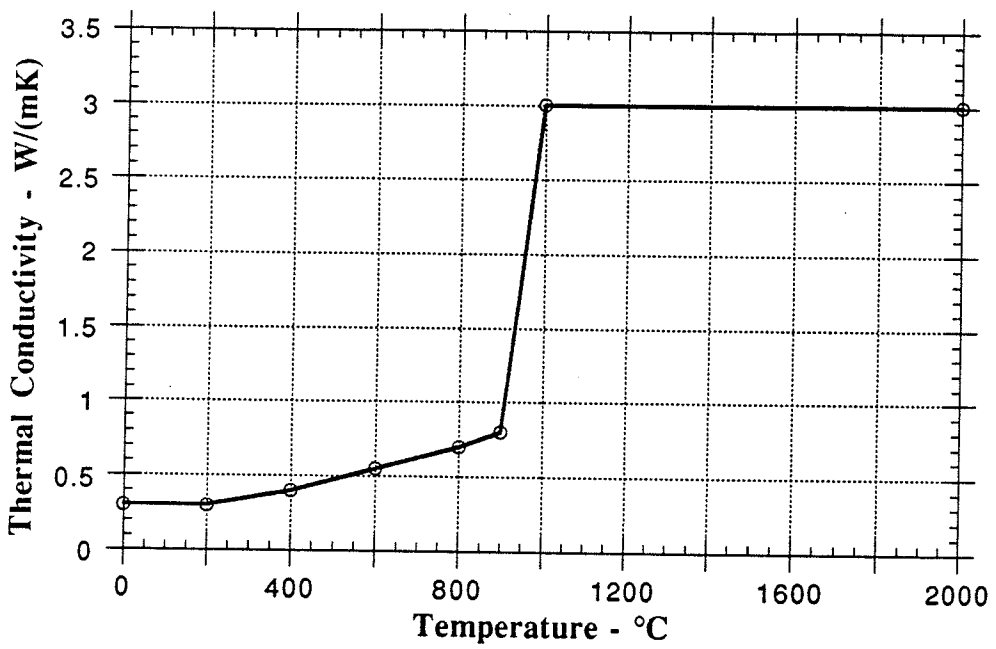

Figure 4.16 - Standard Thermal Conductivity - Temperature Input Curve

While the variation of thermal conductivity with temperature below the melting point is well characterized, the high temperature behavior is not. As discussed in section 2.1.3.2, suitable models for thermal conductivity variation above the melting point are not available, and there is

conflicting opinion in the available literature. It is apparent that the only practical way of handling thermal conductivity at elevated temperature is to enhance the base value to account for additional heat transport due to radiation in the liquid flux. Physically also, this approach seems to work, as reported by several authors (see section 2.1.3.2).

The reader is directed to additional publications [26, 33, 47] to contrast the conductivity-temperature curves given therein with those presented here as model inputs. In addition to the discussion presented immediately above, the reader is also directed to section 2.1.3.2 for other explanations for the difference between the curves given here and those shown in Nagata publications, as well as for reasons those curves were not used. More specifically however, the low temperature portion of the thermal conductivity-temperature curve is obtained from work by Taylor and Mills[2] for powders used in slab casting. The value of 3.0 W/(m.K) for effective thermal conductivity is an average value for thermal conductivity above the melting point of the flux, as reported by Mikrovas *et. al.* [27] and Susa *et. al.*[48].

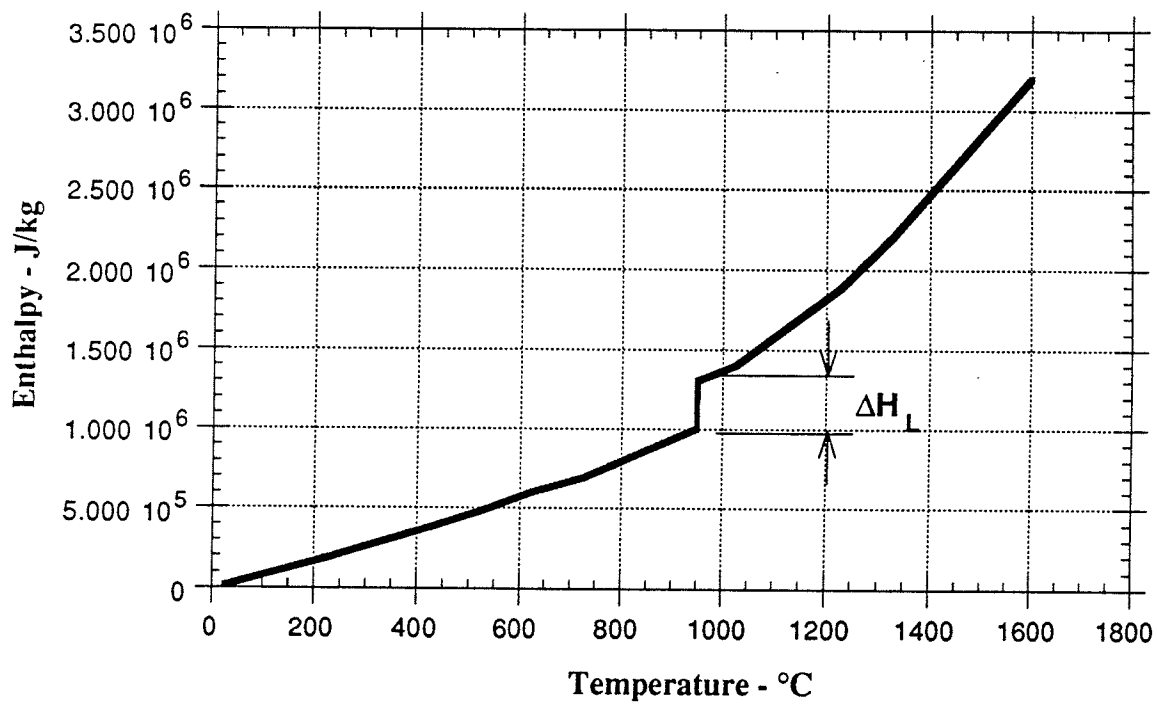

Figure 4.17 - Enthalpy-Temperature Input Curve

4.2.3 Specific Heat

The enthalpy-temperature input curve is shown in Figure 4.17[26, 49]. The finite element code is capable of computing the specific heat at any temperature using enthalpy - temperature data as given in Figure 4.17. The melting point shown in the figure is 950°C. At that temperature there is a sudden "jump" in the enthalpy-temperature curve corresponding to the enthalpy of fusion (or latent heat of fusion). The value used for the enthalpy of fusion is 350 kJ/kg [13]. Thus in addition to the viscosity variation at 950°C, solidification is modeled by incorporating this discontinuity in the enthalpy-temperature curve.

4.3 SOLUTION METHODOLOGY

4.3.1 Method

A three-step process, summarized in Figure 4.18, is used to ensure convergence of the model in the fastest time possible. The main idea behind this method is to provide the program with the best possible initial guess of the velocity and temperature fields which is then used to begin the iterative solution process. If no initial guess is explicitly provided, the code utilizes one of stationary fluid at 0 °C. This is typically a bad guess, which may easily result in either divergence of the solution or a greater than optimal solution time.

The analysis to be performed is a weakly coupled one in which the fluid flow and temperature fields are interdependent. In this type of analysis, buoyancy forces are ignored, but temperature dependent properties, including viscosity are incorporated. As the first step in this process, an isothermal laminar (Re = 70) flow problem is solved with all of the flow boundary conditions of velocity and stress incorporated. Here, the energy equation is discarded and the Navier-Stokes and Continuity Equations only are solved for the variables of velocity and pressure. While the velocity field obtained in the isothermal analysis is not expected to resemble that of the final solution, it usually is a much better initial condition than that of the stationary fluid.

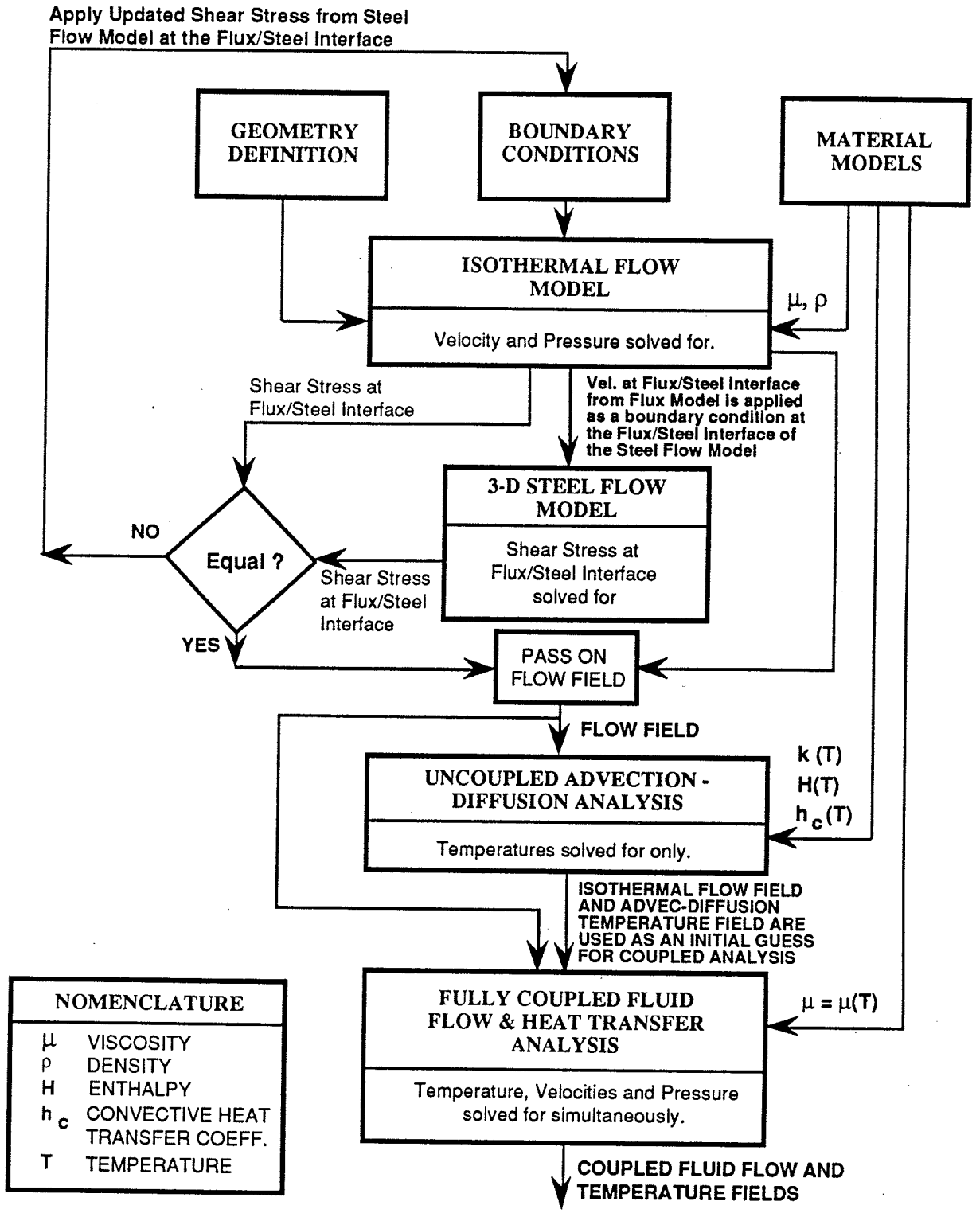

Figure 4.18 - Schematic of Solution Methodology

The isothermal velocity field is then used as input to an advection-diffusion problem in which the thermal boundary conditions of temperature and heat flux are imposed. In this analysis, the momentum equations are not solved. Instead only the energy equation is solved for the temperatures, assuming that the supplied velocity field is unvarying in time. Thus while the velocities have an effect on the temperature distribution, the converse is not true in this type of analysis.

Finally, the temperature-dependent viscosity is incorporated into the input file, and both the isothermal velocity field and the advection-diffusion temperature field are used as input to the weakly-coupled problem. The energy, Navier-Stokes and continuity equations are all re-solved using the improved initial conditions provided. The output of the coupled analysis is the model of the melting and flow behavior of the flux.

4.3.2 Solution Specifics

Table 4.1 below summarizes the specific solution parameters used in this simulation. The solution time is obtained on a Silicon Graphics Personal Iris 4D-25 (20MHz microprocessor and 64MB RAM). Total disk space usage was 180 MB during solution and 15 MB after solution for the coupled model.

Successive Substitution (Picard Iteration) is the commonly used solution method because of its wide radius of convergence. The Residual Convergence Tolerance value is the value of the residual at which the solution is considered to be converged. The smaller this value, the more accurate the solution at which the computer stops iterating. However, the smaller the number, the higher the computational cost, so a balance between accuracy and time is sought when choosing the convergence tolerance. It was possible within one solution run to attain the residual values of 1e-4 for the Isothermal and Advection-Diffusion problems. As can be seen from Table 4.1 however, the residual convergence value chosen for the coupled problem is significantly larger at 1e-1. This was done because solution times were so much larger in this case.

TABLE 4.1 - Summary of Solution Parameters

Problem Type	Relaxation Factor	Residual Convergence Tolerance	Disk Space (MB)	Total Number of Iterations	Total Solution Time (CPU s)
Isothermal	0.6	0.0001	57	40	28,800
Adv-Diff	0.6	0.0001	18	58	10,440
Coupled	0.8 (initial) 0.9 (final)	0.1	220	225	406,080

4.4 RESULTS

WIDE FACE MODEL

Prior to obtaining the fully coupled heat transfer and fluid flow solution, some results were obtained which assisted in establishing the correct boundary conditions. Figure 4.19 shows the results of the iteration process between the 2D isothermal flux flow model and the 3D steel flow model (see step 1, Figure 4.18). Iteration 4 profile is the one used as the stress boundary condition at the steel-flux interface.

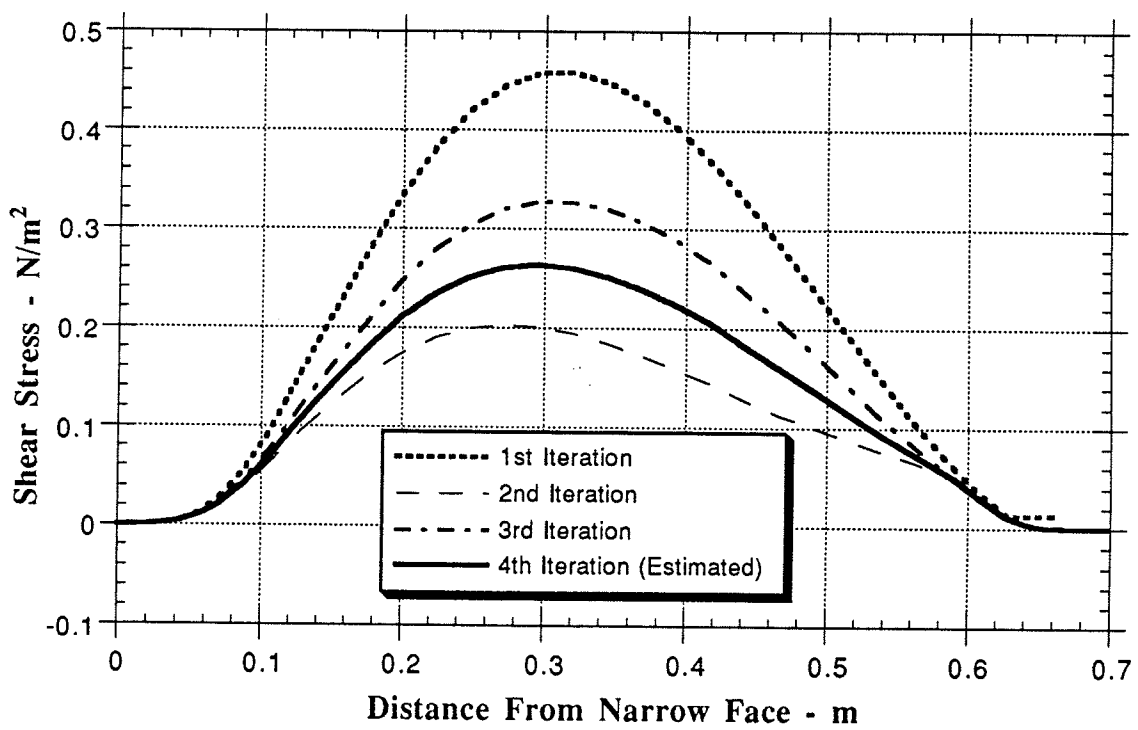

Figure 4.19 - Shear Stress Profile along Steel-Flux Interface as a Function of Iteration Number between Flux Model and 3-D Slab Model.

Figure 4.20 shows the variation of tangential velocity along the steel flux interface. These velocities are calculated based on a shear stress boundary condition as given in Figure 4.19 as the 4th Iteration. This resulting velocity profile is compared to the profile calculated by the 3D slab model at the steel-flux interface using the free surface (zero shear stress) assumption.

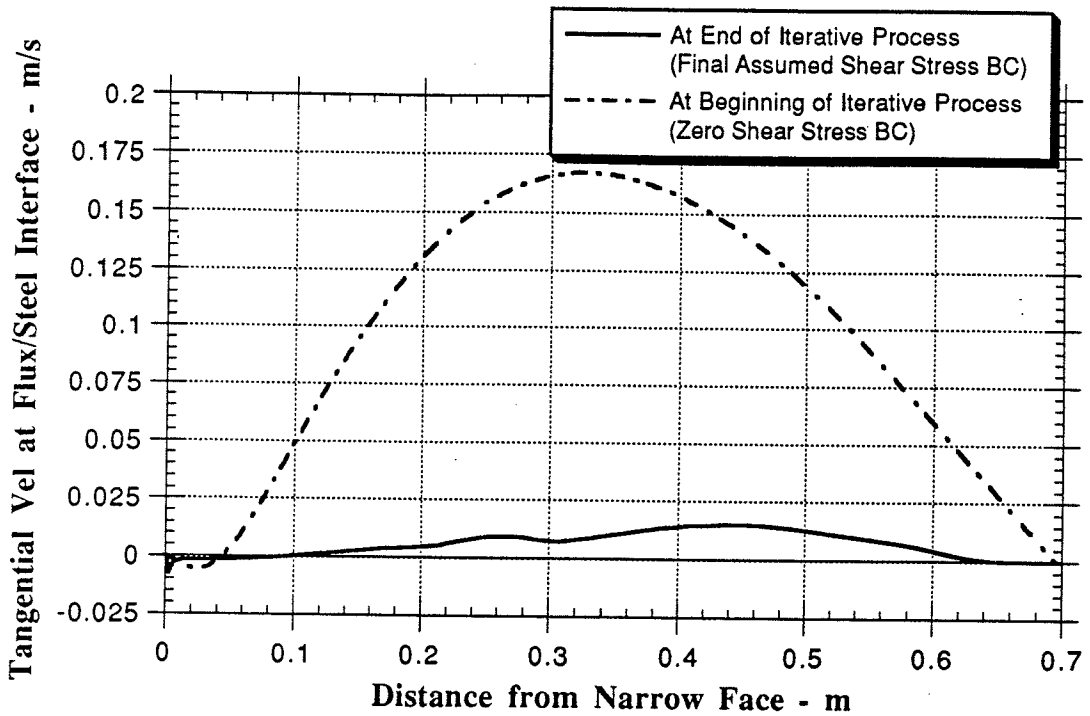

Figure 4.20 - Change in Tangential Velocity Profile at Flux-Steel Interface due to Iteration between Isthermal Flux Flow Model and 3D Steel Model

4.4.1 Flow Pattern

Figure 4.21 is the streamline contour plot for the standard case superimposed on the temperature distribution plot. This figure shows the significant features of the flow pattern developed in the flux. In the lower region of the domain, where the flux is predominantly liquid, two recirculation zones are formed. Flux has to leave the domain through the mold-strand gap, resulting in material flow towards the left side of Figure 4.21 in the upper region of the domain. However the steel flow at the flux-steel interface causes flux in the lower region of the domain to flow towards the submerged entry nozzle (SEN) to the right of Figure 4.21.

This counter-current flow which exists in the upper and lower regions of the domain results in the formation of recirculation zones. The mass of fluid which stagnates in these zones is calculated to be approximately 2 kg. Thus, once these stagnation zones have been developed, all the mass that enters at the top simply flows along above the zones towards the gap at the left of Figure 4.21.

Figure 4.21 also shows the magnitude and direction of the fluid velocity in the meniscus region of the domain. It can be seen, as expected, that the velocity of the flux increases as the temperature increases due to the decrease in flux viscosity with increasing temperature. Solid flux, such as that attached to the mold wall as the "flux rim" can be seen to be immobile.

Along the top surface of the flux, there is a small component of velocity in the negative x-direction. This implies that the flux moves away from the SEN towards the narrow face of the mold even at the very top of the powder layer. This result is consistent with the plant observations that more powder needs to be added at regions close to the SEN as compared to the mold narrow face region. Figure 4.22 shows the variation of the horizontal component of velocity with position.

An average value of the residence time in the mold for new flux, added at the top surface, may be calculated based on the consumption rate and the gap-outlet cross sectional area. This residence time is estimated to be about 83 seconds. The reader is directed to Appendix B for details of this calculation.

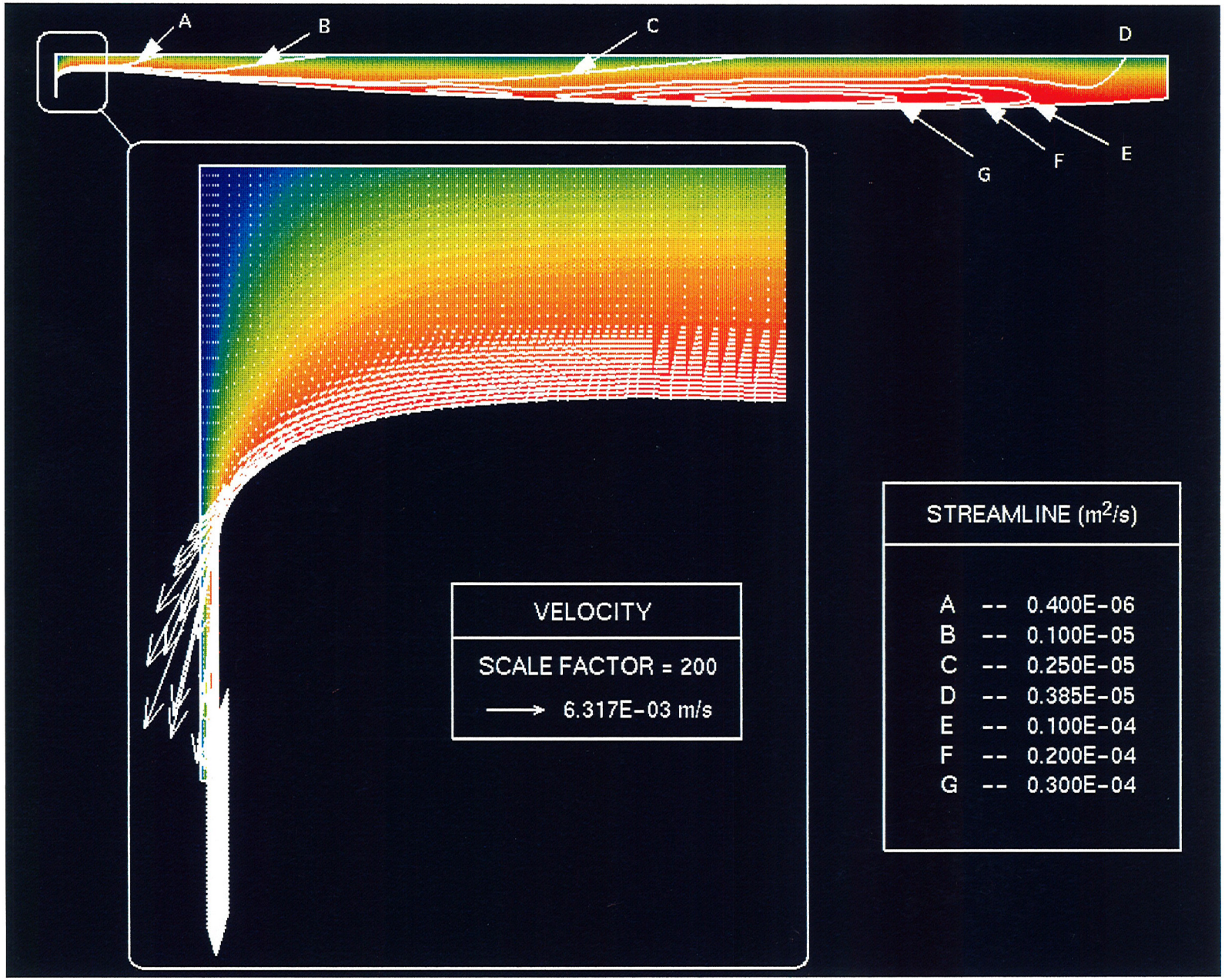

Figure 4.21: Wideface Model - Overall & Meniscus Tempreature Distribution and Flow Pattern

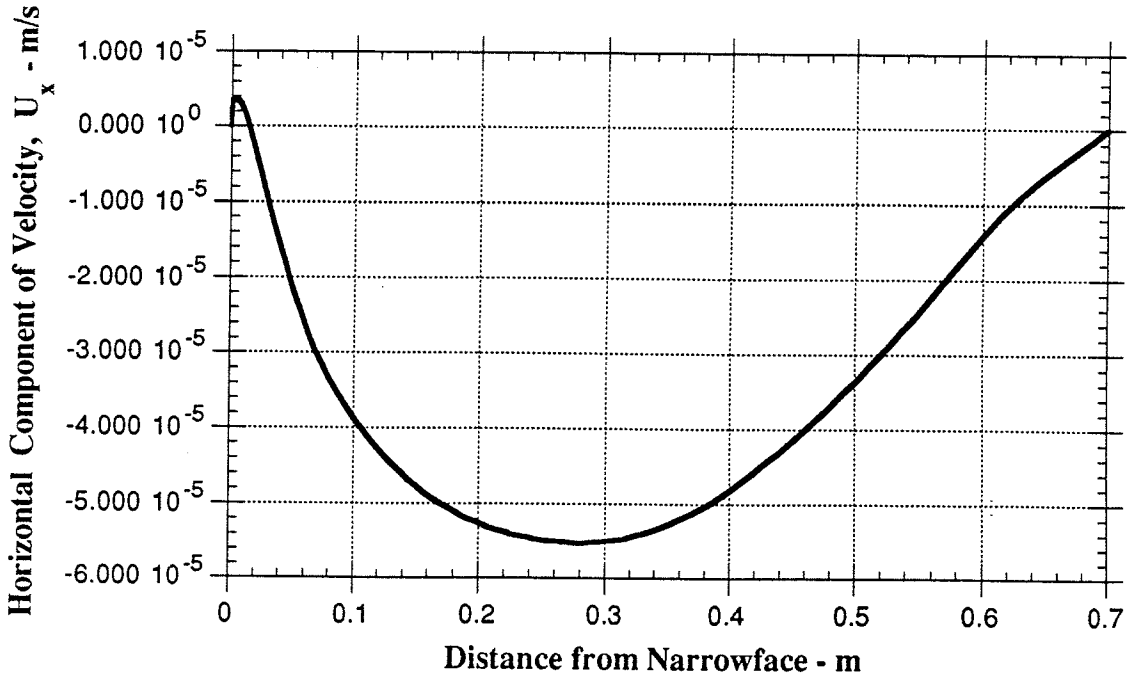

Figure 4.22 - Variation of Horizontal Component of Velocity with location at Top Surface of Powder

4.4.1 Gap Flow and Heat Transfer

In the first step of the solution, using the isothermal flow model, an interesting and significant result of the program's attempt to balance the mass flow in the domain, is an indication of whether the dimension of the gap is correct. The mass inlet is calculated based on overall flux consumption independently of the outlet dimension (see section 4.1.3.1). However, if the outlet dimension is too large, additional mass has to be taken into the domain, and this can only occur at the gap outlet where the velocities are unspecified. This intake of mass results in recirculation in the gap (as shown in Figure 4.23) which is clearly not realistic. Alternatively, as shown in Figure 4.24, the velocity profile produced for the smaller gap size is that theoretically expected for viscous fluid flow between one moving and one stationary plate. Hence, the gap size was adjusted until the flow in the gap is fully in the outlet direction only as shown in Figure 4.14 for d_g = 0.79 mm. This procedure is necessary to get convergence with the isothermal model.

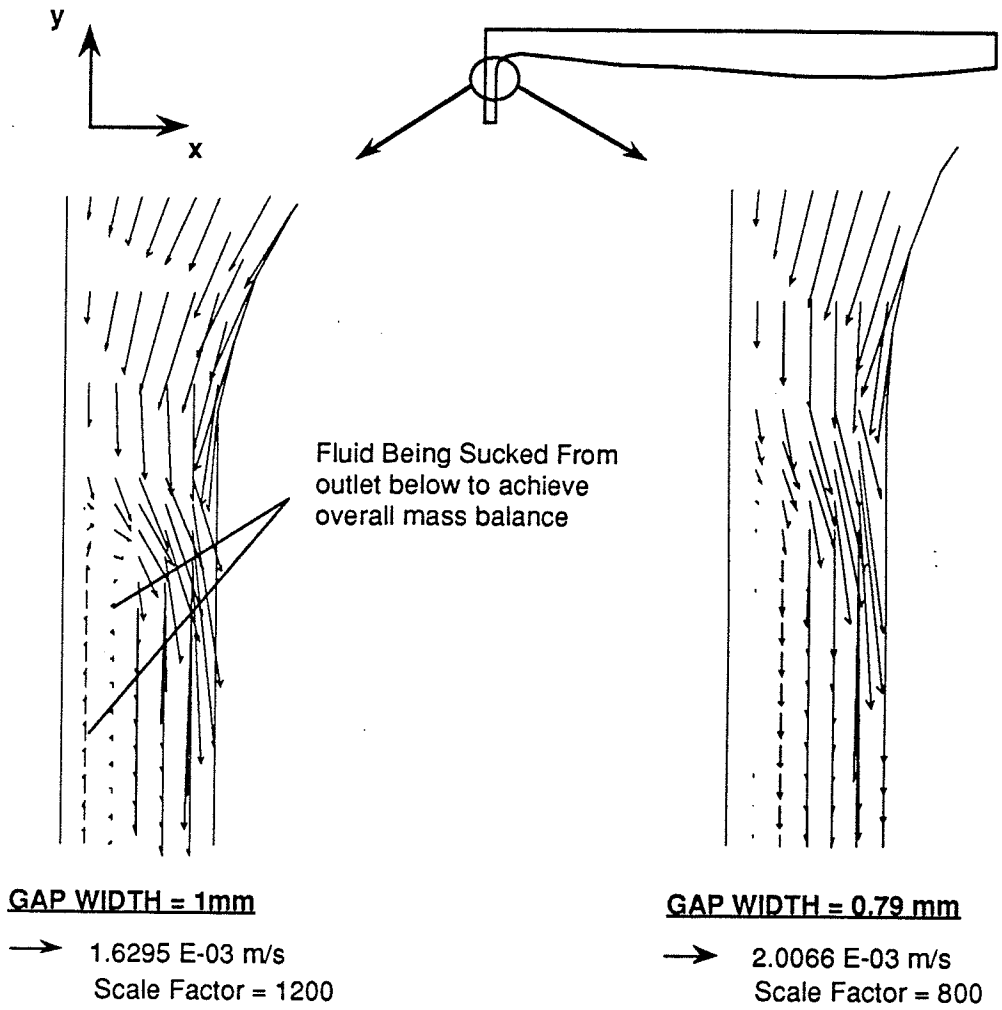

Figure 4.23 - Isothermal Flow in Gap

While the behavior of the flux in the mold-strand gap is not the focus of this study, some basic information on the flow and heat transfer features for the flux in this region may be extracted from the coupled simulation. Figures 4.25 and 4.26 show the variation of temperature across the gap and the flow of flux through it. Figure 4.27 shows the location of the flux melt interface for the flux down the mold-strand gap below the meniscus.

Figures 4.25 and 4.26 give the temperature and flow profiles respectively across the gap at three positions down the mold. In Figure 4.25, the temperature profile is linear across the liquid domain and slightly curved in the solid domain, which corresponds to the temperature dependence of thermal conductivity which was used as an input to the model. This indicates that

convection does not play a significant role in heat transport in the gap, because the temperature profile in the liquid region would have been more curved if convection were important.

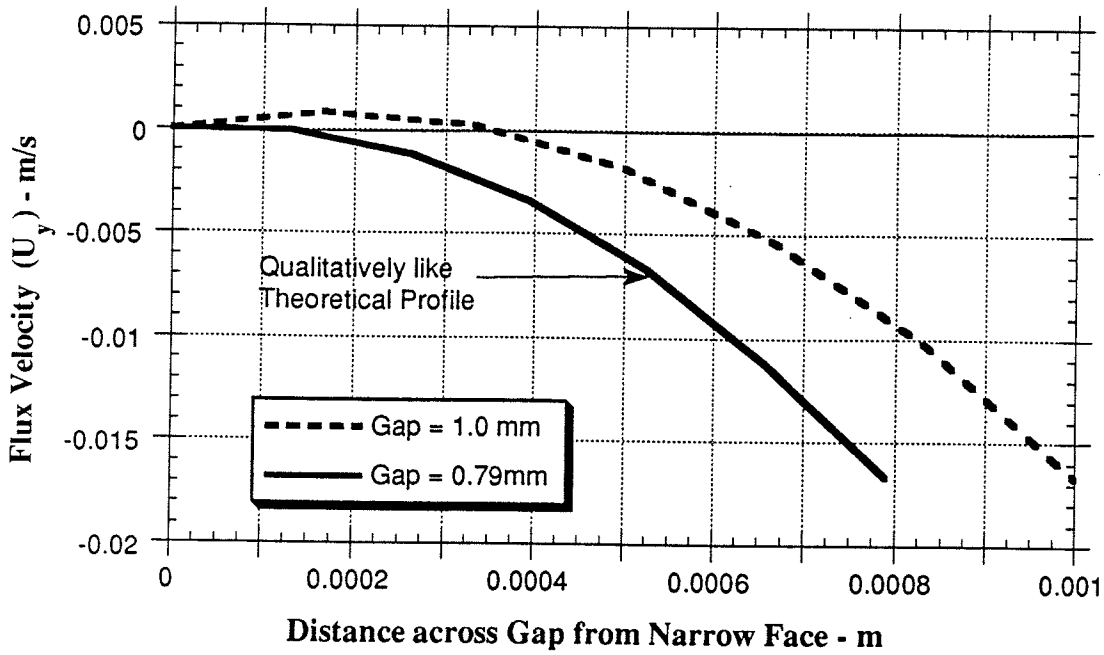

Figure 4.24 -Flux Velocity Profiles in Mold-Strand Gap as a Function of Gap Width, d_g, for Isothermal Flow

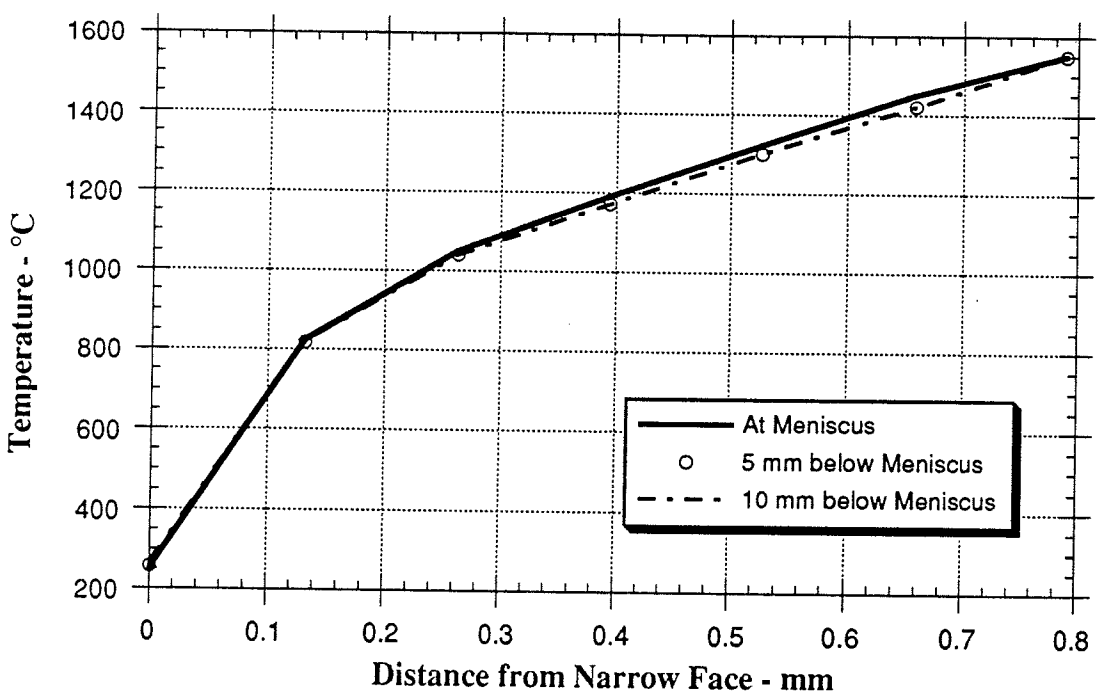

Figure 4.25 - Variation of Temperature Profile in Mold-Strand Gap

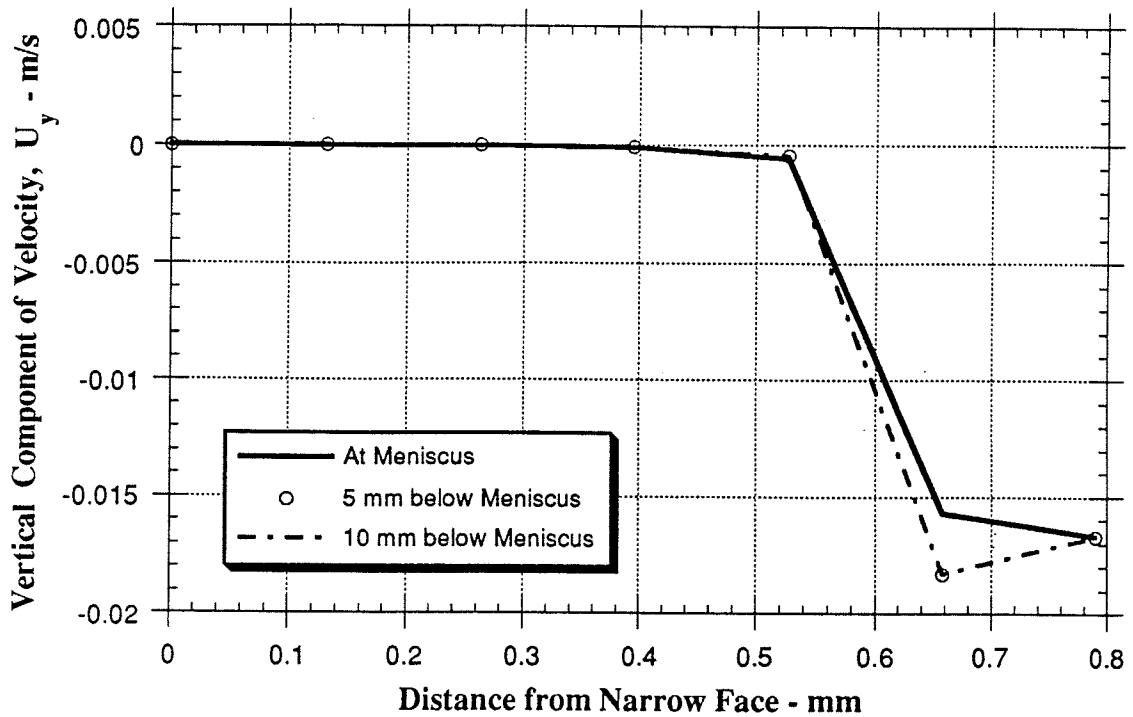

Figure 4.26 - Variation of Velocity Profile in Mold-Strand Gap

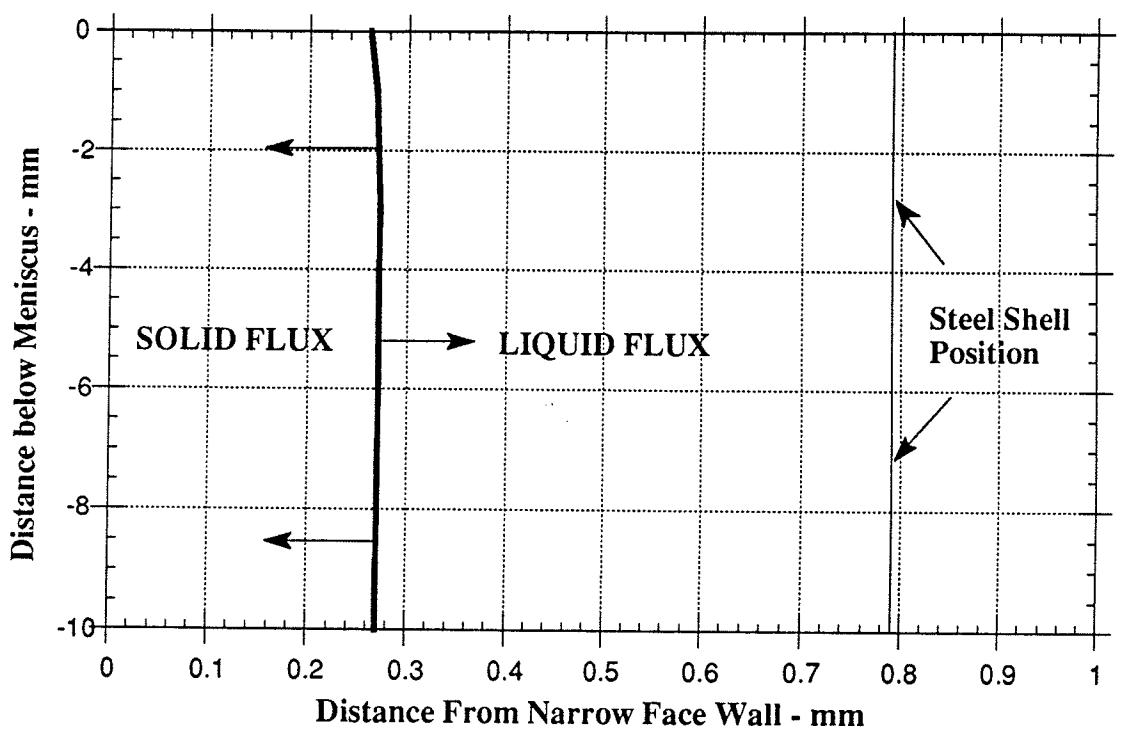

Figure 4.27 - Variation of Flux Layer Thicknesses down the Mold-Strand Gap

The velocity distribution in the gap, as shown in Figure 4.26, resembles the profile expected according to Ho [15]. That is, the velocity is expected to be constant across the solid flux at either a low value or zero, and is expected to increase hyperbolically to the casting speed at the shell across the liquid flux. It can be seen that while this is approximately the profile obtained by the model as given in Figure 4.26, the match with the theoretical profile is not exact. There are three possibilities for this discrepancy.

The first is that the gap size chosen is too small. While the gap size was chosen to give the theoretically accurate velocity profile for the isothermal flow model (≈ 0.79 mm), it is not an appropriate choice for the coupled model because the effective gap width is reduced due to solidification of the flux on the mold wall. Therefore the flux mass balance must occur within the smaller effective gap (≈ 0.52 mm as shown by Figure 4.26). This is the reason the velocity just adjacent to the steel shell exceeds the casting speed imposed at the shell. If the effective gap size after solidification was equal to 0.79 mm, then the proper theoretical profile might have been obtained similar to that given in Figure 4.24.

Secondly, the mesh density in the gap is too low. A better match with the theoretical profile could be obtained with refinement of the mesh in the gap region.

Thirdly, the solid flux moves with the mold wall, so the appropriate boundary condition at the mold wall-flux interface should be the vertical velocity of oscillation of the mold. This value of velocity, however, changes in magnitude and direction during the oscillation cycle, and therefore cannot be incorporated into this steady state model.

For the steady state model, it is suggested, therefore, that an iterative procedure is necessary to determine the correct inital gap size. That is, the initial gap size (i.e. mesh width) should be adjusted so that the effective gap width, after solidification of flux on to the mold, to be equal to 0.79 mm. With the final effective gap size equal to 0.79 mm, the theoretically expected gap flow profile should be obtained. Also, the mesh should be refined.

4.4.3 Temperature Distribution

Figure 4.28 shows the steady state temperature distribution developed in the flux. The distribution of temperature is dependent on the flow pattern developed, which is discussed in the following section. The melting zone of the flux is taken to be centered around a temperature of 1050°C, which is approximately 70°C above the softening point of the flux considered. The melt interface is given therefore by the 1050°C isotherm in Figure 4.28.

Solid flux exists in regions close to the mold wall due to the cooler temperatures there. The shape of the temperature contours close to the mold wall are consistent with the shape of the solid "flux-rim" which is observed to cling to the mold wall in the meniscus region, and are in agreement with the results of previous analytical work [50]. Because the exact shape of the flux rim is expected to be influenced by mold-wall oscillation, this steady state model can only predict the approximate time-averaged shape of the rim in the absense of oscillation.

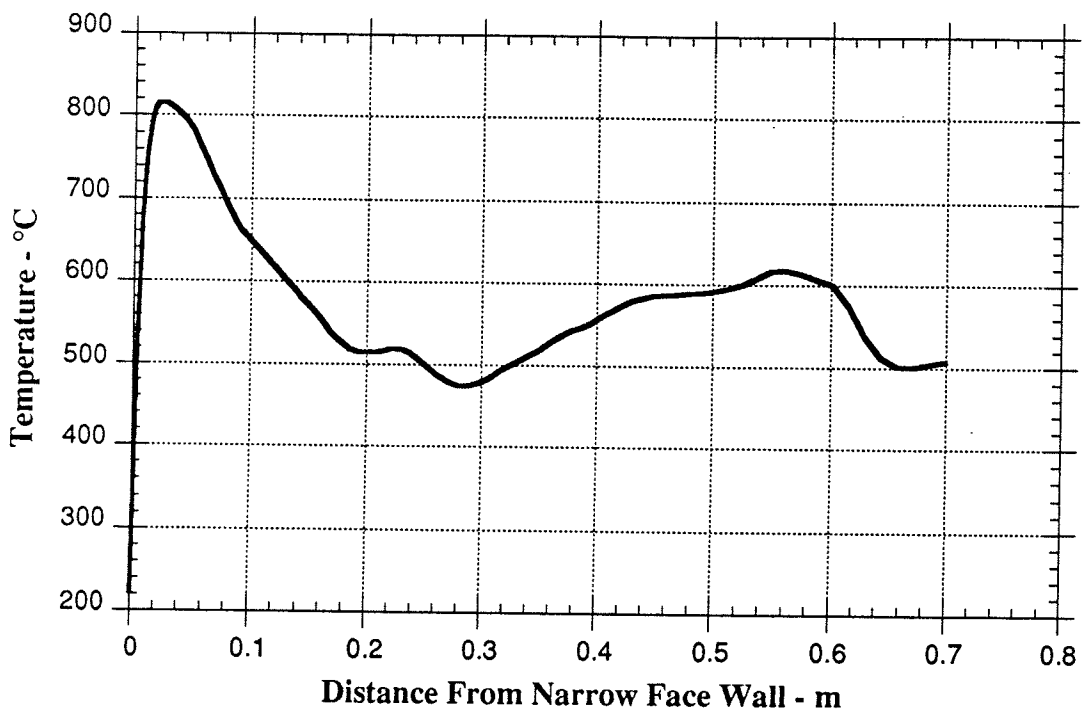

Figure 4.29 - Temperature Profile at Top Surface of Flux

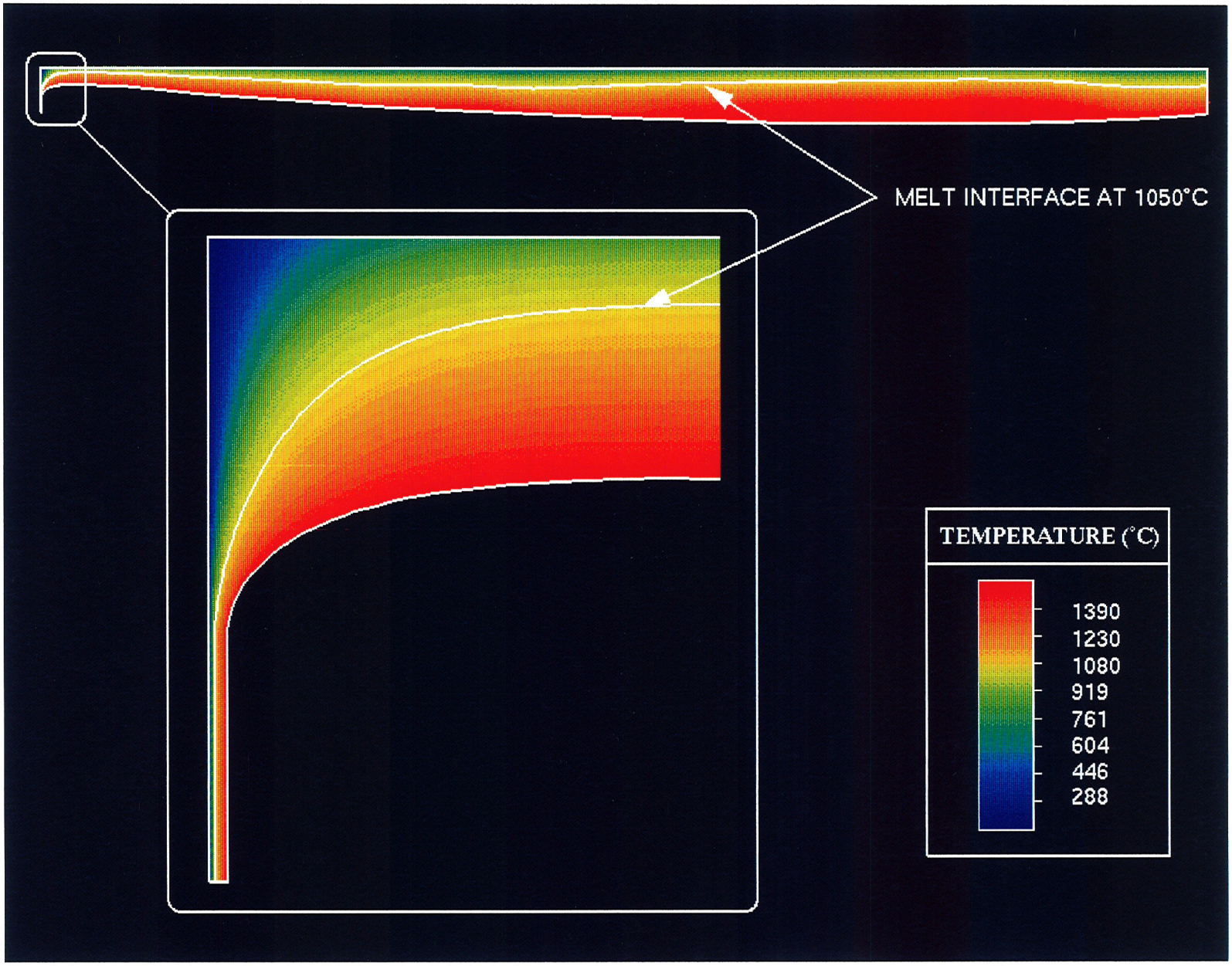

Figure 4.28: Wideface Model - Overall & Meniscus Melt Interface (1050 C Contour)

The temperature profile along the top surface of the flux is given in Figure 4.29. There is a peak in the surface temperature about 25 mm from the narrowface wall. This peak in the temperature profile may result from hot liquid flux being pushed towards the surface as a result of the developed flow pattern, as well as the proximity of the high-temperature liquid-steel interface to the upper flux surface in the meniscus region. The heat flux follows the same trend as the temperature, with the peak in heat flux being sharper than that for temperature. Thus a sharp increase in heat loss from the top surface of the powder is expected at about 50 mm from the narrow face wall.

Close to the meniscus, but beyond 20 mm from the mold wall, the temperature contours are parallel to the x-direction, indicating one dimensional heat transfer. Because the fluid motion is in the x-direction, perpendicular to the direction of heat transport, convection in the y-direction is practically zero. Temperature profiles through the thickness of the flux within the approximate range 20 mm to 60 mm from the mold wall confirm this, by being linear in the liquid domain (see Figure 4.30).

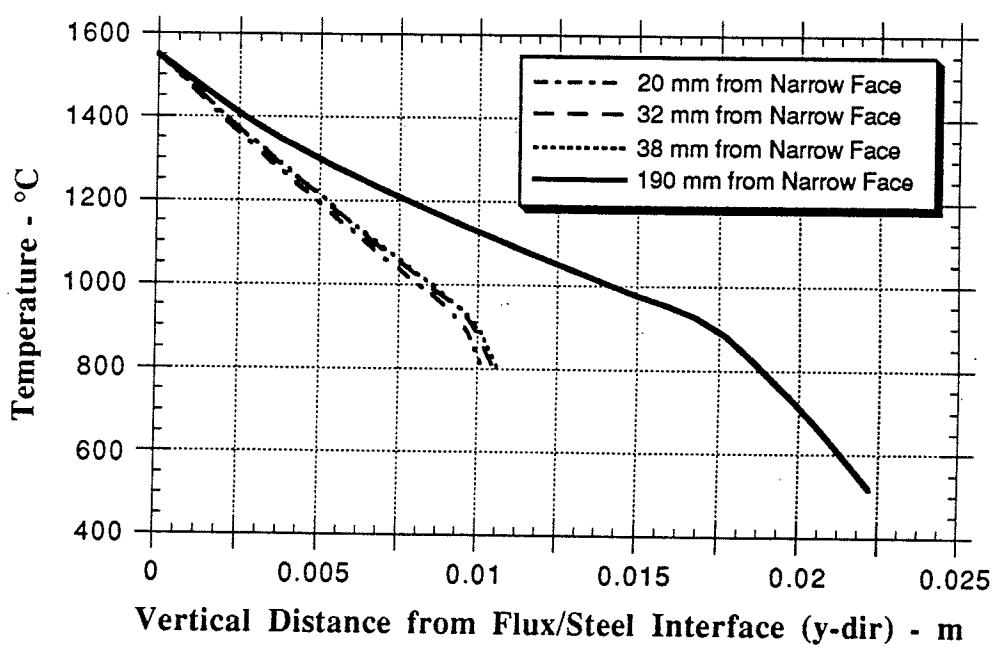

Figure 4.30 - Temperature Profiles through Flux Layers as a Function of Distance from Narrow Face

In contrast the temperature profile through the flux 190 mm from the mold wall is distinctly curved in the liquid domain, indicating that the effects of convection in the y-direction increases as one moves away from the mold wall.

NARROW FACE MODEL

As mentioned previously, all the boundary conditions both thermal and fluid flow, for the narrow face model are exactly the same as those for the wide-face model except at the flux-steel interface. At that interface, the steel flow is normal to the plane being modeled unlike that for the wide-face model. Therefore, the steel flow is not expected to affect flow in the plane being modeled. Thus, the tangential stress is specified as zero at the flux-steel interface. The normal component of velocity is also specified as zero to prevent flux penetration into the steel domain. The thermal boundary condition is fixed temperature at 1550 °C as before.

4.4.4 Flow Pattern

In this case, the driving force for fluid motion is only the imposed casting speed at the mold-strand gap, without the shear stress at the flux-steel interface as before. Thus fluid enters the domain and is drawn towards the mold-strand gap, resulting in the streamlines shown in Figure 4.31. Most of the flux which enters at the surface, flows towards the flux/steel interface, before being pulled to the mold-strand gap, as a liquid. A small portion of the flux entering at the top surface flows directly into the

Figure 4.32 shows the velocity vectors in the meniscus region of the domain, with the 1050°C temperature contour superimposed. In this region, the maximum fluid velocity of 0.03484 m/s is attained, as the flux flow through the smaller effective gap between immobile solid flux and the steel shell. Just away from the meniscus, the flow is parallel to the flux steel interface and therefore perpendicular to heat flow in this region.

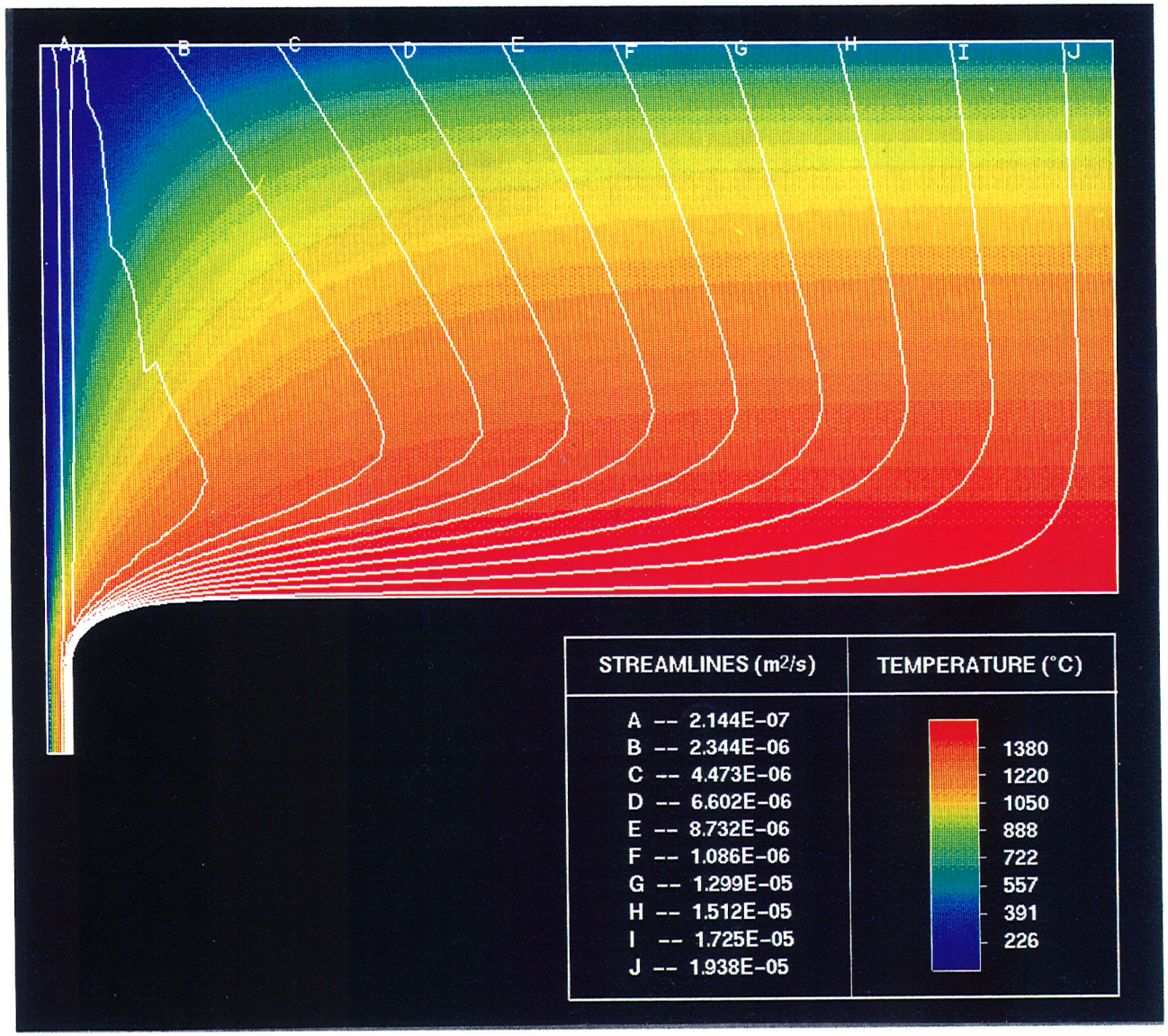

Figure 4.31: **Narrowface Model - Overall Temperature Distribution and Flow Pattern**

4.4.5 Temperature Distribution

The temperature contours shown in Figure 4.31 are essentially horizontal and parallel away from the meniscus but over most of the domain. This pattern indicates that heat flow is essentially one-dimensional. Cold surface temperatures are expected because fluid flow is almost directly opposite to heat flow in the upper regions of the flux. Additionally, because fluid flow is approximately perpendicular to heat flow in the lower regions of the domain, one-dimensional conduction of heat in the y-direction in the liquid, while one dimensional convection through the powder is expected. The temperature profile through the flux in the y-direction at mid-domain (Figure 4.33) confirms the form of heat transfer conclusion, being linear in the liquid domain and curved in the powder domain. The temperature distribution at the top surface is given in Figure 4.34. There is no sharp peak in the temperature profile like that for the wide-face model. Also, it appears that the flux rim is larger on the wideface (to the left of the narrow face domain) than on the narrowface for the same conditions.

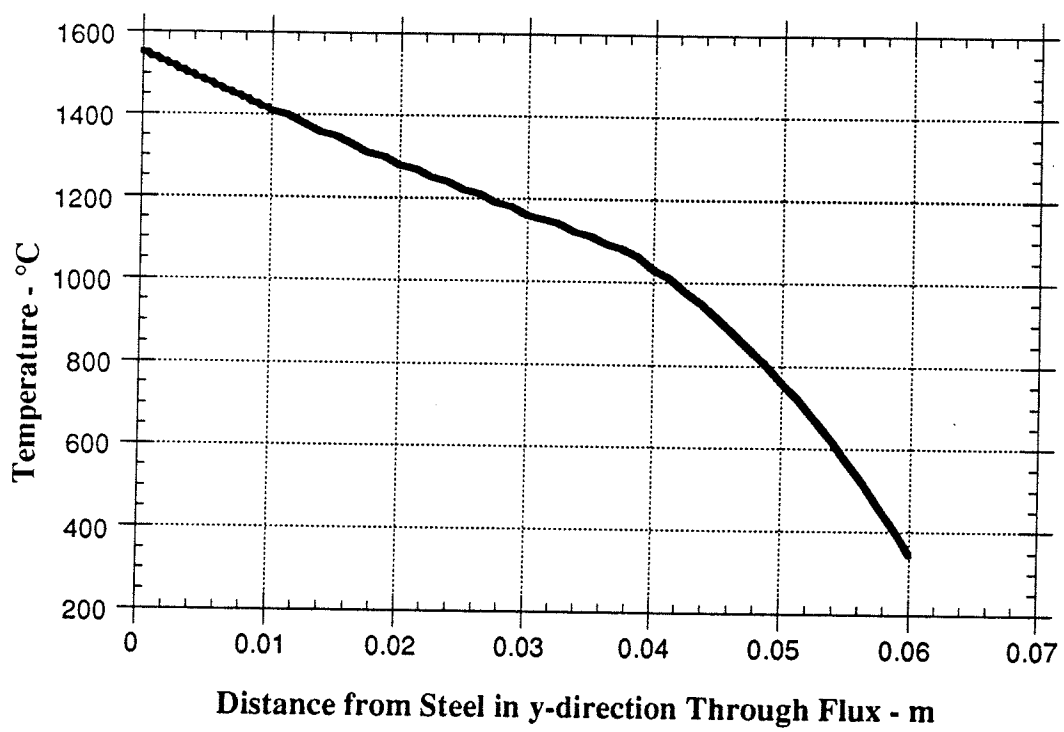

Figure 4.33 - Temperature Profile through Flux at Mid-domain (x=0.057 m)

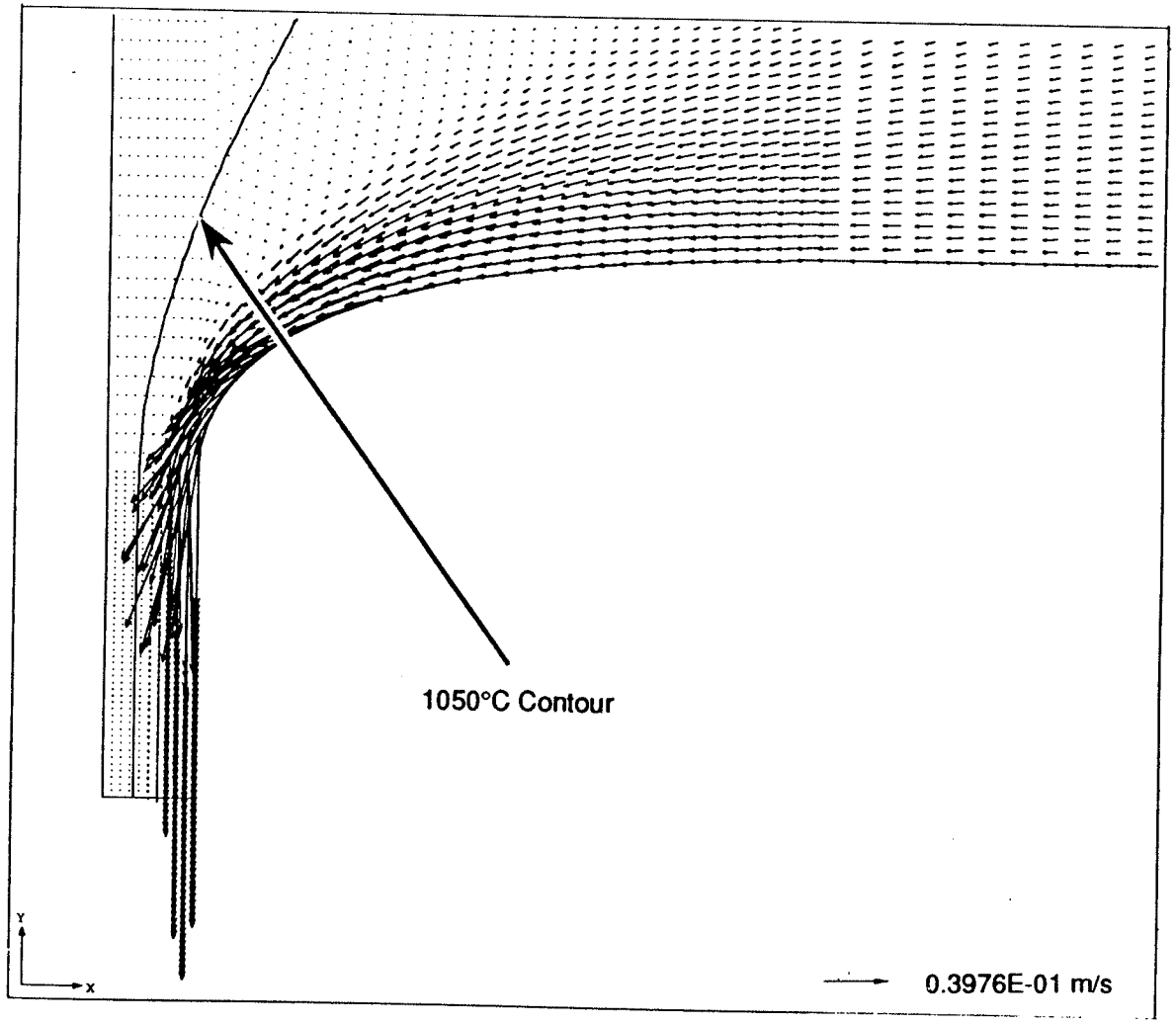

Figure 4.32: Narrowface Model - Menicus Velocity Vectors and 1050°C Contour

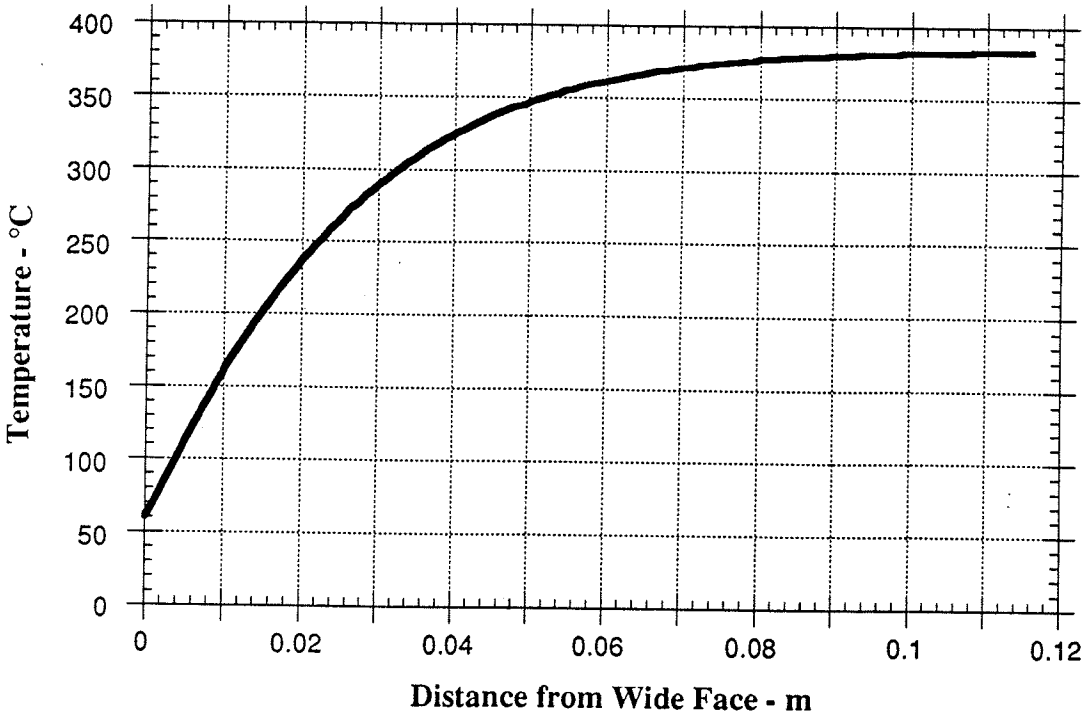

Figure 4.34 - Top Surface Temperature Profile for Narrow Face Model

CHAPTER 5

EXPERIMENTAL METHODOLOGY AND DATA

5.1 OVERVIEW

The aim of the this study is to be able to predict the thermal and flow behavior of the lubricating flux as it melts and infiltrates the mold-strand gap. When reasonable confidence in the results of the model has been attained, an attempt may then be made to predict the behavior of the flux as a function of the casting conditions or to optimize the performance of the flux, in terms of the liquid layer thickness developed (for example). It is therefore essential that the model is calibrated to ensure that most, if not all, significant physical phenomena have been incorporated. In this way can one be reasonably confident that the model has applicability over a wide range of conditions.

Numerical models such as the one proposed for this work may be verified in several ways. In one method, an approximate analytical model may be developed, and its results compared to those of the numerical model. Alternatively, experimental data may be gathered and compared to the values for those variables given by the numerical model. Finally, a combination of these two methods may be used, where an analytical model is created as a tool in the development of the complete numerical model.

To assist in the verification of the model proposed by this work, experimental data for the mold flux was collected at a steel plant. Measurements of powder layer and liquid layer thicknesses at the upper surface of the mold were the primary objective of the experiment. Layer thickness is one output of the model that is easily verifiable. In addition, the measurement technique used can also provide the steady state shape of the liquid steel at the upper surface. This may avoid the need to compute the shape of this surface with another model, which would require significant extra computational effort.

Due to the nature of the model being developed, it is important to know whether the experimental data being obtained for verification is measured under transient or steady-state conditions. While the measurements may be influenced to some extent by such time varying phenomenon like the oscillation of the mold, it is assumed that the thicknesses of powder and liquid can attain some steady value due solely to heat transfer coupled with some overall average mass consumption as a result of the oscillation. Thus, the process of powder melting is considered transient, for example, during the initial period after the addition of new powder, during a casting speed change or change in the oscillation frequency or stroke. Hence, in addition to measurement of the layer thicknesses, it is also important to record the time the readings were taken based on a reference like the time of addition of new powder.

At the steel plant at which the readings were taken, the mold flux powder is added manually by the operators as shown in Figures 5.1 (a) and (b) below. Thus the frequency at which powder is added varies depending on the practice of the individual operator.

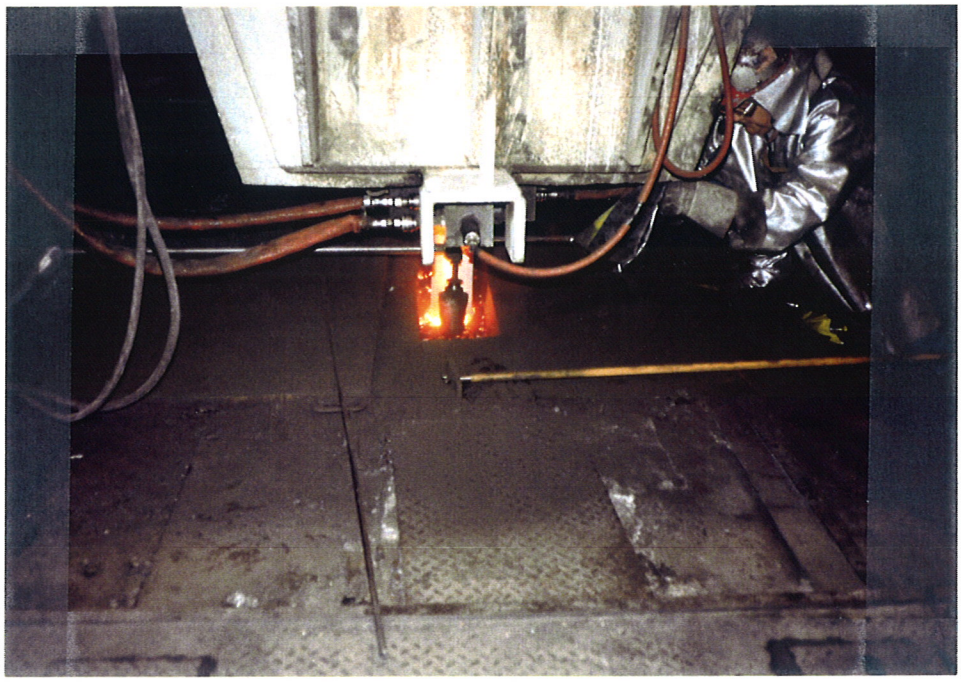

Figure 5.1(a): Manual Mold Powder Addition

Figure 5.1(b): Manual Mold Powder Addition

5.2 APPARATUS

Ideally, the powder and liquid flux layer thicknesses may be indirectly determined based on a temperature profile produced by thermocouples inserted into the flux pool at the steel surface. Additionally, this measurement technique would provide the temperature data which can be directly used to verify the numerical model. This method was not possible at the steel plant where the readings were taken. However, a very simple technique which is readily repeatable was used to obtain the powder and liquid layer thicknesses. Commonly called the 'nail board' test, this method consists of inserting a wooden board containing steel nails and aluminum or copper wire into the mold. A schematic illustration of the method is shown in Figure 5.2 while actual photographs of the measurement process are given in Figures 5.3 (a) and (b) to illustrate the difficulties and possible sources of error encountered when taking the readings.

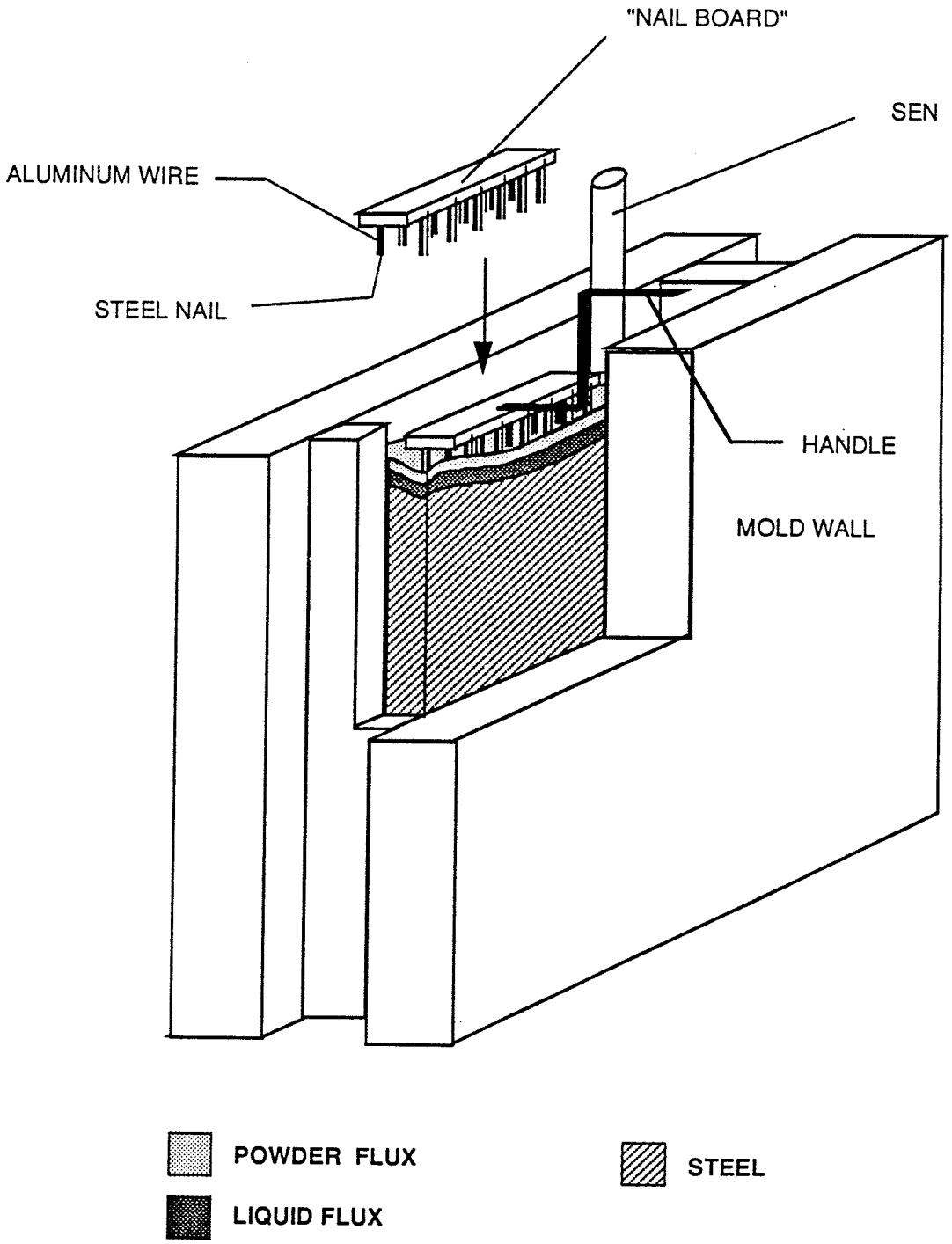

Figure 5.2 - Schematic showing Layer Thickness Measurement Method

5.3 METHODOLOGY

The nail board is inserted for a short time (approximately 1 - 3 seconds) into the mold such that the underside of the board just rests on the upper surface of the mold powder. The liquid steel coats the nail up to its level, while the liquid flux melts the aluminum wire to some point higher than the steel level. The difference in the levels from the end of the aluminum wire to the steel level on the nail gives an indication of the liquid flux thickness (see Figure 5.4). Aluminum melts at approximately 660°C, while the typical flux melting point is about 1000°C. The aluminum wire that remains when the board is extracted from the mold is always pointed at its end. This indicates that the immersion time was too short to allow complete melting of the aluminum, and that the portion of wire that was removed was melted very quickly. Such fast melting must be the result of the wire being subjected to an ambient fluid temperature considerably higher than the liquidus temperature of aluminum. Hence the assumption that the end of the aluminum wire indicates the location of the melt interface for the flux, and not of the 660°C isotherm.

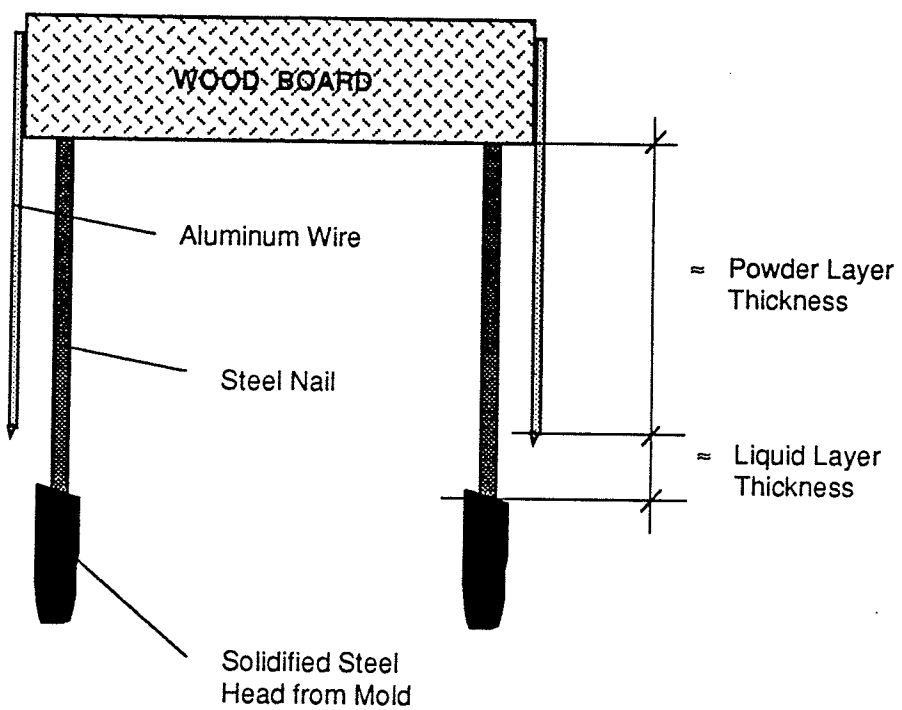

Figure 5.4 - Schematic Showing How Thicknesses are Obtained

Figure 5.3(a): Measurement Method

Figure 5.3(b): Measurement Method

In addition to the values of the liquid and powdered flux layers, the nail-board test can also give an idea of the flow pattern developed in the steel. The solidified head of steel at the ends of the nails are formed when liquid steel impinges on the nail. On the side of the nail to which steel is flowing (i.e. the leading edge), the solid steel level is higher while it is lower on the trailing edge of the nail. Therefore the direction of the steel flow may be determined approximately as illustrated in Figure 5.5.

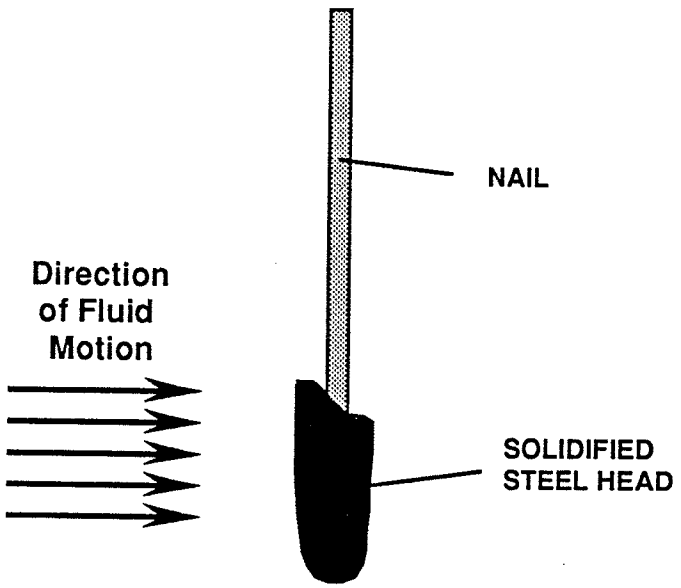

Figure 5.5 - Illustration of Qualitative Determination of Flow Direction

5.4 TYPICAL RESULTS

Two sets of readings were taken. In the first case, shorter boards were used to obtain measurements in the mold narrowface direction, or, in other words, across the thickness of the mold. Within experimental error, given the inherent difficulty in taking the readings, it was determined that, at steady state, there is no significant variation in the layer thicknesses in the thickness direction of the mold (see Figure 5.6). However, there does seem to be a trend in the results shown in Figure 5.6, in which the absolute steel level is higher on the inner radius (distance = 0) than at the outer radius. This results in a downward incline of approximately 5° from the inner radius to the outer.

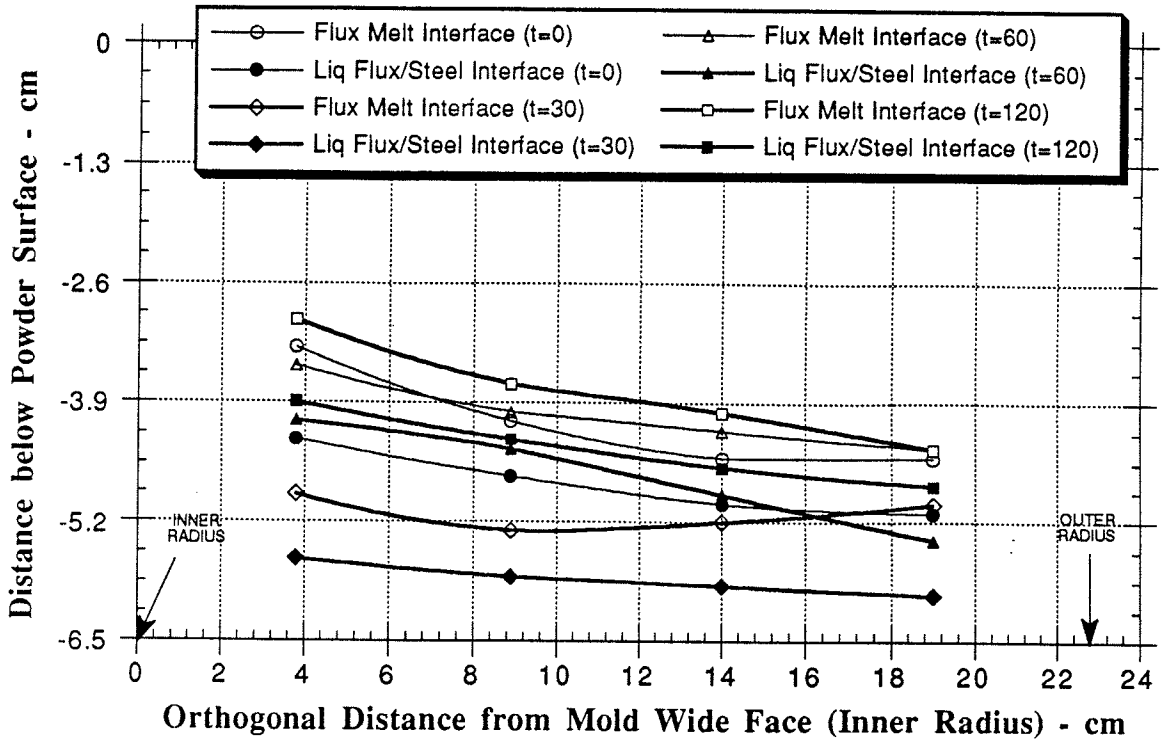

Figure 5.6 - Variation of Layer Thickness as Functions of Time and Position for Short Boards

It is difficult to say, however, whether this trend actually exists, or whether it is the result of flaw in experimental technique. The person taking the measurement must stand on the inner-radius side of the mold, and must rotate the board upwards towards himself when withdrawing it from the mold. This procedure causes the nails and aluminum wires on the inner-radius side of the board to remain longer in the mold than those on the outer-radius side. Additionally with such a rotation of the board, the inner-radius side will tend to push deeper into the flux, than it should be. The comination of these two occurrences will result in further melting of the aluminum wire and coating of the steel nail to a higher level, thereby producing the perceived trend mentioned above. On the other hand, the trend may actually exist, because several factors can cause this trend, including sloshing in the mold, misalignment of the nozzle and instability in the flow pattern in the steel.

Figure 5.7 shows the variation of powder flux and liquid flux layer thicknesses with time, for four different locations in the mold (two locations close to the meniscus and two close to the SEN). The reader is directed to Appendix B (Figure B.3) for illustration of measurement locations. The figure shows that close to the meniscus (positions 1 and 2) there is a slight increase in powder layer thickness, while there is a decrease close to the SEN (positions 3 and 4) over the same time span (i.e. within 60 seconds of new powder addition). This tends to indicate that flux is being moved from the SEN regions towards the narrow face wall, because the powder was added more or less evenly across the mold.

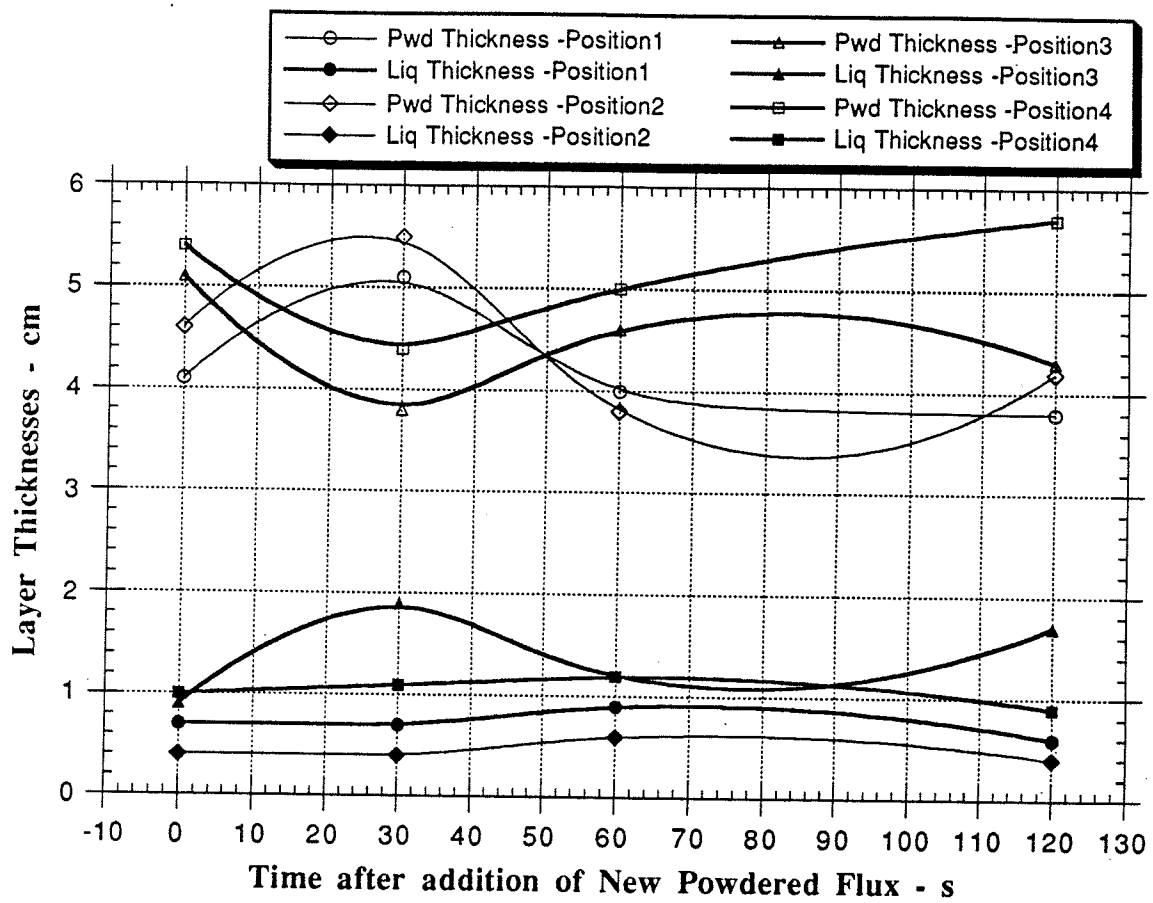

Figure 5.7 - Variation of Flux Thicknesses with Time and Position for Short Boards

On the other hand, the liquid layer thicknesses remained roughly constant, being thicker closer to the SEN (positions 3 and 4).

The readings taken in the mold width direction, or parallel to the mold wide face, agreed with the data presented by Ho, qualitatively, in terms of the profile of flux-steel interface obtained [15]. Additionally, the expected trend in which liquid layers are thicker closer to the SEN was obtained.

5.5 EXPERIMENTAL ERROR AND SENSITIVITY

There are several sources of error for measurements taken using this nail-board test. Difficulties in maintaining a level board, in withdrawing the board from the mold, and inconsistency in placement of the boards and in the construction of the board all contribute to unreliability of the results. Some of these factors are more serious than others. Specifically, maintaining the board level while taking the reading is far more critical than slight variation in the placement of the nails on the board. The combination of the manual nature of the test coupled with the non-standard, uncontrollable and non-constant conditions of the steel plant environment make it difficult to determine a numerical limit on error in the data.

The readings are obtained by measuring the length of the aluminum wire from the underside of the board to the base of the pointed end and from the underside of the board to the midpoint between the high and low sides of the steel coating for the nail. Small error due to irregular coating of the nail and in melting of the aluminum wire produces no more than ± 1 mm of variation in the results.

Finally, the immersion time for the specimens was on average 2 seconds. This is sufficiently long to give the time averaged position of interfaces of interest. Level fluctuations are therefore "evened-out" over that time span. Calculation of the melting time ranges for the wire needs to be done to determine a numerical limit to the possible variation of the actual levels from the measured wire lengths.

CHAPTER 6

MODEL VERIFICATION

6.1 COMPARISON WITH 1-D ANALYTICAL MODEL

Verification of the models with measurements of liquid flux interface position, liquid flux layer thickness and solid flux layer thickness were taken on both the wide face and narrow face. Temperature instrumentation was not available. However, liquid and solid flux depth measurements are available both in the mold wide-face and narrow-face directions.

TABLE 6.1 - Standard Simulation Conditions for 1-D Model

PROPERTY	VALUE	PROPERTY	VALUE
Solid Conductivity, $\frac{W}{m.K}$	0.9	Flux Consumption, $\frac{kg}{m^2}$	0.6
Flux Melting Point, K	1373	Slab Thickness, m	0.2286
Stefan-Boltzman Constant, $\frac{W}{m^2.K^4}$	5.67E-8	Casting Speed, m/min	1.0
Flux Emissivity	0.8	Consumption Rate , $\frac{kg}{s}$	0.0326†
Ambient Temperature, K	300	Steel Temperature, K	1823
Acceleration due to Gravity, $\frac{m}{s^2}$	9.81	Enthalpy of Fusion, $\frac{J}{g}$	450
Slab Width, m	1.4	Liquid Flux Conductivity, $\frac{W}{m.K}$	1.0

† **Calculated Values**

Using the overall depth of flux (equals liquid plus solid layer thickness) as an input to the 1-D analytical model discussed in Chapter 4, the corresponding liquid and solid flux layer thicknesses were calculated. The overall thickness was input for two reasons. First, the overall thickness is fixed in the finite element model, second, it is the controllable operating variable,

and thirdly, it is known with the greatest of certainty. The inputs to the 1-D model used for verification are summarized in Table 6.1.

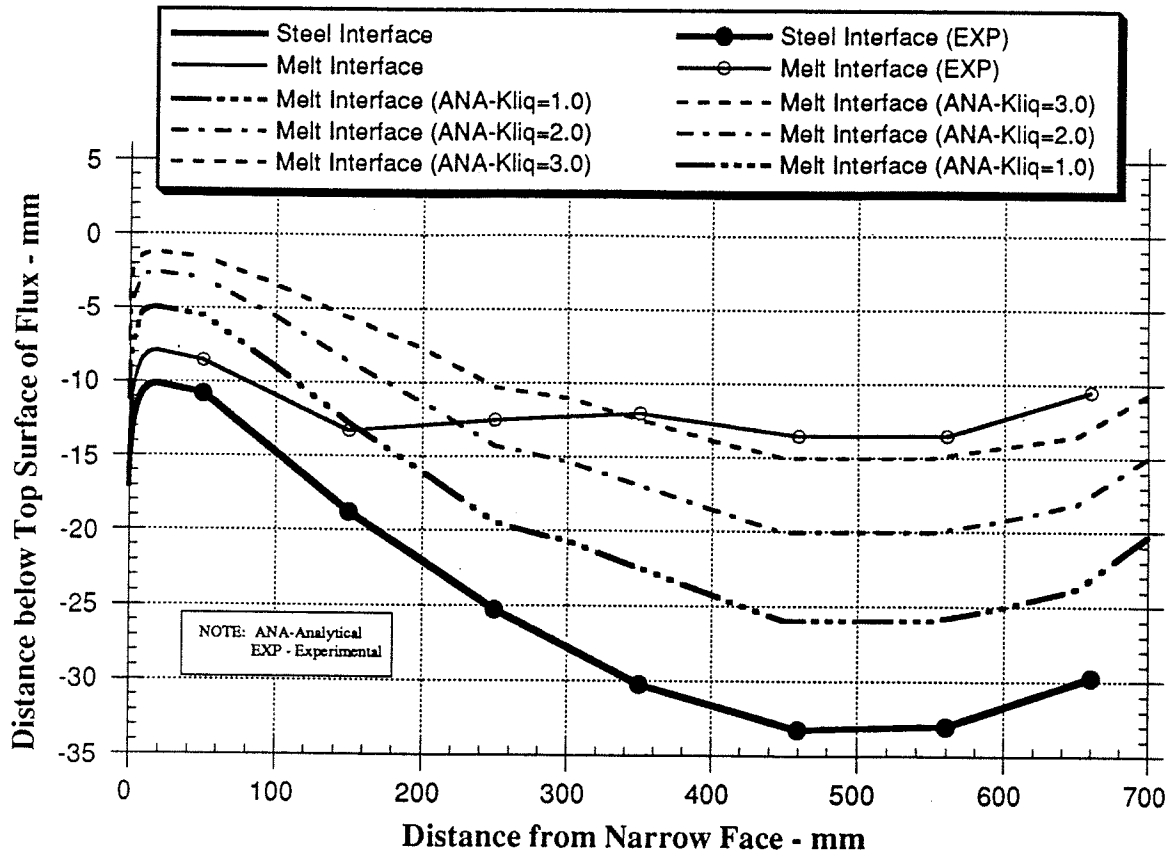

Figure 6.1 - Comparison of 1-D Analytical Results with Experimental Data for k_{liq} = 1.0 (Standard Case), 2.0 and 3.0 $\frac{W}{m.K}$

Figure 6.1 compares the location of the melt interface obtained experimentally with that obtained with the 1-D analytical model. As can be seen, the analytical 1-D conduction model under-predicts the thickness of the liquid flux layer over the center region, comprising most of the mold surface, while it over-estimates the liquid thickness in the meniscus region. Over the majority of the domain, therefore, it is clear that some other phenomena, namely fluid flow, not incorporated in the 1D stead state conduction model, must control the thickness of the flux layers.

6.2 COMPARISON WITH 2-D FINITE ELEMENT MODEL

The reader will recall that three different boundary conditions for simulating the flux-steel interface were applied (see section 4.1.3.6.1). It is believed that the final method which employs a shear stress boundary condition is the most reasonable. However, the results obtained with the other two boundary conditions will also be presented here for comparison with the experimental results. Dimensional and operational parameters are given in Table 6.1, but the material properties are given in Chapter 4.

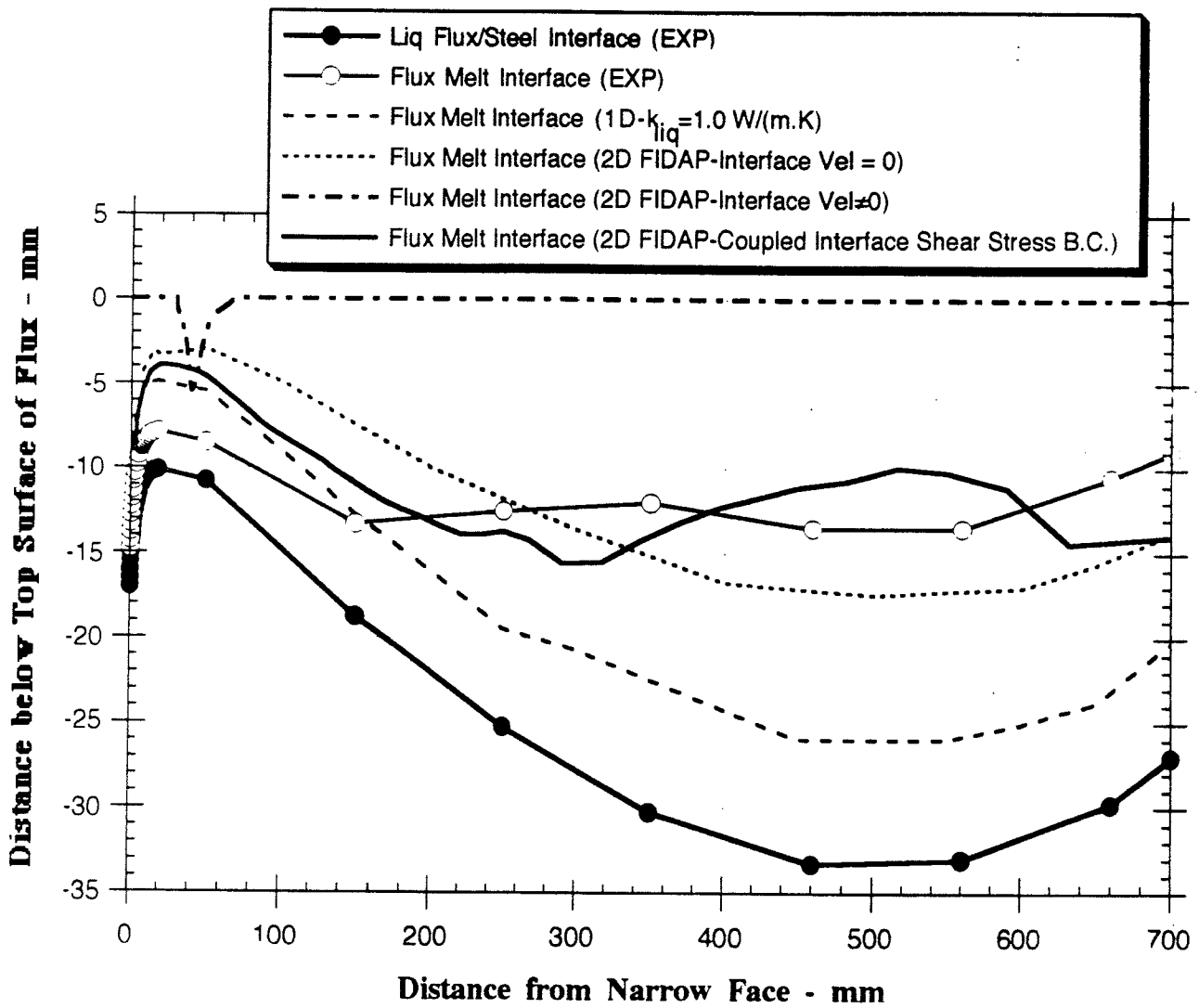

Figure 6.2: Comparison of 2-D FIDAP Results with Experimental Data

Figure 6.2 compares the locations of the flux melting interface as determined by the same model using three different boundary conditions at the steel-flux interface. When the zero velocity boundary condition (described in Method 1 in Chapter 4) is used, under-prediction of liquid layer thickness at the center region and overprediction at the mensicus results. While the 1-D model also underpredicts the liquid layer thickness, the disparity is much greater than for the numerical model with the zero velocity boundary condition. The thicker liquid layer developed in the latter is probably the result of viscous dissipation in addition to conduction, while the 1-D model accounts for conduction only.

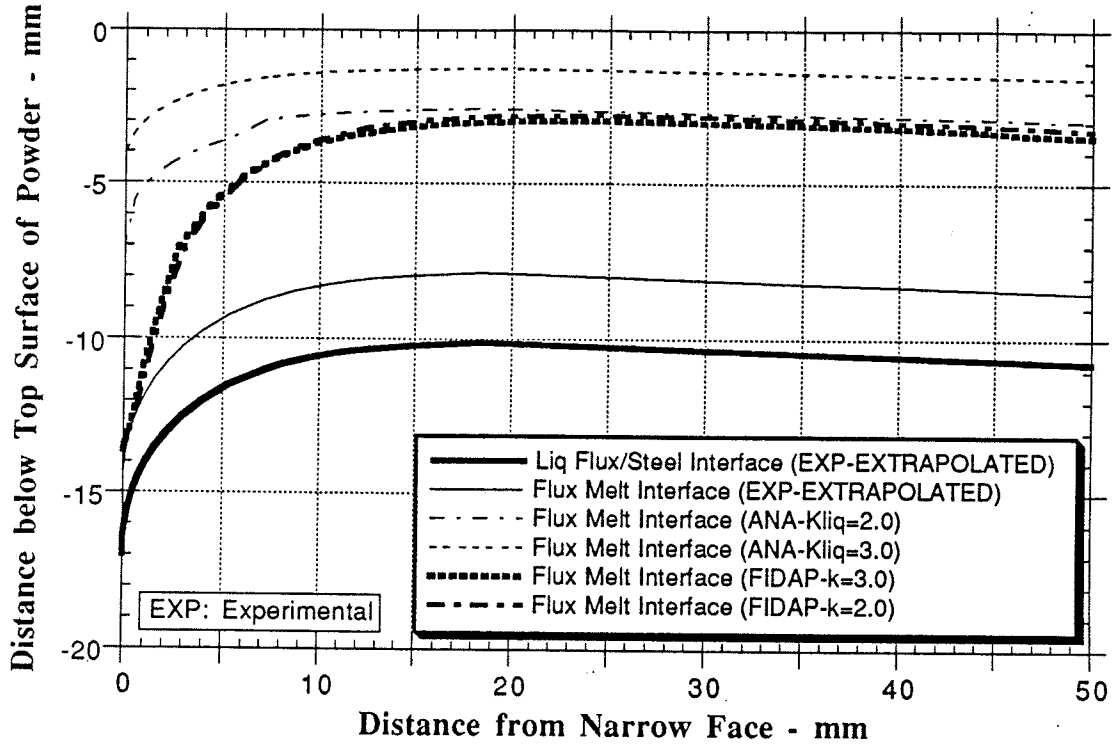

Figure 6.3 - Location of Melt Interface in Meniscus Region as a Function of Material Properties and Model used.

When the full 3-D model velocities, which assumes zero shear stress on the top surface of the steel, are imposed as a boundary condition (Method 2) at the flux steel interface, vast over-prediction of the liquid layer thickness results. This feature is expected because of the high convective component of heat transfer as a result of the large velocities resulting from too high a

velocity being imposed at the flux/steel interface. However, as discussed previously, these 3-D values cannot be the correct velocities at the flux-steel interface because they are calculated assuming, incorrectly, that the steel is in contact with air at the top surface. When the shear stress, calculated by coupling the flux and steel models at the flux/steel interface, is applied, the best agreement with the experimental results occurs.

It is important to note, however, that none of the models or methods produce results which match the experimental data in the meniscus region. In each case, there is over-prediction of the liquid layer thickness. Figure 6.3 is an enlargement at the meniscus and shows the location of the melt interface as predicted by both models under different conditions.

In the meniscus region, there is general agreement between the flux melt interfaces for the analytical model and those predicted by the 2D model for the thermal conductivities given. Because these interfaces, essentially temperature contours, are approximately parallel to the flux-steel interface (which is approximately horizontal), heat transport is expected to be one-dimensional, in a direction normal to the contours. Because the flow is also one-dimensional in this region (in a direction normal to the heat flux), fluid flow has no effect on the thermal distribution in the near meniscus region. Hence the agreement between the analytical (1D) results and those of the 2D model in this region.

The general overprediction of liquid layer thickness in the meniscus region is the result of having all the flux leave through the narrowface gap, whereas in reality considerable amounts of flux leaves towards the wideface as well.. This condition is a necessary approximation of the 2-D model, and one needs to go to a 3-D model to avoid this non-physical effect in the meniscus region. The agreement between the 1-D and 2-D results ceases at a distance of 15 mm from the narrow face wall. At points within this distance the two-dimensional affect of heat transfer close to the cold mold wall takes affect, causing divergence between the 1D and 2D results.

CHAPTER 7

THREE-DIMENSIONAL MODEL

With reference to Figures 6.1 and 6.2, it is evident that neither the analytical nor the numerical models presented previously are capable of matching the experimental data at regions close to the narrowface wall. All previous models over-predict the liquid layer thickness in this region. It is postulated that this discrepancy may be due to the fact that no account is taken of the heat and liquid mass removed by flux flowing towards the wideface wall.

Based on uniform consumption around the mold, 6.1 times as much flux leaves towards the wideface as that removed at the narrowface. It is conceivable that such a large mass removal in the wideface direction, will have a significant effect close to the meniscus in particular. It was shown that in the meniscus region, the flow velocity is low, and essentially one-dimensional. Thus, mass removal to the wide face should significantly influence the flow pattern in the meniscus region, as well as the net liquid layer depth developed.

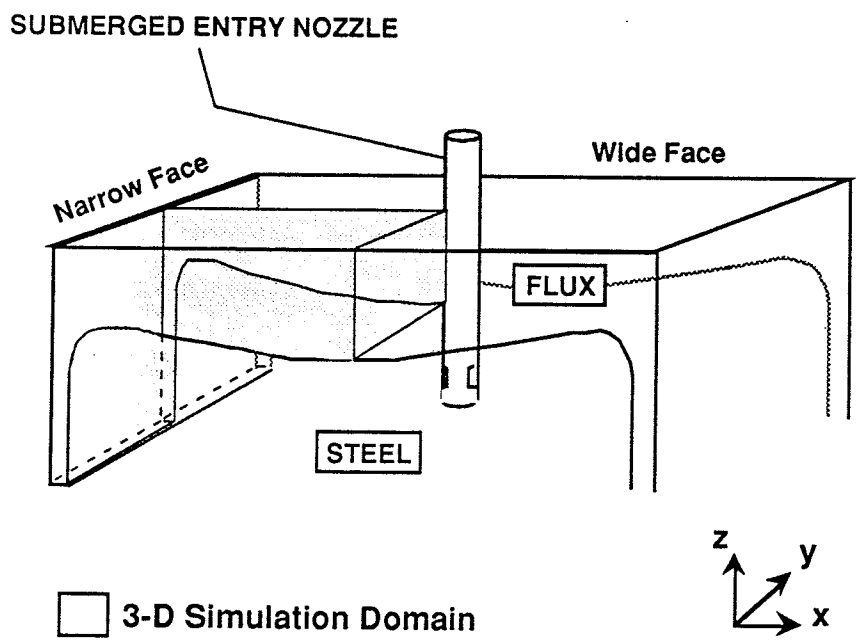

Figure 7.1 - Identification of 3-D Simulation Domain

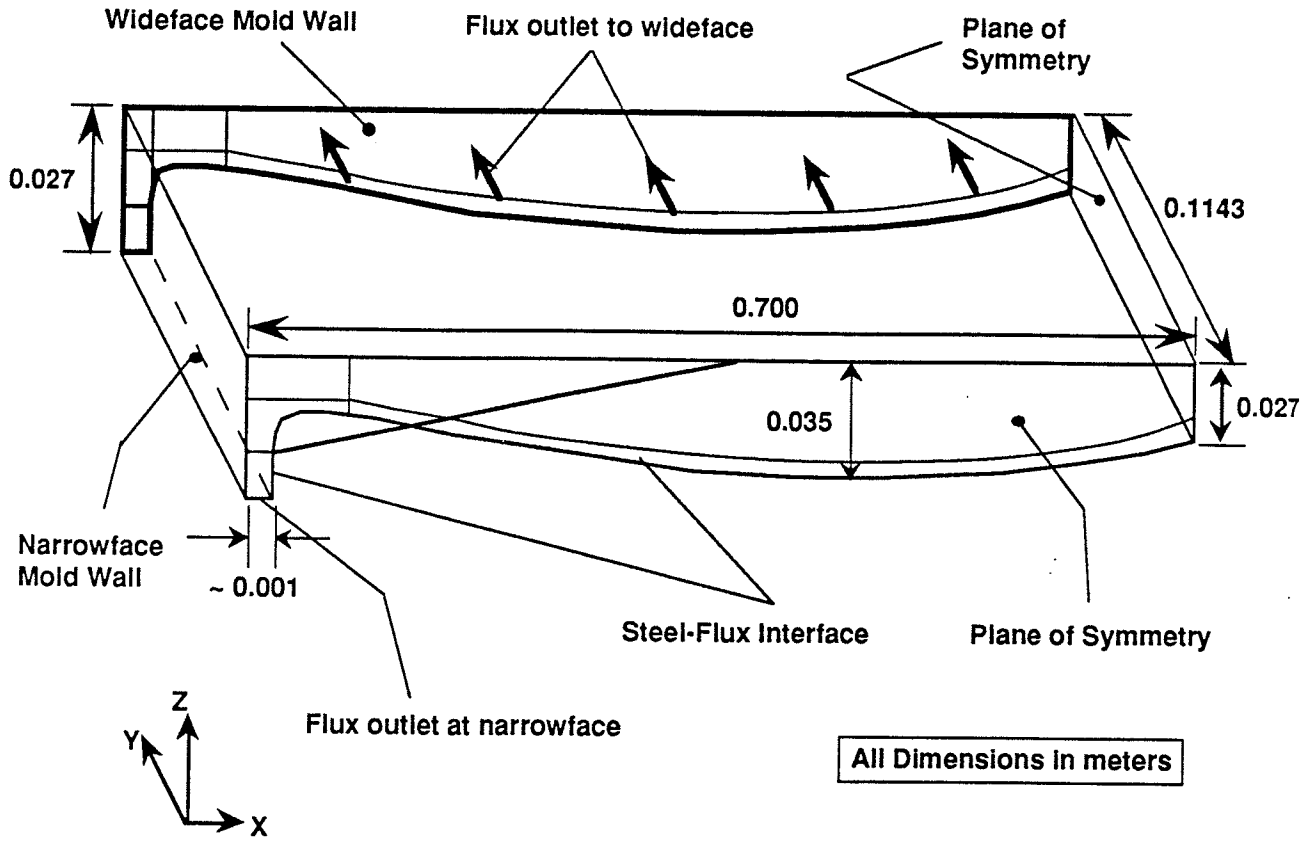

Figure 7.2 - Dimensions for 3-D Simulation Domain

7.1 MODEL FORMULATION

7.1.1 Geometry Definition

For the reasons outlined above, a three-dimensional model was constructed to evaluate the effects of the significant mass flow of flux in the third direction. Figure 7.1 identifies the domain used in this three-dimensional model. Taking advantage of bi-fold symmetry, only one quarter of the physical domain needs to be used for the simulation domain. Essentially, the three-dimensional model was generated by projecting the domain for the 2-D model in the y-direction. Thus the thickness of the domain in the y-direction is half of the mold thickness (≈ 0.1143 m) and the length in the x-direction is half the mold width (≈ 0.7 m).

Figure 7.2 gives some of the essential physical features of the domain including the overall dimensions. Additionally, the reader is directed to Chapter 4 and Figure 4.3 in particular,

for details of the dimensions of this 3-D model, as this model is based on the 2-D model presented previously.

Projection of the 2-D geometry in the y-direction proved to be the simplest way to generate a reasonable 3-D domain. It is clear, though, that the domain is not exact, as the meniscus region at the wideface wall, as well as the wideface shell-mold gap is not explicitly included in the domain. However, the model domain is valid for all regions except very near to the wideface mold wall, where there are significant variations in temperature and flow, due to the presence of the meniscus and the low mold wall temperature.

7.1.2 Fluid Flow Boundary Conditions

Figure 7.2 shows the flow boundary conditions imposed on the three dimensional model. The conditions are virtually identical to those imposed for the two-dimensional model previously. The only new additions are that a second plane of symmetry is now included, as is the wideface wall. Additionally, the flux consumption to the wideface is simulated by imposing a velocity in the y-direction (i.e. normal to the wideface plane) which is calculated based on the amount of mass that leaves through the wideface gap. This mass flow will be calculated later.

7.1.2.1 Planes of Symmetry

In the three-dimensional model, there are two planes of symmetry. One is parallel to the wideface mold wall, and is located at the center-plane in the thickness direction of the mold. The other is parallel to the narrow face mold wall and is located at the mid-plane in the width direction. The fluid-flow boundary conditions are the standard zero normal velocity, and zero shear stress.

7.1.2.2 Narrowface Mold Wall

No slip fluid boundary condition is used at the narrowface mold wall.

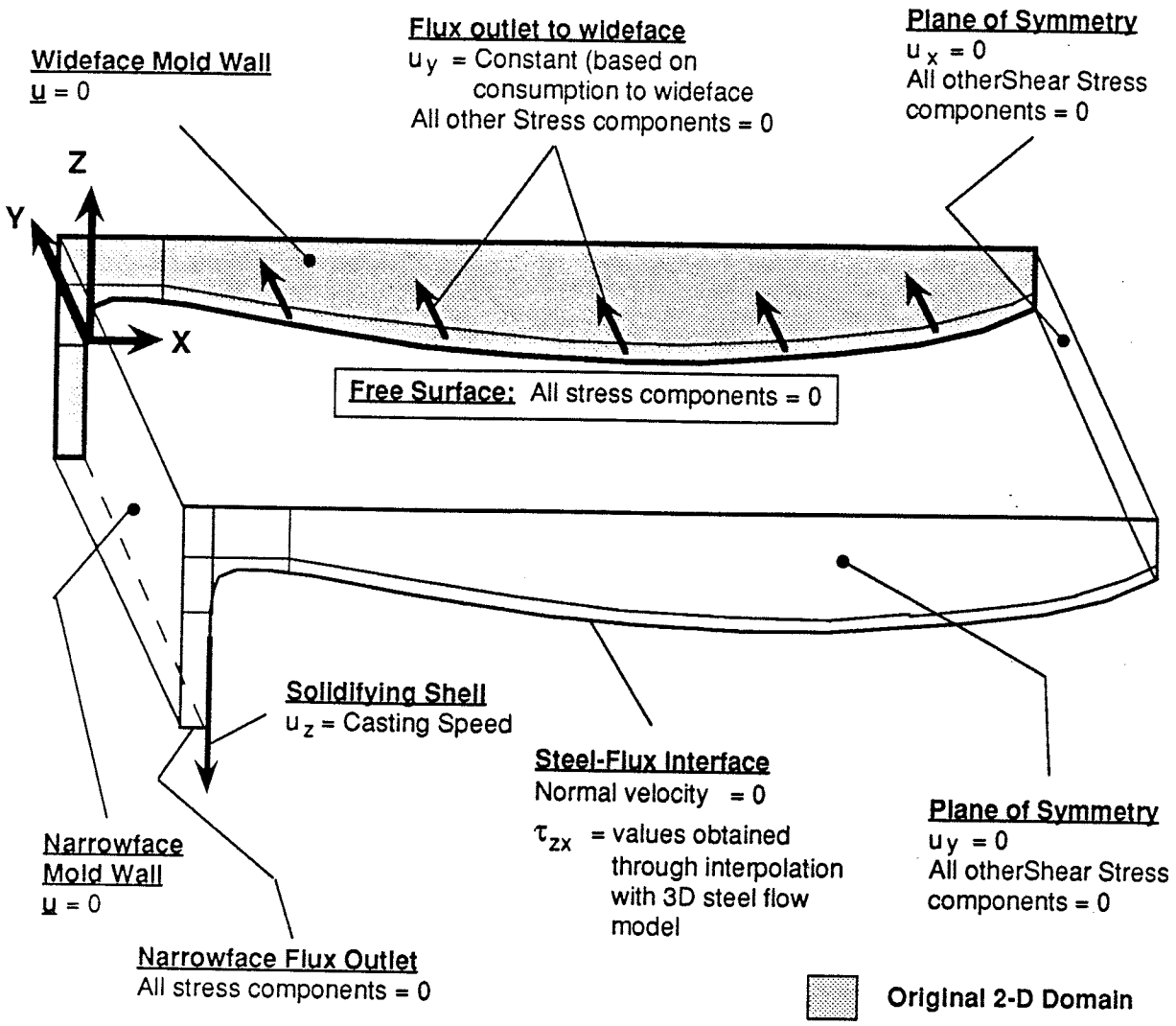

Figure 7.3 - Schematic showing Fluid Flow Boundary Conditions

7.1.2.3 Wideface Mold Wall

As mentioned previously, the boundary of the simulation domain at the narrowface mold wall is a geometric approximation to the physical domain in this location. While the geometry is an approximation, the boundary conditions should be as close to the actual case as possible, to give similar results as if the geometry were accurate. This method is less complicated than the effort required in generating the actual geometry.

At the wideface, the domain boundary is split into two sections. The upper section, which consists of the majority of the boundary is given the actual mold wall boundary conditions of zero-slip. However, the lower section is given an assigned normal velocity, to simulate the flux flow to the narrowface. In the absence of cross flow, this boundary condition is believed to give similar results as would the correct velocity and geometry. Conceptually, this method may be demonstrated using schematics of the previous 2D narrowface models as shown in Figure 7.3.

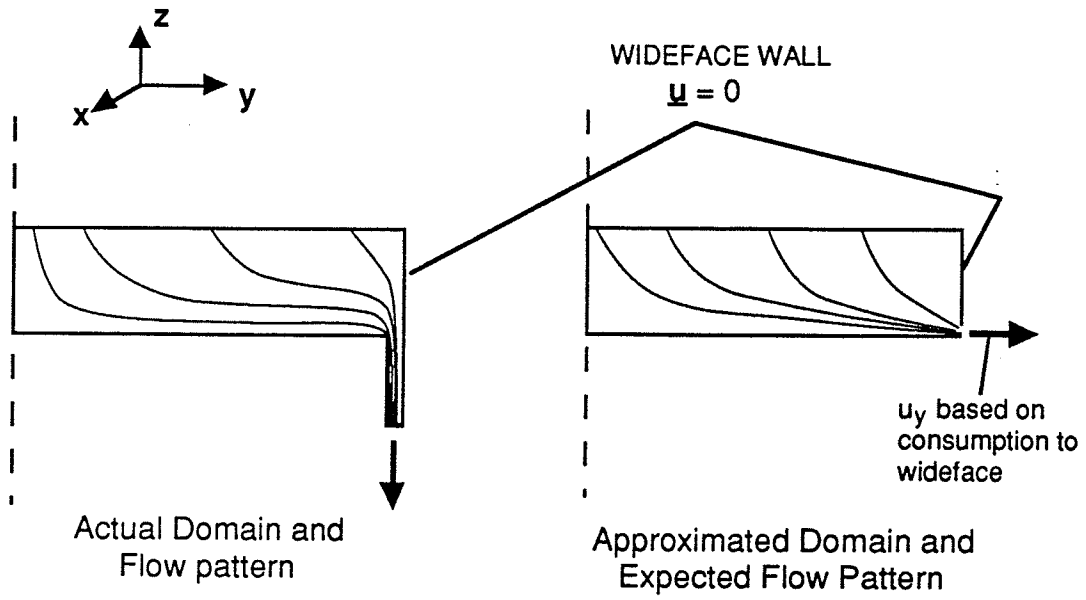

Two 2-D Planes parallel to Mold Narrow Face

Figure 7.4 - Schematic showing the approximation made at the wide face wall, to eliminate the need for the vertical gap between the shell and mold wall in the 3-D computational domain.

The lower section is defined by a separate group of elements in the discretization to ease the imposition of the appropriate boundary conditions. This choice also makes it possible to accurately calculate the area of the boundary, across which the mass has to flow, thus enabling an accurate calculation of the normal velocity to be imposed. The calculation of the normal velocity to simulate mass flow to the wideface is given below.

7.1.2.3.1 Calculation of Mass Flow to Wideface

In chapter 4, calculations of the mass distribution of the flux were performed and schematically illustrated. The relevant figure is repeated here (Figure 7.4). Based on this mass distribution, the velocity normal to the boundary at the wideface, over the lower section element faces, may be calculated as follows.

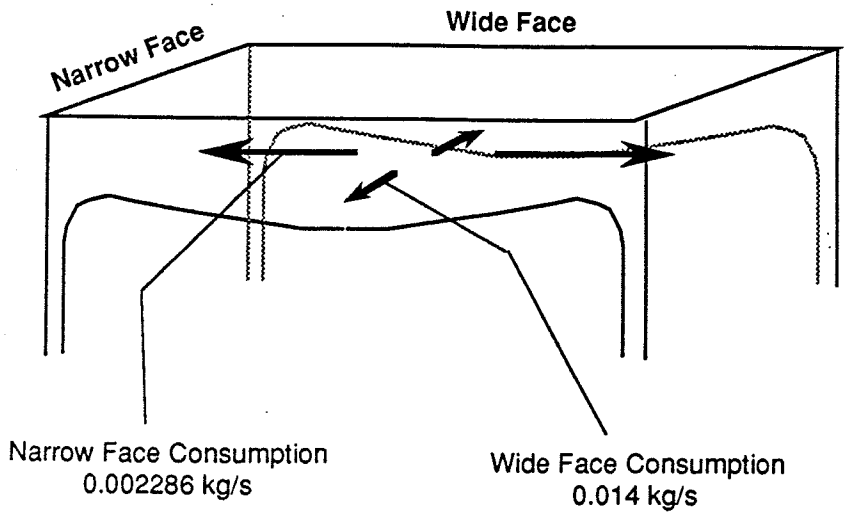

Figure 7.5 - Schematic Showing Distribution of Mass To Wide & Narrow Faces

Thus, the total mass flow in = 2x0.002286 + 2x0.014 = 0.0326 kg/s

Assuming constant density of 2500 kg/m^3, Volume flow in $= \frac{0.0326}{2500}$

$= 1.30288\text{x}10^{-5}$ m^3/s

Ave. velocity in at top surface therefore $= \frac{1.30288\text{x}10^{-5}}{1.4 \text{ x } 0.2286}$

$= 4.070991\text{x}10^{-5}$ m/s

This is the value of the z-direction velocity at the top surface.

For 1/4 mold, the volume inflow = $4.070991\text{x}10^{-5}$ x 0.7 x 0.1143

$= 3.2572\text{x}10^{-6}$ m^3/s

Volume outflow at wide face for 1/4 mold $= \frac{0.014/2}{2500}$

$= 2.8\text{x}10^{-6}$ m^3/s

Area of outlet at wide face = Area of element faces in lower section of elements (calculated by FIDAP)

$$= 0.29383 \times 10^{-2}\ m^2$$

Therefore, the uniform velocity in y-direction that must be imposed for the consumption to the wide face

$$= \frac{2.8 \times 10^{-6}}{0.29383 \times 10^{-2}}$$

$$= 0.000953\ m/s$$

The consumption to the narrowface is not enforced in this way. Because no approximation in the geometry of the narrowface meniscus region was made, it is possible to supply the acutal boundary condition for the flux outlet at the narrowface, which is the casting speed at the solidifying steel shell.

7.1.2.4 Flux-Steel Interface

A specified shear stress (τ_{zx}) boundary condition is used at the flux-steel interface. The reader is directed to chapter 4 (section 4.1.3.6) for full details of this boundary condition. This shear stress is assumed to be uniform in the y-direction

7.1.2.5 Top Surface of Flux

The top surface of the flux (powder layer) is a free surface, so zero normal and shear stresses are used for all but one component. A velocity in the z-direction of 4.071×10^{-5} m/s (as calculated above) is imposed to simulate uniform, steady addition of new powder at the top surface.

7.1.2.6 Solidifying Steel Shell

The casting speed is imposed at this boundary for reasons given for the 2-D model (see section 4.1.3.3).

7.1.2.7 Narrowface - Gap Outlet

See section 4.1.3.4.1

7.1.3 Thermal Boundary Conditions

7.1.3.1 Planes of Symmetry

Zero heat flux is the default boundary condition for planes of symmetry

7.1.3.2 Narrow Face Mold Wall

Specified temperature based on results of previous work [15] using a 1-D step-wise transient heat transfer model of the mold-gap-strand region is applied to the narrowface mold wall.

7.1.3.3 Wideface Mold Wall

A zero heat flux boundary condition is applied to the domain at the wideface. This condition is also an approximation because the actual boundary condition at the wideface should be the same as at the narrowface, which is one of specified nodal temperature. However, the zero flux boundary condition is used for two reasons. First, the simulation domain does not actually extend all the way to the wideface. The mold-strand gap and the meniscus region have been neglected. Thus the zero heat flux condition must be used to account for the fact that the domain has been truncated as such. The model is therefore not strictly valid for those regions very close to the wideface mold wall.

7.1.3.4 Flux-Steel Interface

The flux-steel interface is set at a typical steel liquidus temperature of 1550°C.

7.1.3.5 Top Surface of Flux

A mixed boundary condition is used at the top surface of the flux which is exposed to the atmosphere. Radiant heat loss is the predominant mode of heat transfer for this boundary. The reader is directed to section 4.1.3.5.2.

7.1.3.6 Solidifying Steel Shell

The steel liquidus temperature of 1550°C is also applied to this boundary.

7.1.3.7 Narrowface - Gap Outlet

See section 4.1.3.4.2.

7.2 STANDARD INPUT MATERIAL PROPERTIES

7.2.1 Viscosity

The general trends in and modeling of viscosity were discussed previously (see section 2.1.3.1). Presented in Figure 7.7 are the new viscosity-temperature input curves for base case runs. Here, a two material model is used to represent all three of the basic forms of the flux, i.e. powder, liquid and glassy solid. The curves were generated by combining the data obtained from the manufacturer (high temperature data only was available) with that obtained from the available literature for a flux of the same nominal composition [9]. Figure 7.6 illustrates which zones of the 3-D simulation domain are assigned the material types 1 and 2.

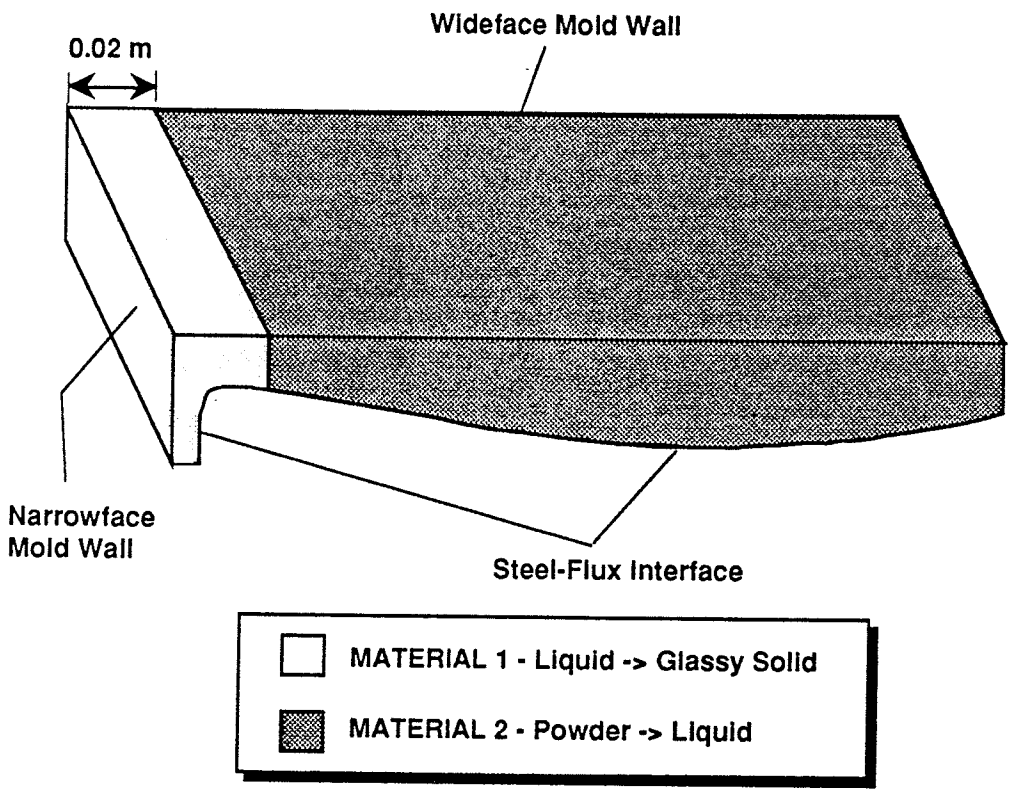

Figure 7.6 - Zones of 3-D Simulation Domain assigned Material Types 1 & 2

Of much interest is the characterization of the viscosity of the flux when it is in the powdered form. It is reasonable to think that the powder does have some resistance to shearing forces which would be analogous to fluid viscosity. The resistance is a type of internal friction between particles caused by static forces such as electrostatic attraction, Van der Waals forces and cpailllary forces as well as the dynamic forces due to particle motion[51]. Fortunately, many researchers in the field of fluidization, powder dynamics and pneumatic transport of particulate solid, agree with this postualtion and have been able to measure an apparent viscosity with standard instruments like the Brookfield, Concentric Cylinder or Stormer Viscometers[52-55].

Much of the past work in the field of fluidization, related to the viscosity of powders was summarized by Rietema[51]. Without delving into the underlying theory, it has been found that the viscosity of the powders is dependent on the particle size, bulk density, and fluidizing gas velocity. Based on these, and assuming a mean particle size of 250μm (actual for Chi-Vit powder flux varied between 200 and 325 μm), bulk density of 2500 kg/m^3 and minimal fluidization, the viscosity of the powder may reasonably be estimated at 0.1 - 0.4 Pa.s[51, 56, 57]

Material 1 (Mat1 in Figure 7.7) represents the behavior of the flux as it solidifies from the liquid form into the glassy solid form against the mold wall. The glassy form is totally immobile and it adheres to the mold wall. Hence the flux is given a large viscosity below the melting point for this material. In the liquid phase, the flux viscosity decrease with temperature, and the values used are those from an available reference [9].

Material 2 (Mat2 in Figure 7.7) represents the behavior of the flux during the sintering process, and then during subsequent melting. As the powder densifies with increasing temperature, the viscosity increases. Additionally, the melting of carbonaecous material around the same temperature further contributes to the increased viscosity, because of its "gummy" consistency at these temperatures. It should be noted that no literature containing viscosity measurements for the sintering and melting process was found. All researchers measured

viscosity as a funtion of decreasing temperature, i.e. during the solidification process from liquid to glass. The two processes of solidification and melting are not equivalent for this material.

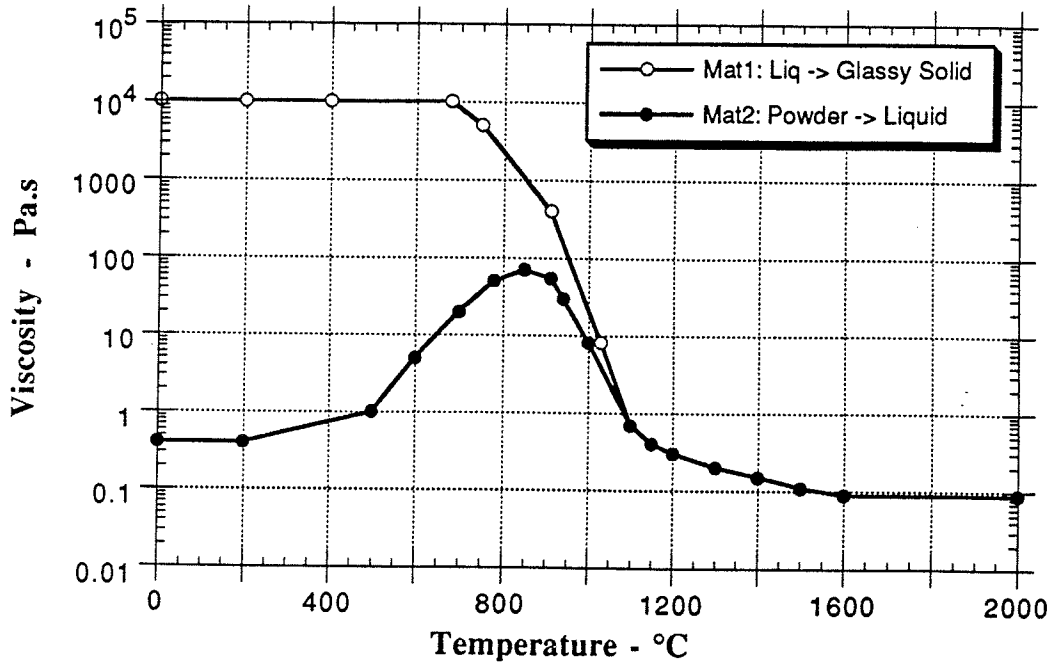

Figure 7.7 - Two Material Model for Viscosity used in 3D Numerical Model

Subesequent to the sintering process, the viscosity then decreases with increasing temperature above the melting point, as the liquid becomes more "runny". Above the melting point, when the flux is fully liquid, Materials 1 & 2 are identical.

7.2.2 Thermal Conductivity

Figure 7.8 shows the thermal conductivity curve used as input to the model for the base case. Two curves are given because it is necessary to use a two-material model to represent all three of the basic forms of the flux, i.e. powder, liquid and glassy solid. During the sintering process in which the powder consolidates, the thermal conductivity of the powder increases, as air spaces slowly disappear. At the melting point, there is a significant increase in the thermal conductivity due to the combined effects of radiation and conduction through the transparent liquid. Above the melting point, a constant value as reported in the literature [26, 27, 36] for

effective thermal conductivity is used. Below 900°C, the values for powder as reported by Taylor and Mills is used [2]. This behavior is represented by material 2 (Mat2 in Figure 7.8).

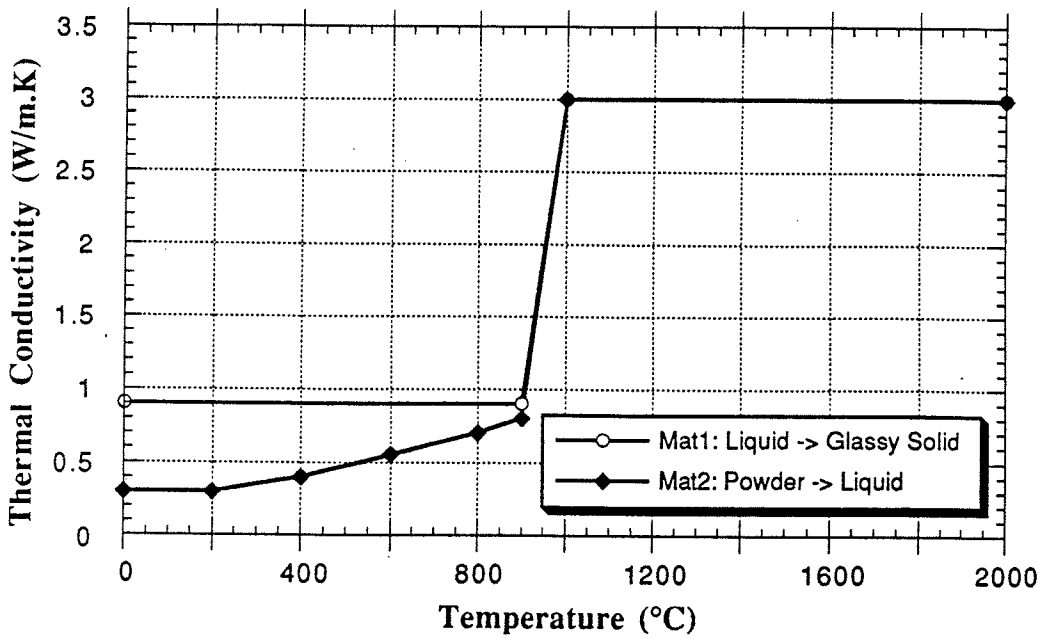

Figure 7.8 - Standard Thermal Conductivity - Temperature Input Curve, using a Two-Material Model

Material 1 (Mat1 in Figure 7.8) represents the behavior of the flux as it solidifies from the liquid to the solid glassy form. In this case there are simply two conductivity values used, one for the liquid state and one for the solidified glassy state, according to Taylor and Mills [2]and Nagata *et. al.* [33]. Nagata and Goto also showed that the value for solidifed flux is larger than for the powder on average. Hence the curve for Material1 in Figure 7.8.

7.3 SOLUTION METHODOLOGY

7.3.1 Method

As before, a three-step solution process is used to obtain the final solution of the coupled heat transfer and fluid flow problem. The first "run" is an isothermal one, the results of which are supplied as a flow field for an advection-diffusion analysis. In the advection-diffusion analysis, only the energy equation is solved. The isothermal flow pattern is assumed as the

constant flow field which contributes to the convective term in the energy equation. The temperature solution of this analysis, coupled with the isothermal flow field is used as an initial guess for the iterative solution of the non-linear, coupled thermal flow problem which this melting process is. The momentum equation is coupled to the energy equation through a temperature dependent viscosity, and the reverse coupling is through the convective term of the energy equation. Thus, continuity, momentum and energy balances must be simultaneously satisfied. The reader is directed to 4.18 for a graphical representation of this three-step process.

7.3.2 Solution Specifics

Obtaining a solution to a fully coupled three-dimensional problem presented several new challenges that were not encountered with the two dimensional model. With the addition of the third dimension, another degree of freedom was created. This posed significant implications on memory and storage requirements. Thus several models had to be created to test the limits of mesh refinement given the requirements of a plausible solution, efficient convergence, memory and fixed disk storage. That is, a sufficiently refined mesh has to be created to produce a good solution given the limitations of the available resources.

It became immediately apparent that the existing workstations, which include a 20 MHz Silicon Graphics IRIS 4D/25 with 64 MB of RAM and over 600MB of free space, were not capable of handling even the coarsest 3-D mesh. The problem had to be run solely on the CRAY Y-MP supercomputer. Pre- and post-processing was performed on the workstations.

7.3.2.1 Mesh Study

27-Node Isoparametric Brick elements were used to discretize the domain. These elements utilize quadratic interpolation for all degrees of freedom except pressure, for which the interpolation is linear. An early mesh study showed that the quadratic 2-D elements gave better results close to the narrowface wall than did the linear elements. In this region, the flow direction and velocity changes rapidly, and the fluid pressure increases rapidly.

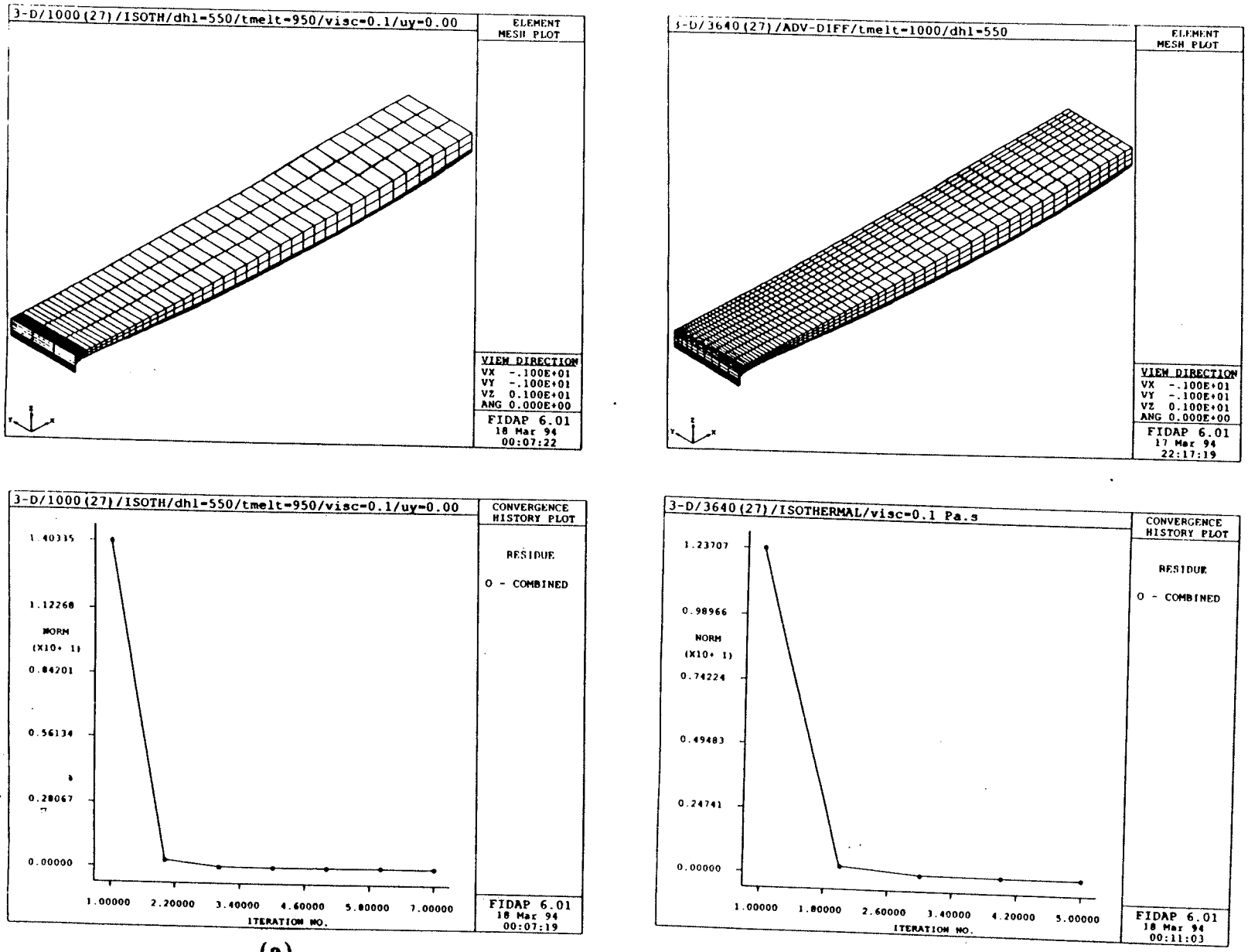

(a) (b)

Figure 7.9: (a) Coarse Mesh (1000 27-Node Quadratic Elements) and Convergence History (b) Finer Mesh (3640 27-Node Quadratic Elements) and Convergence History

Pressure is not independently discretized (or even solved for) when the linear elements are used and this may lead to the poor solution in regions where pressure is believed to be changing rapidly. However, this postulation was not rigorously verified.

The two major considerations when choosing a mesh density are:

(i) Can the mesh give a reasonable solution ?

(ii) What regions of the domain are rapid variations in field variables expected?

Wrapped up in these considerations are the other important issues of convergence and computational expense. Based on consideration (i) alone, a "suitable" mesh would be chosen if a converged solution is obtained using it. Considering only the isothermal model, a converged solution was obtained with only 7 iterations using a relatively coarse mesh of 1000 elements. This mesh has three elements in the thickness direction of the mold.

While convergence is obtained, the mesh is too coarse to reveal significant aspects of the flow, e.g. at the near wall region for the wideface. Secondly, it was postulated, and later found to be true, that the mesh is not sufficiently refined in directions in which significant gradients in temperature are expected to exist. For example, the z-dimension is the smallest (on average) and therefore conductive heat flux is expected to be largest in this direction. Additionally, large velocity gradients occur in this direction as well, because the flow reverses forming a recirculation zone. Thus, the convective term of the energy equation will be large, and significantly affect the convergence behavior of the thermal model.

Based on consideration (ii) above, the mesh was refined and graded (mesh size varies as the domain is traversed in one direction). Finally a mesh of 3640 elements was used. Figure 7.9 compares the convergence histories for the coarse and fine meshes. It can be seen that the finer mesh takes fewer iterations to attain the same level of convergence (relative error norm for residue = 1e-4) as the coarse mesh. There was a trade-off in the CPU time per iteration. On the CRAY Y-MP the coarse mesh took 240 CPU seconds while the finer takes 710 CPU seconds per

iteration. Additionally, the storage and memory requirement increased from 300MB and 2.7MW to 990 MB and 7.2MW in going from the coarse to the fine mesh. It must be emphasized that many mesh densities in between the two shown in Figure 7.9 were used. All were discarded because of convergence difficulties with the thermal model (even the advection-diffusion one).

7.3.2.2 Convergence Criteria

Reduction of the relative error norm for the residue is used as the criterion for convergence rather than relative error in the primitive variable (e.g. temperature, T). This former parameter is used because it produces a more reliable indication of convergence, given that the problem is highly nonlinear. That is, it is entirely possible for the relative error in T to be small while the relative error in the residue remains large due to the latter's dependence on the material functions used as input. Such a situation occurs frequently, and observations of the solution verify the fact that the model is indeed not converged.

Thus, a model is considered to be converged when the relative error norm for the residue is reduced to some small value, or when it has been reduced by several orders of magnitude. The latter criterion is dependent on the appearance of the actual solution. If there is no significant change in the solution (e.g. velocity vectors) as further iterations are performed, the solution process is stopped and the model considered converged. This criterion is used mainly to reduce the computational expense associated with further iteration. Thus different convergence tolerances are used for different models, depending on computing expense, as shown in Table 7.1.

7.3.2.3 Computational Requirements

It is important to note that all computational requirements quoted thus far are required when the direct solver of the code is used. With the direct solver, a large portion of the global stiffness matrix consisting of and the full column vector of nodal variables is utilized. The direct resolution of these coupled nodal equations requires tremendous storage requirements and CPU time.

However, another method to solve the large system of linear equations is to use a segregated solver. This solver decouples the nodal equations, such that each can be solved independently. Only a small portion of the global stiffness matrix is stored and overall CPU times per iteration are drastically reduced. The drawback is that many times more iterations are required than for the direct solver. Typically anywhere from 200 to 400 iterations would be required to reach the same level of convergence. This assertion was tested with the isothermal model. Using the segregated solver, the CPU time for the fine mesh was reduced to 48 CPU seconds. However, there was scarcely any change in the residual after 10 iterations. Assuming that a minimum of 100 iterations (very conservative) would be required to reach the same level of convergence, the total solution time for the segregated solver would be 4800 CPU seconds vs. 3500 CPU seconds for the direct solver. Thus, only if disk space limitations became critical would the segregated solver be employed in this case.

TABLE 7.1 - Solution Times the 3-D Coupled Model

Problem Type	Relaxation Factor	Residual Convergence Tolerance	Disk Space (MB)	Total Number of Iterations	Total Solution Time (CPUs)†
Isothermal	None	0.001	990	5	3500
Adv-Diff	0.6	0.01	59	110	4320
Coupled	0.7	0.1	1,800	45	67,500

† *CPU - seconds on the CRAY Y-MP*

Based on the test with the isothermal model, it was decided that employment of the direct solver was the most efficient choice for this problem and final mesh density. Using the direct solver, the times recorded in Table 7.1 were obtained using successive substitution.

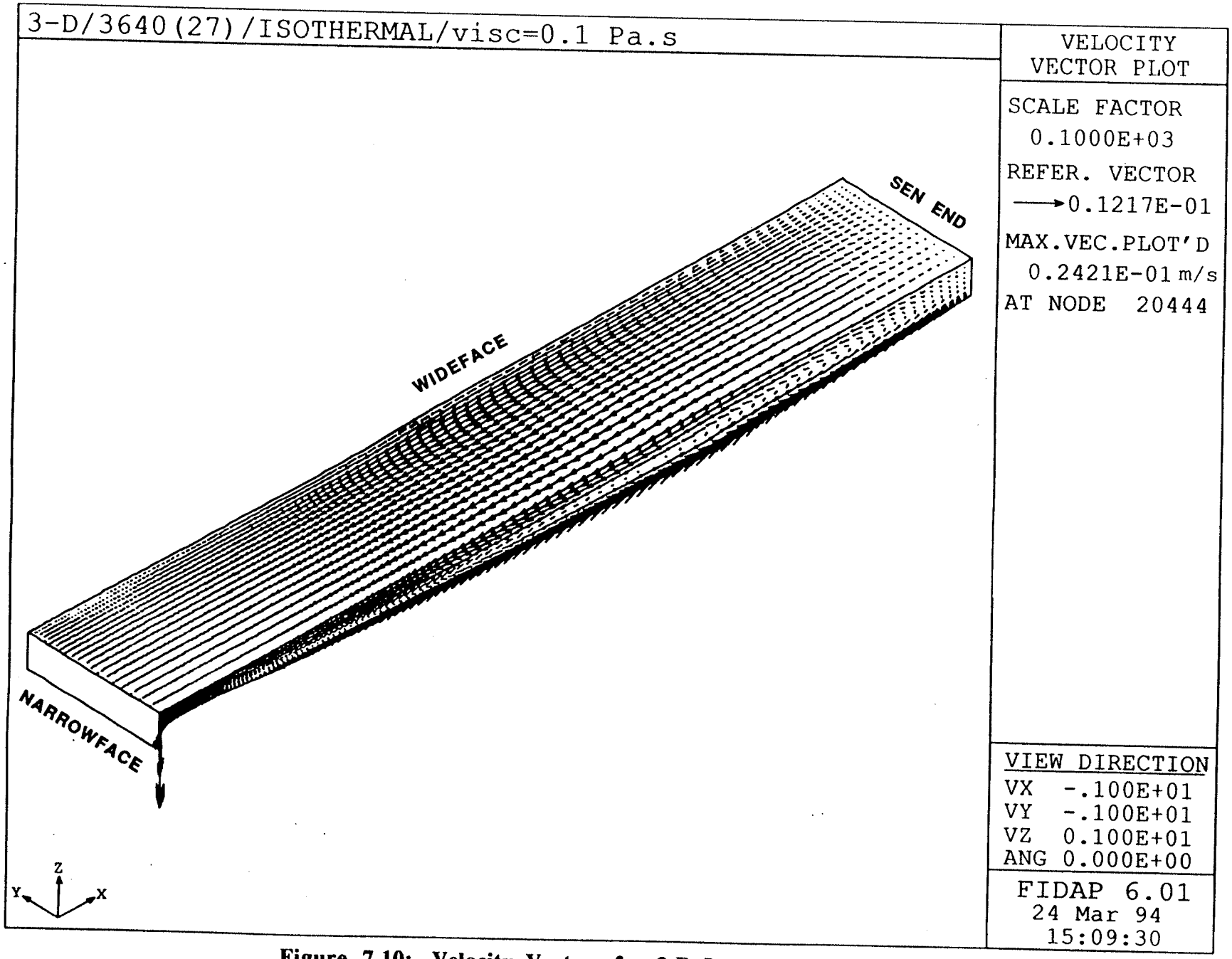

Figure 7.10: Velocity Vectors for 3-D Isothermal Flow

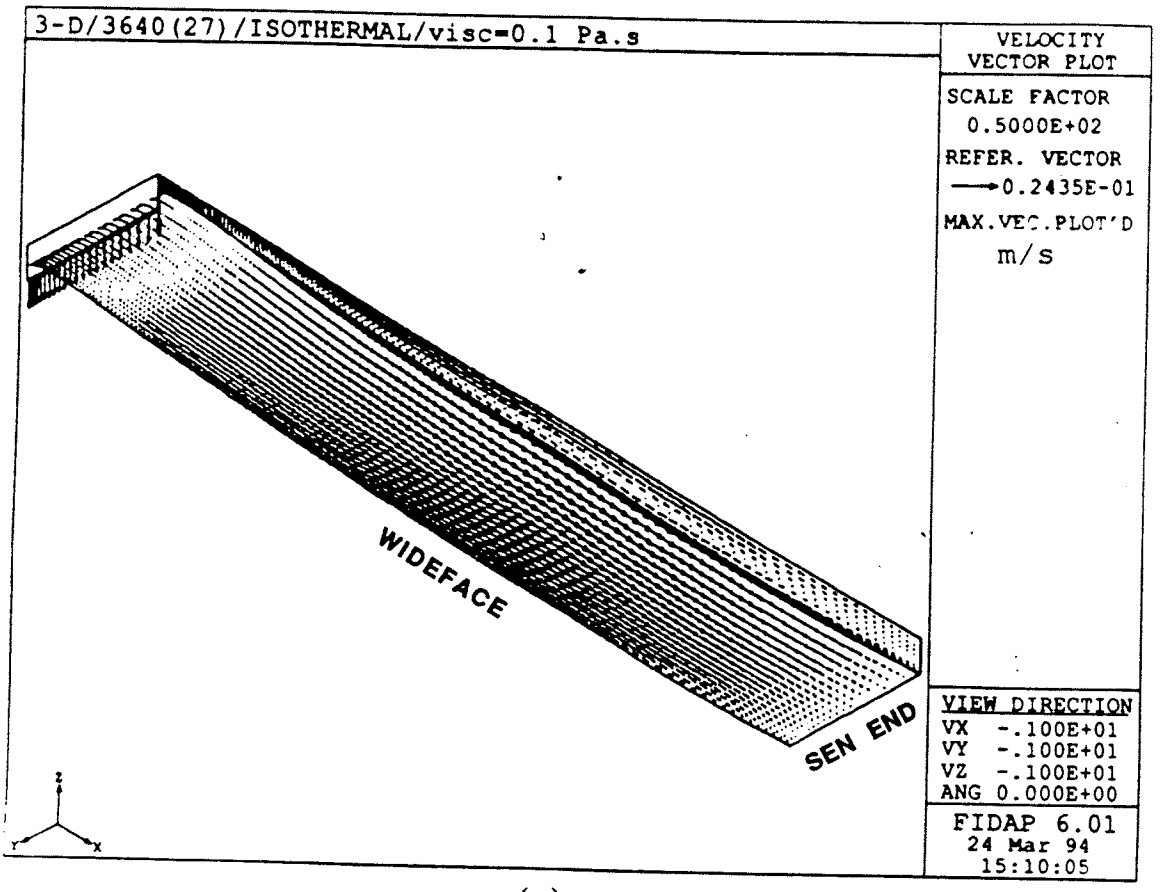

(a)

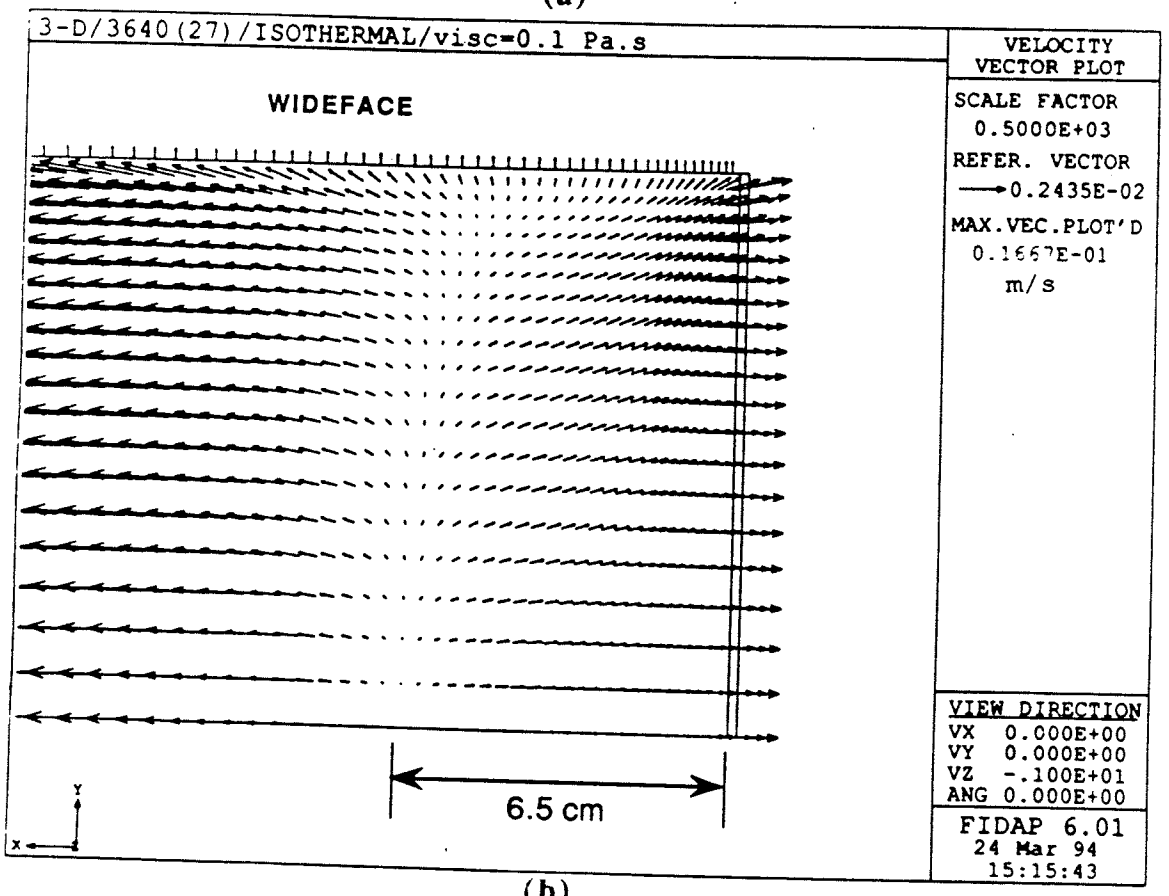

(b)

Figure 7.11: (a) 3-D Isothermal Velocity Vectors (underside view)
(b) Flow Separation in Near-Meniscus Region at Flux/Steel Interface

7.4 RESULTS

At each step of the solution process, results are produced which are themselves solutions of particular models. Each of these individual models, except the last, are incomplete, in that they do not give the entire picture, nor do they incorporate all of the relevant phenomena. However, it is interesting to note the changes which take place when the model goes from being uncoupled to coupled. For this reason the results of the isothermal flow model and the advection-diffusion problem are presented before those for the final model, in which fluid flow and heat transfer are fully coupled.

7.4.1 Isothermal Model

7.4.1.1 Flow Pattern

The flow field given by the isothermal model is used as an initial guess of the flow field for the fully coupled problem. The model simulates the flow of a homogeneous, isotropic medium, with a viscosity of 0.1 Pa.s and density of 2500 kg/m^3, being driven mainly by the shear stress boundary condition at the flux/steel interface. The viscosity was chosen to be close to the value that the liquid flux would have at the interface with the steel.

Figure 7.10 shows the isothermal flow field. Several effects are evident. The first major feature of the flow field is the large recirculation zone formed. Fluid is driven towards the center of the mold (SEN end) under the action of the steel at the flux/steel interface. Additionally, mass attempts to leave, mainly, at the mold-strand gap at the narrowface, under the action of the moving steel shell. These two flows are counter-current, and they result in the strong recirculation zone formed.

Secondly, the applied shear stress at the flux/steel interface increases gradually from zero at the mold-stand gap, to its maximum value at around 0.3 m from the meniscus, while the shear stress developed by fluid flowing into the gap increases as the gap is approached. The stress developed in the leaving fluid acts in the negative x-direction at the steel-flux interface. As a

result, there is a point at which the applied shear stress is balanced by the fluid stress, such that the resultant shear stress in the x-direction is zero. At this location, the driving force on the fluid is provided by the mass flow to the wideface in the y-direction. This results in a distinct flow towards the wideface, over the entire mold width at the flux steel interface (see Figures 7.11(a) & 7.11(b)). The separation in the flow that occurs at this location, produces interesting effects in the temperature distribution, which will be illustrated later. For the case shown, the separation location is approximately 6.5 cm from the meniscus (see Figure 7.11(b)).

7.4.2 3-D Advection-Diffusion Model

The advection-diffusion model produces a thermal solution assuming that the supplied flow field from the isothermal model remains constant in time. Following are the results of the model for temperature distribution and heat flux.

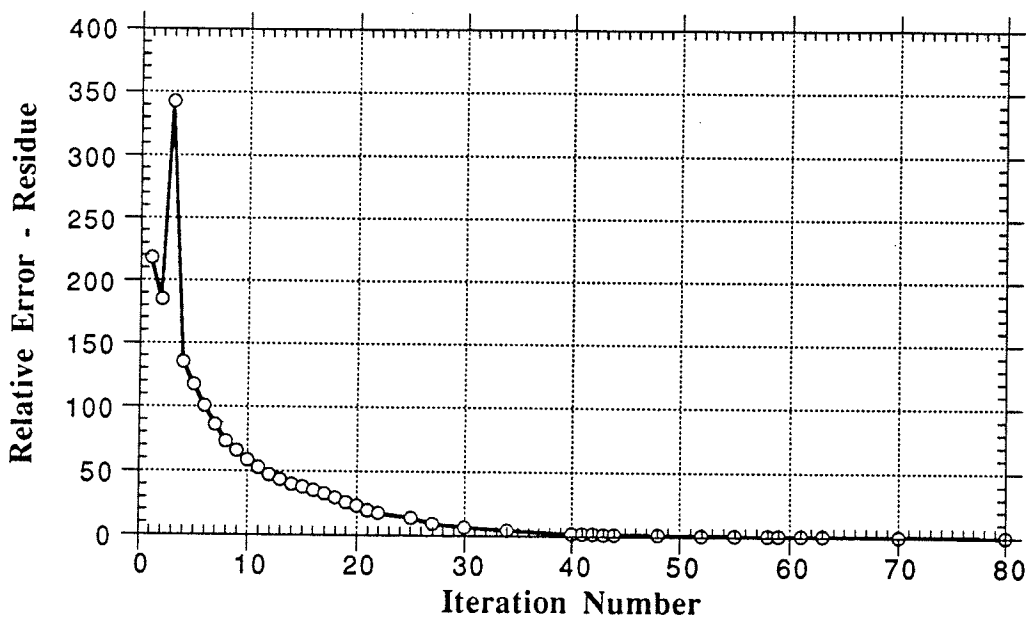

Figure 7.12 - Convergence History for the Advection-Diffusion Problem

7.4.2.1 Temperature Distribution & Heat Flux

Figure 7.12 shows the convergence history for the model. The model is solved directly using successive substitution. Here, the use of under-relaxation is justified; the proof being the convergence history. There was a sharp jump in the relative error norm at the third iteration (see Figure 7.12). If there was no under-relaxation, the fourth iteration could easily have been worse.

The relaxation factor forced the solver to rely more heavily on the previous iteration (in this case iteration 2) when it chose a value for the linearization of the equations before it solved for the fourth iterate. In this way convergence behavior was controlled.

Figure 7.13 shows the temperature contours for the (uncoupled) advection-diffusion problem. Convection currents in the recirculation zone carry hot material at the flux/steel interface up towards the upper surface of the domain. Thus, fairly high temperatures (871 - 1100 °C) develop at the exposed surface of the flux. The surface temperature decreases as the narrowface is approached for two reasons. Firstly, heat is carried away towards the SEN by the convective currents of the main recirculation zone. Secondly, hot material which is delivered to the surface of the domain cools by radiative and convective heat transfer, as it moves towards the narrowface.

An interesting feature in the temperature distribution is the cool region which is developed close to the meniscus. Figure 7.13 (b) gives an enlarged view of this region. Temperature contour "C" represents 419°C, and in Figure 7.13(b) this contour pushes inwards towards the wideface. Additionally, temperature contour "D" which represents the higher temperature of 484°C is observed on either side of the "C" contours. Thus, the temperature does not increase monotonically with distance from the narrowface. Instead there is a dip in the temperature which spatially coincides with the separation in flow at the steel/flux interface (Figure 7.11).

This feature may be the result of the two competing effects of conduction and convection. In the near-meniscus region, the predominant mode of heat transfer in the z-direction is by conduction through the flux. However, hot material is removed continuously towards the wideface, and at the separation point, this flow has the most pronounced effect. Therefore, at the separation point, and close to the wideface, heat is being removed by convection to the wideface faster than it is being conducted up to the surface.

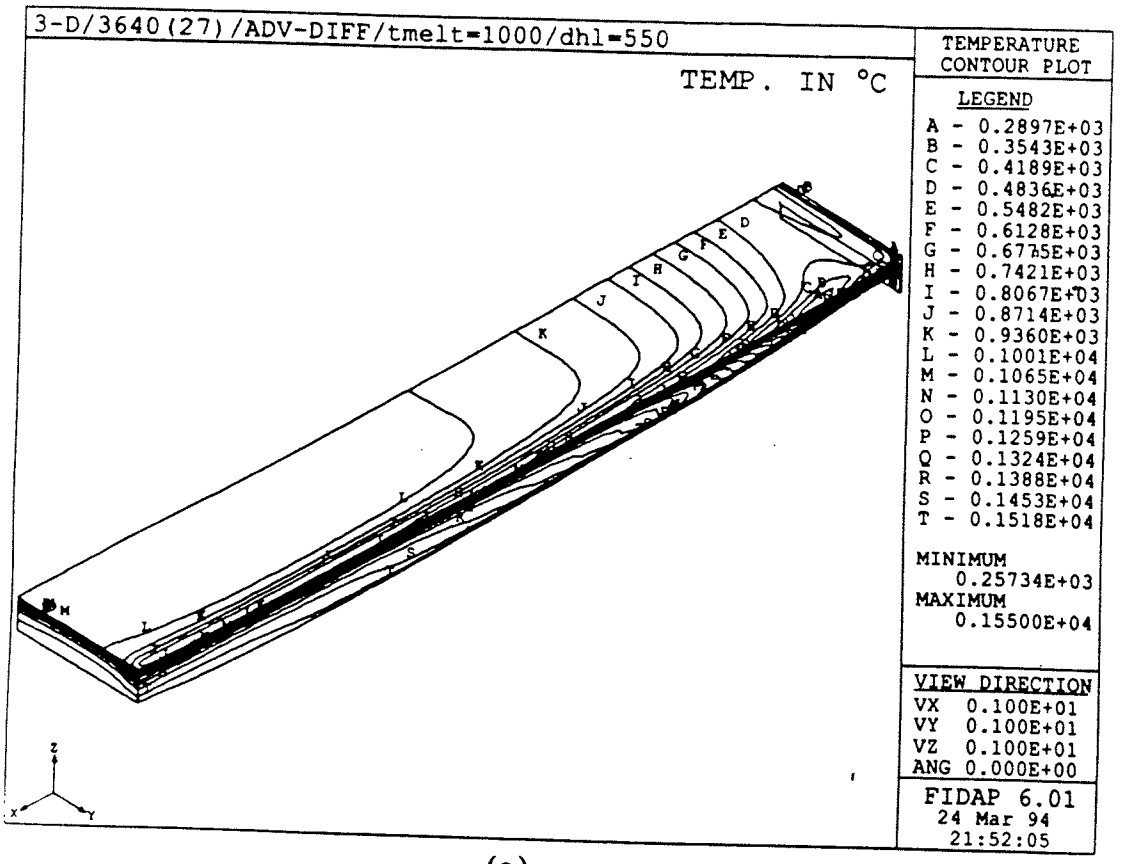

(a)

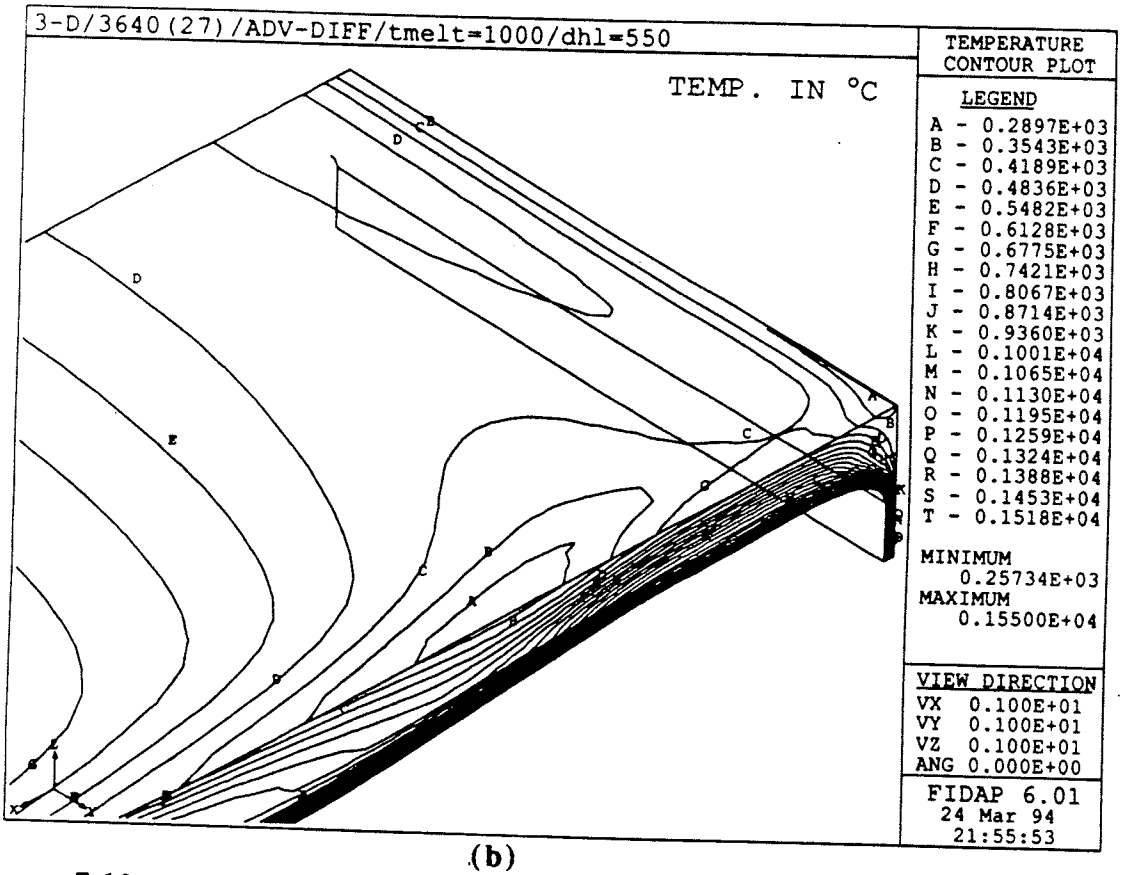

(b)

Figure 7.13: (a) Temperature Contours for 3-D Advection-Diffusion Problem
(b) Enlargement of Near-Mensicus Region (Temperature Distribution)

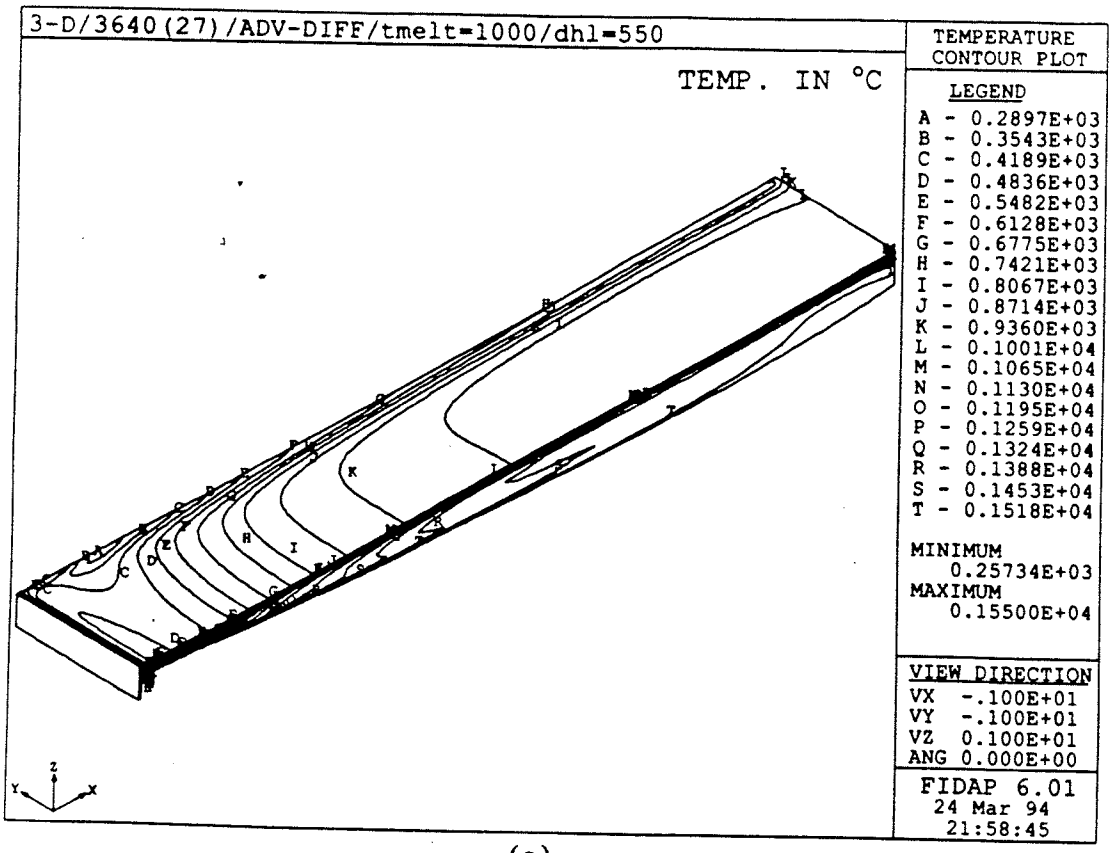

(a)

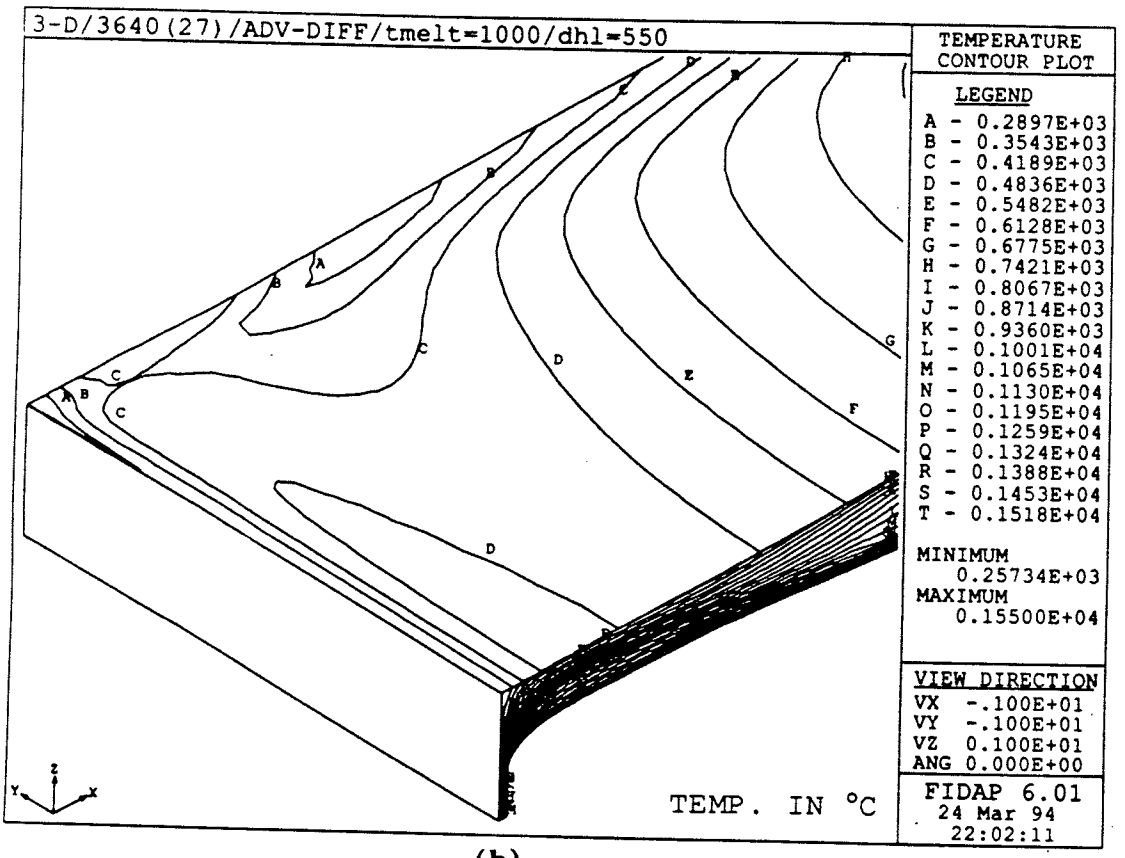

(b)

Figure 7.14: (a) Temperature Contours for 3-D Advection-Diffusion Problem
(b) Enlargement of Near-Mensicus Region (Temperature Distribution)

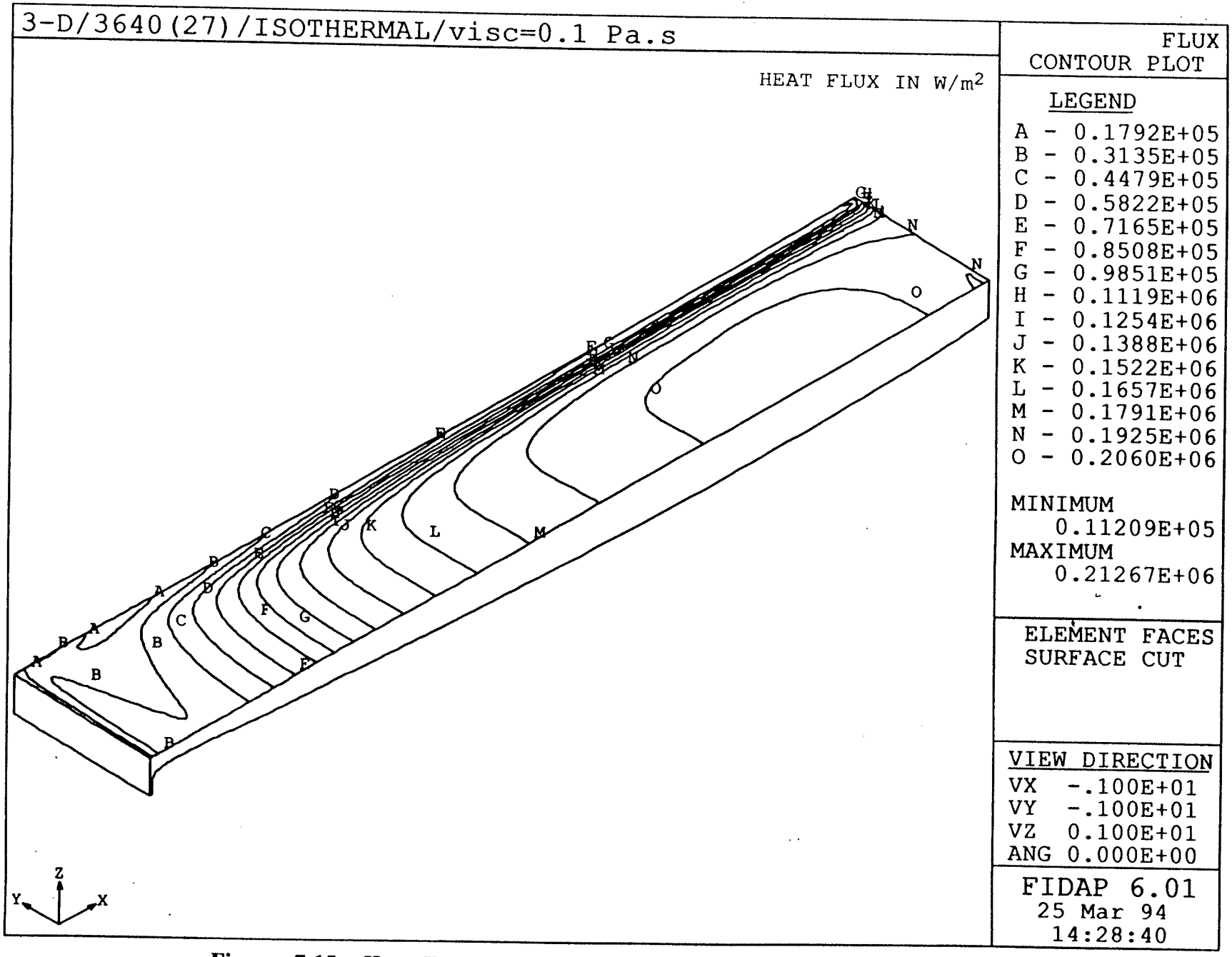

Figure 7.15: Heat Flux Contours for 3-D Advection-Diffusion Problem

Figures 7.14 (a) & (b) are the temperature contours as viewed in the positive y-direction, i.e. from the plane of symmetry to the wideface. Figure 7.15 are the heat flux contours as viewed from the same direction. It can be seen that the magnitude of the heat flux follows patterns similar to the temperature, with the maximum heat flux of 206,000 W/m^2 leaving the top surface of the flux (see flux contour "O" in Figure 7.15).

7.4.3 Coupled Model

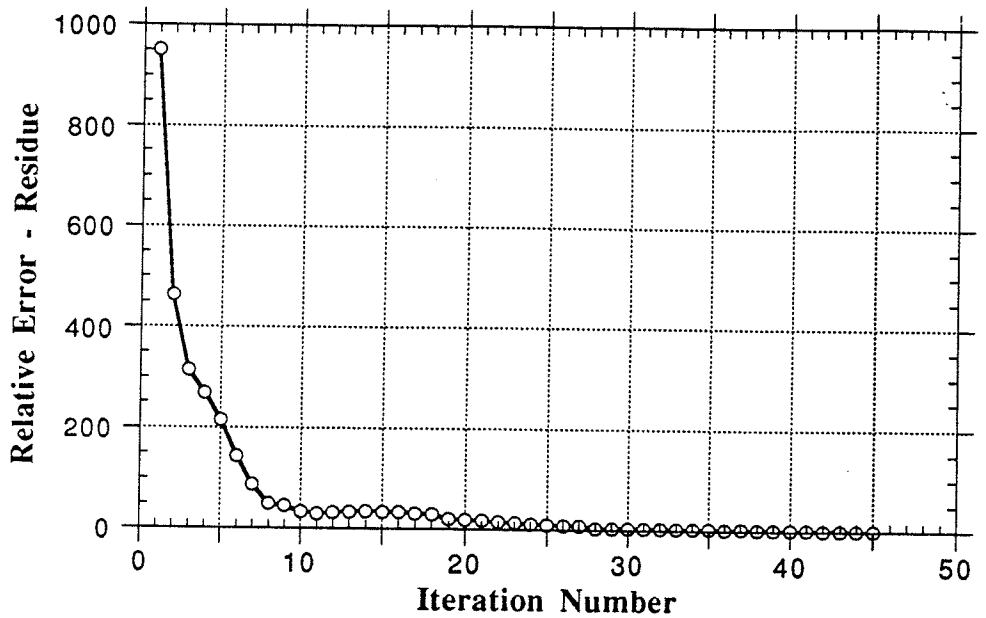

Figure 7.16 - Convergence History for Weakly Coupled Problem

In the weakly-coupled model, the temperature dependence of viscosity is incorporated and the mass, momentum and energy equations are solved in a coupled fashion. It is important to note that it is assumed that the viscosity of the flux is a function of temperature and composition only, and not of strain rate. The effect of temperature on density is ignored in this model.

The convergence history for this model is given in Figure 7.16. The norm of the residue is reduced by three orders of magnitude in 45 iterations. Convergence was not as efficient as in

the previous two 3-D models presented. Two relaxation factors of 0.6 (initial) and 0.7 (final) were used.

7.4.3.1 Flow Pattern

Many of the features of the isothermal flow pattern are evident in the coupled model as well. The presence of a large recirculation zone is evident. However, the extent of the zone is diminished. For example the clearly evident parabolic profile of velocity at the top surface of the flux is now muted due to the higher flux viscosity at the walls. Figure 7.17 shows the overall velocity vector plot for the coupled model. Figure 7.18(a) compares the velocity at the top surface of the flux as a function of orthogonal distance from the wideface wall for the isothermal and coupled models. Not only has the average velocity decresed significantly (from an average of 0.01 to 0.002), but the gradient of velocity between the wideface wall and the center symmetry plane is decresed as a result of the coupling of viscosity and temperature.

Figure 7.18(b) compares the top surface velocity as a function of orthogonal distance from the narrowface wall for the isothermal and coupled models. This figure also shows the reduction in velocity in the range of 0 - 0.56 m from the narrowface wall due to the coupling. Finally, Figure 7.19 compares the flow patterns in the meniscus region for the isothermal and coupled models. The compression of the recirculation zone (from a thickness of 37 mm to 8 mm at a distance of 130 mm from the narrowface wall) and reduction of velocity when viscosity is made to vary with temperature, is clearly evident.

The average flux residence time in the mold, based on the consumption rate to the wideface is approximately 112 s, or roughly 2 minutes. The mass of the flux in the recirculating zone is *estimated* to be equal to 3.65 kg. The reader is directed to appendix B for the details of the calculations of these values.

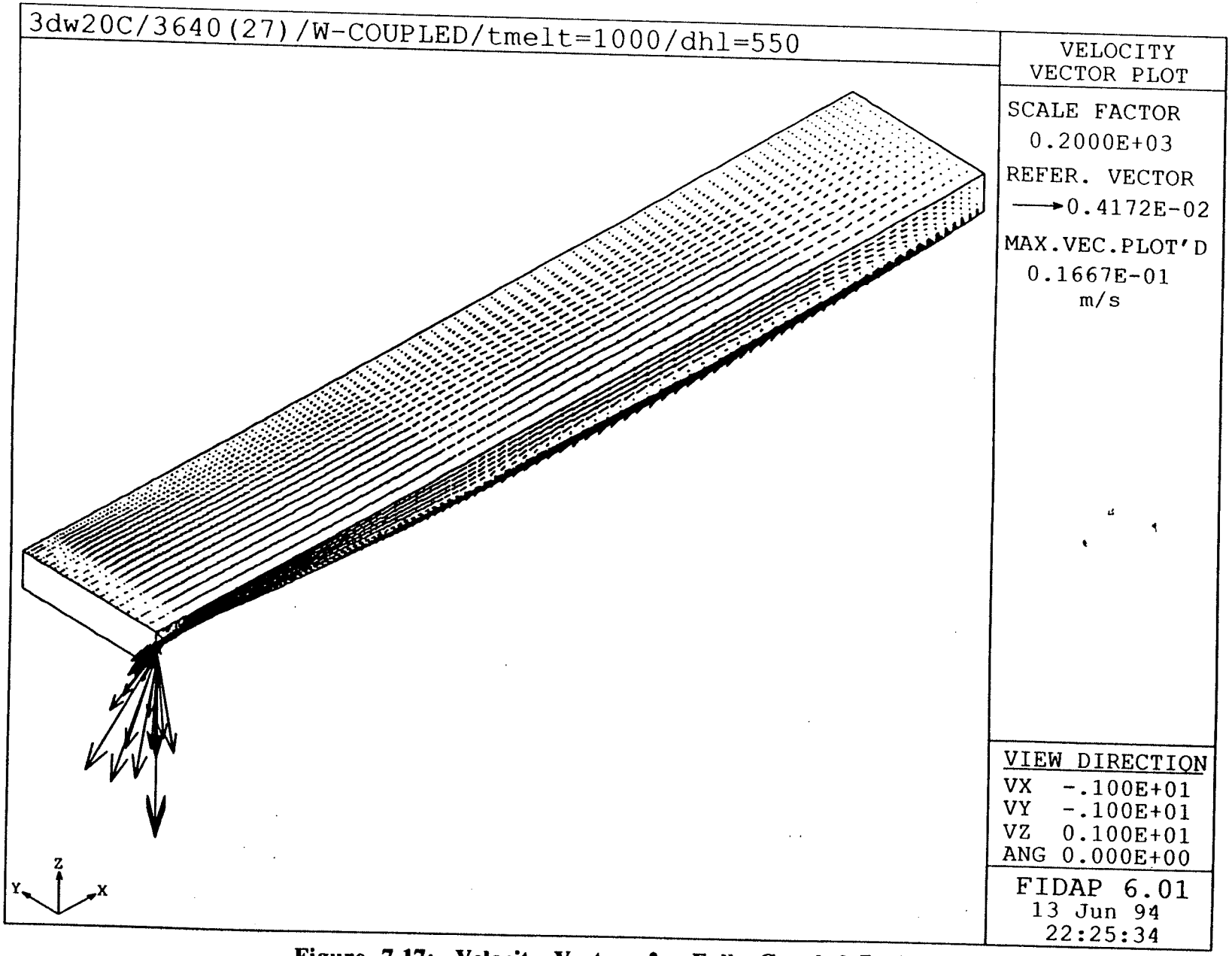

Figure 7.17: Velocity Vectors for Fully Coupled Problem

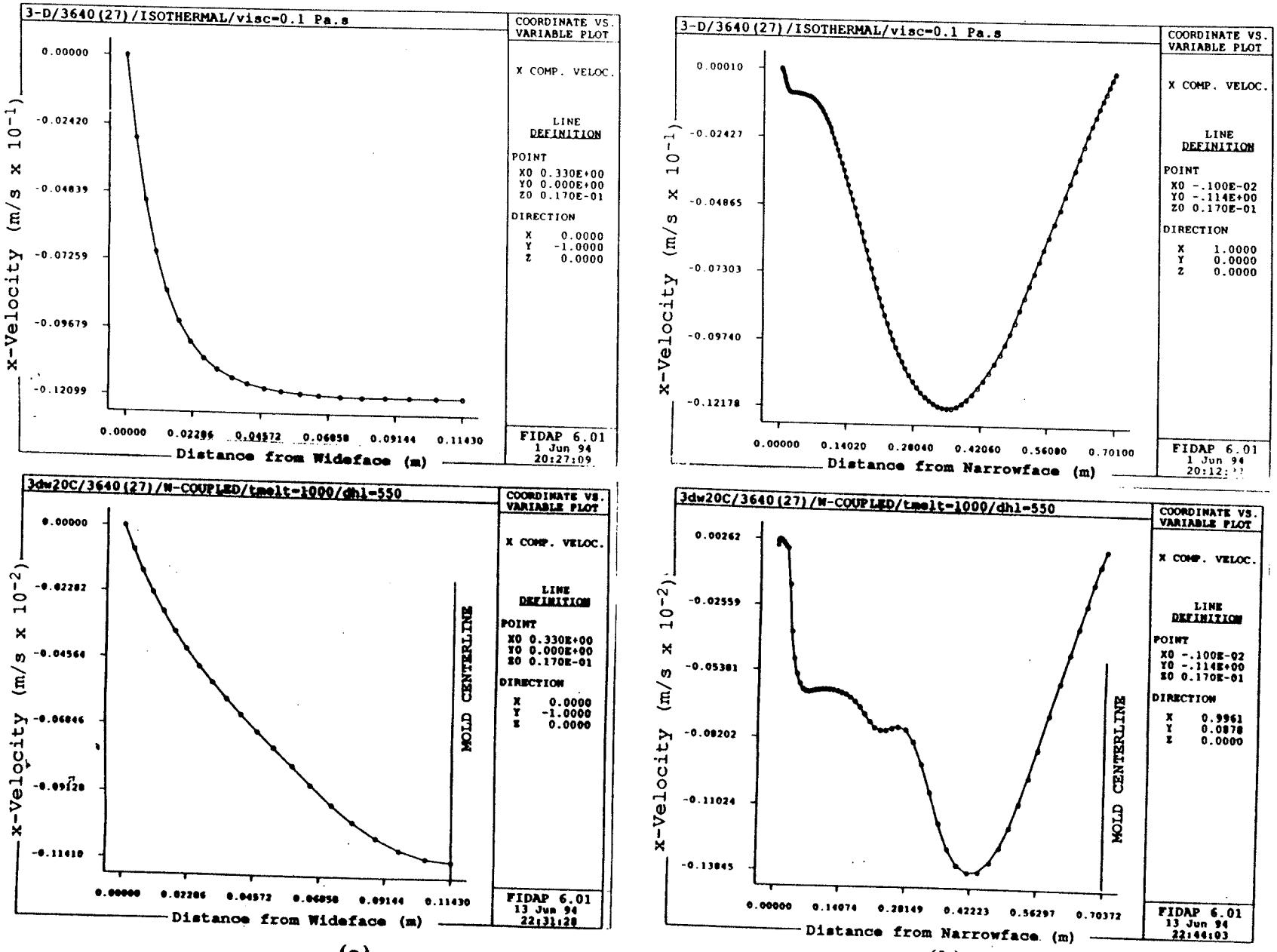

(a) (b)

Figure 7.18: (a) Typical Top Surface Velocity in Mold Thickness Direction for Isothermal and Coupled Flow
(b) Typical Top Surface Velocity in Mold Width Direction for Isothermal and Coupled Flow

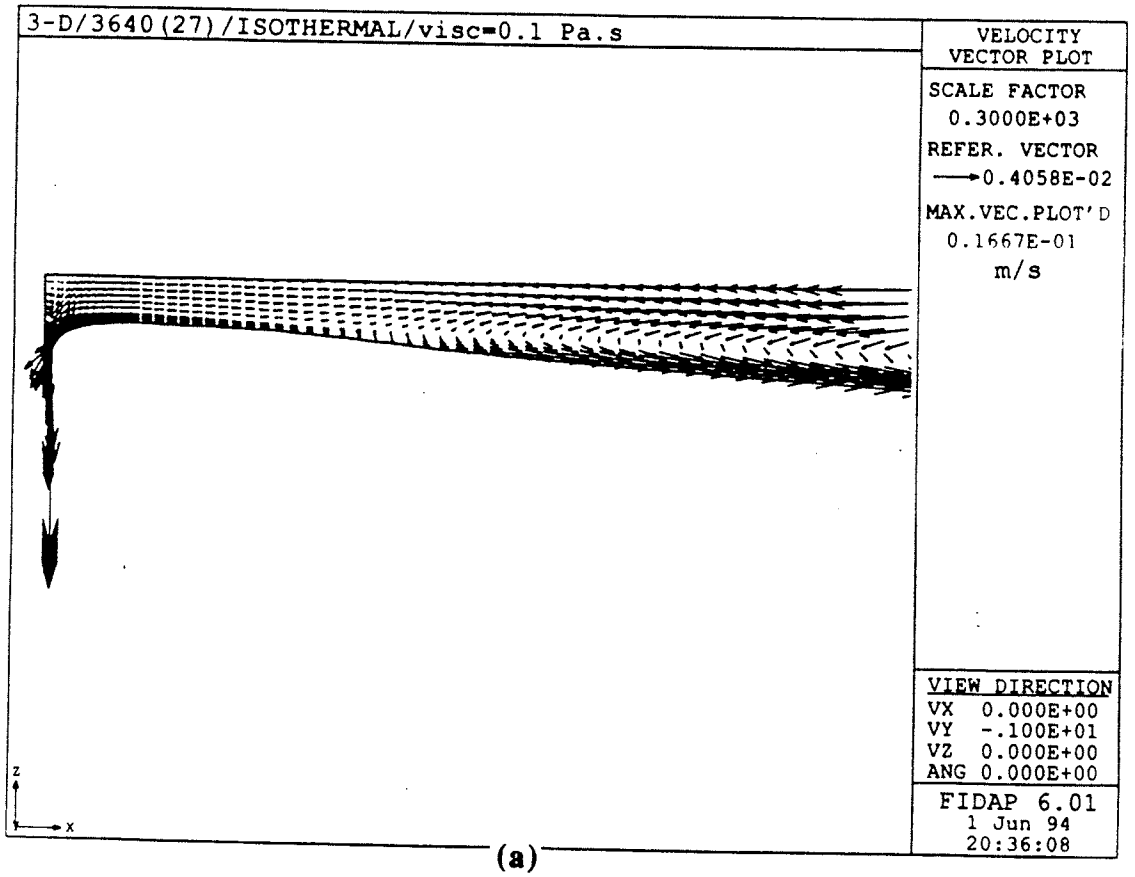

(a)

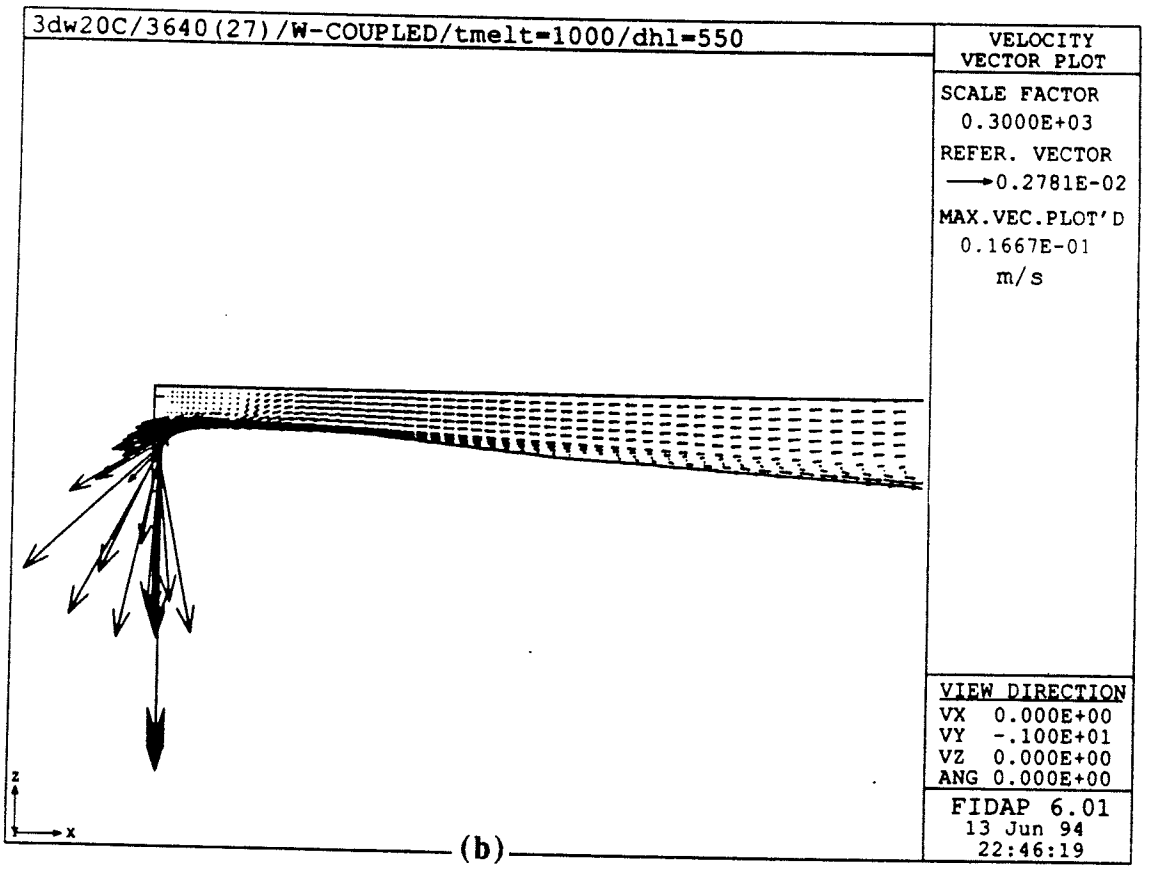

(b)

Figure 7.19: (a) Velocity Distribution in Meniscus Region for Isothermal Flow
(b) Velocity Distribution in Meniscus Region for Coupled Flow

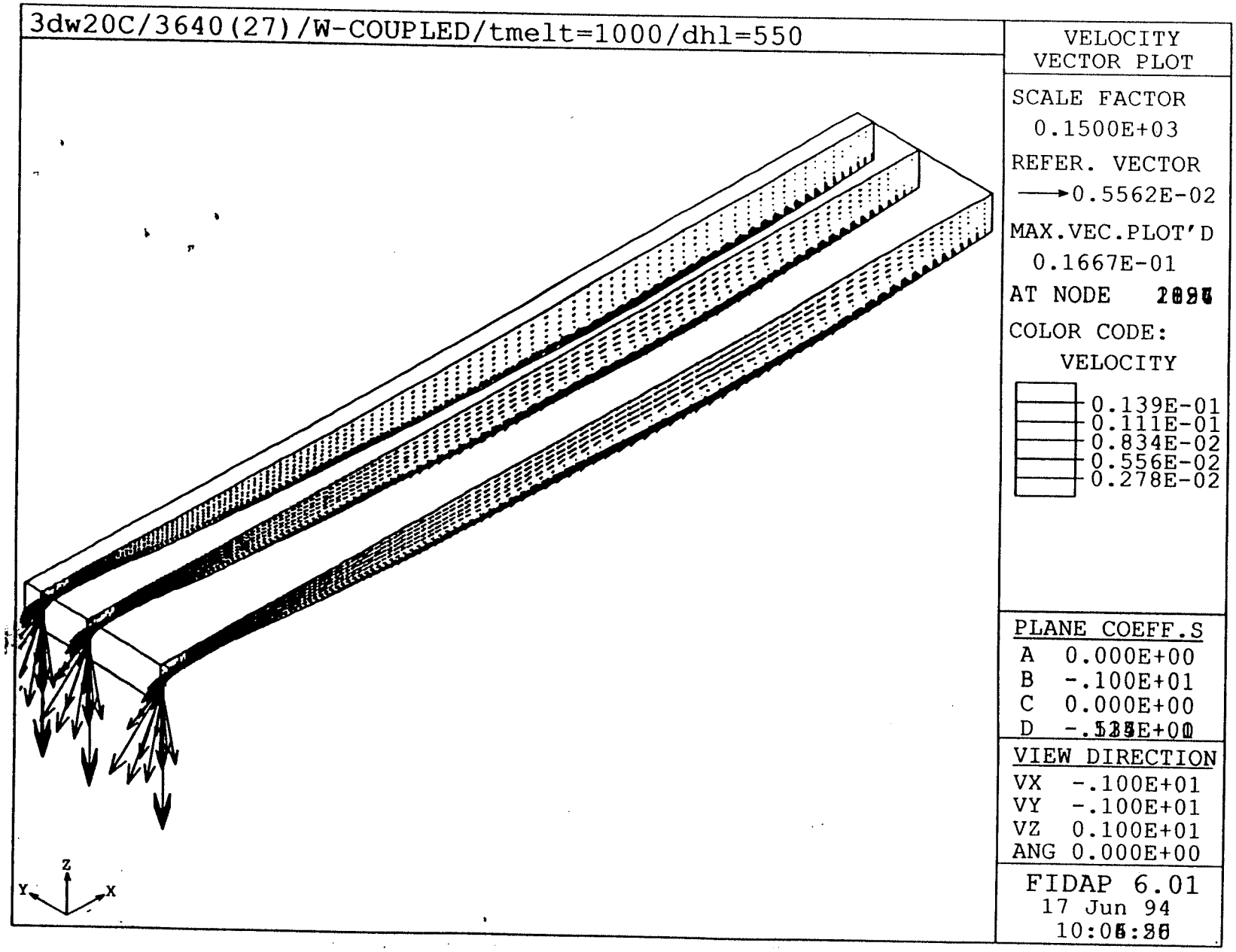

Figure 7.20: Velocity Vectors for Fully Coupled Problem at 3 Locations across the Mold

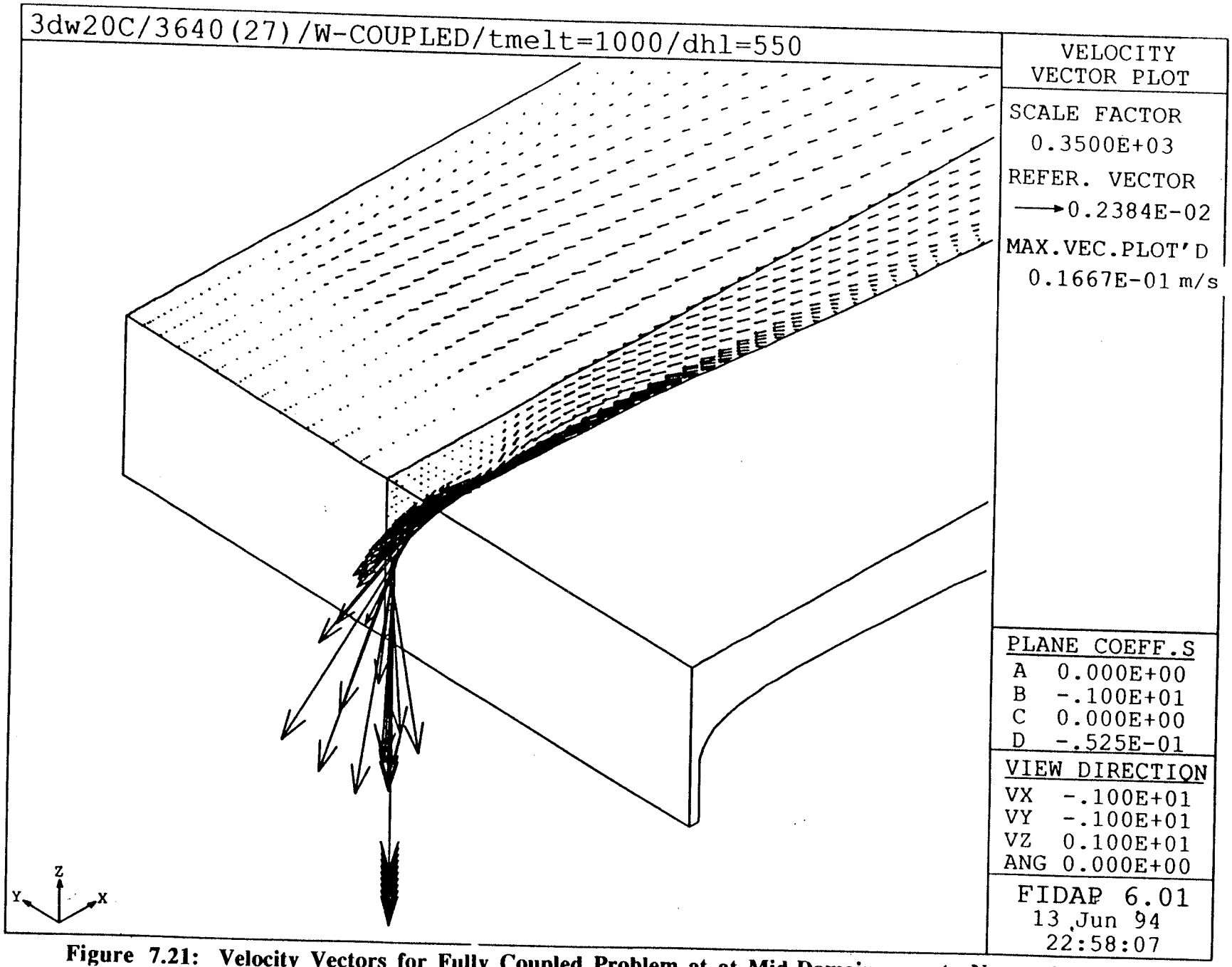

Figure 7.21: Velocity Vectors for Fully Coupled Problem at at Mid-Domain near to Narrowface

Figure 7.20 shows the velocity fields at three different locations across the thickness of the mold. The influence of the consumption cross flow in the positive y-direction is relatively small, as indicated by the small out-of-plane component of velocity in the fluid close to the flux-steel interface.

An examination of the temperature field will explain the reduction of velocity in the regions of the top surface of the flux and close to the meniscus. Lower temperatures in these locations results in higer viscosities according to the material models used. Hence the lower velocities. It is not possible to predict these viscosity variations before hand, because the thermal solution is obtained simultaneously with the flow solution. Figure 7.21 shows an enlarged view of the meniscus region at mid-domain. A solid flux rim is evident. Liquid and some powdered flux squeeze past the rim to flow into the gap. Because the fluid is incompressible, the material accelerates as it flows under the rim, due to the reduction in the cross section of the flow path.

7.4.3.2 Temperature Distribution and Heat Flux

Figure 7.22 gives the overall temperature distribution. It is evident from this plot that the cool surface temperature propagates further into the domain away from the wideface in comparison with the advection-diffusion problem. This is due to the compression in the recirculation zone in the neighborhood of the wideface. Because the zone is smaller, the amount of heat delivered to the surface by hot fluid moving from the flux-steel interface, is less.

This large cold region close to the meniscus, that extends for the entire thickness of the mold, is probably due to the significant amount of heat removed by cross flow to the wideface. As mentioned previously, the imposed consumption velocity is comparable to the x-direction velocity close to the narrowface. Thus, convective removal of heat to the wideface is most significant in this region. Figures 7.23 (a) and (b) illustrate the location of the liquid-solid interface for the flux as the 1000°C isotherm. Figure 7.23 (b) shows that, in general there is less liquid close to the wideface than at the mid-plane. Figure 7.24 gives the total heat flux leaving the top surface.

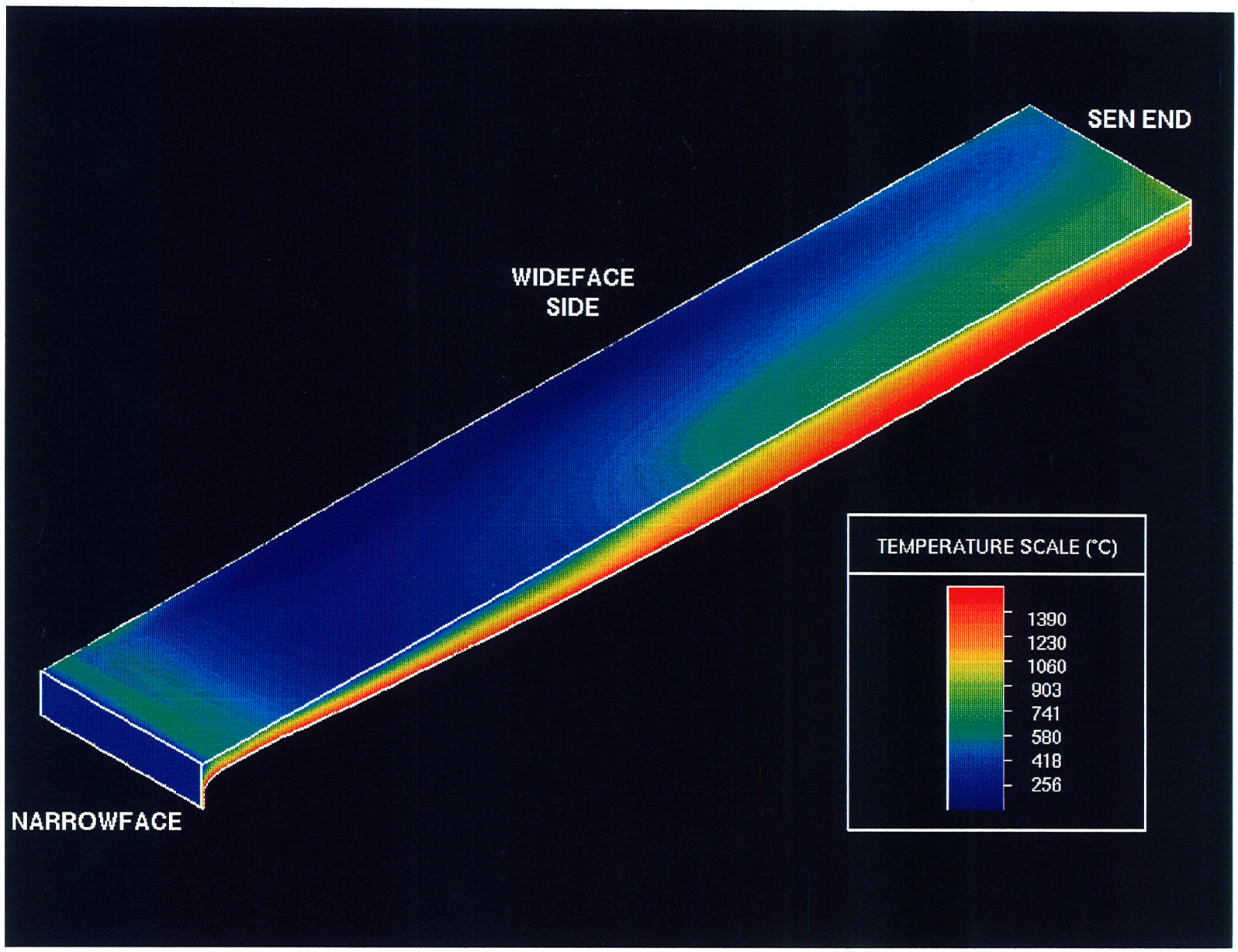

Figure 7.22: Temperature Distribution for Fully-Coupled Problem

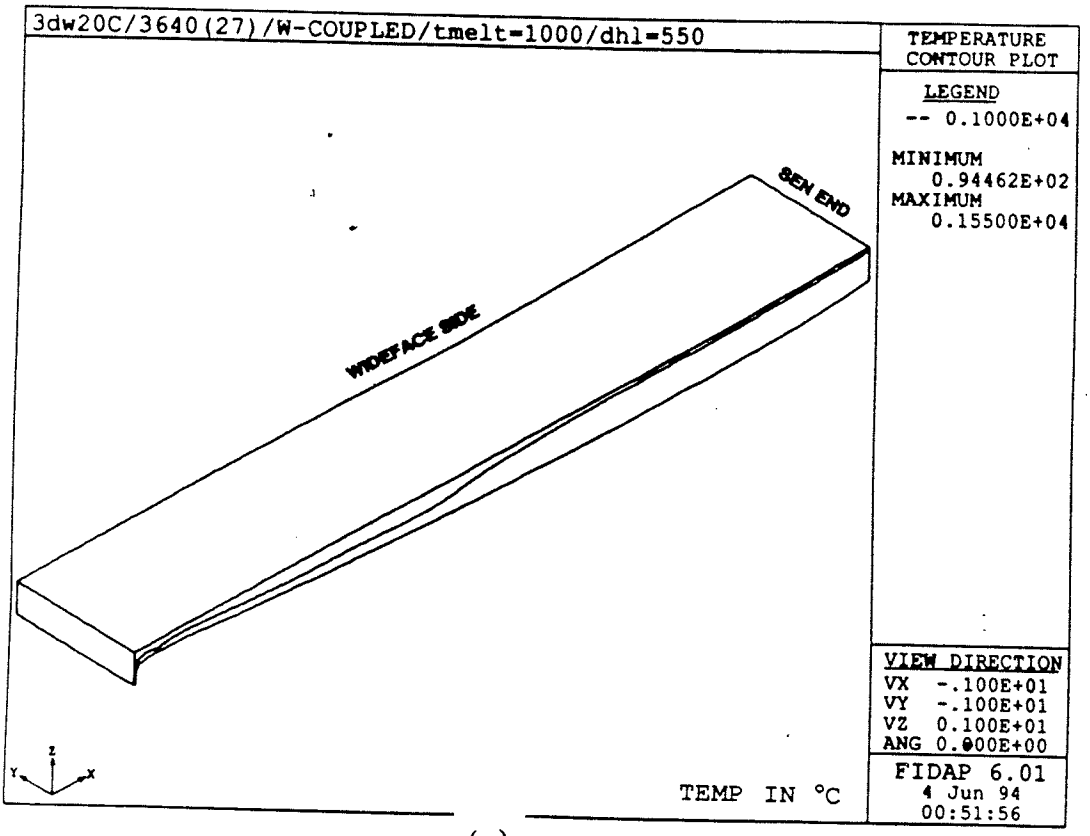

(a)

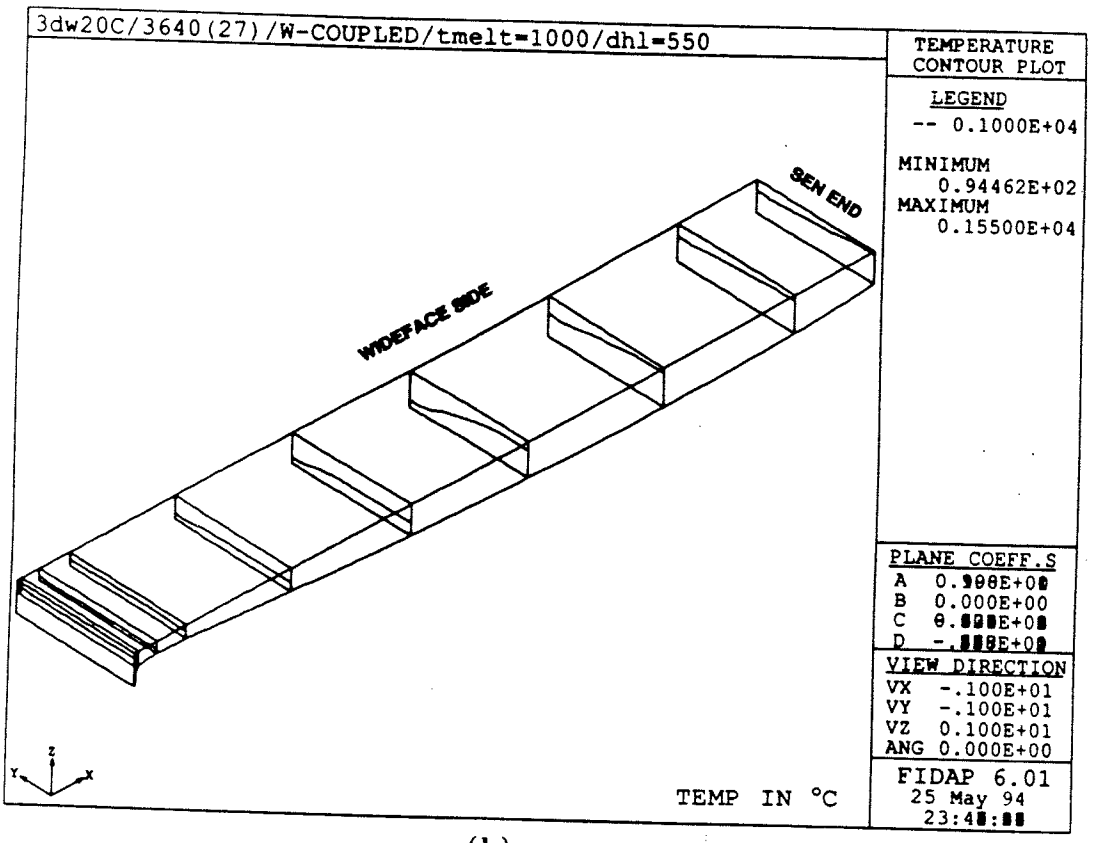

(b)

Figure 7.23: (a) Overall View of Flux Melt Interface
(b) Flux Melt Interface (1000°C contour) at Several Locations in the Mold

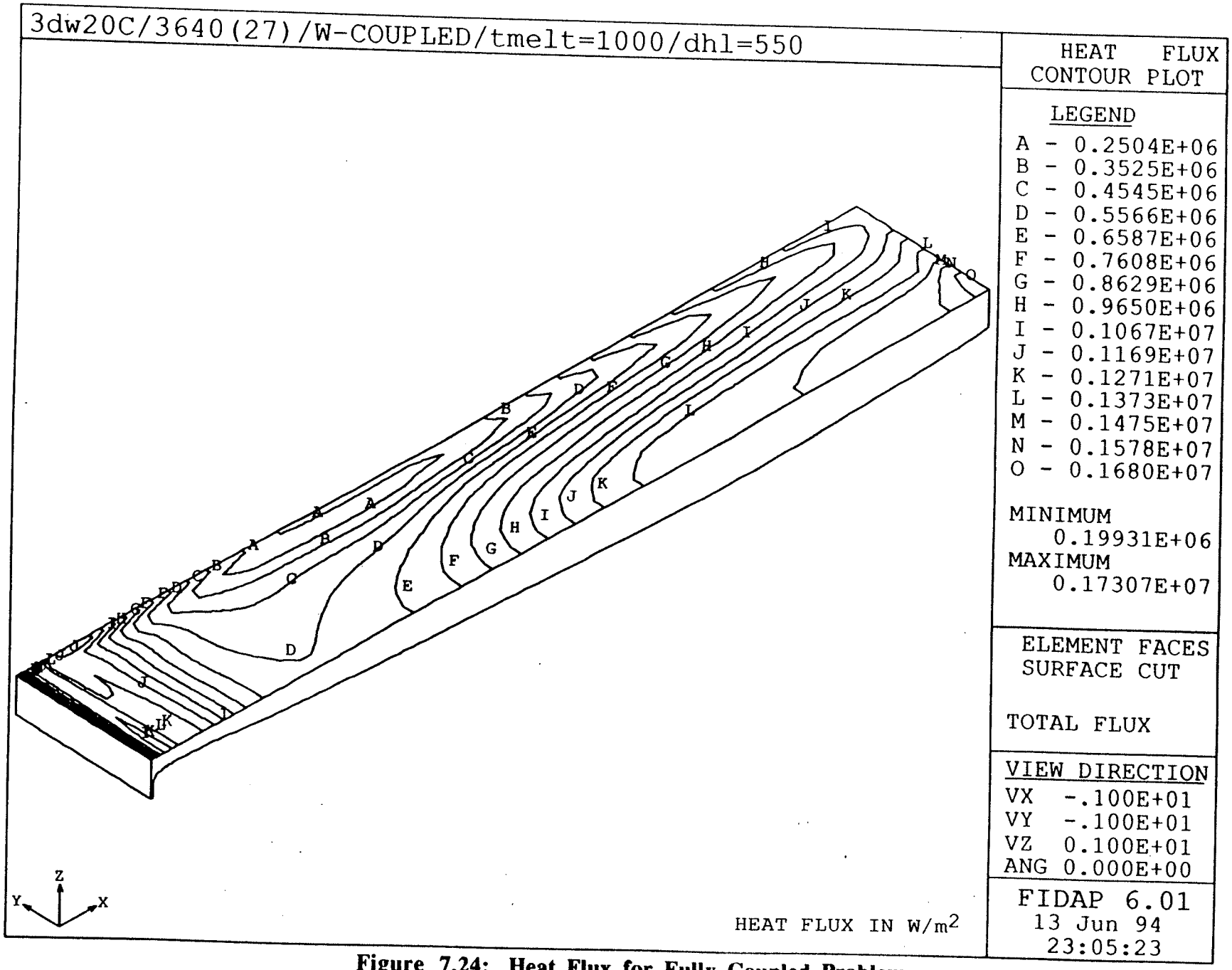

Figure 7.24: Heat Flux for Fully Coupled Problem

7.4.4 Comparison of 3D Results with Experiments

Figure 7.25 compares the prediction of the location of the solid flux/liquid flux interface from the 3D model with that experimentally determined. The 1000 °C istotherm is used to track the location of the flux melt interface. The position of the flux melt interface at the same location in the mold, 80 mm from the wide face wall, was computed. This location corresponds with the location at which the experimental readings were taken. Thus a direct comparison between the experimental and calculated melt interfaces is possible.

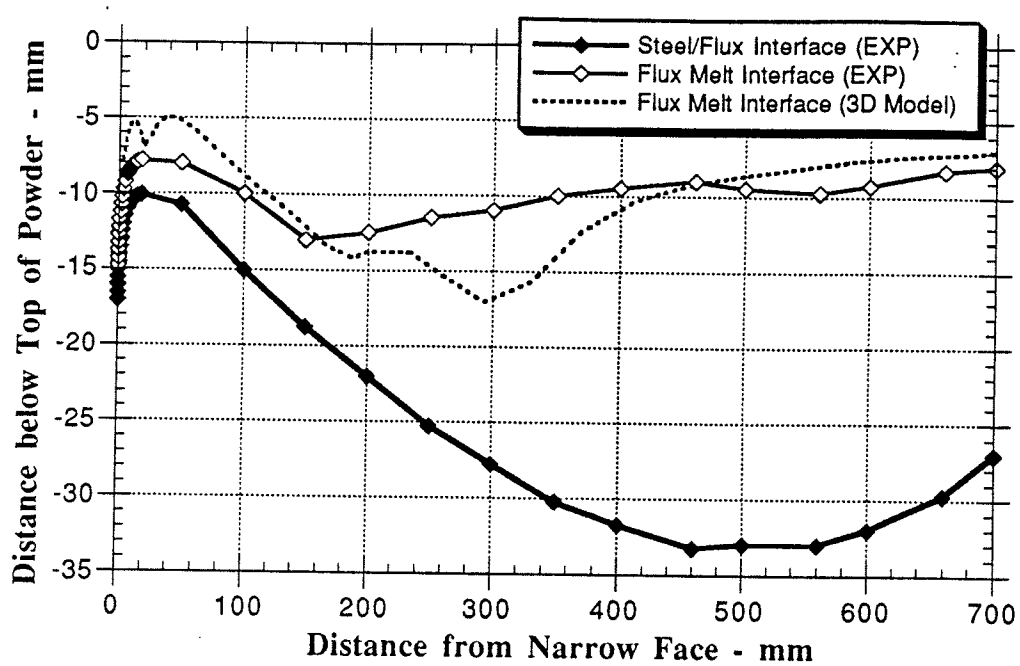

Figure 7.25 -Comparison of Experimentally-Determined and Predicted (3D Model) Profiles of the Flux Melt-Interface

It is clear that the agreement between the predicted and experimental melt profiles is better in this case than in the 2-D model. The maximum disparity between the experimental and predicted profiles is 54% while the average over 20 points is 3.3%. While the maximum error may seem large, it should be noted that the experimental data is taken under less than ideal conditions and with relatively crude instrumentation. Dispite this however, the average disparity is remarkably low.

For instance, the location at which the liquid depth first begins to increase is predicted to be within 25 mm of its actual location. Even more remarkable, the predicted value to which the depth increases is within 4% of the experimentally measured depth. Even the rate of increase of liquid depth is very similar. Figure 7.26 illustrates the trend in the liquid depth as a function of position in the mold, and the similarity between the experimental and predicted results.

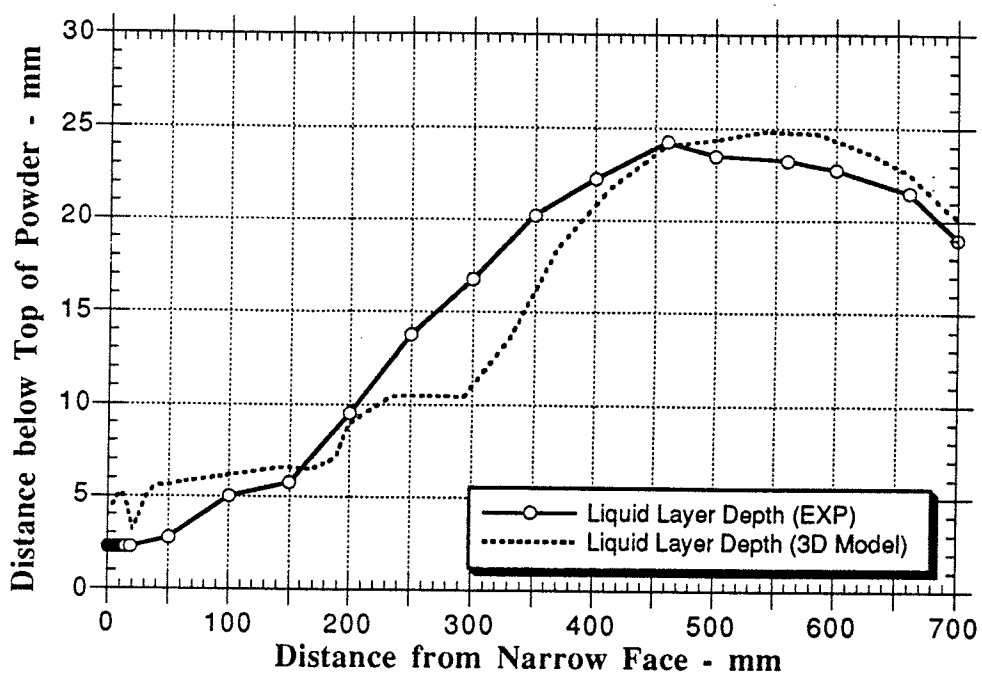

Figure 7.26 - Comparison between the Predicted and Experimental Liquid Layer Depths

Figures 7.27 and 7.28 compare the results obtained by the 2D and 3D models for the location of the flux melt interface. It can be seen that the inclusion of the mass transport to the wideface has resulted in thinner liquid layers in general, as well as better agreement with the experiments than the 2-D model. As can be seen, the overprediction of liquid depth in the meniscus region has been reduced by accounting for the heat that must necessarily leave towards the mold wide face. In fact agreement between the 2-D results and the experiments are only good beyond 250 mm from the narrowface, while the 3-D model gives acceptable agreement over most of the domain. The maximum disparity between the 2-D results and

experiments is 62% and the average is 22% compared with 54% and 3.3% for the 3-D model. Finally, the 3-D model uses a more realistic two-material model for viscosity and thermal conductivity, and is therefore more reliable.

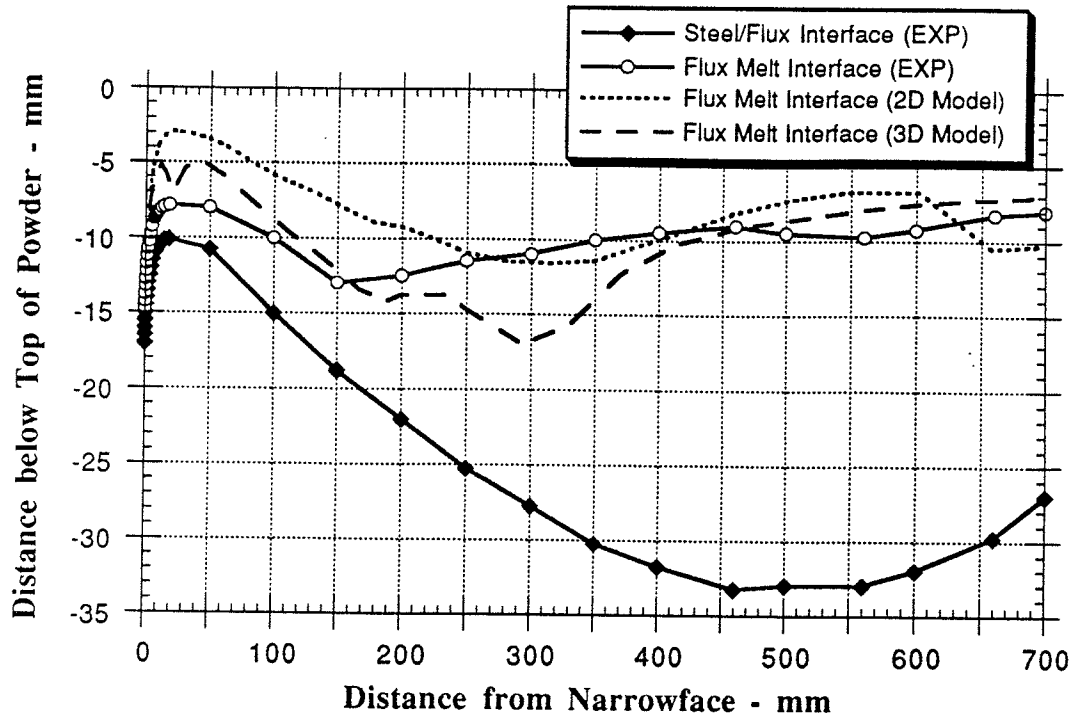

Figure 7.27 - Comparison of 2-D and 3-D Model Results with Experimental Data

7.4.5 Direct Comparison of 2-D and 3-D Models

The use of a single material model in the 2D case was chosen to represent the average thermal and flow behavior of the flux, and it is therefore appropriate to compare the results of that model with the average 3-D results and with the average experimental data. However, for a critical comparison of the two models, it is necessary to evaluate them on an equal basis.

The two-material model was used in the 2-D model, and the results were compared with those for the 3-D model at the center-plane of symmetry. The reader will recall that the original intention of the 2-D model was to simulate the behavior of the flux at the mold center-plane (see Figure 4.1). The comparison is shown in Figure 7.29.

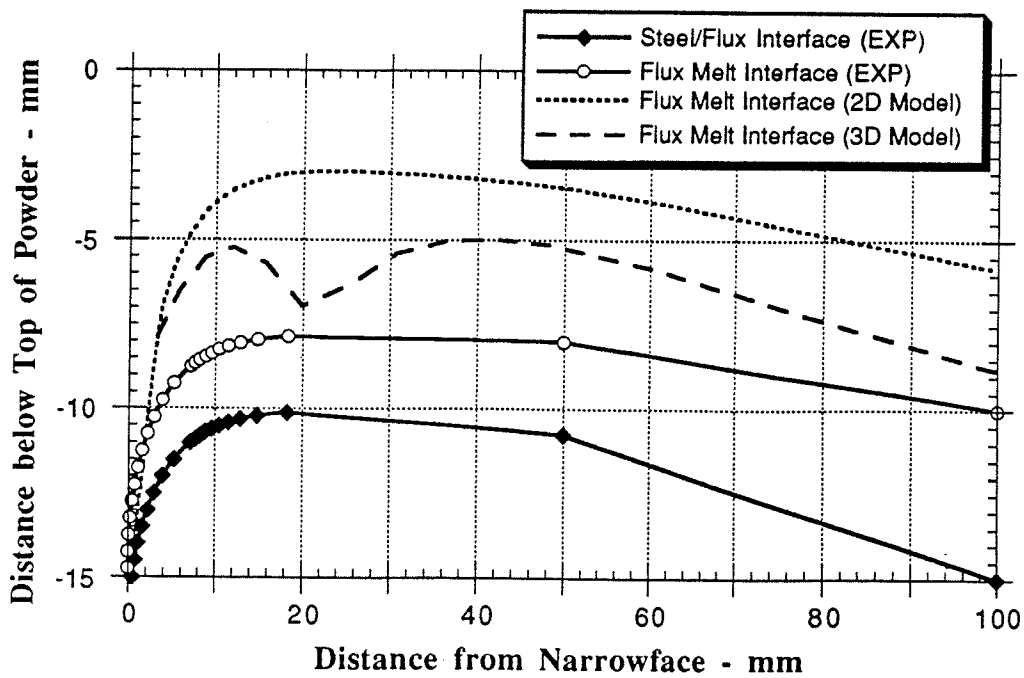

Figure 7.28 - Comparison of 2-D and 3-D Model Results with Experimental Data in Meniscus Region

As a matter of convenience for the author, the results of a previously converged 3-D run were used for the comparison in Figure 7.29, and not the results for the run given in the immediately preceeding sections. The 3-D run used in Figure 7.29 and 7.30 had a lower viscosity in the liquid domain, and the results are presented fully in Chapter 8 (section 8.2), as a parametric variant for the base model presented in the preceeding sections. The important thing however is that the 2-D and 3-D runs compared here had exactly the same material models used as input. It can be seen that the liquid layer depth, in general, is less in the 3-D model. This was the expected result due to the incorporation of mass and thus heat flow to the wideface. An overall energy balance would show that the net heat flowing into the domain in the 3-D model is reduced from that for the 2-D model and the net heat flux out is increased. Thus the overall effect is that the liquid domain will be reduced in size for the 3-D model in comparison with the 2-D model using the same material properties and boundary conditions.

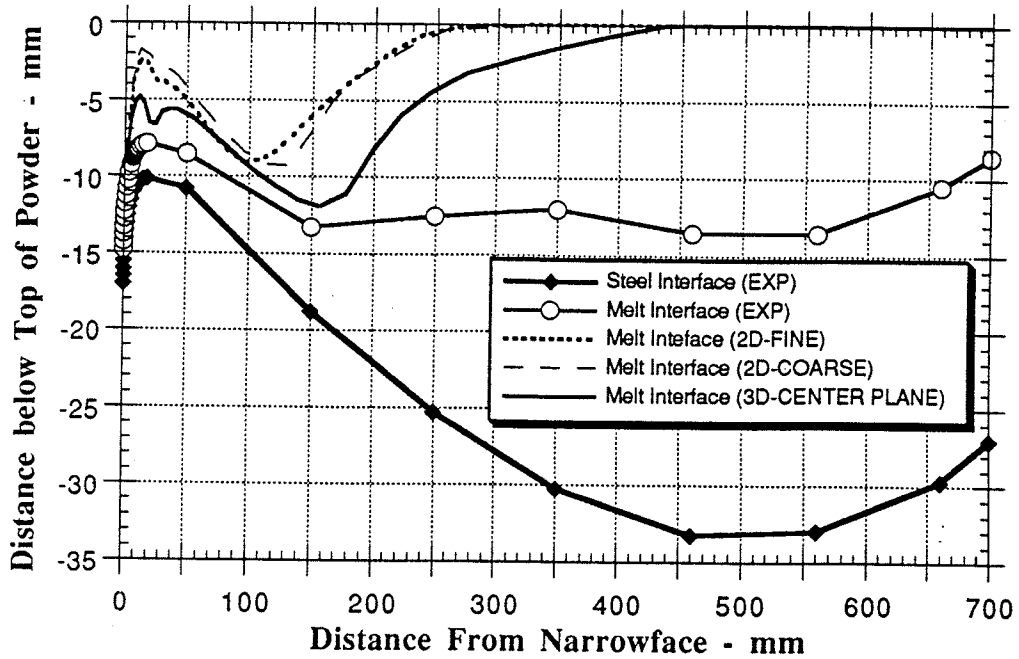

Figure 7.29 - Direct Comparison of 2-D and 3-D Models using Two-Material Model

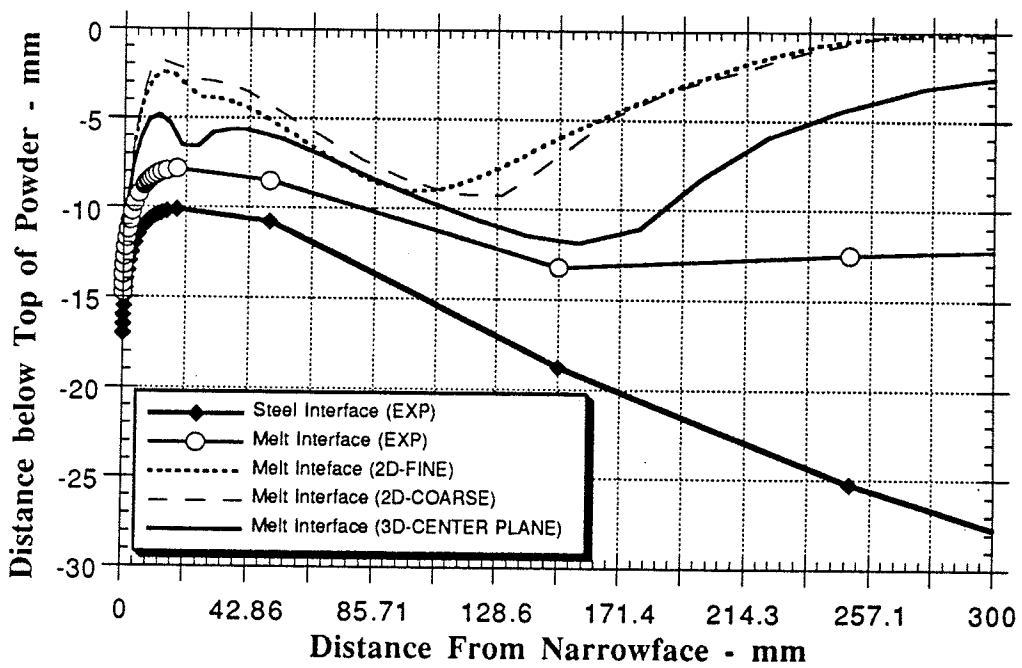

Figure 7.30 - Direct Comparison of 2-D and 3-D Models using Two-Material Model for Viscosity and Thermal Conductivity in the first 300 mm of the mold

Figure 7.30 shows a close up of the first 300 mm from the narrow face wall. The fine 2-D mesh consists of 6400 elements while the coarse mesh consists of 440 elements. The latter

value corresponds to the same discretization in the x and z-directions as was used in the 3-D model. As can be seen, there is a small difference between the coarse-mesh 2-D and fine-mesh 2-D results for liquid layer depth, but this is to be expected given the 16 fold difference in mesh refinement. However, the disparity is always less than 10%. More importantly though, the comparison between the 2-D results for the two mesh densities used indicate that if a finer 3-D mesh is used, the difference in the results would be small. This fact supports the validity of the 3-D model and addresses the questions of convergence and accuracy.

7.4.6 Additional Results

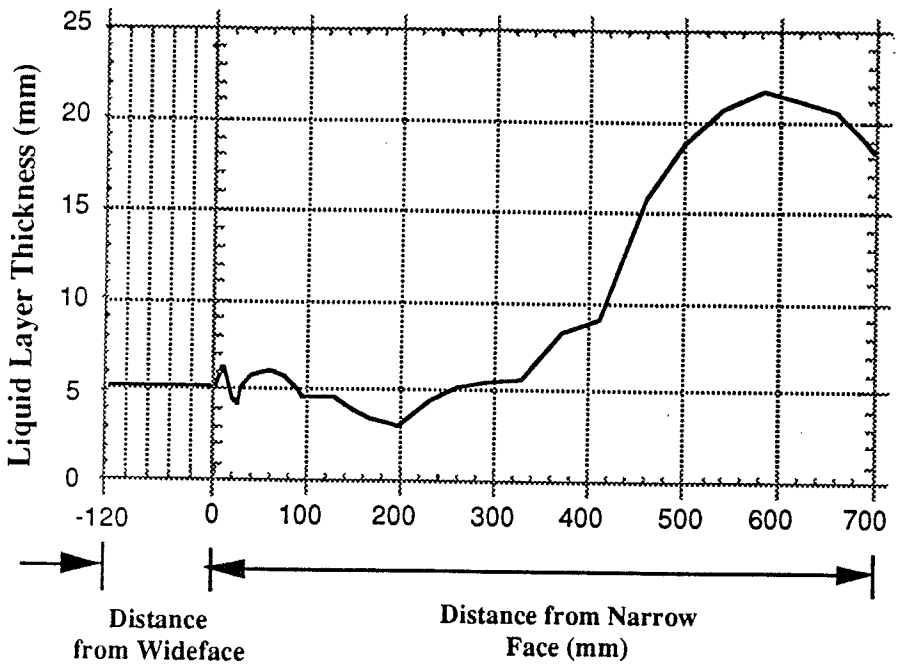

Figure 7.31 - Liquid Layer Thickness at Mold Perimeter

Finally, Figure 7.31 shows the variation of liquid layer thickness as a function of position around the mold. The thinnest liquid layer occurs at approximately 200 mm from the narrowface wall, roughly coinciding with the location of flow separation. Additionally, the dip in the liquid layer thickness at 20 mm from the narrowface is due to cold flux from the upper layers being forced downwards by the solid flux rim on the narrowface, as discussed previously. As expected, the liquid layer thickness along the mold narrowface direction is constant. This trend is due to the one-dimensional nature of the flow in the meniscus region near to the narrowface.

CHAPTER 8

PARAMETRIC STUDY

A parametric study to determine the effect of variation of material properties on flux layer thickness was performed using the 1-D conduction model in Chapter 3. That study provided insight into which properties most significantly affect the conduction of heat in the flux, and was useful in guiding the choice of parameters to be varied in the study with the 2-D coupled model. However, while the information provided by the 1-D model is useful in obtaining an overall picture of the thermal behavior of the flux, it cannot illustrate the effect of these material parameters on the flow pattern developed in the liquid pool. Since we consider the flow pattern to be critically linked to the thermal behavior of the flux and vice-versa, a parametric study using the 2-D finite element model is necessary.

8.1 EFFECT OF CHANGES IN POWDER PROPERTIES

8.1.1 Thermal Conductivity

The one-dimensional conduction model discussed in Chapter 3 predicts a proportional relationship between average liquid thermal conductivity and liquid layer thickness developed for a particular thickness of powder flux. Figure 3.8 quantitatively illustrates this relationship. However, the relationship between the liquid layer thickness, liquid thermal conductivity and overall flux layer thickness (as opposed to powder layer thickness) was not illustrated. Since the overall flux layer thickness is a fixed input to the 2-D finite element model, it will be useful to illustrate the effect of changes in thermal conductivity based on overall layer thickness as predicted by the 1-D model as well. This relationship is shown in Figure 8.1. As shown, the 1-D conduction model predicts that there should be a significant change in the layer thicknesses as the liquid thermal conductivity is changed for the given geometry.

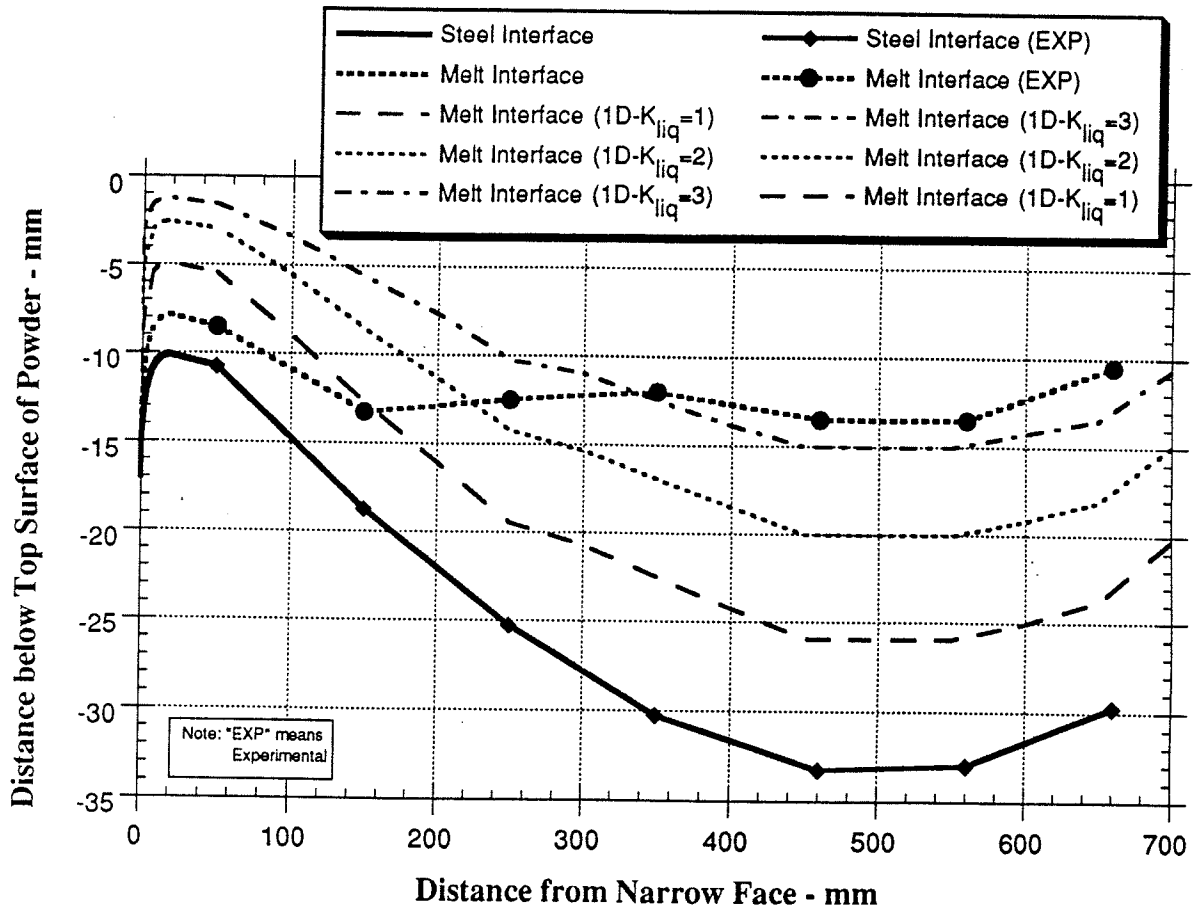

Figure 8.1 - Relationship between Average Liquid Thermal Conductivity (K_{liq}), Overall Flux Layer Thickness, and Liquid Layer Thickness as predicted by 1D Conduction Model

Figure 8.2 shows the effect of changes in the average liquid thermal conductivity on the location of the melt interface. It is clear from this figure that the proportional relationship between liquid thermal conductivity, liquid layer thickness and powder layer thickness does not exist in the 2-D model results as it does for the 1-D conduction model. This was expected due to the interaction between convection and conduction which will vary across the domain, dependent on the magnitude and direction of the velocity at the particular locations. The exact interaction is difficult to predict beforehand, because of the coupled nature of the problem, where velocities and temperatures are interdependent.

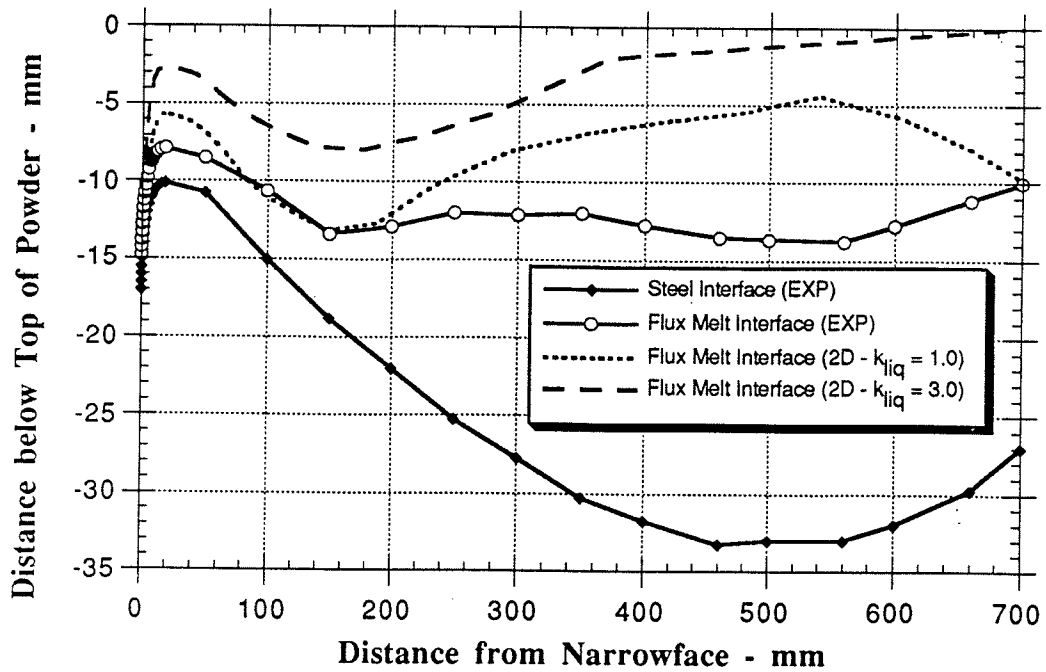

Figure 8.2 - Effect of Changes in Average Liquid Thermal Conductivity on the Location of the Flux Melt Interface as predicted by 2-D Coupled Model

If heat transfer were purely by conduction, a three-fold change in liquid thermal conductivity would produce a three-fold change in liquid layer thickness. As can be seen in Figure 8.2, this proportional relationship between thermal conductivity and liquid layer thickness does not exist. In fact, the change in liquid layer thickness is only 22% (on average) for a 300% change in liquid thermal conductivity, which illustrates the relative importance of convective heat transport.

The location of the flux melt interface is a function of the flow pattern developed. According to figure 8.3, the change in the flow pattern is subtle and consists mainly of a slight compression of the main recirculation zone in the y-direction, as the liquid thermal conductivity is decreased. Generally, the larger the recirculation zone, the larger is the convective component of heat transfer which causes more energy to be transported to the upper regions of the flux. This increased transport results in higher temperatures further away from the steel surface, and consequently a thicker liquid flux layer in some regions.

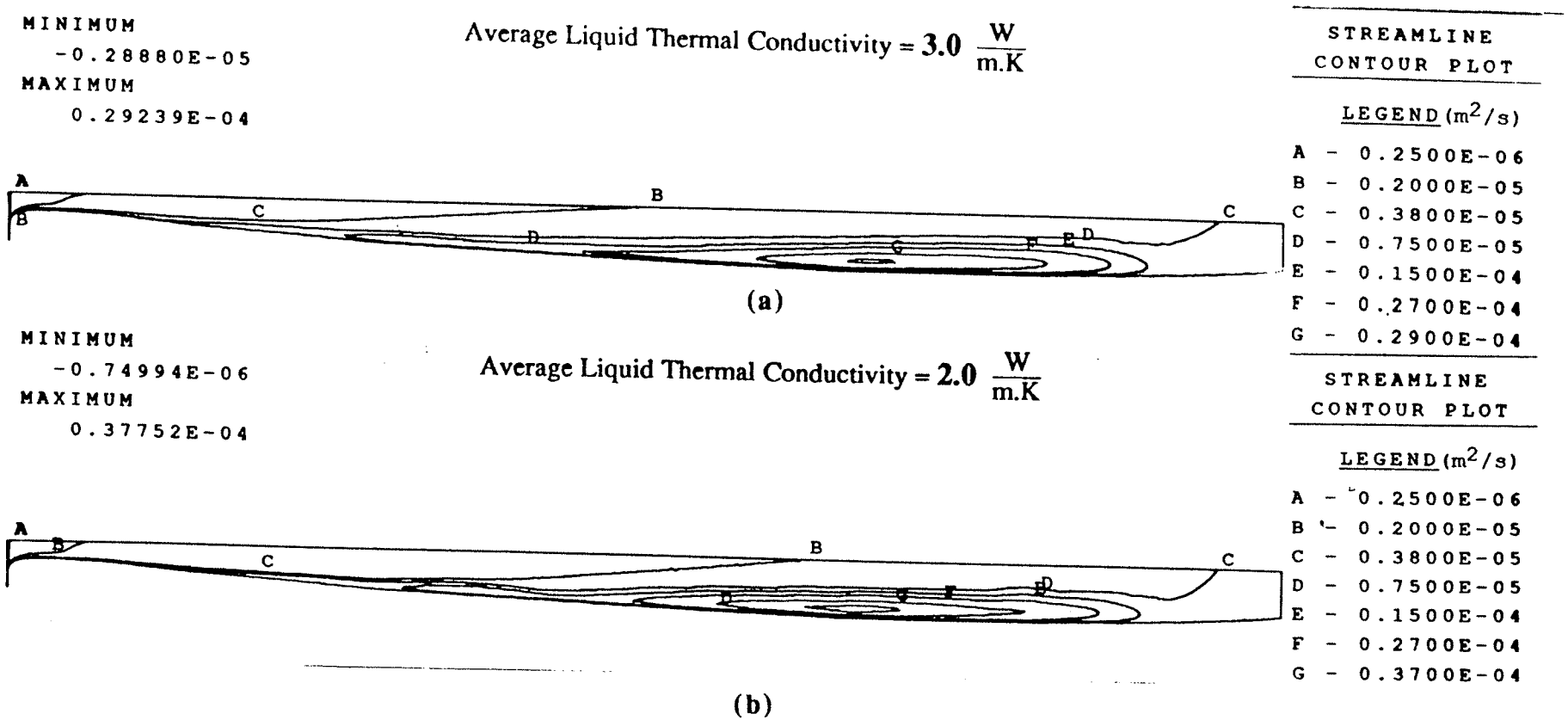

Figure 8.3: Change in Flow Pattern (Streamlines) as a Function of Average Liquid Thermal Conductivity: (a) $k_{liq} = 2.0 \frac{W}{m.K}$, (b) $k_{liq} = 3.0 \frac{W}{m.K}$

The change in the location of the melt interface in the meniscus region, as liquid thermal conductivity is changed, is of special interest. Figure 8.4 shows the flow pattern in the meniscus region and the corresponding temperature distribution, as a function of changing liquid thermal conductivity. In the meniscus region, the model predicts heat transport to be due to a combination of two-dimensional conduction coupled with one dimensional convection. The conductive heat flow is two-dimensional because of the proximity of the flux to the cold narrow face of the mold, which results in conduction in the x-direction. As shown in Figure 8.4, the size of the flux rim, solidified on the mold wall (given approximately by contour F), decreases with increasing liquid thermal conductivity in the meniscus region. This effect seems to be the most significant result of changing average liquid thermal conductivity. Figure 8.4 also shows the effect of changing liquid conductivity on the velocity in the meniscus region. The effect is also minor.

8.1.2 Melting Point

The analytical model also predicts large changes in liquid layer thickness with changes in the melting point of the flux. Thus the effect of changes in this property was investigated with the 2-D model. Figure 8.5 shows the change in the flow pattern when the melting point is increased from 950°C to 1000°C. As shown, a compression of the main recirculation zone occurs, along with the formation of a smaller zone bounded by streamline D for the melting point of 1000°C. Streamline C for the higher melting point shows that powdered flux is pulled slightly deeper into the domain than with the lower melting point.

The change in the location of the melt interface when the melting point is changed from 950 to 1000°C is given in Figure 8.6. Because of the compression of the recirculation zone, cooler flux is able to penetrate deeper into the domain before it is removed to the left of the domain. Hence the melt interface is shifted lower. In contrast to the trend obtained with liquid conductivity changes, the effect of increasing the melting point agrees qualitatively with the prediction of the analytical model.

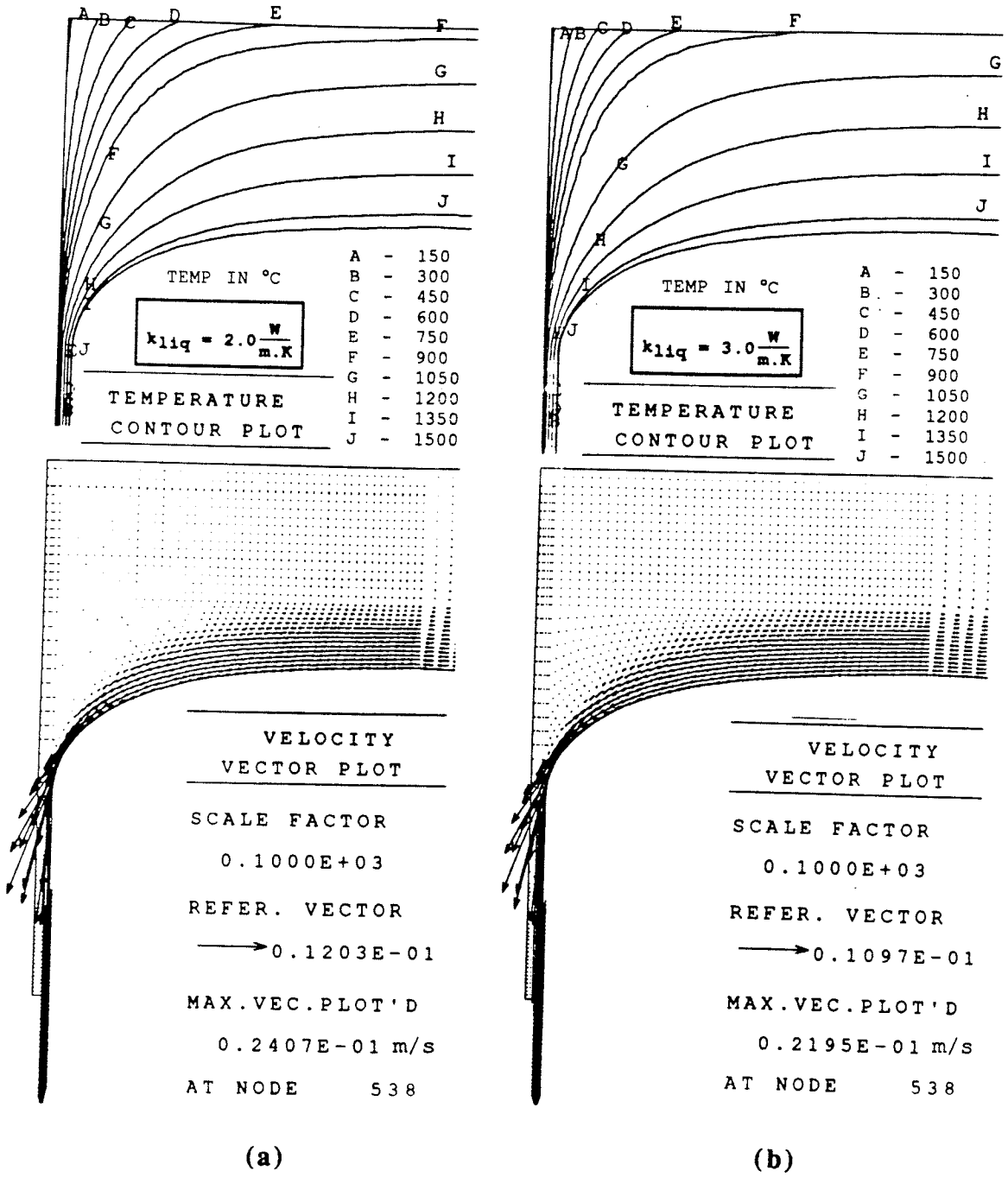

Figure 8.4: Temperature Contours and Velocity Vectors in Meniscus Region as Functions of Average Liquid Thermal Conductivity: (a) k_{liq} = 2.0W/(mK), (b) k_{liq} = 3.0 W/(mK)

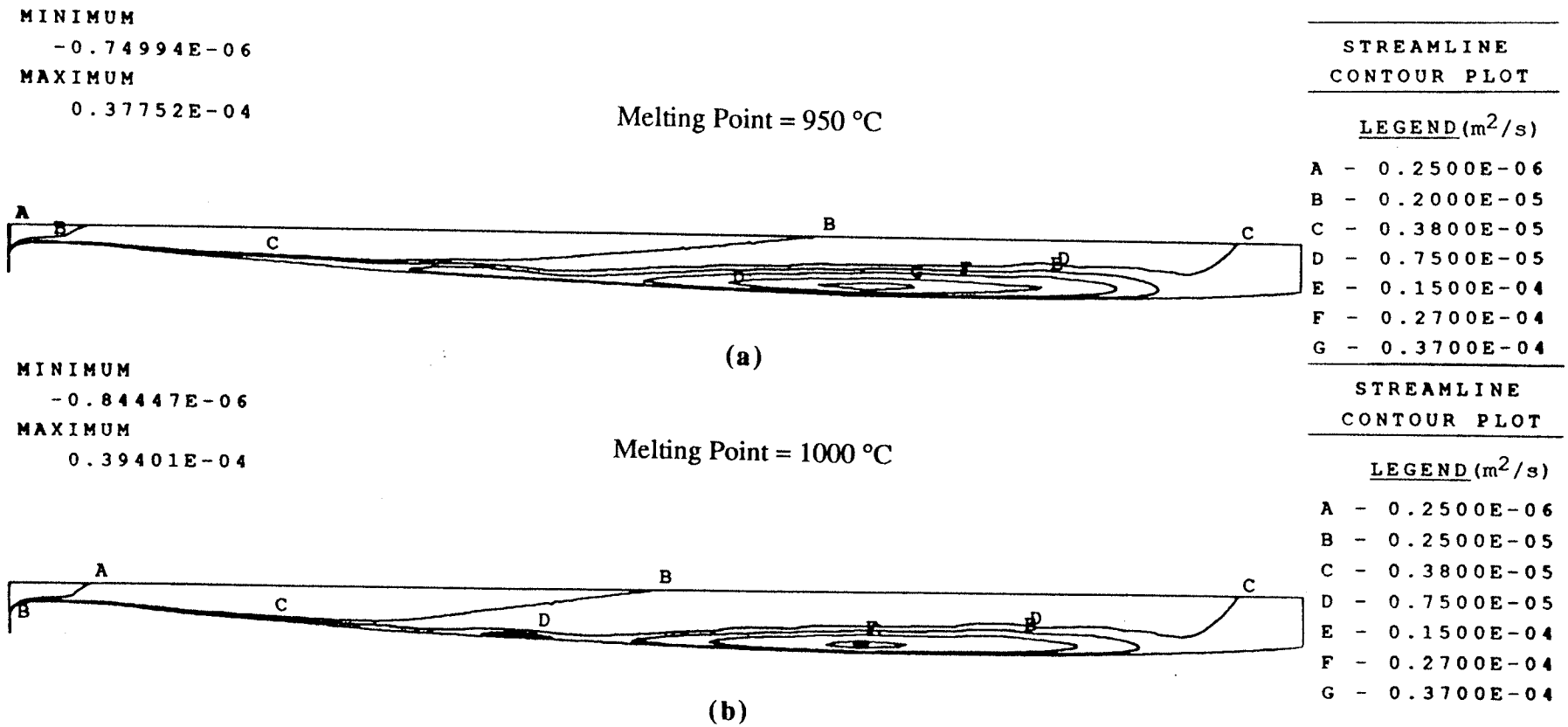

Figure 8.5: Change in Flow Pattern (Streamlines) as a Function of Flux Melting Point: (a) T_{melt} = 950°C, (b) T_{melt} = 1000°C

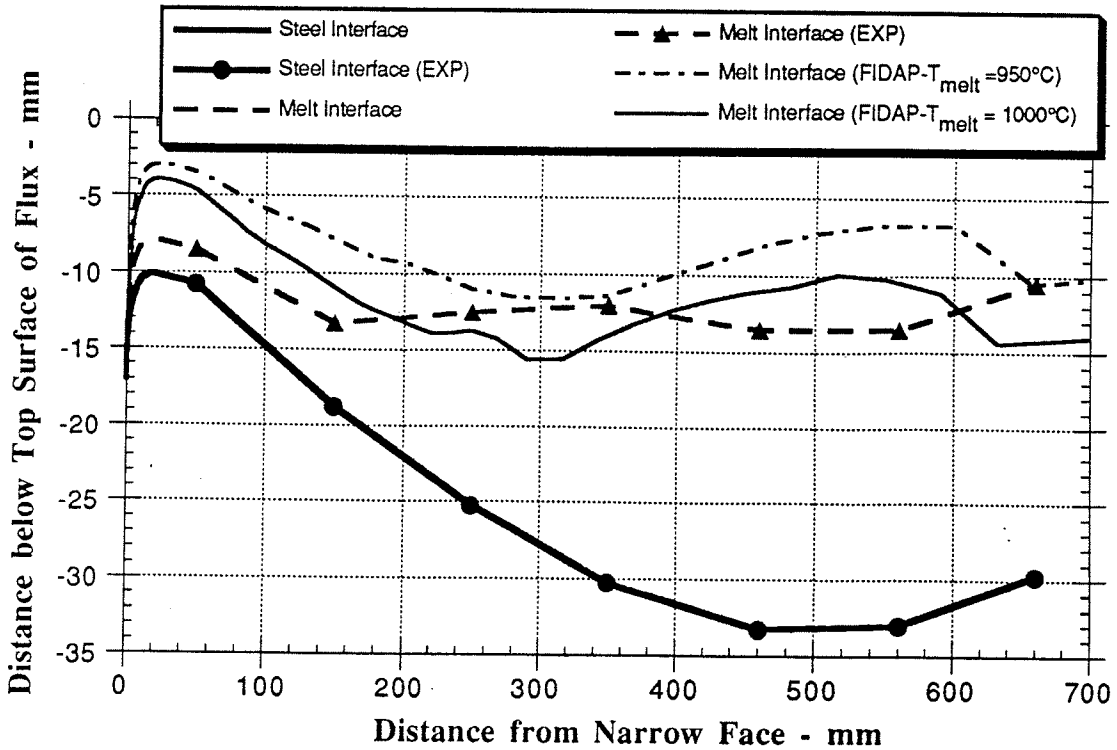

Figure 8.6 - Change in Location of Melt Interface as a Function of Melting Point

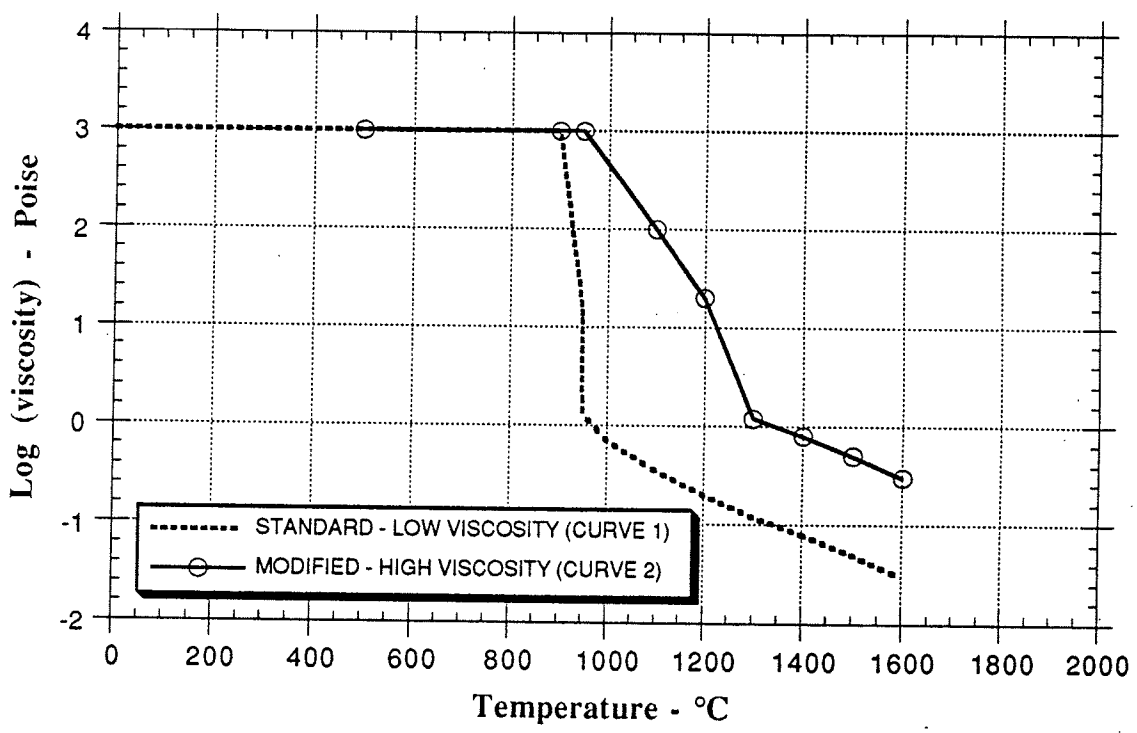

Figure 8.7 - Viscosity - Temperature Curves used in Parametric Study

8.1.3 Flux Viscosity

The parameter viscosity is not contained in the analytical model, so the effect of changing it is unknown thus far. To investigate the effect of such a change, the input viscosity-temperature curve was changed to simulate higher liquid viscosity as shown in Figure 8.7. Figure 8.8 shows the effect of changing the viscosity profile on the location of the liquid/solid interface. The flux liquid/solid inteface is pushed closer to the hot flux/steel interface. Higher viscosity at lower temperature causes the cooler powder that is introduced to act more like a solid coherent mass. The flux is unable to move in any other direction until its temperature is sufficiently high to reduce its viscosity.

The material represented by CURVE1 in Figure 8.7 has a lower viscosity at higher temperature. Generally, therefore, the liquid velocites (i.e. under the shear stress driving force) are higher than for a high viscosity flux. The high liquid velocities results in significant convective mixing and heat transport, and consequently thicker liquid layers. Therefore, in these cases, better feeding of the gap with liquid is expected, consistent with plant observations.

8.2 STUDY WITH 3-D MODEL

Ideally, the parametric study should be performed with the 3-D fully coupled model. However, due to the high cost of running the model, only one run other than the base case was performed. It was necessary to judiciously choose which parameter should be investigated further. The choice was based on the properties which seem to most significantly affect the behavior of the flux. The two parameters which seemed to fit this criterion were the melting point and the flux viscosity. The effect of changes in the melting point was clearly shown in both the 1-D and 2-D models, but viscosity effects were only investigated in the 2-D model. Furhtermore, the parametric study with viscosity in section 8.1.3 did not utilize the more physically plausible 2 material model. Thus, viscosity was chosen to be the parameter that was varied in the 3-D model.

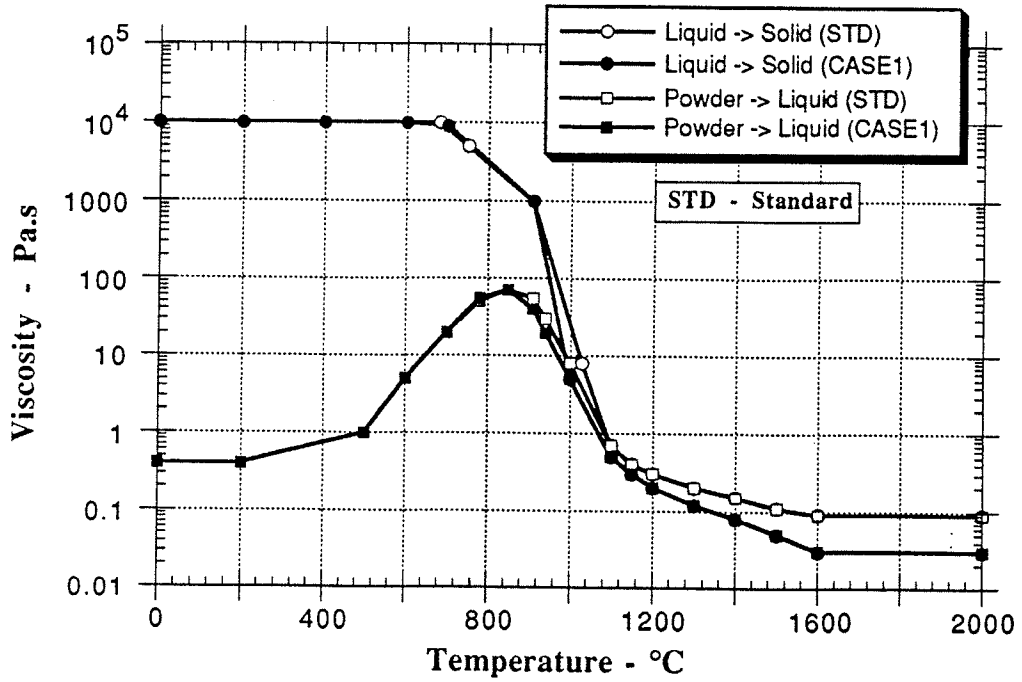

Figure 8.9 - Viscosity-Temperature Curves used In Parametric Study with 3-D Model

Figure 8.9 shows the "new" viscosity-temperature curve (CASE1) in comparison to the curve used in the base case (STD) runs (described in chapter 7). The major change is that, for CASE1, the average viscosity of the liquid was decresed by decreasing (i.e. make more negative) the slope of the viscosity-temperature curve in the temperature range of 1000 - 1600 °C . The results using the new curve in comparison to the standard, follow.

Figures 8.10 through 8.12 compare the temperature contours for the base viscosity (STD) case and for the increased viscosity (CASE1) runs. With reference to Figure 8.10, the surface temperature patterns are similar for both cases, but the temperatures are higher, in general for the decreased viscosity case. Additionally the generic cool region at the top surface of the powder, due to the flow separation in the flux pool is smaller for the decreased viscosity case (see temperature contour 'D' corresponding to 360°C). Figures 8.11 and 8.12 also show the general trend in which temperatures in the upper regions of the flux are higher for the reduced viscosity.

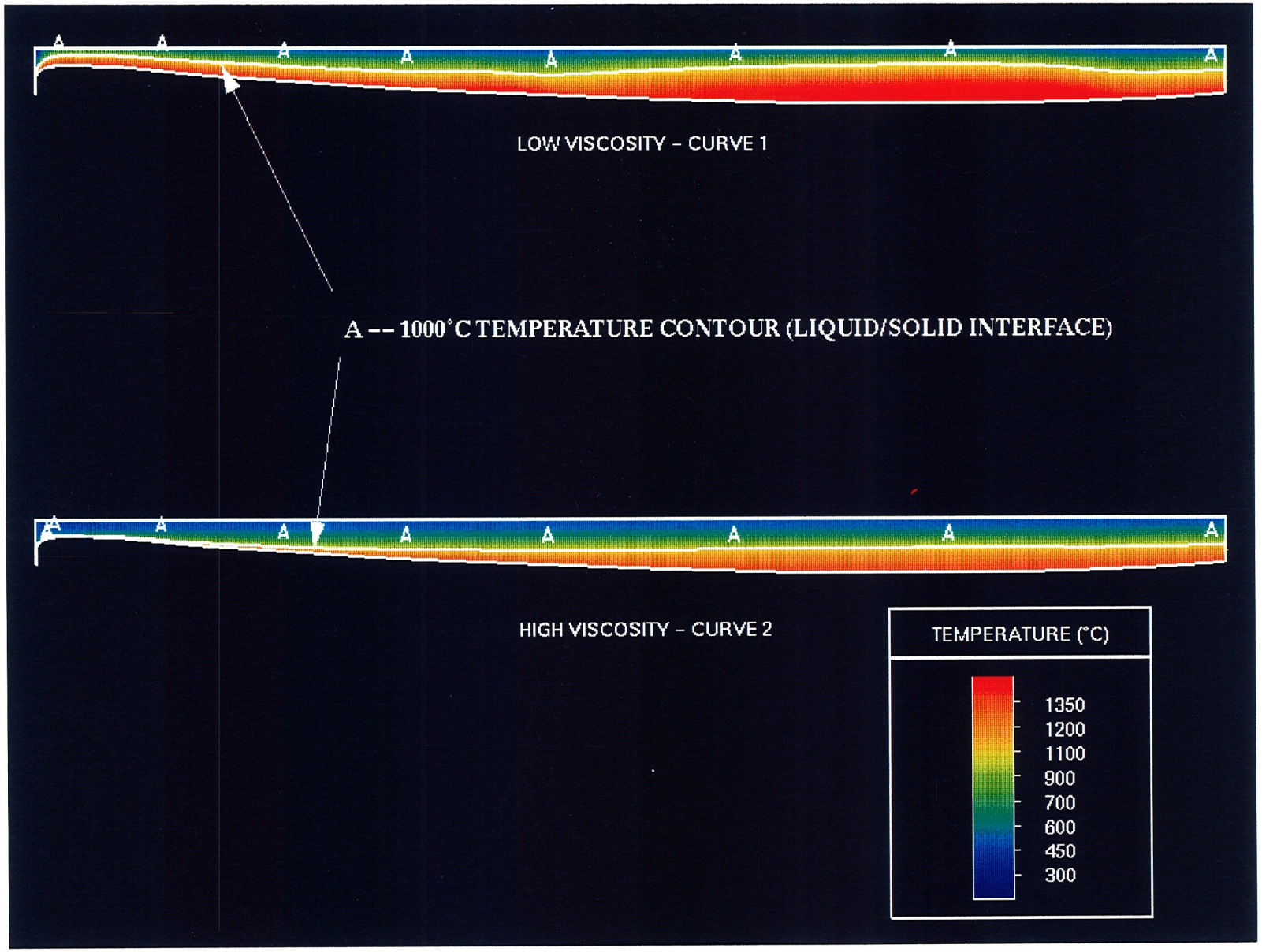

Figure 8.8: Location of Liquid/Solid Interface as a Function of Viscosity Profile

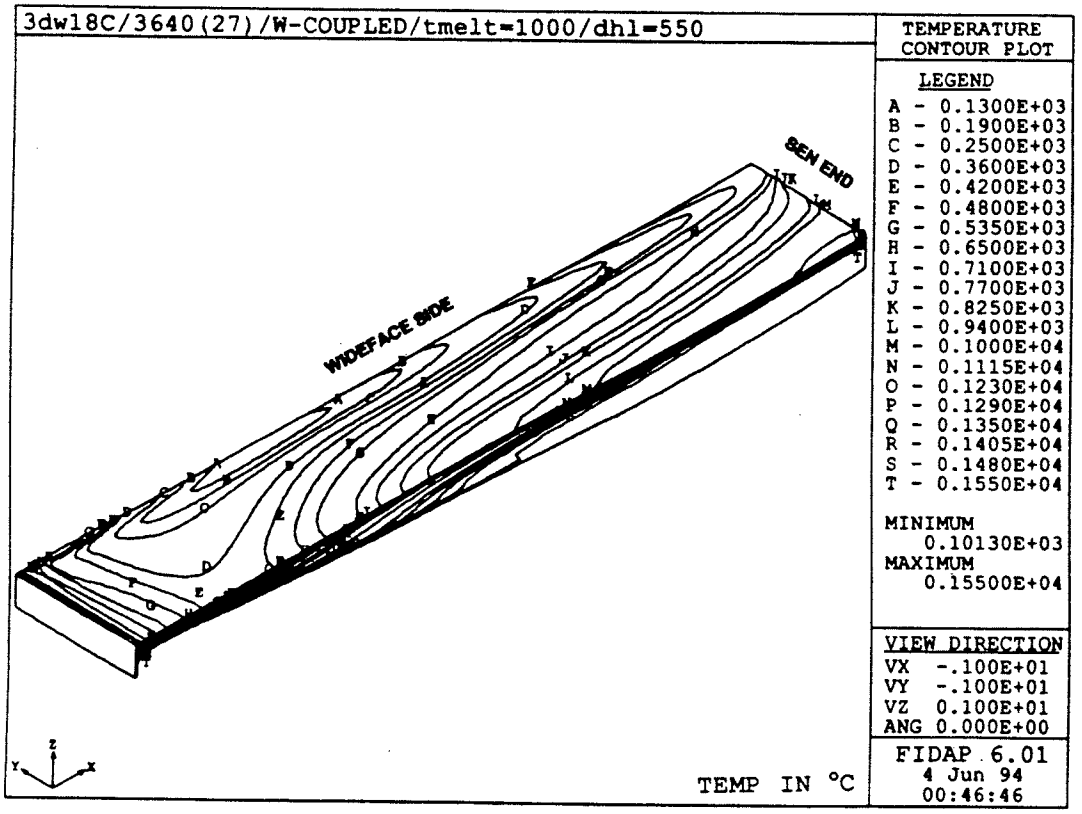

(a)

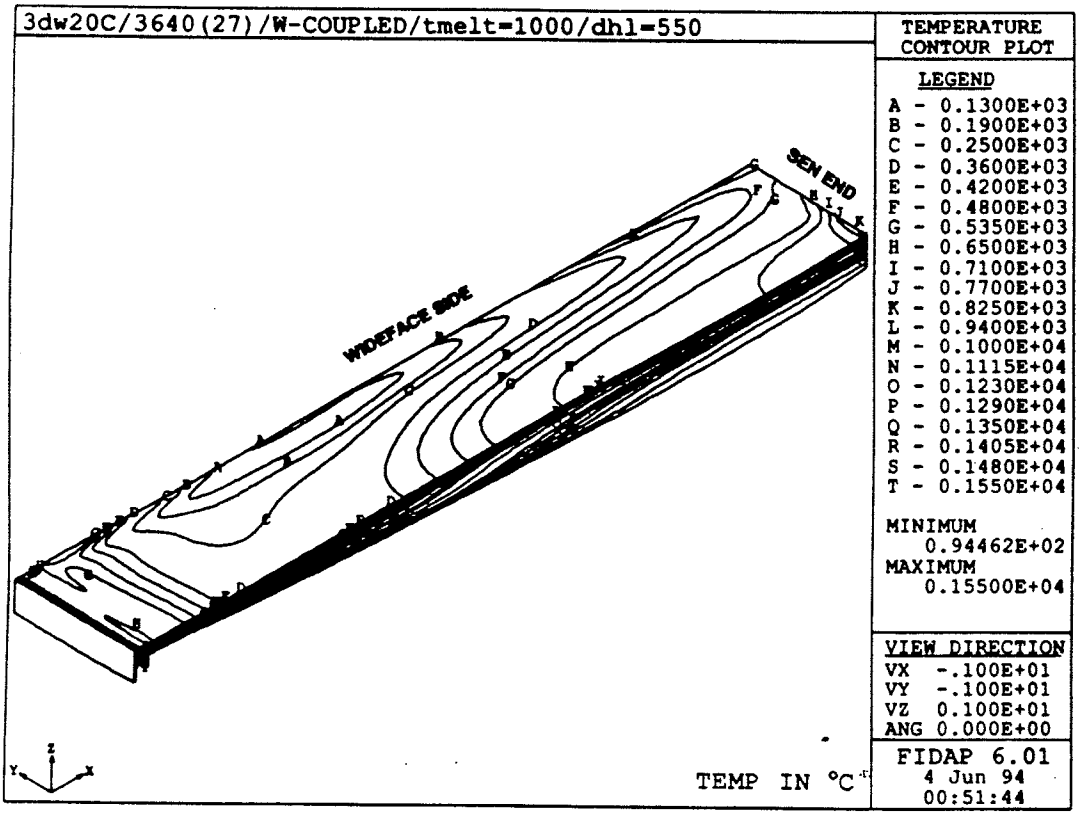

(b)

Figure 8.10: (a) **Temp. Contours for Coupled Problem - Low Viscosity (CASE1)**
(b) **Temp. Contours for Coupled Problem - High Viscosity (STD)**

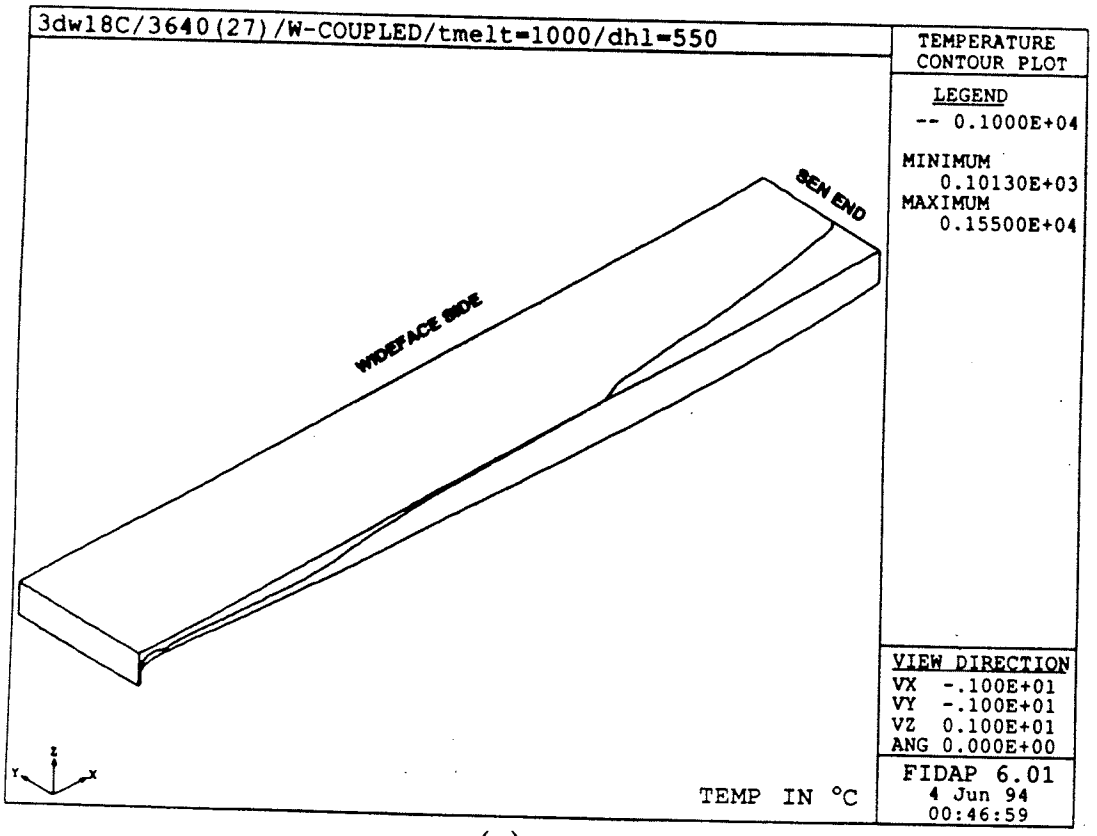

(a)

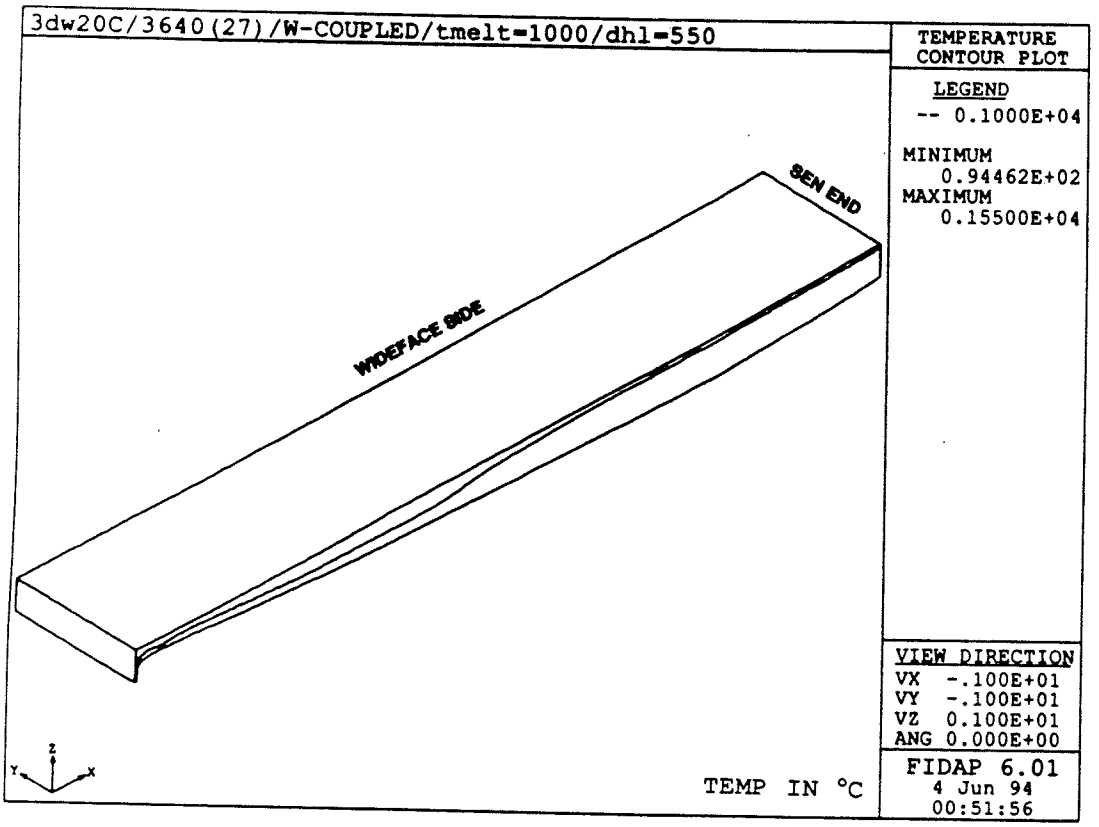

(b)

Figure 8.11: (a) Flux Melt Interface (1000°C Contour) - Low Viscosity (CASE1)
(b) Flux Melt Interface (1000°C Contour) - High Viscosity (STD)

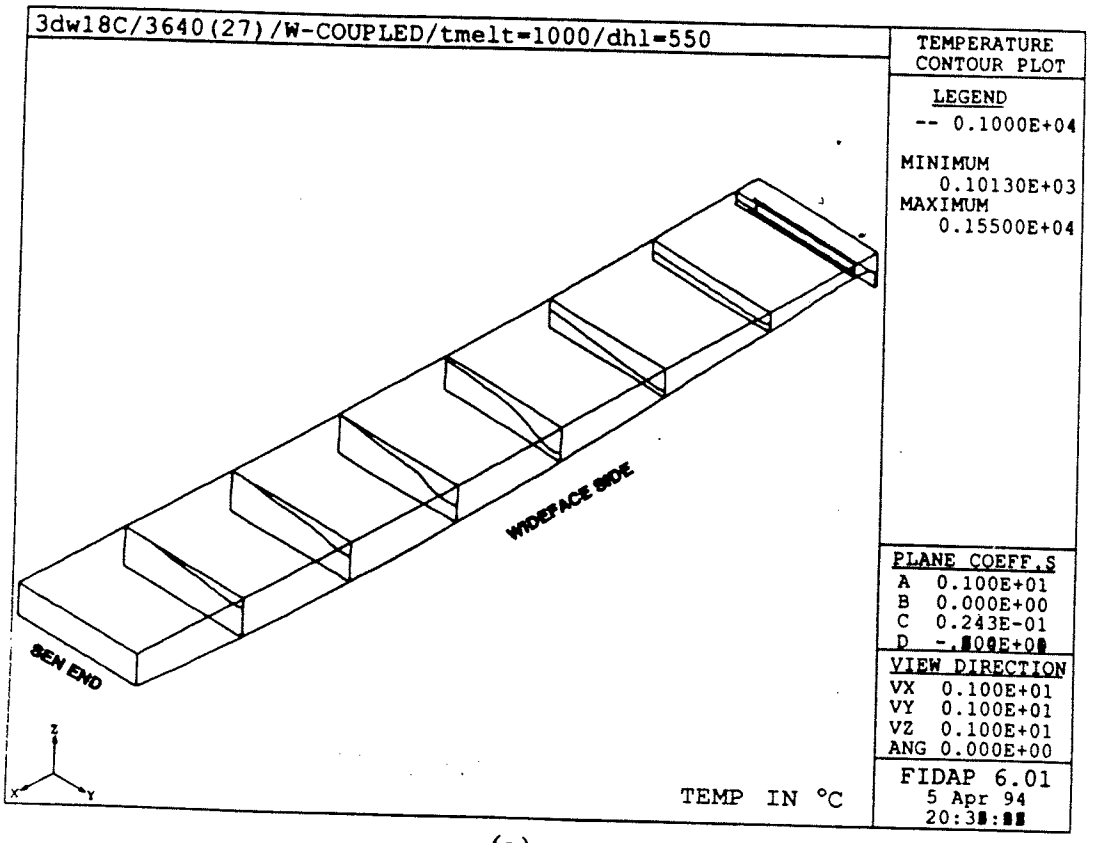

(a)

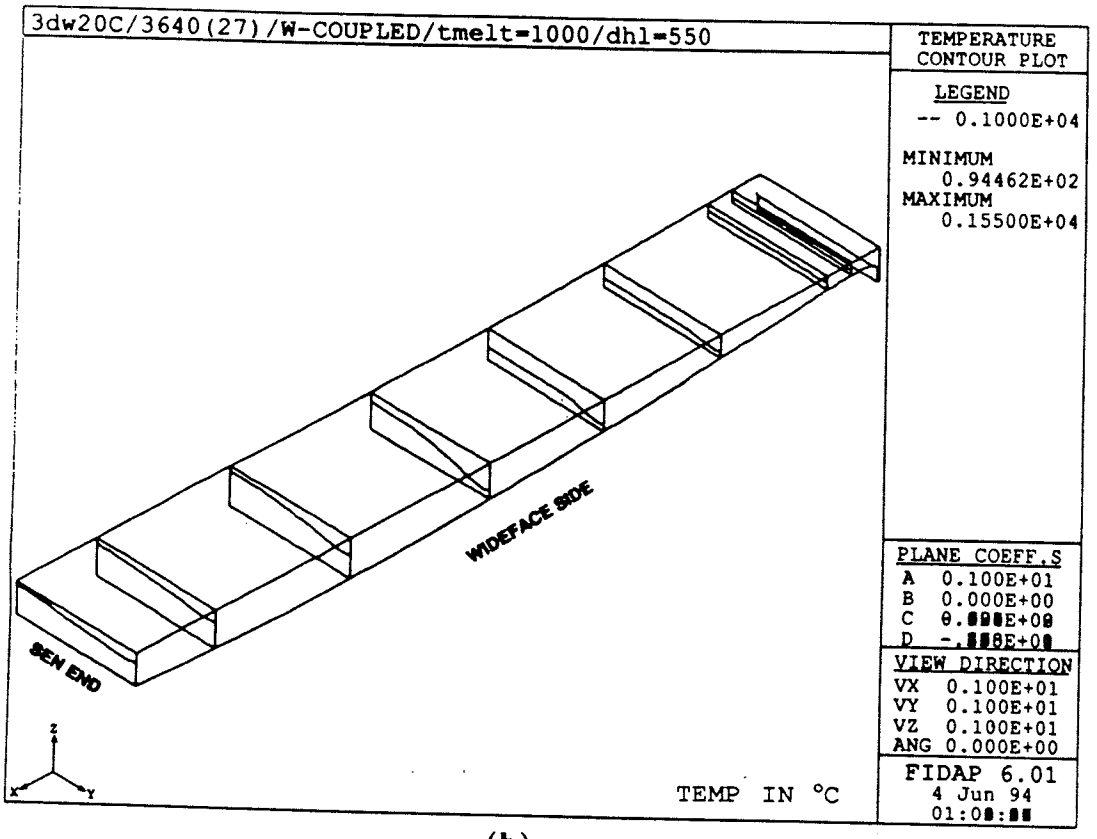

(b)

Figure 8.12: (a) **Flux Melt Int. Variation in x-direction - Low Viscosity (CASE1)**
(b) **Flux Melt Int. Variation in x-direction - Hight Viscosity (STD)**

The decreased viscosity increase liquid velocity because the driving force (i.e. the applied stress at the flux/steel interface) is constant. Higher velocities mean higher convective mixing and thus more (convective) heat transport to the upper layers of the flux. Hence, the higher temperatures in the upper regions of the flux and the upward movement of the flux melt interface. Figure 8.13 quantitatively shows this upward shift in the flux melt interface as the liquid viscosity is increased, leading to higher liquid layer thickness over most of the domain. The three interfaces compared are for the same location in the mold (approximately 80mm from the wideface).

Note that the depression in the melt interface (beteeen 200 - 300 mm from the narrowface) is more severe for the higher viscosity case. Note also that there is little change in the liquid depth in the meniscus region. As mentioned previously, convective heat transport is not important in this region and the change in viscosity can have little effect on the thickness of the liquid layer there.

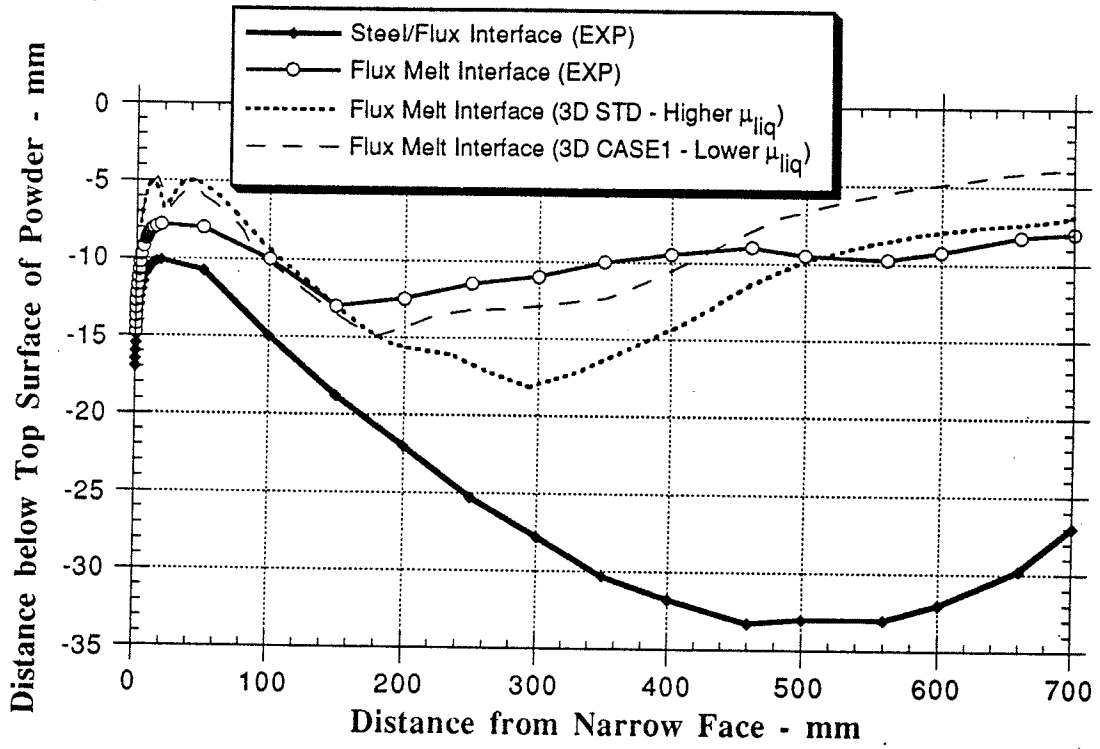

Figure 8.13 - Change in Position of Flux Melt Interface (80 mm from wideface) as a Function of Viscosity

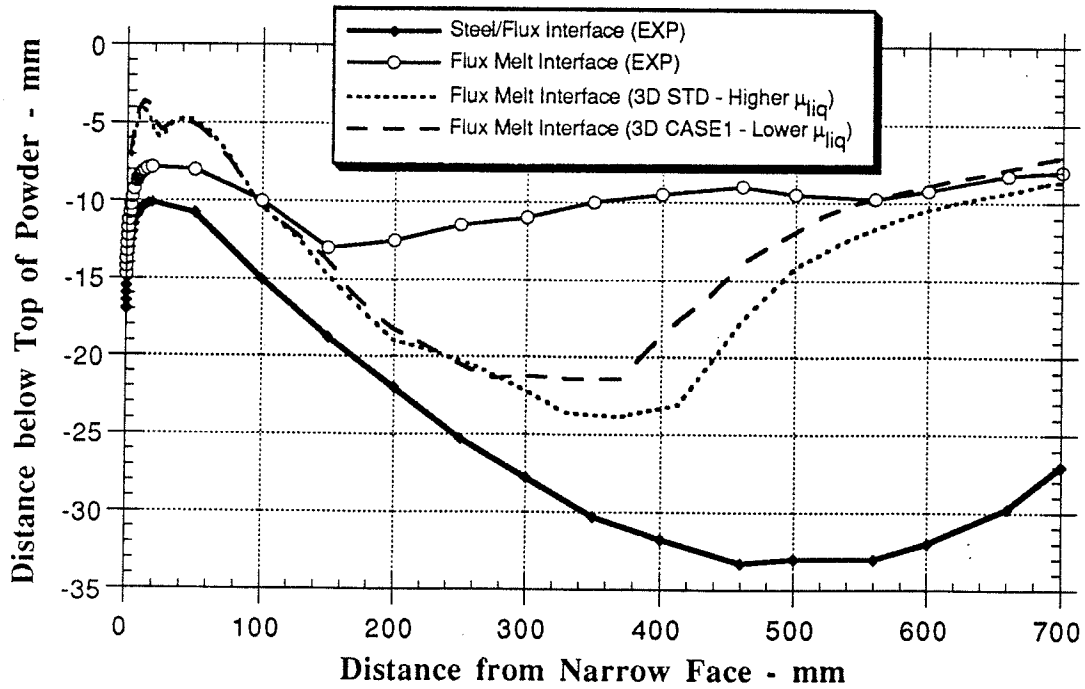

Figure 8.14 - Change in Position of Flux Melt Interface (at Wideface Wall) as a function of Viscosity

Finally, Figure 8.14 shows the effect of an increase in liquid flux viscosity on the position of the flux melt interface at the wideface wall. While the liquid layer at the wideface wall is thinner in general, the trend in the melt interface as the visocity is changed is similar to that for the melt interface at 80mm from the wideface wall. Near to the meniscus at the narrowface, there is practically no change in the liquid layer thickness as the liquid viscosity is change. However, away from the meniscus, where convective transport predominates, the effect is significant.

CHAPTER 9

SUMMARY OF RESULTS

An analytical one-dimensional steady state conduction model was formulated primarily to predict the relationship between the process and material parameters of: Casting Speed, Enthalpy of Fusion, Liquid Thermal Conductivity, Powder Thermal Conductivity, Powder Emissivity, Liquid Depth and Powder Depth. The following results were obtained:

- Liquid layer thickness increases with increasing powder layer thickness, but a practical maximum exists, of about 25 cm of powder, above which further addition of powder does not produce significant increases in liquid depth.

- Radiative heat transfer at the top of the powder is generally much more significant than convective heat loss. The convective component of the overall heat transfer coefficient is approximately 2.1 $\frac{W}{m^2K}$, while the radiative component varies with the third power of absolute temperature, yielding 66 $\frac{W}{m^2K}$, for T = 420°C.

- Powder emissivity does not affect the thickness of the liquid pool.

- Enthalpy of fusion of the powder significantly affects the thickness of the liquid pool. An *increase* in enthalpy of fusion from 250 J/g to 350 J/g *decreases* the liquid depth by 25%.

- The flux melting point is also a critical material property. An *increase* in the melting point from 900 °C to 1000°C *decreases* the liquid layer thickness by 16%.

- The thermal conductivity of the powder (assumed constant in the 1D model) has a small effect on the liquid layer thickness developed. *Doubling* the powder thermal conductivity *decreases* the thickness of the liquid layer by only 16%.

- Liquid thermal conductivity, however, has a significant effect. Increasing the liquid thermal conductivity from 2.0 to 3.0 $\frac{W}{mK}$ increases the liquid depth by 50%

A numerical 1-D model was also formulated to check the consistency of the analytical model. The commercial finite element package FIDAP was used. The 1-D finite element model confirmed the findings of the analytical model for trends in surface temperature and liquid depth produced.

Additionally, a transient 1-D melting model was constructed based on the steady state one. It was used to estimate the time it takes for the melting process to achieve steady state. For the casting conditions used, the model predicts that the steady state liquid depth is achieved in approximately 2 hours.

A two-dimensional model to simulate the thermal and hydrodynamic behavior of the flux under the action of the liquid steel below was constructed. This 2-D model incorporated the effects of convective heat transport which the 1-D model neglects. Additionally, the distribution of liquid and solid depth over the mold domain can be investigated. The model was constructed in three stages: isothermal, advection-diffusion and, fully-coupled. The fully-coupled model simulates the true case in which the flow pattern influences the temperature distribution and the temperature distribution conversely influences the flow pattern. The domain considered is parallel to the mold wideface. The following are the findings of the 2-D model:

- The steel flow is turbulent, while the flux motion is expected to be laminar because of its relatively high viscosity (> 10 times that of liquid steel). Thus, a transition from laminar to turbulent regime occurs at the flux-steel interface. It

was found that the most appropriate boundary condition to be imposed at the flux-steel interface in the 2-D flux model was one of applied shear stress. This stress value is found through an interpolative/iterative process involving an isothermal 2-D flux flow model and a 3-D model of the steel flow in the mold[43].

The alternative, which was found to be unsuitable, was application of the free surface velocity of the 3-D model as the boundary condition at the flux-steel interface in the flux model. These free surface velocities are much too large, as they assume that the steel at the flux-steel interface flows unimpeded. However, the actual case is that the steel is slowed somewhat at this interface because of the relatively high viscosity of the flux above it. By coupling the 2-D flux model and 3-D steel flow models, the true actual velocity at the flux-steel interface was shown to be much less than the predicted "free-surface" velocity. The interpolative process results in the correct interface velocities and shear stress (i.e. non-zero) which may then be applied individually to either the 2-D or 3-D models.

- Recirculation zones develop in the liquid pool because the steel drags liquid flux towards the SEN while the flux must exit at the mold-strand gap in the opposite direction. This cross-current flow produces recirculation zones, the number and size of which depend on the domain and material properties. In the standard cases, one large recirculation zone formed over most of the domain, and a smaller zone formed closer to the meniscus. Approximately 1.9 kg (30% of total) of flux stagnates in the zone.

- Most of the new material added, melts, and then flows along above the main recirculation zone towards the outlet at the narrowface. Very little gets incorporated into the main zone.

- Hot liquid close to the flux-steel interface is delivered to the upper regions of the domain by the currents of the main recirculation zone. This transport provides the thermal energy required to melt new material being introduced at the top surface. Thus convection plays a very important role in the melting process.

- The liquid depth is larger (both absolutely and proportionately) away from the meniscus (> 250 mm from narrowface) than close to the meniscus. Away from the meniscus, convective heat transport in the z-direction is much greater than close to the meniscus. Hence the liquid layer is thicker away from the meniscus.

- The flow of liquid flux in the near-meniscus region (< 100 mm from narrowface) is essentially parallel to the steel/liquid flux interface. (This result may be a function of domain shape)

- Isotherms are parallel in the near-meniscus region. This fact, coupled with the one-dimensional flow characteristics in this region indicate that convective transport in the z-direction (= $v_z\frac{\partial T}{\partial z}$)is not significant there. In fact, because velocities are very small even beyond this region (on average < one-tenth the maximum), convection is probably less significant than conduction until the main recirculation zone is reached.

The results of the 2-D model were compared with experimental measurements of liquid and solid layer thicknesses taken at the steel plant. The following was found.

- Over most of the domain, the location of the liquid/solid interface (given by the melting point isotherm) coincides roughly with the average position of the experimental liquid-solid interface.

There was a significant discrepancy between the depth of the liquid layer at the meniscus, as predicted by the model, and the actual depth measured. The model over-predicts the depth of this liquid layer by 100%.

A three-dimensional finite element model of the melting process of the flux was constructed to evaluate the effect of out-of-plane flow (i.e. normal to the 2-D plane of the previous model). 6.1 times as much material leaves the domain towards the wideface as does to the narrowface. The following results of the fully coupled 3-D model were obtained:

- For most of the domain, strong recirculation zones are established, just as in the 2-D model.

- Near the meniscus, however, the x-direction velocities are low, because the applied stress (at the flux-steel interface) is low. Thus the velocity towards the y-direction due to consumption towards the wideface is comparable to that imposed in the x-direction by the applied shear stress. The balance of these two driving forces results in a location at the flux-steel interface, where the flow separates (65 mm from the narrowface).

- At the separation location, material is moving predominantly in the y-direction towards the wideface outlet. Thus, while heat begins to propagate in the z-direction through the flux, it is removed by convection towards the wideface. This departure from the predominantly one-dimensional flow in the x-direction close to the meniscus, is manifested by an irregularity in the temperature distribution. At the surface of the flux, the temperature is lower at the separation point location than on either side of it, because as much heat is not able to reach the surface at that location as to either side of it.

- As a result of the flow separation at the steel-flux interface, a cool band of material extends from the wideface wall into the domain towards the mid-plane of

symmetry. At positions removed from the separation point, cooler surface temperatures exist only in a narrow band close to the wideface.

- The recirculation zone is larger (i.e. in the z-direction) at the mid-plane of symmetry than in the region close to the wideface wall.

- The liquid/solid interface is depressed close to the wideface wall. Thus the liquid layer thickness decrease in moving from the mid-plane of symmetry towards the wideface (i.e. negative y-direction).

- The coldest surface temperature (~ 100°C) is found at a location approximately 250 mm from the narrowface wall. The thinnest liquid flux layer is found around this location as well. This phenomenon has some implications for the casting process, as the heat loss through the flux at this location is lower than at other locations along the narrowface wall. The non-uniformity in the heat extraction may have some effect on the uniformity in the initially solidified shell along the narrowface wall.

The location of the liquid-solid interface at the wideface as predicted by the 3-D model was compared to the experimental data for liquid layer depth. The following was found:

- The average (i.e. averaged across the mold thickness) location of the interface, predicted and measured, were similar.

- The model just slightly over-predicts the depth of the liquid layer close to the meniscus (by approximately 1 mm). The results of the model show that the isotherms are still parallel (and horizontal) in the close-meniscus region. This feature coupled with the one-dimensional nature of the flow shows that conduction and not convection determines the depth of the liquid domain in this region, after the steady state is achieved.

A parametric study was performed with the numerical 2-D model. Flux melting point, average liquid thermal conductivity and viscosity profile were varied and the effect on the flow pattern and liquid flux layer were investigated.

- Average liquid thermal conductivity did not seem to have a significant effect on the thermal distribution nor on the flow pattern. This behavior is reasonable given the predominance of convection rather than conduction as the mechanism for heat transport. A small difference at the meniscus was observed, likely due to the relative unimportance of convection there.

- A change in the melting point produced a noticeable change in the behavior of the flux. As predicted by the 1-D model, an increase in the melting point decreased the depth of the liquid layer over the entire domain. It seems that the main recirculation zones were compressed a little, as there was less liquid material to establish this zone.

- Flux viscosity changes produced a very significant effect on the behavior of the flux. The case of higher overall viscosity was very difficult to converge because in this case, there was little room to establish the mandatory recirculation zone. The zone must be present, because of the opposition of the two main driving forces. Because of the overall higher viscosity, the liquid can sustain a much larger velocity gradient (i.e. for the fixed applied shear stress). Thus, the x-direction velocity for the initially formed liquid is still small while for the very hot liquid deeper in the pool, it is large. Thus, the predominant motion for initially formed liquid and for the powder is in the negative y-direction, which means that cold material penetrates deeper into the domain than for a low viscosity flux. Hence thinner liquid layers are expected for the high viscosity flux. In fact, the high viscosity case was the only one in which very thin liquid layers, in the meniscus region, were produced using the 2-D model

Finally, another simulation, in addition to the standard case, using the 3-D model was performed. Two features are evident:

- As the average liquid flux viscosity (i.e. over the temperature range of 1000°C - 1500°C) increases, the convective heat transport and hence the liquid layer thickness decreases, in the region of the large recirculation zone. There does not seem to be a significant change in the position of the melt interface at other locations in the mold.

- The surface temperature of the flux, at steady-state is reduced.

CHAPTER 10

CONCLUSIONS AND RECOMMENDATIONS

9.1 CONCLUSIONS

Based on the results of this work, summarised in chapter 9, some conclusions relevant to the actual casting process can be made:

- Flow in the meniscus region is essentially one-dimensional, normal to the heat flux. Therefore heat transfer in this region is conduction dominated, and therefore liquid flux layer thickness is most significantly affected by flux thermal properties like thermal conductivity.

- Due to the combined effects of steel flow towards the SEN and flux consumption flow towards the narrowface, a recirculation zone develops, which results in enhanced convective transport and therefore a deeper liquid layer near the SEN.

- Recirculation flow causes powder added at the SEN to be carried towards the narrowface walls, where it is consumed. This finding implies that more powder needs to be added at the center, even though consumption around the mold perimeter might be uniform.

- Flow separation in the flux layer a distance of approxmately 100mm from the narrow face, results in a very thin liquid layer at the separation point. This generic feature may result in poor feeding of the liquid flux to the mold-strand gap in general, and at the off-corner wideface region in particular. (Refer to Figure 7.31, section 7.4.6 for plots of liquid layer thickness around the perimeter of the mold for the standard 3D case).

- The solidified flux rim on the narrowface wall forces colder, mobile flux (in the upper layers) to flow downwards towards the steel/flux interface, before it can enter the neighbouring mold-strand gap (see Figure 7.21). The result is a dip in the flux melt interface, which corresponds to a decrease in liquid flux thickness at this point, the thinnest liquid layer occuring approximately 20 mm from the narrowface wall.

- Viscosity play a very important role in the thermal and flow behavior of the flux. Lower liquid-flux viscosity produces thicker liquid layers, (due to better convective mixing) which may contribute to the higer consumption and better performance of low viscosity flux. This finding is in apparent agreement with the frequently quoted empirical relationship of μV_c = Constant [17], which states that a lower viscosity is required at higher casting speeds to maintain the same liquid layer thickness.

- Changes in liquid flux viscosity do not seem to have a significant effect on the liquid layer thickness in the near meniscus region.

- Increasing the melting point of the flux decreases the thickness of the liquid flux layer.

- For total flux layer thickness less than 30 mm, addition of more powder will significantly increase the depth of the liquid flux layer. As the powder layer is increased, its thickness has a lessening effect, and for a powder layer thickness greater than 100 mm, the effect on liquid layer thickness is negligible.

- Cold spots develop at the wideface wall around 150 mm from the narrow face. This cold spot is associated with very thin liquid flux layers, and low heat loss through the flux. Lower heat flux implies a thicker flux rim and therefore worse quality problems at these locations

9.2 RECOMMENDATIONS FOR FUTURE WORK

A few ideas for future work are listed below:

- Incorporate the variation of density with temperature into the model. Preliminary work indicates that thermal buoyancy effects as a result of this phenomenon will result in the formation of convection cells. Tentatively, this effect is to be expected because of the high Grashof Number for the problem ($\sim 6 \times 10^5$). Previous works indicate that the critical Grashof number for the formation of multiple cells is approximately 1.2×10^4 [58-60].

- Investigate the effect of casting speed and thus the role of flux/steel interface shape on the position of the melt interface.

- Separate the meniscus region and mold-strand gap from the main flux domain. Using the appropriate boundary conditions obtained from the solution of the complete domain problem, a smaller meniscus model can be created to study the flow and thermal patterns there. It is believed that this region is most critical in the initial shell solidification process and hence on final surface quality.

- Incorporate the periodic oscillation of the mold wall, and make the model transient to study the evolution of waves in the material interfaces (melt and surface). It is postulated that periodic variation in fluid pressure as a result of oscillation may be linked to formation and severity of oscillation marks in the shell surface.

- Use the transient model to investigate the formtion of the slag rim and the role it may play in the deformation of the initially solidified shell.

APPENDIX A

THEORY OF FINITE ELEMENT MODEL FORMULATION

Mathematical modeling of material processing operations has gained momentum in recent years due mostly to the increase in power, efficiency and affordability of computational hardware like workstations. Simple but effective finite difference and spreadsheet models may be implemented even with the personal computers available today. Like all other physical phenomena, materials processing is subject to several governing partial differential equations for fluid flow, heat transfer and stress generation. Because there are rarely any closed-form solution for these equations under realistic conditions, the use of simple spreadsheet models is no longer suitable. Furthermore, finite difference methods are difficult to implement in problems with complex geometries. These shortcomings, therefore, necessitate the use of the more advanced finite element models for physically plausible and accurate numerical solutions to the governing equations. The effective and productive use of these models however requires significant computational power, which is why the upsurge in modeling activity has only occurred recently. This chapter focuses on the implementation of the finite element method (FEM) for modeling of the thermal and fluid flow phenomena which are believed to be at the root of the behavior of the flux.

A.1 GOVERNING EQUATIONS

To mathematically model the behavior of the flux, the governing differential equations for heat and fluid transport must be solved for the variables of velocity, pressure and temperature. These equations may be found in many standard texts [38, 61].

The first of these governing equations is the Continuity Equation for fluid flow, which is the law of conservation of mass applied to a fluid. This equation is given below:

$$\frac{\partial \rho}{\partial t} + \nabla \cdot (\rho \mathbf{V}) = 0 \qquad \text{(A.1)}$$

where: $\mathbf{V}$ = vector of velocity
$= u_x + u_y + u_z$

The first term in equation A.1 is the rate of increase of density in the control volume, while the second term is the rate of mass flux leaving the domain per unit volume. In Cartesian coordinates this equation becomes:

$$\frac{\partial \rho}{\partial t} + \frac{\partial}{\partial x}(\rho u_x) + \frac{\partial}{\partial y}(\rho u_y) + \frac{\partial}{\partial z}(\rho u_z) = 0 \qquad \text{(A.2)}$$

For an incompressible fluid all derivatives of density are zero. Hence, the continuity equation simplifies to:

$$\frac{\partial u_x}{\partial x} + \frac{\partial u_y}{\partial y} + \frac{\partial u_z}{\partial z} = 0 \qquad \text{(A.3)}$$

The second differential equation that must be simultaneously solved with the continuity equation is the Momentum Equation, which is given below in the most general form:

$$\frac{\partial}{\partial t}(\rho \mathbf{V}) + \nabla \cdot \rho \mathbf{V}\mathbf{V} = \rho \mathbf{f} + \nabla \cdot \Pi_{ij} \qquad \text{(A.4)}$$

On a per unit volume basis, the first term is the rate of increase of momentum in the domain; the second term is the rate of momentum lost by convection of the fluid; the third term is the body force (e.g. acceleration due to gravity or Coriolis force or Lorenz force) and the last term represents the surface forces.

Simplifying equation (A.3) using the continuity equation, we get:

$$\rho \frac{\partial \mathbf{V}}{\partial t} + \mathbf{V} \cdot \nabla (\mathbf{V}) = \rho \mathbf{f} + \nabla \cdot \Pi_{ij} \qquad \text{(A.5)}$$

Assuming the flow of the flux is modeled as a continuum, that the flux behaves as a Newtonian Fluid, an expression for the stress tensor, Π_{ij}, may be written as follows:

$$\Pi_{ij} = -\rho\delta_{ij} + \mu\left[\left(\frac{\partial u_i}{\partial x_j} + \frac{\partial u_j}{\partial x_i}\right) - \frac{2}{3}\delta_{ij}\frac{\partial u_k}{\partial x_k}\right] \qquad (A.6)$$

On the right-hand side of equation A.4, the first term is the normal stress tensor, while the second term is the viscous stress tensor, or the tangential stress tensor. Hence:

$$\Pi_{ij} = -\rho\delta_{ij} + \tau_{ij} \qquad (A.7)$$

where: δ_{ij} is the Kronecker delta function

Substituting equation A.6 into the momentum equation A.4, we get the Navier-Stokes Equation:

$$\rho\frac{\partial \mathbf{V}}{\partial t} + \mathbf{V}\bullet\nabla(\mathbf{V}) = \rho\mathbf{f} - \nabla p + \frac{\partial}{\partial x_j}\left[\mu\left(\frac{\partial u_i}{\partial x_j} + \frac{\partial u_j}{\partial x_i}\right) - \frac{2}{3}\delta_{ij}\mu\frac{\partial u_k}{\partial x_k}\right] \qquad (A.8)$$

In Cartesian coordinates, equation (A.8) produces three equations:

$$\rho\frac{\partial u_x}{\partial t} + \mathbf{V}\bullet\nabla(u_x) = \rho f_x - \frac{\partial p}{\partial x} + \frac{\partial}{\partial x}\left[\frac{2}{3}\mu\left(2\frac{\partial u_x}{\partial x} - \frac{\partial u_y}{\partial y} - \frac{\partial u_z}{\partial z}\right)\right]$$

$$+ \frac{\partial}{\partial y}\left[\mu\left(\frac{\partial u_x}{\partial y} + \frac{\partial u_y}{\partial x}\right)\right] + \frac{\partial}{\partial z}\left[\mu\left(\frac{\partial u_z}{\partial x} + \frac{\partial u_x}{\partial z}\right)\right] \qquad (A.9a)$$

$$\rho\frac{\partial u_y}{\partial t} + \mathbf{V}\bullet\nabla(u_y) = \rho f_y - \frac{\partial p}{\partial y} + \frac{\partial}{\partial y}\left[\frac{2}{3}\mu\left(2\frac{\partial u_y}{\partial y} - \frac{\partial u_x}{\partial x} - \frac{\partial u_z}{\partial z}\right)\right]$$

$$+ \frac{\partial}{\partial x}\left[\mu\left(\frac{\partial u_y}{\partial x} + \frac{\partial u_x}{\partial y}\right)\right] + \frac{\partial}{\partial z}\left[\mu\left(\frac{\partial u_y}{\partial z} + \frac{\partial u_z}{\partial y}\right)\right] \qquad (A.9b)$$

$$\rho\frac{\partial u_z}{\partial t} + \mathbf{V}\bullet\nabla(u_z) = \rho f_z - \frac{\partial p}{\partial z} + \frac{\partial}{\partial z}\left[\frac{2}{3}\mu\left(2\frac{\partial u_z}{\partial z} - \frac{\partial u_x}{\partial x} - \frac{\partial u_y}{\partial y}\right)\right]$$

$$+ \frac{\partial}{\partial x}\left[\mu\left(\frac{\partial u_z}{\partial x} + \frac{\partial u_x}{\partial z}\right)\right] + \frac{\partial}{\partial y}\left[\mu\left(\frac{\partial u_y}{\partial z} + \frac{\partial u_z}{\partial y}\right)\right] \qquad (A.9c)$$

Assuming the flow of the flux is modeled as a continuum, that the flux behaves as a Newtonian Fluid, an expression for the stress tensor, Π_{ij}, may be written as follows:

$$\Pi_{ij} = -\rho\delta_{ij} + \mu\left[\left(\frac{\partial u_i}{\partial x_j} + \frac{\partial u_j}{\partial x_i}\right) - \frac{2}{3}\delta_{ij}\frac{\partial u_k}{\partial x_k}\right] \qquad (A.6)$$

On the right-hand side of equation A.4, the first term is the normal stress tensor, while the second term is the viscous stress tensor, or the tangential stress tensor. Hence:

$$\Pi_{ij} = -\rho\delta_{ij} + \tau_{ij} \qquad (A.7)$$

where: δ_{ij} is the Kronecker delta function

Substituting equation A.6 into the momentum equation A.4, we get the Navier-Stokes Equation:

$$\rho\frac{\partial \mathbf{V}}{\partial t} + \mathbf{V}\bullet\nabla(\mathbf{V}) = \rho\mathbf{f} - \nabla p + \frac{\partial}{\partial x_j}\left[\mu\left(\frac{\partial u_i}{\partial x_j} + \frac{\partial u_j}{\partial x_i}\right) - \frac{2}{3}\delta_{ij}\mu\frac{\partial u_k}{\partial x_k}\right] \qquad (A.8)$$

In Cartesian coordinates, equation (A.8) produces three equations:

$$\rho\frac{\partial u_x}{\partial t} + \mathbf{V}\bullet\nabla(u_x) = \rho f_x - \frac{\partial p}{\partial x} + \frac{\partial}{\partial x}\left[\frac{2}{3}\mu\left(2\frac{\partial u_x}{\partial x} - \frac{\partial u_y}{\partial y} - \frac{\partial u_z}{\partial z}\right)\right]$$

$$+ \frac{\partial}{\partial y}\left[\mu\left(\frac{\partial u_x}{\partial y} + \frac{\partial u_y}{\partial x}\right)\right] + \frac{\partial}{\partial z}\left[\mu\left(\frac{\partial u_z}{\partial x} + \frac{\partial u_x}{\partial z}\right)\right] \qquad (A.9a)$$

$$\rho\frac{\partial u_y}{\partial t} + \mathbf{V}\bullet\nabla(u_y) = \rho f_y - \frac{\partial p}{\partial y} + \frac{\partial}{\partial y}\left[\frac{2}{3}\mu\left(2\frac{\partial u_y}{\partial y} - \frac{\partial u_x}{\partial x} - \frac{\partial u_z}{\partial z}\right)\right]$$

$$+ \frac{\partial}{\partial x}\left[\mu\left(\frac{\partial u_y}{\partial x} + \frac{\partial u_x}{\partial y}\right)\right] + \frac{\partial}{\partial z}\left[\mu\left(\frac{\partial u_y}{\partial z} + \frac{\partial u_z}{\partial y}\right)\right] \qquad (A.9b)$$

$$\rho\frac{\partial u_z}{\partial t} + \mathbf{V}\bullet\nabla(u_z) = \rho f_z - \frac{\partial p}{\partial z} + \frac{\partial}{\partial z}\left[\frac{2}{3}\mu\left(2\frac{\partial u_z}{\partial z} - \frac{\partial u_x}{\partial x} - \frac{\partial u_y}{\partial y}\right)\right]$$

$$+ \frac{\partial}{\partial x}\left[\mu\left(\frac{\partial u_z}{\partial x} + \frac{\partial u_x}{\partial z}\right)\right] + \frac{\partial}{\partial y}\left[\mu\left(\frac{\partial u_y}{\partial z} + \frac{\partial u_z}{\partial y}\right)\right] \qquad (A.9c)$$

When equations A.9a, A.9b and A.9c are solved simultaneously along with the continuity equation, each of the independent variables u_x, u_y, u_z and p may be determined.

For coupled heat transfer and fluid flow problems such as the one being studied here, a third equation needs to be solved for the temperature field in the domain being studied. This equation, called the Energy Equation, is the result of applying the First Law of Thermodynamics to fluid passing through an infinitesimal fixed control volume. The total energy equation and the explanation of the terms are given below:

$$\frac{\partial E_t}{\partial t} + \nabla \cdot E_t \mathbf{V} = \frac{\partial Q}{\partial t} - \nabla \cdot q + \rho \mathbf{f} \cdot \mathbf{V} + \nabla \cdot \left(\Pi_{ij} \cdot \mathbf{V}\right) \qquad \text{(A.10)}$$

The first term on the left-hand side of equation A.10 is the total energy accumulation and the second term represents the convective loss of energy. On the right-hand side of the same equation, the first term is the energy generation, the second is conductive loss, the third is the work done due to body forces while the last term is the work done by surface forces.

Re-writing equation A.10 using the continuity equation, we get:

$$\rho \frac{D\left(E_t/\rho\right)}{Dt} = \frac{\partial Q}{\partial t} - \nabla \cdot q + \rho \mathbf{f} \cdot \mathbf{V} + \nabla \cdot \left(\Pi_{ij} \cdot \mathbf{V}\right)$$

$$\Rightarrow \quad \rho \frac{Du}{Dt} + \rho \frac{D\left(V^2/2\right)}{Dt} = \frac{\partial Q}{\partial t} - \nabla \cdot q + \rho \mathbf{f} \cdot \mathbf{V} + \nabla \cdot \left(\Pi_{ij} \cdot \mathbf{V}\right) \qquad \text{(A.11)}$$

Equation A.11 is obtained by considering only internal energy, u, and kinetic energy. Re-writing the momentum equation A.5 and taking the dot product with $\mathbf{V}$, we get:

$$\rho \frac{\partial \mathbf{V}}{\partial t} + \mathbf{V} \cdot \nabla (\mathbf{V}) = \rho \mathbf{f} + \nabla \cdot \Pi_{ij}$$

$$\Rightarrow \quad \rho \frac{D\mathbf{V}}{Dt} = \rho \mathbf{f} + \nabla \cdot \Pi_{ij}$$

$$\Rightarrow \quad \rho \frac{D\mathbf{V}}{Dt} \cdot \mathbf{V} = \rho \mathbf{f} \cdot \mathbf{V} + \left(\nabla \cdot \Pi_{ij}\right) \cdot \mathbf{V}$$

$$\Rightarrow \quad \rho \frac{D\mathbf{V}}{Dt} \cdot \mathbf{V} = \rho \mathbf{f} \cdot \mathbf{V} - \nabla p \cdot \mathbf{V} + (\nabla \cdot \tau_{ij}) \cdot \mathbf{V} \qquad (A.12)$$

Using equation A.12 to express the kinetic energy term in equation A.11, we may re-write the energy equation as follows:

$$\rho \frac{Du}{Dt} + \rho \mathbf{f} \cdot \mathbf{V} - \nabla p \cdot \mathbf{V} + (\nabla \cdot \tau_{ij}) \cdot \mathbf{V} = \frac{\partial Q}{\partial t} - \nabla \cdot q + \rho \mathbf{f} \cdot \mathbf{V} + \nabla \cdot (\Pi_{ij} \cdot \mathbf{V})$$

$$\Rightarrow \quad \rho \frac{Du}{Dt} - \nabla p \cdot \mathbf{V} = \frac{\partial Q}{\partial t} - \nabla \cdot q + \nabla \cdot (\Pi_{ij} \cdot \mathbf{V}) - (\nabla \cdot \tau_{ij}) \cdot \mathbf{V}$$

$$\Rightarrow \quad \rho \frac{Du}{Dt} - \nabla p \cdot \mathbf{V} = \frac{\partial Q}{\partial t} - \nabla \cdot q + \nabla \cdot [(-p + \tau_{ij}) \cdot \mathbf{V}] - (\nabla \cdot \tau_{ij}) \cdot \mathbf{V}$$

$$\Rightarrow \quad \rho \frac{Du}{Dt} - \nabla p \cdot \mathbf{V} = \frac{\partial Q}{\partial t} - \nabla \cdot q + \nabla \cdot (-p.\mathbf{V} + \tau_{ij} \cdot \mathbf{V}) - (\nabla \cdot \tau_{ij}) \cdot \mathbf{V}$$

$$\Rightarrow \quad \rho \frac{Du}{Dt} - \nabla p \cdot \mathbf{V} = \frac{\partial Q}{\partial t} - \nabla \cdot q - \nabla \cdot (p.\mathbf{V}) + \nabla \cdot (\tau_{ij} \cdot \mathbf{V}) - (\nabla \cdot \tau_{ij}) \cdot \mathbf{V}$$

$$\Rightarrow \quad \rho \frac{Du}{Dt} - \nabla p \cdot \mathbf{V} = \frac{\partial Q}{\partial t} - \nabla \cdot q - p(\nabla \cdot \mathbf{V}) - \mathbf{V} \cdot \nabla p + \nabla \cdot (\tau_{ij} \cdot \mathbf{V}) - (\nabla \cdot \tau_{ij}) \cdot \mathbf{V}$$

$$\Rightarrow \quad \rho \frac{Du}{Dt} - p(\nabla \cdot \mathbf{V}) = \frac{\partial Q}{\partial t} - \nabla \cdot q + \nabla \cdot (\tau_{ij} \cdot \mathbf{V}) - (\nabla \cdot \tau_{ij}) \cdot \mathbf{V}$$

(A.13)

The last two terms of equation A.13 may be combined into what is known as the viscous dissipation $\mu\Phi$, as shown below:

$$\mu\Phi = \tau_{ij} \frac{\partial u_i}{\partial x_j} = \nabla \cdot (\tau_{ij} \cdot \mathbf{V}) - (\nabla \cdot \tau_{ij}) \cdot \mathbf{V} \qquad (A.14)$$

where: Φ = Dissipation Rate

$$= 2\left[\left(\frac{\partial u_x}{\partial x}\right)^2 + \left(\frac{\partial u_y}{\partial y}\right)^2 + \left(\frac{\partial u_z}{\partial z}\right)^2\right] + \left(\frac{\partial u_y}{\partial x} + \frac{\partial u_x}{\partial y}\right)^2$$

$$+ \left(\frac{\partial u_z}{\partial y} + \frac{\partial u_y}{\partial z}\right)^2 + \left(\frac{\partial u_x}{\partial z} + \frac{\partial u_z}{\partial x}\right)^2 + \frac{2}{3}(\nabla \cdot \mathbf{V})^2$$

Using the definition of enthalpy:

$$h = u + \frac{p}{\rho} \tag{A.15}$$

and the continuity equation, we may express the energy equation (A.13) as follows:

$$\rho \frac{Dh}{Dt} = \frac{Dp}{Dt} + \frac{\partial Q}{\partial t} - \nabla \cdot q + \mu\Phi \tag{A.16}$$

For incompressible flow and constant thermal conductivity, the energy equation simplifies to:

$$\rho c_p \frac{DT}{Dt} = \nabla \cdot (k\nabla T) + \mu\Phi \tag{A.17}$$

Finally, to close the system of equations (i.e. energy, momentum and continuity), equations of state which relate the transport properties (μ and k) to the thermodynamic variables (p, ρ, T, u, h) must be established. These equations are specific to the problem and are discussed in Chapter 5.

A.2 FINITE ELEMENT METHOD

A.2.1 Problem Discretization

The continuum problem of fluid flow and heat transfer, described by the foregoing differential equations, has an infinite number of degrees of freedom. The purpose of the finite element method (FEM) is to convert this continuous problem into a discrete one, in which there is a limited number of degrees of freedom, and which is described instead by a system of algebraic equations. In the first step, the domain is discretized into several small regions know as elements, the corners of which are called nodes. This allows the problem to be formulated on the elemental basis and then subsequently assembled to represent the entire system being modeled.

The velocity and temperature fields (u_x, u_y, u_z, p and T) within the element are approximated, based on the variable values at the nodal points, using interpolation or shape functions. Figure A.1 is an illustration of the discretization in one dimension. The interpolation

functions $N_j(x)$ and $N_k(x)$ may be linear as shown in Figure A.1 or of a higher order depending on the actual variation of the unknown variable being solved for. All interpolation functions have the value of unity at its own node and zero at every other node. The discretized variable (e.g u^e in Figure A.1) is then expressed as the algebraic sum of the products of the shape functions N and the value of the variable at the nodes (see Figure A.1)

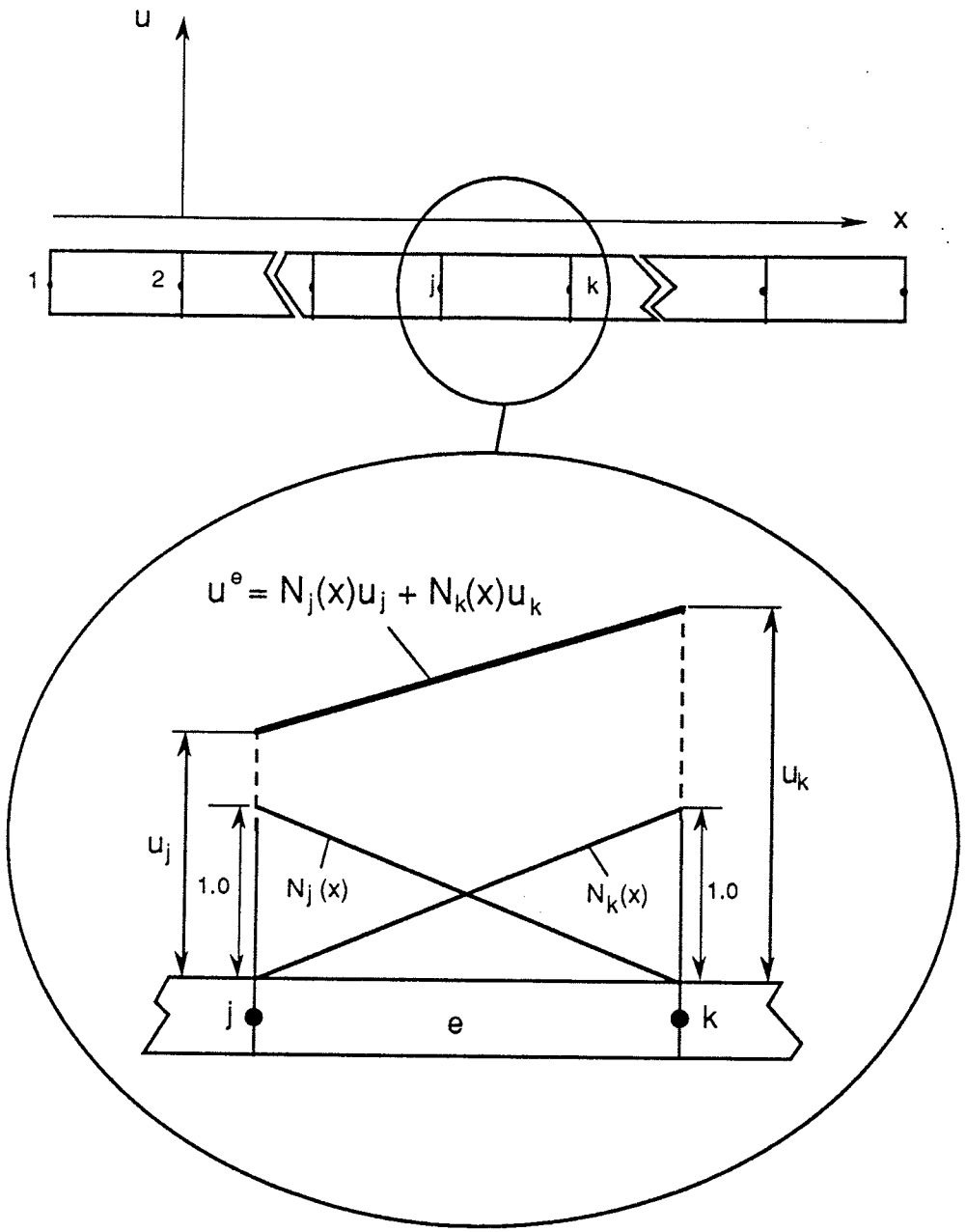

Figure A.1 - Illustration of Domain Discretization for the Finite Element Method[62]

In matrix notation, therefore, we may express the variable u on the element basis as:

$$u^e = [N]\{U^e\} \tag{A.18}$$

where: $[N] = [N_j(x) \quad N_k(x)]$ = Matrix of Shape Functions

$\{U^e\} = \begin{Bmatrix} u_j \\ u_k \end{Bmatrix}$ = Matrix of Nodal Values for the element

Assuming that u satisfies the function $H(u,x) = 0$, substitution of the approximated value u^e (i.e. for each element) into H, gives the following result:

$$H(u^e) = R^e \tag{A.19}$$

where: R^e = Non-zero residual

The next step in the Finite Element Method is to attempt to reduce the residual R to zero for the entire domain. The method generally used is the Galerkin Weighted Residual Method. In weighted residual methods, the residual R is pre-multiplied by some weighting function W(x) and then integrated over the entire domain. In the Galerkin formulation, W(x) is chosen to be equal to the Shape Function N(x). Hence for the entire domain, we obtain the expressions:

$$\sum_{e=1}^{M} \int_{x_j}^{x_k} N_j(x)[R^e(x;u_j,u_k)]\, dx = 0 \tag{A.20a}$$

and

$$\sum_{e=1}^{M} \int_{x_j}^{x_k} N_k(x)[R^e(x;u_j,u_k)]\, dx = 0 \tag{A.20b}$$

where: M = Number of Elements

Combining equations 4.20a and 4.20b, we obtain:

$$\sum_{e=1}^{M} \int_{x_j}^{x_k} [N]^T(x)[R^e(x;u_j,u_k)]\, dx = 0 \qquad (A.21)$$

where: $$[N]^T = \begin{bmatrix} N_j(x) \\ N_k(x) \end{bmatrix}$$

The summation represents the assembly of the expressions for all the elements in the domain, but the analysis may be performed on an element basis for the time being. Replacing Re by the appropriate expression in term of the field variable, and performing the integration, equation A.21 may be expressed (without the summation from 1 to M) as follows:

$$\mathbf{K}^e \{\mathbf{U}^e\} = \mathbf{f}^e \qquad (A.22)$$

where: $\mathbf{K}^e$ = Element stiffness Matrix = $\int_{x_j}^{x_k} \frac{dN^T}{dx} \frac{dN}{dx} dx$

$\{U^e\}$ = Vector of Nodal unknowns (defined previously)

$\mathbf{f}^e$ = element forcing function = $\int_{x_j}^{x_k} N^T H(u,x)\, dx$

Equation A.22 is expressed for each element, and all such relations are assembled into a system of system of algebraic equations. The boundary conditions are applied and the system of equations (A.23) is solved for the nodal unknowns {U}.

$$\mathbf{K}\{\mathbf{U}\} = \mathbf{f} \qquad (A.23)$$

where: $$\{U\} = \begin{Bmatrix} u_1 \\ u_2 \\ \cdot \\ \cdot \\ \cdot \\ u_{n-1} \\ u_n \end{Bmatrix}$$

n = number of nodes

In a similar way, the governing equations for fluid flow and heat transfer may be discretized into a series of algebraic equations to be solved. Within each element the velocity, pressure and temperature fields may be approximated as follows [63]:

$$\left.\begin{aligned} u_i(x,t) &= \varphi^T U_i(t) \\ p(x,t) &= \Psi^T P(t) \\ T(x,t) &= \vartheta^T T(t) \end{aligned}\right\} \qquad (A.24)$$

where: U_i, P, T are column vectors of element nodal point unknowns

φ, Ψ, ϑ are the column vectors of the interpolation functions.

Letting f_1, f_2 and f_3 denote the momentum, continuity and energy equations respectively, upon substitution of the discretized variables (equation A.24), the following is obtained:

$$\left.\begin{aligned} f_1\,(\varphi,\Psi,\vartheta,U_i,P,T) &= R_1 \\ f_2\,(\varphi,U_i) &= R_2 \\ f_3\,(\varphi,\vartheta,U_i,T) &= R_3 \end{aligned}\right\} \qquad (A.25)$$

where: R_1, R_2, and R_3 are the residuals resulting from the use of the approximations given by equation A.24.

Applying the Galerkin formulation to reduce the residuals to zero, the following is obtained:

$$\left.\begin{aligned} (f_1,\varphi) = (R_1,\varphi) &= 0 \\ (f_2,\Psi) = (R_2,\Psi) &= 0 \\ (f_3,\vartheta) = (R_3,\vartheta) &= 0 \end{aligned}\right\} \qquad (A.26)$$

where: (a,b) is defined as $\int_V a.b\, dV$ (V being the volume of the element)

Performing the integrations above in equations A.26, we obtain the following matrix equations for one element:

$$\text{Momentum:} \quad M\dot{U} + A(U)U + K(T,U)U - CP + B(T)T = F(T) \qquad (A.27)$$

$$\text{Continuity:} \quad C^T U = 0 \quad \text{(incompressible)} \qquad (A.28)$$

$$\text{Energy:} \quad N\dot{T} + D(U)T + L(T)T = G(U,T) \qquad (A.29)$$

Expanding the variable vectors U and T and combining into one matrix equation, we obtain the following:

$$\begin{pmatrix} M & 0 & 0 & 0 & 0 \\ 0 & M & 0 & 0 & 0 \\ 0 & 0 & M & 0 & 0 \\ 0 & 0 & 0 & N & 0 \\ 0 & 0 & 0 & 0 & 0 \end{pmatrix} \begin{pmatrix} \dot{U}_1 \\ \dot{U}_2 \\ \dot{U}_3 \\ \dot{T} \\ \dot{P} \end{pmatrix} + \begin{pmatrix} K_1 & K_{12} & K_{13} & B_1 & -C_1 \\ K_{21} & K_2 & K_{23} & B_2 & -C_2 \\ K_{31} & K_{32} & K_3 & B_3 & -C_3 \\ 0 & 0 & 0 & L_1 & 0 \\ -C_1 & -C_2^T & -C_3^T & 0 & 0 \end{pmatrix} \begin{pmatrix} U_1 \\ U_2 \\ U_3 \\ T \\ P \end{pmatrix} +$$

$$\begin{pmatrix} A_{ii} & 0 & 0 & 0 & 0 \\ 0 & A_{ii} & 0 & 0 & 0 \\ 0 & 0 & A_{ii} & 0 & 0 \\ 0 & 0 & 0 & D_{ii} & 0 \\ 0 & 0 & 0 & 0 & 0 \end{pmatrix} \begin{pmatrix} U_1 \\ U_2 \\ U_3 \\ T \\ P \end{pmatrix} = \begin{pmatrix} F_1 \\ F_2 \\ F_3 \\ G \\ 0 \end{pmatrix} \qquad (A.30)$$

where:

$$M = \int_V \rho\varphi\varphi^T \, dV$$

$$N = \int_V \rho c_p \vartheta\vartheta^T \, dV$$

$$K_{ij} = \int_V \mu \frac{\partial\varphi}{\partial x_j} \frac{\partial\varphi^T}{\partial x_i} \, dV$$

$$K_1 = 2K_{11} + K_{22} + K_{33}$$

$$K_2 = K_{11}+2K_{22}+K_{33}$$

$$K_3 = K_{11}+K_{22}+2K_{33}$$

$$C_i = \int_V \frac{\partial \varphi}{\partial x_i} \psi^T \, dV$$

$$L_{ij} = \int_V k \frac{\partial \vartheta}{\partial x_j} \frac{\partial \vartheta^T}{\partial x_i} \, dV$$

$$A_i(U_j) = \int_V \rho \varphi u_j \frac{\partial \varphi^T}{\partial x_i} \, dV$$

$$A_{ii} = A_i(U_i)$$

$$D_i(U_j) = \int_V \rho c_p \vartheta u_j \frac{\partial \vartheta^T}{\partial x_i} \, dV$$

$$D_{ii} = A_i(U_i)$$

$$B_i = \int_V \rho g_i \beta \varphi \vartheta^T \, dV$$

$$F_i = \int_S \bar{t}_i \varphi \, dS + \int_V \rho f_i \varphi \, dV + \int_V \rho g_i \beta T_\infty \varphi \, dV$$

$$G_i = - \int_S (q_a + q_c + q_r)\vartheta \, dS + \int_V q_s \vartheta \, dV + \int_V \mu \Phi \vartheta \, dV$$

The following terms are the result of applying boundary conditions;

q_a = applied heat flux $= k \frac{\Delta t}{\Delta x}$

q_c = convective flux $= h_c (T - T_\infty)$

q_r = radiative heat flux $= \sigma\varepsilon\left(T^4 - T_\infty^4\right)$

q_s = Internal heat generation/unit volume $= \frac{dQ}{dt}$

t_i = Surface Traction forces

f_i = body force terms other than force due to gravity

The effect of density changes in the body force term in the momentum equation may accounted for by the Boussinesq Model which assumes that the density is constant ($= \rho_o$) except

in the presence of a gravitational field. The buoyancy force which exists due to density variations may be represented as follows:

$$f_b = \rho_o[\beta(T - T_\infty)]g_i$$

where: β = volumetric expansion coefficient

T_∞ = Reference Temperature

A.2.2 Solution Procedures

The discretization of the continuum problem using the finite element method generates a system of algebraic equations which requires that a solution algorithm be used for its resolution. The solution method used depends on whether the problem being solved is a steady-state or a transient one. Additionally, in many cases, the problems being solved are non-linear which required iterative procedures for solution. Essentially, the choices for solution of a system of non-linear algebraic equations generated by the finite element method are Successive Substitution and Newton-type methods for steady state problems and implicit or explicit time integration schemes for transient problems.

A.2.2.1 Successive Substitution[63]

Also know as Picard or Fixed Point Iteration, this method requires that the stiffness matrix (i.e. the nonlinearity) be evaluated at the know iterate u_i (or guess of the solution) and may be expressed as follows:

$$\mathbf{K}(u_i)\mathbf{u}_{i+1} = \mathbf{F} \qquad \text{(A.31)}$$

A non-symmetric system of linear equations is thus formed and solved at each iteration, with the values of the iterate u_i approaching the exact value as the number of iterations increases. Convergence towards the exact solution occurs for a wide range of the problems, but the rate of convergence is slow.

A.2.2.2 Newton-Type Methods

Recall that the Galerkin finite element method requires the solution of:

$$R(u) = 0 \tag{A.32}$$

where R is the residual (error) function obtained by using the approximation $u = \mathbf{N}^T\{\mathbf{U}\}$

Expressing the exact solution u in terms of an approximation u*, performing the Taylor series expansion of R(u), and substituting into equation A.32 we obtain:

$$u = u^* + \Delta u$$

$$\Rightarrow \quad R(u) = R(u^*) + \frac{\partial R}{\partial u}(u^*)\,\Delta u = 0$$

(ignoring higher order terms in Δu)

$$\Rightarrow \quad R(u^*) = -\frac{\partial R}{\partial u}(u^*)\,\Delta u$$

$$\Rightarrow \quad R(u_i) = -\frac{\partial R}{\partial u}(u_i)\,(u_{i+1} - u_i)$$

$$\Rightarrow \quad u_{i+1} = u_i - \frac{R(u_i)}{\partial R/\partial u} \tag{A.33}$$

While the rate of convergence is high for method of the Newton type, convergence on the correct solution is highly dependent on the initial guess for the iteration.

A.2.2.3 Implicit Time Integration

In transient problems, the system of finite element equations may be expressed as follows:

$$\mathbf{C}(u)\dot{u} + \mathbf{K}(u)u = F \tag{A.34}$$

The time derivative of the field variable u may be evaluated as:

$$\dot{u} = \frac{u_{n+1} - u_n}{\Delta t} \tag{A.35}$$

However for evaluation of K(u)u and F, a choice of which estimate of u is used, i.e. u_n or u_{n+1} must be made. Fully implicit methods use u_{n+1}.

$$\mathbf{C}(u)\,\frac{u_{n+1} - u_n}{\Delta t} + \mathbf{K}(u)u_{n+1} = \mathbf{F}_{n+1} \qquad \text{(A.36)}$$

The reader is directed to the FIDAP Theoretical Manual [63] for complete details of time integration schemes.

A.2.2.4 Convergence Criterion

To ensure that the solution method converges on an accurate solution without expending extra unnecessary computational effort, a criterion needs to be developed to determine whether an acceptable answer to the problem has been obtained. In general convergence has occurred when the result of one iteration is not significantly different from that of the preceding iteration. The "significance" of the disparity is determined by comparing the difference to some user preset convergence tolerance. Two tolerances may be set. One tolerance, ε_u for the field variable, and another, ε_f for the value of the residual.

A convergence criterion is developed as follows:

If $\Delta u = u_{i+1} - u_i$

Convergence achieved when

$$\left.\begin{array}{ll} \| \Delta u_i \| < \varepsilon_u \| u_{i+1} \| & \text{or} \\ \| R_i \| < \varepsilon_f \| F \| & \end{array}\right\} \qquad \text{(A.34)}$$

where $\| u \|$ = Norm of column vector of variable u

The norm of the variable u may be calculated in two ways:

$$\left.\begin{array}{lll} L_1\text{-Norm:} & \| u_i \| = \max\limits_{i=1}^{N} | u_i | & \text{or} \\ L_2\text{-Norm:} & \| u_i \| = \sqrt{\sum\limits_{i=1}^{N} (\Delta u_i)^2} & \end{array}\right\} \qquad \text{(A.35)}$$

A.2.2.4 Solution Strategy

Given the characteristics of the various solution methods described previously, it is sometimes necessary to take steps to ensure that the method converges and that it converges on the correct solution. Additionally, it is also desirable to control the behavior of the convergence with respect to stability and speed. Numerical solution strategies have be devised to accommodate these needs of fast and accurate solutions.

To increase the stability of a converging steady state solution method, and to avoid oscillation of the solution, the method of under-relaxation is used. In this method, the next guess of an iterate u_{i+1} is a combination of the present and the last most recent iterates (u^* and u_i respectively) according to:

$$\mathbf{K}(u_i)\, u^* = \mathbf{F}_i$$

relaxation: $$a_{i+1} = \alpha a^* + (1-\alpha)\, a_i$$

where: α is a relaxation factor that the user chooses

If α lies between 0 and 1, then the solution is said to be under-relaxed, as described above. If however the value is chosen to be greater than 1, the method is over-relaxed. Over-relaxation or acceleration is used to increase the rate of convergence of the solution method, but may result in instability or divergence if not properly employed.

To improve the efficiency of the solution stage of the finite element problem, a combination of solution methods may be employed. For example, in steady state problems, the Newton methods are desirable because of their high rate of convergence. However because of the high sensitivity to the initial guess, convergence on the correct solution is not assured. However, successive substitution is a more robust method because it will converge for a wide range of problems. The negative side though is its slow rate of convergence. A combination of the two methods should be employed to take advantage of the benefits of both.

APPENDIX B

MODEL ASSUMPTIONS AND BACKGROUND

B.1 ASSUMPTIONS

1. Steady
2. No Body Forces
3. Laminar Flow
4. Density is constant
5. Generalized Newtonian Fluid
6. $H = H(T)$, $k = k(T)$, $\mu = \mu(T)$, $h_c = h_c(T)$

B.2 REYNOLD'S NUMBER CALCULATION

$\rho = 2500\ kg/m^3$

$V = 0.01\ m/s$

L = Equivalent Hydraulic Diameter $= \sqrt{\text{mold width x mold thickness}}$

$= \sqrt{0.7 \times 0.1143} \quad = 0.2829\ m$

$\mu = 0.1\ Pa.s$

$$\Rightarrow \quad Re = \frac{2500 \times 0.01 \times 0.2829}{0.1} \approx 70$$

B.3 CONSISTENT UNIT SET

Unless otherwise noted, **all units are SI**, forming the consistent group given in Table B.1

TABLE B.1 - Consistent Unit Set Used

QUANTITY	UNIT	QUANTITY	UNIT
Length	m	Time	s
Mass	kg	Force	N
Energy	J	Temperature	K
Gravitational Acc.	m/s^2	Density	kg/m^3
Velocity	m/s	Stress (Pressure)	N/m^2 (Pa)
Dynamic Viscosity	Pa.s	Specific Heat	J/(kgK)
Heat Flux	W/m^2	Heat Trans. Coeff.	$W/(m^2.K)$
Thermal Conductivity	W/(m.K)	Thermal Diffusivity	m^2/s

B.4 FLUX RESIDENCE TIME AND MASS IN RECIRCULATION ZONE

2-D MODEL

Referring to the Schematic of Figure B.1,

Cross sectional area of the recirculation zone is estimated to be = 0.006659 m^2

Thickness of mold = 0.1143

=> Volume of recirculating Flux ≈ 0.006659 x 0.1143 = 0.0007611 m3

=> Mass of recirculating flux = Volume x density = 1.9 kg

Mass consumption rate to narrowface = 0.002286 kg/s (see section 4.1.3.5.1)

=> Average residence time $= \frac{\text{recirculating mass}}{\text{mass flow rate (i.e. consumption)}}$

$= \frac{1.9}{0.002286}$ = 83 s

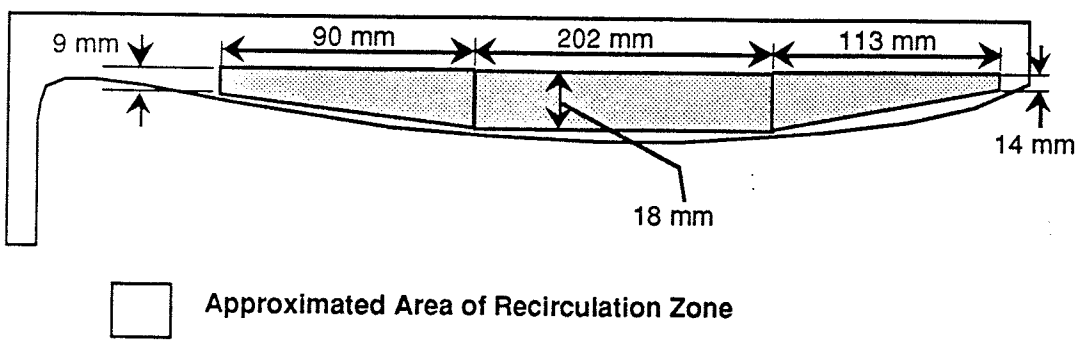

Figure B.1 - Approximation of Cross Sectional Area of Recirculation Zone (2-D)

3-D MODEL

With reference to Figure B.2 -

Area of zone at center plane ≈ 0.01278 m^2

Approximate volume of zone = 0.01278 x 0.1143 = 1.46 E -03

∴ approximate mass in recirculation zone = 1.46 E-03 x 2500

= 3.65 kg

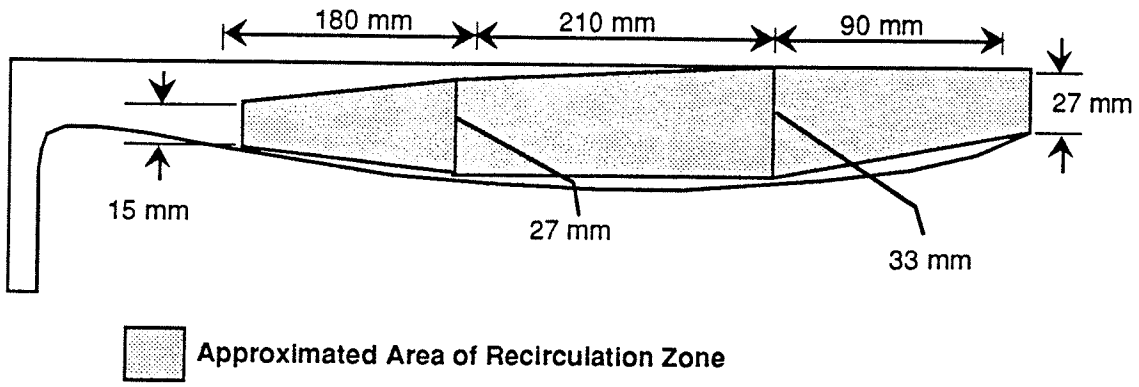

Figure B.2 - Approximation of Area of Recirculation Zone at The Center Plane (3-D)

Total Mass consumption = 0.0326 kg/s

=> Average residence time $= \frac{3.65}{0.03286}$

$= 112$ s

B.5 PLANT MEASUREMENT SCHEMATIC

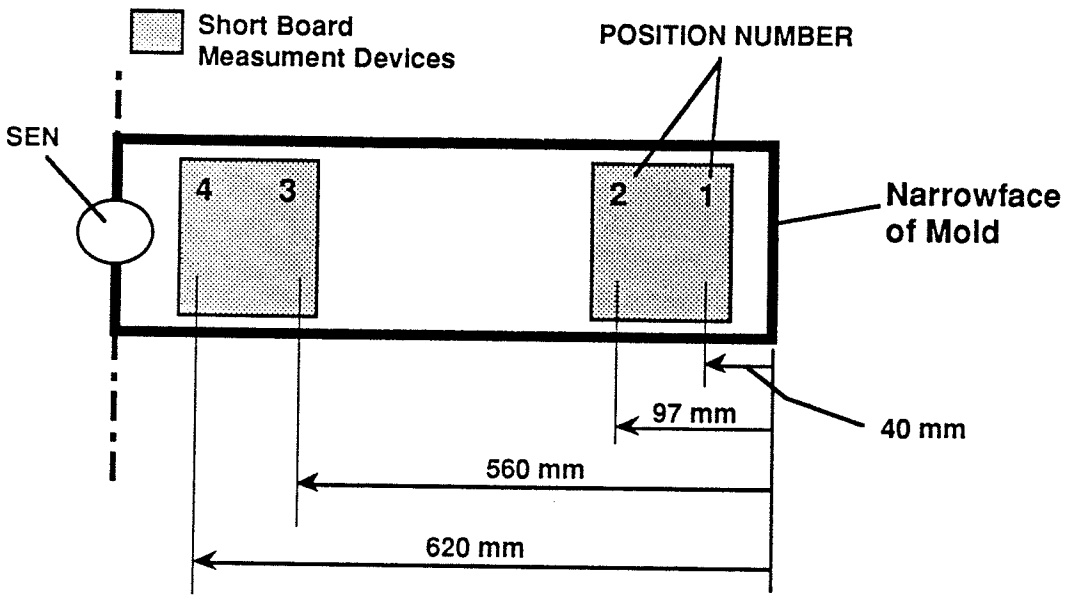

Figure B.3 - Schematic Showing Positions where Flux Measurement at the Plant were taken

APPENDIX C

FIDAP (v6.03) 1-D MODEL INPUT FILES

C.1 STEADY STATE MODEL INPUT FILE

```
*TITLE
  FLUX MELTING - 20 4-N QUAD ELEMENTS/STEADY
*FIMESH (2-D, IMAX=3, JMAX=3)
EXPI
1 2
EXPJ
1 21
POINT
1 1 1 1 0.0 0.0
2 2 1 1 0.0045 0.0
3 2 2 1 0.0045 0.09
4 1 2 1 0.0 0.09
LINE
1 2
2 3
3 4
4 1
NUMBER
2 1
SURFACE
2 4
ELEMENTS (continuum, quadrilateral, nodes=4)
2 4
ELEMENTS (boundary, nodes=2)
3 4
BCNODE (temperature, constant)
1 2 1550.0
BCNODE (ux)
1 2 0.0
2 3 0.0
3 4 0.0
4 1 0.0
BCNODE (uy)
2 4 -5.6243e-5
BCNODE (surface)
3 4 1.0
BCFLUX (heat, nodes=2, constant)
2 3 0.0
4 1 0.0
ICNODE (temperature)
2 4 150.0
END
*FIPREP
PROBLEM (steady, nonlinear, newtonian, 2-D,
laminar, weakly=0)
EXECUTION (newjob)
SOLUTION (n.r.=35, accf=0.4, resconv=0.00001, velconv=0.0001)
PRESSURE (mixed=1.0e-6, discontinuous)
PRINTOUT (all)
DENSITY (set=1, constant=2000)
```

```
VISCOSITY (set=1, curve=7, temperature)
0,   200,  949,   951,  1300,  2000, 2500
1e4, 1e4,  1e4,   2.5,  2.5,   2.5,  2.5
SPECIFICHEAT (set=1, temperature, enthalpy=15, spatial,
tmelt=950, latent=3.5e5)
27,   227,    427,   527,   627,   727,   827,    949,
951,    1027,  1227,   1327,  1600,  2000,  2500
0,    1.8e5,  3.8e5, 4.8e5, 6.0e5, 6.9e5, 8.3e5,  1e6,
1.35e6, 1.4e6, 1.88e6, 2.2e6, 3.2e6, 4.4e6, 6.0e6
CONDUCTIVITY (set=1, curve=12, temperature, isotropic)
0,   200, 400, 600, 800, 900,  950, 1100, 1200, 1400, 1500, 2500
.80, .80 .80, .80,  .80, .80,  1.1, 1.1 , 1.10, 1.10, 1.10, 1.10
NODES (fimesh)
RENUMBER (profile)
HTRANSFER (set=1, curve=10, reftemp=27.0)
-273, 0,  77,  227,  477,  677,  1027,  1327,  1727,  2500
1.2, 4.3, 7.7, 14.1, 28.4, 58.4, 135.1, 231.0, 429.5, 1084.4
ELEMENTS (quadrilateral, nodes=4, fluid, fimesh)
ELEMENTS (convection, nodes=2, mcnv=1, fimesh)
END
*END
```

C.2 TRANSIENT MODEL INPUT FILE

```
*TITLE
  FLUX MELTING IN 2D - 100 4-N QUAD ELEMENTS/TRANSIENT
*FIMESH (2-D, IMAX=3, JMAX=3)
EXPI
1 2
EXPJ
1 21
POINT
1 1 1 1 0.0 0.0
2 2 1 1 0.0025 0.0
3 2 2 1 0.0025 0.05
4 1 2 1 0.0 0.05
LINE
1 2
2 3
3 4
4 1
NUMBER
2 1
SURFACE
2 4
ELEMENTS (continuum, quadrilateral, nodes=4)
2 4
ELEMENTS (boundary, nodes=2)
3 4
BCNODE (temperature, constant)
1 2 1550.0
BCNODE (ux)
1 2 0.0
2 3 0.0
3 4 0.0
4 1 0.0
```

```
BCNODE (uy)
2 4 -5.6243e-5
BCNODE (surface)
3 4 1.0
BCFLUX (heat, nodes=2, constant)
2 3 0.0
4 1 0.0
ICNODE (temperature)
2 4 150.0
END
*FIPREP
PROBLEM (transient, nonlinear, newtonian, 2-D,
laminar, strongly=0)
EXECUTION (restart, rstep=15)
SOLUTION (n.r.=35, accf=0.7, resconv=0.00001, velconv=0.0001)
PRESSURE (mixed=1.0e-8, discontinuous)
TIMEINTEGRATION (trapezoid, nsteps=100, tend=1800,
dt=5.0, variable)
PRINTOUT (all)
DENSITY (set=1, constant=2000)
VISCOSITY (set=1, curve=7, temperature)
0,   200,  949,   951,  1300,  2000, 2500
1e4, 1e4,  1e4,   2.5,  2.5,   2.5,  2.5
SPECIFICHEAT (set=1, temperature, enthalpy=15, spatial,
tmelt=950, latent=3.5e5)
27,   227,    427,   527,   627,   727,   827,    949,
951,    1027,  1227,   1327,  1600,  2000,  2500
0,    1.8e5,  3.8e5, 4.8e5, 6.0e5, 6.9e5, 8.3e5,  1e6,
1.35e6, 1.4e6, 1.88e6, 2.2e6, 3.2e6, 4.4e6, 6.0e6
CONDUCTIVITY (set=1, curve=12, temperature, isotropic)
0,   200, 400, 600, 800, 900,  950, 1100, 1200, 1400, 1500, 2500
.80, .80 .80, .80,  .80, .80,  1.1, 1.1 , 1.10, 1.10, 1.10, 1.10
NODES (fimesh)
RENUMBER (profile)
HTRANSFER (set=1, curve=10, reftemp=27.0)
-273, 0,  77,  227,  477,  677,  1027,  1327,  1727,  2500
1.2, 4.3, 7.7, 14.1, 28.4, 58.4, 135.1, 231.0, 429.5, 1084.4
ELEMENTS (quadrilateral, nodes=4, fluid, fimesh)
ELEMENTS (convection, nodes=2, mcnv=1, fimesh)
END
*END
```

APPENDIX D

FIDAP (v6.03) 2-D MODEL INPUT FILES

D.1 ISOTHERMAL MODEL INPUT FILE

```
*TITLE
W-FACE/6530(9)/ISOTH/dhl=550/tmelt=950/TWO-visc/kl=3
*FIMESH (2-D, IMAX=10, JMAX=10, MXPOINT=750)
EXPI
1 9 57 381 561 621 691
EXPJ
1 51 67 85
POINT
1 1 1 1 -0.0005 -0.01
2 2 1 1 0.001 -0.01
3 2 2 1 0.001 0.00055
4 3 2 1 0.020 0.0069
5 4 2 1 0.260 -0.0088
6 5 2 1 0.460 -0.016
7 6 2 1 0.560 -0.016
8 7 2 1 0.700 -0.0100
9 7 3 1 0.700 -0.001
10 7 4 1 0.700 0.017
11 6 4 1 0.560 0.017
12 5 4 1 0.460 0.017
13 4 4 1 0.260 0.017
14 3 4 1 0.02 0.017
15 2 4 1 0.001 0.017
16 1 4 1 -0.0005 0.017
17 1 3 1 -0.0005 0.01
18 1 2 1 -0.0005 0.00055
19 2 3 1 0.001 0.01
20 3 3 1 0.02 0.01
21 4 3 1 0.260 -0.0006
22 5 3 1 0.460 -0.007
23 6 3 1 0.560 -0.007
CURVE (input)
3 4 21 1.25 3
0.00108507 0.0010
0.00123008 0.0015
0.00144749 0.0020
0.00174240 0.0025
0.00212367 0.0030
0.00260531 0.0035
0.00320916 0.0040
0.0039702 0.0045
0.00494813 0.0050
0.00625592 0.0055
0.00814847 0.0060
0.00864579 0.0061
0.00920358 0.0062
0.00983786 0.0063
0.01057219 0.0064
```

```
0.01144321 0.0065
0.01251268 0.0066
0.01389764 0.0067
0.01586728 0.0068
0.01935433 0.0069
0.0199 0.0069
CURVE (input)
4 5 6
0.050 0.006
0.100 0.001
0.160 -0.003
0.200 -0.0060
0.250 -0.0084
0.258 -0.0087
CURVE (input)
5 6 2
0.360 -0.013
0.459 -0.016
CURVE (input)
6 7 2
0.500 -0.016
0.559 -0.016
CURVE (input)
7 8 3
0.610 -0.015
0.660 -0.013
0.690 -0.011
LINE
1 2
2 3
8 9
9 10
10 11
11 12
12 13
13 14
14 15 0.8 3
15 16
16 17
17 18
18 1
18 3
17 19
19 20 1.25 3
20 21
21 22
22 23
23 9
3 19
19 15
4 20
20 14
5 21
21 13
6 22
22 12
7 23
23 11
```

```
NUMBER
2 1
SURFACE
2 18
3 17
19 16
4 19
20 15
5 20
21 14
6 21
22 13
7 22
23 12
8 23
9 11
AREA
3 9
8 17
8 16
1 3
ELEMENTS (continuum, quadrilateral, nodes=9)
2 18
19 16
20 15
9 14
8 20
ELEMENTS (continuum, triangle, nodes=6)
3 17
4 19
ELEMENTS (boundary, nodes=3)
10 16
3 4
4 8
BCNODE (temperature, constant)
2 3 1550.0
3 4 1550.0
4 5 1550.0
5 6 1550.0
6 7 1550.0
7 8 1550.0
BCNODE (ux)
1 2 0.0
2 3 0.0
8 9 0.0
9 10 0.0
16 17 0.0
17 18 0.0
18 1 0.0
BCNODE (uy)
16 1 0.0
2 3 -0.0166667
10 11 -5.7143e-06
11 12 -5.7143e-06
12 13 -5.7143e-06
13 14 -5.7143e-06
BCFLUX (heat, nodes=3, constant)
8 9 0.0
```

```
9 10 0.0
1 2 0.0
END
*FIPREP
PROBLEM (steady, nonlinear, newtonian, 2-D,
laminar, momentum, isothermal)
EXECUTION (newjob)
SOLUTION (s.s.=15, resconv=1e-4, velconv=1e-9)
PRESSURE (mixed=1.0e-16, continuous)
PRINTOUT (all)
DENSITY (set=1, constant=2500)
VISCOSITY (set=1, constant=0.03)
VISCOSITY (set=2, constant=0.03)
/CONDUCTIVITIES
/Liquid -> Glassy Solid
CONDUCTIVITY (set=1, curve=4, temperature, isotropic)
-9000,  900,  1000, 9000
0.90,   0.9,  3.0,  3.0
/Powder -> Liquid
CONDUCTIVITY (set=2, curve=8, temperature, isotropic)
-9000, 200,  400,  600,   800, 900,  1000, 9000
0.30,  0.30, 0.40, 0.55,  0.7, 0.80, 3.0,  3.0
HTRANSFER (set=1, curve=16, reftemp=27.0)
-3000, -110,  220,  420,  620,  820,  1220,  1420,  1620,  2020,  2420,
2620,   3000,   3500,   4000, 8000
1.1     1.1,  44.7, 65.9, 94.9, 135,  260,   350,   462,   761,   1176,
1434,   2027,   3036,   4341, 4341
NODES (fimesh)
BCFLUX (T, nodes=3)
801 , 766 , 731 ,70, 0.00000E+00
871 , 836 , 801 ,70, 5.35375E-06
941 , 906 , 871 ,70, 1.45232E-05
1011 , 976 , 941 ,70, 2.77153E-05
1081 , 1046 , 1011 ,70, 4.38357E-05
1151 , 1116 , 1081 ,70, 6.23815E-05
1221 , 1186 , 1151 ,70, 8.28796E-05
1291 , 1256 , 1221 ,70, 1.04857E-04
1361 , 1326 , 1291 ,70, 1.27928E-04
1431 , 1396 , 1361 ,70, 1.51798E-04
1501 , 1466 , 1431 ,70, 1.76615E-04
1571 , 1536 , 1501 ,70, 2.02082E-04
1641 , 1606 , 1571 ,70, 2.29221E-04
1711 , 1676 , 1641 ,70, 2.56923E-04
1781 , 1746 , 1711 ,70, 2.84969E-04
1851 , 1816 , 1781 ,70, 3.13454E-04
1921 , 1886 , 1851 ,70, 3.42252E-04
1991 , 1956 , 1921 ,70, 3.71362E-04
2061 , 2026 , 1991 ,70, 4.00786E-04
2131 , 2096 , 2061 ,70, 4.30210E-04
2201 , 2166 , 2131 ,70, 4.80491E-04
2271 , 2236 , 2201 ,70, 5.33943E-04
2341 , 2306 , 2271 ,70, 5.87945E-04
2411 , 2376 , 2341 ,70, 6.41947E-04
2481 , 2446 , 2411 ,70, 6.97051E-04
2551 , 2516 , 2481 ,70, 7.78605E-04
2621 , 2586 , 2551 ,70, 8.60711E-04
2691 , 2656 , 2621 ,70, 9.75945E-04
2761 , 2726 , 2691 ,70, 1.13899E-03
```

```
2831 , 2796 , 2761 ,70, 1.30094E-03
2901 , 2866 , 2831 ,70, 1.46399E-03
2971 , 2936 , 2901 ,70, 1.62594E-03
3041 , 3006 , 2971 ,70, 1.78789E-03
3111 , 3076 , 3041 ,70, 1.95094E-03
3181 , 3146 , 3111 ,70, 2.25346E-03
3251 , 3216 , 3181 ,70, 2.58960E-03
3321 , 3286 , 3251 ,70, 2.92349E-03
3391 , 3356 , 3321 ,70, 3.25964E-03
3461 , 3426 , 3391 ,70, 3.59352E-03
3531 , 3496 , 3461 ,70, 3.92967E-03
3601 , 3566 , 3531 ,70, 4.26356E-03
3671 , 3636 , 3601 ,70, 4.68859E-03
3741 , 3706 , 3671 ,70, 5.33337E-03
3811 , 3776 , 3741 ,70, 5.97382E-03
3881 , 3846 , 3811 ,70, 6.61860E-03
3951 , 3916 , 3881 ,70, 7.25905E-03
4021 , 3986 , 3951 ,70, 7.89517E-03
4091 , 4056 , 4021 ,70, 8.53563E-03
4161 , 4126 , 4091 ,70, 9.17608E-03
4231 , 4196 , 4161 ,70, 9.81653E-03
4301 , 4266 , 4231 ,70, 1.08231E-02
4371 , 4336 , 4301 ,70, 1.19758E-02
4441 , 4406 , 4371 ,70, 1.31286E-02
4511 , 4476 , 4441 ,70, 1.42814E-02
4581 , 4546 , 4511 ,70, 1.54342E-02
4651 , 4616 , 4581 ,70, 1.65792E-02
4721 , 4686 , 4651 ,70, 1.77320E-02
4791 , 4756 , 4721 ,70, 1.88848E-02
4861 , 4826 , 4791 ,70, 2.00375E-02
4931 , 4896 , 4861 ,70, 2.11825E-02
5001 , 4966 , 4931 ,70, 2.28892E-02
5071 , 5036 , 5001 ,70, 2.46233E-02
5141 , 5106 , 5071 ,70, 2.63574E-02
5211 , 5176 , 5141 ,70, 2.80798E-02
5281 , 5246 , 5211 ,70, 2.98139E-02
5351 , 5316 , 5281 ,70, 3.15480E-02
5421 , 5386 , 5351 ,70, 3.32821E-02
5491 , 5456 , 5421 ,70, 3.50045E-02
5561 , 5526 , 5491 ,70, 3.67386E-02
5631 , 5596 , 5561 ,70, 3.84727E-02
5701 , 5666 , 5631 ,70, 4.02069E-02
5771 , 5736 , 5701 ,70, 4.23659E-02
5841 , 5806 , 5771 ,70, 4.45962E-02
5911 , 5876 , 5841 ,70, 4.68417E-02
5981 , 5946 , 5911 ,70, 4.90872E-02
6051 , 6016 , 5981 ,70, 5.13326E-02
6121 , 6086 , 6051 ,70, 5.35629E-02
6191 , 6156 , 6121 ,70, 5.58084E-02
6261 , 6226 , 6191 ,70, 5.80539E-02
6331 , 6296 , 6261 ,70, 6.02841E-02
6401 , 6366 , 6331 ,70, 6.25600E-02
6471 , 6436 , 6401 ,70, 6.48358E-02
6541 , 6506 , 6471 ,70, 6.71116E-02
6611 , 6576 , 6541 ,70, 6.92357E-02
6681 , 6646 , 6611 ,70, 7.18996E-02
6751 , 6716 , 6681 ,70, 7.45100E-02
6821 , 6786 , 6751 ,70, 7.71204E-02
```

```
6891 , 6856 , 6821 ,70, 7.97308E-02
6961 , 6926 , 6891 ,70, 8.21672E-02
7031 , 6996 , 6961 ,70, 8.47776E-02
7101 , 7066 , 7031 ,70, 8.73881E-02
7171 , 7136 , 7101 ,70, 8.99985E-02
7241 , 7206 , 7171 ,70, 9.26089E-02
7311 , 7276 , 7241 ,70, 9.52193E-02
7381 , 7346 , 7311 ,70, 9.76557E-02
7451 , 7416 , 7381 ,70, 1.00266E-01
7521 , 7486 , 7451 ,70, 1.02876E-01
7591 , 7556 , 7521 ,70, 1.05487E-01
7661 , 7626 , 7591 ,70, 1.07881E-01
7731 , 7696 , 7661 ,70, 1.10075E-01
7801 , 7766 , 7731 ,70, 1.12426E-01
7871 , 7836 , 7801 ,70, 1.14777E-01
7941 , 7906 , 7871 ,70, 1.17128E-01
8011 , 7976 , 7941 ,70, 1.19478E-01
8081 , 8046 , 8011 ,70, 1.21829E-01
8151 , 8116 , 8081 ,70, 1.24023E-01
8221 , 8186 , 8151 ,70, 1.26374E-01
8291 , 8256 , 8221 ,70, 1.28725E-01
8361 , 8326 , 8291 ,70, 1.31076E-01
8431 , 8396 , 8361 ,70, 1.33427E-01
8501 , 8466 , 8431 ,70, 1.35621E-01
8571 , 8536 , 8501 ,70, 1.37972E-01
8641 , 8606 , 8571 ,70, 1.40323E-01
8711 , 8676 , 8641 ,70, 1.42673E-01
8781 , 8746 , 8711 ,70, 1.45024E-01
8851 , 8816 , 8781 ,70, 1.47117E-01
8921 , 8886 , 8851 ,70, 1.49150E-01
8991 , 8956 , 8921 ,70, 1.51327E-01
9061 , 9026 , 8991 ,70, 1.53505E-01
9131 , 9096 , 9061 ,70, 1.55682E-01
9201 , 9166 , 9131 ,70, 1.57860E-01
9271 , 9236 , 9201 ,70, 1.59892E-01
9341 , 9306 , 9271 ,70, 1.62070E-01
9411 , 9376 , 9341 ,70, 1.64247E-01
9481 , 9446 , 9411 ,70, 1.66425E-01
9551 , 9516 , 9481 ,70, 1.68603E-01
9621 , 9586 , 9551 ,70, 1.70635E-01
9691 , 9656 , 9621 ,70, 1.72812E-01
9761 , 9726 , 9691 ,70, 1.74990E-01
9831 , 9796 , 9761 ,70, 1.77167E-01
9901 , 9866 , 9831 ,70, 1.79345E-01
9971 , 9936 , 9901 ,70, 1.81160E-01
10041 , 10006 , 9971 ,70, 1.83133E-01
10111 , 10076 , 10041 ,70, 1.85107E-01
10181 , 10146 , 10111 ,70, 1.87080E-01
10251 , 10216 , 10181 ,70, 1.89054E-01
10321 , 10286 , 10251 ,70, 1.91027E-01
10391 , 10356 , 10321 ,70, 1.92869E-01
10461 , 10426 , 10391 ,70, 1.94843E-01
10531 , 10496 , 10461 ,70, 1.96816E-01
10601 , 10566 , 10531 ,70, 1.98790E-01
10671 , 10636 , 10601 ,70, 2.00764E-01
10741 , 10706 , 10671 ,70, 2.02605E-01
10811 , 10776 , 10741 ,70, 2.04579E-01
10881 , 10846 , 10811 ,70, 2.06553E-01
```

```
10951 , 10916 , 10881 ,70, 2.08526E-01
11021 , 10986 , 10951 ,70, 2.10500E-01
11091 , 11056 , 11021 ,70, 2.11987E-01
11161 , 11126 , 11091 ,70, 2.13469E-01
11231 , 11196 , 11161 ,70, 2.14951E-01
11301 , 11266 , 11231 ,70, 2.16432E-01
11371 , 11336 , 11301 ,70, 2.17914E-01
11441 , 11406 , 11371 ,70, 2.19396E-01
11511 , 11476 , 11441 ,70, 2.20778E-01
11581 , 11546 , 11511 ,70, 2.22260E-01
11651 , 11616 , 11581 ,70, 2.23742E-01
11721 , 11686 , 11651 ,70, 2.25223E-01
11791 , 11756 , 11721 ,70, 2.26705E-01
11861 , 11826 , 11791 ,70, 2.28187E-01
11931 , 11896 , 11861 ,70, 2.29570E-01
12001 , 11966 , 11931 ,70, 2.31051E-01
12071 , 12036 , 12001 ,70, 2.32533E-01
12141 , 12106 , 12071 ,70, 2.34014E-01
12211 , 12176 , 12141 ,70, 2.35305E-01
12281 , 12246 , 12211 ,70, 2.36347E-01
12351 , 12316 , 12281 ,70, 2.37319E-01
12421 , 12386 , 12351 ,70, 2.38361E-01
12491 , 12456 , 12421 ,70, 2.39402E-01
12561 , 12526 , 12491 ,70, 2.40444E-01
12631 , 12596 , 12561 ,70, 2.41485E-01
12701 , 12666 , 12631 ,70, 2.42527E-01
12771 , 12736 , 12701 ,70, 2.43499E-01
12841 , 12806 , 12771 ,70, 2.44540E-01
12911 , 12876 , 12841 ,70, 2.45582E-01
12981 , 12946 , 12911 ,70, 2.46623E-01
13051 , 13016 , 12981 ,70, 2.47665E-01
13121 , 13086 , 13051 ,70, 2.48706E-01
13191 , 13156 , 13121 ,70, 2.49678E-01
13261 , 13226 , 13191 ,70, 2.50720E-01
13331 , 13296 , 13261 ,70, 2.51722E-01
13401 , 13366 , 13331 ,70, 2.52310E-01
13471 , 13436 , 13401 ,70, 2.52899E-01
13541 , 13506 , 13471 ,70, 2.53487E-01
13611 , 13576 , 13541 ,70, 2.54036E-01
13681 , 13646 , 13611 ,70, 2.54624E-01
13751 , 13716 , 13681 ,70, 2.55212E-01
13821 , 13786 , 13751 ,70, 2.55801E-01
13891 , 13856 , 13821 ,70, 2.56663E-01
13961 , 13926 , 13891 ,70, 2.57526E-01
14031 , 13996 , 13961 ,70, 2.58428E-01
14101 , 14066 , 14031 ,70, 2.59291E-01
14171 , 14136 , 14101 ,70, 2.60154E-01
14241 , 14206 , 14171 ,70, 2.61016E-01
14311 , 14276 , 14241 ,70, 2.61379E-01
14381 , 14346 , 14311 ,70, 2.61617E-01
14451 , 14416 , 14381 ,70, 2.61855E-01
14521 , 14486 , 14451 ,70, 2.62092E-01
14591 , 14556 , 14521 ,70, 2.62330E-01
14661 , 14626 , 14591 ,70, 2.62579E-01
14731 , 14696 , 14661 ,70, 2.62817E-01
14801 , 14766 , 14731 ,70, 2.63055E-01
14871 , 14836 , 14801 ,70, 2.63293E-01
14941 , 14906 , 14871 ,70, 2.63531E-01
```

15011	14976	14941	70	2.63780E-01
15081	15046	15011	70	2.63500E-01
15151	15116	15081	70	2.63191E-01
15221	15186	15151	70	2.62882E-01
15291	15256	15221	70	2.62559E-01
15361	15326	15291	70	2.62250E-01
15431	15396	15361	70	2.61941E-01
15501	15466	15431	70	2.61631E-01
15571	15536	15501	70	2.61322E-01
15641	15606	15571	70	2.60999E-01
15711	15676	15641	70	2.60690E-01
15781	15746	15711	70	2.60381E-01
15851	15816	15781	70	2.59549E-01
15921	15886	15851	70	2.58694E-01
15991	15956	15921	70	2.57877E-01
16061	16026	15991	70	2.57059E-01
16131	16096	16061	70	2.56242E-01
16201	16166	16131	70	2.55424E-01
16271	16236	16201	70	2.54569E-01
16341	16306	16271	70	2.53751E-01
16411	16376	16341	70	2.52934E-01
16481	16446	16411	70	2.52116E-01
16551	16516	16481	70	2.51264E-01
16621	16586	16551	70	2.50062E-01
16691	16656	16621	70	2.48913E-01
16761	16726	16691	70	2.47763E-01
16831	16796	16761	70	2.46614E-01
16901	16866	16831	70	2.45412E-01
16971	16936	16901	70	2.44262E-01
17041	17006	16971	70	2.43113E-01
17111	17076	17041	70	2.41963E-01
17181	17146	17111	70	2.40814E-01
17251	17216	17181	70	2.39612E-01
17321	17286	17251	70	2.38463E-01
17391	17356	17321	70	2.36949E-01
17461	17426	17391	70	2.35503E-01
17531	17496	17461	70	2.33992E-01
17601	17566	17531	70	2.32546E-01
17671	17636	17601	70	2.31101E-01
17741	17706	17671	70	2.29655E-01
17811	17776	17741	70	2.28144E-01
17881	17846	17811	70	2.26699E-01
17951	17916	17881	70	2.25253E-01
18021	17986	17951	70	2.23808E-01
18091	18056	18021	70	2.22304E-01
18161	18126	18091	70	2.20596E-01
18231	18196	18161	70	2.18963E-01
18301	18266	18231	70	2.17330E-01
18371	18336	18301	70	2.15697E-01
18441	18406	18371	70	2.13989E-01
18511	18476	18441	70	2.12356E-01
18581	18546	18511	70	2.10722E-01
18651	18616	18581	70	2.09089E-01
18721	18686	18651	70	2.07456E-01
18791	18756	18721	70	2.05748E-01
18861	18826	18791	70	2.04115E-01
18931	18896	18861	70	2.02482E-01
19001	18966	18931	70	2.00848E-01

```
19071 , 19036 , 19001 ,70, 1.99141E-01
19141 , 19106 , 19071 ,70, 1.97508E-01
19211 , 19176 , 19141 ,70, 1.95874E-01
19281 , 19246 , 19211 ,70, 1.94241E-01
19351 , 19316 , 19281 ,70, 1.92608E-01
19421 , 19386 , 19351 ,70, 1.90900E-01
19491 , 19456 , 19421 ,70, 1.89267E-01
19561 , 19526 , 19491 ,70, 1.87634E-01
19631 , 19596 , 19561 ,70, 1.86000E-01
19701 , 19666 , 19631 ,70, 1.84293E-01
19771 , 19736 , 19701 ,70, 1.82659E-01
19841 , 19806 , 19771 ,70, 1.81026E-01
19911 , 19876 , 19841 ,70, 1.79393E-01
19981 , 19946 , 19911 ,70, 1.77685E-01
20051 , 20016 , 19981 ,70, 1.76052E-01
20121 , 20086 , 20051 ,70, 1.74419E-01
20191 , 20156 , 20121 ,70, 1.71969E-01
20261 , 20226 , 20191 ,70, 1.69445E-01
20331 , 20296 , 20261 ,70, 1.66995E-01
20401 , 20366 , 20331 ,70, 1.64545E-01
20471 , 20436 , 20401 ,70, 1.62021E-01
20541 , 20506 , 20471 ,70, 1.59571E-01
20611 , 20576 , 20541 ,70, 1.57121E-01
20681 , 20646 , 20611 ,70, 1.54596E-01
20751 , 20716 , 20681 ,70, 1.52146E-01
20821 , 20786 , 20751 ,70, 1.49697E-01
20891 , 20856 , 20821 ,70, 1.47172E-01
20961 , 20926 , 20891 ,70, 1.44722E-01
21031 , 20996 , 20961 ,70, 1.42272E-01
21101 , 21066 , 21031 ,70, 1.39748E-01
21171 , 21136 , 21101 ,70, 1.37298E-01
21241 , 21206 , 21171 ,70, 1.34848E-01
21311 , 21276 , 21241 ,70, 1.32324E-01
21381 , 21346 , 21311 ,70, 1.29874E-01
21451 , 21416 , 21381 ,70, 1.27424E-01
21521 , 21486 , 21451 ,70, 1.24900E-01
21591 , 21556 , 21521 ,70, 1.22450E-01
21661 , 21626 , 21591 ,70, 1.20000E-01
21731 , 21696 , 21661 ,70, 1.17476E-01
21801 , 21766 , 21731 ,70, 1.15026E-01
21871 , 21836 , 21801 ,70, 1.12576E-01
21941 , 21906 , 21871 ,70, 1.10052E-01
22011 , 21976 , 21941 ,70, 1.07602E-01
22081 , 22046 , 22011 ,70, 1.05152E-01
22151 , 22116 , 22081 ,70, 1.02628E-01
22221 , 22186 , 22151 ,70, 1.00178E-01
22291 , 22256 , 22221 ,70, 9.72084E-02
22361 , 22326 , 22291 ,70, 9.42387E-02
22431 , 22396 , 22361 ,70, 9.12691E-02
22501 , 22466 , 22431 ,70, 8.82995E-02
22571 , 22536 , 22501 ,70, 8.53299E-02
22641 , 22606 , 22571 ,70, 8.23602E-02
22711 , 22676 , 22641 ,70, 7.93906E-02
22781 , 22746 , 22711 ,70, 7.64210E-02
22851 , 22816 , 22781 ,70, 7.34513E-02
22921 , 22886 , 22851 ,70, 7.04817E-02
22991 , 22956 , 22921 ,70, 6.75121E-02
23061 , 23026 , 22991 ,70, 6.45425E-02
```

```
23131 , 23096 , 23061 ,70, 6.14986E-02
23201 , 23166 , 23131 ,70, 5.85290E-02
23271 , 23236 , 23201 ,70, 5.55593E-02
23341 , 23306 , 23271 ,70, 5.25897E-02
23411 , 23376 , 23341 ,70, 4.96201E-02
23481 , 23446 , 23411 ,70, 4.66504E-02
23551 , 23516 , 23481 ,70, 4.36808E-02
23621 , 23586 , 23551 ,70, 4.07112E-02
23691 , 23656 , 23621 ,70, 3.77416E-02
23761 , 23726 , 23691 ,70, 3.47719E-02
23831 , 23796 , 23761 ,70, 3.18023E-02
23901 , 23866 , 23831 ,70, 2.88327E-02
23971 , 23936 , 23901 ,70, 2.58630E-02
24041 , 24006 , 23971 ,70, 2.28934E-02
24111 , 24076 , 24041 ,70, 1.99238E-02
24181 , 24146 , 24111 ,70, 1.69542E-02
24251 , 24216 , 24181 ,70, 1.39845E-02
24321 , 24286 , 24251 ,70, 1.10891E-02
24391 , 24356 , 24321 ,70, 8.11951E-03
24461 , 24426 , 24391 ,70, 5.14989E-03
24531 , 24496 , 24461 ,70, 2.18026E-03
24601 , 24566 , 24531 ,  , 0.00000E+00
BCNODE (un)
731,35,0.0
24601,,0.0
RENUMBER (profile)
ELEMENTS (quadrilateral, nodes=9, fluid, mvisc=1, mcond=1, fimesh)
ELEMENTS (quadrilateral, nodes=9, fluid, mvisc=1, mcond=1, fimesh)
ELEMENTS (quadrilateral, nodes=9, fluid, mvisc=1, mcond=1, fimesh)
ELEMENTS (quadrilateral, nodes=9, fluid, mvisc=2, mcond=2, fimesh)
ELEMENTS (quadrilateral, nodes=9, fluid, mvisc=2, mcond=2, fimesh)
ELEMENTS (triangle, nodes=6, fluid, mvisc=1, mcond=1, fimesh)
ELEMENTS (triangle, nodes=6, fluid, mvisc=2, mcond=2, fimesh)
ELEMENTS (convection, nodes=3, mcnv=1, fimesh)
ELEMENTS (slip, nodes=3, attach=7, fimesh)
ELEMENTS (slip, nodes=3, attach=5, fimesh)
END
*END
```

D.2 ADVECTION-DIFFUSION MODEL INPUT FILE

```
*TITLE
W-FACE/6530(9)/ADV-DIFF/dhl=550/tmelt=950/TWO-visc/kl=3
*FIMESH (2-D, IMAX=10, JMAX=10, MXPOINT=750)
EXPI
1 9 57 381 561 621 691
EXPJ
1 51 67 85
POINT
1 1 1 1 -0.0005 -0.01
2 2 1 1 0.001 -0.01
3 2 2 1 0.001 0.00055
4 3 2 1 0.020 0.0069
5 4 2 1 0.260 -0.0088
6 5 2 1 0.460 -0.016
7 6 2 1 0.560 -0.016
```

```
8 7 2 1 0.700 -0.0100
9 7 3 1 0.700 -0.001
10 7 4 1 0.700 0.017
11 6 4 1 0.560 0.017
12 5 4 1 0.460 0.017
13 4 4 1 0.260 0.017
14 3 4 1 0.02 0.017
15 2 4 1 0.001 0.017
16 1 4 1 -0.0005 0.017
17 1 3 1 -0.0005 0.01
18 1 2 1 -0.0005 0.00055
19 2 3 1 0.001 0.01
20 3 3 1 0.02 0.01
21 4 3 1 0.260 -0.0006
22 5 3 1 0.460 -0.007
23 6 3 1 0.560 -0.007
CURVE (input)
3 4 21 1.25 3
0.00108507 0.0010
0.00123008 0.0015
0.00144749 0.0020
0.00174240 0.0025
0.00212367 0.0030
0.00260531 0.0035
0.00320916 0.0040
0.0039702 0.0045
0.00494813 0.0050
0.00625592 0.0055
0.00814847 0.0060
0.00864579 0.0061
0.00920358 0.0062
0.00983786 0.0063
0.01057219 0.0064
0.01144321 0.0065
0.01251268 0.0066
0.01389764 0.0067
0.01586728 0.0068
0.01935433 0.0069
0.0199 0.0069
CURVE (input)
4 5 6
0.050 0.006
0.100 0.001
0.160 -0.003
0.200 -0.0060
0.250 -0.0084
0.258 -0.0087
CURVE (input)
5 6 2
0.360 -0.013
0.459 -0.016
CURVE (input)
6 7 2
0.500 -0.016
0.559 -0.016
CURVE (input)
7 8 3
0.610 -0.015
```

```
0.660 -0.013
0.690 -0.011
LINE
1 2
2 3
8 9
9 10
10 11
11 12
12 13
13 14
14 15 0.8 3
15 16
16 17
17 18
18 1
18 3
17 19
19 20 1.25 3
20 21
21 22
22 23
23 9
3 19
19 15
4 20
20 14
5 21
21 13
6 22
22 12
7 23
23 11
NUMBER
2 1
SURFACE
2 18
3 17
19 16
4 19
20 15
5 20
21 14
6 21
22 13
7 22
23 12
8 23
9 11
AREA
3 9
8 17
8 16
1 3
ELEMENTS (continuum, quadrilateral, nodes=9)
2 18
19 16
20 15
```

```
9 14
8 20
ELEMENTS (continuum, triangle, nodes=6)
3 17
4 19
ELEMENTS (boundary, nodes=3)
10 16
3 4
4 8
BCNODE (temperature, constant)
2 3 1550.0
3 4 1550.0
4 5 1550.0
5 6 1550.0
6 7 1550.0
7 8 1550.0
BCNODE (ux)
1 2 0.0
2 3 0.0
8 9 0.0
9 10 0.0
16 17 0.0
17 18 0.0
18 1 0.0
BCNODE (uy)
16 1 0.0
2 3 -0.0166667
10 11 -5.7143e-06
11 12 -5.7143e-06
12 13 -5.7143e-06
13 14 -5.7143e-06
BCFLUX (heat, nodes=3, constant)
8 9 0.0
9 10 0.0
1 2 0.0
END
*FIPREP
PROBLEM (steady, nonlinear, newtonian, 2-D,
laminar, nomomentum, weakly=0)
EXECUTION (newjob)
SOLUTION (s.s.=5, resconv=1e-4, velconv=1e-9)
PRESSURE (mixed=1.0e-16, continuous)
PRINTOUT (all)
DENSITY (set=1, constant=2500)
VISCOSITY (set=1, constant =0.03)
VISCOSITY (set=2, constant =0.03)
/CONDUCTIVITIES
/Liquid -> Glassy Solid
CONDUCTIVITY (set=1, curve=4, temperature, isotropic)
-9000,  900,  1000, 9000
0.90,   0.9,  3.0,  3.0
/Powder -> Liquid
CONDUCTIVITY (set=2, curve=8, temperature, isotropic)
-9000, 200,  400,  600,   800, 900,  1000, 9000
0.30,  0.30, 0.40, 0.55,  0.7, 0.80, 3.0,  3.0
SPECIFICHEAT (set=1, temperature, enthalpy=18, spatial)
-9000, 27,      227,    427,   527,   627,   727,   827,    950,
999,    1001,  1227,   1327,   1600,   2000,  2500,  3500,  9000
```

```
0,      1.0e4,    1.8e5,   3.8e5, 4.8e5, 6.0e5, 6.9e5, 8.3e5,   1e6,
1.10e6, 1.65e6, 2.0e6, 2.15e6, 2.55e6, 3.2e6, 4.0e6, 4.8e6, 4.8e6
HTRANSFER (set=1, curve=16, reftemp=27.0)
-3000, -110,  220,  420,  620,  820,  1220,  1420,  1620,  2020,  2420,
2620,   3000,   3500,   4000, 8000
1.1     1.1,  44.7, 65.9, 94.9, 135,  260,   350,   462,   761,   1176,
1434,   2027,   3036,   4341, 4341
ICNODE(velocity, read)
NODES (fimesh)
BCFLUX (T, nodes=3)
801 , 766 , 731 ,70, 0.00000E+00
871 , 836 , 801 ,70, 5.35375E-06
941 , 906 , 871 ,70, 1.45232E-05
1011 , 976 , 941 ,70, 2.77153E-05
1081 , 1046 , 1011 ,70, 4.38357E-05
1151 , 1116 , 1081 ,70, 6.23815E-05
1221 , 1186 , 1151 ,70, 8.28796E-05
1291 , 1256 , 1221 ,70, 1.04857E-04
1361 , 1326 , 1291 ,70, 1.27928E-04
1431 , 1396 , 1361 ,70, 1.51798E-04
1501 , 1466 , 1431 ,70, 1.76615E-04
1571 , 1536 , 1501 ,70, 2.02082E-04
1641 , 1606 , 1571 ,70, 2.29221E-04
1711 , 1676 , 1641 ,70, 2.56923E-04
1781 , 1746 , 1711 ,70, 2.84969E-04
1851 , 1816 , 1781 ,70, 3.13454E-04
1921 , 1886 , 1851 ,70, 3.42252E-04
1991 , 1956 , 1921 ,70, 3.71362E-04
2061 , 2026 , 1991 ,70, 4.00786E-04
2131 , 2096 , 2061 ,70, 4.30210E-04
2201 , 2166 , 2131 ,70, 4.80491E-04
2271 , 2236 , 2201 ,70, 5.33943E-04
2341 , 2306 , 2271 ,70, 5.87945E-04
2411 , 2376 , 2341 ,70, 6.41947E-04
2481 , 2446 , 2411 ,70, 6.97051E-04
2551 , 2516 , 2481 ,70, 7.78605E-04
2621 , 2586 , 2551 ,70, 8.60711E-04
2691 , 2656 , 2621 ,70, 9.75945E-04
2761 , 2726 , 2691 ,70, 1.13899E-03
2831 , 2796 , 2761 ,70, 1.30094E-03
2901 , 2866 , 2831 ,70, 1.46399E-03
2971 , 2936 , 2901 ,70, 1.62594E-03
3041 , 3006 , 2971 ,70, 1.78789E-03
3111 , 3076 , 3041 ,70, 1.95094E-03
3181 , 3146 , 3111 ,70, 2.25346E-03
3251 , 3216 , 3181 ,70, 2.58960E-03
3321 , 3286 , 3251 ,70, 2.92349E-03
3391 , 3356 , 3321 ,70, 3.25964E-03
3461 , 3426 , 3391 ,70, 3.59352E-03
3531 , 3496 , 3461 ,70, 3.92967E-03
3601 , 3566 , 3531 ,70, 4.26356E-03
3671 , 3636 , 3601 ,70, 4.68859E-03
3741 , 3706 , 3671 ,70, 5.33337E-03
3811 , 3776 , 3741 ,70, 5.97382E-03
3881 , 3846 , 3811 ,70, 6.61860E-03
3951 , 3916 , 3881 ,70, 7.25905E-03
4021 , 3986 , 3951 ,70, 7.89517E-03
4091 , 4056 , 4021 ,70, 8.53563E-03
```

```
4161 , 4126 , 4091 ,70, 9.17608E-03
4231 , 4196 , 4161 ,70, 9.81653E-03
4301 , 4266 , 4231 ,70, 1.08231E-02
4371 , 4336 , 4301 ,70, 1.19758E-02
4441 , 4406 , 4371 ,70, 1.31286E-02
4511 , 4476 , 4441 ,70, 1.42814E-02
4581 , 4546 , 4511 ,70, 1.54342E-02
4651 , 4616 , 4581 ,70, 1.65792E-02
4721 , 4686 , 4651 ,70, 1.77320E-02
4791 , 4756 , 4721 ,70, 1.88848E-02
4861 , 4826 , 4791 ,70, 2.00375E-02
4931 , 4896 , 4861 ,70, 2.11825E-02
5001 , 4966 , 4931 ,70, 2.28892E-02
5071 , 5036 , 5001 ,70, 2.46233E-02
5141 , 5106 , 5071 ,70, 2.63574E-02
5211 , 5176 , 5141 ,70, 2.80798E-02
5281 , 5246 , 5211 ,70, 2.98139E-02
5351 , 5316 , 5281 ,70, 3.15480E-02
5421 , 5386 , 5351 ,70, 3.32821E-02
5491 , 5456 , 5421 ,70, 3.50045E-02
5561 , 5526 , 5491 ,70, 3.67386E-02
5631 , 5596 , 5561 ,70, 3.84727E-02
5701 , 5666 , 5631 ,70, 4.02069E-02
5771 , 5736 , 5701 ,70, 4.23659E-02
5841 , 5806 , 5771 ,70, 4.45962E-02
5911 , 5876 , 5841 ,70, 4.68417E-02
5981 , 5946 , 5911 ,70, 4.90872E-02
6051 , 6016 , 5981 ,70, 5.13326E-02
6121 , 6086 , 6051 ,70, 5.35629E-02
6191 , 6156 , 6121 ,70, 5.58084E-02
6261 , 6226 , 6191 ,70, 5.80539E-02
6331 , 6296 , 6261 ,70, 6.02841E-02
6401 , 6366 , 6331 ,70, 6.25600E-02
6471 , 6436 , 6401 ,70, 6.48358E-02
6541 , 6506 , 6471 ,70, 6.71116E-02
6611 , 6576 , 6541 ,70, 6.92357E-02
6681 , 6646 , 6611 ,70, 7.18996E-02
6751 , 6716 , 6681 ,70, 7.45100E-02
6821 , 6786 , 6751 ,70, 7.71204E-02
6891 , 6856 , 6821 ,70, 7.97308E-02
6961 , 6926 , 6891 ,70, 8.21672E-02
7031 , 6996 , 6961 ,70, 8.47776E-02
7101 , 7066 , 7031 ,70, 8.73881E-02
7171 , 7136 , 7101 ,70, 8.99985E-02
7241 , 7206 , 7171 ,70, 9.26089E-02
7311 , 7276 , 7241 ,70, 9.52193E-02
7381 , 7346 , 7311 ,70, 9.76557E-02
7451 , 7416 , 7381 ,70, 1.00266E-01
7521 , 7486 , 7451 ,70, 1.02876E-01
7591 , 7556 , 7521 ,70, 1.05487E-01
7661 , 7626 , 7591 ,70, 1.07881E-01
7731 , 7696 , 7661 ,70, 1.10075E-01
7801 , 7766 , 7731 ,70, 1.12426E-01
7871 , 7836 , 7801 ,70, 1.14777E-01
7941 , 7906 , 7871 ,70, 1.17128E-01
8011 , 7976 , 7941 ,70, 1.19478E-01
8081 , 8046 , 8011 ,70, 1.21829E-01
8151 , 8116 , 8081 ,70, 1.24023E-01
```

```
8221 , 8186 , 8151 ,70, 1.26374E-01
8291 , 8256 , 8221 ,70, 1.28725E-01
8361 , 8326 , 8291 ,70, 1.31076E-01
8431 , 8396 , 8361 ,70, 1.33427E-01
8501 , 8466 , 8431 ,70, 1.35621E-01
8571 , 8536 , 8501 ,70, 1.37972E-01
8641 , 8606 , 8571 ,70, 1.40323E-01
8711 , 8676 , 8641 ,70, 1.42673E-01
8781 , 8746 , 8711 ,70, 1.45024E-01
8851 , 8816 , 8781 ,70, 1.47117E-01
8921 , 8886 , 8851 ,70, 1.49150E-01
8991 , 8956 , 8921 ,70, 1.51327E-01
9061 , 9026 , 8991 ,70, 1.53505E-01
9131 , 9096 , 9061 ,70, 1.55682E-01
9201 , 9166 , 9131 ,70, 1.57860E-01
9271 , 9236 , 9201 ,70, 1.59892E-01
9341 , 9306 , 9271 ,70, 1.62070E-01
9411 , 9376 , 9341 ,70, 1.64247E-01
9481 , 9446 , 9411 ,70, 1.66425E-01
9551 , 9516 , 9481 ,70, 1.68603E-01
9621 , 9586 , 9551 ,70, 1.70635E-01
9691 , 9656 , 9621 ,70, 1.72812E-01
9761 , 9726 , 9691 ,70, 1.74990E-01
9831 , 9796 , 9761 ,70, 1.77167E-01
9901 , 9866 , 9831 ,70, 1.79345E-01
9971 , 9936 , 9901 ,70, 1.81160E-01
10041 , 10006 , 9971 ,70, 1.83133E-01
10111 , 10076 , 10041 ,70, 1.85107E-01
10181 , 10146 , 10111 ,70, 1.87080E-01
10251 , 10216 , 10181 ,70, 1.89054E-01
10321 , 10286 , 10251 ,70, 1.91027E-01
10391 , 10356 , 10321 ,70, 1.92869E-01
10461 , 10426 , 10391 ,70, 1.94843E-01
10531 , 10496 , 10461 ,70, 1.96816E-01
10601 , 10566 , 10531 ,70, 1.98790E-01
10671 , 10636 , 10601 ,70, 2.00764E-01
10741 , 10706 , 10671 ,70, 2.02605E-01
10811 , 10776 , 10741 ,70, 2.04579E-01
10881 , 10846 , 10811 ,70, 2.06553E-01
10951 , 10916 , 10881 ,70, 2.08526E-01
11021 , 10986 , 10951 ,70, 2.10500E-01
11091 , 11056 , 11021 ,70, 2.11987E-01
11161 , 11126 , 11091 ,70, 2.13469E-01
11231 , 11196 , 11161 ,70, 2.14951E-01
11301 , 11266 , 11231 ,70, 2.16432E-01
11371 , 11336 , 11301 ,70, 2.17914E-01
11441 , 11406 , 11371 ,70, 2.19396E-01
11511 , 11476 , 11441 ,70, 2.20778E-01
11581 , 11546 , 11511 ,70, 2.22260E-01
11651 , 11616 , 11581 ,70, 2.23742E-01
11721 , 11686 , 11651 ,70, 2.25223E-01
11791 , 11756 , 11721 ,70, 2.26705E-01
11861 , 11826 , 11791 ,70, 2.28187E-01
11931 , 11896 , 11861 ,70, 2.29570E-01
12001 , 11966 , 11931 ,70, 2.31051E-01
12071 , 12036 , 12001 ,70, 2.32533E-01
12141 , 12106 , 12071 ,70, 2.34014E-01
12211 , 12176 , 12141 ,70, 2.35305E-01
```

```
12281 , 12246 , 12211 ,70, 2.36347E-01
12351 , 12316 , 12281 ,70, 2.37319E-01
12421 , 12386 , 12351 ,70, 2.38361E-01
12491 , 12456 , 12421 ,70, 2.39402E-01
12561 , 12526 , 12491 ,70, 2.40444E-01
12631 , 12596 , 12561 ,70, 2.41485E-01
12701 , 12666 , 12631 ,70, 2.42527E-01
12771 , 12736 , 12701 ,70, 2.43499E-01
12841 , 12806 , 12771 ,70, 2.44540E-01
12911 , 12876 , 12841 ,70, 2.45582E-01
12981 , 12946 , 12911 ,70, 2.46623E-01
13051 , 13016 , 12981 ,70, 2.47665E-01
13121 , 13086 , 13051 ,70, 2.48706E-01
13191 , 13156 , 13121 ,70, 2.49678E-01
13261 , 13226 , 13191 ,70, 2.50720E-01
13331 , 13296 , 13261 ,70, 2.51722E-01
13401 , 13366 , 13331 ,70, 2.52310E-01
13471 , 13436 , 13401 ,70, 2.52899E-01
13541 , 13506 , 13471 ,70, 2.53487E-01
13611 , 13576 , 13541 ,70, 2.54036E-01
13681 , 13646 , 13611 ,70, 2.54624E-01
13751 , 13716 , 13681 ,70, 2.55212E-01
13821 , 13786 , 13751 ,70, 2.55801E-01
13891 , 13856 , 13821 ,70, 2.56663E-01
13961 , 13926 , 13891 ,70, 2.57526E-01
14031 , 13996 , 13961 ,70, 2.58428E-01
14101 , 14066 , 14031 ,70, 2.59291E-01
14171 , 14136 , 14101 ,70, 2.60154E-01
14241 , 14206 , 14171 ,70, 2.61016E-01
14311 , 14276 , 14241 ,70, 2.61379E-01
14381 , 14346 , 14311 ,70, 2.61617E-01
14451 , 14416 , 14381 ,70, 2.61855E-01
14521 , 14486 , 14451 ,70, 2.62092E-01
14591 , 14556 , 14521 ,70, 2.62330E-01
14661 , 14626 , 14591 ,70, 2.62579E-01
14731 , 14696 , 14661 ,70, 2.62817E-01
14801 , 14766 , 14731 ,70, 2.63055E-01
14871 , 14836 , 14801 ,70, 2.63293E-01
14941 , 14906 , 14871 ,70, 2.63531E-01
15011 , 14976 , 14941 ,70, 2.63780E-01
15081 , 15046 , 15011 ,70, 2.63500E-01
15151 , 15116 , 15081 ,70, 2.63191E-01
15221 , 15186 , 15151 ,70, 2.62882E-01
15291 , 15256 , 15221 ,70, 2.62559E-01
15361 , 15326 , 15291 ,70, 2.62250E-01
15431 , 15396 , 15361 ,70, 2.61941E-01
15501 , 15466 , 15431 ,70, 2.61631E-01
15571 , 15536 , 15501 ,70, 2.61322E-01
15641 , 15606 , 15571 ,70, 2.60999E-01
15711 , 15676 , 15641 ,70, 2.60690E-01
15781 , 15746 , 15711 ,70, 2.60381E-01
15851 , 15816 , 15781 ,70, 2.59549E-01
15921 , 15886 , 15851 ,70, 2.58694E-01
15991 , 15956 , 15921 ,70, 2.57877E-01
16061 , 16026 , 15991 ,70, 2.57059E-01
16131 , 16096 , 16061 ,70, 2.56242E-01
16201 , 16166 , 16131 ,70, 2.55424E-01
16271 , 16236 , 16201 ,70, 2.54569E-01
```

16341	16306	16271	70	2.53751E-01
16411	16376	16341	70	2.52934E-01
16481	16446	16411	70	2.52116E-01
16551	16516	16481	70	2.51264E-01
16621	16586	16551	70	2.50062E-01
16691	16656	16621	70	2.48913E-01
16761	16726	16691	70	2.47763E-01
16831	16796	16761	70	2.46614E-01
16901	16866	16831	70	2.45412E-01
16971	16936	16901	70	2.44262E-01
17041	17006	16971	70	2.43113E-01
17111	17076	17041	70	2.41963E-01
17181	17146	17111	70	2.40814E-01
17251	17216	17181	70	2.39612E-01
17321	17286	17251	70	2.38463E-01
17391	17356	17321	70	2.36949E-01
17461	17426	17391	70	2.35503E-01
17531	17496	17461	70	2.33992E-01
17601	17566	17531	70	2.32546E-01
17671	17636	17601	70	2.31101E-01
17741	17706	17671	70	2.29655E-01
17811	17776	17741	70	2.28144E-01
17881	17846	17811	70	2.26699E-01
17951	17916	17881	70	2.25253E-01
18021	17986	17951	70	2.23808E-01
18091	18056	18021	70	2.22304E-01
18161	18126	18091	70	2.20596E-01
18231	18196	18161	70	2.18963E-01
18301	18266	18231	70	2.17330E-01
18371	18336	18301	70	2.15697E-01
18441	18406	18371	70	2.13989E-01
18511	18476	18441	70	2.12356E-01
18581	18546	18511	70	2.10722E-01
18651	18616	18581	70	2.09089E-01
18721	18686	18651	70	2.07456E-01
18791	18756	18721	70	2.05748E-01
18861	18826	18791	70	2.04115E-01
18931	18896	18861	70	2.02482E-01
19001	18966	18931	70	2.00848E-01
19071	19036	19001	70	1.99141E-01
19141	19106	19071	70	1.97508E-01
19211	19176	19141	70	1.95874E-01
19281	19246	19211	70	1.94241E-01
19351	19316	19281	70	1.92608E-01
19421	19386	19351	70	1.90900E-01
19491	19456	19421	70	1.89267E-01
19561	19526	19491	70	1.87634E-01
19631	19596	19561	70	1.86000E-01
19701	19666	19631	70	1.84293E-01
19771	19736	19701	70	1.82659E-01
19841	19806	19771	70	1.81026E-01
19911	19876	19841	70	1.79393E-01
19981	19946	19911	70	1.77685E-01
20051	20016	19981	70	1.76052E-01
20121	20086	20051	70	1.74419E-01
20191	20156	20121	70	1.71969E-01
20261	20226	20191	70	1.69445E-01
20331	20296	20261	70	1.66995E-01

```
20401 , 20366 , 20331 ,70, 1.64545E-01
20471 , 20436 , 20401 ,70, 1.62021E-01
20541 , 20506 , 20471 ,70, 1.59571E-01
20611 , 20576 , 20541 ,70, 1.57121E-01
20681 , 20646 , 20611 ,70, 1.54596E-01
20751 , 20716 , 20681 ,70, 1.52146E-01
20821 , 20786 , 20751 ,70, 1.49697E-01
20891 , 20856 , 20821 ,70, 1.47172E-01
20961 , 20926 , 20891 ,70, 1.44722E-01
21031 , 20996 , 20961 ,70, 1.42272E-01
21101 , 21066 , 21031 ,70, 1.39748E-01
21171 , 21136 , 21101 ,70, 1.37298E-01
21241 , 21206 , 21171 ,70, 1.34848E-01
21311 , 21276 , 21241 ,70, 1.32324E-01
21381 , 21346 , 21311 ,70, 1.29874E-01
21451 , 21416 , 21381 ,70, 1.27424E-01
21521 , 21486 , 21451 ,70, 1.24900E-01
21591 , 21556 , 21521 ,70, 1.22450E-01
21661 , 21626 , 21591 ,70, 1.20000E-01
21731 , 21696 , 21661 ,70, 1.17476E-01
21801 , 21766 , 21731 ,70, 1.15026E-01
21871 , 21836 , 21801 ,70, 1.12576E-01
21941 , 21906 , 21871 ,70, 1.10052E-01
22011 , 21976 , 21941 ,70, 1.07602E-01
22081 , 22046 , 22011 ,70, 1.05152E-01
22151 , 22116 , 22081 ,70, 1.02628E-01
22221 , 22186 , 22151 ,70, 1.00178E-01
22291 , 22256 , 22221 ,70, 9.72084E-02
22361 , 22326 , 22291 ,70, 9.42387E-02
22431 , 22396 , 22361 ,70, 9.12691E-02
22501 , 22466 , 22431 ,70, 8.82995E-02
22571 , 22536 , 22501 ,70, 8.53299E-02
22641 , 22606 , 22571 ,70, 8.23602E-02
22711 , 22676 , 22641 ,70, 7.93906E-02
22781 , 22746 , 22711 ,70, 7.64210E-02
22851 , 22816 , 22781 ,70, 7.34513E-02
22921 , 22886 , 22851 ,70, 7.04817E-02
22991 , 22956 , 22921 ,70, 6.75121E-02
23061 , 23026 , 22991 ,70, 6.45425E-02
23131 , 23096 , 23061 ,70, 6.14986E-02
23201 , 23166 , 23131 ,70, 5.85290E-02
23271 , 23236 , 23201 ,70, 5.55593E-02
23341 , 23306 , 23271 ,70, 5.25897E-02
23411 , 23376 , 23341 ,70, 4.96201E-02
23481 , 23446 , 23411 ,70, 4.66504E-02
23551 , 23516 , 23481 ,70, 4.36808E-02
23621 , 23586 , 23551 ,70, 4.07112E-02
23691 , 23656 , 23621 ,70, 3.77416E-02
23761 , 23726 , 23691 ,70, 3.47719E-02
23831 , 23796 , 23761 ,70, 3.18023E-02
23901 , 23866 , 23831 ,70, 2.88327E-02
23971 , 23936 , 23901 ,70, 2.58630E-02
24041 , 24006 , 23971 ,70, 2.28934E-02
24111 , 24076 , 24041 ,70, 1.99238E-02
24181 , 24146 , 24111 ,70, 1.69542E-02
24251 , 24216 , 24181 ,70, 1.39845E-02
24321 , 24286 , 24251 ,70, 1.10891E-02
24391 , 24356 , 24321 ,70, 8.11951E-03
```

```
24461 , 24426 , 24391 ,70, 5.14989E-03
24531 , 24496 , 24461 ,70, 2.18026E-03
24601 , 24566 , 24531 ,  , 0.00000E+00
BCNODE (un)
731,35,0.0
24601,,0.0
BCNODE (temperature)
1 ,1, 275.00
2 ,1, 273.95
3 ,1, 272.89
4 ,1, 271.84
5 ,1, 270.78
6 ,1, 269.73
7 ,1, 268.67
8 ,1, 267.62
9 ,1, 266.56
10 ,1, 265.51
11 ,1, 264.45
12 ,1, 263.40
13 ,1, 262.34
14 ,1, 261.29
15 ,1, 260.23
16 ,1, 259.18
17 ,1, 258.12
18 ,1, 257.07
19 ,1, 256.01
20 ,1, 254.96
21 ,1, 253.90
22 ,1, 252.85
23 ,1, 251.79
24 ,1, 250.74
25 ,1, 249.68
26 ,1, 248.63
27 ,1, 247.57
28 ,1, 246.52
29 ,1, 245.46
30 ,1, 244.41
31 ,1, 243.35
32 ,1, 242.30
33 ,1, 241.24
34 ,1, 240.19
35 ,1, 239.13
36 ,1, 238.08
37 ,1, 237.02
38 ,1, 235.97
39 ,1, 234.91
40 ,1, 233.86
41 ,1, 232.80
42 ,1, 231.75
43 ,1, 230.69
44 ,1, 229.64
45 ,1, 228.58
46 ,1, 227.53
47 ,1, 226.47
48 ,1, 225.42
49 ,1, 224.17
50 ,1, 222.80
51 ,1, 221.43
```

```
 52 ,1, 217.58
 53 ,1, 213.75
 54 ,1, 209.91
 55 ,1, 206.07
 56 ,1, 202.23
 57 ,1, 198.39
 58 ,1, 194.55
 59 ,1, 190.71
 60 ,1, 186.87
 61 ,1, 183.04
 62 ,1, 179.19
 63 ,1, 175.35
 64 ,1, 171.52
 65 ,1, 167.68
 66 ,1, 163.84
 67 ,1, 160.00
 68 ,1, 158.36
 69 ,1, 156.72
 70 ,1, 155.09
 71 ,1, 153.45
 72 ,1, 151.85
 73 ,1, 150.21
 74 ,1, 148.58
 75 ,1, 146.94
 76 ,1, 145.30
 77 ,1, 143.66
 78 ,1, 142.02
 79 ,1, 140.39
 80 ,1, 138.75
 81 ,1, 137.15
 82 ,1, 135.51
 83 ,1, 133.88
 84 ,1, 132.24
 85 ,1, 130.60
RENUMBER (profile)
ELEMENTS (quadrilateral, nodes=9, fluid, mvisc=1, mcond=1, fimesh)
ELEMENTS (quadrilateral, nodes=9, fluid, mvisc=1, mcond=1, fimesh)
ELEMENTS (quadrilateral, nodes=9, fluid, mvisc=1, mcond=1, fimesh)
ELEMENTS (quadrilateral, nodes=9, fluid, mvisc=2, mcond=2, fimesh)
ELEMENTS (quadrilateral, nodes=9, fluid, mvisc=2, mcond=2, fimesh)
ELEMENTS (triangle, nodes=6, fluid, mvisc=1, mcond=1, fimesh)
ELEMENTS (triangle, nodes=6, fluid, mvisc=2, mcond=2, fimesh)
ELEMENTS (convection, nodes=3, mcnv=1, fimesh)
ELEMENTS (slip, nodes=3, attach=7, fimesh)
ELEMENTS (slip, nodes=3, attach=5, fimesh)
END
*END
```

D.3 WEAKLY-COUPLED MODEL INPUT FILE

```
*TITLE
W-FACE/6530(9)/W-CPL/dhl=550/tmelt=950/TWO-visc/kl=3
*FIMESH (2-D, IMAX=10, JMAX=10, MXPOINT=750)
EXPI
1 9 57 381 561 621 691
EXPJ
1 51 67 85
```

```
POINT
1 1 1 1 -0.0005 -0.01
2 2 1 1 0.001 -0.01
3 2 2 1 0.001 0.00055
4 3 2 1 0.020 0.0069
5 4 2 1 0.260 -0.0088
6 5 2 1 0.460 -0.016
7 6 2 1 0.560 -0.016
8 7 2 1 0.700 -0.0100
9 7 3 1 0.700 -0.001
10 7 4 1 0.700 0.017
11 6 4 1 0.560 0.017
12 5 4 1 0.460 0.017
13 4 4 1 0.260 0.017
14 3 4 1 0.02 0.017
15 2 4 1 0.001 0.017
16 1 4 1 -0.0005 0.017
17 1 3 1 -0.0005 0.01
18 1 2 1 -0.0005 0.00055
19 2 3 1 0.001 0.01
20 3 3 1 0.02 0.01
21 4 3 1 0.260 -0.0006
22 5 3 1 0.460 -0.007
23 6 3 1 0.560 -0.007
CURVE (input)
3 4 21 1.25 3
0.00108507 0.0010
0.00123008 0.0015
0.00144749 0.0020
0.00174240 0.0025
0.00212367 0.0030
0.00260531 0.0035
0.00320916 0.0040
0.0039702 0.0045
0.00494813 0.0050
0.00625592 0.0055
0.00814847 0.0060
0.00864579 0.0061
0.00920358 0.0062
0.00983786 0.0063
0.01057219 0.0064
0.01144321 0.0065
0.01251268 0.0066
0.01389764 0.0067
0.01586728 0.0068
0.01935433 0.0069
0.0199 0.0069
CURVE (input)
4 5 6
0.050 0.006
0.100 0.001
0.160 -0.003
0.200 -0.0060
0.250 -0.0084
0.258 -0.0087
CURVE (input)
5 6 2
0.360 -0.013
```

```
0.459 -0.016
CURVE (input)
6 7 2
0.500 -0.016
0.559 -0.016
CURVE (input)
7 8 3
0.610 -0.015
0.660 -0.013
0.690 -0.011
LINE
1 2
2 3
8 9
9 10
10 11
11 12
12 13
13 14
14 15 0.8 3
15 16
16 17
17 18
18 1
18 3
17 19
19 20 1.25 3
20 21
21 22
22 23
23 9
3 19
19 15
4 20
20 14
5 21
21 13
6 22
22 12
7 23
23 11
NUMBER
2 1
SURFACE
2 18
3 17
19 16
4 19
20 15
5 20
21 14
6 21
22 13
7 22
23 12
8 23
9 11
AREA
```

```
3 9
8 17
8 16
1 3
ELEMENTS (continuum, quadrilateral, nodes=9)
2 18
19 16
20 15
9 14
8 20
ELEMENTS (continuum, triangle, nodes=6)
3 17
4 19
ELEMENTS (boundary, nodes=3)
10 16
3 4
4 8
BCNODE (temperature, constant)
2 3 1550.0
3 4 1550.0
4 5 1550.0
5 6 1550.0
6 7 1550.0
7 8 1550.0
BCNODE (ux)
1 2 0.0
2 3 0.0
8 9 0.0
9 10 0.0
16 17 0.0
17 18 0.0
18 1 0.0
BCNODE (uy)
16 1 0.0
2 3 -0.0166667
10 11 -5.7143e-06
11 12 -5.7143e-06
12 13 -5.7143e-06
13 14 -5.7143e-06
BCFLUX (heat, nodes=3, constant)
8 9 0.0
9 10 0.0
1 2 0.0
END
*FIPREP
PROBLEM (steady, nonlinear, newtonian, 2-D,
laminar, momentum, weakly=0)
EXECUTION (newjob)
SOLUTION (s.s.=25, resconv=1e-4, velconv=1e-9)
PRESSURE (mixed=1.0e-16, continuous)
PRINTOUT (all)
DENSITY (set=1, constant=2500)
/VISCOSITIES
/Liquid -> Glassy solid
VISCOSITY (set=1, curve=14, temperature)
-9000, 500,  700,  900,  1000,  1050,  1100, 1150, 1200, 1300,
1400, 1500, 1600, 9000
1e8,   1e8,  1e8,  1e8,   5.0,  1.00,  0.50, 0.30, 0.20, 0.12,
```

```
0.08, 0.05, 0.03, 0.03
/Powder -> Liquid
VISCOSITY (set=2, curve=14, temperature)
-9000, 500,  700,  900,  1000, 1050,  1100, 1150, 1200, 1300,
1400, 1500, 1600, 9000
10.0,  10.0, 10.0, 5.0,  2.0,  1.00,  0.50, 0.30, 0.20, 0.12,
0.08, 0.05, 0.03, 0.03
/CONDUCTIVITIES
/Liquid -> Glassy Solid
CONDUCTIVITY (set=1, curve=4, temperature, isotropic)
-9000,  900,  1000, 9000
0.90,   0.9,  3.0,  3.0
/Powder -> Liquid
CONDUCTIVITY (set=2, curve=8, temperature, isotropic)
-9000, 200,  400,  600,   800, 900,  1000, 9000
0.30,  0.30, 0.40, 0.55,  0.7, 0.80, 3.0,  3.0
SPECIFICHEAT (set=1, temperature, enthalpy=18, spatial)
-9000, 27,      227,    427,   527,   627,   727,   827,    950,
999,    1001,  1227,   1327,   1600,   2000,  2500,  3500,  9000
0,     1.0e4,   1.8e5,  3.8e5, 4.8e5, 6.0e5, 6.9e5, 8.3e5,  1e6,
1.10e6, 1.65e6, 2.0e6, 2.15e6, 2.55e6, 3.2e6, 4.0e6, 4.8e6, 4.8e6
HTRANSFER (set=1, curve=16, reftemp=27.0)
-3000, -110,  220,  420,  620,  820,  1220,  1420,  1620,  2020,  2420,
2620,   3000,   3500,   4000, 8000
1.1     1.1,  44.7, 65.9, 94.9, 135,  260,   350,   462,   761,   1176,
1434,   2027,   3036,   4341, 4341
ICNODE (temperature, read)
ICNODE(velocity, read)
NODES (fimesh)
BCFLUX (T, nodes=3)
801 , 766 , 731 ,70, 0.00000E+00
871 , 836 , 801 ,70, 5.35375E-06
941 , 906 , 871 ,70, 1.45232E-05
1011 , 976 , 941 ,70, 2.77153E-05
1081 , 1046 , 1011 ,70, 4.38357E-05
1151 , 1116 , 1081 ,70, 6.23815E-05
1221 , 1186 , 1151 ,70, 8.28796E-05
1291 , 1256 , 1221 ,70, 1.04857E-04
1361 , 1326 , 1291 ,70, 1.27928E-04
1431 , 1396 , 1361 ,70, 1.51798E-04
1501 , 1466 , 1431 ,70, 1.76615E-04
1571 , 1536 , 1501 ,70, 2.02082E-04
1641 , 1606 , 1571 ,70, 2.29221E-04
1711 , 1676 , 1641 ,70, 2.56923E-04
1781 , 1746 , 1711 ,70, 2.84969E-04
1851 , 1816 , 1781 ,70, 3.13454E-04
1921 , 1886 , 1851 ,70, 3.42252E-04
1991 , 1956 , 1921 ,70, 3.71362E-04
2061 , 2026 , 1991 ,70, 4.00786E-04
2131 , 2096 , 2061 ,70, 4.30210E-04
2201 , 2166 , 2131 ,70, 4.80491E-04
2271 , 2236 , 2201 ,70, 5.33943E-04
2341 , 2306 , 2271 ,70, 5.87945E-04
2411 , 2376 , 2341 ,70, 6.41947E-04
2481 , 2446 , 2411 ,70, 6.97051E-04
2551 , 2516 , 2481 ,70, 7.78605E-04
2621 , 2586 , 2551 ,70, 8.60711E-04
2691 , 2656 , 2621 ,70, 9.75945E-04
```

```
2761 , 2726 , 2691 ,70, 1.13899E-03
2831 , 2796 , 2761 ,70, 1.30094E-03
2901 , 2866 , 2831 ,70, 1.46399E-03
2971 , 2936 , 2901 ,70, 1.62594E-03
3041 , 3006 , 2971 ,70, 1.78789E-03
3111 , 3076 , 3041 ,70, 1.95094E-03
3181 , 3146 , 3111 ,70, 2.25346E-03
3251 , 3216 , 3181 ,70, 2.58960E-03
3321 , 3286 , 3251 ,70, 2.92349E-03
3391 , 3356 , 3321 ,70, 3.25964E-03
3461 , 3426 , 3391 ,70, 3.59352E-03
3531 , 3496 , 3461 ,70, 3.92967E-03
3601 , 3566 , 3531 ,70, 4.26356E-03
3671 , 3636 , 3601 ,70, 4.68859E-03
3741 , 3706 , 3671 ,70, 5.33337E-03
3811 , 3776 , 3741 ,70, 5.97382E-03
3881 , 3846 , 3811 ,70, 6.61860E-03
3951 , 3916 , 3881 ,70, 7.25905E-03
4021 , 3986 , 3951 ,70, 7.89517E-03
4091 , 4056 , 4021 ,70, 8.53563E-03
4161 , 4126 , 4091 ,70, 9.17608E-03
4231 , 4196 , 4161 ,70, 9.81653E-03
4301 , 4266 , 4231 ,70, 1.08231E-02
4371 , 4336 , 4301 ,70, 1.19758E-02
4441 , 4406 , 4371 ,70, 1.31286E-02
4511 , 4476 , 4441 ,70, 1.42814E-02
4581 , 4546 , 4511 ,70, 1.54342E-02
4651 , 4616 , 4581 ,70, 1.65792E-02
4721 , 4686 , 4651 ,70, 1.77320E-02
4791 , 4756 , 4721 ,70, 1.88848E-02
4861 , 4826 , 4791 ,70, 2.00375E-02
4931 , 4896 , 4861 ,70, 2.11825E-02
5001 , 4966 , 4931 ,70, 2.28892E-02
5071 , 5036 , 5001 ,70, 2.46233E-02
5141 , 5106 , 5071 ,70, 2.63574E-02
5211 , 5176 , 5141 ,70, 2.80798E-02
5281 , 5246 , 5211 ,70, 2.98139E-02
5351 , 5316 , 5281 ,70, 3.15480E-02
5421 , 5386 , 5351 ,70, 3.32821E-02
5491 , 5456 , 5421 ,70, 3.50045E-02
5561 , 5526 , 5491 ,70, 3.67386E-02
5631 , 5596 , 5561 ,70, 3.84727E-02
5701 , 5666 , 5631 ,70, 4.02069E-02
5771 , 5736 , 5701 ,70, 4.23659E-02
5841 , 5806 , 5771 ,70, 4.45962E-02
5911 , 5876 , 5841 ,70, 4.68417E-02
5981 , 5946 , 5911 ,70, 4.90872E-02
6051 , 6016 , 5981 ,70, 5.13326E-02
6121 , 6086 , 6051 ,70, 5.35629E-02
6191 , 6156 , 6121 ,70, 5.58084E-02
6261 , 6226 , 6191 ,70, 5.80539E-02
6331 , 6296 , 6261 ,70, 6.02841E-02
6401 , 6366 , 6331 ,70, 6.25600E-02
6471 , 6436 , 6401 ,70, 6.48358E-02
6541 , 6506 , 6471 ,70, 6.71116E-02
6611 , 6576 , 6541 ,70, 6.92357E-02
6681 , 6646 , 6611 ,70, 7.18996E-02
6751 , 6716 , 6681 ,70, 7.45100E-02
```

```
6821 , 6786 , 6751 ,70, 7.71204E-02
6891 , 6856 , 6821 ,70, 7.97308E-02
6961 , 6926 , 6891 ,70, 8.21672E-02
7031 , 6996 , 6961 ,70, 8.47776E-02
7101 , 7066 , 7031 ,70, 8.73881E-02
7171 , 7136 , 7101 ,70, 8.99985E-02
7241 , 7206 , 7171 ,70, 9.26089E-02
7311 , 7276 , 7241 ,70, 9.52193E-02
7381 , 7346 , 7311 ,70, 9.76557E-02
7451 , 7416 , 7381 ,70, 1.00266E-01
7521 , 7486 , 7451 ,70, 1.02876E-01
7591 , 7556 , 7521 ,70, 1.05487E-01
7661 , 7626 , 7591 ,70, 1.07881E-01
7731 , 7696 , 7661 ,70, 1.10075E-01
7801 , 7766 , 7731 ,70, 1.12426E-01
7871 , 7836 , 7801 ,70, 1.14777E-01
7941 , 7906 , 7871 ,70, 1.17128E-01
8011 , 7976 , 7941 ,70, 1.19478E-01
8081 , 8046 , 8011 ,70, 1.21829E-01
8151 , 8116 , 8081 ,70, 1.24023E-01
8221 , 8186 , 8151 ,70, 1.26374E-01
8291 , 8256 , 8221 ,70, 1.28725E-01
8361 , 8326 , 8291 ,70, 1.31076E-01
8431 , 8396 , 8361 ,70, 1.33427E-01
8501 , 8466 , 8431 ,70, 1.35621E-01
8571 , 8536 , 8501 ,70, 1.37972E-01
8641 , 8606 , 8571 ,70, 1.40323E-01
8711 , 8676 , 8641 ,70, 1.42673E-01
8781 , 8746 , 8711 ,70, 1.45024E-01
8851 , 8816 , 8781 ,70, 1.47117E-01
8921 , 8886 , 8851 ,70, 1.49150E-01
8991 , 8956 , 8921 ,70, 1.51327E-01
9061 , 9026 , 8991 ,70, 1.53505E-01
9131 , 9096 , 9061 ,70, 1.55682E-01
9201 , 9166 , 9131 ,70, 1.57860E-01
9271 , 9236 , 9201 ,70, 1.59892E-01
9341 , 9306 , 9271 ,70, 1.62070E-01
9411 , 9376 , 9341 ,70, 1.64247E-01
9481 , 9446 , 9411 ,70, 1.66425E-01
9551 , 9516 , 9481 ,70, 1.68603E-01
9621 , 9586 , 9551 ,70, 1.70635E-01
9691 , 9656 , 9621 ,70, 1.72812E-01
9761 , 9726 , 9691 ,70, 1.74990E-01
9831 , 9796 , 9761 ,70, 1.77167E-01
9901 , 9866 , 9831 ,70, 1.79345E-01
9971 , 9936 , 9901 ,70, 1.81160E-01
10041 , 10006 , 9971 ,70, 1.83133E-01
10111 , 10076 , 10041 ,70, 1.85107E-01
10181 , 10146 , 10111 ,70, 1.87080E-01
10251 , 10216 , 10181 ,70, 1.89054E-01
10321 , 10286 , 10251 ,70, 1.91027E-01
10391 , 10356 , 10321 ,70, 1.92869E-01
10461 , 10426 , 10391 ,70, 1.94843E-01
10531 , 10496 , 10461 ,70, 1.96816E-01
10601 , 10566 , 10531 ,70, 1.98790E-01
10671 , 10636 , 10601 ,70, 2.00764E-01
10741 , 10706 , 10671 ,70, 2.02605E-01
10811 , 10776 , 10741 ,70, 2.04579E-01
```

```
10881 , 10846 , 10811 ,70, 2.06553E-01
10951 , 10916 , 10881 ,70, 2.08526E-01
11021 , 10986 , 10951 ,70, 2.10500E-01
11091 , 11056 , 11021 ,70, 2.11987E-01
11161 , 11126 , 11091 ,70, 2.13469E-01
11231 , 11196 , 11161 ,70, 2.14951E-01
11301 , 11266 , 11231 ,70, 2.16432E-01
11371 , 11336 , 11301 ,70, 2.17914E-01
11441 , 11406 , 11371 ,70, 2.19396E-01
11511 , 11476 , 11441 ,70, 2.20778E-01
11581 , 11546 , 11511 ,70, 2.22260E-01
11651 , 11616 , 11581 ,70, 2.23742E-01
11721 , 11686 , 11651 ,70, 2.25223E-01
11791 , 11756 , 11721 ,70, 2.26705E-01
11861 , 11826 , 11791 ,70, 2.28187E-01
11931 , 11896 , 11861 ,70, 2.29570E-01
12001 , 11966 , 11931 ,70, 2.31051E-01
12071 , 12036 , 12001 ,70, 2.32533E-01
12141 , 12106 , 12071 ,70, 2.34014E-01
12211 , 12176 , 12141 ,70, 2.35305E-01
12281 , 12246 , 12211 ,70, 2.36347E-01
12351 , 12316 , 12281 ,70, 2.37319E-01
12421 , 12386 , 12351 ,70, 2.38361E-01
12491 , 12456 , 12421 ,70, 2.39402E-01
12561 , 12526 , 12491 ,70, 2.40444E-01
12631 , 12596 , 12561 ,70, 2.41485E-01
12701 , 12666 , 12631 ,70, 2.42527E-01
12771 , 12736 , 12701 ,70, 2.43499E-01
12841 , 12806 , 12771 ,70, 2.44540E-01
12911 , 12876 , 12841 ,70, 2.45582E-01
12981 , 12946 , 12911 ,70, 2.46623E-01
13051 , 13016 , 12981 ,70, 2.47665E-01
13121 , 13086 , 13051 ,70, 2.48706E-01
13191 , 13156 , 13121 ,70, 2.49678E-01
13261 , 13226 , 13191 ,70, 2.50720E-01
13331 , 13296 , 13261 ,70, 2.51722E-01
13401 , 13366 , 13331 ,70, 2.52310E-01
13471 , 13436 , 13401 ,70, 2.52899E-01
13541 , 13506 , 13471 ,70, 2.53487E-01
13611 , 13576 , 13541 ,70, 2.54036E-01
13681 , 13646 , 13611 ,70, 2.54624E-01
13751 , 13716 , 13681 ,70, 2.55212E-01
13821 , 13786 , 13751 ,70, 2.55801E-01
13891 , 13856 , 13821 ,70, 2.56663E-01
13961 , 13926 , 13891 ,70, 2.57526E-01
14031 , 13996 , 13961 ,70, 2.58428E-01
14101 , 14066 , 14031 ,70, 2.59291E-01
14171 , 14136 , 14101 ,70, 2.60154E-01
14241 , 14206 , 14171 ,70, 2.61016E-01
14311 , 14276 , 14241 ,70, 2.61379E-01
14381 , 14346 , 14311 ,70, 2.61617E-01
14451 , 14416 , 14381 ,70, 2.61855E-01
14521 , 14486 , 14451 ,70, 2.62092E-01
14591 , 14556 , 14521 ,70, 2.62330E-01
14661 , 14626 , 14591 ,70, 2.62579E-01
14731 , 14696 , 14661 ,70, 2.62817E-01
14801 , 14766 , 14731 ,70, 2.63055E-01
14871 , 14836 , 14801 ,70, 2.63293E-01
```

```
14941 , 14906 , 14871 ,70, 2.63531E-01
15011 , 14976 , 14941 ,70, 2.63780E-01
15081 , 15046 , 15011 ,70, 2.63500E-01
15151 , 15116 , 15081 ,70, 2.63191E-01
15221 , 15186 , 15151 ,70, 2.62882E-01
15291 , 15256 , 15221 ,70, 2.62559E-01
15361 , 15326 , 15291 ,70, 2.62250E-01
15431 , 15396 , 15361 ,70, 2.61941E-01
15501 , 15466 , 15431 ,70, 2.61631E-01
15571 , 15536 , 15501 ,70, 2.61322E-01
15641 , 15606 , 15571 ,70, 2.60999E-01
15711 , 15676 , 15641 ,70, 2.60690E-01
15781 , 15746 , 15711 ,70, 2.60381E-01
15851 , 15816 , 15781 ,70, 2.59549E-01
15921 , 15886 , 15851 ,70, 2.58694E-01
15991 , 15956 , 15921 ,70, 2.57877E-01
16061 , 16026 , 15991 ,70, 2.57059E-01
16131 , 16096 , 16061 ,70, 2.56242E-01
16201 , 16166 , 16131 ,70, 2.55424E-01
16271 , 16236 , 16201 ,70, 2.54569E-01
16341 , 16306 , 16271 ,70, 2.53751E-01
16411 , 16376 , 16341 ,70, 2.52934E-01
16481 , 16446 , 16411 ,70, 2.52116E-01
16551 , 16516 , 16481 ,70, 2.51264E-01
16621 , 16586 , 16551 ,70, 2.50062E-01
16691 , 16656 , 16621 ,70, 2.48913E-01
16761 , 16726 , 16691 ,70, 2.47763E-01
16831 , 16796 , 16761 ,70, 2.46614E-01
16901 , 16866 , 16831 ,70, 2.45412E-01
16971 , 16936 , 16901 ,70, 2.44262E-01
17041 , 17006 , 16971 ,70, 2.43113E-01
17111 , 17076 , 17041 ,70, 2.41963E-01
17181 , 17146 , 17111 ,70, 2.40814E-01
17251 , 17216 , 17181 ,70, 2.39612E-01
17321 , 17286 , 17251 ,70, 2.38463E-01
17391 , 17356 , 17321 ,70, 2.36949E-01
17461 , 17426 , 17391 ,70, 2.35503E-01
17531 , 17496 , 17461 ,70, 2.33992E-01
17601 , 17566 , 17531 ,70, 2.32546E-01
17671 , 17636 , 17601 ,70, 2.31101E-01
17741 , 17706 , 17671 ,70, 2.29655E-01
17811 , 17776 , 17741 ,70, 2.28144E-01
17881 , 17846 , 17811 ,70, 2.26699E-01
17951 , 17916 , 17881 ,70, 2.25253E-01
18021 , 17986 , 17951 ,70, 2.23808E-01
18091 , 18056 , 18021 ,70, 2.22304E-01
18161 , 18126 , 18091 ,70, 2.20596E-01
18231 , 18196 , 18161 ,70, 2.18963E-01
18301 , 18266 , 18231 ,70, 2.17330E-01
18371 , 18336 , 18301 ,70, 2.15697E-01
18441 , 18406 , 18371 ,70, 2.13989E-01
18511 , 18476 , 18441 ,70, 2.12356E-01
18581 , 18546 , 18511 ,70, 2.10722E-01
18651 , 18616 , 18581 ,70, 2.09089E-01
18721 , 18686 , 18651 ,70, 2.07456E-01
18791 , 18756 , 18721 ,70, 2.05748E-01
18861 , 18826 , 18791 ,70, 2.04115E-01
18931 , 18896 , 18861 ,70, 2.02482E-01
```

```
19001 , 18966 , 18931 ,70, 2.00848E-01
19071 , 19036 , 19001 ,70, 1.99141E-01
19141 , 19106 , 19071 ,70, 1.97508E-01
19211 , 19176 , 19141 ,70, 1.95874E-01
19281 , 19246 , 19211 ,70, 1.94241E-01
19351 , 19316 , 19281 ,70, 1.92608E-01
19421 , 19386 , 19351 ,70, 1.90900E-01
19491 , 19456 , 19421 ,70, 1.89267E-01
19561 , 19526 , 19491 ,70, 1.87634E-01
19631 , 19596 , 19561 ,70, 1.86000E-01
19701 , 19666 , 19631 ,70, 1.84293E-01
19771 , 19736 , 19701 ,70, 1.82659E-01
19841 , 19806 , 19771 ,70, 1.81026E-01
19911 , 19876 , 19841 ,70, 1.79393E-01
19981 , 19946 , 19911 ,70, 1.77685E-01
20051 , 20016 , 19981 ,70, 1.76052E-01
20121 , 20086 , 20051 ,70, 1.74419E-01
20191 , 20156 , 20121 ,70, 1.71969E-01
20261 , 20226 , 20191 ,70, 1.69445E-01
20331 , 20296 , 20261 ,70, 1.66995E-01
20401 , 20366 , 20331 ,70, 1.64545E-01
20471 , 20436 , 20401 ,70, 1.62021E-01
20541 , 20506 , 20471 ,70, 1.59571E-01
20611 , 20576 , 20541 ,70, 1.57121E-01
20681 , 20646 , 20611 ,70, 1.54596E-01
20751 , 20716 , 20681 ,70, 1.52146E-01
20821 , 20786 , 20751 ,70, 1.49697E-01
20891 , 20856 , 20821 ,70, 1.47172E-01
20961 , 20926 , 20891 ,70, 1.44722E-01
21031 , 20996 , 20961 ,70, 1.42272E-01
21101 , 21066 , 21031 ,70, 1.39748E-01
21171 , 21136 , 21101 ,70, 1.37298E-01
21241 , 21206 , 21171 ,70, 1.34848E-01
21311 , 21276 , 21241 ,70, 1.32324E-01
21381 , 21346 , 21311 ,70, 1.29874E-01
21451 , 21416 , 21381 ,70, 1.27424E-01
21521 , 21486 , 21451 ,70, 1.24900E-01
21591 , 21556 , 21521 ,70, 1.22450E-01
21661 , 21626 , 21591 ,70, 1.20000E-01
21731 , 21696 , 21661 ,70, 1.17476E-01
21801 , 21766 , 21731 ,70, 1.15026E-01
21871 , 21836 , 21801 ,70, 1.12576E-01
21941 , 21906 , 21871 ,70, 1.10052E-01
22011 , 21976 , 21941 ,70, 1.07602E-01
22081 , 22046 , 22011 ,70, 1.05152E-01
22151 , 22116 , 22081 ,70, 1.02628E-01
22221 , 22186 , 22151 ,70, 1.00178E-01
22291 , 22256 , 22221 ,70, 9.72084E-02
22361 , 22326 , 22291 ,70, 9.42387E-02
22431 , 22396 , 22361 ,70, 9.12691E-02
22501 , 22466 , 22431 ,70, 8.82995E-02
22571 , 22536 , 22501 ,70, 8.53299E-02
22641 , 22606 , 22571 ,70, 8.23602E-02
22711 , 22676 , 22641 ,70, 7.93906E-02
22781 , 22746 , 22711 ,70, 7.64210E-02
22851 , 22816 , 22781 ,70, 7.34513E-02
22921 , 22886 , 22851 ,70, 7.04817E-02
22991 , 22956 , 22921 ,70, 6.75121E-02
```

```
23061 , 23026 , 22991 ,70, 6.45425E-02
23131 , 23096 , 23061 ,70, 6.14986E-02
23201 , 23166 , 23131 ,70, 5.85290E-02
23271 , 23236 , 23201 ,70, 5.55593E-02
23341 , 23306 , 23271 ,70, 5.25897E-02
23411 , 23376 , 23341 ,70, 4.96201E-02
23481 , 23446 , 23411 ,70, 4.66504E-02
23551 , 23516 , 23481 ,70, 4.36808E-02
23621 , 23586 , 23551 ,70, 4.07112E-02
23691 , 23656 , 23621 ,70, 3.77416E-02
23761 , 23726 , 23691 ,70, 3.47719E-02
23831 , 23796 , 23761 ,70, 3.18023E-02
23901 , 23866 , 23831 ,70, 2.88327E-02
23971 , 23936 , 23901 ,70, 2.58630E-02
24041 , 24006 , 23971 ,70, 2.28934E-02
24111 , 24076 , 24041 ,70, 1.99238E-02
24181 , 24146 , 24111 ,70, 1.69542E-02
24251 , 24216 , 24181 ,70, 1.39845E-02
24321 , 24286 , 24251 ,70, 1.10891E-02
24391 , 24356 , 24321 ,70, 8.11951E-03
24461 , 24426 , 24391 ,70, 5.14989E-03
24531 , 24496 , 24461 ,70, 2.18026E-03
24601 , 24566 , 24531 ,  , 0.00000E+00
BCNODE (un)
731,35,0.0
24601,,0.0
BCNODE (temperature)
1 ,1, 275.00
2 ,1, 273.95
3 ,1, 272.89
4 ,1, 271.84
5 ,1, 270.78
6 ,1, 269.73
7 ,1, 268.67
8 ,1, 267.62
9 ,1, 266.56
10 ,1, 265.51
11 ,1, 264.45
12 ,1, 263.40
13 ,1, 262.34
14 ,1, 261.29
15 ,1, 260.23
16 ,1, 259.18
17 ,1, 258.12
18 ,1, 257.07
19 ,1, 256.01
20 ,1, 254.96
21 ,1, 253.90
22 ,1, 252.85
23 ,1, 251.79
24 ,1, 250.74
25 ,1, 249.68
26 ,1, 248.63
27 ,1, 247.57
28 ,1, 246.52
29 ,1, 245.46
30 ,1, 244.41
31 ,1, 243.35
```

```
 32 ,1, 242.30
 33 ,1, 241.24
 34 ,1, 240.19
 35 ,1, 239.13
 36 ,1, 238.08
 37 ,1, 237.02
 38 ,1, 235.97
 39 ,1, 234.91
 40 ,1, 233.86
 41 ,1, 232.80
 42 ,1, 231.75
 43 ,1, 230.69
 44 ,1, 229.64
 45 ,1, 228.58
 46 ,1, 227.53
 47 ,1, 226.47
 48 ,1, 225.42
 49 ,1, 224.17
 50 ,1, 222.80
 51 ,1, 221.43
 52 ,1, 217.58
 53 ,1, 213.75
 54 ,1, 209.91
 55 ,1, 206.07
 56 ,1, 202.23
 57 ,1, 198.39
 58 ,1, 194.55
 59 ,1, 190.71
 60 ,1, 186.87
 61 ,1, 183.04
 62 ,1, 179.19
 63 ,1, 175.35
 64 ,1, 171.52
 65 ,1, 167.68
 66 ,1, 163.84
 67 ,1, 160.00
 68 ,1, 158.36
 69 ,1, 156.72
 70 ,1, 155.09
 71 ,1, 153.45
 72 ,1, 151.85
 73 ,1, 150.21
 74 ,1, 148.58
 75 ,1, 146.94
 76 ,1, 145.30
 77 ,1, 143.66
 78 ,1, 142.02
 79 ,1, 140.39
 80 ,1, 138.75
 81 ,1, 137.15
 82 ,1, 135.51
 83 ,1, 133.88
 84 ,1, 132.24
 85 ,1, 130.60
RENUMBER (profile)
ELEMENTS (quadrilateral, nodes=9, fluid, mvisc=1, mcond=1, fimesh)
ELEMENTS (quadrilateral, nodes=9, fluid, mvisc=1, mcond=1, fimesh)
ELEMENTS (quadrilateral, nodes=9, fluid, mvisc=1, mcond=1, fimesh)
```

```
ELEMENTS (quadrilateral, nodes=9, fluid, mvisc=2, mcond=2, fimesh)
ELEMENTS (quadrilateral, nodes=9, fluid, mvisc=2, mcond=2, fimesh)
ELEMENTS (triangle, nodes=6, fluid, mvisc=1, mcond=1, fimesh)
ELEMENTS (triangle, nodes=6, fluid, mvisc=2, mcond=2, fimesh)
ELEMENTS (convection, nodes=3, mcnv=1, fimesh)
ELEMENTS (slip, nodes=3, attach=7, fimesh)
ELEMENTS (slip, nodes=3, attach=5, fimesh)
END
*END
```

APPENDIX E

3-D (v6.03) MODEL INPUT FILES

E1. ISOTHERMAL FLOW MODEL

```
*NOINTERACTIVE
/   Visc = 0.1 Pa.s,
/   Uy for wideface consumption = 0.00090
/   28539 nodes
/   MUST run on the CRAY
/   10 elements in y-dir
/   Mesh graded to make finer in some regions
/   Approx 720 CPUs/iter
/   990 MB Disk Space
*TITLE
3-D/3640(27)/ISOTHERMAL/visc=0.1 Pa.s
*FIMESH (3-D, IMAX=10, JMAX=5, KMAX=5, MXPOINT=150)
EXPI
1 5 17 73 93 103 119
EXPJ
1 11 21
EXPK
1 11 15 21
POINT
/# I J K     X          Y         Z
1 1 1 1     -0.0010    0.00     -0.01
2 2 1 1     0.001      0.00     -0.01
3 2 1 2     0.001      0.00      0.00055
4 3 1 2     0.020      0.00      0.0069
5 4 1 2     0.260      0.00     -0.0088
6 5 1 2     0.460      0.00     -0.016
7 6 1 2     0.560      0.00     -0.016
8 7 1 2     0.700      0.00     -0.0100
9 7 1 3     0.700      0.00     -0.006
10 7 1 4    0.700      0.00      0.017
11 6 1 4    0.560      0.00      0.017
12 5 1 4    0.460      0.00      0.017
13 4 1 4    0.260      0.00      0.017
14 3 1 4    0.02       0.00      0.017
15 2 1 4    0.001      0.00      0.017
16 1 1 4    -0.0010    0.00      0.017
17 1 1 3    -0.0010    0.00      0.009
18 1 1 2    -0.0010    0.00      0.00055
19 2 1 3    0.001      0.00      0.009
20 3 1 3    0.02       0.00      0.009
21 4 1 3    0.260      0.00     -0.004
22 5 1 3    0.460      0.00     -0.012
23 6 1 3    0.560      0.00     -0.012
24 1 2 1    -0.0010   -0.05715  -0.01
25 1 2 2    -0.0010   -0.05715   0.00055
26 2 2 2    0.001     -0.05715   0.00055
27 1 3 1    -0.0010   -0.1143   -0.01
28 2 3 1    0.001     -0.1143   -0.01
29 2 3 2    0.001     -0.1143    0.00055
30 7 3 2    0.700     -0.1143   -0.0100
31 7 3 3    0.700     -0.1143   -0.006
32 7 3 4    0.700     -0.1143    0.017
```

```
33 2 3 4   0.001     -0.1143   0.017
34 1 3 4   -0.0010   -0.1143   0.017
35 1 3 3   -0.0010   -0.1143   0.009
36 1 3 2   -0.0010   -0.1143   0.00055
37 2 3 3   0.001     -0.1143   0.009
38 3 3 4   0.02      -0.1143   0.017
39 3 3 3   0.02      -0.1143   0.009
40 3 3 2   0.020     -0.1143   0.0069
41 5 3 2   0.460     -0.1143  -0.016
42 5 3 3   0.460     -0.1143  -0.012
43 6 3 2   0.560     -0.1143  -0.016
44 6 3 3   0.560     -0.1143  -0.012
CURVE (input)
3 4 21 1.25 3
0.00108507 0.0 0.0010
0.00123008 0.0 0.0015
0.00144749 0.0 0.0020
0.00174240 0.0 0.0025
0.00212367 0.0 0.0030
0.00260531 0.0 0.0035
0.00320916 0.0 0.0040
0.00397020 0.0 0.0045
0.00494813 0.0 0.0050
0.00625592 0.0 0.0055
0.00814847 0.0 0.0060
0.00864579 0.0 0.0061
0.00920358 0.0 0.0062
0.00983786 0.0 0.0063
0.01057219 0.0 0.0064
0.01144321 0.0 0.0065
0.01251268 0.0 0.0066
0.01389764 0.0 0.0067
0.01586728 0.0 0.0068
0.01935433 0.0 0.0069
0.01990000 0.0 0.0069
CURVE (input)
4 5 6 2.5 3
0.050 0.0  0.006
0.100 0.0  0.001
0.160 0.0 -0.003
0.200 0.0 -0.0060
0.250 0.0 -0.0084
0.258 0.0 -0.0087
CURVE (input)
5 6 2 1.5 3
0.360 0.0 -0.013
0.459 0.0 -0.016
CURVE (input)
6 7 2
0.500 0.0 -0.016
0.559 0.0 -0.016
CURVE (input)
7 8 3 0.5 3
0.610 0.0 -0.015
0.660 0.0 -0.013
0.690 0.0 -0.011
LINE
1 2
```

```
2 3
8 9
9 10
10 11 2.0 3
11 12
12 13 0.66666666 3
13 14 0.4 3
14 15 0.5 3
15 16
16 17
17 18
18 1
18 3
17 19
19 20 2.0 3
20 21 2.5 3
21 22 1.5 3
22 23
23 9 0.5 3
3 19
19 15
4 20
20 14
5 21
21 13
6 22
22 12
7 23
23 11
1 27 3.0 3
18 36 3.0 3
3 29 3.0 3
NUMBER
3 2 1
SURFACE
2 18
3 16
8 15
CDRIVE (parallel)
1 3 1 27
18 15 18 36
3 10 3 29
AREA
3 9
4 9
ELEMENTS (continuum, brick, nodes=27)
2 34
20 33
4 37
9 38
8 39
ELEMENTS (boundary, quadrilateral, nodes=9)
34 10 16
29 4 3
40 8 4
BCNODE (ux)
1 3 0.0
4 9 0.0
```

```
18 15 0.0
19 10 0.0
3 20 0.0
1 28 0.0
2 29 0.0
8 32 0.0
1 34 0.0
BCNODE (uy)
27 29 0.0
36 33 0.0
29 32 0.0
1 3 0.0
18 15 0.0
3 14 0.0
20 10 0.0
1 34 0.0
1 28 0.0
BCNODE (uz)
4 9 0.0
1 34 0.0
1 3 0.0
18 15 0.0
3 20 0.0
19 10 0.0
2 29 -0.0166667
10 34 -4.1e-05
BCNODE (coordinate)
29 8 1
BCNODE (temperature, constant)
2 29 1550.0
3 30 1550.0
1 34 300.0
BCFLUX (heat, nodes=9, constant)
8 32 0.0
1 28 0.0
27 29 0.0
36 33 0.0
29 38 0.0
40 32 0.0
1 3 0.0
18 15 0.0
3 10 0.0
END
*FIPREP
PROBLEM (steady, nonlinear, newtonian, 3-D,
laminar, momentum, isothermal)
EXECUTION (newjob)
SOLUTION (s.s.=5, resconv=1e-2, velconv=1e-6)
OPTIONS (upwinding)
PRESSURE (mixed=1.0e-14, continuous)
PRINTOUT (all)
DENSITY (set=1, constant=2500)
VISCOSITY (set=1, constant=0.1)
VISCOSITY (set=2, constant=0.1)
/VISCOSITIES
/Liquid -> Glassy solid
/VISCOSITY (set=1, curve=12, temperature)
/-20000, 500,  700,  900,  1100, 1150, 1200, 1300,
```

```
/1400, 1500, 1600, 20000
/1e8,   1e8,  1e8,  1e8,   0.50, 0.30, 0.20, 0.12,
/0.08, 0.05, 0.03, 0.03
/Powder -> Liquid
/VISCOSITY (set=2, curve=14, temperature)
/-20000, 500,  700,  900,  1000, 1050,  1100, 1150, 1200, 1300,
/1400, 1500, 1600, 20000
/10.0,  10.0, 10.0, 5.0,  2.0,  1.00,  0.50, 0.30, 0.20, 0.12,
/0.08, 0.05, 0.03, 0.03
/CONDUCTIVITIES
/Liquid -> Glassy Solid
/CONDUCTIVITY (set=1, curve=4, temperature, isotropic)
/-20000, 1000, 1200, 20000
/0.90,   0.9,  3.0,  3.0
/Powder -> Liquid
/CONDUCTIVITY (set=2, curve=16, temperature, isotropic)
/-15000, 0.0,  200,  400,  600,   800, 900,  940, 970, 1000, 1200, 1560,
/1590,  1650,  1750,  15000
/0.15,  0.20, 0.30, 0.42, 0.55,  0.7, 0.82, 0.9, 1.0, 1.10, 2.70, 2.80,
/2.88,  2.95,  3.00,  3.00
/HTRANSFER (set=1, curve=16, reftemp=27.0)
/-15000, -110,  220,  420,  620,  820,  1220, 1420, 1620, 2020, 2420,
/2620,   3000,   3500,   4000, 15000
/1.1     1.1,  44.7, 65.9, 94.9, 135,  260,  350,  462,  761,  1176,
/1434,   2027,   3036,   4341, 4341
/SPECIFICHEAT (set=1, temperature, enthalpy=17, spatial)
/-15000, 27,      227,    427,   527,   627,   727,   827,    950,
/1000,   1100,   1227,   1327,   1600,   2000,  2100,  15000
/0,     1.0e4,   1.8e5,  3.8e5, 4.8e5, 6.0e5, 6.9e5, 8.3e5,  1e6,
/1.10e6, 1.65e6, 1.85e6, 1.95e6, 2.2e6, 2.6e6, 2.65e6, 2.65e6
NODES (fimesh)
BCNODE (uy)
1775,21,0.0
2195,,0.0
/  Impose wideface consumption using uy velocity component
BCNODE (uy)
2437,231,-0.00090
28309,,-0.00090
BCNODE (uy)
2438,231,0.00090
28310,,0.00090
BCNODE (uy)
2439,231,0.00090
28311,,0.00090
BCNODE (uy)
2440,231,0.00090
28312,,0.00090
BCNODE (uy)
2441,231,0.00090
28313,,0.00090
/  Constrain velocity along flux/steel edge at wideface
BCNODE (uz)
2437,231,0.0
28309,,0.0
/  Constrain velocity normal to flux/steel interface
BCNODE (un3)
1775,21,0.0
2195,,0.0
```

```
BCNODE (un3)
2206,11,0.0
28529,,0.0
/  Second tangential direction defined as always in the
/  y-direction -- Needed for definition of stress on the curved
/  flux/steel interface.  BCSYSTEM is used in conjunction with
/  BCNODE (coordinate) card (see FIMESH input)
BCSYSTEM (set=1, 2tangential)
0, 0, 0, 0, 0, 0, 0, -0.001, 0
BCFLUX (T1, NODES=9)
2437 2448 2459 2690 2921 2910 2899 2668 2679 462 4.3374E-05
2899 2910 2921 3152 3383 3372 3361 3130 3141 462 1.2693E-04
3361 3372 3383 3614 3845 3834 3823 3592 3603 462 2.2794E-04
3823 3834 3845 4076 4307 4296 4285 4054 4065 462 3.4101E-04
4285 4296 4307 4538 4769 4758 4747 4516 4527 462 4.7931E-04
4747 4758 4769 5000 5231 5220 5209 4978 4989 462 6.9705E-04
5209 5220 5231 5462 5693 5682 5671 5440 5451 462 1.0672E-03
5671 5682 5693 5924 6155 6144 6133 5902 5913 462 1.6649E-03
6133 6144 6155 6386 6617 6606 6595 6364 6375 462 2.6040E-03
6595 6606 6617 6848 7079 7068 7057 6826 6837 462 3.9213E-03
7057 7068 7079 7310 7541 7530 7519 7288 7299 462 6.0039E-03
7519 7530 7541 7772 8003 7992 7981 7750 7761 462 8.6960E-03
7981 7992 8003 8234 8465 8454 8443 8212 8223 462 1.2665E-02
8443 8454 8465 8696 8927 8916 8905 8674 8685 462 1.7838E-02
8905 8916 8927 9158 9389 9378 9367 9136 9147 462 2.4168E-02
9367 9378 9389 9620 9851 9840 9829 9598 9609 462 3.2486E-02
9829 9840 9851 10082 10313 10302 10291 10060 10071 462 4.1259E-02
10291 10302 10313 10544 10775 10764 10753 10522 10533 462 5.2772E-02
10753 10764 10775 11006 11237 11226 11215 10984 10995 462 6.4693E-02
11215 11226 11237 11468 11699 11688 11677 11446 11457 462 7.8232E-02
11677 11688 11699 11930 12161 12150 12139 11908 11919 462 9.2866E-02
12139 12150 12161 12392 12623 12612 12601 12370 12381 462 1.0779E-01
12601 12612 12623 12854 13085 13074 13063 12832 12843 462 1.2188E-01
13063 13074 13085 13316 13547 13536 13525 13294 13305 462 1.3644E-01
13525 13536 13547 13778 14009 13998 13987 13756 13767 462 1.5094E-01
13987 13998 14009 14240 14471 14460 14449 14218 14229 462 1.6535E-01
14449 14460 14471 14702 14933 14922 14911 14680 14691 462 1.8014E-01
14911 14922 14933 15164 15395 15384 15373 15142 15153 462 1.9410E-01
15373 15384 15395 15626 15857 15846 15835 15604 15615 462 2.0854E-01
15835 15846 15857 16088 16319 16308 16297 16066 16077 462 2.2035E-01
16297 16308 16319 16550 16781 16770 16759 16528 16539 462 2.3195E-01
16759 16770 16781 17012 17243 17232 17221 16990 17001 462 2.4125E-01
17221 17232 17243 17474 17705 17694 17683 17452 17463 462 2.4997E-01
17683 17694 17705 17936 18167 18156 18145 17914 17925 462 2.5580E-01
18145 18156 18167 18398 18629 18618 18607 18376 18387 462 2.6146E-01
18607 18618 18629 18860 19091 19080 19069 18838 18849 462 2.6331E-01
19069 19080 19091 19322 19553 19542 19531 19300 19311 462 2.6191E-01
19531 19542 19553 19784 20015 20004 19993 19762 19773 462 2.5750E-01
19993 20004 20015 20246 20477 20466 20455 20224 20235 462 2.4983E-01
20455 20466 20477 20708 20939 20928 20917 20686 20697 462 2.3923E-01
20917 20928 20939 21170 21401 21390 21379 21148 21159 462 2.2545E-01
21379 21390 21401 21632 21863 21852 21841 21610 21621 462 2.0940E-01
21841 21852 21863 22094 22325 22314 22303 22072 22083 462 1.9228E-01
22303 22314 22325 22556 22787 22776 22765 22534 22545 462 1.7442E-01
22765 22776 22787 23018 23249 23238 23227 22996 23007 462 1.5957E-01
23227 23238 23249 23480 23711 23700 23689 23458 23469 462 1.4472E-01
23689 23700 23711 23942 24173 24162 24151 23920 23931 462 1.2987E-01
24151 24162 24173 24404 24635 24624 24613 24382 24393 462 1.1503E-01
```

```
24613 24624 24635 24866 25097 25086 25075 24844 24855 462 1.0018E-01
25075 25086 25097 25328 25559 25548 25537 25306 25317 462 8.2603E-02
25537 25548 25559 25790 26021 26010 25999 25768 25779 462 6.6580E-02
25999 26010 26021 26252 26483 26472 26461 26230 26241 462 5.1977E-02
26461 26472 26483 26714 26945 26934 26923 26692 26703 462 3.8665E-02
26923 26934 26945 27176 27407 27396 27385 27154 27165 462 2.6529E-02
27385 27396 27407 27638 27869 27858 27847 27616 27627 462 1.5479E-02
27847 27858 27869 28100 28331 28320 28309 28078 28089 462 5.4053E-03
BCFLUX (T1, NODES=9)
2459 2470 2481 2712 2943 2932 2921 2690 2701 462 4.3374E-05
2921 2932 2943 3174 3405 3394 3383 3152 3163 462 1.2693E-04
3383 3394 3405 3636 3867 3856 3845 3614 3625 462 2.2794E-04
3845 3856 3867 4098 4329 4318 4307 4076 4087 462 3.4101E-04
4307 4318 4329 4560 4791 4780 4769 4538 4549 462 4.7931E-04
4769 4780 4791 5022 5253 5242 5231 5000 5011 462 6.9705E-04
5231 5242 5253 5484 5715 5704 5693 5462 5473 462 1.0672E-03
5693 5704 5715 5946 6177 6166 6155 5924 5935 462 1.6649E-03
6155 6166 6177 6408 6639 6628 6617 6386 6397 462 2.6040E-03
6617 6628 6639 6870 7101 7090 7079 6848 6859 462 3.9213E-03
7079 7090 7101 7332 7563 7552 7541 7310 7321 462 6.0039E-03
7541 7552 7563 7794 8025 8014 8003 7772 7783 462 8.6960E-03
8003 8014 8025 8256 8487 8476 8465 8234 8245 462 1.2665E-02
8465 8476 8487 8718 8949 8938 8927 8696 8707 462 1.7838E-02
8927 8938 8949 9180 9411 9400 9389 9158 9169 462 2.4168E-02
9389 9400 9411 9642 9873 9862 9851 9620 9631 462 3.2486E-02
9851 9862 9873 10104 10335 10324 10313 10082 10093 462 4.1259E-02
10313 10324 10335 10566 10797 10786 10775 10544 10555 462 5.2772E-02
10775 10786 10797 11028 11259 11248 11237 11006 11017 462 6.4693E-02
11237 11248 11259 11490 11721 11710 11699 11468 11479 462 7.8232E-02
11699 11710 11721 11952 12183 12172 12161 11930 11941 462 9.2866E-02
12161 12172 12183 12414 12645 12634 12623 12392 12403 462 1.0779E-01
12623 12634 12645 12876 13107 13096 13085 12854 12865 462 1.2188E-01
13085 13096 13107 13338 13569 13558 13547 13316 13327 462 1.3644E-01
13547 13558 13569 13800 14031 14020 14009 13778 13789 462 1.5094E-01
14009 14020 14031 14262 14493 14482 14471 14240 14251 462 1.6535E-01
14471 14482 14493 14724 14955 14944 14933 14702 14713 462 1.8014E-01
14933 14944 14955 15186 15417 15406 15395 15164 15175 462 1.9410E-01
15395 15406 15417 15648 15879 15868 15857 15626 15637 462 2.0854E-01
15857 15868 15879 16110 16341 16330 16319 16088 16099 462 2.2035E-01
16319 16330 16341 16572 16803 16792 16781 16550 16561 462 2.3195E-01
16781 16792 16803 17034 17265 17254 17243 17012 17023 462 2.4125E-01
17243 17254 17265 17496 17727 17716 17705 17474 17485 462 2.4997E-01
17705 17716 17727 17958 18189 18178 18167 17936 17947 462 2.5580E-01
18167 18178 18189 18420 18651 18640 18629 18398 18409 462 2.6146E-01
18629 18640 18651 18882 19113 19102 19091 18860 18871 462 2.6331E-01
19091 19102 19113 19344 19575 19564 19553 19322 19333 462 2.6191E-01
19553 19564 19575 19806 20037 20026 20015 19784 19795 462 2.5750E-01
20015 20026 20037 20268 20499 20488 20477 20246 20257 462 2.4983E-01
20477 20488 20499 20730 20961 20950 20939 20708 20719 462 2.3923E-01
20939 20950 20961 21192 21423 21412 21401 21170 21181 462 2.2545E-01
21401 21412 21423 21654 21885 21874 21863 21632 21643 462 2.0940E-01
21863 21874 21885 22116 22347 22336 22325 22094 22105 462 1.9228E-01
22325 22336 22347 22578 22809 22798 22787 22556 22567 462 1.7442E-01
22787 22798 22809 23040 23271 23260 23249 23018 23029 462 1.5957E-01
23249 23260 23271 23502 23733 23722 23711 23480 23491 462 1.4472E-01
23711 23722 23733 23964 24195 24184 24173 23942 23953 462 1.2987E-01
24173 24184 24195 24426 24657 24646 24635 24404 24415 462 1.1503E-01
24635 24646 24657 24888 25119 25108 25097 24866 24877 462 1.0018E-01
```

```
25097 25108 25119 25350 25581 25570 25559 25328 25339 462 8.2603E-02
25559 25570 25581 25812 26043 26032 26021 25790 25801 462 6.6580E-02
26021 26032 26043 26274 26505 26494 26483 26252 26263 462 5.1977E-02
26483 26494 26505 26736 26967 26956 26945 26714 26725 462 3.8665E-02
26945 26956 26967 27198 27429 27418 27407 27176 27187 462 2.6529E-02
27407 27418 27429 27660 27891 27880 27869 27638 27649 462 1.5479E-02
27869 27880 27891 28122 28353 28342 28331 28100 28111 462 5.4053E-03
BCFLUX (T1, NODES=9)
2481 2492 2503 2734 2965 2954 2943 2712 2723 462 4.3374E-05
2943 2954 2965 3196 3427 3416 3405 3174 3185 462 1.2693E-04
3405 3416 3427 3658 3889 3878 3867 3636 3647 462 2.2794E-04
3867 3878 3889 4120 4351 4340 4329 4098 4109 462 3.4101E-04
4329 4340 4351 4582 4813 4802 4791 4560 4571 462 4.7931E-04
4791 4802 4813 5044 5275 5264 5253 5022 5033 462 6.9705E-04
5253 5264 5275 5506 5737 5726 5715 5484 5495 462 1.0672E-03
5715 5726 5737 5968 6199 6188 6177 5946 5957 462 1.6649E-03
6177 6188 6199 6430 6661 6650 6639 6408 6419 462 2.6040E-03
6639 6650 6661 6892 7123 7112 7101 6870 6881 462 3.9213E-03
7101 7112 7123 7354 7585 7574 7563 7332 7343 462 6.0039E-03
7563 7574 7585 7816 8047 8036 8025 7794 7805 462 8.6960E-03
8025 8036 8047 8278 8509 8498 8487 8256 8267 462 1.2665E-02
8487 8498 8509 8740 8971 8960 8949 8718 8729 462 1.7838E-02
8949 8960 8971 9202 9433 9422 9411 9180 9191 462 2.4168E-02
9411 9422 9433 9664 9895 9884 9873 9642 9653 462 3.2486E-02
9873 9884 9895 10126 10357 10346 10335 10104 10115 462 4.1259E-02
10335 10346 10357 10588 10819 10808 10797 10566 10577 462 5.2772E-02
10797 10808 10819 11050 11281 11270 11259 11028 11039 462 6.4693E-02
11259 11270 11281 11512 11743 11732 11721 11490 11501 462 7.8232E-02
11721 11732 11743 11974 12205 12194 12183 11952 11963 462 9.2866E-02
12183 12194 12205 12436 12667 12656 12645 12414 12425 462 1.0779E-01
12645 12656 12667 12898 13129 13118 13107 12876 12887 462 1.2188E-01
13107 13118 13129 13360 13591 13580 13569 13338 13349 462 1.3644E-01
13569 13580 13591 13822 14053 14042 14031 13800 13811 462 1.5094E-01
14031 14042 14053 14284 14515 14504 14493 14262 14273 462 1.6535E-01
14493 14504 14515 14746 14977 14966 14955 14724 14735 462 1.8014E-01
14955 14966 14977 15208 15439 15428 15417 15186 15197 462 1.9410E-01
15417 15428 15439 15670 15901 15890 15879 15648 15659 462 2.0854E-01
15879 15890 15901 16132 16363 16352 16341 16110 16121 462 2.2035E-01
16341 16352 16363 16594 16825 16814 16803 16572 16583 462 2.3195E-01
16803 16814 16825 17056 17287 17276 17265 17034 17045 462 2.4125E-01
17265 17276 17287 17518 17749 17738 17727 17496 17507 462 2.4997E-01
17727 17738 17749 17980 18211 18200 18189 17958 17969 462 2.5580E-01
18189 18200 18211 18442 18673 18662 18651 18420 18431 462 2.6146E-01
18651 18662 18673 18904 19135 19124 19113 18882 18893 462 2.6331E-01
19113 19124 19135 19366 19597 19586 19575 19344 19355 462 2.6191E-01
19575 19586 19597 19828 20059 20048 20037 19806 19817 462 2.5750E-01
20037 20048 20059 20290 20521 20510 20499 20268 20279 462 2.4983E-01
20499 20510 20521 20752 20983 20972 20961 20730 20741 462 2.3923E-01
20961 20972 20983 21214 21445 21434 21423 21192 21203 462 2.2545E-01
21423 21434 21445 21676 21907 21896 21885 21654 21665 462 2.0940E-01
21885 21896 21907 22138 22369 22358 22347 22116 22127 462 1.9228E-01
22347 22358 22369 22600 22831 22820 22809 22578 22589 462 1.7442E-01
22809 22820 22831 23062 23293 23282 23271 23040 23051 462 1.5957E-01
23271 23282 23293 23524 23755 23744 23733 23502 23513 462 1.4472E-01
23733 23744 23755 23986 24217 24206 24195 23964 23975 462 1.2987E-01
24195 24206 24217 24448 24679 24668 24657 24426 24437 462 1.1503E-01
24657 24668 24679 24910 25141 25130 25119 24888 24899 462 1.0018E-01
25119 25130 25141 25372 25603 25592 25581 25350 25361 462 8.2603E-02
```

```
25581 25592 25603 25834 26065 26054 26043 25812 25823 462 6.6580E-02
26043 26054 26065 26296 26527 26516 26505 26274 26285 462 5.1977E-02
26505 26516 26527 26758 26989 26978 26967 26736 26747 462 3.8665E-02
26967 26978 26989 27220 27451 27440 27429 27198 27209 462 2.6529E-02
27429 27440 27451 27682 27913 27902 27891 27660 27671 462 1.5479E-02
27891 27902 27913 28144 28375 28364 28353 28122 28133 462 5.4053E-03
BCFLUX (T1, NODES=9)
2503 2514 2525 2756 2987 2976 2965 2734 2745 462 4.3374E-05
2965 2976 2987 3218 3449 3438 3427 3196 3207 462 1.2693E-04
3427 3438 3449 3680 3911 3900 3889 3658 3669 462 2.2794E-04
3889 3900 3911 4142 4373 4362 4351 4120 4131 462 3.4101E-04
4351 4362 4373 4604 4835 4824 4813 4582 4593 462 4.7931E-04
4813 4824 4835 5066 5297 5286 5275 5044 5055 462 6.9705E-04
5275 5286 5297 5528 5759 5748 5737 5506 5517 462 1.0672E-03
5737 5748 5759 5990 6221 6210 6199 5968 5979 462 1.6649E-03
6199 6210 6221 6452 6683 6672 6661 6430 6441 462 2.6040E-03
6661 6672 6683 6914 7145 7134 7123 6892 6903 462 3.9213E-03
7123 7134 7145 7376 7607 7596 7585 7354 7365 462 6.0039E-03
7585 7596 7607 7838 8069 8058 8047 7816 7827 462 8.6960E-03
8047 8058 8069 8300 8531 8520 8509 8278 8289 462 1.2665E-02
8509 8520 8531 8762 8993 8982 8971 8740 8751 462 1.7838E-02
8971 8982 8993 9224 9455 9444 9433 9202 9213 462 2.4168E-02
9433 9444 9455 9686 9917 9906 9895 9664 9675 462 3.2486E-02
9895 9906 9917 10148 10379 10368 10357 10126 10137 462 4.1259E-02
10357 10368 10379 10610 10841 10830 10819 10588 10599 462 5.2772E-02
10819 10830 10841 11072 11303 11292 11281 11050 11061 462 6.4693E-02
11281 11292 11303 11534 11765 11754 11743 11512 11523 462 7.8232E-02
11743 11754 11765 11996 12227 12216 12205 11974 11985 462 9.2866E-02
12205 12216 12227 12458 12689 12678 12667 12436 12447 462 1.0779E-01
12667 12678 12689 12920 13151 13140 13129 12898 12909 462 1.2188E-01
13129 13140 13151 13382 13613 13602 13591 13360 13371 462 1.3644E-01
13591 13602 13613 13844 14075 14064 14053 13822 13833 462 1.5094E-01
14053 14064 14075 14306 14537 14526 14515 14284 14295 462 1.6535E-01
14515 14526 14537 14768 14999 14988 14977 14746 14757 462 1.8014E-01
14977 14988 14999 15230 15461 15450 15439 15208 15219 462 1.9410E-01
15439 15450 15461 15692 15923 15912 15901 15670 15681 462 2.0854E-01
15901 15912 15923 16154 16385 16374 16363 16132 16143 462 2.2035E-01
16363 16374 16385 16616 16847 16836 16825 16594 16605 462 2.3195E-01
16825 16836 16847 17078 17309 17298 17287 17056 17067 462 2.4125E-01
17287 17298 17309 17540 17771 17760 17749 17518 17529 462 2.4997E-01
17749 17760 17771 18002 18233 18222 18211 17980 17991 462 2.5580E-01
18211 18222 18233 18464 18695 18684 18673 18442 18453 462 2.6146E-01
18673 18684 18695 18926 19157 19146 19135 18904 18915 462 2.6331E-01
19135 19146 19157 19388 19619 19608 19597 19366 19377 462 2.6191E-01
19597 19608 19619 19850 20081 20070 20059 19828 19839 462 2.5750E-01
20059 20070 20081 20312 20543 20532 20521 20290 20301 462 2.4983E-01
20521 20532 20543 20774 21005 20994 20983 20752 20763 462 2.3923E-01
20983 20994 21005 21236 21467 21456 21445 21214 21225 462 2.2545E-01
21445 21456 21467 21698 21929 21918 21907 21676 21687 462 2.0940E-01
21907 21918 21929 22160 22391 22380 22369 22138 22149 462 1.9228E-01
22369 22380 22391 22622 22853 22842 22831 22600 22611 462 1.7442E-01
22831 22842 22853 23084 23315 23304 23293 23062 23073 462 1.5957E-01
23293 23304 23315 23546 23777 23766 23755 23524 23535 462 1.4472E-01
23755 23766 23777 24008 24239 24228 24217 23986 23997 462 1.2987E-01
24217 24228 24239 24470 24701 24690 24679 24448 24459 462 1.1503E-01
24679 24690 24701 24932 25163 25152 25141 24910 24921 462 1.0018E-01
25141 25152 25163 25394 25625 25614 25603 25372 25383 462 8.2603E-02
25603 25614 25625 25856 26087 26076 26065 25834 25845 462 6.6580E-02
```

```
26065 26076 26087 26318 26549 26538 26527 26296 26307 462 5.1977E-02
26527 26538 26549 26780 27011 27000 26989 26758 26769 462 3.8665E-02
26989 27000 27011 27242 27473 27462 27451 27220 27231 462 2.6529E-02
27451 27462 27473 27704 27935 27924 27913 27682 27693 462 1.5479E-02
27913 27924 27935 28166 28397 28386 28375 28144 28155 462 5.4053E-03
BCFLUX (T1, NODES=9)
2525 2536 2547 2778 3009 2998 2987 2756 2767 462 4.3374E-05
2987 2998 3009 3240 3471 3460 3449 3218 3229 462 1.2693E-04
3449 3460 3471 3702 3933 3922 3911 3680 3691 462 2.2794E-04
3911 3922 3933 4164 4395 4384 4373 4142 4153 462 3.4101E-04
4373 4384 4395 4626 4857 4846 4835 4604 4615 462 4.7931E-04
4835 4846 4857 5088 5319 5308 5297 5066 5077 462 6.9705E-04
5297 5308 5319 5550 5781 5770 5759 5528 5539 462 1.0672E-03
5759 5770 5781 6012 6243 6232 6221 5990 6001 462 1.6649E-03
6221 6232 6243 6474 6705 6694 6683 6452 6463 462 2.6040E-03
6683 6694 6705 6936 7167 7156 7145 6914 6925 462 3.9213E-03
7145 7156 7167 7398 7629 7618 7607 7376 7387 462 6.0039E-03
7607 7618 7629 7860 8091 8080 8069 7838 7849 462 8.6960E-03
8069 8080 8091 8322 8553 8542 8531 8300 8311 462 1.2665E-02
8531 8542 8553 8784 9015 9004 8993 8762 8773 462 1.7838E-02
8993 9004 9015 9246 9477 9466 9455 9224 9235 462 2.4168E-02
9455 9466 9477 9708 9939 9928 9917 9686 9697 462 3.2486E-02
9917 9928 9939 10170 10401 10390 10379 10148 10159 462 4.1259E-02
10379 10390 10401 10632 10863 10852 10841 10610 10621 462 5.2772E-02
10841 10852 10863 11094 11325 11314 11303 11072 11083 462 6.4693E-02
11303 11314 11325 11556 11787 11776 11765 11534 11545 462 7.8232E-02
11765 11776 11787 12018 12249 12238 12227 11996 12007 462 9.2866E-02
12227 12238 12249 12480 12711 12700 12689 12458 12469 462 1.0779E-01
12689 12700 12711 12942 13173 13162 13151 12920 12931 462 1.2188E-01
13151 13162 13173 13404 13635 13624 13613 13382 13393 462 1.3644E-01
13613 13624 13635 13866 14097 14086 14075 13844 13855 462 1.5094E-01
14075 14086 14097 14328 14559 14548 14537 14306 14317 462 1.6535E-01
14537 14548 14559 14790 15021 15010 14999 14768 14779 462 1.8014E-01
14999 15010 15021 15252 15483 15472 15461 15230 15241 462 1.9410E-01
15461 15472 15483 15714 15945 15934 15923 15692 15703 462 2.0854E-01
15923 15934 15945 16176 16407 16396 16385 16154 16165 462 2.2035E-01
16385 16396 16407 16638 16869 16858 16847 16616 16627 462 2.3195E-01
16847 16858 16869 17100 17331 17320 17309 17078 17089 462 2.4125E-01
17309 17320 17331 17562 17793 17782 17771 17540 17551 462 2.4997E-01
17771 17782 17793 18024 18255 18244 18233 18002 18013 462 2.5580E-01
18233 18244 18255 18486 18717 18706 18695 18464 18475 462 2.6146E-01
18695 18706 18717 18948 19179 19168 19157 18926 18937 462 2.6331E-01
19157 19168 19179 19410 19641 19630 19619 19388 19399 462 2.6191E-01
19619 19630 19641 19872 20103 20092 20081 19850 19861 462 2.5750E-01
20081 20092 20103 20334 20565 20554 20543 20312 20323 462 2.4983E-01
20543 20554 20565 20796 21027 21016 21005 20774 20785 462 2.3923E-01
21005 21016 21027 21258 21489 21478 21467 21236 21247 462 2.2545E-01
21467 21478 21489 21720 21951 21940 21929 21698 21709 462 2.0940E-01
21929 21940 21951 22182 22413 22402 22391 22160 22171 462 1.9228E-01
22391 22402 22413 22644 22875 22864 22853 22622 22633 462 1.7442E-01
22853 22864 22875 23106 23337 23326 23315 23084 23095 462 1.5957E-01
23315 23326 23337 23568 23799 23788 23777 23546 23557 462 1.4472E-01
23777 23788 23799 24030 24261 24250 24239 24008 24019 462 1.2987E-01
24239 24250 24261 24492 24723 24712 24701 24470 24481 462 1.1503E-01
24701 24712 24723 24954 25185 25174 25163 24932 24943 462 1.0018E-01
25163 25174 25185 25416 25647 25636 25625 25394 25405 462 8.2603E-02
25625 25636 25647 25878 26109 26098 26087 25856 25867 462 6.6580E-02
26087 26098 26109 26340 26571 26560 26549 26318 26329 462 5.1977E-02
```

```
26549 26560 26571 26802 27033 27022 27011 26780 26791 462 3.8665E-02
27011 27022 27033 27264 27495 27484 27473 27242 27253 462 2.6529E-02
27473 27484 27495 27726 27957 27946 27935 27704 27715 462 1.5479E-02
27935 27946 27957 28188 28419 28408 28397 28166 28177 462 5.4053E-03
BCFLUX (T1, NODES=9)
2547 2558 2569 2800 3031 3020 3009 2778 2789 462 4.3374E-05
3009 3020 3031 3262 3493 3482 3471 3240 3251 462 1.2693E-04
3471 3482 3493 3724 3955 3944 3933 3702 3713 462 2.2794E-04
3933 3944 3955 4186 4417 4406 4395 4164 4175 462 3.4101E-04
4395 4406 4417 4648 4879 4868 4857 4626 4637 462 4.7931E-04
4857 4868 4879 5110 5341 5330 5319 5088 5099 462 6.9705E-04
5319 5330 5341 5572 5803 5792 5781 5550 5561 462 1.0672E-03
5781 5792 5803 6034 6265 6254 6243 6012 6023 462 1.6649E-03
6243 6254 6265 6496 6727 6716 6705 6474 6485 462 2.6040E-03
6705 6716 6727 6958 7189 7178 7167 6936 6947 462 3.9213E-03
7167 7178 7189 7420 7651 7640 7629 7398 7409 462 6.0039E-03
7629 7640 7651 7882 8113 8102 8091 7860 7871 462 8.6960E-03
8091 8102 8113 8344 8575 8564 8553 8322 8333 462 1.2665E-02
8553 8564 8575 8806 9037 9026 9015 8784 8795 462 1.7838E-02
9015 9026 9037 9268 9499 9488 9477 9246 9257 462 2.4168E-02
9477 9488 9499 9730 9961 9950 9939 9708 9719 462 3.2486E-02
9939 9950 9961 10192 10423 10412 10401 10170 10181 462 4.1259E-02
10401 10412 10423 10654 10885 10874 10863 10632 10643 462 5.2772E-02
10863 10874 10885 11116 11347 11336 11325 11094 11105 462 6.4693E-02
11325 11336 11347 11578 11809 11798 11787 11556 11567 462 7.8232E-02
11787 11798 11809 12040 12271 12260 12249 12018 12029 462 9.2866E-02
12249 12260 12271 12502 12733 12722 12711 12480 12491 462 1.0779E-01
12711 12722 12733 12964 13195 13184 13173 12942 12953 462 1.2188E-01
13173 13184 13195 13426 13657 13646 13635 13404 13415 462 1.3644E-01
13635 13646 13657 13888 14119 14108 14097 13866 13877 462 1.5094E-01
14097 14108 14119 14350 14581 14570 14559 14328 14339 462 1.6535E-01
14559 14570 14581 14812 15043 15032 15021 14790 14801 462 1.8014E-01
15021 15032 15043 15274 15505 15494 15483 15252 15263 462 1.9410E-01
15483 15494 15505 15736 15967 15956 15945 15714 15725 462 2.0854E-01
15945 15956 15967 16198 16429 16418 16407 16176 16187 462 2.2035E-01
16407 16418 16429 16660 16891 16880 16869 16638 16649 462 2.3195E-01
16869 16880 16891 17122 17353 17342 17331 17100 17111 462 2.4125E-01
17331 17342 17353 17584 17815 17804 17793 17562 17573 462 2.4997E-01
17793 17804 17815 18046 18277 18266 18255 18024 18035 462 2.5580E-01
18255 18266 18277 18508 18739 18728 18717 18486 18497 462 2.6146E-01
18717 18728 18739 18970 19201 19190 19179 18948 18959 462 2.6331E-01
19179 19190 19201 19432 19663 19652 19641 19410 19421 462 2.6191E-01
19641 19652 19663 19894 20125 20114 20103 19872 19883 462 2.5750E-01
20103 20114 20125 20356 20587 20576 20565 20334 20345 462 2.4983E-01
20565 20576 20587 20818 21049 21038 21027 20796 20807 462 2.3923E-01
21027 21038 21049 21280 21511 21500 21489 21258 21269 462 2.2545E-01
21489 21500 21511 21742 21973 21962 21951 21720 21731 462 2.0940E-01
21951 21962 21973 22204 22435 22424 22413 22182 22193 462 1.9228E-01
22413 22424 22435 22666 22897 22886 22875 22644 22655 462 1.7442E-01
22875 22886 22897 23128 23359 23348 23337 23106 23117 462 1.5957E-01
23337 23348 23359 23590 23821 23810 23799 23568 23579 462 1.4472E-01
23799 23810 23821 24052 24283 24272 24261 24030 24041 462 1.2987E-01
24261 24272 24283 24514 24745 24734 24723 24492 24503 462 1.1503E-01
24723 24734 24745 24976 25207 25196 25185 24954 24965 462 1.0018E-01
25185 25196 25207 25438 25669 25658 25647 25416 25427 462 8.2603E-02
25647 25658 25669 25900 26131 26120 26109 25878 25889 462 6.6580E-02
26109 26120 26131 26362 26593 26582 26571 26340 26351 462 5.1977E-02
26571 26582 26593 26824 27055 27044 27033 26802 26813 462 3.8665E-02
```

```
27033 27044 27055 27286 27517 27506 27495 27264 27275 462 2.6529E-02
27495 27506 27517 27748 27979 27968 27957 27726 27737 462 1.5479E-02
27957 27968 27979 28210 28441 28430 28419 28188 28199 462 5.4053E-03
BCFLUX (T1, NODES=9)
2569 2580 2591 2822 3053 3042 3031 2800 2811 462 4.3374E-05
3031 3042 3053 3284 3515 3504 3493 3262 3273 462 1.2693E-04
3493 3504 3515 3746 3977 3966 3955 3724 3735 462 2.2794E-04
3955 3966 3977 4208 4439 4428 4417 4186 4197 462 3.4101E-04
4417 4428 4439 4670 4901 4890 4879 4648 4659 462 4.7931E-04
4879 4890 4901 5132 5363 5352 5341 5110 5121 462 6.9705E-04
5341 5352 5363 5594 5825 5814 5803 5572 5583 462 1.0672E-03
5803 5814 5825 6056 6287 6276 6265 6034 6045 462 1.6649E-03
6265 6276 6287 6518 6749 6738 6727 6496 6507 462 2.6040E-03
6727 6738 6749 6980 7211 7200 7189 6958 6969 462 3.9213E-03
7189 7200 7211 7442 7673 7662 7651 7420 7431 462 6.0039E-03
7651 7662 7673 7904 8135 8124 8113 7882 7893 462 8.6960E-03
8113 8124 8135 8366 8597 8586 8575 8344 8355 462 1.2665E-02
8575 8586 8597 8828 9059 9048 9037 8806 8817 462 1.7838E-02
9037 9048 9059 9290 9521 9510 9499 9268 9279 462 2.4168E-02
9499 9510 9521 9752 9983 9972 9961 9730 9741 462 3.2486E-02
9961 9972 9983 10214 10445 10434 10423 10192 10203 462 4.1259E-02
10423 10434 10445 10676 10907 10896 10885 10654 10665 462 5.2772E-02
10885 10896 10907 11138 11369 11358 11347 11116 11127 462 6.4693E-02
11347 11358 11369 11600 11831 11820 11809 11578 11589 462 7.8232E-02
11809 11820 11831 12062 12293 12282 12271 12040 12051 462 9.2866E-02
12271 12282 12293 12524 12755 12744 12733 12502 12513 462 1.0779E-01
12733 12744 12755 12986 13217 13206 13195 12964 12975 462 1.2188E-01
13195 13206 13217 13448 13679 13668 13657 13426 13437 462 1.3644E-01
13657 13668 13679 13910 14141 14130 14119 13888 13899 462 1.5094E-01
14119 14130 14141 14372 14603 14592 14581 14350 14361 462 1.6535E-01
14581 14592 14603 14834 15065 15054 15043 14812 14823 462 1.8014E-01
15043 15054 15065 15296 15527 15516 15505 15274 15285 462 1.9410E-01
15505 15516 15527 15758 15989 15978 15967 15736 15747 462 2.0854E-01
15967 15978 15989 16220 16451 16440 16429 16198 16209 462 2.2035E-01
16429 16440 16451 16682 16913 16902 16891 16660 16671 462 2.3195E-01
16891 16902 16913 17144 17375 17364 17353 17122 17133 462 2.4125E-01
17353 17364 17375 17606 17837 17826 17815 17584 17595 462 2.4997E-01
17815 17826 17837 18068 18299 18288 18277 18046 18057 462 2.5580E-01
18277 18288 18299 18530 18761 18750 18739 18508 18519 462 2.6146E-01
18739 18750 18761 18992 19223 19212 19201 18970 18981 462 2.6331E-01
19201 19212 19223 19454 19685 19674 19663 19432 19443 462 2.6191E-01
19663 19674 19685 19916 20147 20136 20125 19894 19905 462 2.5750E-01
20125 20136 20147 20378 20609 20598 20587 20356 20367 462 2.4983E-01
20587 20598 20609 20840 21071 21060 21049 20818 20829 462 2.3923E-01
21049 21060 21071 21302 21533 21522 21511 21280 21291 462 2.2545E-01
21511 21522 21533 21764 21995 21984 21973 21742 21753 462 2.0940E-01
21973 21984 21995 22226 22457 22446 22435 22204 22215 462 1.9228E-01
22435 22446 22457 22688 22919 22908 22897 22666 22677 462 1.7442E-01
22897 22908 22919 23150 23381 23370 23359 23128 23139 462 1.5957E-01
23359 23370 23381 23612 23843 23832 23821 23590 23601 462 1.4472E-01
23821 23832 23843 24074 24305 24294 24283 24052 24063 462 1.2987E-01
24283 24294 24305 24536 24767 24756 24745 24514 24525 462 1.1503E-01
24745 24756 24767 24998 25229 25218 25207 24976 24987 462 1.0018E-01
25207 25218 25229 25460 25691 25680 25669 25438 25449 462 8.2603E-02
25669 25680 25691 25922 26153 26142 26131 25900 25911 462 6.6580E-02
26131 26142 26153 26384 26615 26604 26593 26362 26373 462 5.1977E-02
26593 26604 26615 26846 27077 27066 27055 26824 26835 462 3.8665E-02
27055 27066 27077 27308 27539 27528 27517 27286 27297 462 2.6529E-02
```

```
27517 27528 27539 27770 28001 27990 27979 27748 27759 462 1.5479E-02
27979 27990 28001 28232 28463 28452 28441 28210 28221 462 5.4053E-03
BCFLUX (T1, NODES=9)
2591 2602 2613 2844 3075 3064 3053 2822 2833 462 4.3374E-05
3053 3064 3075 3306 3537 3526 3515 3284 3295 462 1.2693E-04
3515 3526 3537 3768 3999 3988 3977 3746 3757 462 2.2794E-04
3977 3988 3999 4230 4461 4450 4439 4208 4219 462 3.4101E-04
4439 4450 4461 4692 4923 4912 4901 4670 4681 462 4.7931E-04
4901 4912 4923 5154 5385 5374 5363 5132 5143 462 6.9705E-04
5363 5374 5385 5616 5847 5836 5825 5594 5605 462 1.0672E-03
5825 5836 5847 6078 6309 6298 6287 6056 6067 462 1.6649E-03
6287 6298 6309 6540 6771 6760 6749 6518 6529 462 2.6040E-03
6749 6760 6771 7002 7233 7222 7211 6980 6991 462 3.9213E-03
7211 7222 7233 7464 7695 7684 7673 7442 7453 462 6.0039E-03
7673 7684 7695 7926 8157 8146 8135 7904 7915 462 8.6960E-03
8135 8146 8157 8388 8619 8608 8597 8366 8377 462 1.2665E-02
8597 8608 8619 8850 9081 9070 9059 8828 8839 462 1.7838E-02
9059 9070 9081 9312 9543 9532 9521 9290 9301 462 2.4168E-02
9521 9532 9543 9774 10005 9994 9983 9752 9763 462 3.2486E-02
9983 9994 10005 10236 10467 10456 10445 10214 10225 462 4.1259E-02
10445 10456 10467 10698 10929 10918 10907 10676 10687 462 5.2772E-02
10907 10918 10929 11160 11391 11380 11369 11138 11149 462 6.4693E-02
11369 11380 11391 11622 11853 11842 11831 11600 11611 462 7.8232E-02
11831 11842 11853 12084 12315 12304 12293 12062 12073 462 9.2866E-02
12293 12304 12315 12546 12777 12766 12755 12524 12535 462 1.0779E-01
12755 12766 12777 13008 13239 13228 13217 12986 12997 462 1.2188E-01
13217 13228 13239 13470 13701 13690 13679 13448 13459 462 1.3644E-01
13679 13690 13701 13932 14163 14152 14141 13910 13921 462 1.5094E-01
14141 14152 14163 14394 14625 14614 14603 14372 14383 462 1.6535E-01
14603 14614 14625 14856 15087 15076 15065 14834 14845 462 1.8014E-01
15065 15076 15087 15318 15549 15538 15527 15296 15307 462 1.9410E-01
15527 15538 15549 15780 16011 16000 15989 15758 15769 462 2.0854E-01
15989 16000 16011 16242 16473 16462 16451 16220 16231 462 2.2035E-01
16451 16462 16473 16704 16935 16924 16913 16682 16693 462 2.3195E-01
16913 16924 16935 17166 17397 17386 17375 17144 17155 462 2.4125E-01
17375 17386 17397 17628 17859 17848 17837 17606 17617 462 2.4997E-01
17837 17848 17859 18090 18321 18310 18299 18068 18079 462 2.5580E-01
18299 18310 18321 18552 18783 18772 18761 18530 18541 462 2.6146E-01
18761 18772 18783 19014 19245 19234 19223 18992 19003 462 2.6331E-01
19223 19234 19245 19476 19707 19696 19685 19454 19465 462 2.6191E-01
19685 19696 19707 19938 20169 20158 20147 19916 19927 462 2.5750E-01
20147 20158 20169 20400 20631 20620 20609 20378 20389 462 2.4983E-01
20609 20620 20631 20862 21093 21082 21071 20840 20851 462 2.3923E-01
21071 21082 21093 21324 21555 21544 21533 21302 21313 462 2.2545E-01
21533 21544 21555 21786 22017 22006 21995 21764 21775 462 2.0940E-01
21995 22006 22017 22248 22479 22468 22457 22226 22237 462 1.9228E-01
22457 22468 22479 22710 22941 22930 22919 22688 22699 462 1.7442E-01
22919 22930 22941 23172 23403 23392 23381 23150 23161 462 1.5957E-01
23381 23392 23403 23634 23865 23854 23843 23612 23623 462 1.4472E-01
23843 23854 23865 24096 24327 24316 24305 24074 24085 462 1.2987E-01
24305 24316 24327 24558 24789 24778 24767 24536 24547 462 1.1503E-01
24767 24778 24789 25020 25251 25240 25229 24998 25009 462 1.0018E-01
25229 25240 25251 25482 25713 25702 25691 25460 25471 462 8.2603E-02
25691 25702 25713 25944 26175 26164 26153 25922 25933 462 6.6580E-02
26153 26164 26175 26406 26637 26626 26615 26384 26395 462 5.1977E-02
26615 26626 26637 26868 27099 27088 27077 26846 26857 462 3.8665E-02
27077 27088 27099 27330 27561 27550 27539 27308 27319 462 2.6529E-02
27539 27550 27561 27792 28023 28012 28001 27770 27781 462 1.5479E-02
```

```
28001 28012 28023 28254 28485 28474 28463 28232 28243 462 5.4053E-03
BCFLUX (T1, NODES=9)
2613 2624 2635 2866 3097 3086 3075 2844 2855 462 4.3374E-05
3075 3086 3097 3328 3559 3548 3537 3306 3317 462 1.2693E-04
3537 3548 3559 3790 4021 4010 3999 3768 3779 462 2.2794E-04
3999 4010 4021 4252 4483 4472 4461 4230 4241 462 3.4101E-04
4461 4472 4483 4714 4945 4934 4923 4692 4703 462 4.7931E-04
4923 4934 4945 5176 5407 5396 5385 5154 5165 462 6.9705E-04
5385 5396 5407 5638 5869 5858 5847 5616 5627 462 1.0672E-03
5847 5858 5869 6100 6331 6320 6309 6078 6089 462 1.6649E-03
6309 6320 6331 6562 6793 6782 6771 6540 6551 462 2.6040E-03
6771 6782 6793 7024 7255 7244 7233 7002 7013 462 3.9213E-03
7233 7244 7255 7486 7717 7706 7695 7464 7475 462 6.0039E-03
7695 7706 7717 7948 8179 8168 8157 7926 7937 462 8.6960E-03
8157 8168 8179 8410 8641 8630 8619 8388 8399 462 1.2665E-02
8619 8630 8641 8872 9103 9092 9081 8850 8861 462 1.7838E-02
9081 9092 9103 9334 9565 9554 9543 9312 9323 462 2.4168E-02
9543 9554 9565 9796 10027 10016 10005 9774 9785 462 3.2486E-02
10005 10016 10027 10258 10489 10478 10467 10236 10247 462 4.1259E-02
10467 10478 10489 10720 10951 10940 10929 10698 10709 462 5.2772E-02
10929 10940 10951 11182 11413 11402 11391 11160 11171 462 6.4693E-02
11391 11402 11413 11644 11875 11864 11853 11622 11633 462 7.8232E-02
11853 11864 11875 12106 12337 12326 12315 12084 12095 462 9.2866E-02
12315 12326 12337 12568 12799 12788 12777 12546 12557 462 1.0779E-01
12777 12788 12799 13030 13261 13250 13239 13008 13019 462 1.2188E-01
13239 13250 13261 13492 13723 13712 13701 13470 13481 462 1.3644E-01
13701 13712 13723 13954 14185 14174 14163 13932 13943 462 1.5094E-01
14163 14174 14185 14416 14647 14636 14625 14394 14405 462 1.6535E-01
14625 14636 14647 14878 15109 15098 15087 14856 14867 462 1.8014E-01
15087 15098 15109 15340 15571 15560 15549 15318 15329 462 1.9410E-01
15549 15560 15571 15802 16033 16022 16011 15780 15791 462 2.0854E-01
16011 16022 16033 16264 16495 16484 16473 16242 16253 462 2.2035E-01
16473 16484 16495 16726 16957 16946 16935 16704 16715 462 2.3195E-01
16935 16946 16957 17188 17419 17408 17397 17166 17177 462 2.4125E-01
17397 17408 17419 17650 17881 17870 17859 17628 17639 462 2.4997E-01
17859 17870 17881 18112 18343 18332 18321 18090 18101 462 2.5580E-01
18321 18332 18343 18574 18805 18794 18783 18552 18563 462 2.6146E-01
18783 18794 18805 19036 19267 19256 19245 19014 19025 462 2.6331E-01
19245 19256 19267 19498 19729 19718 19707 19476 19487 462 2.6191E-01
19707 19718 19729 19960 20191 20180 20169 19938 19949 462 2.5750E-01
20169 20180 20191 20422 20653 20642 20631 20400 20411 462 2.4983E-01
20631 20642 20653 20884 21115 21104 21093 20862 20873 462 2.3923E-01
21093 21104 21115 21346 21577 21566 21555 21324 21335 462 2.2545E-01
21555 21566 21577 21808 22039 22028 22017 21786 21797 462 2.0940E-01
22017 22028 22039 22270 22501 22490 22479 22248 22259 462 1.9228E-01
22479 22490 22501 22732 22963 22952 22941 22710 22721 462 1.7442E-01
22941 22952 22963 23194 23425 23414 23403 23172 23183 462 1.5957E-01
23403 23414 23425 23656 23887 23876 23865 23634 23645 462 1.4472E-01
23865 23876 23887 24118 24349 24338 24327 24096 24107 462 1.2987E-01
24327 24338 24349 24580 24811 24800 24789 24558 24569 462 1.1503E-01
24789 24800 24811 25042 25273 25262 25251 25020 25031 462 1.0018E-01
25251 25262 25273 25504 25735 25724 25713 25482 25493 462 8.2603E-02
25713 25724 25735 25966 26197 26186 26175 25944 25955 462 6.6580E-02
26175 26186 26197 26428 26659 26648 26637 26406 26417 462 5.1977E-02
26637 26648 26659 26890 27121 27110 27099 26868 26879 462 3.8665E-02
27099 27110 27121 27352 27583 27572 27561 27330 27341 462 2.6529E-02
27561 27572 27583 27814 28045 28034 28023 27792 27803 462 1.5479E-02
28023 28034 28045 28276 28507 28496 28485 28254 28265 462 5.4053E-03
```

```
BCFLUX (T1, NODES=9)
2635 2646 2657 2888 3119 3108 3097 2866 2877 462 4.3374E-05
3097 3108 3119 3350 3581 3570 3559 3328 3339 462 1.2693E-04
3559 3570 3581 3812 4043 4032 4021 3790 3801 462 2.2794E-04
4021 4032 4043 4274 4505 4494 4483 4252 4263 462 3.4101E-04
4483 4494 4505 4736 4967 4956 4945 4714 4725 462 4.7931E-04
4945 4956 4967 5198 5429 5418 5407 5176 5187 462 6.9705E-04
5407 5418 5429 5660 5891 5880 5869 5638 5649 462 1.0672E-03
5869 5880 5891 6122 6353 6342 6331 6100 6111 462 1.6649E-03
6331 6342 6353 6584 6815 6804 6793 6562 6573 462 2.6040E-03
6793 6804 6815 7046 7277 7266 7255 7024 7035 462 3.9213E-03
7255 7266 7277 7508 7739 7728 7717 7486 7497 462 6.0039E-03
7717 7728 7739 7970 8201 8190 8179 7948 7959 462 8.6960E-03
8179 8190 8201 8432 8663 8652 8641 8410 8421 462 1.2665E-02
8641 8652 8663 8894 9125 9114 9103 8872 8883 462 1.7838E-02
9103 9114 9125 9356 9587 9576 9565 9334 9345 462 2.4168E-02
9565 9576 9587 9818 10049 10038 10027 9796 9807 462 3.2486E-02
10027 10038 10049 10280 10511 10500 10489 10258 10269 462 4.1259E-02
10489 10500 10511 10742 10973 10962 10951 10720 10731 462 5.2772E-02
10951 10962 10973 11204 11435 11424 11413 11182 11193 462 6.4693E-02
11413 11424 11435 11666 11897 11886 11875 11644 11655 462 7.8232E-02
11875 11886 11897 12128 12359 12348 12337 12106 12117 462 9.2866E-02
12337 12348 12359 12590 12821 12810 12799 12568 12579 462 1.0779E-01
12799 12810 12821 13052 13283 13272 13261 13030 13041 462 1.2188E-01
13261 13272 13283 13514 13745 13734 13723 13492 13503 462 1.3644E-01
13723 13734 13745 13976 14207 14196 14185 13954 13965 462 1.5094E-01
14185 14196 14207 14438 14669 14658 14647 14416 14427 462 1.6535E-01
14647 14658 14669 14900 15131 15120 15109 14878 14889 462 1.8014E-01
15109 15120 15131 15362 15593 15582 15571 15340 15351 462 1.9410E-01
15571 15582 15593 15824 16055 16044 16033 15802 15813 462 2.0854E-01
16033 16044 16055 16286 16517 16506 16495 16264 16275 462 2.2035E-01
16495 16506 16517 16748 16979 16968 16957 16726 16737 462 2.3195E-01
16957 16968 16979 17210 17441 17430 17419 17188 17199 462 2.4125E-01
17419 17430 17441 17672 17903 17892 17881 17650 17661 462 2.4997E-01
17881 17892 17903 18134 18365 18354 18343 18112 18123 462 2.5580E-01
18343 18354 18365 18596 18827 18816 18805 18574 18585 462 2.6146E-01
18805 18816 18827 19058 19289 19278 19267 19036 19047 462 2.6331E-01
19267 19278 19289 19520 19751 19740 19729 19498 19509 462 2.6191E-01
19729 19740 19751 19982 20213 20202 20191 19960 19971 462 2.5750E-01
20191 20202 20213 20444 20675 20664 20653 20422 20433 462 2.4983E-01
20653 20664 20675 20906 21137 21126 21115 20884 20895 462 2.3923E-01
21115 21126 21137 21368 21599 21588 21577 21346 21357 462 2.2545E-01
21577 21588 21599 21830 22061 22050 22039 21808 21819 462 2.0940E-01
22039 22050 22061 22292 22523 22512 22501 22270 22281 462 1.9228E-01
22501 22512 22523 22754 22985 22974 22963 22732 22743 462 1.7442E-01
22963 22974 22985 23216 23447 23436 23425 23194 23205 462 1.5957E-01
23425 23436 23447 23678 23909 23898 23887 23656 23667 462 1.4472E-01
23887 23898 23909 24140 24371 24360 24349 24118 24129 462 1.2987E-01
24349 24360 24371 24602 24833 24822 24811 24580 24591 462 1.1503E-01
24811 24822 24833 25064 25295 25284 25273 25042 25053 462 1.0018E-01
25273 25284 25295 25526 25757 25746 25735 25504 25515 462 8.2603E-02
25735 25746 25757 25988 26219 26208 26197 25966 25977 462 6.6580E-02
26197 26208 26219 26450 26681 26670 26659 26428 26439 462 5.1977E-02
26659 26670 26681 26912 27143 27132 27121 26890 26901 462 3.8665E-02
27121 27132 27143 27374 27605 27594 27583 27352 27363 462 2.6529E-02
27583 27594 27605 27836 28067 28056 28045 27814 27825 462 1.5479E-02
28045 28056 28067 28298 28529 28518 28507 28276 28287 462 5.4053E-03
RENUMBER (profile)
```

```
ELEMENTS (brick, nodes=27, fluid, mvisc=1, mcond=2, fimesh)
ELEMENTS (brick, nodes=27, fluid, mvisc=1, mcond=2, fimesh)
ELEMENTS (brick, nodes=27, fluid, mvisc=1, mcond=2, fimesh)
ELEMENTS (brick, nodes=27, fluid, mvisc=2, mcond=2, fimesh)
ELEMENTS (brick, nodes=27, fluid, mvisc=2, mcond=2, fimesh)
ELEMENTS (convection, nodes=9, mcnv=1, fimesh)
ELEMENTS (slip, nodes=9, attach=3, fimesh)
ELEMENTS (slip, nodes=9, attach=5, fimesh)
END
*END
```

E2. ADVECTION-DIFFUSION MODEL

```
* NOINTERACTIVE
/   Visc = 0.1 Pa.s,
/   Uy for wideface consumption = 0.00090
/   28539 nodes
/   MUST run on the CRAY
/   10 elements in y-dir
/   Mesh graded to make finer in some regions
/   Approx 54 CPUs/iter
/   59 MB Disk Space
*TITLE
3-D/3640(27)/ISOTHERMAL/visc=0.1 Pa.s
*FIMESH (3-D, IMAX=10, JMAX=5, KMAX=5, MXPOINT=150)
EXPI
1 5 17 73 93 103 119
EXPJ
1 11 21
EXPK
1 11 15 21
POINT
/# I J K      X          Y         Z
1 1 1 1     -0.0010    0.00     -0.01
2 2 1 1     0.001      0.00     -0.01
3 2 1 2     0.001      0.00      0.00055
4 3 1 2     0.020      0.00      0.0069
5 4 1 2     0.260      0.00     -0.0088
6 5 1 2     0.460      0.00     -0.016
7 6 1 2     0.560      0.00     -0.016
8 7 1 2     0.700      0.00     -0.0100
9 7 1 3     0.700      0.00     -0.006
10 7 1 4    0.700      0.00      0.017
11 6 1 4    0.560      0.00      0.017
12 5 1 4    0.460      0.00      0.017
13 4 1 4    0.260      0.00      0.017
14 3 1 4    0.02       0.00      0.017
15 2 1 4    0.001      0.00      0.017
16 1 1 4    -0.0010    0.00      0.017
17 1 1 3    -0.0010    0.00      0.009
18 1 1 2    -0.0010    0.00      0.00055
19 2 1 3    0.001      0.00      0.009
20 3 1 3    0.02       0.00      0.009
21 4 1 3    0.260      0.00     -0.004
22 5 1 3    0.460      0.00     -0.012
23 6 1 3    0.560      0.00     -0.012
24 1 2 1    -0.0010   -0.05715  -0.01
```

```
25 1 2 2   -0.0010  -0.05715  0.00055
26 2 2 2   0.001    -0.05715  0.00055
27 1 3 1   -0.0010  -0.1143  -0.01
28 2 3 1   0.001    -0.1143  -0.01
29 2 3 2   0.001    -0.1143   0.00055
30 7 3 2   0.700    -0.1143  -0.0100
31 7 3 3   0.700    -0.1143  -0.006
32 7 3 4   0.700    -0.1143   0.017
33 2 3 4   0.001    -0.1143   0.017
34 1 3 4   -0.0010  -0.1143   0.017
35 1 3 3   -0.0010  -0.1143   0.009
36 1 3 2   -0.0010  -0.1143   0.00055
37 2 3 3   0.001    -0.1143   0.009
38 3 3 4   0.02     -0.1143   0.017
39 3 3 3   0.02     -0.1143   0.009
40 3 3 2   0.020    -0.1143   0.0069
41 5 3 2   0.460    -0.1143  -0.016
42 5 3 3   0.460    -0.1143  -0.012
43 6 3 2   0.560    -0.1143  -0.016
44 6 3 3   0.560    -0.1143  -0.012
CURVE (input)
3 4 21 1.25 3
0.00108507 0.0 0.0010
0.00123008 0.0 0.0015
0.00144749 0.0 0.0020
0.00174240 0.0 0.0025
0.00212367 0.0 0.0030
0.00260531 0.0 0.0035
0.00320916 0.0 0.0040
0.00397020 0.0 0.0045
0.00494813 0.0 0.0050
0.00625592 0.0 0.0055
0.00814847 0.0 0.0060
0.00864579 0.0 0.0061
0.00920358 0.0 0.0062
0.00983786 0.0 0.0063
0.01057219 0.0 0.0064
0.01144321 0.0 0.0065
0.01251268 0.0 0.0066
0.01389764 0.0 0.0067
0.01586728 0.0 0.0068
0.01935433 0.0 0.0069
0.01990000 0.0 0.0069
CURVE (input)
4 5 6 2.5 3
0.050 0.0  0.006
0.100 0.0  0.001
0.160 0.0 -0.003
0.200 0.0 -0.0060
0.250 0.0 -0.0084
0.258 0.0 -0.0087
CURVE (input)
5 6 2 1.5 3
0.360 0.0 -0.013
0.459 0.0 -0.016
CURVE (input)
6 7 2
0.500 0.0 -0.016
```

```
0.559 0.0 -0.016
CURVE (input)
7 8 3 0.5 3
0.610 0.0 -0.015
0.660 0.0 -0.013
0.690 0.0 -0.011
LINE
1 2
2 3
8 9
9 10
10 11 2.0 3
11 12
12 13 0.66666666 3
13 14 0.4 3
14 15 0.5 3
15 16
16 17
17 18
18 1
18 3
17 19
19 20 2.0 3
20 21 2.5 3
21 22 1.5 3
22 23
23 9 0.5 3
3 19
19 15
4 20
20 14
5 21
21 13
6 22
22 12
7 23
23 11
1 27 3.0 3
18 36 3.0 3
3 29 3.0 3
NUMBER
3 2 1
SURFACE
2 18
3 16
8 15
CDRIVE (parallel)
1 3 1 27
18 15 18 36
3 10 3 29
AREA
3 9
4 9
ELEMENTS (continuum, brick, nodes=27)
2 34
20 33
4 37
9 38
```

```
8 39
ELEMENTS (boundary, quadrilateral, nodes=9)
34 10 16
29 4 3
40 8 4
BCNODE (ux)
1 3 0.0
4 9 0.0
18 15 0.0
19 10 0.0
3 20 0.0
1 28 0.0
2 29 0.0
8 32 0.0
1 34 0.0
BCNODE (uy)
27 29 0.0
36 33 0.0
29 32 0.0
1 3 0.0
18 15 0.0
3 14 0.0
20 10 0.0
1 34 0.0
1 28 0.0
BCNODE (uz)
4 9 0.0
1 34 0.0
1 3 0.0
18 15 0.0
3 20 0.0
19 10 0.0
2 29 -0.0166667
10 34 -4.1e-05
BCNODE (coordinate)
29 8 1
BCNODE (temperature, constant)
2 29 1550.0
3 30 1550.0
1 34 300.0
BCFLUX (heat, nodes=9, constant)
8 32 0.0
1 28 0.0
27 29 0.0
36 33 0.0
29 38 0.0
40 32 0.0
1 3 0.0
18 15 0.0
3 10 0.0
ICNODE (temperature)
1 34 500.0
4 33 700.0
9 38 800.0
8 39 1000.0
END
*FIPREP
PROBLEM (steady, nonlinear, newtonian, 3-D,
```

```
laminar, nomomentum, weakly=0)
EXECUTION (newjob)
SOLUTION (s.s.=40, accf=0.85, resconv=1e-2, velconv=1e-6)
OPTIONS (upwinding)
PRESSURE (mixed=1.0e-14, continuous)
PRINTOUT (all)
DENSITY (set=1, constant=2500)
VISCOSITY (set=1, constant=0.1)
VISCOSITY (set=2, constant=0.1)
/VISCOSITIES
/Liquid -> Glassy solid
/VISCOSITY (set=1, curve=12, temperature)
/-20000, 500,  700,  900,  1100, 1150, 1200, 1300,
/1400, 1500, 1600, 20000
/1e8,   1e8,  1e8,  1e8,   0.50, 0.30, 0.20, 0.12,
/0.08, 0.05, 0.03, 0.03
/Powder -> Liquid
/VISCOSITY (set=2, curve=14, temperature)
/-20000, 500,  700,  900,  1000, 1050,  1100, 1150, 1200, 1300,
/1400, 1500, 1600, 20000
/10.0,  10.0, 10.0, 5.0,  2.0,  1.00,  0.50, 0.30, 0.20, 0.12,
/0.08, 0.05, 0.03, 0.03
/CONDUCTIVITIES
/Liquid -> Glassy Solid
/CONDUCTIVITY (set=1, curve=4, temperature, isotropic)
/-20000, 1000, 1200, 20000
/0.90,   0.9,  3.0,  3.0
/Powder -> Liquid
CONDUCTIVITY (set=2, curve=16, temperature, isotropic)
-15000, 0.0,  200,  400,  600,   800, 900,  940, 970, 1000, 1200, 1560,
1590,  1650,  1750,  15000
0.15,  0.20, 0.30, 0.42, 0.55,  0.7, 0.82, 0.9, 1.0, 1.10, 2.70, 2.80,
2.88,  2.95,  3.00,  3.00
HTRANSFER (set=1, curve=16, reftemp=27.0)
-15000, -110,  220,  420,  620,  820,  1220, 1420, 1620, 2020, 2420,
2620,   3000,   3500,   4000, 15000
1.1     1.1,  44.7, 65.9, 94.9, 135,  260,  350,  462,  761,  1176,
1434,   2027,   3036,   4341, 4341
SPECIFICHEAT (set=1, temperature, enthalpy=17, spatial)
-15000, 27,      227,    427,   527,   627,   727,   827,    950,
1000,   1100,   1227,   1327,   1600,   2000,  2100,  15000
0,     1.0e4,   1.8e5,  3.8e5, 4.8e5, 6.0e5, 6.9e5, 8.3e5,  1e6,
1.10e6, 1.65e6, 1.85e6, 1.95e6, 2.2e6, 2.6e6, 2.65e6, 2.65e6
ICNODE (velocity, read)
NODES (fimesh)
BCNODE (uy)
1775,21,0.0
2195,,0.0
/  Impose wideface consumption using uy velocity component
BCNODE (uy)
2437,231,-0.00090
28309,,-0.00090
BCNODE (uy)
2438,231,0.00090
28310,,0.00090
BCNODE (uy)
2439,231,0.00090
28311,,0.00090
```

```
BCNODE (uy)
2440,231,0.00090
28312,,0.00090
BCNODE (uy)
2441,231,0.00090
28313,,0.00090
/  Constrain velocity along flux/steel edge at wideface
BCNODE (uz)
2437,231,0.0
28309,,0.0
/  Constrain velocity normal to flux/steel interface
BCNODE (un3)
1775,21,0.0
2195,,0.0
BCNODE (un3)
2206,11,0.0
28529,,0.0
/  Second tangential direction defined as always in the
/  y-direction -- Needed for definition of stress on the curved
/  flux/steel interface.  BCSYSTEM is used in conjunction with
/  BCNODE (coordinate) card (see FIMESH input)
BCSYSTEM (set=1, 2tangential)
0, 0, 0, 0, 0, 0, 0, -0.001, 0
BCFLUX (T1, NODES=9)
2437 2448 2459 2690 2921 2910 2899 2668 2679 462 4.3374E-05
2899 2910 2921 3152 3383 3372 3361 3130 3141 462 1.2693E-04
3361 3372 3383 3614 3845 3834 3823 3592 3603 462 2.2794E-04
3823 3834 3845 4076 4307 4296 4285 4054 4065 462 3.4101E-04
4285 4296 4307 4538 4769 4758 4747 4516 4527 462 4.7931E-04
4747 4758 4769 5000 5231 5220 5209 4978 4989 462 6.9705E-04
5209 5220 5231 5462 5693 5682 5671 5440 5451 462 1.0672E-03
5671 5682 5693 5924 6155 6144 6133 5902 5913 462 1.6649E-03
6133 6144 6155 6386 6617 6606 6595 6364 6375 462 2.6040E-03
6595 6606 6617 6848 7079 7068 7057 6826 6837 462 3.9213E-03
7057 7068 7079 7310 7541 7530 7519 7288 7299 462 6.0039E-03
7519 7530 7541 7772 8003 7992 7981 7750 7761 462 8.6960E-03
7981 7992 8003 8234 8465 8454 8443 8212 8223 462 1.2665E-02
8443 8454 8465 8696 8927 8916 8905 8674 8685 462 1.7838E-02
8905 8916 8927 9158 9389 9378 9367 9136 9147 462 2.4168E-02
9367 9378 9389 9620 9851 9840 9829 9598 9609 462 3.2486E-02
9829 9840 9851 10082 10313 10302 10291 10060 10071 462 4.1259E-02
10291 10302 10313 10544 10775 10764 10753 10522 10533 462 5.2772E-02
10753 10764 10775 11006 11237 11226 11215 10984 10995 462 6.4693E-02
11215 11226 11237 11468 11699 11688 11677 11446 11457 462 7.8232E-02
11677 11688 11699 11930 12161 12150 12139 11908 11919 462 9.2866E-02
12139 12150 12161 12392 12623 12612 12601 12370 12381 462 1.0779E-01
12601 12612 12623 12854 13085 13074 13063 12832 12843 462 1.2188E-01
13063 13074 13085 13316 13547 13536 13525 13294 13305 462 1.3644E-01
13525 13536 13547 13778 14009 13998 13987 13756 13767 462 1.5094E-01
13987 13998 14009 14240 14471 14460 14449 14218 14229 462 1.6535E-01
14449 14460 14471 14702 14933 14922 14911 14680 14691 462 1.8014E-01
14911 14922 14933 15164 15395 15384 15373 15142 15153 462 1.9410E-01
15373 15384 15395 15626 15857 15846 15835 15604 15615 462 2.0854E-01
15835 15846 15857 16088 16319 16308 16297 16066 16077 462 2.2035E-01
16297 16308 16319 16550 16781 16770 16759 16528 16539 462 2.3195E-01
16759 16770 16781 17012 17243 17232 17221 16990 17001 462 2.4125E-01
17221 17232 17243 17474 17705 17694 17683 17452 17463 462 2.4997E-01
17683 17694 17705 17936 18167 18156 18145 17914 17925 462 2.5580E-01
```

```
18145 18156 18167 18398 18629 18618 18607 18376 18387 462 2.6146E-01
18607 18618 18629 18860 19091 19080 19069 18838 18849 462 2.6331E-01
19069 19080 19091 19322 19553 19542 19531 19300 19311 462 2.6191E-01
19531 19542 19553 19784 20015 20004 19993 19762 19773 462 2.5750E-01
19993 20004 20015 20246 20477 20466 20455 20224 20235 462 2.4983E-01
20455 20466 20477 20708 20939 20928 20917 20686 20697 462 2.3923E-01
20917 20928 20939 21170 21401 21390 21379 21148 21159 462 2.2545E-01
21379 21390 21401 21632 21863 21852 21841 21610 21621 462 2.0940E-01
21841 21852 21863 22094 22325 22314 22303 22072 22083 462 1.9228E-01
22303 22314 22325 22556 22787 22776 22765 22534 22545 462 1.7442E-01
22765 22776 22787 23018 23249 23238 23227 22996 23007 462 1.5957E-01
23227 23238 23249 23480 23711 23700 23689 23458 23469 462 1.4472E-01
23689 23700 23711 23942 24173 24162 24151 23920 23931 462 1.2987E-01
24151 24162 24173 24404 24635 24624 24613 24382 24393 462 1.1503E-01
24613 24624 24635 24866 25097 25086 25075 24844 24855 462 1.0018E-01
25075 25086 25097 25328 25559 25548 25537 25306 25317 462 8.2603E-02
25537 25548 25559 25790 26021 26010 25999 25768 25779 462 6.6580E-02
25999 26010 26021 26252 26483 26472 26461 26230 26241 462 5.1977E-02
26461 26472 26483 26714 26945 26934 26923 26692 26703 462 3.8665E-02
26923 26934 26945 27176 27407 27396 27385 27154 27165 462 2.6529E-02
27385 27396 27407 27638 27869 27858 27847 27616 27627 462 1.5479E-02
27847 27858 27869 28100 28331 28320 28309 28078 28089 462 5.4053E-03
BCFLUX (T1, NODES=9)
2459 2470 2481 2712 2943 2932 2921 2690 2701 462 4.3374E-05
2921 2932 2943 3174 3405 3394 3383 3152 3163 462 1.2693E-04
3383 3394 3405 3636 3867 3856 3845 3614 3625 462 2.2794E-04
3845 3856 3867 4098 4329 4318 4307 4076 4087 462 3.4101E-04
4307 4318 4329 4560 4791 4780 4769 4538 4549 462 4.7931E-04
4769 4780 4791 5022 5253 5242 5231 5000 5011 462 6.9705E-04
5231 5242 5253 5484 5715 5704 5693 5462 5473 462 1.0672E-03
5693 5704 5715 5946 6177 6166 6155 5924 5935 462 1.6649E-03
6155 6166 6177 6408 6639 6628 6617 6386 6397 462 2.6040E-03
6617 6628 6639 6870 7101 7090 7079 6848 6859 462 3.9213E-03
7079 7090 7101 7332 7563 7552 7541 7310 7321 462 6.0039E-03
7541 7552 7563 7794 8025 8014 8003 7772 7783 462 8.6960E-03
8003 8014 8025 8256 8487 8476 8465 8234 8245 462 1.2665E-02
8465 8476 8487 8718 8949 8938 8927 8696 8707 462 1.7838E-02
8927 8938 8949 9180 9411 9400 9389 9158 9169 462 2.4168E-02
9389 9400 9411 9642 9873 9862 9851 9620 9631 462 3.2486E-02
9851 9862 9873 10104 10335 10324 10313 10082 10093 462 4.1259E-02
10313 10324 10335 10566 10797 10786 10775 10544 10555 462 5.2772E-02
10775 10786 10797 11028 11259 11248 11237 11006 11017 462 6.4693E-02
11237 11248 11259 11490 11721 11710 11699 11468 11479 462 7.8232E-02
11699 11710 11721 11952 12183 12172 12161 11930 11941 462 9.2866E-02
12161 12172 12183 12414 12645 12634 12623 12392 12403 462 1.0779E-01
12623 12634 12645 12876 13107 13096 13085 12854 12865 462 1.2188E-01
13085 13096 13107 13338 13569 13558 13547 13316 13327 462 1.3644E-01
13547 13558 13569 13800 14031 14020 14009 13778 13789 462 1.5094E-01
14009 14020 14031 14262 14493 14482 14471 14240 14251 462 1.6535E-01
14471 14482 14493 14724 14955 14944 14933 14702 14713 462 1.8014E-01
14933 14944 14955 15186 15417 15406 15395 15164 15175 462 1.9410E-01
15395 15406 15417 15648 15879 15868 15857 15626 15637 462 2.0854E-01
15857 15868 15879 16110 16341 16330 16319 16088 16099 462 2.2035E-01
16319 16330 16341 16572 16803 16792 16781 16550 16561 462 2.3195E-01
16781 16792 16803 17034 17265 17254 17243 17012 17023 462 2.4125E-01
17243 17254 17265 17496 17727 17716 17705 17474 17485 462 2.4997E-01
17705 17716 17727 17958 18189 18178 18167 17936 17947 462 2.5580E-01
18167 18178 18189 18420 18651 18640 18629 18398 18409 462 2.6146E-01
```

```
18629 18640 18651 18882 19113 19102 19091 18860 18871 462 2.6331E-01
19091 19102 19113 19344 19575 19564 19553 19322 19333 462 2.6191E-01
19553 19564 19575 19806 20037 20026 20015 19784 19795 462 2.5750E-01
20015 20026 20037 20268 20499 20488 20477 20246 20257 462 2.4983E-01
20477 20488 20499 20730 20961 20950 20939 20708 20719 462 2.3923E-01
20939 20950 20961 21192 21423 21412 21401 21170 21181 462 2.2545E-01
21401 21412 21423 21654 21885 21874 21863 21632 21643 462 2.0940E-01
21863 21874 21885 22116 22347 22336 22325 22094 22105 462 1.9228E-01
22325 22336 22347 22578 22809 22798 22787 22556 22567 462 1.7442E-01
22787 22798 22809 23040 23271 23260 23249 23018 23029 462 1.5957E-01
23249 23260 23271 23502 23733 23722 23711 23480 23491 462 1.4472E-01
23711 23722 23733 23964 24195 24184 24173 23942 23953 462 1.2987E-01
24173 24184 24195 24426 24657 24646 24635 24404 24415 462 1.1503E-01
24635 24646 24657 24888 25119 25108 25097 24866 24877 462 1.0018E-01
25097 25108 25119 25350 25581 25570 25559 25328 25339 462 8.2603E-02
25559 25570 25581 25812 26043 26032 26021 25790 25801 462 6.6580E-02
26021 26032 26043 26274 26505 26494 26483 26252 26263 462 5.1977E-02
26483 26494 26505 26736 26967 26956 26945 26714 26725 462 3.8665E-02
26945 26956 26967 27198 27429 27418 27407 27176 27187 462 2.6529E-02
27407 27418 27429 27660 27891 27880 27869 27638 27649 462 1.5479E-02
27869 27880 27891 28122 28353 28342 28331 28100 28111 462 5.4053E-03
BCFLUX (T1, NODES=9)
2481 2492 2503 2734 2965 2954 2943 2712 2723 462 4.3374E-05
2943 2954 2965 3196 3427 3416 3405 3174 3185 462 1.2693E-04
3405 3416 3427 3658 3889 3878 3867 3636 3647 462 2.2794E-04
3867 3878 3889 4120 4351 4340 4329 4098 4109 462 3.4101E-04
4329 4340 4351 4582 4813 4802 4791 4560 4571 462 4.7931E-04
4791 4802 4813 5044 5275 5264 5253 5022 5033 462 6.9705E-04
5253 5264 5275 5506 5737 5726 5715 5484 5495 462 1.0672E-03
5715 5726 5737 5968 6199 6188 6177 5946 5957 462 1.6649E-03
6177 6188 6199 6430 6661 6650 6639 6408 6419 462 2.6040E-03
6639 6650 6661 6892 7123 7112 7101 6870 6881 462 3.9213E-03
7101 7112 7123 7354 7585 7574 7563 7332 7343 462 6.0039E-03
7563 7574 7585 7816 8047 8036 8025 7794 7805 462 8.6960E-03
8025 8036 8047 8278 8509 8498 8487 8256 8267 462 1.2665E-02
8487 8498 8509 8740 8971 8960 8949 8718 8729 462 1.7838E-02
8949 8960 8971 9202 9433 9422 9411 9180 9191 462 2.4168E-02
9411 9422 9433 9664 9895 9884 9873 9642 9653 462 3.2486E-02
9873 9884 9895 10126 10357 10346 10335 10104 10115 462 4.1259E-02
10335 10346 10357 10588 10819 10808 10797 10566 10577 462 5.2772E-02
10797 10808 10819 11050 11281 11270 11259 11028 11039 462 6.4693E-02
11259 11270 11281 11512 11743 11732 11721 11490 11501 462 7.8232E-02
11721 11732 11743 11974 12205 12194 12183 11952 11963 462 9.2866E-02
12183 12194 12205 12436 12667 12656 12645 12414 12425 462 1.0779E-01
12645 12656 12667 12898 13129 13118 13107 12876 12887 462 1.2188E-01
13107 13118 13129 13360 13591 13580 13569 13338 13349 462 1.3644E-01
13569 13580 13591 13822 14053 14042 14031 13800 13811 462 1.5094E-01
14031 14042 14053 14284 14515 14504 14493 14262 14273 462 1.6535E-01
14493 14504 14515 14746 14977 14966 14955 14724 14735 462 1.8014E-01
14955 14966 14977 15208 15439 15428 15417 15186 15197 462 1.9410E-01
15417 15428 15439 15670 15901 15890 15879 15648 15659 462 2.0854E-01
15879 15890 15901 16132 16363 16352 16341 16110 16121 462 2.2035E-01
16341 16352 16363 16594 16825 16814 16803 16572 16583 462 2.3195E-01
16803 16814 16825 17056 17287 17276 17265 17034 17045 462 2.4125E-01
17265 17276 17287 17518 17749 17738 17727 17496 17507 462 2.4997E-01
17727 17738 17749 17980 18211 18200 18189 17958 17969 462 2.5580E-01
18189 18200 18211 18442 18673 18662 18651 18420 18431 462 2.6146E-01
18651 18662 18673 18904 19135 19124 19113 18882 18893 462 2.6331E-01
```

```
19113 19124 19135 19366 19597 19586 19575 19344 19355 462 2.6191E-01
19575 19586 19597 19828 20059 20048 20037 19806 19817 462 2.5750E-01
20037 20048 20059 20290 20521 20510 20499 20268 20279 462 2.4983E-01
20499 20510 20521 20752 20983 20972 20961 20730 20741 462 2.3923E-01
20961 20972 20983 21214 21445 21434 21423 21192 21203 462 2.2545E-01
21423 21434 21445 21676 21907 21896 21885 21654 21665 462 2.0940E-01
21885 21896 21907 22138 22369 22358 22347 22116 22127 462 1.9228E-01
22347 22358 22369 22600 22831 22820 22809 22578 22589 462 1.7442E-01
22809 22820 22831 23062 23293 23282 23271 23040 23051 462 1.5957E-01
23271 23282 23293 23524 23755 23744 23733 23502 23513 462 1.4472E-01
23733 23744 23755 23986 24217 24206 24195 23964 23975 462 1.2987E-01
24195 24206 24217 24448 24679 24668 24657 24426 24437 462 1.1503E-01
24657 24668 24679 24910 25141 25130 25119 24888 24899 462 1.0018E-01
25119 25130 25141 25372 25603 25592 25581 25350 25361 462 8.2603E-02
25581 25592 25603 25834 26065 26054 26043 25812 25823 462 6.6580E-02
26043 26054 26065 26296 26527 26516 26505 26274 26285 462 5.1977E-02
26505 26516 26527 26758 26989 26978 26967 26736 26747 462 3.8665E-02
26967 26978 26989 27220 27451 27440 27429 27198 27209 462 2.6529E-02
27429 27440 27451 27682 27913 27902 27891 27660 27671 462 1.5479E-02
27891 27902 27913 28144 28375 28364 28353 28122 28133 462 5.4053E-03
BCFLUX (T1, NODES=9)
2503 2514 2525 2756 2987 2976 2965 2734 2745 462 4.3374E-05
2965 2976 2987 3218 3449 3438 3427 3196 3207 462 1.2693E-04
3427 3438 3449 3680 3911 3900 3889 3658 3669 462 2.2794E-04
3889 3900 3911 4142 4373 4362 4351 4120 4131 462 3.4101E-04
4351 4362 4373 4604 4835 4824 4813 4582 4593 462 4.7931E-04
4813 4824 4835 5066 5297 5286 5275 5044 5055 462 6.9705E-04
5275 5286 5297 5528 5759 5748 5737 5506 5517 462 1.0672E-03
5737 5748 5759 5990 6221 6210 6199 5968 5979 462 1.6649E-03
6199 6210 6221 6452 6683 6672 6661 6430 6441 462 2.6040E-03
6661 6672 6683 6914 7145 7134 7123 6892 6903 462 3.9213E-03
7123 7134 7145 7376 7607 7596 7585 7354 7365 462 6.0039E-03
7585 7596 7607 7838 8069 8058 8047 7816 7827 462 8.6960E-03
8047 8058 8069 8300 8531 8520 8509 8278 8289 462 1.2665E-02
8509 8520 8531 8762 8993 8982 8971 8740 8751 462 1.7838E-02
8971 8982 8993 9224 9455 9444 9433 9202 9213 462 2.4168E-02
9433 9444 9455 9686 9917 9906 9895 9664 9675 462 3.2486E-02
9895 9906 9917 10148 10379 10368 10357 10126 10137 462 4.1259E-02
10357 10368 10379 10610 10841 10830 10819 10588 10599 462 5.2772E-02
10819 10830 10841 11072 11303 11292 11281 11050 11061 462 6.4693E-02
11281 11292 11303 11534 11765 11754 11743 11512 11523 462 7.8232E-02
11743 11754 11765 11996 12227 12216 12205 11974 11985 462 9.2866E-02
12205 12216 12227 12458 12689 12678 12667 12436 12447 462 1.0779E-01
12667 12678 12689 12920 13151 13140 13129 12898 12909 462 1.2188E-01
13129 13140 13151 13382 13613 13602 13591 13360 13371 462 1.3644E-01
13591 13602 13613 13844 14075 14064 14053 13822 13833 462 1.5094E-01
14053 14064 14075 14306 14537 14526 14515 14284 14295 462 1.6535E-01
14515 14526 14537 14768 14999 14988 14977 14746 14757 462 1.8014E-01
14977 14988 14999 15230 15461 15450 15439 15208 15219 462 1.9410E-01
15439 15450 15461 15692 15923 15912 15901 15670 15681 462 2.0854E-01
15901 15912 15923 16154 16385 16374 16363 16132 16143 462 2.2035E-01
16363 16374 16385 16616 16847 16836 16825 16594 16605 462 2.3195E-01
16825 16836 16847 17078 17309 17298 17287 17056 17067 462 2.4125E-01
17287 17298 17309 17540 17771 17760 17749 17518 17529 462 2.4997E-01
17749 17760 17771 18002 18233 18222 18211 17980 17991 462 2.5580E-01
18211 18222 18233 18464 18695 18684 18673 18442 18453 462 2.6146E-01
18673 18684 18695 18926 19157 19146 19135 18904 18915 462 2.6331E-01
19135 19146 19157 19388 19619 19608 19597 19366 19377 462 2.6191E-01
```

```
19597 19608 19619 19850 20081 20070 20059 19828 19839 462 2.5750E-01
20059 20070 20081 20312 20543 20532 20521 20290 20301 462 2.4983E-01
20521 20532 20543 20774 21005 20994 20983 20752 20763 462 2.3923E-01
20983 20994 21005 21236 21467 21456 21445 21214 21225 462 2.2545E-01
21445 21456 21467 21698 21929 21918 21907 21676 21687 462 2.0940E-01
21907 21918 21929 22160 22391 22380 22369 22138 22149 462 1.9228E-01
22369 22380 22391 22622 22853 22842 22831 22600 22611 462 1.7442E-01
22831 22842 22853 23084 23315 23304 23293 23062 23073 462 1.5957E-01
23293 23304 23315 23546 23777 23766 23755 23524 23535 462 1.4472E-01
23755 23766 23777 24008 24239 24228 24217 23986 23997 462 1.2987E-01
24217 24228 24239 24470 24701 24690 24679 24448 24459 462 1.1503E-01
24679 24690 24701 24932 25163 25152 25141 24910 24921 462 1.0018E-01
25141 25152 25163 25394 25625 25614 25603 25372 25383 462 8.2603E-02
25603 25614 25625 25856 26087 26076 26065 25834 25845 462 6.6580E-02
26065 26076 26087 26318 26549 26538 26527 26296 26307 462 5.1977E-02
26527 26538 26549 26780 27011 27000 26989 26758 26769 462 3.8665E-02
26989 27000 27011 27242 27473 27462 27451 27220 27231 462 2.6529E-02
27451 27462 27473 27704 27935 27924 27913 27682 27693 462 1.5479E-02
27913 27924 27935 28166 28397 28386 28375 28144 28155 462 5.4053E-03
BCFLUX (T1, NODES=9)
2525 2536 2547 2778 3009 2998 2987 2756 2767 462 4.3374E-05
2987 2998 3009 3240 3471 3460 3449 3218 3229 462 1.2693E-04
3449 3460 3471 3702 3933 3922 3911 3680 3691 462 2.2794E-04
3911 3922 3933 4164 4395 4384 4373 4142 4153 462 3.4101E-04
4373 4384 4395 4626 4857 4846 4835 4604 4615 462 4.7931E-04
4835 4846 4857 5088 5319 5308 5297 5066 5077 462 6.9705E-04
5297 5308 5319 5550 5781 5770 5759 5528 5539 462 1.0672E-03
5759 5770 5781 6012 6243 6232 6221 5990 6001 462 1.6649E-03
6221 6232 6243 6474 6705 6694 6683 6452 6463 462 2.6040E-03
6683 6694 6705 6936 7167 7156 7145 6914 6925 462 3.9213E-03
7145 7156 7167 7398 7629 7618 7607 7376 7387 462 6.0039E-03
7607 7618 7629 7860 8091 8080 8069 7838 7849 462 8.6960E-03
8069 8080 8091 8322 8553 8542 8531 8300 8311 462 1.2665E-02
8531 8542 8553 8784 9015 9004 8993 8762 8773 462 1.7838E-02
8993 9004 9015 9246 9477 9466 9455 9224 9235 462 2.4168E-02
9455 9466 9477 9708 9939 9928 9917 9686 9697 462 3.2486E-02
9917 9928 9939 10170 10401 10390 10379 10148 10159 462 4.1259E-02
10379 10390 10401 10632 10863 10852 10841 10610 10621 462 5.2772E-02
10841 10852 10863 11094 11325 11314 11303 11072 11083 462 6.4693E-02
11303 11314 11325 11556 11787 11776 11765 11534 11545 462 7.8232E-02
11765 11776 11787 12018 12249 12238 12227 11996 12007 462 9.2866E-02
12227 12238 12249 12480 12711 12700 12689 12458 12469 462 1.0779E-01
12689 12700 12711 12942 13173 13162 13151 12920 12931 462 1.2188E-01
13151 13162 13173 13404 13635 13624 13613 13382 13393 462 1.3644E-01
13613 13624 13635 13866 14097 14086 14075 13844 13855 462 1.5094E-01
14075 14086 14097 14328 14559 14548 14537 14306 14317 462 1.6535E-01
14537 14548 14559 14790 15021 15010 14999 14768 14779 462 1.8014E-01
14999 15010 15021 15252 15483 15472 15461 15230 15241 462 1.9410E-01
15461 15472 15483 15714 15945 15934 15923 15692 15703 462 2.0854E-01
15923 15934 15945 16176 16407 16396 16385 16154 16165 462 2.2035E-01
16385 16396 16407 16638 16869 16858 16847 16616 16627 462 2.3195E-01
16847 16858 16869 17100 17331 17320 17309 17078 17089 462 2.4125E-01
17309 17320 17331 17562 17793 17782 17771 17540 17551 462 2.4997E-01
17771 17782 17793 18024 18255 18244 18233 18002 18013 462 2.5580E-01
18233 18244 18255 18486 18717 18706 18695 18464 18475 462 2.6146E-01
18695 18706 18717 18948 19179 19168 19157 18926 18937 462 2.6331E-01
19157 19168 19179 19410 19641 19630 19619 19388 19399 462 2.6191E-01
19619 19630 19641 19872 20103 20092 20081 19850 19861 462 2.5750E-01
```

```
20081 20092 20103 20334 20565 20554 20543 20312 20323 462 2.4983E-01
20543 20554 20565 20796 21027 21016 21005 20774 20785 462 2.3923E-01
21005 21016 21027 21258 21489 21478 21467 21236 21247 462 2.2545E-01
21467 21478 21489 21720 21951 21940 21929 21698 21709 462 2.0940E-01
21929 21940 21951 22182 22413 22402 22391 22160 22171 462 1.9228E-01
22391 22402 22413 22644 22875 22864 22853 22622 22633 462 1.7442E-01
22853 22864 22875 23106 23337 23326 23315 23084 23095 462 1.5957E-01
23315 23326 23337 23568 23799 23788 23777 23546 23557 462 1.4472E-01
23777 23788 23799 24030 24261 24250 24239 24008 24019 462 1.2987E-01
24239 24250 24261 24492 24723 24712 24701 24470 24481 462 1.1503E-01
24701 24712 24723 24954 25185 25174 25163 24932 24943 462 1.0018E-01
25163 25174 25185 25416 25647 25636 25625 25394 25405 462 8.2603E-02
25625 25636 25647 25878 26109 26098 26087 25856 25867 462 6.6580E-02
26087 26098 26109 26340 26571 26560 26549 26318 26329 462 5.1977E-02
26549 26560 26571 26802 27033 27022 27011 26780 26791 462 3.8665E-02
27011 27022 27033 27264 27495 27484 27473 27242 27253 462 2.6529E-02
27473 27484 27495 27726 27957 27946 27935 27704 27715 462 1.5479E-02
27935 27946 27957 28188 28419 28408 28397 28166 28177 462 5.4053E-03
BCFLUX (T1, NODES=9)
2547 2558 2569 2800 3031 3020 3009 2778 2789 462 4.3374E-05
3009 3020 3031 3262 3493 3482 3471 3240 3251 462 1.2693E-04
3471 3482 3493 3724 3955 3944 3933 3702 3713 462 2.2794E-04
3933 3944 3955 4186 4417 4406 4395 4164 4175 462 3.4101E-04
4395 4406 4417 4648 4879 4868 4857 4626 4637 462 4.7931E-04
4857 4868 4879 5110 5341 5330 5319 5088 5099 462 6.9705E-04
5319 5330 5341 5572 5803 5792 5781 5550 5561 462 1.0672E-03
5781 5792 5803 6034 6265 6254 6243 6012 6023 462 1.6649E-03
6243 6254 6265 6496 6727 6716 6705 6474 6485 462 2.6040E-03
6705 6716 6727 6958 7189 7178 7167 6936 6947 462 3.9213E-03
7167 7178 7189 7420 7651 7640 7629 7398 7409 462 6.0039E-03
7629 7640 7651 7882 8113 8102 8091 7860 7871 462 8.6960E-03
8091 8102 8113 8344 8575 8564 8553 8322 8333 462 1.2665E-02
8553 8564 8575 8806 9037 9026 9015 8784 8795 462 1.7838E-02
9015 9026 9037 9268 9499 9488 9477 9246 9257 462 2.4168E-02
9477 9488 9499 9730 9961 9950 9939 9708 9719 462 3.2486E-02
9939 9950 9961 10192 10423 10412 10401 10170 10181 462 4.1259E-02
10401 10412 10423 10654 10885 10874 10863 10632 10643 462 5.2772E-02
10863 10874 10885 11116 11347 11336 11325 11094 11105 462 6.4693E-02
11325 11336 11347 11578 11809 11798 11787 11556 11567 462 7.8232E-02
11787 11798 11809 12040 12271 12260 12249 12018 12029 462 9.2866E-02
12249 12260 12271 12502 12733 12722 12711 12480 12491 462 1.0779E-01
12711 12722 12733 12964 13195 13184 13173 12942 12953 462 1.2188E-01
13173 13184 13195 13426 13657 13646 13635 13404 13415 462 1.3644E-01
13635 13646 13657 13888 14119 14108 14097 13866 13877 462 1.5094E-01
14097 14108 14119 14350 14581 14570 14559 14328 14339 462 1.6535E-01
14559 14570 14581 14812 15043 15032 15021 14790 14801 462 1.8014E-01
15021 15032 15043 15274 15505 15494 15483 15252 15263 462 1.9410E-01
15483 15494 15505 15736 15967 15956 15945 15714 15725 462 2.0854E-01
15945 15956 15967 16198 16429 16418 16407 16176 16187 462 2.2035E-01
16407 16418 16429 16660 16891 16880 16869 16638 16649 462 2.3195E-01
16869 16880 16891 17122 17353 17342 17331 17100 17111 462 2.4125E-01
17331 17342 17353 17584 17815 17804 17793 17562 17573 462 2.4997E-01
17793 17804 17815 18046 18277 18266 18255 18024 18035 462 2.5580E-01
18255 18266 18277 18508 18739 18728 18717 18486 18497 462 2.6146E-01
18717 18728 18739 18970 19201 19190 19179 18948 18959 462 2.6331E-01
19179 19190 19201 19432 19663 19652 19641 19410 19421 462 2.6191E-01
19641 19652 19663 19894 20125 20114 20103 19872 19883 462 2.5750E-01
20103 20114 20125 20356 20587 20576 20565 20334 20345 462 2.4983E-01
```

```
20565 20576 20587 20818 21049 21038 21027 20796 20807 462 2.3923E-01
21027 21038 21049 21280 21511 21500 21489 21258 21269 462 2.2545E-01
21489 21500 21511 21742 21973 21962 21951 21720 21731 462 2.0940E-01
21951 21962 21973 22204 22435 22424 22413 22182 22193 462 1.9228E-01
22413 22424 22435 22666 22897 22886 22875 22644 22655 462 1.7442E-01
22875 22886 22897 23128 23359 23348 23337 23106 23117 462 1.5957E-01
23337 23348 23359 23590 23821 23810 23799 23568 23579 462 1.4472E-01
23799 23810 23821 24052 24283 24272 24261 24030 24041 462 1.2987E-01
24261 24272 24283 24514 24745 24734 24723 24492 24503 462 1.1503E-01
24723 24734 24745 24976 25207 25196 25185 24954 24965 462 1.0018E-01
25185 25196 25207 25438 25669 25658 25647 25416 25427 462 8.2603E-02
25647 25658 25669 25900 26131 26120 26109 25878 25889 462 6.6580E-02
26109 26120 26131 26362 26593 26582 26571 26340 26351 462 5.1977E-02
26571 26582 26593 26824 27055 27044 27033 26802 26813 462 3.8665E-02
27033 27044 27055 27286 27517 27506 27495 27264 27275 462 2.6529E-02
27495 27506 27517 27748 27979 27968 27957 27726 27737 462 1.5479E-02
27957 27968 27979 28210 28441 28430 28419 28188 28199 462 5.4053E-03
BCFLUX (T1, NODES=9)
2569 2580 2591 2822 3053 3042 3031 2800 2811 462 4.3374E-05
3031 3042 3053 3284 3515 3504 3493 3262 3273 462 1.2693E-04
3493 3504 3515 3746 3977 3966 3955 3724 3735 462 2.2794E-04
3955 3966 3977 4208 4439 4428 4417 4186 4197 462 3.4101E-04
4417 4428 4439 4670 4901 4890 4879 4648 4659 462 4.7931E-04
4879 4890 4901 5132 5363 5352 5341 5110 5121 462 6.9705E-04
5341 5352 5363 5594 5825 5814 5803 5572 5583 462 1.0672E-03
5803 5814 5825 6056 6287 6276 6265 6034 6045 462 1.6649E-03
6265 6276 6287 6518 6749 6738 6727 6496 6507 462 2.6040E-03
6727 6738 6749 6980 7211 7200 7189 6958 6969 462 3.9213E-03
7189 7200 7211 7442 7673 7662 7651 7420 7431 462 6.0039E-03
7651 7662 7673 7904 8135 8124 8113 7882 7893 462 8.6960E-03
8113 8124 8135 8366 8597 8586 8575 8344 8355 462 1.2665E-02
8575 8586 8597 8828 9059 9048 9037 8806 8817 462 1.7838E-02
9037 9048 9059 9290 9521 9510 9499 9268 9279 462 2.4168E-02
9499 9510 9521 9752 9983 9972 9961 9730 9741 462 3.2486E-02
9961 9972 9983 10214 10445 10434 10423 10192 10203 462 4.1259E-02
10423 10434 10445 10676 10907 10896 10885 10654 10665 462 5.2772E-02
10885 10896 10907 11138 11369 11358 11347 11116 11127 462 6.4693E-02
11347 11358 11369 11600 11831 11820 11809 11578 11589 462 7.8232E-02
11809 11820 11831 12062 12293 12282 12271 12040 12051 462 9.2866E-02
12271 12282 12293 12524 12755 12744 12733 12502 12513 462 1.0779E-01
12733 12744 12755 12986 13217 13206 13195 12964 12975 462 1.2188E-01
13195 13206 13217 13448 13679 13668 13657 13426 13437 462 1.3644E-01
13657 13668 13679 13910 14141 14130 14119 13888 13899 462 1.5094E-01
14119 14130 14141 14372 14603 14592 14581 14350 14361 462 1.6535E-01
14581 14592 14603 14834 15065 15054 15043 14812 14823 462 1.8014E-01
15043 15054 15065 15296 15527 15516 15505 15274 15285 462 1.9410E-01
15505 15516 15527 15758 15989 15978 15967 15736 15747 462 2.0854E-01
15967 15978 15989 16220 16451 16440 16429 16198 16209 462 2.2035E-01
16429 16440 16451 16682 16913 16902 16891 16660 16671 462 2.3195E-01
16891 16902 16913 17144 17375 17364 17353 17122 17133 462 2.4125E-01
17353 17364 17375 17606 17837 17826 17815 17584 17595 462 2.4997E-01
17815 17826 17837 18068 18299 18288 18277 18046 18057 462 2.5580E-01
18277 18288 18299 18530 18761 18750 18739 18508 18519 462 2.6146E-01
18739 18750 18761 18992 19223 19212 19201 18970 18981 462 2.6331E-01
19201 19212 19223 19454 19685 19674 19663 19432 19443 462 2.6191E-01
19663 19674 19685 19916 20147 20136 20125 19894 19905 462 2.5750E-01
20125 20136 20147 20378 20609 20598 20587 20356 20367 462 2.4983E-01
20587 20598 20609 20840 21071 21060 21049 20818 20829 462 2.3923E-01
```

```
21049 21060 21071 21302 21533 21522 21511 21280 21291 462 2.2545E-01
21511 21522 21533 21764 21995 21984 21973 21742 21753 462 2.0940E-01
21973 21984 21995 22226 22457 22446 22435 22204 22215 462 1.9228E-01
22435 22446 22457 22688 22919 22908 22897 22666 22677 462 1.7442E-01
22897 22908 22919 23150 23381 23370 23359 23128 23139 462 1.5957E-01
23359 23370 23381 23612 23843 23832 23821 23590 23601 462 1.4472E-01
23821 23832 23843 24074 24305 24294 24283 24052 24063 462 1.2987E-01
24283 24294 24305 24536 24767 24756 24745 24514 24525 462 1.1503E-01
24745 24756 24767 24998 25229 25218 25207 24976 24987 462 1.0018E-01
25207 25218 25229 25460 25691 25680 25669 25438 25449 462 8.2603E-02
25669 25680 25691 25922 26153 26142 26131 25900 25911 462 6.6580E-02
26131 26142 26153 26384 26615 26604 26593 26362 26373 462 5.1977E-02
26593 26604 26615 26846 27077 27066 27055 26824 26835 462 3.8665E-02
27055 27066 27077 27308 27539 27528 27517 27286 27297 462 2.6529E-02
27517 27528 27539 27770 28001 27990 27979 27748 27759 462 1.5479E-02
27979 27990 28001 28232 28463 28452 28441 28210 28221 462 5.4053E-03
BCFLUX (T1, NODES=9)
2591 2602 2613 2844 3075 3064 3053 2822 2833 462 4.3374E-05
3053 3064 3075 3306 3537 3526 3515 3284 3295 462 1.2693E-04
3515 3526 3537 3768 3999 3988 3977 3746 3757 462 2.2794E-04
3977 3988 3999 4230 4461 4450 4439 4208 4219 462 3.4101E-04
4439 4450 4461 4692 4923 4912 4901 4670 4681 462 4.7931E-04
4901 4912 4923 5154 5385 5374 5363 5132 5143 462 6.9705E-04
5363 5374 5385 5616 5847 5836 5825 5594 5605 462 1.0672E-03
5825 5836 5847 6078 6309 6298 6287 6056 6067 462 1.6649E-03
6287 6298 6309 6540 6771 6760 6749 6518 6529 462 2.6040E-03
6749 6760 6771 7002 7233 7222 7211 6980 6991 462 3.9213E-03
7211 7222 7233 7464 7695 7684 7673 7442 7453 462 6.0039E-03
7673 7684 7695 7926 8157 8146 8135 7904 7915 462 8.6960E-03
8135 8146 8157 8388 8619 8608 8597 8366 8377 462 1.2665E-02
8597 8608 8619 8850 9081 9070 9059 8828 8839 462 1.7838E-02
9059 9070 9081 9312 9543 9532 9521 9290 9301 462 2.4168E-02
9521 9532 9543 9774 10005 9994 9983 9752 9763 462 3.2486E-02
9983 9994 10005 10236 10467 10456 10445 10214 10225 462 4.1259E-02
10445 10456 10467 10698 10929 10918 10907 10676 10687 462 5.2772E-02
10907 10918 10929 11160 11391 11380 11369 11138 11149 462 6.4693E-02
11369 11380 11391 11622 11853 11842 11831 11600 11611 462 7.8232E-02
11831 11842 11853 12084 12315 12304 12293 12062 12073 462 9.2866E-02
12293 12304 12315 12546 12777 12766 12755 12524 12535 462 1.0779E-01
12755 12766 12777 13008 13239 13228 13217 12986 12997 462 1.2188E-01
13217 13228 13239 13470 13701 13690 13679 13448 13459 462 1.3644E-01
13679 13690 13701 13932 14163 14152 14141 13910 13921 462 1.5094E-01
14141 14152 14163 14394 14625 14614 14603 14372 14383 462 1.6535E-01
14603 14614 14625 14856 15087 15076 15065 14834 14845 462 1.8014E-01
15065 15076 15087 15318 15549 15538 15527 15296 15307 462 1.9410E-01
15527 15538 15549 15780 16011 16000 15989 15758 15769 462 2.0854E-01
15989 16000 16011 16242 16473 16462 16451 16220 16231 462 2.2035E-01
16451 16462 16473 16704 16935 16924 16913 16682 16693 462 2.3195E-01
16913 16924 16935 17166 17397 17386 17375 17144 17155 462 2.4125E-01
17375 17386 17397 17628 17859 17848 17837 17606 17617 462 2.4997E-01
17837 17848 17859 18090 18321 18310 18299 18068 18079 462 2.5580E-01
18299 18310 18321 18552 18783 18772 18761 18530 18541 462 2.6146E-01
18761 18772 18783 19014 19245 19234 19223 18992 19003 462 2.6331E-01
19223 19234 19245 19476 19707 19696 19685 19454 19465 462 2.6191E-01
19685 19696 19707 19938 20169 20158 20147 19916 19927 462 2.5750E-01
20147 20158 20169 20400 20631 20620 20609 20378 20389 462 2.4983E-01
20609 20620 20631 20862 21093 21082 21071 20840 20851 462 2.3923E-01
21071 21082 21093 21324 21555 21544 21533 21302 21313 462 2.2545E-01
```

```
21533 21544 21555 21786 22017 22006 21995 21764 21775 462 2.0940E-01
21995 22006 22017 22248 22479 22468 22457 22226 22237 462 1.9228E-01
22457 22468 22479 22710 22941 22930 22919 22688 22699 462 1.7442E-01
22919 22930 22941 23172 23403 23392 23381 23150 23161 462 1.5957E-01
23381 23392 23403 23634 23865 23854 23843 23612 23623 462 1.4472E-01
23843 23854 23865 24096 24327 24316 24305 24074 24085 462 1.2987E-01
24305 24316 24327 24558 24789 24778 24767 24536 24547 462 1.1503E-01
24767 24778 24789 25020 25251 25240 25229 24998 25009 462 1.0018E-01
25229 25240 25251 25482 25713 25702 25691 25460 25471 462 8.2603E-02
25691 25702 25713 25944 26175 26164 26153 25922 25933 462 6.6580E-02
26153 26164 26175 26406 26637 26626 26615 26384 26395 462 5.1977E-02
26615 26626 26637 26868 27099 27088 27077 26846 26857 462 3.8665E-02
27077 27088 27099 27330 27561 27550 27539 27308 27319 462 2.6529E-02
27539 27550 27561 27792 28023 28012 28001 27770 27781 462 1.5479E-02
28001 28012 28023 28254 28485 28474 28463 28232 28243 462 5.4053E-03
BCFLUX (T1, NODES=9)
2613 2624 2635 2866 3097 3086 3075 2844 2855 462 4.3374E-05
3075 3086 3097 3328 3559 3548 3537 3306 3317 462 1.2693E-04
3537 3548 3559 3790 4021 4010 3999 3768 3779 462 2.2794E-04
3999 4010 4021 4252 4483 4472 4461 4230 4241 462 3.4101E-04
4461 4472 4483 4714 4945 4934 4923 4692 4703 462 4.7931E-04
4923 4934 4945 5176 5407 5396 5385 5154 5165 462 6.9705E-04
5385 5396 5407 5638 5869 5858 5847 5616 5627 462 1.0672E-03
5847 5858 5869 6100 6331 6320 6309 6078 6089 462 1.6649E-03
6309 6320 6331 6562 6793 6782 6771 6540 6551 462 2.6040E-03
6771 6782 6793 7024 7255 7244 7233 7002 7013 462 3.9213E-03
7233 7244 7255 7486 7717 7706 7695 7464 7475 462 6.0039E-03
7695 7706 7717 7948 8179 8168 8157 7926 7937 462 8.6960E-03
8157 8168 8179 8410 8641 8630 8619 8388 8399 462 1.2665E-02
8619 8630 8641 8872 9103 9092 9081 8850 8861 462 1.7838E-02
9081 9092 9103 9334 9565 9554 9543 9312 9323 462 2.4168E-02
9543 9554 9565 9796 10027 10016 10005 9774 9785 462 3.2486E-02
10005 10016 10027 10258 10489 10478 10467 10236 10247 462 4.1259E-02
10467 10478 10489 10720 10951 10940 10929 10698 10709 462 5.2772E-02
10929 10940 10951 11182 11413 11402 11391 11160 11171 462 6.4693E-02
11391 11402 11413 11644 11875 11864 11853 11622 11633 462 7.8232E-02
11853 11864 11875 12106 12337 12326 12315 12084 12095 462 9.2866E-02
12315 12326 12337 12568 12799 12788 12777 12546 12557 462 1.0779E-01
12777 12788 12799 13030 13261 13250 13239 13008 13019 462 1.2188E-01
13239 13250 13261 13492 13723 13712 13701 13470 13481 462 1.3644E-01
13701 13712 13723 13954 14185 14174 14163 13932 13943 462 1.5094E-01
14163 14174 14185 14416 14647 14636 14625 14394 14405 462 1.6535E-01
14625 14636 14647 14878 15109 15098 15087 14856 14867 462 1.8014E-01
15087 15098 15109 15340 15571 15560 15549 15318 15329 462 1.9410E-01
15549 15560 15571 15802 16033 16022 16011 15780 15791 462 2.0854E-01
16011 16022 16033 16264 16495 16484 16473 16242 16253 462 2.2035E-01
16473 16484 16495 16726 16957 16946 16935 16704 16715 462 2.3195E-01
16935 16946 16957 17188 17419 17408 17397 17166 17177 462 2.4125E-01
17397 17408 17419 17650 17881 17870 17859 17628 17639 462 2.4997E-01
17859 17870 17881 18112 18343 18332 18321 18090 18101 462 2.5580E-01
18321 18332 18343 18574 18805 18794 18783 18552 18563 462 2.6146E-01
18783 18794 18805 19036 19267 19256 19245 19014 19025 462 2.6331E-01
19245 19256 19267 19498 19729 19718 19707 19476 19487 462 2.6191E-01
19707 19718 19729 19960 20191 20180 20169 19938 19949 462 2.5750E-01
20169 20180 20191 20422 20653 20642 20631 20400 20411 462 2.4983E-01
20631 20642 20653 20884 21115 21104 21093 20862 20873 462 2.3923E-01
21093 21104 21115 21346 21577 21566 21555 21324 21335 462 2.2545E-01
21555 21566 21577 21808 22039 22028 22017 21786 21797 462 2.0940E-01
```

```
22017 22028 22039 22270 22501 22490 22479 22248 22259 462 1.9228E-01
22479 22490 22501 22732 22963 22952 22941 22710 22721 462 1.7442E-01
22941 22952 22963 23194 23425 23414 23403 23172 23183 462 1.5957E-01
23403 23414 23425 23656 23887 23876 23865 23634 23645 462 1.4472E-01
23865 23876 23887 24118 24349 24338 24327 24096 24107 462 1.2987E-01
24327 24338 24349 24580 24811 24800 24789 24558 24569 462 1.1503E-01
24789 24800 24811 25042 25273 25262 25251 25020 25031 462 1.0018E-01
25251 25262 25273 25504 25735 25724 25713 25482 25493 462 8.2603E-02
25713 25724 25735 25966 26197 26186 26175 25944 25955 462 6.6580E-02
26175 26186 26197 26428 26659 26648 26637 26406 26417 462 5.1977E-02
26637 26648 26659 26890 27121 27110 27099 26868 26879 462 3.8665E-02
27099 27110 27121 27352 27583 27572 27561 27330 27341 462 2.6529E-02
27561 27572 27583 27814 28045 28034 28023 27792 27803 462 1.5479E-02
28023 28034 28045 28276 28507 28496 28485 28254 28265 462 5.4053E-03
BCFLUX (T1, NODES=9)
2635 2646 2657 2888 3119 3108 3097 2866 2877 462 4.3374E-05
3097 3108 3119 3350 3581 3570 3559 3328 3339 462 1.2693E-04
3559 3570 3581 3812 4043 4032 4021 3790 3801 462 2.2794E-04
4021 4032 4043 4274 4505 4494 4483 4252 4263 462 3.4101E-04
4483 4494 4505 4736 4967 4956 4945 4714 4725 462 4.7931E-04
4945 4956 4967 5198 5429 5418 5407 5176 5187 462 6.9705E-04
5407 5418 5429 5660 5891 5880 5869 5638 5649 462 1.0672E-03
5869 5880 5891 6122 6353 6342 6331 6100 6111 462 1.6649E-03
6331 6342 6353 6584 6815 6804 6793 6562 6573 462 2.6040E-03
6793 6804 6815 7046 7277 7266 7255 7024 7035 462 3.9213E-03
7255 7266 7277 7508 7739 7728 7717 7486 7497 462 6.0039E-03
7717 7728 7739 7970 8201 8190 8179 7948 7959 462 8.6960E-03
8179 8190 8201 8432 8663 8652 8641 8410 8421 462 1.2665E-02
8641 8652 8663 8894 9125 9114 9103 8872 8883 462 1.7838E-02
9103 9114 9125 9356 9587 9576 9565 9334 9345 462 2.4168E-02
9565 9576 9587 9818 10049 10038 10027 9796 9807 462 3.2486E-02
10027 10038 10049 10280 10511 10500 10489 10258 10269 462 4.1259E-02
10489 10500 10511 10742 10973 10962 10951 10720 10731 462 5.2772E-02
10951 10962 10973 11204 11435 11424 11413 11182 11193 462 6.4693E-02
11413 11424 11435 11666 11897 11886 11875 11644 11655 462 7.8232E-02
11875 11886 11897 12128 12359 12348 12337 12106 12117 462 9.2866E-02
12337 12348 12359 12590 12821 12810 12799 12568 12579 462 1.0779E-01
12799 12810 12821 13052 13283 13272 13261 13030 13041 462 1.2188E-01
13261 13272 13283 13514 13745 13734 13723 13492 13503 462 1.3644E-01
13723 13734 13745 13976 14207 14196 14185 13954 13965 462 1.5094E-01
14185 14196 14207 14438 14669 14658 14647 14416 14427 462 1.6535E-01
14647 14658 14669 14900 15131 15120 15109 14878 14889 462 1.8014E-01
15109 15120 15131 15362 15593 15582 15571 15340 15351 462 1.9410E-01
15571 15582 15593 15824 16055 16044 16033 15802 15813 462 2.0854E-01
16033 16044 16055 16286 16517 16506 16495 16264 16275 462 2.2035E-01
16495 16506 16517 16748 16979 16968 16957 16726 16737 462 2.3195E-01
16957 16968 16979 17210 17441 17430 17419 17188 17199 462 2.4125E-01
17419 17430 17441 17672 17903 17892 17881 17650 17661 462 2.4997E-01
17881 17892 17903 18134 18365 18354 18343 18112 18123 462 2.5580E-01
18343 18354 18365 18596 18827 18816 18805 18574 18585 462 2.6146E-01
18805 18816 18827 19058 19289 19278 19267 19036 19047 462 2.6331E-01
19267 19278 19289 19520 19751 19740 19729 19498 19509 462 2.6191E-01
19729 19740 19751 19982 20213 20202 20191 19960 19971 462 2.5750E-01
20191 20202 20213 20444 20675 20664 20653 20422 20433 462 2.4983E-01
20653 20664 20675 20906 21137 21126 21115 20884 20895 462 2.3923E-01
21115 21126 21137 21368 21599 21588 21577 21346 21357 462 2.2545E-01
21577 21588 21599 21830 22061 22050 22039 21808 21819 462 2.0940E-01
22039 22050 22061 22292 22523 22512 22501 22270 22281 462 1.9228E-01
```

```
22501 22512 22523 22754 22985 22974 22963 22732 22743 462 1.7442E-01
22963 22974 22985 23216 23447 23436 23425 23194 23205 462 1.5957E-01
23425 23436 23447 23678 23909 23898 23887 23656 23667 462 1.4472E-01
23887 23898 23909 24140 24371 24360 24349 24118 24129 462 1.2987E-01
24349 24360 24371 24602 24833 24822 24811 24580 24591 462 1.1503E-01
24811 24822 24833 25064 25295 25284 25273 25042 25053 462 1.0018E-01
25273 25284 25295 25526 25757 25746 25735 25504 25515 462 8.2603E-02
25735 25746 25757 25988 26219 26208 26197 25966 25977 462 6.6580E-02
26197 26208 26219 26450 26681 26670 26659 26428 26439 462 5.1977E-02
26659 26670 26681 26912 27143 27132 27121 26890 26901 462 3.8665E-02
27121 27132 27143 27374 27605 27594 27583 27352 27363 462 2.6529E-02
27583 27594 27605 27836 28067 28056 28045 27814 27825 462 1.5479E-02
28045 28056 28067 28298 28529 28518 28507 28276 28287 462 5.4053E-03
RENUMBER (profile)
ELEMENTS (brick, nodes=27, fluid, mvisc=1, mcond=2, fimesh)
ELEMENTS (brick, nodes=27, fluid, mvisc=1, mcond=2, fimesh)
ELEMENTS (brick, nodes=27, fluid, mvisc=1, mcond=2, fimesh)
ELEMENTS (brick, nodes=27, fluid, mvisc=2, mcond=2, fimesh)
ELEMENTS (brick, nodes=27, fluid, mvisc=2, mcond=2, fimesh)
ELEMENTS (convection, nodes=9, mcnv=1, fimesh)
ELEMENTS (slip, nodes=9, attach=3, fimesh)
ELEMENTS (slip, nodes=9, attach=5, fimesh)
END
*END
```

E3. WEAKLY-COUPLED MODEL

```
*NOINTERACTIVE
/   Visc = 0.1 Pa.s,
/   Uy for wideface consumption = 0.00090
/   28539 nodes
/   MUST run on the CRAY
/   10 elements in y-dir
/   Mesh graded to make finer in some regions
/   Approx 1500 CPUs/iteration
/   1800 MB Disk Space
*TITLE
3dw18C/3640(27)/W-COUPLED/tmelt=1000/dhl=550
*FIMESH (3-D, IMAX=10, JMAX=5, KMAX=5, MXPOINT=150)
EXPI
1 5 17 73 93 103 119
EXPJ
1 11 21
EXPK
1 11 15 21
POINT
/# I J K      X          Y        Z
1 1 1 1     -0.0010    0.00     -0.01
2 2 1 1     0.001      0.00     -0.01
3 2 1 2     0.001      0.00      0.00055
4 3 1 2     0.020      0.00      0.0069
5 4 1 2     0.260      0.00     -0.0088
6 5 1 2     0.460      0.00     -0.016
7 6 1 2     0.560      0.00     -0.016
8 7 1 2     0.700      0.00     -0.0100
9 7 1 3     0.700      0.00     -0.006
10 7 1 4    0.700      0.00      0.017
```

```
11 6 1 4   0.560      0.00      0.017
12 5 1 4   0.460      0.00      0.017
13 4 1 4   0.260      0.00      0.017
14 3 1 4   0.02       0.00      0.017
15 2 1 4   0.001      0.00      0.017
16 1 1 4   -0.0010    0.00      0.017
17 1 1 3   -0.0010    0.00      0.009
18 1 1 2   -0.0010    0.00      0.00055
19 2 1 3   0.001      0.00      0.009
20 3 1 3   0.02       0.00      0.009
21 4 1 3   0.260      0.00     -0.004
22 5 1 3   0.460      0.00     -0.012
23 6 1 3   0.560      0.00     -0.012
24 1 2 1   -0.0010   -0.05715 -0.01
25 1 2 2   -0.0010   -0.05715  0.00055
26 2 2 2   0.001     -0.05715  0.00055
27 1 3 1   -0.0010   -0.1143  -0.01
28 2 3 1   0.001     -0.1143  -0.01
29 2 3 2   0.001     -0.1143   0.00055
30 7 3 2   0.700     -0.1143  -0.0100
31 7 3 3   0.700     -0.1143  -0.006
32 7 3 4   0.700     -0.1143   0.017
33 2 3 4   0.001     -0.1143   0.017
34 1 3 4   -0.0010   -0.1143   0.017
35 1 3 3   -0.0010   -0.1143   0.009
36 1 3 2   -0.0010   -0.1143   0.00055
37 2 3 3   0.001     -0.1143   0.009
38 3 3 4   0.02      -0.1143   0.017
39 3 3 3   0.02      -0.1143   0.009
40 3 3 2   0.020     -0.1143   0.0069
41 5 3 2   0.460     -0.1143  -0.016
42 5 3 3   0.460     -0.1143  -0.012
43 6 3 2   0.560     -0.1143  -0.016
44 6 3 3   0.560     -0.1143  -0.012
CURVE (input)
3 4 21 1.25 3
0.00108507 0.0 0.0010
0.00123008 0.0 0.0015
0.00144749 0.0 0.0020
0.00174240 0.0 0.0025
0.00212367 0.0 0.0030
0.00260531 0.0 0.0035
0.00320916 0.0 0.0040
0.00397020 0.0 0.0045
0.00494813 0.0 0.0050
0.00625592 0.0 0.0055
0.00814847 0.0 0.0060
0.00864579 0.0 0.0061
0.00920358 0.0 0.0062
0.00983786 0.0 0.0063
0.01057219 0.0 0.0064
0.01144321 0.0 0.0065
0.01251268 0.0 0.0066
0.01389764 0.0 0.0067
0.01586728 0.0 0.0068
0.01935433 0.0 0.0069
0.01990000 0.0 0.0069
CURVE (input)
```

```
4 5 6 2.5 3
0.050 0.0  0.006
0.100 0.0  0.001
0.160 0.0 -0.003
0.200 0.0 -0.0060
0.250 0.0 -0.0084
0.258 0.0 -0.0087
CURVE (input)
5 6 2 1.5 3
0.360 0.0 -0.013
0.459 0.0 -0.016
CURVE (input)
6 7 2
0.500 0.0 -0.016
0.559 0.0 -0.016
CURVE (input)
7 8 3 0.5 3
0.610 0.0 -0.015
0.660 0.0 -0.013
0.690 0.0 -0.011
LINE
1 2
2 3
8 9
9 10
10 11 2.0 3
11 12
12 13 0.66666666 3
13 14 0.4 3
14 15 0.5 3
15 16
16 17
17 18
18 1
18 3
17 19
19 20 2.0 3
20 21 2.5 3
21 22 1.5 3
22 23
23 9 0.5 3
3 19
19 15
4 20
20 14
5 21
21 13
6 22
22 12
7 23
23 11
1 27 3.0 3
18 36 3.0 3
3 29 3.0 3
NUMBER
3 2 1
SURFACE
2 18
```

```
3 16
8 15
CDRIVE (parallel)
1 3 1 27
18 15 18 36
3 10 3 29
AREA
3 9
4 9
ELEMENTS (continuum, brick, nodes=27)
2 34
20 33
4 37
9 38
8 39
ELEMENTS (boundary, quadrilateral, nodes=9)
34 10 16
29 4 3
40 8 4
BCNODE (ux)
1 3 0.0
4 9 0.0
18 15 0.0
19 10 0.0
3 20 0.0
1 28 0.0
2 29 0.0
8 32 0.0
1 34 0.0
BCNODE (uy)
27 29 0.0
36 33 0.0
29 32 0.0
1 3 0.0
18 15 0.0
3 14 0.0
20 10 0.0
1 34 0.0
1 28 0.0
BCNODE (uz)
4 9 0.0
1 34 0.0
1 3 0.0
18 15 0.0
3 20 0.0
19 10 0.0
2 29 -0.0166667
10 34 -4.1e-05
BCNODE (coordinate)
29 8 1
BCNODE (temperature, constant)
2 29 1550.0
3 30 1550.0
1 34 300.0
BCFLUX (heat, nodes=9, constant)
8 32 0.0
1 28 0.0
27 29 0.0
```

```
36 33 0.0
29 38 0.0
40 32 0.0
1 3 0.0
18 15 0.0
3 10 0.0
END
*FIPREP
PROBLEM (steady, nonlinear, newtonian, 3-D,
laminar, momentum, weakly=0)
EXECUTION (restart)
SOLUTION (s.s.=9, accf=0.6, resconv=1e-2, velconv=1e-6)
OPTIONS (upwinding)
PRESSURE (mixed=1.0e-16, continuous)
PRINTOUT (all)
DENSITY (set=1, constant=2500)
/ VISCOSITIES
/ Liquid -> Glassy solid
VISCOSITY (set=1, curve=15, temperature)
-20000, 200, 400, 600, 700, 900, 1000, 1100, 1150, 1200, 1300,
1400, 1500, 1600, 20000
1e4,   1e4,  1e4, 1e4, 9e3, 1e3, 5.0,  0.5,  0.3,  0.2,  0.12,
0.08, 0.05, 0.03, 0.03
/ Powder -> Liquid
VISCOSITY (set=2, curve=16, temperature)
-20000, 500,  700,  780,  850,  910,  940,  1000, 1100, 1150,
1200, 1300, 1400, 1500, 1600, 20000
20.0,   20.0, 30.0, 55.0, 70.0, 40.0, 20.0, 5.0,  0.5,  0.3,
0.2, 0.12, 0.08, 0.05, 0.03, 0.03
/ CONDUCTIVITIES
/ Liquid -> Glassy Solid
CONDUCTIVITY (set=1, curve=10, temperature, isotropic)
-20000, 200, 800, 880, 940, 1050, 1100, 1200, 1300, 20000
0.90,   0.9, 0.9, 1.0, 1.25, 2.7, 2.9,  3.0,  3.0,  3.0
/ Powder -> Liquid
CONDUCTIVITY (set=2, curve=17, temperature, isotropic)
-20000, 0.0,  200,  400,  600,  650,  700,  750, 800, 850, 920, 1000,
1050,  1100,  1200,  1500, 20000
0.15,   0.20, 0.30, 0.42, 0.55, 0.6,  0.65, 0.7, 0.8, 0.95, 1.4, 2.4,
2.75,  2.91,  3.00,  3.00, 3.00
HTRANSFER (set=1, curve=16, reftemp=27.0)
-20000, -110,  220,  420,  620,  820,  1220, 1420, 1620, 2020, 2420,
2620,   3000,   3500,   4000, 20000
1.1     1.1,  44.7, 65.9, 94.9, 135,  260,  350,  462,  761,  1176,
1434,   2027,   3036,   4341, 4341
SPECIFICHEAT (set=1, temperature, enthalpy=19, spatial)
-20000, 27,      227,    427,   527,   627,   727,   827,    950,
1000,   1100,   1227,   1327,   1600,   2000,  3000,  4000, 5000, 20000
0,     1.0e4,   1.8e5,  3.8e5, 4.8e5, 6.0e5, 6.9e5, 8.3e5,  1e6,
1.10e6, 1.65e6, 1.85e6, 1.95e6, 2.2e6, 2.5e6, 3.20e6, 3.9e6, 4.6e6 4.6e6
NODES (fimesh)
BCNODE (uy)
1775,21,0.0
2195,,0.0
/  Impose wideface consumption using uy velocity component
BCNODE (uy)
2437,231,-0.00090
28309,,-0.00090
```

```
BCNODE (uy)
2438,231,0.00090
28310,,0.00090
BCNODE (uy)
2439,231,0.00090
28311,,0.00090
BCNODE (uy)
2440,231,0.00090
28312,,0.00090
BCNODE (uy)
2441,231,0.00090
28313,,0.00090
/  Constrain velocity along flux/steel edge at wideface
BCNODE (uz)
2437,231,0.0
28309,,0.0
/  Constrain velocity normal to flux/steel interface
BCNODE (un3)
1775,21,0.0
2195,,0.0
BCNODE (un3)
2206,11,0.0
28529,,0.0
/  Second tangential direction defined as always in the
/  y-direction -- Needed for definition of stress on the curved
/  flux/steel interface.  BCSYSTEM is used in conjunction with
/  BCNODE (coordinate) card (see FIMESH input)
BCSYSTEM (set=1, 2tangential)
0, 0, 0, 0, 0, 0, 0, -0.001, 0
BCFLUX (T1, NODES=9)
2437 2448 2459 2690 2921 2910 2899 2668 2679 462 4.3374E-05
2899 2910 2921 3152 3383 3372 3361 3130 3141 462 1.2693E-04
3361 3372 3383 3614 3845 3834 3823 3592 3603 462 2.2794E-04
3823 3834 3845 4076 4307 4296 4285 4054 4065 462 3.4101E-04
4285 4296 4307 4538 4769 4758 4747 4516 4527 462 4.7931E-04
4747 4758 4769 5000 5231 5220 5209 4978 4989 462 6.9705E-04
5209 5220 5231 5462 5693 5682 5671 5440 5451 462 1.0672E-03
5671 5682 5693 5924 6155 6144 6133 5902 5913 462 1.6649E-03
6133 6144 6155 6386 6617 6606 6595 6364 6375 462 2.6040E-03
6595 6606 6617 6848 7079 7068 7057 6826 6837 462 3.9213E-03
7057 7068 7079 7310 7541 7530 7519 7288 7299 462 6.0039E-03
7519 7530 7541 7772 8003 7992 7981 7750 7761 462 8.6960E-03
7981 7992 8003 8234 8465 8454 8443 8212 8223 462 1.2665E-02
8443 8454 8465 8696 8927 8916 8905 8674 8685 462 1.7838E-02
8905 8916 8927 9158 9389 9378 9367 9136 9147 462 2.4168E-02
9367 9378 9389 9620 9851 9840 9829 9598 9609 462 3.2486E-02
9829 9840 9851 10082 10313 10302 10291 10060 10071 462 4.1259E-02
10291 10302 10313 10544 10775 10764 10753 10522 10533 462 5.2772E-02
10753 10764 10775 11006 11237 11226 11215 10984 10995 462 6.4693E-02
11215 11226 11237 11468 11699 11688 11677 11446 11457 462 7.8232E-02
11677 11688 11699 11930 12161 12150 12139 11908 11919 462 9.2866E-02
12139 12150 12161 12392 12623 12612 12601 12370 12381 462 1.0779E-01
12601 12612 12623 12854 13085 13074 13063 12832 12843 462 1.2188E-01
13063 13074 13085 13316 13547 13536 13525 13294 13305 462 1.3644E-01
13525 13536 13547 13778 14009 13998 13987 13756 13767 462 1.5094E-01
13987 13998 14009 14240 14471 14460 14449 14218 14229 462 1.6535E-01
14449 14460 14471 14702 14933 14922 14911 14680 14691 462 1.8014E-01
14911 14922 14933 15164 15395 15384 15373 15142 15153 462 1.9410E-01
```

```
15373 15384 15395 15626 15857 15846 15835 15604 15615 462 2.0854E-01
15835 15846 15857 16088 16319 16308 16297 16066 16077 462 2.2035E-01
16297 16308 16319 16550 16781 16770 16759 16528 16539 462 2.3195E-01
16759 16770 16781 17012 17243 17232 17221 16990 17001 462 2.4125E-01
17221 17232 17243 17474 17705 17694 17683 17452 17463 462 2.4997E-01
17683 17694 17705 17936 18167 18156 18145 17914 17925 462 2.5580E-01
18145 18156 18167 18398 18629 18618 18607 18376 18387 462 2.6146E-01
18607 18618 18629 18860 19091 19080 19069 18838 18849 462 2.6331E-01
19069 19080 19091 19322 19553 19542 19531 19300 19311 462 2.6191E-01
19531 19542 19553 19784 20015 20004 19993 19762 19773 462 2.5750E-01
19993 20004 20015 20246 20477 20466 20455 20224 20235 462 2.4983E-01
20455 20466 20477 20708 20939 20928 20917 20686 20697 462 2.3923E-01
20917 20928 20939 21170 21401 21390 21379 21148 21159 462 2.2545E-01
21379 21390 21401 21632 21863 21852 21841 21610 21621 462 2.0940E-01
21841 21852 21863 22094 22325 22314 22303 22072 22083 462 1.9228E-01
22303 22314 22325 22556 22787 22776 22765 22534 22545 462 1.7442E-01
22765 22776 22787 23018 23249 23238 23227 22996 23007 462 1.5957E-01
23227 23238 23249 23480 23711 23700 23689 23458 23469 462 1.4472E-01
23689 23700 23711 23942 24173 24162 24151 23920 23931 462 1.2987E-01
24151 24162 24173 24404 24635 24624 24613 24382 24393 462 1.1503E-01
24613 24624 24635 24866 25097 25086 25075 24844 24855 462 1.0018E-01
25075 25086 25097 25328 25559 25548 25537 25306 25317 462 8.2603E-02
25537 25548 25559 25790 26021 26010 25999 25768 25779 462 6.6580E-02
25999 26010 26021 26252 26483 26472 26461 26230 26241 462 5.1977E-02
26461 26472 26483 26714 26945 26934 26923 26692 26703 462 3.8665E-02
26923 26934 26945 27176 27407 27396 27385 27154 27165 462 2.6529E-02
27385 27396 27407 27638 27869 27858 27847 27616 27627 462 1.5479E-02
27847 27858 27869 28100 28331 28320 28309 28078 28089 462 5.4053E-03
BCFLUX (T1, NODES=9)
2459 2470 2481 2712 2943 2932 2921 2690 2701 462 4.3374E-05
2921 2932 2943 3174 3405 3394 3383 3152 3163 462 1.2693E-04
3383 3394 3405 3636 3867 3856 3845 3614 3625 462 2.2794E-04
3845 3856 3867 4098 4329 4318 4307 4076 4087 462 3.4101E-04
4307 4318 4329 4560 4791 4780 4769 4538 4549 462 4.7931E-04
4769 4780 4791 5022 5253 5242 5231 5000 5011 462 6.9705E-04
5231 5242 5253 5484 5715 5704 5693 5462 5473 462 1.0672E-03
5693 5704 5715 5946 6177 6166 6155 5924 5935 462 1.6649E-03
6155 6166 6177 6408 6639 6628 6617 6386 6397 462 2.6040E-03
6617 6628 6639 6870 7101 7090 7079 6848 6859 462 3.9213E-03
7079 7090 7101 7332 7563 7552 7541 7310 7321 462 6.0039E-03
7541 7552 7563 7794 8025 8014 8003 7772 7783 462 8.6960E-03
8003 8014 8025 8256 8487 8476 8465 8234 8245 462 1.2665E-02
8465 8476 8487 8718 8949 8938 8927 8696 8707 462 1.7838E-02
8927 8938 8949 9180 9411 9400 9389 9158 9169 462 2.4168E-02
9389 9400 9411 9642 9873 9862 9851 9620 9631 462 3.2486E-02
9851 9862 9873 10104 10335 10324 10313 10082 10093 462 4.1259E-02
10313 10324 10335 10566 10797 10786 10775 10544 10555 462 5.2772E-02
10775 10786 10797 11028 11259 11248 11237 11006 11017 462 6.4693E-02
11237 11248 11259 11490 11721 11710 11699 11468 11479 462 7.8232E-02
11699 11710 11721 11952 12183 12172 12161 11930 11941 462 9.2866E-02
12161 12172 12183 12414 12645 12634 12623 12392 12403 462 1.0779E-01
12623 12634 12645 12876 13107 13096 13085 12854 12865 462 1.2188E-01
13085 13096 13107 13338 13569 13558 13547 13316 13327 462 1.3644E-01
13547 13558 13569 13800 14031 14020 14009 13778 13789 462 1.5094E-01
14009 14020 14031 14262 14493 14482 14471 14240 14251 462 1.6535E-01
14471 14482 14493 14724 14955 14944 14933 14702 14713 462 1.8014E-01
14933 14944 14955 15186 15417 15406 15395 15164 15175 462 1.9410E-01
15395 15406 15417 15648 15879 15868 15857 15626 15637 462 2.0854E-01
```

```
15857 15868 15879 16110 16341 16330 16319 16088 16099 462 2.2035E-01
16319 16330 16341 16572 16803 16792 16781 16550 16561 462 2.3195E-01
16781 16792 16803 17034 17265 17254 17243 17012 17023 462 2.4125E-01
17243 17254 17265 17496 17727 17716 17705 17474 17485 462 2.4997E-01
17705 17716 17727 17958 18189 18178 18167 17936 17947 462 2.5580E-01
18167 18178 18189 18420 18651 18640 18629 18398 18409 462 2.6146E-01
18629 18640 18651 18882 19113 19102 19091 18860 18871 462 2.6331E-01
19091 19102 19113 19344 19575 19564 19553 19322 19333 462 2.6191E-01
19553 19564 19575 19806 20037 20026 20015 19784 19795 462 2.5750E-01
20015 20026 20037 20268 20499 20488 20477 20246 20257 462 2.4983E-01
20477 20488 20499 20730 20961 20950 20939 20708 20719 462 2.3923E-01
20939 20950 20961 21192 21423 21412 21401 21170 21181 462 2.2545E-01
21401 21412 21423 21654 21885 21874 21863 21632 21643 462 2.0940E-01
21863 21874 21885 22116 22347 22336 22325 22094 22105 462 1.9228E-01
22325 22336 22347 22578 22809 22798 22787 22556 22567 462 1.7442E-01
22787 22798 22809 23040 23271 23260 23249 23018 23029 462 1.5957E-01
23249 23260 23271 23502 23733 23722 23711 23480 23491 462 1.4472E-01
23711 23722 23733 23964 24195 24184 24173 23942 23953 462 1.2987E-01
24173 24184 24195 24426 24657 24646 24635 24404 24415 462 1.1503E-01
24635 24646 24657 24888 25119 25108 25097 24866 24877 462 1.0018E-01
25097 25108 25119 25350 25581 25570 25559 25328 25339 462 8.2603E-02
25559 25570 25581 25812 26043 26032 26021 25790 25801 462 6.6580E-02
26021 26032 26043 26274 26505 26494 26483 26252 26263 462 5.1977E-02
26483 26494 26505 26736 26967 26956 26945 26714 26725 462 3.8665E-02
26945 26956 26967 27198 27429 27418 27407 27176 27187 462 2.6529E-02
27407 27418 27429 27660 27891 27880 27869 27638 27649 462 1.5479E-02
27869 27880 27891 28122 28353 28342 28331 28100 28111 462 5.4053E-03
BCFLUX (T1, NODES=9)
2481 2492 2503 2734 2965 2954 2943 2712 2723 462 4.3374E-05
2943 2954 2965 3196 3427 3416 3405 3174 3185 462 1.2693E-04
3405 3416 3427 3658 3889 3878 3867 3636 3647 462 2.2794E-04
3867 3878 3889 4120 4351 4340 4329 4098 4109 462 3.4101E-04
4329 4340 4351 4582 4813 4802 4791 4560 4571 462 4.7931E-04
4791 4802 4813 5044 5275 5264 5253 5022 5033 462 6.9705E-04
5253 5264 5275 5506 5737 5726 5715 5484 5495 462 1.0672E-03
5715 5726 5737 5968 6199 6188 6177 5946 5957 462 1.6649E-03
6177 6188 6199 6430 6661 6650 6639 6408 6419 462 2.6040E-03
6639 6650 6661 6892 7123 7112 7101 6870 6881 462 3.9213E-03
7101 7112 7123 7354 7585 7574 7563 7332 7343 462 6.0039E-03
7563 7574 7585 7816 8047 8036 8025 7794 7805 462 8.6960E-03
8025 8036 8047 8278 8509 8498 8487 8256 8267 462 1.2665E-02
8487 8498 8509 8740 8971 8960 8949 8718 8729 462 1.7838E-02
8949 8960 8971 9202 9433 9422 9411 9180 9191 462 2.4168E-02
9411 9422 9433 9664 9895 9884 9873 9642 9653 462 3.2486E-02
9873 9884 9895 10126 10357 10346 10335 10104 10115 462 4.1259E-02
10335 10346 10357 10588 10819 10808 10797 10566 10577 462 5.2772E-02
10797 10808 10819 11050 11281 11270 11259 11028 11039 462 6.4693E-02
11259 11270 11281 11512 11743 11732 11721 11490 11501 462 7.8232E-02
11721 11732 11743 11974 12205 12194 12183 11952 11963 462 9.2866E-02
12183 12194 12205 12436 12667 12656 12645 12414 12425 462 1.0779E-01
12645 12656 12667 12898 13129 13118 13107 12876 12887 462 1.2188E-01
13107 13118 13129 13360 13591 13580 13569 13338 13349 462 1.3644E-01
13569 13580 13591 13822 14053 14042 14031 13800 13811 462 1.5094E-01
14031 14042 14053 14284 14515 14504 14493 14262 14273 462 1.6535E-01
14493 14504 14515 14746 14977 14966 14955 14724 14735 462 1.8014E-01
14955 14966 14977 15208 15439 15428 15417 15186 15197 462 1.9410E-01
15417 15428 15439 15670 15901 15890 15879 15648 15659 462 2.0854E-01
15879 15890 15901 16132 16363 16352 16341 16110 16121 462 2.2035E-01
```

```
16341 16352 16363 16594 16825 16814 16803 16572 16583 462 2.3195E-01
16803 16814 16825 17056 17287 17276 17265 17034 17045 462 2.4125E-01
17265 17276 17287 17518 17749 17738 17727 17496 17507 462 2.4997E-01
17727 17738 17749 17980 18211 18200 18189 17958 17969 462 2.5580E-01
18189 18200 18211 18442 18673 18662 18651 18420 18431 462 2.6146E-01
18651 18662 18673 18904 19135 19124 19113 18882 18893 462 2.6331E-01
19113 19124 19135 19366 19597 19586 19575 19344 19355 462 2.6191E-01
19575 19586 19597 19828 20059 20048 20037 19806 19817 462 2.5750E-01
20037 20048 20059 20290 20521 20510 20499 20268 20279 462 2.4983E-01
20499 20510 20521 20752 20983 20972 20961 20730 20741 462 2.3923E-01
20961 20972 20983 21214 21445 21434 21423 21192 21203 462 2.2545E-01
21423 21434 21445 21676 21907 21896 21885 21654 21665 462 2.0940E-01
21885 21896 21907 22138 22369 22358 22347 22116 22127 462 1.9228E-01
22347 22358 22369 22600 22831 22820 22809 22578 22589 462 1.7442E-01
22809 22820 22831 23062 23293 23282 23271 23040 23051 462 1.5957E-01
23271 23282 23293 23524 23755 23744 23733 23502 23513 462 1.4472E-01
23733 23744 23755 23986 24217 24206 24195 23964 23975 462 1.2987E-01
24195 24206 24217 24448 24679 24668 24657 24426 24437 462 1.1503E-01
24657 24668 24679 24910 25141 25130 25119 24888 24899 462 1.0018E-01
25119 25130 25141 25372 25603 25592 25581 25350 25361 462 8.2603E-02
25581 25592 25603 25834 26065 26054 26043 25812 25823 462 6.6580E-02
26043 26054 26065 26296 26527 26516 26505 26274 26285 462 5.1977E-02
26505 26516 26527 26758 26989 26978 26967 26736 26747 462 3.8665E-02
26967 26978 26989 27220 27451 27440 27429 27198 27209 462 2.6529E-02
27429 27440 27451 27682 27913 27902 27891 27660 27671 462 1.5479E-02
27891 27902 27913 28144 28375 28364 28353 28122 28133 462 5.4053E-03
BCFLUX (T1, NODES=9)
2503 2514 2525 2756 2987 2976 2965 2734 2745 462 4.3374E-05
2965 2976 2987 3218 3449 3438 3427 3196 3207 462 1.2693E-04
3427 3438 3449 3680 3911 3900 3889 3658 3669 462 2.2794E-04
3889 3900 3911 4142 4373 4362 4351 4120 4131 462 3.4101E-04
4351 4362 4373 4604 4835 4824 4813 4582 4593 462 4.7931E-04
4813 4824 4835 5066 5297 5286 5275 5044 5055 462 6.9705E-04
5275 5286 5297 5528 5759 5748 5737 5506 5517 462 1.0672E-03
5737 5748 5759 5990 6221 6210 6199 5968 5979 462 1.6649E-03
6199 6210 6221 6452 6683 6672 6661 6430 6441 462 2.6040E-03
6661 6672 6683 6914 7145 7134 7123 6892 6903 462 3.9213E-03
7123 7134 7145 7376 7607 7596 7585 7354 7365 462 6.0039E-03
7585 7596 7607 7838 8069 8058 8047 7816 7827 462 8.6960E-03
8047 8058 8069 8300 8531 8520 8509 8278 8289 462 1.2665E-02
8509 8520 8531 8762 8993 8982 8971 8740 8751 462 1.7838E-02
8971 8982 8993 9224 9455 9444 9433 9202 9213 462 2.4168E-02
9433 9444 9455 9686 9917 9906 9895 9664 9675 462 3.2486E-02
9895 9906 9917 10148 10379 10368 10357 10126 10137 462 4.1259E-02
10357 10368 10379 10610 10841 10830 10819 10588 10599 462 5.2772E-02
10819 10830 10841 11072 11303 11292 11281 11050 11061 462 6.4693E-02
11281 11292 11303 11534 11765 11754 11743 11512 11523 462 7.8232E-02
11743 11754 11765 11996 12227 12216 12205 11974 11985 462 9.2866E-02
12205 12216 12227 12458 12689 12678 12667 12436 12447 462 1.0779E-01
12667 12678 12689 12920 13151 13140 13129 12898 12909 462 1.2188E-01
13129 13140 13151 13382 13613 13602 13591 13360 13371 462 1.3644E-01
13591 13602 13613 13844 14075 14064 14053 13822 13833 462 1.5094E-01
14053 14064 14075 14306 14537 14526 14515 14284 14295 462 1.6535E-01
14515 14526 14537 14768 14999 14988 14977 14746 14757 462 1.8014E-01
14977 14988 14999 15230 15461 15450 15439 15208 15219 462 1.9410E-01
15439 15450 15461 15692 15923 15912 15901 15670 15681 462 2.0854E-01
15901 15912 15923 16154 16385 16374 16363 16132 16143 462 2.2035E-01
16363 16374 16385 16616 16847 16836 16825 16594 16605 462 2.3195E-01
```

```
16825 16836 16847 17078 17309 17298 17287 17056 17067 462 2.4125E-01
17287 17298 17309 17540 17771 17760 17749 17518 17529 462 2.4997E-01
17749 17760 17771 18002 18233 18222 18211 17980 17991 462 2.5580E-01
18211 18222 18233 18464 18695 18684 18673 18442 18453 462 2.6146E-01
18673 18684 18695 18926 19157 19146 19135 18904 18915 462 2.6331E-01
19135 19146 19157 19388 19619 19608 19597 19366 19377 462 2.6191E-01
19597 19608 19619 19850 20081 20070 20059 19828 19839 462 2.5750E-01
20059 20070 20081 20312 20543 20532 20521 20290 20301 462 2.4983E-01
20521 20532 20543 20774 21005 20994 20983 20752 20763 462 2.3923E-01
20983 20994 21005 21236 21467 21456 21445 21214 21225 462 2.2545E-01
21445 21456 21467 21698 21929 21918 21907 21676 21687 462 2.0940E-01
21907 21918 21929 22160 22391 22380 22369 22138 22149 462 1.9228E-01
22369 22380 22391 22622 22853 22842 22831 22600 22611 462 1.7442E-01
22831 22842 22853 23084 23315 23304 23293 23062 23073 462 1.5957E-01
23293 23304 23315 23546 23777 23766 23755 23524 23535 462 1.4472E-01
23755 23766 23777 24008 24239 24228 24217 23986 23997 462 1.2987E-01
24217 24228 24239 24470 24701 24690 24679 24448 24459 462 1.1503E-01
24679 24690 24701 24932 25163 25152 25141 24910 24921 462 1.0018E-01
25141 25152 25163 25394 25625 25614 25603 25372 25383 462 8.2603E-02
25603 25614 25625 25856 26087 26076 26065 25834 25845 462 6.6580E-02
26065 26076 26087 26318 26549 26538 26527 26296 26307 462 5.1977E-02
26527 26538 26549 26780 27011 27000 26989 26758 26769 462 3.8665E-02
26989 27000 27011 27242 27473 27462 27451 27220 27231 462 2.6529E-02
27451 27462 27473 27704 27935 27924 27913 27682 27693 462 1.5479E-02
27913 27924 27935 28166 28397 28386 28375 28144 28155 462 5.4053E-03
BCFLUX (T1, NODES=9)
2525 2536 2547 2778 3009 2998 2987 2756 2767 462 4.3374E-05
2987 2998 3009 3240 3471 3460 3449 3218 3229 462 1.2693E-04
3449 3460 3471 3702 3933 3922 3911 3680 3691 462 2.2794E-04
3911 3922 3933 4164 4395 4384 4373 4142 4153 462 3.4101E-04
4373 4384 4395 4626 4857 4846 4835 4604 4615 462 4.7931E-04
4835 4846 4857 5088 5319 5308 5297 5066 5077 462 6.9705E-04
5297 5308 5319 5550 5781 5770 5759 5528 5539 462 1.0672E-03
5759 5770 5781 6012 6243 6232 6221 5990 6001 462 1.6649E-03
6221 6232 6243 6474 6705 6694 6683 6452 6463 462 2.6040E-03
6683 6694 6705 6936 7167 7156 7145 6914 6925 462 3.9213E-03
7145 7156 7167 7398 7629 7618 7607 7376 7387 462 6.0039E-03
7607 7618 7629 7860 8091 8080 8069 7838 7849 462 8.6960E-03
8069 8080 8091 8322 8553 8542 8531 8300 8311 462 1.2665E-02
8531 8542 8553 8784 9015 9004 8993 8762 8773 462 1.7838E-02
8993 9004 9015 9246 9477 9466 9455 9224 9235 462 2.4168E-02
9455 9466 9477 9708 9939 9928 9917 9686 9697 462 3.2486E-02
9917 9928 9939 10170 10401 10390 10379 10148 10159 462 4.1259E-02
10379 10390 10401 10632 10863 10852 10841 10610 10621 462 5.2772E-02
10841 10852 10863 11094 11325 11314 11303 11072 11083 462 6.4693E-02
11303 11314 11325 11556 11787 11776 11765 11534 11545 462 7.8232E-02
11765 11776 11787 12018 12249 12238 12227 11996 12007 462 9.2866E-02
12227 12238 12249 12480 12711 12700 12689 12458 12469 462 1.0779E-01
12689 12700 12711 12942 13173 13162 13151 12920 12931 462 1.2188E-01
13151 13162 13173 13404 13635 13624 13613 13382 13393 462 1.3644E-01
13613 13624 13635 13866 14097 14086 14075 13844 13855 462 1.5094E-01
14075 14086 14097 14328 14559 14548 14537 14306 14317 462 1.6535E-01
14537 14548 14559 14790 15021 15010 14999 14768 14779 462 1.8014E-01
14999 15010 15021 15252 15483 15472 15461 15230 15241 462 1.9410E-01
15461 15472 15483 15714 15945 15934 15923 15692 15703 462 2.0854E-01
15923 15934 15945 16176 16407 16396 16385 16154 16165 462 2.2035E-01
16385 16396 16407 16638 16869 16858 16847 16616 16627 462 2.3195E-01
16847 16858 16869 17100 17331 17320 17309 17078 17089 462 2.4125E-01
```

```
17309 17320 17331 17562 17793 17782 17771 17540 17551 462 2.4997E-01
17771 17782 17793 18024 18255 18244 18233 18002 18013 462 2.5580E-01
18233 18244 18255 18486 18717 18706 18695 18464 18475 462 2.6146E-01
18695 18706 18717 18948 19179 19168 19157 18926 18937 462 2.6331E-01
19157 19168 19179 19410 19641 19630 19619 19388 19399 462 2.6191E-01
19619 19630 19641 19872 20103 20092 20081 19850 19861 462 2.5750E-01
20081 20092 20103 20334 20565 20554 20543 20312 20323 462 2.4983E-01
20543 20554 20565 20796 21027 21016 21005 20774 20785 462 2.3923E-01
21005 21016 21027 21258 21489 21478 21467 21236 21247 462 2.2545E-01
21467 21478 21489 21720 21951 21940 21929 21698 21709 462 2.0940E-01
21929 21940 21951 22182 22413 22402 22391 22160 22171 462 1.9228E-01
22391 22402 22413 22644 22875 22864 22853 22622 22633 462 1.7442E-01
22853 22864 22875 23106 23337 23326 23315 23084 23095 462 1.5957E-01
23315 23326 23337 23568 23799 23788 23777 23546 23557 462 1.4472E-01
23777 23788 23799 24030 24261 24250 24239 24008 24019 462 1.2987E-01
24239 24250 24261 24492 24723 24712 24701 24470 24481 462 1.1503E-01
24701 24712 24723 24954 25185 25174 25163 24932 24943 462 1.0018E-01
25163 25174 25185 25416 25647 25636 25625 25394 25405 462 8.2603E-02
25625 25636 25647 25878 26109 26098 26087 25856 25867 462 6.6580E-02
26087 26098 26109 26340 26571 26560 26549 26318 26329 462 5.1977E-02
26549 26560 26571 26802 27033 27022 27011 26780 26791 462 3.8665E-02
27011 27022 27033 27264 27495 27484 27473 27242 27253 462 2.6529E-02
27473 27484 27495 27726 27957 27946 27935 27704 27715 462 1.5479E-02
27935 27946 27957 28188 28419 28408 28397 28166 28177 462 5.4053E-03
BCFLUX (T1, NODES=9)
2547 2558 2569 2800 3031 3020 3009 2778 2789 462 4.3374E-05
3009 3020 3031 3262 3493 3482 3471 3240 3251 462 1.2693E-04
3471 3482 3493 3724 3955 3944 3933 3702 3713 462 2.2794E-04
3933 3944 3955 4186 4417 4406 4395 4164 4175 462 3.4101E-04
4395 4406 4417 4648 4879 4868 4857 4626 4637 462 4.7931E-04
4857 4868 4879 5110 5341 5330 5319 5088 5099 462 6.9705E-04
5319 5330 5341 5572 5803 5792 5781 5550 5561 462 1.0672E-03
5781 5792 5803 6034 6265 6254 6243 6012 6023 462 1.6649E-03
6243 6254 6265 6496 6727 6716 6705 6474 6485 462 2.6040E-03
6705 6716 6727 6958 7189 7178 7167 6936 6947 462 3.9213E-03
7167 7178 7189 7420 7651 7640 7629 7398 7409 462 6.0039E-03
7629 7640 7651 7882 8113 8102 8091 7860 7871 462 8.6960E-03
8091 8102 8113 8344 8575 8564 8553 8322 8333 462 1.2665E-02
8553 8564 8575 8806 9037 9026 9015 8784 8795 462 1.7838E-02
9015 9026 9037 9268 9499 9488 9477 9246 9257 462 2.4168E-02
9477 9488 9499 9730 9961 9950 9939 9708 9719 462 3.2486E-02
9939 9950 9961 10192 10423 10412 10401 10170 10181 462 4.1259E-02
10401 10412 10423 10654 10885 10874 10863 10632 10643 462 5.2772E-02
10863 10874 10885 11116 11347 11336 11325 11094 11105 462 6.4693E-02
11325 11336 11347 11578 11809 11798 11787 11556 11567 462 7.8232E-02
11787 11798 11809 12040 12271 12260 12249 12018 12029 462 9.2866E-02
12249 12260 12271 12502 12733 12722 12711 12480 12491 462 1.0779E-01
12711 12722 12733 12964 13195 13184 13173 12942 12953 462 1.2188E-01
13173 13184 13195 13426 13657 13646 13635 13404 13415 462 1.3644E-01
13635 13646 13657 13888 14119 14108 14097 13866 13877 462 1.5094E-01
14097 14108 14119 14350 14581 14570 14559 14328 14339 462 1.6535E-01
14559 14570 14581 14812 15043 15032 15021 14790 14801 462 1.8014E-01
15021 15032 15043 15274 15505 15494 15483 15252 15263 462 1.9410E-01
15483 15494 15505 15736 15967 15956 15945 15714 15725 462 2.0854E-01
15945 15956 15967 16198 16429 16418 16407 16176 16187 462 2.2035E-01
16407 16418 16429 16660 16891 16880 16869 16638 16649 462 2.3195E-01
16869 16880 16891 17122 17353 17342 17331 17100 17111 462 2.4125E-01
17331 17342 17353 17584 17815 17804 17793 17562 17573 462 2.4997E-01
```

```
17793 17804 17815 18046 18277 18266 18255 18024 18035 462 2.5580E-01
18255 18266 18277 18508 18739 18728 18717 18486 18497 462 2.6146E-01
18717 18728 18739 18970 19201 19190 19179 18948 18959 462 2.6331E-01
19179 19190 19201 19432 19663 19652 19641 19410 19421 462 2.6191E-01
19641 19652 19663 19894 20125 20114 20103 19872 19883 462 2.5750E-01
20103 20114 20125 20356 20587 20576 20565 20334 20345 462 2.4983E-01
20565 20576 20587 20818 21049 21038 21027 20796 20807 462 2.3923E-01
21027 21038 21049 21280 21511 21500 21489 21258 21269 462 2.2545E-01
21489 21500 21511 21742 21973 21962 21951 21720 21731 462 2.0940E-01
21951 21962 21973 22204 22435 22424 22413 22182 22193 462 1.9228E-01
22413 22424 22435 22666 22897 22886 22875 22644 22655 462 1.7442E-01
22875 22886 22897 23128 23359 23348 23337 23106 23117 462 1.5957E-01
23337 23348 23359 23590 23821 23810 23799 23568 23579 462 1.4472E-01
23799 23810 23821 24052 24283 24272 24261 24030 24041 462 1.2987E-01
24261 24272 24283 24514 24745 24734 24723 24492 24503 462 1.1503E-01
24723 24734 24745 24976 25207 25196 25185 24954 24965 462 1.0018E-01
25185 25196 25207 25438 25669 25658 25647 25416 25427 462 8.2603E-02
25647 25658 25669 25900 26131 26120 26109 25878 25889 462 6.6580E-02
26109 26120 26131 26362 26593 26582 26571 26340 26351 462 5.1977E-02
26571 26582 26593 26824 27055 27044 27033 26802 26813 462 3.8665E-02
27033 27044 27055 27286 27517 27506 27495 27264 27275 462 2.6529E-02
27495 27506 27517 27748 27979 27968 27957 27726 27737 462 1.5479E-02
27957 27968 27979 28210 28441 28430 28419 28188 28199 462 5.4053E-03
BCFLUX (T1, NODES=9)
2569 2580 2591 2822 3053 3042 3031 2800 2811 462 4.3374E-05
3031 3042 3053 3284 3515 3504 3493 3262 3273 462 1.2693E-04
3493 3504 3515 3746 3977 3966 3955 3724 3735 462 2.2794E-04
3955 3966 3977 4208 4439 4428 4417 4186 4197 462 3.4101E-04
4417 4428 4439 4670 4901 4890 4879 4648 4659 462 4.7931E-04
4879 4890 4901 5132 5363 5352 5341 5110 5121 462 6.9705E-04
5341 5352 5363 5594 5825 5814 5803 5572 5583 462 1.0672E-03
5803 5814 5825 6056 6287 6276 6265 6034 6045 462 1.6649E-03
6265 6276 6287 6518 6749 6738 6727 6496 6507 462 2.6040E-03
6727 6738 6749 6980 7211 7200 7189 6958 6969 462 3.9213E-03
7189 7200 7211 7442 7673 7662 7651 7420 7431 462 6.0039E-03
7651 7662 7673 7904 8135 8124 8113 7882 7893 462 8.6960E-03
8113 8124 8135 8366 8597 8586 8575 8344 8355 462 1.2665E-02
8575 8586 8597 8828 9059 9048 9037 8806 8817 462 1.7838E-02
9037 9048 9059 9290 9521 9510 9499 9268 9279 462 2.4168E-02
9499 9510 9521 9752 9983 9972 9961 9730 9741 462 3.2486E-02
9961 9972 9983 10214 10445 10434 10423 10192 10203 462 4.1259E-02
10423 10434 10445 10676 10907 10896 10885 10654 10665 462 5.2772E-02
10885 10896 10907 11138 11369 11358 11347 11116 11127 462 6.4693E-02
11347 11358 11369 11600 11831 11820 11809 11578 11589 462 7.8232E-02
11809 11820 11831 12062 12293 12282 12271 12040 12051 462 9.2866E-02
12271 12282 12293 12524 12755 12744 12733 12502 12513 462 1.0779E-01
12733 12744 12755 12986 13217 13206 13195 12964 12975 462 1.2188E-01
13195 13206 13217 13448 13679 13668 13657 13426 13437 462 1.3644E-01
13657 13668 13679 13910 14141 14130 14119 13888 13899 462 1.5094E-01
14119 14130 14141 14372 14603 14592 14581 14350 14361 462 1.6535E-01
14581 14592 14603 14834 15065 15054 15043 14812 14823 462 1.8014E-01
15043 15054 15065 15296 15527 15516 15505 15274 15285 462 1.9410E-01
15505 15516 15527 15758 15989 15978 15967 15736 15747 462 2.0854E-01
15967 15978 15989 16220 16451 16440 16429 16198 16209 462 2.2035E-01
16429 16440 16451 16682 16913 16902 16891 16660 16671 462 2.3195E-01
16891 16902 16913 17144 17375 17364 17353 17122 17133 462 2.4125E-01
17353 17364 17375 17606 17837 17826 17815 17584 17595 462 2.4997E-01
17815 17826 17837 18068 18299 18288 18277 18046 18057 462 2.5580E-01
```

```
18277 18288 18299 18530 18761 18750 18739 18508 18519 462 2.6146E-01
18739 18750 18761 18992 19223 19212 19201 18970 18981 462 2.6331E-01
19201 19212 19223 19454 19685 19674 19663 19432 19443 462 2.6191E-01
19663 19674 19685 19916 20147 20136 20125 19894 19905 462 2.5750E-01
20125 20136 20147 20378 20609 20598 20587 20356 20367 462 2.4983E-01
20587 20598 20609 20840 21071 21060 21049 20818 20829 462 2.3923E-01
21049 21060 21071 21302 21533 21522 21511 21280 21291 462 2.2545E-01
21511 21522 21533 21764 21995 21984 21973 21742 21753 462 2.0940E-01
21973 21984 21995 22226 22457 22446 22435 22204 22215 462 1.9228E-01
22435 22446 22457 22688 22919 22908 22897 22666 22677 462 1.7442E-01
22897 22908 22919 23150 23381 23370 23359 23128 23139 462 1.5957E-01
23359 23370 23381 23612 23843 23832 23821 23590 23601 462 1.4472E-01
23821 23832 23843 24074 24305 24294 24283 24052 24063 462 1.2987E-01
24283 24294 24305 24536 24767 24756 24745 24514 24525 462 1.1503E-01
24745 24756 24767 24998 25229 25218 25207 24976 24987 462 1.0018E-01
25207 25218 25229 25460 25691 25680 25669 25438 25449 462 8.2603E-02
25669 25680 25691 25922 26153 26142 26131 25900 25911 462 6.6580E-02
26131 26142 26153 26384 26615 26604 26593 26362 26373 462 5.1977E-02
26593 26604 26615 26846 27077 27066 27055 26824 26835 462 3.8665E-02
27055 27066 27077 27308 27539 27528 27517 27286 27297 462 2.6529E-02
27517 27528 27539 27770 28001 27990 27979 27748 27759 462 1.5479E-02
27979 27990 28001 28232 28463 28452 28441 28210 28221 462 5.4053E-03
BCFLUX (T1, NODES=9)
2591 2602 2613 2844 3075 3064 3053 2822 2833 462 4.3374E-05
3053 3064 3075 3306 3537 3526 3515 3284 3295 462 1.2693E-04
3515 3526 3537 3768 3999 3988 3977 3746 3757 462 2.2794E-04
3977 3988 3999 4230 4461 4450 4439 4208 4219 462 3.4101E-04
4439 4450 4461 4692 4923 4912 4901 4670 4681 462 4.7931E-04
4901 4912 4923 5154 5385 5374 5363 5132 5143 462 6.9705E-04
5363 5374 5385 5616 5847 5836 5825 5594 5605 462 1.0672E-03
5825 5836 5847 6078 6309 6298 6287 6056 6067 462 1.6649E-03
6287 6298 6309 6540 6771 6760 6749 6518 6529 462 2.6040E-03
6749 6760 6771 7002 7233 7222 7211 6980 6991 462 3.9213E-03
7211 7222 7233 7464 7695 7684 7673 7442 7453 462 6.0039E-03
7673 7684 7695 7926 8157 8146 8135 7904 7915 462 8.6960E-03
8135 8146 8157 8388 8619 8608 8597 8366 8377 462 1.2665E-02
8597 8608 8619 8850 9081 9070 9059 8828 8839 462 1.7838E-02
9059 9070 9081 9312 9543 9532 9521 9290 9301 462 2.4168E-02
9521 9532 9543 9774 10005 9994 9983 9752 9763 462 3.2486E-02
9983 9994 10005 10236 10467 10456 10445 10214 10225 462 4.1259E-02
10445 10456 10467 10698 10929 10918 10907 10676 10687 462 5.2772E-02
10907 10918 10929 11160 11391 11380 11369 11138 11149 462 6.4693E-02
11369 11380 11391 11622 11853 11842 11831 11600 11611 462 7.8232E-02
11831 11842 11853 12084 12315 12304 12293 12062 12073 462 9.2866E-02
12293 12304 12315 12546 12777 12766 12755 12524 12535 462 1.0779E-01
12755 12766 12777 13008 13239 13228 13217 12986 12997 462 1.2188E-01
13217 13228 13239 13470 13701 13690 13679 13448 13459 462 1.3644E-01
13679 13690 13701 13932 14163 14152 14141 13910 13921 462 1.5094E-01
14141 14152 14163 14394 14625 14614 14603 14372 14383 462 1.6535E-01
14603 14614 14625 14856 15087 15076 15065 14834 14845 462 1.8014E-01
15065 15076 15087 15318 15549 15538 15527 15296 15307 462 1.9410E-01
15527 15538 15549 15780 16011 16000 15989 15758 15769 462 2.0854E-01
15989 16000 16011 16242 16473 16462 16451 16220 16231 462 2.2035E-01
16451 16462 16473 16704 16935 16924 16913 16682 16693 462 2.3195E-01
16913 16924 16935 17166 17397 17386 17375 17144 17155 462 2.4125E-01
17375 17386 17397 17628 17859 17848 17837 17606 17617 462 2.4997E-01
17837 17848 17859 18090 18321 18310 18299 18068 18079 462 2.5580E-01
18299 18310 18321 18552 18783 18772 18761 18530 18541 462 2.6146E-01
```

```
18761 18772 18783 19014 19245 19234 19223 18992 19003 462 2.6331E-01
19223 19234 19245 19476 19707 19696 19685 19454 19465 462 2.6191E-01
19685 19696 19707 19938 20169 20158 20147 19916 19927 462 2.5750E-01
20147 20158 20169 20400 20631 20620 20609 20378 20389 462 2.4983E-01
20609 20620 20631 20862 21093 21082 21071 20840 20851 462 2.3923E-01
21071 21082 21093 21324 21555 21544 21533 21302 21313 462 2.2545E-01
21533 21544 21555 21786 22017 22006 21995 21764 21775 462 2.0940E-01
21995 22006 22017 22248 22479 22468 22457 22226 22237 462 1.9228E-01
22457 22468 22479 22710 22941 22930 22919 22688 22699 462 1.7442E-01
22919 22930 22941 23172 23403 23392 23381 23150 23161 462 1.5957E-01
23381 23392 23403 23634 23865 23854 23843 23612 23623 462 1.4472E-01
23843 23854 23865 24096 24327 24316 24305 24074 24085 462 1.2987E-01
24305 24316 24327 24558 24789 24778 24767 24536 24547 462 1.1503E-01
24767 24778 24789 25020 25251 25240 25229 24998 25009 462 1.0018E-01
25229 25240 25251 25482 25713 25702 25691 25460 25471 462 8.2603E-02
25691 25702 25713 25944 26175 26164 26153 25922 25933 462 6.6580E-02
26153 26164 26175 26406 26637 26626 26615 26384 26395 462 5.1977E-02
26615 26626 26637 26868 27099 27088 27077 26846 26857 462 3.8665E-02
27077 27088 27099 27330 27561 27550 27539 27308 27319 462 2.6529E-02
27539 27550 27561 27792 28023 28012 28001 27770 27781 462 1.5479E-02
28001 28012 28023 28254 28485 28474 28463 28232 28243 462 5.4053E-03
BCFLUX (T1, NODES=9)
2613 2624 2635 2866 3097 3086 3075 2844 2855 462 4.3374E-05
3075 3086 3097 3328 3559 3548 3537 3306 3317 462 1.2693E-04
3537 3548 3559 3790 4021 4010 3999 3768 3779 462 2.2794E-04
3999 4010 4021 4252 4483 4472 4461 4230 4241 462 3.4101E-04
4461 4472 4483 4714 4945 4934 4923 4692 4703 462 4.7931E-04
4923 4934 4945 5176 5407 5396 5385 5154 5165 462 6.9705E-04
5385 5396 5407 5638 5869 5858 5847 5616 5627 462 1.0672E-03
5847 5858 5869 6100 6331 6320 6309 6078 6089 462 1.6649E-03
6309 6320 6331 6562 6793 6782 6771 6540 6551 462 2.6040E-03
6771 6782 6793 7024 7255 7244 7233 7002 7013 462 3.9213E-03
7233 7244 7255 7486 7717 7706 7695 7464 7475 462 6.0039E-03
7695 7706 7717 7948 8179 8168 8157 7926 7937 462 8.6960E-03
8157 8168 8179 8410 8641 8630 8619 8388 8399 462 1.2665E-02
8619 8630 8641 8872 9103 9092 9081 8850 8861 462 1.7838E-02
9081 9092 9103 9334 9565 9554 9543 9312 9323 462 2.4168E-02
9543 9554 9565 9796 10027 10016 10005 9774 9785 462 3.2486E-02
10005 10016 10027 10258 10489 10478 10467 10236 10247 462 4.1259E-02
10467 10478 10489 10720 10951 10940 10929 10698 10709 462 5.2772E-02
10929 10940 10951 11182 11413 11402 11391 11160 11171 462 6.4693E-02
11391 11402 11413 11644 11875 11864 11853 11622 11633 462 7.8232E-02
11853 11864 11875 12106 12337 12326 12315 12084 12095 462 9.2866E-02
12315 12326 12337 12568 12799 12788 12777 12546 12557 462 1.0779E-01
12777 12788 12799 13030 13261 13250 13239 13008 13019 462 1.2188E-01
13239 13250 13261 13492 13723 13712 13701 13470 13481 462 1.3644E-01
13701 13712 13723 13954 14185 14174 14163 13932 13943 462 1.5094E-01
14163 14174 14185 14416 14647 14636 14625 14394 14405 462 1.6535E-01
14625 14636 14647 14878 15109 15098 15087 14856 14867 462 1.8014E-01
15087 15098 15109 15340 15571 15560 15549 15318 15329 462 1.9410E-01
15549 15560 15571 15802 16033 16022 16011 15780 15791 462 2.0854E-01
16011 16022 16033 16264 16495 16484 16473 16242 16253 462 2.2035E-01
16473 16484 16495 16726 16957 16946 16935 16704 16715 462 2.3195E-01
16935 16946 16957 17188 17419 17408 17397 17166 17177 462 2.4125E-01
17397 17408 17419 17650 17881 17870 17859 17628 17639 462 2.4997E-01
17859 17870 17881 18112 18343 18332 18321 18090 18101 462 2.5580E-01
18321 18332 18343 18574 18805 18794 18783 18552 18563 462 2.6146E-01
18783 18794 18805 19036 19267 19256 19245 19014 19025 462 2.6331E-01
```

```
19245 19256 19267 19498 19729 19718 19707 19476 19487 462 2.6191E-01
19707 19718 19729 19960 20191 20180 20169 19938 19949 462 2.5750E-01
20169 20180 20191 20422 20653 20642 20631 20400 20411 462 2.4983E-01
20631 20642 20653 20884 21115 21104 21093 20862 20873 462 2.3923E-01
21093 21104 21115 21346 21577 21566 21555 21324 21335 462 2.2545E-01
21555 21566 21577 21808 22039 22028 22017 21786 21797 462 2.0940E-01
22017 22028 22039 22270 22501 22490 22479 22248 22259 462 1.9228E-01
22479 22490 22501 22732 22963 22952 22941 22710 22721 462 1.7442E-01
22941 22952 22963 23194 23425 23414 23403 23172 23183 462 1.5957E-01
23403 23414 23425 23656 23887 23876 23865 23634 23645 462 1.4472E-01
23865 23876 23887 24118 24349 24338 24327 24096 24107 462 1.2987E-01
24327 24338 24349 24580 24811 24800 24789 24558 24569 462 1.1503E-01
24789 24800 24811 25042 25273 25262 25251 25020 25031 462 1.0018E-01
25251 25262 25273 25504 25735 25724 25713 25482 25493 462 8.2603E-02
25713 25724 25735 25966 26197 26186 26175 25944 25955 462 6.6580E-02
26175 26186 26197 26428 26659 26648 26637 26406 26417 462 5.1977E-02
26637 26648 26659 26890 27121 27110 27099 26868 26879 462 3.8665E-02
27099 27110 27121 27352 27583 27572 27561 27330 27341 462 2.6529E-02
27561 27572 27583 27814 28045 28034 28023 27792 27803 462 1.5479E-02
28023 28034 28045 28276 28507 28496 28485 28254 28265 462 5.4053E-03
BCFLUX (T1, NODES=9)
2635 2646 2657 2888 3119 3108 3097 2866 2877 462 4.3374E-05
3097 3108 3119 3350 3581 3570 3559 3328 3339 462 1.2693E-04
3559 3570 3581 3812 4043 4032 4021 3790 3801 462 2.2794E-04
4021 4032 4043 4274 4505 4494 4483 4252 4263 462 3.4101E-04
4483 4494 4505 4736 4967 4956 4945 4714 4725 462 4.7931E-04
4945 4956 4967 5198 5429 5418 5407 5176 5187 462 6.9705E-04
5407 5418 5429 5660 5891 5880 5869 5638 5649 462 1.0672E-03
5869 5880 5891 6122 6353 6342 6331 6100 6111 462 1.6649E-03
6331 6342 6353 6584 6815 6804 6793 6562 6573 462 2.6040E-03
6793 6804 6815 7046 7277 7266 7255 7024 7035 462 3.9213E-03
7255 7266 7277 7508 7739 7728 7717 7486 7497 462 6.0039E-03
7717 7728 7739 7970 8201 8190 8179 7948 7959 462 8.6960E-03
8179 8190 8201 8432 8663 8652 8641 8410 8421 462 1.2665E-02
8641 8652 8663 8894 9125 9114 9103 8872 8883 462 1.7838E-02
9103 9114 9125 9356 9587 9576 9565 9334 9345 462 2.4168E-02
9565 9576 9587 9818 10049 10038 10027 9796 9807 462 3.2486E-02
10027 10038 10049 10280 10511 10500 10489 10258 10269 462 4.1259E-02
10489 10500 10511 10742 10973 10962 10951 10720 10731 462 5.2772E-02
10951 10962 10973 11204 11435 11424 11413 11182 11193 462 6.4693E-02
11413 11424 11435 11666 11897 11886 11875 11644 11655 462 7.8232E-02
11875 11886 11897 12128 12359 12348 12337 12106 12117 462 9.2866E-02
12337 12348 12359 12590 12821 12810 12799 12568 12579 462 1.0779E-01
12799 12810 12821 13052 13283 13272 13261 13030 13041 462 1.2188E-01
13261 13272 13283 13514 13745 13734 13723 13492 13503 462 1.3644E-01
13723 13734 13745 13976 14207 14196 14185 13954 13965 462 1.5094E-01
14185 14196 14207 14438 14669 14658 14647 14416 14427 462 1.6535E-01
14647 14658 14669 14900 15131 15120 15109 14878 14889 462 1.8014E-01
15109 15120 15131 15362 15593 15582 15571 15340 15351 462 1.9410E-01
15571 15582 15593 15824 16055 16044 16033 15802 15813 462 2.0854E-01
16033 16044 16055 16286 16517 16506 16495 16264 16275 462 2.2035E-01
16495 16506 16517 16748 16979 16968 16957 16726 16737 462 2.3195E-01
16957 16968 16979 17210 17441 17430 17419 17188 17199 462 2.4125E-01
17419 17430 17441 17672 17903 17892 17881 17650 17661 462 2.4997E-01
17881 17892 17903 18134 18365 18354 18343 18112 18123 462 2.5580E-01
18343 18354 18365 18596 18827 18816 18805 18574 18585 462 2.6146E-01
18805 18816 18827 19058 19289 19278 19267 19036 19047 462 2.6331E-01
19267 19278 19289 19520 19751 19740 19729 19498 19509 462 2.6191E-01
```

```
19729 19740 19751 19982 20213 20202 20191 19960 19971 462 2.5750E-01
20191 20202 20213 20444 20675 20664 20653 20422 20433 462 2.4983E-01
20653 20664 20675 20906 21137 21126 21115 20884 20895 462 2.3923E-01
21115 21126 21137 21368 21599 21588 21577 21346 21357 462 2.2545E-01
21577 21588 21599 21830 22061 22050 22039 21808 21819 462 2.0940E-01
22039 22050 22061 22292 22523 22512 22501 22270 22281 462 1.9228E-01
22501 22512 22523 22754 22985 22974 22963 22732 22743 462 1.7442E-01
22963 22974 22985 23216 23447 23436 23425 23194 23205 462 1.5957E-01
23425 23436 23447 23678 23909 23898 23887 23656 23667 462 1.4472E-01
23887 23898 23909 24140 24371 24360 24349 24118 24129 462 1.2987E-01
24349 24360 24371 24602 24833 24822 24811 24580 24591 462 1.1503E-01
24811 24822 24833 25064 25295 25284 25273 25042 25053 462 1.0018E-01
25273 25284 25295 25526 25757 25746 25735 25504 25515 462 8.2603E-02
25735 25746 25757 25988 26219 26208 26197 25966 25977 462 6.6580E-02
26197 26208 26219 26450 26681 26670 26659 26428 26439 462 5.1977E-02
26659 26670 26681 26912 27143 27132 27121 26890 26901 462 3.8665E-02
27121 27132 27143 27374 27605 27594 27583 27352 27363 462 2.6529E-02
27583 27594 27605 27836 28067 28056 28045 27814 27825 462 1.5479E-02
28045 28056 28067 28298 28529 28518 28507 28276 28287 462 5.4053E-03
RENUMBER (profile)
ELEMENTS (brick, nodes=27, fluid, mvisc=1, mcond=1, fimesh)
ELEMENTS (brick, nodes=27, fluid, mvisc=1, mcond=1, fimesh)
ELEMENTS (brick, nodes=27, fluid, mvisc=1, mcond=1, fimesh)
ELEMENTS (brick, nodes=27, fluid, mvisc=2, mcond=2, fimesh)
ELEMENTS (brick, nodes=27, fluid, mvisc=2, mcond=2, fimesh)
ELEMENTS (convection, nodes=9, mcnv=1, fimesh)
ELEMENTS (slip, nodes=9, attach=3, fimesh)
ELEMENTS (slip, nodes=9, attach=5, fimesh)
END
*END
```

APPENDIX F
TRANSIENT EXPERIMENTAL DATA

HEAT # 79815					
STRAND #1					
BOARD TYPE - LONG					
GRADE -					
T = O SECONDS					
RAW DATA					
	1	2	3	4	5
x-position (in)	12.25	9.625	7	4.375	1.75
y -position (in)	3.3125	3.3125	3.3125	3.3125	3.3125
I (cm)	2.6	3.7	3.6	2.7	3.3
II (cm)	3.4	4.2	4.4	4.9	4.7
	10	9	8	7	6
x-position (in)	12.25	9.625	7	4.375	1.75
y -position (in)	4.5	4.5	4.5	4.5	4.5
I (cm)	3	3.5	3.3	3.1	3
II (cm)	3.5	4.2	3.9	5	5
CALCULATED DATA					
	1	2	3	4	5
x-position (cm)	31.115	24.4475	17.78	11.1125	4.445
y-position (cm)	8.41375	8.41375	8.41375	8.41375	8.41375
POWDER (cm)	2.6	3.7	3.6	2.7	3.3
LIQUID (cm)	0.8	0.5	0.8	2.2	1.4
	10	9	8	7	6
x-position (cm)	31.115	24.4475	17.78	11.1125	4.445
y-position (cm)	11.43	11.43	11.43	11.43	11.43
POWDER (cm)	3	3.5	3.3	3.1	3
LIQUID (cm)	0.5	0.7	0.6	1.9	2
Ave powder thickne	2.8	3.6	3.45	2.9	3.15
Ave liquid thickness	0.65	0.6	0.7	2.05	1.7
T = 30.0 SECONDS					
RAW DATA					
	1	2	3	4	5
x-position (in)	12.25	9.625	7	4.375	1.75
y -position (in)	3.3125	3.3125	3.3125	3.3125	3.3125
I (cm)	2.9	3.7	3.8	4.5	4.3
II (cm)	3.6	4.3	4.9	5.4	4.9
	10	9	8	7	6
x-position (in)	12.25	9.625	7	4.375	1.75
y -position (in)	4.5	4.5	4.5	4.5	4.5
I (cm)	3.7	4	4.3	5.1	6.1

II (cm)	3.7	4.6	5.4	5.9	6.3
CALCULATED DATA					
	1	2	3	4	5
x-position (cm)	31.115	24.4475	17.78	11.1125	4.445
y-position (cm)	8.41375	8.41375	8.41375	8.41375	8.41375
POWDER (cm)	2.9	3.7	3.8	4.5	4.3
LIQUID (cm)	0.7	0.6	1.1	0.9	0.6
	10	9	8	7	6
x-position (cm)	31.115	24.4475	17.78	11.1125	4.445
y-position (cm)	11.43	11.43	11.43	11.43	11.43
POWDER (cm)	3.7	4	4.3	5.1	6.1
LIQUID (cm)	0	0.6	1.1	0.8	0.2
Ave powder thickne	3.3	3.85	4.05	4.8	5.2
Ave liquid thicknes	0.35	0.6	1.1	0.85	0.4
T = 60.0 SECONDS					
RAW DATA					
	1	2	3	4	5
x-position (in)	12.25	9.625	7	4.375	1.75
y -position (in)	3.3125	3.3125	3.3125	3.3125	3.3125
I (cm)	2.2	2.3	2.3	2.7	2
II (cm)	3	3.5	3.6	3.6	4.4
	10	9	8	7	6
x-position (in)	12.25	9.625	7	4.375	1.75
y -position (in)	4.5	4.5	4.5	4.5	4.5
I (cm)	2.3	2.4	3	3	3.1
II (cm)	2.9	3.6	4	4.3	4.4
CALCULATED DATA					
	1	2	3	4	5
x-position (cm)	31.115	24.4475	17.78	11.1125	4.445
y-position (cm)	8.41375	8.41375	8.41375	8.41375	8.41375
POWDER (cm)	2.2	2.3	2.3	2.7	2
LIQUID (cm)	0.8	1.2	1.3	0.9	2.4
	10	9	8	7	6
x-position (cm)	31.115	24.4475	17.78	11.1125	4.445
y-position (cm)	11.43	11.43	11.43	11.43	11.43
POWDER (cm)	2.3	2.4	3	3	3.1
LIQUID (cm)	0.6	1.2	1	1.3	1.3
Ave powder thickne	2.25	2.35	2.65	2.85	2.55
Ave liquid thicknes	0.7	1.2	1.15	1.1	1.85

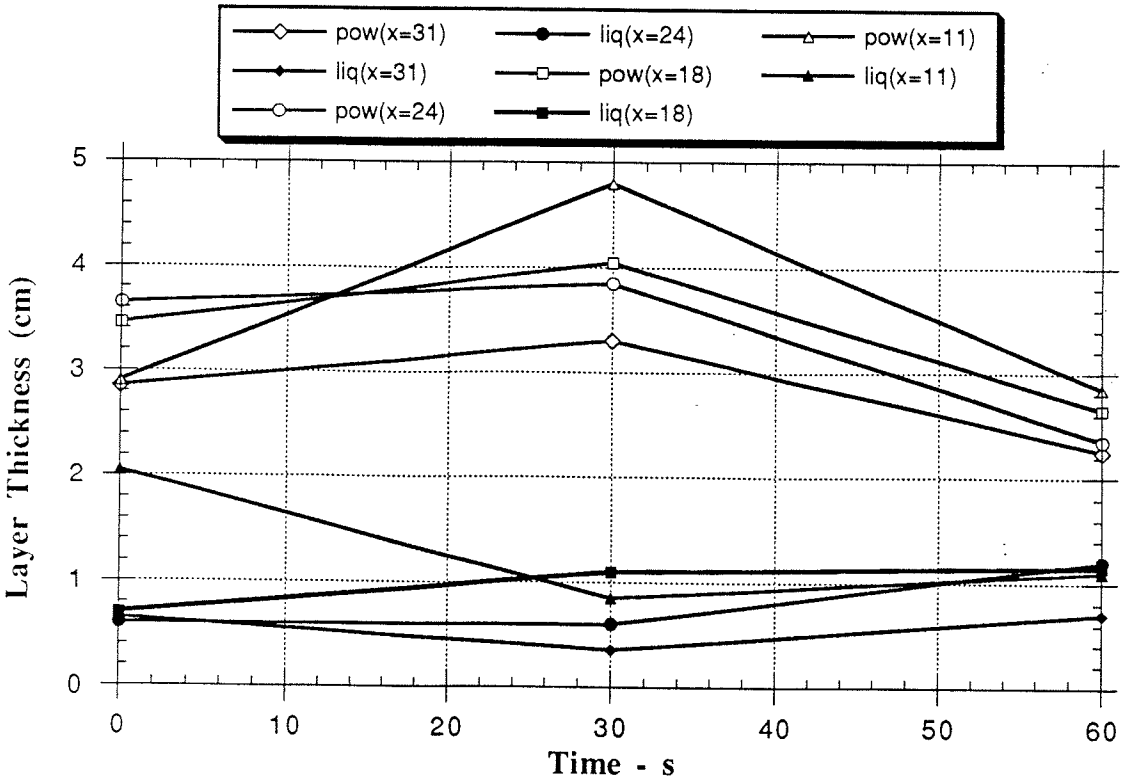

Figure F.1: **Transient Powder and Liquid Layer Thickness (Heat#: 79815)**

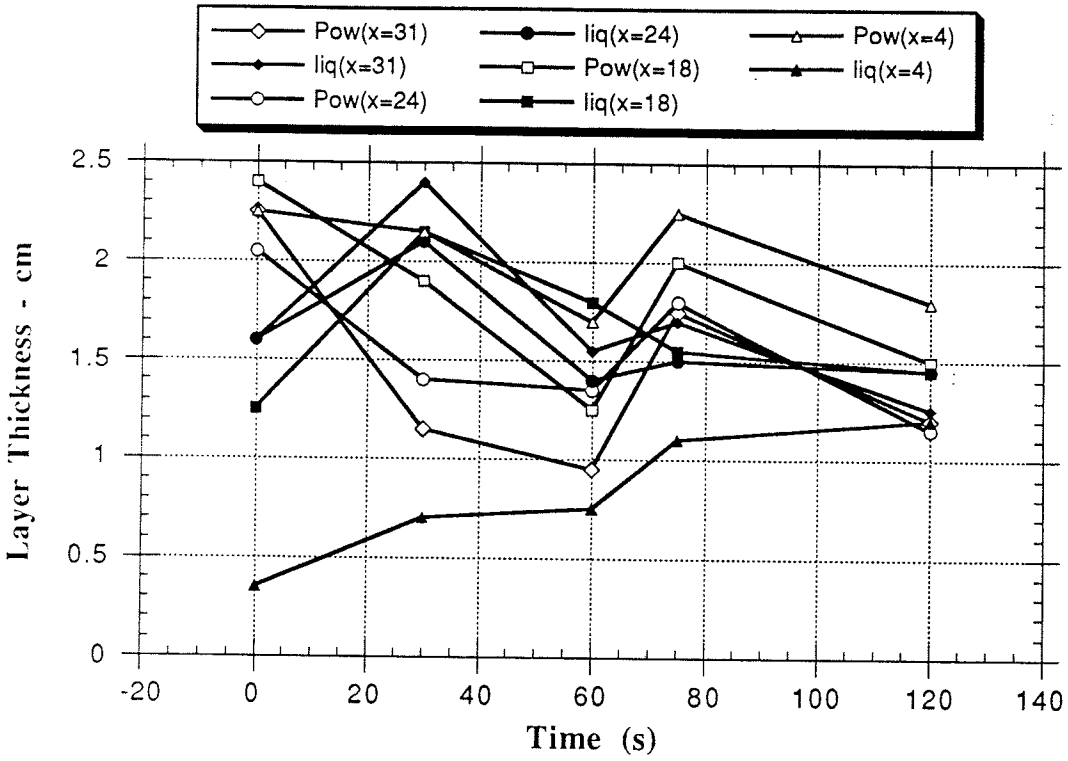

Figure F.2: **Transient Powder and Liquid Layer Thickness (Heat#: 79797)**

HEAT # 79797					
STRAND #2					
BOARD TYPE - LONG					
GRADE -					
T = O SECONDS					
RAW DATA					
	1	2	3	4	5
x-position (in)	12.25	9.625	7	4.375	1.75
y -position (in)	3.3125	3.3125	3.3125	3.3125	3.3125
I (cm)	1.6	1.8	2	2	2.2
II (cm)	3.2	3.4	3.5	3.7	2.8
	10	9	8	7	6
x-position (in)	12.25	9.625	7	4.375	1.75
y -position (in)	4.5	4.5	4.5	4.5	4.5
I (cm)	2.9	2.3	2.8	2.5	2.5
II (cm)		3.9	3.8	3.4	2.6
CALCULATED DATA					
	1	2	3	4	5
x-position (cm)	31.115	24.4475	17.78	11.1125	4.445
y-position (cm)	8.41375	8.41375	8.41375	8.41375	8.41375
POWDER (cm)	1.6	1.8	2	2	2.2
LIQUID (cm)	1.6	1.6	1.5	1.7	0.6
	10	9	8	7	6
x-position (cm)	31.115	24.4475	17.78	11.1125	4.445
y-position (cm)	11.43	11.43	11.43	11.43	11.43
POWDER (cm)	2.9	2.3	2.8	2.5	2.5
LIQUID (cm)		1.6	1	0.9	0.1
Ave Powder Thick	2.25	2.05	2.4	2.25	2.35
Average Liq Thick	1.6	1.6	1.25	1.3	0.35
T = 30.0 SECONDS					
RAW DATA					
	1	2	3	4	5
x-position (in)	12.25	9.625	7	4.375	1.75
y -position (in)	3.3125	3.3125	3.3125	3.3125	3.3125
I (cm)	1	1.6	2	2.6	2.2
II (cm)	3.4	3.5	4	3.7	3.2
	10	9	8	7	6
x-position (in)	12.25	9.625	7	4.375	1.75

y -position (in)	4.5	4.5	4.5	4.5	4.5
I (cm)	1.3	1.2	1.8	2.2	2.1
II (cm)		3.5	4.1	4	2.5
CALCULATED DATA					
	1	2	3	4	5
x-position (cm)	31.115	24.4475	17.78	11.1125	4.445
y-position (cm)	8.41375	8.41375	8.41375	8.41375	8.41375
POWDER (cm)	1	1.6	2	2.6	2.2
LIQUID (cm)	2.4	1.9	2	1.1	1
	10	9	8	7	6
x-position (cm)	31.115	24.4475	17.78	11.1125	4.445
y-position (cm)	11.43	11.43	11.43	11.43	11.43
POWDER (cm)	1.3	1.2	1.8	2.2	2.1
LIQUID (cm)		2.3	2.3	1.8	0.4
Ave Powder Thick	1.15	1.4	1.9	2.4	2.15
Average Liq Thick	2.4	2.1	2.15	1.45	0.7
T = 60.0 SECONDS					
RAW DATA					
	1	2	3	4	5
x-position (in)	12.25	9.625	7	4.375	1.75
y -position (in)	3.3125	3.3125	3.3125	3.3125	3.3125
I (cm)	0.9	1.7	1.3	1.5	2
II (cm)	2.4	2.8	3.1	3.3	2.8
	10	9	8	7	6
x-position (in)	12.25	9.625	7	4.375	1.75
y -position (in)	4.5	4.5	4.5	4.5	4.5
I (cm)	1	1	1.2	1.4	1.4
II (cm)	2.6	2.7	3	2.8	2.1
CALCULATED DATA					
	1	2	3	4	5
x-position (cm)	31.115	24.4475	17.78	11.1125	4.445
y-position (cm)	8.41375	8.41375	8.41375	8.41375	8.41375
POWDER (cm)	0.9	1.7	1.3	1.5	2
LIQUID (cm)	1.5	1.1	1.8	1.8	0.8
	10	9	8	7	6
x-position (cm)	31.115	24.4475	17.78	11.1125	4.445
y-position (cm)	11.43	11.43	11.43	11.43	11.43
POWDER (cm)	1	1	1.2	1.4	1.4
LIQUID (cm)	1.6	1.7	1.8	1.4	0.7
Ave Powder Thick	0.95	1.35	1.25	1.45	1.7
Average Liq Thick	1.55	1.4	1.8	1.6	0.75

T = 75.0 SECONDS					
RAW DATA					
	1	2	3	4	5
x-position (in)	12.25	9.625	7	4.375	1.75
y -position (in)	3.3125	3.3125	3.3125	3.3125	3.3125
I (cm)	2	1.8	2	2.3	2.4
II (cm)	3.7	3.5	3.6	3.9	3.5
	10	9	8	7	6
x-position (in)	12.25	9.625	7	4.375	1.75
y -position (in)	4.5	4.5	4.5	4.5	4.5
I (cm)	1.5	1.8	2	2	2.1
II (cm)	3.2	3.1	3.5	3.5	
CALCULATED DATA					
	1	2	3	4	5
x-position (cm)	31.115	24.4475	17.78	11.1125	4.445
y-position (cm)	8.41375	8.41375	8.41375	8.41375	8.41375
POWDER (cm)	2	1.8	2	2.3	2.4
LIQUID (cm)	1.7	1.7	1.6	1.6	1.1
	10	9	8	7	6
x-position (cm)	31.115	24.4475	17.78	11.1125	4.445
y-position (cm)	11.43	11.43	11.43	11.43	11.43
POWDER (cm)	1.5	1.8	2	2	2.1
LIQUID (cm)	1.7	1.3	1.5	1.5	
Ave Powder Thick	1.75	1.8	2	2.15	2.25
Average Liq Thick	1.7	1.5	1.55	1.55	1.1
T = 120.0 SECONDS					
RAW DATA					
	1	2	3	4	5
x-position (in)	12.25	9.625	7	4.375	1.75
y -position (in)	3.3125	3.3125	3.3125	3.3125	3.3125
I (cm)	1	0.9	1.5	1.5	1.5
II (cm)	2.2	2.4	2.8	2.8	2.7
	10	9	8	7	6
x-position (in)	12.25	9.625	7	4.375	1.75
y -position (in)	4.5	4.5	4.5	4.5	4.5
I (cm)	1.4	1.4	1.5	2.1	2.1
II (cm)	2.7	2.8	3.1	3.1	2.8
CALCULATED DATA					

	1	2	3	4	5
x-position (cm)	31.115	24.4475	17.78	11.1125	4.445
y-position (cm)	8.41375	8.41375	8.41375	8.41375	8.41375
POWDER (cm)	1	0.9	1.5	1.5	1.5
LIQUID (cm)	1.2	1.5	1.3	1.3	1.2
	10	9	8	7	6
x-position (cm)	31.115	24.4475	17.78	11.1125	4.445
y-position (cm)	11.43	11.43	11.43	11.43	11.43
POWDER (cm)	1.4	1.4	1.5	2.1	2.1
LIQUID (cm)	1.3	1.4	1.6	1	
Ave Powder Thick	1.2	1.15	1.5	1.8	1.8
Average Liq Thick	1.25	1.45	1.45	1.15	1.2

REFERENCES

1. *Percentage of Crude Steel Continuously Cast.* Iron and Steelmaker. 18 - 16, 1991.

2. Taylor, R., Mills. K.C.: *"Physical Porperties of Casting Powders: Part 3 - Thermal Conductivities of Casting Powders"*, Ironmaking and Steelmaking, 1988, vol. 15 (4), pp. 187 - 194.

3. Branion, R.V.: *"Mold Fluxes for Continuous Casting"*, Steelmaking Conference Proceedings, Iron and Steel Society of AIME, Warrendale, PA, 1986, Vol. 69, pp. 95 - 105.

4. Mahapatra, R.B., Brimacombe, J.K. et. al: *"Mold Behavior and Its Influence on Quality in the Continuous Casting of Steel Slabs: Part I. - Industrial Trials, Mold Temperature Measurements, and Mathematical Modeling"*, Metallurgical Transactions B, 1991, vol. 22B, pp. 861 - 874.

5. Kwon, O.D., Choi, J., et. al.: *"Optimization of Mold Oscillation Pattern for the Improvement of Surface Quality and Lubrication in Slab Continuous Casting"*, Steelmaking Conference Proceedings, 1991, Vol. 74, pp. 561 - 568.

6. Machingawuta, N.C., Bagha, S., Grievson, P.: *"Heat Transfer Simulation for Continuous Casting"*, Steelmaking Conference Proceedings, Iron and Steel Society of AIME, Warrendale, PA, 1991, Vol. 74, pp. 163.

7. Jimbo, I., Ozturk, B., et. al.: *"Some Aspects of Chemical Phenomena in the Mold of a Continuous Slab Caster"*, Steelmaking Conference Proceedings, Iron and Steel Society of AIME, Warrendale, PA, 1991, Vol. 74, pp. 117 - 126.

8. Nakato, H., Takeuchi, S., et. al.: *"Characteristics of New Mold Fluxes for Strand Casting of Low and Ultra Low Carbon Steel Slabs"*, Steelmaking Conference Proceedings, Iron and Steel Society of AIME, Warrendale, PA, 1991, Vol. 74, pp. 639 - 646.

9. Bommaraju, R., Saad, E.: *"Mathematical Modeling of Lubrication Capacity of Mold Fluxes"*, Steelmaking Conference Proceedings, Iron and Steel Society of AIME, Warrendale, PA, 1990, Vol. 73, pp. 281 - 296.

10. Delhalle, A., Larrecq, M., et. al.: *"Slag Melting and Behavior at Meniscus Level in a Continuous Casting Mold"*, Steelmaking Conference Proceedings, Iron and Steel Society of AIME, Warrendale, PA, 1986, Vol. 68, pp. 145 - 152.

11. Mills, K.C., Grieveson, P., et. al.: *"Effect of Casting Powder on Heat transfer in Continuous Casting"*, Continuous Casting 1985, The Institute of Metals, London, U.K., 1985, pp. 57.1 - 57.7.

12. Moore, J.A., Phillips, R.J., Gibbs, T.R.: *"An Overview for the Requirements of Continuous Casting Mold Fluxes"*, Steelmaking Conference Proceedings, Iron and Steel Society of AIME, Warrendale, PA, 1991, Vol. 74, pp. 615 - 621.

13. Mills, K.C., Olusanya, A. et. al.: *"Physical Properties of Casting Powders: Part 4 - Physical Properties Relevant ot Fluid and Thermal Flow"*, Ironmaking and Steelmaking, 1988, vol. 15 (5), pp. 257 - 264.

14. Sardemann, J., Schrewe, H.: *"The Influence of Casting Powder on the Formation of Cracks in Continuous Slab Casting"*, Steelmaking Conference, Iron and Steel Society of AIME, Warrendale, PA, 1991, Vol. 74, pp. 719 - 729.

15. Ho, B.: *Characterization of Interfacial Heat Transfer in the Continuous Slab Casting Process*, Masters Thesis, University of Illinois at Urbana-Champaign, 1991.

16. Xie, B., Wu, J., and Gan, Y.: *"Study on Amount and Scheme of Carbon Mixed in Continuous Casting Mold Fluxes"*, Steelmaking Conference Proceedings, Iron and Steel Society of AIME, Warrendale, PA, 1991, Vol. 74, pp. 647 - 651.

17. Koyama, K., Nagano, K., et. al.: *"Design for Chemcial and Physical Properties of Continuous Casting Powders"*, Nippon Steel Technical Report, 1987, vol. 34 (7), pp. 41 - 47.

18. Lee, I.R., Choi, J., et. al.: *"Optimization Technology of Mold Powder according to Casting Conditions"*, Steelmaking Conference Proceedings, Iron and Steel Institute of the AIME, Warrendale, PA, 1988, Vol. 71, pp. 175 - 181.

19. Saucedo, I.G.: *"Improving the Casting Conditions at the Meniscus"*, Steelmaking Conference Proceedings, Iron and Steel Society of the AIME, Warrendale, PA, 1987, Vol. 70, pp. 449 - 459.

20. Turkdogan, E.T., Bills, A. M.: *"A Critical Review of Viscosity of CaO-MgO-Al_2O_3-SiO_2 Melts"*, American Ceramics Society Bulletin, 1960, vol. 39 (11), pp. 682 - 687.

21. Kingery, W.D., Bowen, H.K. and Uhlmann, D.R.: *Introduction to Ceramics*, Second ed., Wiley Series on the Science and Technology of Materials, E. Burke Chalmers, B., Krumhansl, J.A., eds., John Wiley & Sons, New York, 1976, pp. 477.

22. Bommaraju, R.: *"Optimum Selection and Application of Mold Fluxes for Carbon Steels"*, Steelmaking Conference Proceedings, Iron and Steel Society of AIME, Warrendale, PA, 1991, Vol. 74, pp. 131 - 146.

23. McCauley, W.L., Apelian, D.: *"Temperature Dependence of the Viscosity of Liquids"*, Proceedings of 2nd International Symposium on Metallurgical Slags and Fluxes, H.A.a.G. Fine D.R., eds., Metallurgical Society of AIME, Warrendale, PA, 1984, pp. 925 - 947.

24. Saxton, H.J., Sherby , O.D.: *"Viscosity and Atomic Mobility in Liquid Metals"*, Transactions of the ASM, 1962, vol. 55, pp. 862.

25. Riboud, P.V., Olette, M., et. al.: *"Continuous Casting Slags: Theoretical Analysis of Their Behavior and Industrial Performances"*, Steelmaking Conference Proceedings, Iron and Steel Society of AIME, Warrendale, PA, 1978, Vol. 61, pp. 411 - 417.

26. Kishimoto, M., Maeda, M., et. al.: *"Thermal Conductivity and Specific Heat of Metallurgical Slags"*, Proceedings of 2nd International Symposium on Metallurgical Slags and Fluxes, H.A. Fine Gaskell, D.R., eds., Metallurgical Society of AIME, Warrendale, PA, 1984, pp. 891 - 905.

27. Mikrovas, A.C., Argyropoulos, S.A., and Sommerville, I.D.: *"Measurements of the Effective Thermal Conductivity of Liquid Slags"*, Iron and Steelmaker, 1991, vol. 18 (12), pp. 51 - 61.

28. Siegel, R., Howell, J.R.: *Thermal Radiation Heat Transfer*, 2nd ed., McGraw-Hill, New York, 1981.

29. Ohmiya, S., Tacke, K.-H., Schwerdtfeger: *"Heat Transfer Through Layers of Casting fluxes"*, Ironmaking and Steelmaking, 1983, vol. 10 (1), pp. 24 - 30.

30. Turkdogan, E.T.: *Physicochemical Properties of Molten Slags and Glasses*, The Metals Society, London, London, 1983, pp. 58.

31. Chui, G.K.a.G., R: *"Interaction of Radiation and Conduction in Glass"*, Journal of the American Ceramic Society, 1969, vol. 52 (10), pp. 548 - 553.

32. Walther, A., Dorr, J., and Eller, E.: IBID, 1953, vol. 26, pp. 133.

33. Nagata, K., Goto, K.S.: *"Heat Conductivity and Mean Free Path of Phonons in Metallurgical Slags"*, International Symposium on Metallurgical Slags and Fluxes, H.A.a.G. Fine O.R., eds., Metallurgical Society of AIME, Warrendale, PA, 1984, pp. 875 - 889.

34. Kittel, C.: *"Interpretation of the Thermal Conductivity of Glasses"*, Physical Review, 1949, vol. 75 (6), pp. 972 - 974.

35. Nakato, H., Sakuraya, T., et. al.: *"Physical and Chemical Properties of Casting Powders affecting the Mold Lubrication during Continuous Casting"*, Steelmaking Conference Proceedings, Iron and Steel Society of AIME, Warrendale, PA, 1986, Vol. 69, pp. 137 - 143.

36. Nakano, T., Nagano, K, Masuo, N., et. al.: *"Model Analysis of Melting Process of Mold Powder for Continuous Casting of Steel"*, 1987, ,

37. Anzai, E., Shigezumi, T., et. al.: *"Hydrodynamic Behavior of Molten Powder in Meniscus Zone of Continuous Casting Mold"*, 1987, ,

38. Kakaç, S., Shah, R.K. and Aung Win: *Handbook of Single-Phase Convective Heat Transfer*, John Wiley & Sons, New York, 1987, pp. 1.21 - 1.35.

39. Incopera, F.P., DeWitt, D.P.: *Introduction to Heat Transfer*, John Wiley & Sons, New York, NY, 1985.

40. Moitra, A. *Personal Communication.* 1993.

41. Emi, T., et. al.: *"Influence of Physical and Chemical Properties of Mold Powders on the Solidification and Occurrence of Surface Defects of Strand Cast Slabs"*, Steelmaking Conference, Iron and Steel Society of AIME, Warrendale, PA, 1978, Vol. 61, pp. 350 - 360.

42. Tomono, H., Kurz, W. and Heinemann, W.: *"The Liquid Steel Meniscus in Molds and its Relevance to the Surface Quality of Castings"*, Metallurgical Transactions B, 1981, vol. 12, pp. 409 - 411.

43. Huang, X. *Personal Communication.* 1993.

44. Launder, B.E.: *"On The Computation of Convective Heat Transfer in Complex Turbulent Flows"*, Journal of Heat Transfer - Transactions of the ASME, 1988, vol. 110, pp. 1112 - 1128.

45. Khalil, E.E.: *Modelling of Furnaces and Combustors*, Abacus Press, Kent, UK, Tundbridge Wells, 1982, pp. 21 - 51.

46. Launder, B.E., Shima, N.: *"Second-Moment Closure for the Near-Wall Sublayer: Development and Application"*, Journal of the American Institute of Aeronautics and Astronautics, 1988, vol. 27 (10), pp. 1319 - 1325.

47. Nagata, K., Susa, M. and Goto, K.S.: *"Thermal Conductivities of Slags for Ironmakng and Steelmaking"*, Transactions of the ISIJ (Tetsu-to-Hagane), 1983, vol. 69, pp. 1417 - 1424.

48. Susa, M., Li F., Nagata, K.: *"Thermal Conductivity, Thermal Diffusivity and Specific Heat of Slags containing Iron Oxides"*, Ironmaking and Steelmaking 1993, 1993, vol. 20 (3), pp. 201 - 206.

49. Ponsford, F.H., K.C., Mills, et. al.: *"Physical and Thermal Properties of Aluminate Slags"*, 3rd International Conference on Molten Slags and Fluxes, 1988.

50. Ken-Ichi, T., Birat, J.P., Riboud, P., et. al: *"Modeling of Slag Rim Formation and Pressure in Molten Flux near the Meniscus"*, Transactions of the Iron and Steel Institute of Japan (ISIJ), 1984, vol. 24, pp. B-382.

51. Reitema, K.: *The Dynamics of Fine Powders: Rheology of Fluidized Powders (Chapter 9)*, Elsevier Science, New York, 1991.

52. Woodruff, H.C.: *"Rheological Properties of Plastic-Mineral Composite Powders Affecting Fluidization and Air Transport"*, Powder Technology, 1973, vol. 8, pp. 283-291.

53. Matheson, G.L., Herbst, W.A., Holt, P.H.: *"Fluid-Solid Systems"*, Industrial and Engineering Chemistry, 1949, vol. 41, pp. 1099.

54. Ashwin, B.S., Hagyard, T., et. al.: *"Viscometers Having Damped Torsional Oscillation"*, Journal of Scientific Instruments, 1960, vol. 37, pp. 480 - 485.

55. Botterill, J.S.M., Van der Kolk, M., et. al.: *"The Flow of Fluidized Solids"*, Powder Technology, 1972, vol. 6, pp. 343 - 351.

56. Adewumi, M.A., Arastoopour, H.: *"Two Dimensional Steady State Hydrodynamics Analysis of Gas-Solids Flow in Vertical Pneumatic Conveying Systems"*, World Congress Particle Technology, K. Leschonski, eds., NMA Nürnberger Messe- und Austellungsgesselschaft mbH, 1986, Vol. Part III: Mechanics of Particulate Solids Pneumatic and Hydraulic Conveying Mixing.

57. Arastoopour, H., Cutchin III, J.H.: *"Measurement and Analyis of Particle-Particle Interaction in a Co-current Flow of Particles in a Dilute Gas-Solid System"*, Chemical Engineering Science, 1985, vol. 40 (7), pp. 1135 - 1143.

58. Chikhaoui, A., Bontoux, P., et. al.: *"Steady Three-Dimensional Thermal Convectionin a Vertical Rectangular Enclosure: Transitionto Multicellular Flow"*, FIDAP User's Conference, M.S. Engleman, eds., Fluid Dynamics International, 1987, pp. 4.1 - 4.19.

59. Yee, Y., Korpela, S.A.: *"Multicellular Natural Convection in a Vertical Slot"*, Journal of Fluid Mechanics, 1983, vol. 126, pp. 91 - 121.

60. Dantzig, J.A.: *"Modelling Liquid-Solid Phase Changes with Melt Convection"*, International Journal for Numerical Methods in Engineering, 1989, vol. 28, pp. 1769-1785.

61. Anderson, D.A., Tannehill, J.C. and Pletcher, R.H.: *Computational Fluid Mechanics and Heat Transfer*, 1st ed., Computational Mehtods in Mechanics and Thermal Sciences, W.J. Minkowycz Sparrow, E.M., eds., McGraw-Hill, New York, 1984, pp. 181 - 190.

62. Stasa, F.L.: *Applied Finite Element Analysis for Engineers*, 1st ed., HRW Series in Mechanical Engineering, L.S. Fletcher, eds., Holt, Rinehart and Winston, New York, 1985, pp. 133 - 157.

63. Engleman, M.S.: *FIDAP Theoretical Manual - Revision 6.0*, Fluid Dynamics International, Inc., Evanston, IL, 1991, pp. 3.1 - 3.4.